AD-A194 954 PIEZOELECTRIC AND ELECTROSTRICTIVE MATERIALS FOR TRANSDUCER APPLICATIONS(U) PENNSYLVANIA STATE UNIV UNIVERSITY PARK MATERIALS RESEARCH LAB

1/3

UNCLASSIFIED L E CROSS ET AL. JAN 88 N00014-82-K-0339 F/G 20/3 NL

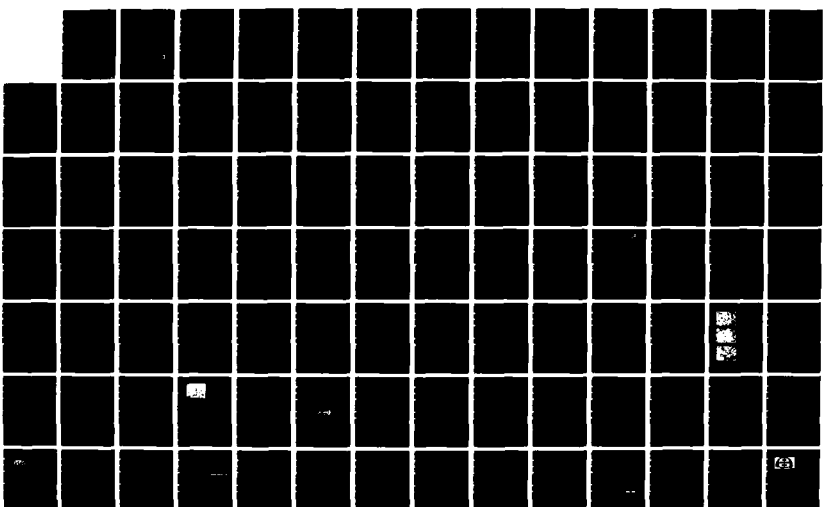

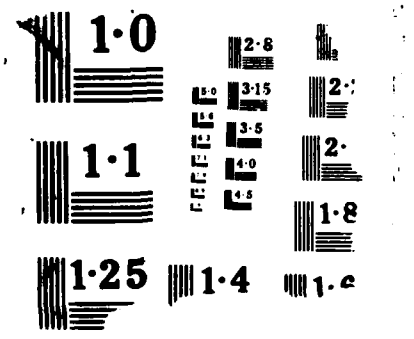
1·0
1·1
1·25
1·4
2·8
3·15
3·5
4·0
4·5
2·
1·8

PIEZOELECTRIC AND ELECTROSTRICTIVE MATERIALS FOR TRANSDUCER APPLICATIONS

Period January 1 to December 31, 1986

Annual Report

OFFICE OF NAVAL RESEARCH

Contract No. N00014-82-K0339

APPROVED FOR PUBLIC RELEASE--DISTRIBUTION UNLIMITED

L.E. Cross
R.E. Newnham
G.R. Barsch
J.V. Biggers

January 1988

THE MATERIALS RESEARCH LABORATORY

THE PENNSYLVANIA STATE UNIVERSITY

UNIVERSITY PARK, PENNSYLVANIA

TABLE OF CONTENTS

SECURITY CLASSIFICATION OF THIS PAGE

REPORT DOCUMENTATION PAGE

1a. REPORT SECURITY CLASSIFICATION	1b. RESTRICTIVE MARKINGS
2a. SECURITY CLASSIFICATION AUTHORITY	3. DISTRIBUTION/AVAILABILITY OF REPORT: Reproduction in whole or in part is permitted for any purpose of the United States Government.
2b. DECLASSIFICATION/DOWNGRADING SCHEDULE	
4. PERFORMING ORGANIZATION REPORT NUMBER(S): N00014-82-K0339	5. MONITORING ORGANIZATION REPORT NUMBER(S)
6a. NAME OF PERFORMING ORGANIZATION: Materials Research Laboratory; 6b. OFFICE SYMBOL (If applicable)	7a. NAME OF MONITORING ORGANIZATION
6c. ADDRESS (City, State and ZIP Code): The Pennsylvania State University, University Park, PA 16802	7b. ADDRESS (City, State and ZIP Code)
8a. NAME OF FUNDING/SPONSORING ORGANIZATION: Office of Naval Research; 8b. OFFICE SYMBOL (If applicable)	9. PROCUREMENT INSTRUMENT IDENTIFICATION NUMBER
8c. ADDRESS (City, State and ZIP Code): 619 Ballston Tower, 800 N. Quincy Street, Arlington, VA 22217	10. SOURCE OF FUNDING NOS.

PROGRAM ELEMENT NO.	PROJECT NO.	TASK NO.	WORK UNIT NO.

11. TITLE (Include Security Classification): Piezoelectric and Electrostrictive Mtls. for Transducer Appls.

12. PERSONAL AUTHOR(S): L.E. Cross, R.E. Newnham, G.R. Barsch, J.V. Biggers

13a. TYPE OF REPORT	13b. TIME COVERED	14. DATE OF REPORT (Yr., Mo., Day)	15. PAGE COUNT
Annual	FROM 2/86 TO 1/87		

16. SUPPLEMENTARY NOTATION

17. COSATI CODES			18. SUBJECT TERMS (Continue on reverse if necessary and identify by block number)
FIELD	GROUP	SUB. GR.	

19. ABSTRACT (Continue on reverse if necessary and identify by block number)

This annual report documents work carried out over the first year (Jan. 31, 1986 to Feb. 1, 1987) of a new three-year extension of ONR contract No. N00014-82-K-0399 Piezoelectric and Electrostrictive Materials for Transducer Applications. Three major topic areas have provided the focus for the year. Piezoelectric and Related Composites, Electrostrictive Materials, Phenomenology and Properties of Conventional Ceramic Piezoelectrics. A short section is also appended covering preparative studies and related programs. During the year, personnel from the program took a major role in the technical organization of ISAF'86, the International Meeting on Applications of Ferroelectrics held at Lehigh University. Dr. R.E. Newnham was program chairman and four of the eight program committee were from this laboratory.

In the composite structures, the emphasis has been primarily upon 0:3 connected structures with a major effort ot develop more perfect powders and more effective poling procedures. The improvement in filling factor imparted by a low temperature pre-firing

20. DISTRIBUTION/AVAILABILITY OF ABSTRACT	21. ABSTRACT SECURITY CLASSIFICATION	
UNCLASSIFIED/UNLIMITED ☐ SAME AS RPT. ☐ DTIC USERS ☐		
22a. NAME OF RESPONSIBLE INDIVIDUAL	22b. TELEPHONE NUMBER (Include Area Code)	22c. OFFICE SYMBOL

DD FORM 1473, 83 APR EDITION OF 1 JAN 73 IS OBSOLETE.

SECURITY CLASSIFICATION OF THIS PAGE

to produce a pseudo 3:0 structure has been further explored and it appears that a more complete range of properties between these of pure polymer piezoelectrics and those of pure ceramic are now accessible.

For the basic theory of electrostriction it has become clear that the earlier simple models are not applicable and effort is now being directed to developing the mathematical framework for a charge transfer model. Measurements of electrostriction in simple low permittivity solids using the converse method have been extended to the perovskite $KMnF_3$ and temperature dependence of second and third order elastic constants have been measured to complete the data needed for the theory. For practical electrostrictors, an extensive study of aging in aliovalent doped lead magnesium niobate:lead titanate has been completed and has proven that a pure compound can be made which shows no aging.

In the phenomenological study of the PZT structure family, the octahedron tilting has been inserted as a new order parameter and the problem solved for both high (untilted) and low temperature (oxygen tilted) structures. The two sublattice formalism required to describe the antiferroelectric $PbZrO_3$ rich phases has been developed and it is expected that a complete phenomenology for the whole PZT phas diagram will be completed next year.

Low temperature dielectric and piezoelectric measurements upon well defined pure PZTs have continued to permit separation of extrinsic domain and defect related contributions to the response.

Work on the high anisotropy lead titanate based ceramics has progressed to the point that it is now very clear that complex e, d and s constants are needed to fully characterize the system, and that there is a genuine zero crossing in the real part of d_{31} leading to a true zero in K_{31} at a temperature which is dependent on both poling and processing conditions.

In the associated programs, extensive preparative work has been essential to 'back up' the ongoing studies reported above. Crystal growth work has continued on the lead barium niobate bronze compositions required for morphotropic phase boundary studies, and upon the $KMnF_3$ crystals required for electrostriction studies.

1.0 INTRODUCTION

This annual report documents the work carried out on the first year (January 31, 1986 to February 1, 1987) of a new three-year extension of ONR Contract No. N00014-82-K-0339 "Piezoelectric and Electrostrictive Materials for Transducer Applications." Following already well-established custom, the work is documented largely through reprints of papers published by investigators on the program and this method is continued in this current report. To key this rather large assemblage of information carried in reprint form in the technical appendices, a brief overview summary is given to highlight the points of major progress. For convenience in accessing the data which is now circulated to more than 160 users both the summary and the appendices are divided into four major topic areas:

1. Piezoelectric and Related Composites
2. Electrostrictive Materials
3. Phenomenology and Properties of Conventional Ceramic Piezoelectrics
4. Associated Programs

During the year, personnel from the program took a major role in the technical organization of ISAF86. Dr. R.E. Newnham was program chairman, and four of the eight program committee were from this Laboratory. Focus on this program accounts for the 'bulge' in the number of papers presented this year.

2.0 PIEZOELECTRIC AND RELATED COMPOSITES

2.1 Introduction

The balance of topics under study has not changed significantly since last year. Major emphasis is still upon the 0-3 connected composites, but in view of the importance of the filler powders, more emphasis has been placed upon preparation of more perfect powders and upon characterizing the poling and performance quantitatively.

For the newer 3-0 connectivity, the higher filling factor (~ 70 vol%) give the possibility of generating a more complete family of composites--grading properties almost continuously from pure ceramic to those of pure polymer phases.

2.2 0-3 Connected Ceramic:Polymer Composites

To further test the hypothesis that the properties of 0-3 ceramic polymer composites are markedly dependent on the homogeneity and perfection of the ceramic powder, mixed oxide, sol-gel and chemical co-precipitation routes have been used to prepare high purity lead titanate

powders. As starting chemicals $Pb(C_2H_3O_2)_2 \cdot 3H_2O$ and $Ti(OC_3H_7)_4$ were used in the sol-gel method, $Pb(NO_3)_2$ and $TiCl_4$ in the co-precipitation method and PbO and TiO_2 as mixed oxides.

For all three methods, final calcining was in the range of 800-900°C. SEM studies showed that the co-precipitation method produced highly crystalline clean powder with a narrow size distribution about 5 μ meters. The sol-gel powders were also highly crystalline with a much broader size distribution containing obvious hard aggregates. As expected the mixed oxide powder was less well-crystallized with a broad size distribution.

Fabrication was with Eccogel 1365-0 polymer at a 70% volume loading of the lead titanate. Poling was effected between painted air-drying silver electrodes at the maximum field permitted which was in the range 80-115 KV/cm at 75°C.

Poling was checked using the 001 and 100 x-ray line intensities from the lead titanate diffraction pattern. Both sol-gel and co-precipitated powder composites could be more completely poled at lower fields than the mixed oxide prepared materials.

From the physical measurements d_{33}, d_{31}, d_h, K_{33}, g_h and the $d_h g_h$ product were superior in the co-precipitated powder as compared to sol-gel or oxide generated material. Both d_h and g_h showed no pressure dependence up to 1000 psi, and the co-precipitated material showed no significant aging. The best figure of merit $d_h g_h$ was over $4{,}000 \times 10^{-15}$ M^2/N.

Work is now in progress to explore hydrothermal preparation of the $PbTiO_3$ which should produce even more perfect crystallinity.

2.3 Piezoelectric Paints

0-3 ceramic-polymer composites have been produced using a paint technology with a water based methacrylic co-polymer emulsion, modified by suitable surfactants and rheology agents. Loading of the PZT or lead titanate powders was in the range 60 to 70 volume % for the final dried film. The paint was cast onto a roughened brass plate air dried for 24 hours, then oven dried at 110°C for an additional 24 hours to remove all water. Gold electrodes were sputter deposited onto the dried films for poling and measurement. After poling using fields in the range 50 to 140 KV/cm d_{33} values up to 40 pc/N were achieved.

2.4 3-0 Fired Composites

Composites with more than 70 volume % ceramic loading have been prepared by a new method. In this technique, the pressed ceramic powder is pre-fired at a relatively low (800°C) temperature, then the polymer filler is vacuum impregnated into the pre-fired ceramic. Using this method, higher density and improved connectivity is achieved. Suitably prepared samples could be corona poled to yield d_{33} values up to 90 pc/N and $d_h g_h$ values of $1{,}750$ 10^{-15} M^2/N.

We believe that by further development of this method it may be possible to produce a range of composites intermediate between the conventional 0-3 and the full ceramic PZTs which may find use as both transmitting and receiving elements.

2.5 Etched Piezoelectric Structures

Photo-resist techniques have been used to define small scale structures in piezoelectric PZT ceramics using etchants which attack preferentially at the grain boundary. Very small scale bar resonators have been defined with flexure modes in the frequency range 10 to 100 KHz and lengthwise resonances from 200 KHz to 1 MHz. Use of the transducers in micro density meters and in viscometers has been explored. The method has also been used to generate spiral delay lines, and thickness mode resonators which show no coupling into harmonics of the radial modes.

2.6 Related Studies

Work has continued jointly with NSF support and GTE collaboration, to explore the possible application of the Fresnoite structure modified polar glass ceramics to the problem of an inexpensive but temperature compensated surface acoustic wave (SAW) substrate for TV line filter applications. Using a TiO_2 modifier SAW coupling factors over 1% were achieved with temperature coefficients of -7 ppm/^oC and attenuation of only 10 dB/cm.

3.0 ELECTROSTRICTION

3.1 Introduction

In basic theory the Mathematical Framework for Lattice Dynamics in the harmonic approximation based on the charge transfer model is being worked out and an extension to the anharmonic properties, including electrostriction attempted.

Experimentally the temperature dependence of second and third order elastic constants has been determined for $KMnF_3$, needed data for input to the theory and a complete determination of the electrostriction tensor components for single crystal $KMnF_3$ has been completed using the compressometer designed in out laboratory.

For more practical electrostrictors, the compressometer method has been used to explore electrostriction in a range of alkali silicate, aluminosilicate and borosilicate glasses. In the lead magnesium niobate lead titanate ceramics, an extended study of the aging behavior revealed that aging could be eliminated by very careful stoichiometry control.

To enlarge the family of available relaxor ferroelectrics which would be available for electrostrictive applications considerable work has been done in exploring phase stability in the

lead zinc niobate (PZN) family, and on techniques for improving the stability of the useful perovskite phase by minor additions of $PbTiO_3$ and $BaTiO_3$.

3.2 Basic Theory

Effort during the contract period was concentrated upon working out the mathematics for lattice dynamics in the harmonic approximation based on the charge transfer model. This work was essentially completed, but to be useful in the context of the present study it has to be extended to anharmonic properties and that work is now in progress, so that electrostriction can be handled. In view of the mathematical complexity initial application will be only to the simplest of structures such as alkali halides and perovskites.

In a spin-off from the earlier considerations of electrostriction in $SrTiO_3$ calculations have been made of the thickness and of the energy density in the improper ferroelastic domain walls in $SrTiO_3$ at temperatures below the R point instability at 110°K.

3.3 Experimental Studies

3.3.1 Elastic Properties of $KMnF_3$

Using single crystals of $KMnF_3$ grown under this program, acoustic time of flight experiments have been used to measure the elastic constants c^s_{11}, c^s_{12}, c^s_{44} as a function of temperature over the range from 200 to 400°C. Pressure derivatives of the elastic constants were used to derive the third order constants c_{111}, c_{123} and c_{166} and to explore unusual temperature dependence in c_{144}, c_{456} and c_{112}.

A comparison to other measured third order elastic constants in perovskite trifluorides Table 3.1 shows that $KMnF_3$ is not highly anomalous.

Table 3.1
Comparison of third order elastic constants for some perovskite compounds at room temperature [units of 10^{10} N/M^2]

	$SrTiO_3$	$KZnF_3$	$KMnF_3$	$RbMnF_3$	$CsCdF_3$
a(Å)	3.905	4.055	4.19	4.25	4.465
c_{111}	-496±43	-166	-137	-184	-132
c_{112}	-77±16	-47.5	-2.5	-24	-45.5
c_{166}	-30±12	-17.9	-14	-18	-6.9
c_{123}	2±43	32	-44	4	26
c_{144}	-81±24	-5.2	1.2	-6	-31.2
c_{456}	9±27	-68.7	-2.1	-5	-38

3.3.2 Electrostriction in $KMnF_3$

For the single crystals grown in our laboratory, the original compressometer designed by Meng and Cross had to be modified to accept smaller samples. After careful testing to assure that stray capacitances could be kept under control, the guard circuit was not used and two terminal measurements carried through. The data for $KMnF_3$ is summarized in Table 3.2.

Table 3.2
Electrostriction coefficients of single crystals

	M_{11}	M_{12}	M_{44}	M_h	Q_{11}	Q_{12}	Q_{44}	Q_h
$KMnF_3$	2.72	-.538	6.58	1.64	.453	-.0896	1.10	.274**
$BaTiO_3$		.11					-0.45	.02**
CaF_2¶	-1.32	1.17	5.07	1.02	-.508	.450	1.95	.392
SrF_2¶	-1.16	1.09	5.38	1.02	-.331	.311	1.53	.291
BaF_2¶	-1.07	1.23	5.94	1.39	-.340	.390	1.88	.441

M: coefficients are in unit of 10^{-21} $M^{-2}V^2$ and Q in M^4C^{-2}.
*: from Uchino, et al., 1984.
**: from Uchino, et al., 1980.
¶: from Meng, Sun and Cross, 1984.

3.3.3 Electrostriction in Glass

Measurements on trisilicate and aluminosilicate glasses are summarized in appendices.

3.3.4 Aging Studies on Lead Magnesium Niobate

In view of the already large scale use of lead magnesium niobate:lead titanate compositions for actuators in precise surface deformable mirror applications it was important to prove that the dielectric aging effects (which would affect dimensions) observed in PLZT relaxors could be avoided in PMN and PMN:PT compositions. The studies in appendices shows very clearly that carefully made PMN:PT does not age, but that aging as in the PLZTs can be introduced either by aliovalent impurities (MnO doping) or by going off stoichiometry (excess PbO) in processing.

3.3.5 Compositions Based on Lead Zinc Niobate

Studies on lead zinc niobate (PZN) based compositions have focussed upon the basic problem of stabilizing this exciting material in the proper perovskite phase. From electronegativity and Goldschmidt tolerance factor considerations it is clear that PZN and PIN are right on the limit of stability of the perovskite vs. a pyrochlore form.

Stabilization has been achieved in the powder by quenching from a melt using excess PbO flux, in the ceramic stabilization can be achieved using a 5% addition of $BaTiO_3$ or 10% $SrTiO_3$. A number of interesting ceramic compositions in the PZN:BT:PT solid solution system have been explored.

4.0 REGULAR PIEZOELECTRICS

4.1 Introduction

Work on the phenomenological theory for the PZT family has been extended to cover all phases up to the antiferroelectric lead zirconate rich compositions. The theory accounts well for the morphotropic phase boundary, the single cell:multi-cell rhombohedral phases and the tricritical behavior near PZT 92:8. A new tricritical point is now also predicted in the tetragonal phase region.

Dielectric and piezoelectric measurements on undoped PZTs have now been extended to helium temperatures to freeze out extrinsic domain effects and to provide data for the averaged properties in random ensembles of single domain states.

Switching studies have been carried through on soft PZTs to explore the effects of hydrostatic pressure, and thus the possible changes in speed for actuator devices using P_S changes.

In related studies extensive work upon the highly anisotropic piezoelectric effects in modified lead titanates have been shown to reside primarily in intrinsic anisotropy, but the final near zero values for d_{31} and K_{31} contain important extrinsic contributions and it is shown that for a complete explanation real and imaginary components of ϵ, s and d must be considered.

4.2 Phenomenology of the PZT System

The Landau-Ginsburg-Devonshire phenomenology for PZT has now been completed for all phases up to the antiferroelectric $PbZrO_3$ rich compositions. The two sub-lattice theory for the $PbZrO_3$ has been developed, but experimental data has not yet been inserted to define the thermodynamic constants.

For the morphotropic phase boundary compositions the fitting is little changed from earlier work by Amin. In the rhombohedral phase, the octahedral tilt angle θ is inserted as a new variable and equations are solved for the spontaneous tilts in the low temperature multi-cell rhombohedral phase.

Rotostriction coupling constants to the tilt angles are necessary to describe the shape change, and contrary to initial expectation rotostriction and electrostriction are not mutually reinforcing. The first tricritical point in the PZT near the 8% $PbTiO_3$ composition is well reflected in the phenomenology, and a second tri-critical point is now indicated over in the tetragonal phase region. The long range of second order behavior embracing most of the rhombohedral compositions was not expected.

4.3 Dielectric and Piezoelectric Measurements on PZTs

Low temperature measurements on pure very carefully prepared PZT compositions confirm the trend observed earlier in doped hard and soft compositions. Freeze out of the domain contribution was however, now confirmed by observation of dielectric hysteresis where the coercivity is found to increase rapidly below ~ 35°K. The data for a wide range of sol-gel prepared compositions is being used to define the sixth order stiffness parameters in the LGD formalism.

4.4 Polarization Switching Studies

Polarization switching studies were carried through on a soft PZT 501A under a range of hydrostatic pressure from 0 to 6 K-bar. In all specimens P_S and E_C decreased with increasing pressure. For coarse grain ~ 10 μ samples the effects were linear, however in fine grain samples the effect was much steeper and non-linear. The effect was traced to the influence of grain size on the phase distribution for compositions like the 501A which is very close to morphotropy.

4.5 Lead Titanate Based Compositions (Related Studies)

Both samarium and calcium modified $PbTiO_3$ ceramic have most unusual highly anisotropic piezoelectric character in poled ceramic form. In properly chosen compositions $K_{33} \sim 50\%$ while K_{31} the transverse coefficient is almost zero. The anisotropy is observed to change with temperature and the zero crossing temperature for K_{31} is a complex function of both poling and processing variables.

Our studies have shown that the anomaly may be traced to a zero crossing of the real part of d_{31}, but that complex ϵ, s and d are essential to describe the resonance behavior precisely.

A disadvantage of the original samarium and calcium modified compositions was the low ϵ_{33} which makes drive electronics expensive in simple electromedical applications. By changing composition to the $Pb_{0.66}Ca_{0.34}Ti_{0.94}(Co_{1/2}W_{1/2})_{0.06}O_3$ + 0.01 MnO composition we were able to increase ϵ_{33} to 456 and to still maintain an $k_t/k_p \sim \infty$.

5.0 ASSOCIATED PROGRAMS

Extensive work has been carried out in ceramic preparation, most of which is described in the topical papers presented earlier. A broad review of the processing characteristics of relaxor ferroelectrics is appended, as these materials are of major importance both for transducer/actuator structures and in multilayer ceramic capacitors.

Crystal growth work has been divided between the tungsten bronze crystals in the lead barium niobate family and the perovskite trifluorides needed for the electrostriction measurements.

To confirm Japanese reports of very exciting properties in crystals of PZN:PT at compositions close to the morphotropic phase boundary, single crystals of 0.9 $PbZn_{1/3}Nb_{2/3}O_3$ - 0.1 $PbTiO_3$ were grown from lead oxide flux. Dielectric studies confirmed the phase boundary and the very high permittivity in the poled state suggests very large coupling coefficients.

6.0 PUBLICATIONS, PRESENTATIONS, HONORS, AND AWARDS

6.1 Publications

1. R.E. Newnham. "Composite Electroceramics," Ann. Rev. Mater. Sci., 1986, 16:47-68.
2. R.E. Newnham, A. Safari, C. Sa-gong, J. Giniewicz. "Flexible Composite Piezoelectric Sensors."
3. Robert E. Newnham. "Transducers, Sensors, and Actuators," Proceedings of 6th Symp. on Ultrasonic Electronics, Tokyo, 1985, Japanese J. of Appl. Phys., Vol. 25 (1986), Supplement 25-1, pp. 9-14.
4. J.R. Giniewicz, K. Duscha, R.E. Newnham, A. Safari. "$(Pb_{1-x},Bi_x)(Ti_{1-x},(Fe_{1-y},Mn_y)_x)O_3$-Polymer 0-3 Composites for Hydrophone Applications." pp. 323.
5. Y.H. Lee, M.J. Haun, A. Safari, R.E. Newnham. "Preparation of $PbTiO_3$ Powder for a Flexible 0-3 Piezoelectric Composite." pp. 318.
6. K.A. Klein, A. Safari, R.E. Newnham, J. Runt. "Composite Piezoelectric Paints." pp. 285.
7. S.M. Pilgrim, R.E. Newnham. "3:0 A New Composite Connectivity," Mat. Res. Bull., Vol. 21, pp. 1447-1454, 1986.
8. S.M. Pilgrim, R.E. Newnham. "3-0: A New Composite Connectivity." pp. 314.
9. A. Safari, T.R. Gururaja, C. Hakun, A. Halliyal, R.E. Newnham. "0-3 Piezoelectric Ceramic-Polymer Composites Prepared by a New Method: Fired Composites." pp. 305.
10. G. Sa-Gong, A. Safari, R.E. Newnham. "Poling Study of $PbTiO_3$-Polymer Composites." pp. 281.
11. S. Trolier, C. Geist, A. Safari, R.E. Newnham, Q.C. Xu. "Etched Piezoelectric Structures." pp. 707.
12. J.M. Browne, C.W. Lee, J.R. McColl, E. Ylo, A. Halliyal, A.S. Bhalla. "Piezoelectric Glass-Ceramics as Low Temperature-Coefficient Saw Substrate Materials." pp. 300.
13. E.E. Ylo, III, M. Wheeler, A. Halliyal, A.S. Bhalla, R.E. Newnham. "Piezoelectric Properties of Microstructure of Glass-Ceramics in the BaO-SrO-SiO_2-TiO_2 System." pp. 406.
14. K.A. Hu, J. Runt, A. Safari, R.E. Newnham. "TiO-Epoxy Composite Thermistors," Phase Trans., 1986, Vol. 7, pp. 1-4.
15. D. Moffatt, J. Runt, A. Safari, R.E. Newnham. "V_2O_3 Composite Thermistors." pp. 673.
16. Y. Sun, W.W. Cao, W.Y. Pan, Z.P. Chang, L.E. Cross. "Complete Determination of Electrostriction Tensor Components of $KMnF_3$ Single Crystals at Room Temperature." pp. 735.

17. Y. Sun, W.W. Cao, L.E. Cross. "Electrostriction Effect in Glass," Materials Letters, Vol. 4, No. 8, 9, 1986.

18. Y. Sun, L.E. Cross. "Investigations of Electrostriction Effects in Glass by Uniaxial Stress Compressometer."

19. Wuyi Pan, E. Furman, G.O. Dayton, L.E. Cross. "Dielectric ageing effects in doped lead magnesium niobate:lead titanate relaxor ferroelectric ceramics," J. Mat. Sci. Ltrs., 5, 1986, 647-649.

20. S.L. Swartz, G.O. Dayton, D.K. Laubscher. "Low-Temperature Fired Lead Magnesium Niobate." pp. 153.

21. W. Pan, G.O. Dayton, L.E. Cross. "Dielectric Aging Effects in Doped Lead Magnesium Niobate:Lead Titanate Relaxor Ferroelectric Ceramics." pp. 645.

22. A. Halliyal, T.R. Gururaja, U. Kumar, A. Safari. "Stability of Perovskite Phase in $Pb(Zn_{1/2}Nb_{2/3})O_3$ and Other $A(B'B'')O_3$ Perovskites." pp. 437.

23. S.L. Baumler, A. Halliyal, R.E. Newnham. "Dielectric and Piezoelectric Properties of $Pb(Zn_{1/2}Nb_{2/3})O_3$-$PbTiO_3$-$BaTiO_3$ Ceramics." pp. 418.

24. M.J. Haun, Z.Q, Zhuang, S.J. Jang, H.A. McKinstry, L.E. Cross. "A Phenomenological Theory for the Second Order Transition Region of the PZT Solid Solution System." pp. 398.

25. U. Kumar, A. Halliyal, L.E. Cross. "Modified Lead Zinc Niobate Ceramic Electrostrictors for Micropositioner Applications." pp. 633.

26. W.B. Carlson, S.E. Trolier, A. Safari, R.E. Newnham, L.E. Cross. "Multilayer Actuator Design." pp. 641.

27. Z.Q. Zhuang, M.J. Haun, S.J. Jang, L.E. Cross. "Low Temperature Dielectric, Piezoelectric and Elastic Properties of Pure (Undoped) PZT Ceramics." pp. 394.

28. D.N. Huang, Z.W. Yin, L.E. Cross. "Electrical Properties of Grain-Grown PLZT Ceramics." pp. 159.

29. Q. Li, W.Y. Pan, L.E. Cross. "The Effects of Hydrostatic Pressure on Polarization Reversal in Soft Nb:PZT Ceramics," J. Wave-Mat. Inter., Vol. 1, No. 3, 1986.

30. D. Damjanovic, T.R. Gururaja, S.J. Jang, L.E. Cross. "Temperature Behavior of the Complex Piezoelectric d_{31} Coefficient in Modified Lead Titanate Ceramics," Mat. Ltrs., Vol. 4, No. 10, 1986.

31. D. Damjanovic, T.R. Gururaja, S.J. Jang, L.E. Cross. "Electromechanical Anisotropy in Modified Lead Titanate Ceramics." pp. 344.

32. K. Takeuchi, D. Damjanovic, T.R. Gururaja, S.J. Jang, L.E. Cross. "Electromechanical Properties of Calcium Modified Lead Titanate Ceramics." pp. 402.

33. W. Pan and L.E. Cross. "Antiferroelectric to Ferroelectric Switching in Lead Zirconate Titanate Stannate Ceramics." pp. 633.

34. Thomas R. Shrout and Arvind Halliyal. "A Review of the Fabrication of Lead-Based Ferroelectric Relaxors for Capacitors."

35. M. Adachi, S.G. Sankar, A.S. Bhalla, Z.P. Chang, L.E. Cross. "Growth and Dielectric Properties of Lead Barium Niobate Single Crystals and Morphotropic Phase Boundary." pp. 169.

36. X.S, Lin, A.S, Bhalla, L.E. Cross. "Growth and Pyroelectric Properties of Alanine and Phosphorus Substituted Triglycine Selenate (TGSe) Single Crystals." pp. 192.

37. Z.P. Chang, A.S. Bhalla, L.E. Cross. "Growth, Dielectric and Pyroelectric Properties of $0.9Pb(Zn_{1/3}Nb_{2/3})O_3$-$0.1PbTiO_3$ Single Crystals." pp. 482.

38. P.K. Ghosh, A.S. Bhalla, L.E. Cross. "Dielectric Properties of RF Sputtered Bismuth Titanate Thin Films." pp. 596.

39. C.W. Nies, T.R. Gururaja, R.E. Newnham. "Testing Techniques for Sonochemistry in Flow-Through Transducers." pp. 700.

40. Z.Q. Zhuang, M.P. Harmer, D.M. Smyth. "The Effect of Octahedrally-Coordinated Calcium on the Ferroelectric Transition of $BaTiO_3$." pp. 122.

41. N.S. Dalal, A.S. Bhalla, L.E. Cross. "Investigations of Charge Compensation in the Phosphate, Arsenate, and Chromate-Doped Triglycine Sulphate (TGS) Crystals: Mechanism of Enhancement of Pyroelectric Properties." pp. 188.

6.2 Presentations at National and International Meetings

1. W.Y. Pan, L.E. Cross. "Aging Effects in Doped Lead Magnesium Niobate:Lead Titanate Relaxor Ferroelectric Ceramics," Amer. Ceram. Soc. Annual Mtg. (1986).
2. C.W. Nies, T.R. Gururaja, R.E. Newnham. "Flow Through Transducers for On-Line Sonication," Amer. Ceram. Soc. Annual Mtg. (1986).
3. M.T. Lanagan, D.M. Moffatt, D.A. Anderson, R.E. Newnham. "Dielectric and Piezoelectric Properties of $PbTiO_3$-$PbZrO_3$-$Pb(Zn_{1/3}Nb_{2/3})O_3$ Ceramics," Amer. Ceram. Soc. Annual Mtg. (1986).
4. S.M. Pilgrim, R.E. Newnham. "3:0 A New Composite Connectivity," Amer. Ceram. Soc. Annual Mtg. (1986).
5. S.M. Pilgrim, W. Thompson, R.E. Newnham, A.E. Semple. "Complex Dynamic Moduli of Ceramic-Polymer Composites by the Transfer Function Method," Amer. Ceram. Soc. Annual Mtg. (1986).

6. S.M. Pilgrim, A.E. Semple, W. Thompson, R.E. Newnham. "Wave Absorption in Piezoelectric Composites, Tailoring Multiphase and Composite Ceramics," Amer. Ceram. Soc. Annual Mtg. (1986).
7. W.B. Carlson, R.E. Newnham, A. Safari. "Numerical Analysis of the Design of Electrostrictive Ceramic Devices," Amer. Ceram. Soc. Annual Mtg. (1986).
8. S. DaVanzo, W. Carlson, R.E. Newnham, A. Safari. "Finite Element/Finite Difference Modeling of Electroceramics," 21st University Conf. in Tailoring Multiphase and Composite Ceramics, Penn State (1985).
9. W.B. Carlson, R.E. Newnham. "Electrical Field Modeling in Flawed Ceramic Capacitors," Amer. Ceram. Soc. Annual Mtg. (1986).
10. K.A. Hu, J. Runt, D.A. Moffatt, A. Safari, R.E. Newnham. "Composite Thermistors," Amer. Chem. Soc. (1986).
11. K.A. Hu, J. Runt, R.E. Newnham, A. Safari. "Composite Thermistors," Amer. Phys. Soc. (1986).
12. K.A. Hu, J. Runt, D.A. Moffatt, A. Safari, R.E. Newnham. "Electroceramic-Polymer Composite Thermistors." Polymer Symp., Penn State (1985).
13. A. Safari, G. Giniewicz, T.R. Gururaja, J. Runt, R.E. Newnham. "Piezoelectric Polymer Composites," Polymer Symp., Penn State (1985).
14. Y. Sun, L.E. Cross. "Electrostrictive Effects in Glass," Amer. Ceram. Soc. Annual Mtg. (1986).
15. Y. Sun, L.E. Cross. "Investigations of Electrostrictive Effects in Glass by Uniaxial Stress Compressometer."
16. M.J. Haun, T.R. Halemane, R.E. Newnham, L.E. Cross. "A Phenomenological Theory for the $PbZrO_3$:$PbTiO_3$ Solid Solution System," Amer. Ceram. Soc. Annual Mtg. (1986).
17. M.J. Haun, S.J. Jang, H.A. McKinstry, R.E. Newnham, L.E. Cross. "A Phenomenological Theory for the Second Order Transition Region of the PZT Solid Solution System," Amer. Ceram. Soc. Annual Mtg. (1986).
18. Z.Q. Zhuang, M.J. Haun, S.J. Jang, L.E. Cross. "Low Temperature Piezoelectric, Dielectric, and Elastic Properties of Pure (Undoped) PZT Ceramics," Amer. Ceram. Soc. Annual Mtg. (1986).
19. Y.H. Lee, M.J. Haun, A. Safari, R.E. Newnham. "Filler Preparation for $PbTiO_3$-Polymer Piezoelectric Composites," Amer. Ceram. Soc. Annual Mtg. (1986).
20. M.J. Haun, Y.H. Lee, H.A. McKinstry, L.E. Cross. "High Temperature X-ray Diffraction Study of $Pb(Zr_{1-x}Ti_x)O_3$ Compositions," 35th Conf. on Appl. of X-ray Analysis, Denver (1986).

21. S. Trolier, C. Geist, S. DaVanzo, A. Safari, R.E. Newnham. "Etched Piezoelectric Structures," Amer. Ceram. Soc. Annual Mtg. (1986).

22. E. Ylo, M. Wheeler, A. Halliyal, A.S. Bhalla, R.E. Newnham. "Piezoelectric Properties and Microstructure of Fresnoite Glass-Ceramics," Amer. Ceram. Soc. Annual Mtg. (1986).

23. T.R. Shrout. "Processing of Relaxor Ferroelectrics," Amer. Ceram. Soc. Annual Mtg. (1986).

24. R. Guo, F. Liu. "Resistance Leakage Current and Power Loss of Zinc Oxide Varistors," Amer. Ceram. Soc. Annual Mtg. (1986).

25. K.A. Klein, A. Safari, R.E. Newnham, J. Runt. "Thin Film Polymer-Electroceramic Composites," Penn State Polymer Symp. (1986).

26. D. Moffatt, L. Rohlfing, A. Safari, J. Runt, R.E. Newnham. "Composite Thermistors," Penn State Polymer Symp. (1986).

27. D. Lei, A. Safari, R.E. Newnham, J. Runt. "Dielectric Properties of Dye-Polymer Composites," Penn State Polymer Symp. (1986).

28. S.M. Pilgrim, R.E. Newnham, W. Thompson, A.E. Semple. "Complex Dynamic Moduli of Ceramic-Polymer Composites by the Transfer Function Method." Penn State Polymer Symp. (1986).

29. A. Halliyal, U. Kumar, R.E. Newnham. "Stabilization of Perovskite Phase in the PZN-$PbTiO_3$-$BaTiO_3$ System and Dielectric and Piezoelectric Properties," Amer. Ceram. Soc. Annual Mtg. (1986).

30. U. Kumar, A. Halliyal, L.E. Cross. "Modified Lead Zinc Niobate Ceramics for Micropositioner Applications," Amer. Ceram. Soc. Annual Mtg. (1986).

31. S.L. Baumler, A. Halliyal, R.E. Newnham. "Dielectric and Piezoelectric Properties of PZN-$PbTiO_3$-$BaTiO_3$ Ceramics," Amer. Ceram. Soc. Annual Mtg. (1986).

32. A. Safari, T.R. Gururaja, C. Hakun, A. Halliyal, R.E. Newnham. "Alternative Way of Fabrication and Poling 0-3 Piezoelectric-Polymer Composites," Amer. Ceram. Soc. Annual Mtg. (1986).

33. T.R. Gururaja, A. Safari, A. Halliyal. "Preparation of Perovskite PZN-PT Ceramic Powders Near the Morphotropic Phase Boundary," Amer. Ceram. Soc. Annual Mtg. (1986).

34. R.E. Newnham. "Electrostriction and Actuators," Amer. Crystallographic Association Annual Mtg. (1986).

35. F.J. Rotella, M.H. Mueller, D. Damjanovic, R.E. Newnham. "A Neutron Powder Diffraction Study of Doped $PbTiO_3$ Ceramics," Amer. Crystallographic Association Annual Mtg. (1986).

36. R.E. Newnham. Presidential Address, "Crystals and the National Economy," Amer. Crystallographic Association (1986).

37. J.K. Yamamoto, A.S. Bhalla, R.E. Newnham. "Microwave Dielectric Properties of Microporus Silica," Amer. Ceram. Soc. Annual Mtg. (1986).

38. S. DaVanzo, L. Pardo, A. Safari, R.E. Newnham. "A Conductive Cubes Model for 0-3 Piezoelectric Composites," Amer. Ceram. Soc. Annual Mtg. (1986).

39. J.R. Giniewicz, K. Duscha, R.E. Newnham, A. Safari, "$(Pb_{1-x}Bi_x)(Ti_{1-x}Fe_x)O_3$/Polymer 0-3 Composites," Amer. Ceram. Soc. Annual Mtg. (1986).

40. D. Moffatt, A. Safari, J. Runt, R.E. Newnham. "V_2O_3 Composite Thermistors," Amer. Ceram. Soc. Annual Mtg. (1986).

41. B.V. Hiremath, R.E. Newnham. "Fabrication and Characterization of a Multilayer Thermistor," Amer. Ceram. Soc. Annual Mtg. (1986).

42. D.L. Boucher, J.H. Kim, S.J. Jang, R.E. Newnham. "Dielectric Properties of Silicates at Microwave Frequencies," Amer. Ceram. Soc. Annual Mtg. (1986).

43. L.E. Cross, R.E. Newnham. "Ferroelectric Ceramics," Amer. Ceram. Soc. Annual Mtg. (1986).

44. R.E. Newnham. "Holey Crystals," Amer. Ceram. Soc. Annual Mtg. (1986).

45. S.A. Markgraf, A.S. Bhalla, R.E. Newnham. "Polar Properties of Hemimorphite," Amer. Crystallographic Association Mtg. (1985).

46. A. Halliyal, E. Ylo, S.A. Markgraf, A.S. Bhalla, R.E. Newnham. "Polar Glass-Ceramics for Piezoelectric and Pyroelectric Devices," Symp. on Composite Materials, Penn State (1985).

47. A.S. Bhalla. "New Materials for Sensor Applications," Keynote Speaker, Lecture at the Canadian Ceramic Society (1986).

48. J. Yamamoto, J.H. Kim, A.S. Bhalla, R.E. Newnham. "Microwave Dielectric Properties of Microporus Silica," Amer. Ceram. Soc. Annual Mtg. (1986).

49. H.M. Chan, M.P. Harmer, A.S. Bhalla, L.E. Cross. "Transmission Electron Microscopy of Undoped and Mn-Doped Lead Magnesium Niobate:Lead Titanate $Pb(Mg_{1/2}Nb_{2/3})O_3$:$PbTiO_3$ Relaxor Ferroelectrics," Amer. Ceram. Soc. Annual Mtg. (1986).

50. L.E. Cross, A.S. Bhalla, P. Asadipour. "Polarization Mechanism in Relaxor Ferroelectrics," (Invited) Amer. Ceram. Soc. Annual Mtg. (1986).

51. H.M. Chan, M.P. Harmer, A.S. Bhalla, L.E. Cross. "TEM of the Relaxor Material $Pb(Sc_{0.5}Ta_{0.5})O_3$," Amer. Ceram. Soc. Annual Mtg. (1986).

52. A.S. Bhalla, S.L. Swartz, L.E. Cross. "Dielectric Properties of Al_2O_3/Al Composites Formed by Oxidizing Al Alloys," Amer. Ceram. Soc. Annual Mtg. (1986).

53. W.Y. Pan, L.E. Cross, G.O. Dayton. "Antiferroelectric to Ferroelectric Switching in Lead Zirconate Titanate Stannate Ceramics," Intl. Symp. Appl. Ferroelectrics (1986).

54. W.Y. Pan, L.E. Cross, G.O. Dayton. "Dielectric Aging Effects in Doped Lead Magnesium Niobate:Lead Titanate Relaxor Ferroelectric Ceramics," Intl. Symp. Appl. Ferroelectrics (1986).

55. C.W. Nies, T.R. Gururaja, R.E. Newnham. "Flow Through Transducers for On-Line Sonication," Intl. Symp. Appl. Ferroelectrics (1986).

56. S.M. Pilgrim, R.E. Newnham. "3:0 A New Composite Connectivity," Intl. Symp. Appl. Ferroelectrics (1986).

57. W.B. Carlson, R.E. Newnham, A. Safari. "Multilayer Actuator Design," Intl. Symp. Appl. Ferroelectrics (1986).

58. D.A. Moffatt, J. Runt, A. Safari, R.E. Newnham. "V_2O_3 Composite Thermistors," Intl. Symp. Appl. Ferroelectrics (1986).

59. K. Klein, J. Runt, A. Safari, R.E. Newnham. "Composite Piezoelectric Points," Intl. Symp. Appl. Ferroelectrics (1986).

60. Y. Sun, L.E. Cross. "Investigations of Electrostrictive Effects in Glass by Uniaxial Stress Compressometer," Intl. Symp. Appl. Ferroelectrics (1986).

61. S. Markgraf, A.S. Bhalla, R.E. Newnham. "Hemimorphite, A Strong Nonferroelectric Pyroelectric," Intl. Symp. Appl. Ferroelectrics (1986).

62. M.J. Haun, Z.Q. Zhuang, S.J. Jang, H.A. McKinstry, L.E. Cross. "A Phenomenological Theory for the Second Order Transition Region of the PZT Solid Solution System," Intl. Symp. Appl. Ferroelectrics (1986).

63. Z.Q. Zhuang, M.J. Haun, S.J. Jang, L.E. Cross. "Low Temperature Dielectric, Piezoelectric and Elastic Properties of Pure (Undoped) PZT Ceramics," Intl. Symp. Appl. Ferroelectrics (1986).

64. Y.H. Le, M.J. Haun, A. Safari, R.E. Newnham. "Preparation of $PbTiO_3$ Powder for a Flexible 0-3 Piezoelectric Composite," Intl. Symp. Appl. Ferroelectrics (1986).

65. S. Trolier, C. Geist, A. Safari, R.E. Newnham, Q.C. Xu. "Etched Piezoelectric Structures," Intl. Symp. Appl. Ferroelectrics (1986).

66. X.S. Lin, A.S. Bhalla, L.E. Cross. "Growth and Pyroelectric Properties of LATGSeP Single Crystals," Intl. Symp. Appl. Ferroelectrics (1986).

67. D.N. Huang, Z.W. Yin, L.E. Cross. "Electrical Properties of Grain-Grown PLZT Ceramics," Intl. Symp. Appl. Ferroelectrics (1986).

68. E. Ylo, M. Wheeler, A. Halliyal, A.S. Bhalla, R.E. Newnham. "Piezoelectric Properties and Microstructure of Fresnoite Glass-Ceramics," Intl. Symp. Appl. Ferroelectrics (1986).

69. J.M. Browne, C.W. Lee, J.R. McColl, E. Ylo, A. Halliyal, A.S. Bhalla. "Piezoelectric Glass-Ceramics as Low Temperature Coefficient SAW Substrate Materials," Intl. Symp. Appl. Ferroelectrics (1986).

70. R.E. Newnham. "Ferroelectric Composites," Intl. Symp. Appl. Ferroelectrics (1986).

71. B.V. Hiremath, R.E. Newnham, L.E. Cross, J.V. Biggers. "$Ba_{1-x}Bi_xPbO_3$-A New Materials for Barrier Layer Capacitors," Intl. Symp. Appl. Ferroelectrics (1986).

72. G. Sa-Gong, A. Safari, S.J. Jang, R.E. Newnham. "Easily Poled Flexible Piezoelectric Composites," Intl. Symp. Appl. Ferroelectrics (1986).

73. K.A. Klein, A. Safari, R.E. Newnham, J. Runt. "Composite Piezoelectric Paints," Intl. Symp. Appl. Ferroelectrics (1986).

74. B.V. Hiremath, R.E. Newnham. "Fabrication and Characterization of a New Multilayer Thermistor," Intl. Symp. Appl. Ferroelectrics (1986).

75. D. Moffatt, A. Safari, J. Runt, R.E. Newnham. "V_2O_3 Composite Thermistors," Intl. Symp. Appl. Ferroelectrics (1986).

76. A. Safari, T.R. Gururaja, C. Hakun, A. Halliyal, R.E. Newnham. "Alternative Way of Fabrication and Poling 0-3 Piezoelectric-Polymer Composites," Intl. Symp. Appl. Ferroelectrics (1986).

77. A. Halliyal, T.R. Gururaja, U. Kumar, A. Safari. "Stability of Perovskite Phase in PZN and Other $A(B'B'')O_3$ Perovskites," Intl. Symp. Appl. Ferroelectrics (1986).

78. S.L. Baumler, A. Halliyal, R.E. Newnham. "Dielectric and Piezoelectric Properties of PZN-$PbTiO_3$-$BaTiO_3$ Ceramics," Intl. Symp. Appl. Ferroelectrics (1986).

79. U. Kumar, A. Halliyal, L.E. Cross. "Modified Lead Zinc Niobate Ceramic Electrostrictors for Micropositioner Applications," Intl. Symp. Appl. Ferroelectrics (1986).

80. T.R. Gururaja, A. Safari, A. Halliyal. "Preparation of Perovskite PZN-PT Ceramic Powders Near the Morphotropic Phase Boundary," Intl. Symp. Appl. Ferroelectrics (1986).

81. D. Damjanovic, T.R. Gururaja, S.J. Jang, L.E. Cross. "Electromechanical Anisotropy in Modified Lead Titanate Ceramics," Intl. Symp. Appl. Ferroelectrics (1986).

82. Z.Q. Zhuang, M.P. Harmer, D.M. Smyth, R.E. Newnham. "The Effect of Octahedrally Coordinated Calcium Ion on the Ferroelectric Transition in $BaTiO_3$," Intl. Symp. Appl. Ferroelectrics (1986).

83. M. Adachi, S.G. Sankar, A.S. Bhalla, Z.P. Chang, L.E. Cross. "Growth and Dielectric Properties of Orthorhombic Lead Barium Niobate Single Crystals Near Morphotropic Phase Boundaries," Intl. Symp. Appl. Ferroelectrics (1986).

84. J.R. Giniewicz, K. Duscha, R.E. Newnham, A. Safari, "$(Pb_{1-x}Bi_x)(Ti_{1-x}F_x)O_3$/Polymer 0-3 Composites," Intl. Symp. Appl. Ferroelectrics (1986).

85. G.O. Dayton, S.L. Swartz, D. Laubscher. "Fast Firing of Lead Magnesium Niobate Ceramics," Intl. Symp. Appl. Ferroelectrics (1986).

86. N.S. Dalal, A.S. Bhalla, L.E. Cross. "Investigation of Structural Change in Phosphate, Arsenate and Chromate-Substituted TGS," Intl. Symp. Appl. Ferroelectrics (1986).

87. L.E. Cross. "Electrostrictive Materials and Applications," Intl. Symp. Appl. Ferroelectrics (1986).

88. P.K. Ghosh, A.S. Bhalla, L.E. Cross. "Dielectric Properties of RF Sputtered Bismuth Titanate Thin Films," Intl. Symp. Appl. Ferroelectrics (1986).

89. E. Furman, L.E. Cross. "Dielectric Breakdown and Related Properties of PLZT," Intl. Symp. Appl. Ferroelectrics (1986).

90. K. Takeuchi, D. Damjanovic, T.R. Gururaja, S.J. Jang, L.E. Cross. "Electromechanical Coupling Properties of Calcium Doped Lead Titanate Ceramics," Intl. Symp. Appl. Ferroelectrics (1986).

91. X.S. Lin. A.S. Bhalla, L.E. Cross. "Growth and Pyroelectric Properties of Alanine and Phosphorus Substituted TGSe Single Crystals," Intl. Symp. Appl. Ferroelectrics (1986).

92. Z.P. Chang, A.S. Bhalla, L.E. Cross. "Growth, Dielectric and Pyroelectric Properties of 0.91 PZN-0.1 PT Single Crystals," Intl. Symp. Appl. Ferroelectrics (1986).

Books

R.E. Newnham, S.A. Markgraf. Classic Crystals: A Book of Models, The Pennsylvania State University (1986).

6.3 Honors and Awards

L. Eric Cross	Honorary Doctor Degree from Xian Jiaotong University, China
R.E. Newnham	Colorado State University Outstanding Alumnus Award

T.R. Gururaja W.A. Schulze L.E. Cross R.E. Newnham B. Auld J. Wang	Best Paper Award for 1985 Ultrasonics Ferroelectrics and Frequency Control Society of the IEEE
S.L. Swartz	Ph.D. Xerox Award
J. Giniewicz	M.S. Xerox Award
J. Belsick	B.S. Xerox Award
S. Trolier	Time Magazine Best Student Award 1986

6.4 Degrees Earned

May 1986	S.P. DaVanzo Finite Element Modeling of PZT Composites for Hydrophone Applications	Ph.D. in Solid State Science
June 1986	Wenwu Cao Non-linear and Non-local Lattice Dynamical Effects in $O^1{}_h$-$D^{18}{}_{4h}$ Improper Ferroelastic Phase Transitions	Ph.D. in Physics
August 1986	P.K. Ghosh Dielectric Thin Films	Ph.D. in Solid State Science
May 1986	S.M. Baumler Dielectric and Piezoelectric Properties of $Pb(Zn_{1/3}Nb_{2/3})O_3$:$PbTiO_3$-$BaTiO_3$ Ceramics	M.S. in Solid State Science
May 1986	P. Asadipour Polarization Mechanisms in Relaxor Ferroelectrics	M.S. in Electrical Engineering

August 1986	K. Takeuchi Electromechanical Properties of Modified Lead Titanates	M.S. in Electrical Engineering

6.5 Applied Science Apprenticeships

It is the purpose of this program to provide opportunity for high school students to become acquainted, during their summer break, with the workings of a major research laboratory and the fascination of research and discover. The objective is to have a maximum of four students in this category who could work closely with the post-doctoral fellows and graduate assistants in the Materials Research Laboratory on problems associated with our ONR program in the Center and Dielectric Studies and on the program of research on Piezoelectric and Electrostrictive Materials for Transducer Applications. These programs which encompasses the preparation, characterization, and measurement of properties of a wide range of new electroceramic and ceramic-plastic composites offer many opportunities in which the "extra pair of hands" and quick perceptions of a well-motivated high school student provides invaluable assistance.

We believe that the relaxed atmosphere and constant interchange between faculty, post-doctoral fellows, graduate assistants, and technical aides, and the continuous presence of many eminent foreign visiting scientists provides a very stimulating environment for the young student who may be at a critical juncture in making decisions as to longer range career plans.

A secondary but not insignificant advantage of the program is in the additional component which it provides in the education of our graduate students. Most of these young men and women will go out into responsible positions in Government and Industry where they will be called upon to organize and supervise the work of many junior engineers and technicians. This program, which attaches the technical aid to a graduate assistant, gives him the chance to organize the work of a second person to speed his own program, but also the responsibility of the associated human problems of scheduling and humane management. We believe it has been a most valuable experience for the graduate assistants who have participated and has given them very useful insights into both the problems and the rewards of "people management."

For the last three years, we have developed a much closer relationship with the University's Upward Bound Program, who are able to draw well-motivated black students from the Philadelphia School System. Over the years it has become our custom to issue each student participant a certificate on completion of the term at a small internal ceremony in MRL. Copies of certificates given to our last three successful apprentices are appended.

THE MATERIALS RESEARCH LABORATORY

THE PENNSYLVANIA STATE UNIVERSITY

1986

Office of Naval Research
Apprentice Program Certification

for successful completion of the 7 week project/study program
in Electronic Ceramica

Tanya Fredrick

The Pennsylvania State University

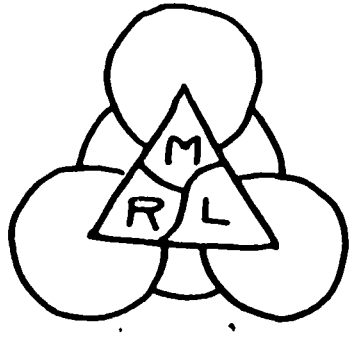

THE MATERIALS RESEARCH LABORATORY

THE PENNSYLVANIA STATE UNIVERSITY

1986

Office of Naval Research
Apprentice Program Certification

for successful completion of the 7 week project/study program
in Electronic Ceramica

Keith Scriven

The Pennsylvania State University

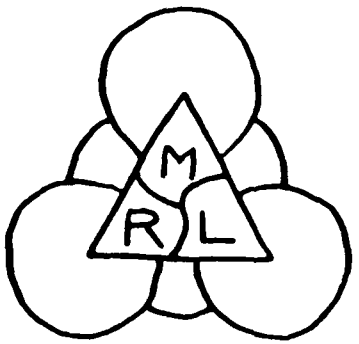

THE MATERIALS RESEARCH LABORATORY

THE PENNSYLVANIA STATE UNIVERSITY

1986

Office of Naval Research
Apprentice Program Certification

for successful completion of the 7 week project/study program
in Electronic Ceramica

Yuri Brown

The Pennsylvania State University

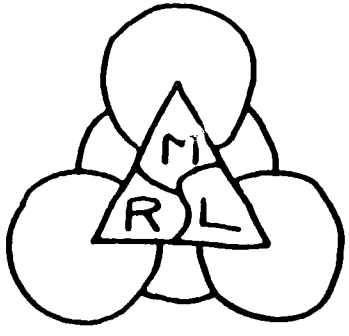

PIEZOELECTRIC AND RELATED COMPOSITES

Ann. Rev. Mater. Sci. 1986. 16: 47–68

COMPOSITE ELECTROCERAMICS

R. E. Newnham

Materials Research Laboratory, Pennsylvania State University, University Park, Pennsylvania 16802

INTRODUCTION

Composite materials have found a number of structural applications in the aircraft and automobile industries, but their use in electronics is also surprisingly widespread. Such applications of electroceramics include their use in multilayer capacitors, piezoelectric transducers, packages for integrated circuits, high voltage insulators, magnetic tape, varistors for lightning arrestors, and chemical sensors.

In this paper we review some of the basic ideas underlying composite electroceramics: sum and product properties; connectivity patterns, which determine field and force concentration; the importance of periodicity and scale in resonant structures; the symmetry of composite materials and its influence on physical properties; polychromatic percolation and coupled conduction paths in composites; varistor action and other interfacial effects; coupled phase transformation phenomena in composites; and the important role that porosity and inner surface area play in many composites.

PROPERTIES OF COMPOSITE MATERIALS

For convenience, the physical and chemical properties of composites can be classified as sum properties, combination properties, and product properties. The basic ideas underlying sum and product properties were introduced by van Suchtelen (1). For a *sum property*, the composite property coefficient depends on the corresponding coefficients of its constituent phases. Thus the stiffness of a composite is governed by the elastic stiffnesses of its component phases and the mixing rule appropriate

0084–6600/86/0801-0047$02.00

to its geometry. In general, the property coefficient of the composite will be between those of its constituent phases.

This is not true for *combination properties*, which involve two or more different coefficients. Poisson's ratio is a good example of a combination property since it is equal to the ratio of two compliance coefficients. Some composite materials, e.g. wood (2), have extremely small Poisson ratios, even smaller than those of the materials used to make the composite.

Product properties are more complex and more interesting. The product properties of a composite involve different properties in its constituent phases: the interactions between the phases often causing unexpected results.

Sum Properties

The dielectric constant will be used to illustrate a simple sum property. Series and parallel mixing rules delimit the bounding conditions for the dielectric constant $\bar{K}$ of a diphasic composite:

$$\bar{K}^n = V_1 K_1^n + V_2 K_2^n + \ldots,$$

where K_1 and K_2 are the dielectric constants of the constituent phases, and V_1 and V_2 are their volume fractions. The exponent n is $+1$ for parallel mixing and -1 for series mixing. For many composites, the geometric arrangement is partly series and partly parallel, in which case $\bar{K}$ can often be described by a logarithmic mixing rule for which the exponent $n \approx 0$.

There are, of course, many other mixing rules in addition to the series and parallel models. These represent only the limiting conditio A more complete discussion of the dielectric properties of heterogeneou materials is given in the classic article by van Beek (3).

As examples of composite ferroelectrics, let us consider the temperature dependence of capacitors. *Depressors* are materials that are added to a high K capacitor formulation to depress its peak at the Curie point, thus producing a flatter temperature dependence curve. Bismuth stannate and magnesium zirconate are often used as depressors for barium titanate multilayer ceramics. These additives form a second phase in the grain boundary regions of the ceramic. The grain boundary phase has a much lower dielectric constant than $BaTiO_3$ and depresses the dielectric constant of the ceramic, largely through the series mixing rule. Low K boundary phases in series with high K grains have a much greater effect on the permittivity than do those in parallel. The brick-wall model gives a good description of diphasic ceramic dielectrics (4).

Composite ceramics are also useful in high voltage applications. The dielectric ceramics of $BaTiO_3$ multilayer capacitors decreases substantially under high voltage fields, often by 100% or more. This is normal

behavior for ferroelectric materials in which the polarization saturates, but antiferroelectric substances such as $NaNbO_3$ behave differently. The dielectric constant of sodium niobate is nearly independent of bias field as its metastable ferroelectric structure begins to influence the permittivity under high fields.

Capacitor compositions with enhanced permittivity at high fields have been manufactured from composites made from $BaTiO_3$ and $NaNbO_3$. Fast-firing a mixture of $BaTiO_3$ and $NaNbO_3$ causes the $NaNbO_3$ to melt and coat the grains of $BaTiO_3$, producing a composite structure with ferroelectric grains embedded in an antiferroelectric matrix. By adjusting the composition and firing schedule, a capacitor with field-independent permittivity can be produced (4).

Insulators with low dielectric constants are required for microwave lead-through seals (5). By introducing 60 vol.% porosity in a foamed lithium aluminum silicate glass, its dielectric constant is reduced from 5.6 to 2.1. Decreasing the dielectric constant increases the speed of electromagnetic waves traveling along conducting wires embedded in the composite. The speed is doubled by replacing alumina ($K \sim 9$) with porous glass ($K \sim 2$).

Combination Properties

For simple mixing rules the properties of a composite lie between those of its constituent phases, but combination properties involve two or more coefficients which may average in a different way.

For example, acoustic wave velocity determines the resonant frequency of piezoelectric devices. The velocity of waves propagating along the length of a long, thin rod is $v = (E\rho)^{1/2}$, where E is Young's modulus and ρ is the rod's density. Fiber-reinforced composites often have very anisotropic wave velocities. Consider a compliant matrix material reinforced with parallel fibers. Long, thin rods fashioned from the composite have different properties when the fibers are oriented parallel or perpendicular to the length of the rod. The wave velocities are much faster for rods with longitudinally oriented (v_L) fibers than for those with transversely oriented (v_T) ones.

Experimental data (6) for composites made from steel filaments embedded in epoxy conform closely to the equations for v_L and v_T. It is interesting to note that v_T, the wave velocity for waves traveling transverse to the fibers, is less than the velocity of both epoxy and steel, the two phases that make up the composite. The slowness of this wave results from the different dependencies of density and stiffness on volume fraction. This difference in mixing rules for E and ρ cause the combination property v_T to lie outside the range of the end members. The longitudinal wave, v_L,

behaves more normally: E and ρ follow the same mixing rule and the values for v_L lie between those of the end members.

Product Properties

The interaction of different properties in the two phases of a composite result in yet a third property, a product property. The combination of different properties of two or more constituents sometimes yields surprisingly large product properties. Indeed, in a few cases, product properties are found in composites that were entirely absent in the phases that make up the composite. Table 1 lists a few of the hundreds of possible product properties (1), including several described in this article.

Several of the most sensitive magnetic field sensors are composite materials that utilize product properties. In the magnetoresistive field plate (7) a composite of InSb and NiSb is directionally solidified to form parallel NiSb needles in an InSb matrix. A long rectangular segment of the composite is electroded across the ends with the NiSb fibers parallel to the electrodes and transverse to the length of the composite. InSb is a semiconductor with a large Hall effect and NiSb is metallic and highly electrically conductive.

When an electric current flows along the length of the bar and a magnetic field is applied perpendicular to the current and perpendicular to the NiSb needles the current is deflected because of the Hall effect. Normally this would result in an electrical field transverse to the current and the magnetic field, but the NiSb needles short out the field. Electric current continues to be deflected as long as the magnetic field is present. The resulting product property is a large magnetoresistance effect.

Magnetic field probes are also made from ferroelectric $BaTiO_3$ and ferrimagnetic cobalt titanium ferrite (8,9). A dense eutectic mixture of the perovskite and spinel-structure phases was obtained by directional solidification, and then was electrically poled to make the $BaTiO_3$ phase

Table 1 Examples of product properties (1)

Property of phase 1	Property of phase 2	Composite product property
Thermal expansion	Electrical conductivity	Thermistor
Magnetostriction	Piezoelectricity	Magnetoelectricity
Hall effect	Electrical conductivity	Magnetoresistance
Photoconductivity	Electrostriction	Photostriction
Superconductivity	Adiabatic demagnetization	Electrothermal effect
Piezoelectricity	Thermal expansion	Pyroelectricity

piezoelectric. When a magnetic field is applied to the composite the ferrite grains change shape because of magnetostriction, and the strain is passed along to the piezoelectric grains, resulting in an electrical polarization. Magnetoelectric effects a hundred times larger than those in Cr_2O_3 are obtained in this way. Further research in this area led to the development of a broadband magnetic field probe with an exceptionally flat frequency response up to 650 kHz (10).

SYMMETRY OF COMPOSITE MATERIALS

A wide variety of symmetries are found in composite materials, including crystallographic groups, Curie groups, black-and-white groups, and color groups. In describing the symmetry of composite materials, the basic idea is Curie's principle of symmetry superposition: A composite material will exhibit only those symmetry elements that are common to its constituent phases and their geometrical arrangement. The practical importance of Curie's principle rests upon the resulting influence on physical properties. Generalizing Neumann's law from crystal physics: The symmetry elements of any physical property of a composite must include the symmetry elements of the point group of the composite.

Crystallographic Groups

Laminated composites are good examples of composite materials that conform to crystallographic symmetry. In a unidirectional laminate the glass fibers are aligned parallel to one another, such that a laminate has orthorhombic symmetry (crystallographic point group mmm). Mirror planes are oriented perpendicular to the laminate normal and perpendicular to an axis formed by the intersection of the other two mirrors. The physical properties of a unidirectional laminate must therefore include the symmetry elements of point group mmm. If the laminate is heated it will change shape because of thermal expansion. Less expansion will take place parallel to the fiber axis because glass has a lower thermal expansion and greater stiffness than does the polymer. The laminate will therefore expand anisotropically but will not change its symmetry, i.e. the heated laminate continues to conform to point group mmm.

A cross-ply laminate is made up of two unidirectional laminates bonded together with the fiber axes at 90°. Such a laminate belongs to tetragonal point group $\bar{4}2m$, as indicated in Table 2. Laminated composites with $\pm\theta$ angle-ply alignment exhibit orthorhombic symmetry, which is consistent with point group 222 characteristics.

Other types of symmetry elements can also be introduced during processing. The extruded honeycomb ceramics used as catalytic substrates

Table 2 Symmetry groups of representative composites

Composite type	Symmetry group
Unidirectional laminate	mmm
Cross-ply laminate	42m
Angle-ply laminate	222
Tetragonal honeycomb extrusion	
Unpoled	4 mmm
Longitudinally poled	4mm
Transversely poled	mm2
Glass-ceramic	∞ ∞ m
Polar glass-ceramic	∞ m
Ferroelectric-ferromagnetic composite	
Unpoled, unmagnetized	∞ ∞ m
Poled, unmagnetized	∞ m
Unpoled, magnetized	∞ mm'
Parallel poled and magnetized	∞ m'
Transverse poled and magnetized	2'mm'

are an interesting example (11). By suitably altering the die used in extruding the ceramic slip, a large number of different symmetries can be incorporated into the composite body when the extruded form is filled with a second phase.

Lead zirconate titanate (PZT) honeycomb ceramics have been transformed into piezoelectric transducers by electroding and poling. The symmetry of the honeycomb transducers depends on the symmetry of the extruded honeycomb and also on the poling direction. For a square honeycomb pattern, the symmetry of the unpoled ceramic is tetragonal (4 mmm) with a fourfold axis parallel to the extrusion direction. When poled parallel to the same direction (12), the symmetry changes to 4mm. Transversely poled composites filled with epoxy are especially sensitive to hydrostatic pressure waves (13), and in this case the symmetry belongs to orthorhombic point group mm2.

Curie Groups and Magnetic Symmetry

The piezoelectric properties and symmetry of natural composites, such as wood and bone, conform to their texture symmetries (14). Some texture symmetry groups belong to the 32 crystallographic point groups, but others do not. Composite bodies with texture may also belong to one of the Curie groups: ∞ ∞ m, ∞ ∞, ∞ mm, ∞ m, ∞ m, ∞ 2, and ∞. Polar glass ceramics with conical symmetry can be used to illustrate this idea (15). A glass can be crystallized under a strong temperature gradient such

that polar crystals grow like icicles into the interior from the surface. Certain glass-ceramic systems, such as $Ba_2TiSi_2O_8$ and $Li_2Si_2O_5$, show sizable pyroelectric and piezoelectric effects when prepared in this manner. Polar glass ceramics belong to the Curie point group ∞m, the point group of a polar vector. As the glass is crystallized in a temperature gradient, its symmetry changes from spherical ($\infty\infty m$) to conical (∞m), the same symmetry found in a poled ferroelectric ceramic.

To describe the magnetic fields and properties it is necessary to introduce the black-and-white Curie groups. Magnetic fields are represented by axial vectors with symmetry ∞/mm'. The symbol m′ indicates that the mirror planes parallel to the magnetic field are accompanied by time reversal.

The magnetoelectric composite described previously is an excellent illustration of the importance of symmetry in composite materials. In combining a magnetized ceramic (symmetry group ∞/mm'), the symmetry of the composite is obtained by retaining the symmetry of elements common to both groups: $\infty m'$.

An interesting feature of this symmetry description is its effect on physical properties. According to Neumann's law, the symmetry of a physical property of a material must include the symmetry elements of the point group. The symmetry of a magnetized ceramic and a poled ferroelectric both forbid the occurrence of magnetoelectricity, but their combined symmetry ($\infty m'$) allows it. By incorporating materials of suitable symmetry in a composite, new and interesting product properties can be expected to occur.

The symmetry of a magnetoresistive field plate with current flowing perpendicular to the fibers is $2'mm'$, the same symmetry group found in crossed electric and magnetic fields.

MAGNETIC COMPOSITES

Plastic magnets are made by embedding ferrimagnetic ceramic grains in a plastic matrix. The processing is carried out by rolling, extrusion, or injection molding. Barium ferrite fillers in nylon 6/10 or polyphenylene sulfide have sufficient mechanical strength to withstand normal load-bearing environments. To obtain maximum alignment, the ferrite particles are physically rotated in a magnetic field during the molding process. BH energy products equivalent to those of a cobalt steel are obtained in this way (16). In addition to simple mechanical clamps and latches, molded plastic magnets are used as bearing sleeves, timing-motor rotors, beam-focusing devices for television receivers, and magnetic sensors.

Magnetic Tape

Composite magnetic recording media consist of submicroscopic, single domain particles of magnetic oxides or metals immersed in a polymeric binder that separates the particles and binds them to the substrate. The substrates used in tapes, magnetic cards, and floppy disks are generally made from polyethylene terephthalate, while rigid disks are fabricated from an Al-Mg alloy. Among the advantages of the particulate composites are low cost, high yields, high roll-coating speeds, and independent control of the magnetic, mechanical, and thermal properties of the recording media.

Particles of γ-Fe_2O_3 have been used in tapes for more than 50 years, but as the bit length of recorded signals becomes shorter, further improvements in coercivity are required. Coercive fields have been raised from 100 to 500 A/m by impregnating the surface of the iron oxide particles with cobalt.

The market for tapes and disks has grown to eight billion dollars a year, but a number of unanswered questions remain (17): What are the relationships among particle size distribution, switching fields, and the overwrite performance of tapes and disks? Why is surface impregnation of cobalt on γ-Fe_2O_3 particles superior to bulk impregnation? Why does surface treatment with sodium metabisulfite cause a threefold increase in coercivity? And finally, how can mixed assemblies of particles with various anisotropies best be utilized in magnetic recording?

Ferromagnetic-Antiferromagnetic Composites

Exchange anisotropy can be developed in composites by exchange coupling at the interfaces between ferromagnetic and antiferromagnetic crystallites (18). Interfacial coupling can produce an exchange anisotropy so great that the magnetization cannot be changed by magnetic fields of 80 kA/m.

Exchange coupling to the antiferromagnetic phase introduces a bias in the hysteresis loop that shifts it along the magnetic field axis. The antiferromagnetic phase plays the role of a bias field. Among the antiferromagnetic-ferromagnetic pairs investigated are CoO-Co, NiO-Ni, NiFeMn-NiFe, and Cr_2O_3NiFe (19). Exchange coupled systems have been used in thermomagnetic recording (20).

TRANSPORT PROPERTIES

Conductor-filled composites are discussed in this section; we emphasize the importance of percolation in random and segregated mixes. Differential thermal expansion between matrix and filler sometimes leads to remark-

able variations in resistance with temperature. Composite positive (PTC) and negative (NTC) temperature coefficient thermistors and chemical sensors based on these ideas have been fabricated.

Percolation in Thick Film Resistors

Most composite conductors are made up of conducting metal particles suspended in an insulating polymer matrix. Particle contact and percolation require a larger volume fraction when the metal and polymer grains are comparable in size. When the conducting particles are small they are forced into interstitial regions between the insulating particles; this forces the conducting particles into contact with one another, which results in a low percolation limit.

These ideas were borne out by experiments on copper particles embedded in a matrix of polyvinylchloride (21). The critical volume fraction decreased markedly when the Cu particles were far smaller than the polymer particles. When the size ratio was 35 : 1 the critical volume percent was only 4% Cu. This highly segregated mixing establishes contact between conducting copper particles at a very low ratio of conductor to insulator.

Commercial thick film resistors are prepared from an ink consisting of coarse (~ 5 μm) glass particles and fine (< 1 μm) metallic particles suspended in an organic liquid. Lead borosilicate glasses and ruthenium oxides (RuO_2 or $Bi_2Ru_2O_7$) are commonly employed. After screen printing on an alumina substrate, the ink is dried and slowly fired at temperatures up to 850°C. Micrographs of the fired resistors reveal a glassy matrix with a network of connected metal particles.

Conduction takes place through the metallic chains in thick film resistors (22). For commercial systems the electrical conductivity changes over many orders of magnitude with metallic particle volume fraction v_M. It conforms to a power law $\sigma = K(v_m - v_o)^t$, where K, v_o, and t are constants for a given system. Experimentally it has been observed that the constant v_o is very small (0.01–0.1), while t is unusually large (2–7). The functional dependence of the conductivity is similar to that predicted by theoretical models for a resistor lattice just above the percolation threshold (22), but the constants are different. According to theory, v_o is 0.25 for a simple cubic lattice and t is about 1.6 for many types of resistor lattices.

Pike (23) has reconciled theory and experiment by proposing a model more consistent with the observed microstructure. The modified percolation model consists of large close-packed glass particles with tiny metal particles connecting the interstitial sites.

Polychromatic Percolation

Transport by percolation through two or more materials can be visualized in terms of colors. Black and white patterns illustrate percolation in a diphasic solid. Three kinds of percolation are possible: (*a*) percolation through an all-white path, (*b*) percolation through an all-black path, and (*c*) percolation through a combined black and white path. From a composite point of view, the third path is the most interesting because it offers the possibility of discovering phenomena not present in either phase individually. Foremost among these effects are the interfacial phenomena, which arise from the insertion of a thin insulating layer between particles with high electrical conductivity. Varistors, PTC thermistors, and boundary layer capacitors are examples of such materials. In ceramic varistors conducting ZnO grains are surrounded by thin layers of Bi_2O_3 insulation. The tunneling of electrons through this barrier gives rise to the varistor effect.

For three-color systems, a multitude of conduction paths are possible. Connectivity requirements for polychromatic percolation have been discussed from a theoretical viewpoint by Zallen (24). An example of such a system is an easy-poling piezoelectric composite made up of two kinds of particles mixed in an insulating polymer matrix (25). The first kind of particulate phase in a piezoelectric composite is PZT (lead zirconate titanate), a ferroelectric ceramic phase that must be poled to make it piezoelectrically active. Poling is difficult because the PZT grains are not in good electrical contact, and when shielded by a polymer, only a small fraction of the poling field penetrates into the ferroelectric PZT particles. A small amount of a second conductive filler material is added to facilitate poling. When a conductor is added and the composite is stressed, electrical contact is established between the ferroelectric grains, making poling possible. Pressure sensors of remarkable sensitivity can be obtained in this way.

Composite Thermistors

A second interesting effect is the dependence of electrical resistance on temperature. PTC thermistors are characterized by a positive temperature coefficient of electrical resistance. Doped barium titanate ($BaTiO_3$) has a useful PTC effect in which the resistance undergoes a sudden increase of four orders of magnitude just above the ferroelectric Curie temperature (130°C). The PTC effect is caused by insulating Schottky barriers created by oxidizing the grain boundary regions between conducting grains of rare earth-doped $BaTiO_3$ (26).

Similar PTC effects are observed when polymers are loaded near the percolation limit with a conducting filler. The Polyswitch overload protector (27) is made from high density polyethylene with carbon filler. At room temperature the carbon particles are in contact, giving resistivities of only 1 Ω-cm, but on heating the polymer expands more rapidly than carbon, pulling the carbon grains apart and raising the resistivity. Polyethylene expands very rapidly near 130°C, which results in a pronounced PTC effect comparable to that of $BaTiO_3$. A rapid increase in resistivity of six orders of magnitude occurs over a 30° temperature rise.

As pointed out by Doljack (27), the carbon-polyethylene PTC thermistor has several advantages over $BaTiO_3$: (*a*) its room temperature resistivity is lower, (*b*) it shows PTC behavior at high temperature, (*c*) its resistance is insensitive to voltage, and (*d*) the device has good thermal shock resistance. The principal drawback of Polyswitch composites seems to be the slow recovery time. Several hours are required for the resistance to return to within 10% of its initial value at room temperature. The slow recovery of base resistance is caused by polymer melting followed by secondary recrystallization and gradual reformation of the carbon black chains responsible for conduction.

Combined NTC-PTC composites have also been constructed (28). Vanadium sesquioxide (V_2O_3) has a metal-semiconductor transition near −110°C with a large increase in conductivity on heating. This material can be incorporated in a composite by mixing V_2O_3 powder in an epoxy matrix. The filler particles are in contact at low temperatures and exhibit an NTC resistance change similar to that observed in V_2O_3 crystals and single phase ceramics. On heating above room temperature, the polymer matrix expands rapidly, pulling the V_2O_3 grains apart and raising the resistance by many orders of magnitude. This produces a PTC effect similar to the Polyswitch composite. The net result is an NTC-PTC thermistor with a conduction "window" in the range −100°C to +100°C. This is a good example of the use of coupled phase transformations in composites.

POROUS SENSORS

Many kinds of porous ceramic sensors are under development for measuring humidity, methane gas concentration, temperature, and pressure. Superb PTC thermistors have been made from porous $BaTiO_3$ semiconductors doped with antimony (29). A maximum step in resistivity of 10^4 occurred for ceramics with about 20% connected porosity and very small grain size (near 1 μm). Oxygen diffusion is essential in forming

insulating Schottky barriers between the conducting ceramic grains, and porosity enhances the accessibility of grain boundaries to the atmosphere during the critical cooling process following sintering.

Composite humidity sensors have been synthesized by loading lithium fluoride with alumina (30). Differential thermal contraction of the LiF matrix and Al_2O_3 filler causes internal microcracks to open within the composite. The electrical resistance of this material is very sensitive to humidity. Moisture penetrates into the microcracks and affects the surface resistance. Conduction probably occurs by the Grotthus mechanism ($H_3O^+ \rightarrow H_2O + H^+$) at low humidity levels, and by Li^+ ion conduction in adsorbed water layers at high humidity. The ceramic alumina particles play an interesting role in the composite: Their presence initiates the microcracking responsible for increased surface conduction.

Composite gas sensors have been constructed based on similar principles (31). The addition of Al_2O_3 to ZnO ceramics stabilizes it in a porous microstructure ideal for use in adsorption/desorption-type gas sensors. The porous texture enhances the electrical conductivity to such an extent that the sensitivity to flammable gases is adversely affected, but soaking the porous structure in a lithium-containing solution increases its resistivity, resulting in a reproducible gas sensor sensitive to methane, propane, and other hydrocarbon gases.

As pointed out by Yanagida (32), interactions between two different materials can give rise to very unusual phenomena. Dispersing a basic refractory ($MgCr_2O_4$) in an acid refractory (TiO_2) produces a composite humidity sensor suitable for monitoring cooking in electric ovens.

Contacts between p- and n-type ceramic grains are also sensitive to humidity (33). The I–V characteristics of ZnO (n-type) and NiO (p-type) junctions change markedly with humidity and exposure to flammable gases.

Catalytic Coatings

The sensitivities of many chemical sensors are affected by catalytic coatings. A large change in conductivity occurs in rare earth perovskites after chemisorption of flammable gases (34). $LaCoO_3$ and similar oxides have high electrical conductivity and exhibit oxidation-reduction catalytic behavior. In the oxidation reaction of carbon monoxide or alcohols, the reactive gases cause a change in the oxygen balance of the ceramic when the gases come into contact with the surface at elevated temperature: $CO + O^{2-} \rightarrow CO_2 + 2e^-$. The resulting change in electrical resistance can be used to sense the presence of reducing gases adsorbed on the surface.

Ferroelectric polarization is known to affect adsorptive and catalytic properties in certain systems. Studies of carbon monoxide oxidation over

Pd deposited on $LiNbO_3$ crystals show that the positive polar surface interacts strongly with small Pd particles and effectively reduces the CO adsorption bond (35). Electron transfer from the dispersed metal to the ferroelectric leads to an *electron-deficient state of the metal*, which weakens the metal-CO bonding. In order to verify the polarization effects, it is important to investigate other metal-ferroelectric combinations.

Additional chemical reactivity can be stimulated ultrasonically (36) by initiating ligand dissociation and activating catalysts. Sonocatalysis can produce intermediate chemical species that are inaccessible to more conventional preparative techniques. Piezoelectric transducers with large surface areas are of interest as vibrating substrates for catalyzed chemical reactions.

Fractal Nature of Interface

Interface area is important in a number of electric applications. In a boundary layer capacitor or an electrolytic capacitor, for instance, the capacitance is directly proportional to the area of a thin insulating layer. To maximize capacitance one must maximize area, and this can best be done by roughening the interface. The highly etched surface of a tantalum electrolytic capacitor is a good example of a nodular surface.

Electrical conductivity across an interface barrier is also proportional to surface area. Increasing the surface area lowers the electrical resistance. An example of this phenomenon can be found in the surface resistance of a humidity sensor.

For these reasons, as well as others, the irregularity of inner surfaces is of great interest in composites. The fractal dimension D is a way of characterizing geometric irregularities (37). For straight lines $D = 1$ and for flat surfaces $D = 2$. Boundary lines lie in the range $1 \leq D < 2$, and for surfaces $2 \leq D < 3$. The higher the D value of a surface, the more wrinkled and space-filling it is.

Measurements of real surfaces have been reported by Avnir and coworkers (38). The fractal theory of surfaces makes use of the relation $n \sim r^{-D}$, where n is the number of yardsticks of size r necessary to cover the surface area under investigation. For flat surfaces $n \sim r^{-2}$. The yardsticks are molecules of different size that are adsorbed on the surface.

Silica gel has a highly irregular surface ($D = 2.94 \pm 0.04$) while graphite is nearly flat ($D = 2.07 \pm 0.01$) because of its pronounced cleavage. The surface regularity of composite components can have any value between $2 \leq D < 3$. The various forms of carbon, for instance, range from 2.0 to 2.8 (38). Such variations can be expected to have a profound effect on the physical and chemical properties related to surface area.

CONNECTIVITY

Connectivity (39) is a key feature in property development in multiphase solids because their physical properties can change by many orders of magnitude depending on the manner in which connections are made.

Each phase in a composite may be self-connected in zero, one, two, or three dimensions. It is natural to focus attention on three perpendicular axes because all property tensors are referred to orthogonal systems. If we limit the discussion to diphasic composites, there are ten connectivities: 0-0, 1-0, 2-0, 3-0, 1-1, 2-1, 3-1, 2-2, 2-3, and 3-3. Connectivity patterns for more than two phases are similar to the diphasic patterns, but far more numerous. There are 20 three-phase patterns and 35 four-phase patterns. For n phases the number of connectivity patterns is $(n+3)!/3!n!$.

During the past few years we have been developing processing techniques for making piezoelectric composites with different connectivities (40). Extrusion, tape casting, injection molding, and fugitive phase methods have been especially successful. The 3-1 connectivity pattern, for instance, is ideally suited to extrusion processing. A ceramic slip is extruded through a die to yield a three-dimensionally connected pattern with one-dimensional holes, which can later be filled with a second phase. Another type of connectivity well-suited to processing is the 2-2 pattern, made up of alternating layers of the two phases. The tape casting of multilayer capacitors with alternating layers of metal and ceramic is a way of producing 2-2 connectivity. In this arrangement both phases are self-connected in the lateral directions but not self-connected perpendicular to the layer.

Stress Concentration

The importance of stress concentration in composite materials is well known from structural studies, but its relevance to electroceramics is not so obvious. Stress concentration is a key feature of many of the piezoelectric composites made from polymers and ferroelectric ceramics (40). By focusing the stress on the piezoelectric phase, some of the piezoelectric coefficients can be enhanced and others reduced.

For example, consider the hydrostatic voltage coefficient $g_h = (d_{31} + d_{32} + d_{33})/\varepsilon_{33}$ in a 1-2-3-0 composite. This composite is made up of PZT fibers in the poling direction (X_3) and glass fibers in the X_1 and X_2 directions. The fibers are embedded in a foamed polymer matrix. In terms of the 1-2-3-0 symbol, the PZT is self-connected in one dimension, the glass fibers in two dimensions, and the polymer in three dimensions, and the voids in none.

Hydrostatic stress waves are converted to uniaxial stresses inside the

composite. Stress components in the X_1 and X_2 directions are carried by the glass fibers, while stresses along X_3 act upon the PZT. Because of its greater compliance, the polymer matrix transfers stress to the fibers. Foaming the polymer reduces the Poisson ratio of the composite, preventing transfer of stress between the X_3(poling) direction and the orthogonal X_1 and X_2 directions. As a result d_{33} is kept large while d_{31} and d_{32} are reduced. This improves g_h because normally d_{31} and d_{32} are opposite in sign from d_{33}. As an added benefit, the dielectric permittivity ε_{33} is reduced by eliminating much of the ferroelectric PZT from the transducer. Improvements in g_h of two orders of magnitude have been demonstrated (41).

Advantageous internal stress transfer can also be utilized in pyroelectric coefficients. If the two phases have different thermal expansion coefficients, there is stress transfer between the phases, which generates electrical polarization through the piezoelectric effect. In this way it is possible to make a composite pyroelectric that is not piezoelectric (42).

Stress redistribution also occurs in the piezoelectric bimorphs and unimorphs used as fans, printers, and speakers (43). Unimorphs are made by bonding a thin piezoelectric ceramic to a steel shim and driving it in resonance. The steel shim restricts extension of the piezoelectric, causing a large bending motion. Force is traded off for displacement in the unimorph and bimorph.

Electric Field Concentration

The multilayer design used for ceramic capacitors is an effective configuration for concentrating electric fields. By interleaving metal electrodes and ceramic dielectrics in a 2-2 connectivity pattern, relatively modest voltages can produce high electric fields.

Multilayer piezoelectric transducers are made in the same way as multilayer capacitors (44). The oxide powder is mixed with an organic binder and tape-cast using a doctor blade configuration. After drying, the tape is stripped from the substrate and electrodes are applied with a screen printer and electrode ink. A number of pieces of tape are then stacked, pressed, and fired to produce a ceramic with internal electrodes. After attaching leads, the multilayer transducer is packaged and poled. When compared to a simple piezoelectric transducer, the multilayer transducer offers a number of advantages: (*a*) The internal electrodes make it possible to generate larger fields for smaller voltages, eliminating the need for transformers for high-power transmitters. Ten volts across a tape-case layer 100 μm thick produces an electric field of 10^5 V/m, a value not far from the depoling field of PZT. (*b*) The higher capacitance inherent in a multilayer design often improves acoustic impedance matching. (*c*)

Many different electrode designs can be incorporated in the transducer to shape poling patterns, which in turn control the mode of vibration and the ultrasonic beam pattern. (*d*) Additional design flexibility can be achieved by interleaving layers of different composition. One can alternate ferroelectric and antiferroelectric layers, for instance, thereby increasing the depoling field. (*e*) Grain-oriented piezoelectric ceramics can also be tape cast into multilayer transducers. Enhanced piezoelectric properties are obtained by aligning the crystallites parallel to the internal electrodes. (*f*) Another advantage of the thin dielectric layers in a multilayer transducer is improved electric breakdown strength. The dc breakdown field for ceramics 1 cm thick was less than that of 1-mm-thick samples. It is likely that the trend toward thinner specimens will continue, leading to improved poling and more reliable transducers.

Multilayer Thermistors

For many applications it is desirable to lower the room temperature resistance because the thermistor elements are often connected in series with the circuit elements they are designed to protect. It is possible, of course, to lower the resistivity of the composite by altering the components, but the resistivity cannot be lowered indefinitely without degrading the PTC thermistor effect.

The introduction of internal electrodes offers a way to reduce the resistance per unit volume without affecting the temperature characteristics. Thermistor devices are presently being fabricated as ceramic discs or as composite wafers. Recently a way of making multilayer $BaTiO_3$ PTC thermistors (45) has been developed that greatly lowers the room temperature resistance. Barium titanate powder doped with rare-earth ions is mixed with an organic binder and is tape cast on glass slides. Electrodes are screen-printed on the tapes, which are then stacked, pressed, and fired. The internal electrode configuration is very similar to that in multilayer capacitors.

The basic idea involves comparing a single layer disk thermistor with a multilayer thermistor of the same external dimensions. The multilayer device is assumed to have n ceramic layers and $n+1$ electrodes. Let A represent the area of the single layer disk thermistor, t its thickness, and ρ the resistivity. The resistance of the disk thermistor is $R_s = \rho t/A$. For the multilayer thermistor the total electroded area is nA (neglecting margins) and the thickness is t/n (neglecting the electrode thickness). The resistance of the multilayer device is $R_M = \rho(t/n)/nA = R_s/n^2$. The resistivity of the thermistor is lowered by a factor of $1/n^2$ with $n-1$ internal electrodes.

The feasibility of this idea has been demonstrated with a multilayer device containing four tape cast layers. As predicted, the resistance of the multilayer specimen is approximately $n^2 (= 16)$ times smaller with very little change in the temperature characteristic.

SCALE AND PERIODICITY

A good deal has been written about the importance of scale in magnetic, optical, and semiconductor materials. Many of the same effects occur in ferroelectrics: critical domain sizes, resonance phenomena, electron tunneling, and nonlinear effects.

Intrinsic Size Effects

In ferromagnetic materials, there are three kinds of magnetic structures for small particles (46). *Multidomain* structures are common for particles larger than a critical size; magnetization in large particles takes place through domain wall motion. Below this critical size, *single domain* particles are observed, and switching takes place by rotation rather than wall movement, thereby raising the coercive field. Very small particles exhibit a *supermagnetic* effect in which the spins rotate in unison under thermal excitation. Only modest magnetic fields are required to align the spins of adjacent particles.

Analogous behavior in ferroelectric particles has yet to be fully established, but a variety of interesting experimental results are accumulating (47). In $BaTiO_3$ ceramics, single domain behavior is observed in grains less than ~ 1 μm (48), while dielectric phenomena resembling those found in superparamagnetism are found in relaxor ferroelectrics. The fluctuating microdomains in this superparaelectric state are about 20 nm across (49).

Composite materials made up of single domain and superparaelectric particles have yet to be investigated in a systematic way with proper control of the connectivity and surrounding environment. The controlled synthesis of submicrometer ferroelectric grains will do much to stimulate research in this area.

Surface treatment of the ferroelectric phase allows control of the mechanical boundary conditions. Titanyl coupling agents are effective in bonding PZT to epoxy (50). Mechanical pull tests have been used to demonstrate the strength of the ceramic-polymer bond. Improved stress transfer and large piezoelectric coefficients in 1-3 and 0-3 piezoelectric composites are obtained as a result of better bonding.

Polymers are about a hundred times more compliant than ceramics. If

a ceramic grain is surrounded by polymer the mechanical constraints are relatively small. This means that more complete poling is possible, as demonstrated in 0-3 ferroelectric composites (51).

Electrical boundary conditions can also be controlled by adjusting the dielectric constant and conductivity of the surrounding phase.

Resonant Structures

Periodicity and scale are important factors when composites are to be used at high frequencies where resonance and interference effects occur. When the wavelengths are on the same scale as the component dimensions, the composite no longer behaves like a uniform solid.

An interesting example of unusual wave behavior occurs in composite transducers made from poled ferroelectric fibers embedded in an epoxy matrix (52). When driven in thickness resonance, the regularly spaced fibers excite resonance modes in the polymer matrix, causing the matrix to vibrate with much larger amplitude than the piezoelectric fibers. The difference in compliance coefficents causes the nonpiezoelectric phase to respond far more than the stiff ceramic piezoelectric. Composite materials are therefore capable of mechanical amplification. Multiply poled piezoelectric transducers (MUPPETS) have been fabricated from pre-poled PZT fibers mounted in a polymer matrix (53).

Domain-divided transducers operate on a similar principle (54). Multidomain crystals and ceramics have been used as acoustic phase plates and high frequency transducers. Optical analogs occur in the twinned acentric crystals used to phase-match fundamental and second harmonic wavelengths (55).

Nonlinear Phenomena

Second harmonic generation and other nonlinear optical effects are well known, but the corresponding low frequency phenomena have not been thoroughly investigated. The recent surge of interest in actuators (56) is changing this situation. Electrostriction is a second-order electromechanical coupling between strain and electronic field. For small fields electrostrictive strains are small compared to piezoelectric strain, but this is not true for the high fields generated in composite transducers.

Multilayer electrostrictive transducers (57) made from relaxor ferroelectrics, such as lead magnesium niobate (PMN), are capable of generating strains larger than PZT. Since there are no macrodomains in PMN there are no "walk-off" effects in electrostrictive micropositioners. Moreover, poling is not required and there are no aging effects. The concentration of electric fields in composite transducers makes nonlinear effects increasingly important.

SUMMARY

Some of the basic ideas underlying composite electroceramics have been illustrated in this paper. By way of summary, we might state them as Ten Commandments:

1. *Sum properties* involve the averaging of similar properties in the component phases, with the mixing rules bounded by the series and parallel models. For a simple sum property such as the dielectric constant, the dielectric constant of the composite lies between those of the individual phases. This is not true for *combination properties*, which are based on two or more properties. Acoustic velocity depends on stiffness and density, and since the mixing rules for these two properties are often different, the acoustic velocity of a composite can be smaller than those of its constituent phases.
2. *Product properties* are even more complex because three properties are involved: Different properties in the constituent combine to yield a third property in the composite. In a magnetoelectric composite, the piezoelectric effect in barium titanate acts on the magnetostrictive effect of cobalt ferrite to produce a composite magnetoelectric effect.
3. *Connectivity patterns* are a key feature of composite electroceramics. The self-connection of the phases determines whether series or parallel models apply, and thereby minimizes or maximizes the properties of the composite. The three-dimensional nature of the connectivity patterns makes it possible to minimize some tensor components while maximizing others. Piezoelectric composites made from parallel ferroelectric fibers have large d_{33} coefficients and small d_{31} values.
4. *Concentrated field and force patterns* are possible with carefully selected connectivities. Using internal electrodes, electrostrictive ceramics are capable of producing strains comparable to the best piezoelectrics. Stress concentration is achieved by combining stiff and compliant phases in parallel. A number of different hydrophone designs are based on this principle.
5. *Periodicity and scale* are important factors when composites are to be used at high frequencies, where resonance and interference effects occur. When the wavelengths are on the same scale as the component dimension, the composite no longer behaves like a uniform solid. The colorful interference phenomena observed in opal and feldspar minerals are interesting examples of natural composites. Acoustic analogs occur in the PZT-polymer composites used as biomedical transducers.
6. *Symmetry* governs the physical properties of composites just as it

does in single crystals. The Curie Principle of symmetry superposition and Neumann's Law can be generalized to cover fine-scale composites, thereby elucidating the nature of their tensor properties. As in the case of magnetoelectric composites, sometimes the composite belongs to a symmetry group that is lower than any of its constituent phases. Unexpected product properties occur under such circumstances.

7. *Interfacial effects* can lead to interesting barrier phenomena in composites. ZnO-Bi_2O_3 varistors and carbon-polymer PTC thermistors are important examples of Schottky barrier effects. Barrier layer capacitors made from conducting grains separated by thin insulating grain boundaries are another example.
8. *Polychromatic percolation* is an interesting concept that has yet to be fully explored. Composites fabricated from two or more conducting phases can have several kinds of transport paths, both single phase and mixed, depending on percolation limits and volume fractions. Carbon-PZT-polymer composites can be poled because polychromatic percolation establishes flux continuity through ferroelectric grains. The SiC-BeO composites under development as substrate ceramics are another example. These diphasic ceramics are simultaneously excellent thermal conductors and poor electrical conductors. A thin layer of BeO-rich carbide separates the SiC grains, insulating them from one another electrically, but providing a good acoustic impedance match ensuring phonon conduction.
9. *Coupled phase transformations* in polyphasic solids introduce additional possibilities. Recently discovered NTC-PTC composites made from V_2O_3 powder and embedded in polyethylene combine matrix and filler materials with complementary properties. At low temperatures the vanadium oxide particles are in a semiconducting state and in intimate contact with one another. On passing through a semiconductor-metal transition, the electrical conductivity increases by five orders of magnitude. Further heating brings the polymer to a phase transformation, causing a rapid expansion in volume, and pulling the V_2O_3 particles apart. As a consequence the electrical conductivity decreases by eight orders of magnitude. In addition to this "window material" with a controlled conductivity range, several other composites with coupled phase transformations were described in the text.
10. *Porosity and inner surfaces* play a special role in many electroceramic composites used as sensors. Humidity sensors made from Al_2O_3 and LiF have high inner surface area because of thermally induced fracture. The high surface area and hygroscopic nature of the salt result in excellent moisture sensitivity of the electrical resistance.

Chemical sensors based on similar principles can be constructed in the same way.

Literature Cited

1. van Suchtelen, J. 1972. *Philips Res. Rep.* 27: 28–37
2. Hearmon, R. F. S. 1961. *Applied Anisotropic Elasticity*, pp. 40–41. London: Oxford Univ. Press. 136 pp.
3. van Beek, L. K. H. 1965. *Prog. Dielectr.* 7: 69–114
4. Payne, D. A. 1973. *Role of internal boundaries upon the dielectric properties of polycrystalline ferroelectric materials.* PhD thesis, Penn. State Univ. 317 pp.
5. Partridge, G. 1983. *Glass Tech.* 24: 293–96
6. Ross, C. A., Sierakowski, R. L. 1975. *Shock Vibration Dig.* 7: 1–00
7. Weiss, H. 1971. *Met. Trans.* 2: 1513–21
8. van den Boomgaard, J., Terrell, D. R., Born, R. A. J., Giller, H. F. J. I. 1974. *J. Mater. Sci.* 9: 1705–9
9. van Run, A. M. J. G., Terrell, D. R., Scholing, J. H. 1974. *J. Mater. Sci.* 9: 1710–14
10. Bracke, L. P. M., van Vliet, R. G. 1981. *Int. J. Elect.* 51: 255–62
11. Lachman, I. M., Bagley, R. D., Lewis, R. M. 1981. *Bull. Am. Ceram. Soc.* 60: 202–5
12. Shrout, T. R., Bowen, L. J., Schulze, W. A. 1980. *Mater. Res. Bull.* 15: 1371–79
13. Safari, A., Halliyal, A., Newnham, R. E., Lachman, I. M. 1982. *Mater. Res. Bull.* 17: 302–8
14. Zheludev, I. S. 1974. *Solid State Phys.* 29: 315–59
15. Gardopee, G. J., Newnham, R. E., Bhalla, A. S. 1981. *Ferroelectrics* 33: 155–66
16. Theberge, J., Arkles, B., Knabb, D. 1977. *Machine Design*, pp. 3–7
17. White, R. M. 1985. *Science* 229: 11–15
18. Meiklejohn, W. H., Bean, C. P. 1956. *Phys. Rev.* 102: 1413–14; 1957. *Phys. Rev.* 105: 904–13
19. Meiklejohn, W. H. 1962. *J. Appl. Phys.* 33: 1328–35
20. Berkowitz, A. E., Meiklejohn, W. H. 1974. *Report No. 74CRD286, General Electric Co.*
21. Bhattacharya, S. K., Chaklader, A. C. D. 1982. *Polymer Plastics Tech. Eng.* 19: 21–36
22. Carcia, P. F., Ferretti, A., Suna, A. 1982. *J. Appl. Phys.* 53: 5282–88
23. Pike, G. E. 1978. *Electrical Transport and Optical Properties of Inhomogeneous Media*, pp. 366–71. New York: Am. Inst. Phys. 416 pp.
24. Zallen, R. 1977. *Phys. Rev. B* 16: 1426–35
25. Newnham, R., Safari, A., Sa-Gong, G., Giniewicz, J. 1984. *Proc. IEEE Ultrasonic Symp., Dallas, Texas*, pp. 501–6
26. Heywang, W. 1961. *Solid State Elec.* 3: 51–58
27. Doljack, F. A. 1981. *IEEE Trans. CHMT* 4: 372–78
28. Hu, K. A., Newnham, R. E., Runt, J. P., Safari, A. 1985. *Proc. Symp. Tailoring Multiphase Composite Ceram., University Park, Penn.*
29. Kuwabara, M. 1981. *J. Am. Ceram. Soc.* 64: 639–44
30. Tofield, B. C., Williams, D. E. 1983. *Solid State Ionics* 83: 1299–1304
31. Takuma, Y., Miyoyama, M., Yanagida, H. 1982. *Chem. Lett.* 1982: 345–48
32. Yanagida, H. 1984. *Bull. Am. Ceram. Soc.* 63: 1135–37
33. Toyoshima, Y., Miayayama, S., Yanagida, H. 1983. *Jpn. J. Appl. Phys.* 22: 1933–38
34. Arakawa, T., K[illegible]uchi, H., Shiokawa, J. 1985. *J. Mater [illegible].* 20: 1207–10
35. Inoue, Y., Yoshioka, I., Sato, K. 1984. *J. Phys. Chem.* [illegible]984: 1148–51
36. Suslick, K. S., Gawienowski, J. J., Schubert, P. F., Wang, H. H. 1984. *Ultrasonics* 23: 33–36
37. Mandelbrot, B. B. 1982. *The Fractal Geometry of Nature.* San Francisco: Freeman
38. Avnir, D., Farin, D., Pfeifer, P. 1984. *Nature* 308: 261–63
39. Newnham, R. E., Skinner, D. P., Cross, L. E. 1978. *Mater. Res. Bull.* 13: 525–36
40. Newnham, R. E., Bowen, L. J., Klicker, K. A., Cross, L. E. 1980. *Mater. Eng.* II: 93–106
41. Haun, M. J. 1983. Transverse Reinforcement of 1-3 and 1-3-0 PZT-Polymer Piezoelectric Composites. MS thesis, Penn. State Univ. 212 pp.
42. Halliyal, A., Bhalla, A. S., Newnham, R. E. 1983. *Mater. Res. Bull.* 18: 1007–19
43. Herbert, J. M. 1982. *Ferroelectric Transducers and Sensors.* London: Gordon & Breach. 437 pp.
44. Dayton, G. O., Schulze, W. A., Shrout, T. R., Swartz, S., Biggers, J. V. 1984. *Adv. Ceram.* 9: 115–24
45. Hiremath, B. V., Hu, K. A., Newnham,

R. E. 1984. *Multilayer PTC Thermistors Ferroelectrics*. In press
46. Rado, G. T., Suhl, H., eds. 1963. *Magnetism*, Vol. III. New York: Academic. 623 pp.
47. Honig, J. M., Rao, C. N. R. 1981. *Preparation and Characterization of Materials*. New York: Academic. 609 pp.
48. Ozaki, Y. 1983. *Ferroelectrics* 49: 285–89
49. Harmer, M. P., Bhalla, A., Fox, B. H., Cross, L. E. 1984. *Mater. Lett.* 2: 278–84
50. Galgoci, E. 1985. *Ceramic-polymer bonding in piezoelectric composites*. PhD thesis, Penn. State Univ. 104 pp.
51. Giniewicz, J. R. 1985. *(Pb, Bi)(Ti, Fe) O_3/Polymer 0-3 composite materials for hydrophone applications*. MS thesis, Penn. State Univ. 170 pp.
52. Gururaja, T. R. 1984. Piezoelectric composite materials for ultrasonic transducer applications. PhD thesis, Penn. State Univ. 223 pp.
53. Gururaja, T. R., Christopher, D., Newnham, R. E., Schulze, W. A. 1983. *Ferroelectrics* 47: 193–200
54. Newnham, R. E., Miller, C. S., Cross, L. E., Cline, T. W. 1975. *Phys. Status Solidi* 32: 69–78
55. Feng, D., Ming, N., Hong, J., Yang, Y., Zhu, J., et al. 1980. *Appl. Phys. Lett.* 37: 607–9
56. Uchino, K. 1984. *Piezoelectric Actuator Development and Applications, Essential Electronics Series No.* 3. Tokyo: Jpn. Eng. Tech. Center. 179 pp.
57. Uchino, K., Nomura, S., Cross, L. E., Newnham, R. E., Jang, S. J. 1981. *J. Mater. Sci.* 16: 569–78

FLEXIBLE COMPOSITE PIEZOELECTRIC SENSORS

R.E. Newnham, A. [illegible], [illegible] and L. [illegible]
Materials Research Laboratory
The Pennsylvania State University
University Park, PA 16802

Abstract

The piezoelectric properties of several different composites with 0-3 connectivity are reviewed. In these composites a piezoelectric ceramic powder such as $PbZr_{1-x}Ti_xO_3$ (PZT), $PbTiO_3$ or $Pb_{1-x}Bi_x$-$Ti_{1-x}Fe_xO_3$ is used as a filler in a polymer matrix. The values of hydrostatic voltage coefficient g_h of these composites are higher than the corresponding properties of *single phase* materials. Composites with $PbTiO_3$ or $(Pb,Bi)(Ti,Fe)O_3$ as fillers have higher piezoelectric voltage coefficients than PZT-polymer composites because of the greater anisotropy and lower dielectric constants of these systems. By adding a small amount of carbon to the piezoelectric composite, poling can be carried out at much lower voltages and shorter poling times, making it possible to mass produce the composites. Fabrication of 0-3 composites is a relatively simple process which can be adapted to the production of piezoelectric fabrics, piezoelectric cables, and piezoelectric paint.

I. Introduction

A hydrophone is an underwater microphone or transducer used to detect underwater sound. The sensitivity of a hydrophone is determined by the voltage that is produced by a hydrostatic pressure wave. The hydrostatic voltage coefficient, g_h, relates the electric field appearing across a transducer to the applied hydrostatic stress, and is therefore a useful parameter for evaluating piezoelectric materials for use in hydrophones. Another piezoelectric coefficient frequently used is the hydrostatic strain coefficient, d_h, which describes the polarization resulting from a change in hydrostatic stress. The g_h coefficient is related to the d_h coefficient by the relative permittivity (K): $g_h = d_h/\varepsilon_o K$, where ε_o is the permittivity of free space.

A useful 'figure of merit' for hydrophone materials is the product of hydrostatic strain coefficient d_h and hydrostatic voltage coefficient g_h. The product $d_h g_h$ has the units of m^2N^{-1}. Other desirable properties for a hydrophone transducer include (i) low density for better acoustical matching with water, (ii) high compliance and flexibility so that the transducer can conform to any surface and withstand mechanical shock. Compliance also leads to large damping coefficients which prevent 'ringing' in a passive transducer, and (iii) little or no variation of the g_h and d_h coefficients with pressure, temperature and frequency.

Lead zirconate titanate (PZT) is widely used as a transducer material because of its high piezoelectric coefficients. However for hydrophones, PZT is a poor choice for several reasons. PZT has a large piezoelectric d_{33} coefficient, but its hydrostatic strain coefficient d_h ($= d_{33} + 2d_{31}$) is small because d_{33} and $2d_{31}$ are opposite in sign, and almost cancel one another. Moreover, the high permittivity of PZT ($K \cong 1800$) lowers the voltage coefficient gh to miniscule values. In addition, the density of PZT (7.9 g/cm_3) makes it difficult to obtain good impedance matching with water. PZT is also a brittle ceramic and for some applications a more compliant material with better shock resistance is desirable.

Other materials used for hydrophone applications are lead metaniobate $PbNb_2O_6$[1] and $PbTiO_3$[2]. Their d_h values are slightly higher than that of PZT (Table I) and the g_h values are an order of magnitude better because of their modest dielectric constants. Unfortunately, $PbNb_2O_6$ and $PbTiO_3$ are also dense, brittle ceramics, which undergo a large volume change at the Curie temperature, often causing fracture during preparation.

Polyvinylidene fluoride ($PVF_2 = (CH_2\text{-}CF_2)_n$) offers several advantages over PZT and other piezoelectric ceramics[2]. It has low density, high flexibility, and although PVF_2 has low d_{33} and d_h, the piezoelectric voltage coefficient g_h is large because of its low relative permittivity.

There are, however, problems associated with the use of PVF_2. The major problem is the difficulty in poling PVF_2. A very high field is necessary to pole PVF_2 (1.2 MV/cm), and this limits the thickness that can be poled. Pyroelectric phenomena in PVF_2 also produces undesirably large polarization fluctuations with temperature.

It is clear that none of the single phase materials are ideal for hydrophones and there is need for better piezoelectric materials.

II. Composite Piezoelectrics

One approach to the problem is to develop composite materials in which the desired properties can be incorporated through use of a combination of materials with different properties. In designing composite materials for hydrophone applications, a logical choice would be a piezoelectric ceramic and a compliant polymer. In such a composite, the ceramic produces a large piezoelectric effect, while the polymer phase lowers the density and permittivity and increases the elastic compliance.

In a composite the electric flux pattern and the mechanical stress distribution, and hence the resulting physical and electromechanical properties, depend strongly on the manner in which the individual phases are interconnected. In this regard the connectivity of a composite, defined as the number of dimensions in which each component phase is continuous[4], is of crucial importance. When referred to in an orthogonal axis system, each phase in a composite may be self-connected in zero, one, two, or three directions. For diphasic composites, there are ten connectivity patterns designated as 0-0, 0-1, 0-2, 0-3, 1-1, 1-2, 1-3, 2-2, 2-3, and 3-3.

During the past few years, a number of investigators have examined piezoelectric ceramic-polymer composites with different connectivity patterns. The method of preparation of these composites covers a wide spectrum of ceramic fabrication processes, and the piezoelectric properties of the composites depend to a large extent, on the connectivity pattern. In this paper, a brief summary of the piezoelectric properties of flexible composites with 0-3 connectivity is presented. A more extensive description of the work on other PZT-polymer composites can be found in recent review papers[5,6].

III. Dielectric Piezoelectric Properties of 0-3 Composites

The simplest type of piezoelectric composite consists of a polymer matrix loaded with ceramic powder. In a composite with 0-3 connectivity, the ceramic particles are not in contact with each other while the polymer phase is self-connected in all three dimensions (Fig. 1). This type of composite does not have the desirable stress concentration factor found in some other connectivity patterns[7], so the hydrostatic figure of merit $d_h \tilde{g}_h$ is not large. In many ways the 0-3 composite is similar to polyvinylidene fluoride (PVF_2). Both consist of a crystalline phase embedded in an amorphous matrix, and both are reasonably flexible.

The first flexible piezoelectric composites were made by embedding PZT particles 5-10 μm in size in a polyurethane film[7]. The d_{33} coefficient of these composites were comparable with PVF_2, but the d_h value was lower than those of solid PZT and PVF_2 polymer (Table 1).

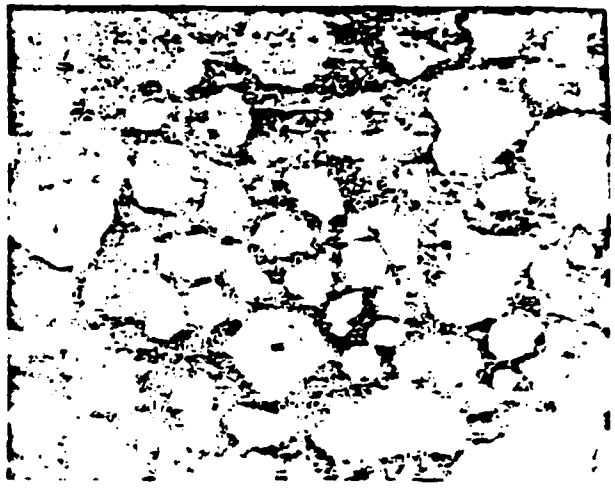

A similar composite (Flex) was developed at Honeywell[8], using 120 μm particles in a silicone-rubber matrix. The d_{33} values obtained with these composites were again comparable to PVF_2. The measured piezoelectric voltage coefficient $\tilde{g}_h$ was low (Table 1) and further improvement of piezoelectric coefficients was necessary. One difficulty with this type of composite is that the piezoelectric particles are smaller in diameter than the thickness of polymer sheet, and poling of the PZT was very poor because the electrodes were not in direct contact with the particles. To improve the properties of these composites Harrison[8] fabricated a composite with much larger PZT particles up to 2.4 mm. Here the particle size approaches the thickness of the composite, and since the PZT particles extend from electrode to electrode, near saturation poling can be achieved. The large rigid PZT particles can also transmit applied stress extremely well, leading to high d_{33} values when measurements are taken across the particles. Permittivity in this composite is lower than that of homogeneous PZT, resulting in an improved voltage coefficient. One problem with this type of composite is that complete poling cannot be achieved and the piezoelectric properties of the composite vary from point to point. An improved version of the 0-3 composite was synthesized by Safari[9]. Flexible piezoelectric composites made from PZT spheres and polymers with 0-3 connectivity were fabricated using several types of polymers. Two techniques were developed for making spheres 0.4 to 4 mm in diameter. The dielectric constant of the composites were 300-400 and the piezoelectric voltage coefficients g_{33} were 45-55 x 10^{-3} Vm/N. The high frequency properties of the composites were measured in both the thickness and radial mode of resonance. The frequency constants and the coupling coefficients of the composites for

Table I. Dielectric and Piezoelectric Properties of Static Phase-Connected Composites

Description of	Dielectric Constant	$\bar{d}_{33}$ $pC\,N^{-1}$	$\bar{g}_{33}$ $(\times 10^{-3}\ V\,m\,N^{-1})$	$\bar{g}_h$ $(\times 10^{-3}\ V\,m\,N^{-1})$	$\bar{d}_h$ $(pC\,N^{-1})$	$\bar{d}_h\bar{g}_h$ $(\times 10^{-3}\ pC\,V\,N^{-1})$	Reference
PZT 501 Ceramic	1800	450	28	2.5	40	100	6
$PbNb_2O_6$ Ceramic	225	85	42	31	67	2100	1
$PbTiO_3$ Ceramic	230	53	26	23	47	1080	2
$PVF_2 = (CH_2\text{-}CF_2)_n$	12	35	329	100	10	1000	3
PZT Particles-Polyurethane Composite	26	10	43	8	2	10	7
PZT Particles-Silicone Rubber Composite (T-flex)	41	8	22	--	--	--	8, 9
Large PZT Particles-Silicone Rubber Composites (S-flex)	100	350	500	1	28	500	4
WO_3 Modified PZT-Chloroprene Rubber	45	--	--	14	5	70	10, 11
Bi_2O_3 Modified $PbTiO_3$-Chloroprene Rubber	43	--	--	24	10	240	10, 12
Pure $PbTiO_3$-Chloroprene Composite	54	60	13	47	22	1000	10, 12
PZT-Eccogel Composite	100	44	50	9	10	90	13
Carbon Filled PZT-Eccogel Composite	120	50	47	32	25	800	13
$Pb(Mn_{1/3}Nb_{2/3})O_3$-$Pb(Zr,Ti)O_3$-Epoxy-Polymer Composite	29	40	156	4	10	40	5

the thickness mode of resonance are comparable with the corresponding values for PZT. Possible applications of the composites as band-pass filters have been developed[10].

But an even better suggestion has been put forward by Banno[11,12]. Rather than using PZT as the ceramic filler, pure or modified lead titanate was employed because of its greater piezoelectric anisotropy. The piezoelectric ceramic fillers used in these composites are $PbTiO_3$, Bi_2O_3-modified $PbTiO_3$ and WO_3-modified PZT. Fine-grained (~ 5 μm) particles of pure $PbTiO_3$ were made by water quenching sintered ceramics, while those of modified $PbTiO_3$ and PZT were made by grinding sintered ceramics. To fabricate the composite bodies, the piezoelectric powders and chloroprene rubber were mixed and rolled down into 0.5 mm thick sheets at 40°C using a hot roller, and then heated at 190°C for 20 minutes under a pressure of 13 kg/cm^2. The composites were poled in a 100-150 kV/cm for 30 minutes.

As shown in Table 1, the hydrostatic voltage coefficient $\tilde{g}_h$ of pure $PbTiO_3$ composites is comparable to that of PVF_2. In Fig. 2 the $\tilde{g}_h$ and $\tilde{d}_h$ of these composites are plotted as a function of hydrostatic pressure up to 35 MPa. (5000 PSI). It is found that $\tilde{g}_h$ and $\tilde{d}_h$ are independent of pressure up to 35 MPa[13].

Recently we have fabricated flexible composites with a more active piezoelectric material. The piezoelectric ceramic filler used in these composites is $Pb_{1-x}Bi_xTi_{1-x}Fe_xO_3$ (BF-PT) which has a very large spontaneous strain.

There are two reasons why large spontaneous strain is advantageous. First, it makes it easy to obtain a loose ceramic powder of extremely fine-grain size. On cooling from high temperature, the BF-PT ceramic undergoes brittle fracture at the Curie point as it transforms from a cubic state to a tetragonal phase with c/a ratio as large as 1.18[14]. Water-quenching accelerates the fracture process, further reducing the particle size, and making it possible to fabricate very thin piezo-films. The second reason is that a large spontaneous strain promotes greater piezoelectric anisotropy. This increases the hydrostatic sensitivity by reducing the cancellation between piezoelectric coefficients d_{33} and d_{31}. Banno[11] found that in 0-3 composite ferroelectrics, pure $PbTiO_3$ has a larger *hydrostatic piezoelectric effect than* $Pb(Zr,Ti)O_3$.

The spontaneous strain in $PbTiO_3$ is about 6%. In PZT compositions near the morphotropic boundary, it is about 2%. And since in BF-PT, the spontaneous strain is as large as 18%, we were not surprised to find a substantial increase in the hydrostatic voltage coefficients of the composites.

To fabricate the composites, the filler powder is synthesized from the system $Pb_{1-x}Bi_xTi_{1-x}Fe_xO_3$ for which there is a continuous solid solution across the entire composition range. The composition of the powders synthesized in this study lie in the range $x \sim 0.5$-0.7. To prepare the filler powder, PbO, TiO_2, Bi_2O_3 and Fe_2O_3 were mixed and ball-milled with zirconia media. The oxides were subjected to a low temperature (700°C-800°C) primary calcination for 1.5 hours, followed by a second high temperature firing (950°C-1050°C). Water quenching produces an average particle size of 5 μm (Fig. 1). To fabricate the composites, piezoelectric ceramic powders and cement polymer[15] were mixed and calendered at 40°C. The calendered material is then cured at 80° under slight pressure. Composites were poled in an 80°C silicone oil bath by applying a field 100-120 kV/cm for 20 minutes. The poled composites exhibits outstanding hydrostatic sensitivity attaining values of g_h and d_hg_h well in excess of the values reported for pure $PbTiO_3$ composites (Table 1). The g_h and d_h values of these composites[13] remain virtually constant over a broad pressure range (Fig. 2).

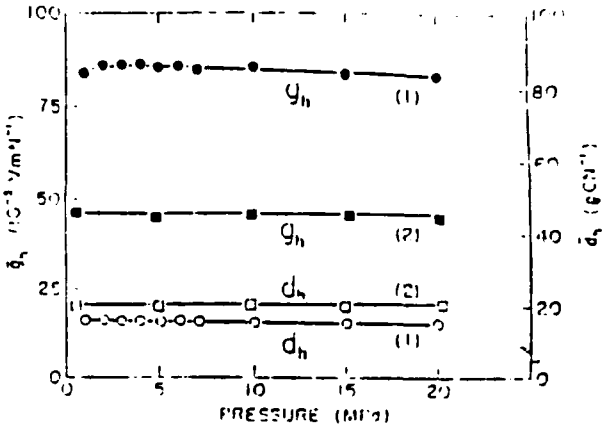

IV. Poling Method

As mentioned earlier, 0-3 composites prepared from PZT, $PbTiO_3$ and $(Pb,Bi)(Ti,Fe)O_3$ powders are poled at very large field strength (100-150 kV/cm) in order to achieve sufficient poling. The reason for the necessity of such large fields will be clear from the following discussion.

For a 0-3 composite consisting of spherical grains embedded in a matrix, the electric field E_1, acting on an isolated spherical grain is given by

$$E_1 = \frac{3K_2}{K_1+3K_2} E_0$$

In this equation, K_1 and K_2 are the dielectric constants of the spherical piezoelectric grains and polymer matrix, respectively, and E_0 is externally applied electric field. For a 0-3

composite of $PbTiO_3$ powder and polymer, $K_1 = 300$ and $K_2 = 5$. For such a composite with an external field of 100 kV/cm, the electric field acting on the piezoelectric particles is only about 5 kV/cm which is insufficient to pole the composite. According to the above equation $F_1 \simeq F_0$ only when the dielectric constant of the piezoelectric phase approaches that of the polymer phase. Most of the ferroelectric materials have very high dielectric constants and hence the above condition cannot be satisfied.

The importance of conductivity to poling can be assessed by applying the Maxwell-Wagner model to the 0-3 composites[16]. The model leads to a relationship between the electric field strength and the conductivities of the two phases.

After applying a DC poling field to the sample for a time long compared to the sample relaxation time, the field distribution in a two-layer capacitor is given by $[E_1/E_2 = \sigma_2/\sigma_1]$. The field acting on the ceramic is controlled by σ_2/σ_1, the ratio of the electrical conductivity of the polymer to that of the ceramic. Since the conductivity of the polymer matrix ($\sim 10^{-14}\ \Omega^{-1}\text{-cm}^{-1}$) is about 100 times smaller than that of the PZT ceramic filler ($\sim 10^{-12}\ \Omega^{-1}\text{-cm}^{-1}$) at room temperature, only a few percent of the poling field acts on the PZT particles. Under normal poling voltages, this is an insufficient field strength for poling the ferroelectric particles.

One way to increase poling is to increase the polymer conductivity close to that of the PZT filler. To do this, we have added a conducting third phase such as carbon to the PZT-polymer composite. In preparing these composites, 68.5 volume percent PZT 501 and 1.5 volume percent carbon were mixed and dry ball-milled. After ball-milling, the fillers were hand-mixed with eccogel polymer, and placed in a mold under pressure. It is found that the PZT polymer composite with small amount of carbon additive can be poled in about five minutes under a field of 35-40 kV/cm at 100°C. Fig. 3 shows the effect of the poling voltage on the d_{33} values of the composites when poling is carried out at 120°C. It is observed that a duration of five minutes is sufficient for full poling of the composites. Piezoelectric and dielectric properties of some of these composites are calculated in Table I along with the properties of composites without conductive phase additive. Further details of the poling method will be reported elsewhere[17].

Flexible 0-3 composite have also been developed at Bell Laboratories by Zipfel[18]. In this composite a polyurethane matrix material is mixed with 30-40 volume percent of a non-ferroelectric filler such as tartaric acid or lithium sulfate monohydrate. The liquid mixture is injected into an evacuated 3 inch diameter steel mold having two broad faces approximately 1.27 mm apart. While the polymer is undergoing polymerization, the composite is polarized by applying hydrostatic pressure and an electric field. In this way the piezoelectric crystals suspended in the liquid co polymer rotate until they are electrically

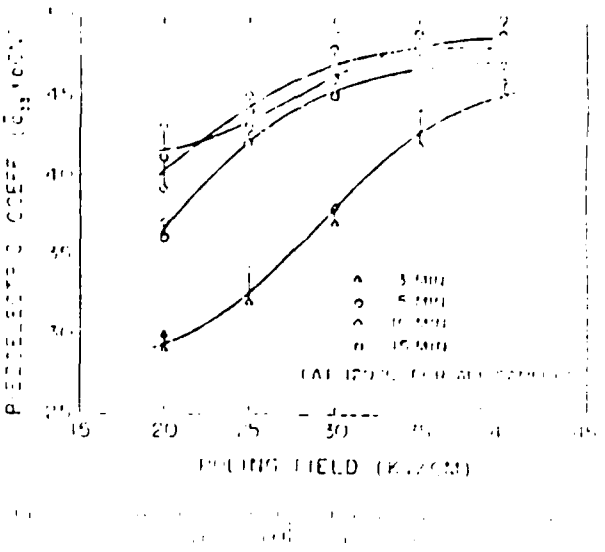

aligned. After polymerization, the resultant rubbery matrix holds the oriented particles in polar alignment for maximum sensitivity. The dielectric constant of this cable hydrophone is typically 4.2 and the piezoelectric sensitivity is stated to be 'comparable with most of the other piezoelectric materials.'

V. Summary

The dielectric and piezoelectric properties of several different types of flexible composites having 0-3 connectivity are described and their figure of merit for hydrophone applications ($d_h g_h$) are discussed. Hydrophones are used at low frequencies where the acoustic signal has a wavelength much larger than the scale of the microstructure of the composite. It is shown that the hydrostatic voltage coefficient g_h and figure of merit $g_h d_h$ of ceramic polymer composites are an order of magnitude higher than those of single phase materials. Composites fabricated with $(Pb,Pi)(Ti,Fe)O_3$ showed higher piezoelectric voltage coefficient than the other composites because of the large spontaneous strain in these systems. Difficulties of poling 0-3 composites can be eased by adding a small volume fraction of conductive phase.

VI. References

1. G. Goodman, J. Am. Ceram. Soc. 36, 368-72 (1953).

2. T.-Y. Tien and W.G. Carlson, J. Am. Ceram. Soc. 45, 567-71 (1962).

3. Y. Wada and R. Hayakawa, Japan J. Appl. Phys. 15, 2041 (1976).

4. R.E. Newnham, D.P. Skinner, and L.E. Cross, Mat. Res. Bull. 13, 525-536 (1978).

5. R.E. Newnham, L.J. Bowen, K.A. Klicker, and L.E. Cross, Mat. in Eng. 112, 93-106 (1980).

6. R.E. Newnham, A. Safari, J. Giniewicz, and B.H. Fox, Ferroelectrics, (to be published).

7. L.A. Pauer. IEEE Int. Conf. Res., p. 1-5 (1973).

8. W.B. Harrison, Proc. of the Workshop on Sonar Transducer Materials, Naval Research Labs. (Feb. 1976).

9. A. Safari, A. Halliyal, L.J. Bowen, and R.E. Newnham, J. Am. Ceram. Soc. 65, 207-9 (1982).

10. L.J. Bowen and T.R. Gururaja, J. Appl. Phys. 51[11], 5661-66 1980).

11. Hisao Banno, Ferroelectrics, Vol. 50, pp. 3-12 (1983).

12. Hisao Banno and Shigeo Saito, Japan J. Appl. Phys., Vol. 22 (1983) Suppl. 22-2 pp. 67-69.

13. R. Tinge, Private Communication.

14. S.A. Fedulov, Yu. N. Venevtsev, G.S. Zhdanov, E.G. Smazhevskaya, and I.S. Rez, Soviet Physics--Cryst. Vol. 7, no. 1, p. 62, July-August 1962.

15. Eccogel 1365 Series [Emerson and Cumming, Dewey and Almy Chemical Division, W.R. Grace and Co.]

16. Arthur R. Von Hippel, Dielectrics and Waves, John Wiley and Sons, 1954, p. 228.

17. G. Sa-gong, A. Safari, R.E. Newnham, (to be published).

18. C.G. Zipfel, Bell Labs Record, Apr. 1983, p. 11-13.

19. J. Giniewicz, A. Safari and R.E. Newnham (applied for patent).

Proceedings of 6th Symposium on Ultrasonic Electronics, Tokyo 1985
Japanese Journal of Applied Physics, Vol. 25 (1986) Supplement 25-1, pp. 9-14

Transducers, Sensors, and Actuators

Robert E. NEWNHAM
IEEE—Sonics and Ultrasonics Group National Lecturer

Materials Research Laboratory, The Pennsylvania State University

(Received December 16, 1985)

We review some of the basic ideas underlying composite electroceramics. The ideas will be illustrated with electromechanical transducers, sonochemical sensors, active vibration absorbers, electronic actuators, and a variety of other applications-both real and imagined.

§1. Introduction

Composite materials have found a number of structural applications but their use in the electronics industry has been relatively limited. As the advantages and disadvantages of electroceramic composites are better understood we can expect this picture to change.

In this paper we review some of the basic ideas underlying composite electroceramics: sum and product properties, connectivity patterns leading to field and force concentration, the importance of periodicity and scale in resonant structures, the symmetry of composite materials and its influence on physical properties, polychromatic percolation and coupled conduction paths in composites, varistor action and other interfacial effects, coupled phase transformation phenomena in composites, and the important role that porosity and inner surface area play in many composites.

§2. Properties of Composite Materials

For convenience in understanding, the physical and chemical properties of composites can be classified as sum properties, combination properties, and product properties. The basic ideas underlying sum and product properties were introduced by Van Suchtelen.[1] For a *sum property*, the composite property coefficient depends on the corresponding coefficients of its constituent phases. Thus the stiffness of a composite is governed by the elastic stiffnesses of its component phases and the mixing rule appropriate to its gometry. In general, the property coefficient of the composite will be between those of its constituent phases.

This is not true for *combination properties* which involve two or more different coefficients. Poisson's ratio is a good example of a combination property since it is equal to the ratio of two compliance coefficients. As is well known, some composite materials have extremely small values of Poisson's ratio, smaller than those of the materials used to make the composite. Wood is a good example from nature.[2]

Product properties are more complex and more interesting. The product properties of a composite involve different properties in its constituent phases with the interactions between the phases often causing unexpected results.

2.1 *Sum properties*

Dielectric constant will be used to illustrate a simple sum property. Series and parallel mixing rules represent bounding conditions for the dielectric constant K^* of a diphasic composite:

$$K^* = V_1 K_1^n + V_2 K_2^n + \cdots$$

where K_1 and K_2 are the dielectric constants of the constituent phases, and V_1 and V_2 are their volume fractions. The exponent n is $+1$ for parallel mixing, and $n=-1$ for series mixing. For many composites, the geometric arrangement is partly series and partly parallel. In this case, K^* can often be described by a logarithmic mixing rule for which the exponent $n \approx 0$.

There are, of course, many other mixing rules in addition to the series and parallel models. These represent only the limiting conditions. A more complete discussion of the dielectric properties of heterogeneous materials is given in the classic article by van Beek.[3]

As examples of composite ferroelectrics, consider the temperature of capacitors. *Depressors* are materials that are added to a high K capacitor formulation to depress the peak at the Curie point, resulting in a flatter temperature dependence. Bismuth stannate and magnesium zirconate are often used as depressors for barium titanate multilayer ceramics. These additives form a second phase in the grain boundary regions of the ceramic. The grain boundary phase has a much lower dielectric constant than $BaTiO_3$ and depresses the dielectric constant of the ceramic, largely through the series mixing rule. Low K boundary phases in series with the high K grains have a much greater effect on the permittivity than do those in parallel. The brick wall model gives a good description of diphasic ceramic dielectrics.[4]

2.2 *Combination properties*

For simple mixing rules, the properties of the composite lie between those of its constituent phases, but combination properties involve two or more coefficients which may average in a different way.

An example of interest is the acoustic wave velocity which determines the resonant frequency of piezoelectric devices. For a long, thin rod, the velocity of waves propagating along the length of the rod is $v=(E\ \rho)^{-1}$ where E is Young's modulus and ρ is the density. Fiber-reinforced composites often have very anisotropic wave

vestigated. The recent upsurge of interest in actuators[26] is changing this situation. Electrostriction is a second order electromechanical coupling between strain and electronic field. For small fields electrostrictive strains are small compared to piezoelectric strain, but this is not true for the high fields generated in composite transducers.

Multilayer electrostrictive transducrs[27] made from relaxor ferroelectrics such as lead magnesium niobate (PMN) are capable of generating strains larger than PZT. Since there are no macrodomains in PMN there are no "walk-off" effects in electrostrictive micropositioners. Moreover, poling is not required and there are no aging effects. The concentration of electric fields in composite transducers make non-linear effects increasingly important.

Table I. Symmetry groups of representative Compositives.

Unidirectional laminate	mmm
Cross-ply laminate	$\bar{4}2m$
Angle-ply laminate	222
Tetragonal honeycomb extrusion	
Unpoled	$\frac{4}{m}mm$
Longitudinally poled	4mm
Transversely poled	mm2
Glass-ceramic	$\infty\infty m$
Polar glass-ceramic	∞m
Ferroelectric-Ferrimagnetic Composite	
Unpoled, unmagnetized	$\infty\infty m$
Poled, unmagnetized	∞m
Unpoled, magnetized	$\infty\ mm'$
Parallel poled and magnetized	$\infty m'$
Transverse poled and magnetized	$2'mm'$

§5. Symmetry of Composite Materials

A wide variety of symmetries are found in composite materials. Examples of crystallographic groups, Curie groups, black-and-white groups, and color groups will be given, and the resulting effect on physical properties discussed.

In describing the symmetry of composite materials, the basic idea is Curie's principle of symmetry superposition: *A composite material will exhibit only those symmetry elements that are common to its constituent phases and their geometrical arrangement.*

The practical importance of Curie's principle rests upon the resulting influence on physical properties. Generalizing Neumann's law from crystal physics:[28] *The symmetry elements of any physical property of a composite must include the symmetry elements of the point group of the composite.*

5.1 *Crystallographic groups*

Laminated composites are good illustrations of composite materials conforming to crystallographic symmetry. In a unidirectional laminate the glass fibers are aligned parallel to one another, such that a laminate has orthorhombic symmetry (crystallographic point group mmm). Mirror planes are oriented perpendicular to the laminate normal, and perpendicular to an axis formed by the intersection of the other two mirrors. The physical properties of a unidirectional laminate must therefore include the symmetry elements of point group mmm. If the laminate is heated, it will change shape because of thermal expansion. Less expansion will take place parallel to the fiber axis because glass has a lower thermal expansion and greater stiffness than that of polymer. The laminate will therefore expand anisotropically but it will not change symmetry. The heated laminate continues to conform to point group mmm.

A cross-ply laminate is made up of two unidirectional laminates bonded together with the fiber axes at 90°. Such a laminate belongs to tetragonal point group $\bar{4}2m$, as indicated in Table I. Laminated composites with $\pm\theta$ angle-ply alignment exhibit orthorhombic symmetry consistent with point group 222.

Other types of symmetry elements can also be introduced during processing. The extruded honeycomb ceramic used as catalytic substrates are an interesting example.[29] By suitably altering the die used in extruding the ceramic slip, a large number of different symmetries can be incorporated into the composite body when the extruded form is filled with a second phase.

Lead zirconate titanate (PZT) honeycomb ceramics have been transformed into piezoelectric transducers by electroding and poling. The symmetry of the honeycomb transducers depends on the symmetry of the extruded honeycomb and also on the poling direction. For a square honeycomb pattern, the symmetry of the unpoled ceramic is tetragonal (4/mmm) with four-fold axis parallel to the extrusion direction. When poled parallel to the same direction,[30] the symmetry changes to 4 mm. Transversely poled composites filled with epoxy are especially sensitive to hydrostatic pressure waves,[31] and in this case the symmetry belongs to orthorhombic point group mm2.

5.2 *Curie groups and magnetic symmetry*

The piezoelectric properties and symmetry of natural composites such as wood and bone are found to conform to texture symmetries.[32] Some texture symmetry groups belong to the 32 crystallographic point groups, but others do not. Composite bodies with texture may also belong to one of the Curie groups: $\infty\infty m$, $\infty\infty$, ∞/mm, ∞m, ∞/m, $\infty 2$, and ∞. Polar glass-ceramics with conical symmetry illustrate the idea.[33] A glass is crystallized under a strong temperature gradient with polar crystals growing like icicles into the interior from the surface. Certain glass-ceramic systems such as $Ba_2TiSi_2O_8$ and $Li_2Si_2O_5$ show sizable pyroelectric and piezoelectric effects when prepared in this manner. Polar glass-ceramics belong to the Curie point group ∞m, the point group of a polar vector. As the glass is crystallized in a temperature gradient, it changes symmetry from spherical ($\infty\infty m$) to conical (∞m), the same as that of a poled ferroelectric ceramic.

To describe the magnetic fields and properties it is necessary to introduce the black-and-white Curie groups. Magnetic fields are represented by axial vectors with symmetry $\infty\ mm'$. The symbol m' indicates that the mirror planes parallel to the magnetic field are accompanied by time reversal.

The magnetoelectric composite described previously is an excellent illustration of the importance of symmetry in

composite materials. In combining a magnetized ceramic (symmetry group ∞/mm') with a poled ferroelectric ceramic (symmetry group ∞m), the symmetry of the composite is obtained by retaining the symmetry elements common to both groups: $\infty m'$.

An interesting feature of this symmetry description is its effect on physical properties. According to Neumann's law, the symmetry of a physical property of a material must include the symmetry elements of the point group. The symmetry of a magnetized ceramic and a poled ferroelectric both forbid the occurrence of magnetoelectricity, but their combined symmetry ($\infty m'$) allows it. By incorporating materials of suitable symmetry in a composite, new and interesting product properties can be expected to occur.

§6. Transport Properties of Composites

Conductor-filled composites are discussed in this section, emphasizing the importance of percolation in random and segregated mixes. Differential thermal expansion between matrix and filler sometimes leads to remarkable variations in resistance with temperature. Composite PTC and NTC thermistors and chemical sensors based on these ideas have been fabricated.

6.1 *Percolation and segregated mixing*

Most composite conductors are made up of conducting metal particles suspended in an insulating polymer matrix. Particle contact and percolation require a larger volume fraction when the metal and polymer grains are comparable in size. When the conducting particles are small, they are forced into interstitial regions between the insulating particles: this forces the conducting particles in contact with one another, resulting in a low percolation limit.

These ideas are borne out by experiments on copper particles embedded in a matrix of polyvinylchloride.[34] The critical volume fraction decreases markedly when the Cu particles are far smaller than the polymer particles. When the size ratio is 35:1, the critical volume percent is only 4%Cu. This highly segregated mixing establishes contact between conducting copper particles at a very low ratio of conductor to insulator.

6.2 *Composite thermistors*

A second interesting efect is the dependence of electrical resistance on temperature. PTC thermistors are characterized by a positive temperature coefficient of electrical resistance. Doped barium titanate ($BaTiO_3$) has a useful PTC effect in which the resistance undergoes a sudden increase of four orders of magnitude just above the ferroelectric Curie temperature (130°C). The PTC effect is caused by insulating Schottky barriers created by oxidizing the grain boundary regions between conducting grains of rare earth-doped $BaTiO_3$.

Similar PTC effects are observed when polymers are loaded near the percolation limit with a conducting filler. The Polyswitch overload protector[35] is made from high density polyethylene with carbon filler. At room temperature the carbon particles are in contact giving resistivities of only 1 Ω-cm, but on heating the polymer expands more rapidly than carbon, pulling the carbon grains apart and raising the resistivity. Polyethylene expands very rapidly near 130°C, resulting in a pronounced PTC effect comparable to that of $BaTiO_3$. A rapid increase in resistivity of six orders of magnitude occurs over a 30° temperature rise.

Combined NTC-PTC composites have also been constructed.[36] Vanadium sesquioxide (V_2O_3) has a metal-semiconductor transition near 160°K with a large increase in conductivity on heating. This material can be incorporated in a composite by mixing V_2O_3 powder in an epoxy matrix. The filler particles are in contact at low temperatures and exhibit an NTC resistance change similar to that observed in V_2O_3 crystals and single phase ceramics. On heating above room temperature, the polymer matrix expands rapidly, pulling the V_2O_3 grains apart and raising the resistance by many orders of magnitude. This produces a PTC effect similar to the Polyswitch composite. The net result is an NTC-PTC thermistor with a conduction "window" in the range −100°C to +100°C. This is a good example of the use of coupled phase transformations in composites.

References

1) J. van Suchtelen: Product Properties: A New Application of Composite Materials, *Philips Res. Repts.*27 (1972) 28.
2) R. F. S. Hearmon: "Applied Anisotropic Elasticity", Oxford University Press, London (1961) pp. 40–41.
3) L. K. H. van Beek: Dielectric Behaviour of Heterogeneous Systems, *Prog. in Diel.*7 (1965) 69.
4) D. A. Payne: Role of Internal Boundaries Upon the Dielectric Properties of Polycrystalline Ferroelectric Materials, Ph.D. Thesis, Pennsylvania State University (1973).
5) C. A. Ross and R. L. Sierakowski: Elastic Waves in Fiber Reinforced Materials, *Shock and Vibration Digest* 7 (1975) 1.
6) J. van den Boomgaard, D. R. Terrell, R. A. J. Born and H. F. J. I. Giller: An in Situ Grown Eutectic Magnetoelectric Composite Material, Part 1, *J. Mat. Sci.*9 (1974) 1705.
7) A. M. J. G. van Run, D. R. Terrell and J. H. Scholing: An in Situ grown Eutectic Magnetoelectric Composite Material, Part 2, *J. Mat. Sci.* 9 (1974) 1710.
8) L. P. M. Bracke and R. G. van Vliet: A Broadband Magnetoelectric Transducer Using a Composite Material, *Int. J. Elec.* 51 (1981) 255.
9) R. E. Newham, D. P. Skinner and L. E. Cross: Connectivity and Piezoelectric-Pyroelectric Composites, *Mat. Res. Bull.* 13 (1978) 525.
10) R. E. Newnham, L. J. Bowen, K. A. Klicker and L. E. Cross: Composite Piezoelectric Transducers, *Mat. in Eng.* II: 93.
11) M. J. Haun: Transverse Reinforcement of 1-3 and 1-3-0 PZT-Polymer Piezoelectric Composites with Glass Fibers, M. S. Thesis, Pennsylvania State University (1983).
12) A. Halliyal, A. S. bhalla and R. E. Newnham: Polar Glass Ceramics—A New Family of Electroceramic Materials: Tailoring the Piezoelectric and Pyroelectric Properties, *Mat. Res. Bull.* 18 (1983) 1007.
13) G. O. Dayton, W. A. Schulze, T. R. Shrout, S. Swartz and J. V. Biggers: Fabrication of Electromechanical Transducer Materials by Tape Casting, *Adv. in Ceramics* 9 (1984) 115.
14) M. Granahan, M. Holmes, W. A. Schulze and R. E. Newnham: Grain-Oriented $PbNb_2O_6$ Ceramics, *J. Amer. Ceram. Soc.* 64 (1981) C68.
15) R. Gerson and T. C. Marshall: Dielectric Breakdown of Porous Ceramics, *J. Appl. Phys.* 30 (1959) 1650.
16) I. S. Jacobs and C. P. Bean: Fine Particles, Thin Films, and Exchange Anisotropy, in: "Magnetism, Vol. III," G. T. Rado and H. Suhl, ed., Academic Press, N.Y. (1963).
17) M. Multani: The Finite Solid State Lattice, *in*: "Preparation and

Characterization of Materials," J. M. Honig and C. N. R. Rao, eds., Academic Press, N.Y. (1981).

18) Y. Ozaki: Ultrafine Electroceramic Powder Preparation from Metal Alkoxides, *Ferroelectrics* **49** (1983) 285.

19) V. A. Bokov and I. E. Myl'nikova: Electrical and Optical Properties of Single Crystals of Ferroelectrics with a Diffused Phase Transition, *Sov. Phys.-Solid State* **3** (1961) 613.

20) E. Galgoci: Ceramic-Polymer bonding in Piezoelectric Composites, Ph.D. Thesis, Pennsylvania State University (1985).

21) J. Giniewicz: (Pb, Bi)(Ti, Fe)O_3 Polymer 0-3 Composite Materials for Hydrophone Applications, M. S. Thesis, Pennsylvania State University (1985).

22) T. R. Gururaja: Piezoelectric Composite Materials for Ultrasonic Transducer Applications, Ph.D. Thesis, Pennsylvania State University (1984).

23) T. R. Gururaja, D. Christopher, R. E. Newnham and W. A. Schulze: Continuous Poling of PZT Fibers and Ribbons and Its Application to New Devices, *Ferroelectrics* **47** (1983) 193.

24) R. E. Newnham, C. S. Miller, L. E. Cross and T. W. Cline: Tailored Domain Patterns in Piezoelectric Crystals, *Phys. Stat. Sol.* **32** (1975) 69.

25) D. Feng, N. Ming, J. Hong, Y. Yang, J. Zhu, Z. Yang and Y. Wang: Enhancement of Second Harmonic Generation in $LiNbO_3$ crystals with Periodic Laminar Ferroelectric Domains, *Appl. Phys. Lett.* **37** (1980) 607.

26) K. Uchino, S. Nomura, L. E. Cross, R. E. Newnham and S. J. Jang: Electrostrictive Effects in Perovskites and ITS Transducer Applications, *J. Mat. Sci.* **16** (1981) 569.

27) L. E. Cross, S. J. Jang, R. E. Newnham, S. Nomura and K. Uchino: Large Electrostriction Effects in Relaxor Ferroelectrics, *Ferroelectrics* **23** (1980) 187.

28) J. F. Nye: "Physical Properties of Crystals," Oxford University Press, London (1957).

29) I. M. Lachman and R. N. McNally: High Temperature Monolithic Supports for Automobile Exhaust Catalysis, *Ceram Eng. Sci. Proc.* **2** (1981) 337.

30) T. R. Shrout, L. J. Bowen and W. A. Schulze: Extruded PZT Polymer Composites for Electromechanical Transducer Applications, *Mat. Res. Bull.* **15** (1980) 1371.

31) A. Safari, A. Halliyal, R. E. Newnham and I. Lachman, Transverse Honeycomb Composite Transducers, *Mat. Res. Bull.* **17** (1982) 301.

32) I. S. Zheludev, Piezoelectricity in Textured Media, *Solid State Physics* **29** (1974) 315.

33) G. J. Gardopee, R. E. Newnham and A. S. Bhalla: Pyroelectric $Li_2Si_2O_5$ Glass-Ceramics, *Ferroelectrics* **33** (19851) 155.

34) S. K. Bhattacharya and A. C. D. Chaklader: Review on Metal-Filled Plastics, Part 1, Electrical Conductivity, *Polym.-Plast. Tech. Eng.* **19** (1982) 21.

35) R. D. Sherman, L. M. Middleman and S. M. Jacobs: Electron Transport Processes in Conductor-Filled Polymers, *Polymer Eng. and Sci.* **23** (1983) 36.

36) K. A. Hu, R. E. Newnham, J. P. Runt and A. Safari (in preparation).

$(Pb_{1-x}Bi_x)(Ti_{1-x}(Fe_{1-y}Mn_y)_x)O_3$ - POLYMER 0-3 COMPOSITES FOR HYDROPHONE APPLICATIONS

J.R. Giniewicz, K. Duscha, R.E. Newnham, and A. Safari
Materials Research Laboratory
The Pennsylvania State University
University Park, PA 16802 USA

Abstract

The hydrostatic piezoelectric response of composite materials incorporating $(Pb_{1-x}Bi_x)(Ti_{1-x}Fe_x)O_3$ ceramic fillers from the highly anisotropic tetragonal region of the solid solution system in the vicinity of the morphotropic phase boundary were measured and compared. The considerable difficulty in poling and, hence, the diminished piezoelectric response encountered as the composition of the filler is shifted closer to the phase boundary was determined to be largely due to the high conductivity of the $BiFeO_3$-rich compositions. The ceramic was modified with Mn in an attempt to lower its conductivity. Composites incorporating the Mn-doped filler poled more efficiently and ultimately achieved hydrostatic figures of merit, $d_h g_h$, significantly better than those observed for the undoped samples. Among the samples investigated, the highest hydrostatic figures of merit were exhibited by samples containing the doped and undoped x=0.5 fillers. The hydrostatic response remains stable over a broad pressure range.

1. Introduction

0-3 piezoceramic/polymer materials consist of a three-dimensionally connected polymer matrix within which the ceramic phase is dispersed as discrete particles. Although less responsive overall than its more elaborately configured relatives, this material has certain distinctly advantageous features. Perhaps one of the most attractive characteristics of the 0-3 design is its versatility in assuming a variety of forms including thin sheets, extruded bars and fibers, and certain molded shapes.

This investigation is concerned with the dielectric and hydrostatic piezoelectric performance of the material in the form of thin sheets prepared by conventional polymer compounding and forming techniques incorporating undoped and Mn-doped fillers from the highly anisotropic phase boundary compositions of the $PbTiO_3$-$BiFeO_3$ solid solution system. The flexible nature of the sheet design makes it a viable candidate for a variety of applications. Piezoelectric sheets are suitable materials for pressure sensitive devices which require a material that is able to conform to the contours of various surfaces. Such devices as pressure sensitive keyboards, transducing gloves, and blood pressure gauges are a few products currently produced from piezoelectric sheet composites.[1,2]

2. Hydrophone Materials: An Overview

A number of poled ceramic materials, such as $Pb(Zr,Ti)O_3$, (PZT)[7], and certain piezoelectric polymers, such as polyvinylidenedifluoride, (PVDF)[8], exhibit a piezoelectric response when subjected to a hydrostatic pressure. Such materials are well-suited for transducer applications, in particular for those devices employed as underwater pressure sensors, hydrophones. Three of the most important properties required of a good transducer are: (1) voltage sensitivity or the material's ability to convert the applied pressure to an electrical signal, (2) low density to enable adequate impedance coupling between the device and the transmitting medium (typically water), and (3) compliance for enhanced durability and conformability. The conventional figure of merit focuses on the sensitivity of the material and is expressed in terms of the hydrostatic piezoelectric voltage coefficient, g_h, and the hydrostatic piezoelectric strain coefficient, d_h, as

$$d_h g_h = (d_{33} + 2d_{31})^2 / K_{33}\varepsilon_o$$

The leading piezoelectric ceramic material, PZT, exhibits only a modest hydrostatic response due to a relatively large negative d_{31} coefficient (-175 pC/N) with respect to its d_{33} coefficient (400 pC/N). The hydrostatic performance of the leading piezoelectric polymer, PVDF, is also limited by a similar inhibition of d_h and a relatively low melting temperature.

Piezoceramic/polymer composites are a class of materials that effectively overcome these limitations and hence are found to be more responsive and versatile transducer devices.[3-5] The composite constituents provide complementary properties which, when combined, produce a superior hydrostatic piezoelectric material. The polymer phase lowers the density of the material providing better acoustic coupling to water than that obtained for a high density homogeneous ceramic. The low dielectric constant of the polymer phase effectively increases the g_h coefficient and the figure of merit. Finally, the piezoelectric properties of the ceramic are easily adjusted within the composite whose constituent phases may be suitably arranged to effectively distribute the applied stresses in a manner that encourages the maximum piezoelectric response.[6]

CH2358-0/86/0000-0323 $1.00

3. The $PbTiO_3$-$BiFeO_3$ System

The $(Pb_{1-x}Bi_x)(Ti_{1-x}Fe_x)O_3$ solid solution system is of particular interest for its promising piezoelectric properties. The system possesses a morphotropic phase boundary ($0.7<x<0.8$) between a tetragonal ($0.0<x<0.7$) and rhombohedral ($0.8<x<1.0$) modification of the perovskite structure (Figure 1) very much analogous to that observed for $PbTiO_3$-$PbZrO_3$.[9,10] The $PbTiO_3$-$BiFeO_3$ system is distinctive, however, for the extremely large structural anisotropy attained for compositions in the tetragonal region.[10] This considerable distortion gives rise to a potential for highly anisotropic piezoelectrics from the composition range near or on the morphotropic phase boundary. Unfortunately, as is the case for $PbTiO_3$, it is this very feature which on the one hand, makes possible an outstanding piezoelectric response, also deters the production of strong, dense ceramics. Samples prepared in the tetragonal range generally fracture upon cooling through the transition temperature, Tc, with the degree of specimen disruption increasing as the composition approaches the phase boundary.

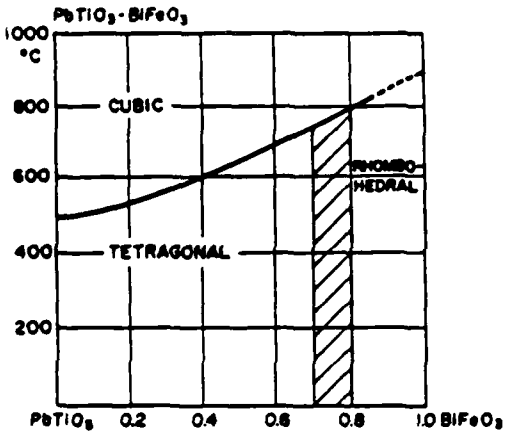

FIGURE 1 $PbTiO_3$ - $BiFeO_3$ structural phase diagram.[10]

The tetragonal lattice parameters c_T and a_T are found to vary quite considerably as the composition approaches the phase boundary.[10] The magnitude of c_T increases dramatically from 4.40 A for x=0.5 to 4.53 A at x=0.7 while a_T decreases in a more gradual manner from 3.85 A for x=0.5 to 3.81 A at the phase boundary. The c_T/a_T ratio is exceptionally high for all the compositions recorded, attaining a maximum value of 1.19 at the morphotropic phase boundary. This represents a strain of nearly 20% present in materials prepared from this portion of the solid solution system which are rarely strong and generally fracture entirely upon cooling through the transition temperature.

All modifications of the solid solution are ferroelectric. No reports appear in the literature, however, regarding the observation of a hysteresis loop for any composition presumably because of a high coercive field and the low resistivity of the material as is the case for $PbTiO_3$. The variation of ferroelectric Curie point with composition as depicted in Figure 1 is seen to increase in a nearly linear fashion from 490°C for $PbTiO_3$ to 850°C for $BiFeO_3$.

The Curie point dielectric constant is depicted in Figure 2a as a function of composition measured at 25°C and a frequency of 530 MHz. Its value is observed to decrease with increasing $BiFeO_3$ content.[11] The dissipation factor is plotted as a function of temperature for selected compositions in Figure 2b. The losses generally increase with increasing $BiFeO_3$ content and are likely due to a substantial n-type conductivity associated with the ferrite.[11] A complex variation of conductivity with composition has been reported and has been attributed to the relative contributions of several possible conductivity mechanisms operating across the composition range.[10] The greatest contributors to the conductivity for compositions with a high $BiFeO_3$ content are likely to be the Fe^{2+} ions present with the Fe^{3+} ions on the B-sites of the perovskite lattice which are oxidized via the reaction

$$Fe^{2+} \longrightarrow Fe^{3+} + e- \qquad (1)$$

thereby liberating electrons to the system.[12-14] Where $PbTiO_3$ and $BiFeO_3$ are both semiconductors, it can be assumed that the high losses at elevated temperatures are primarily conductive.[11]

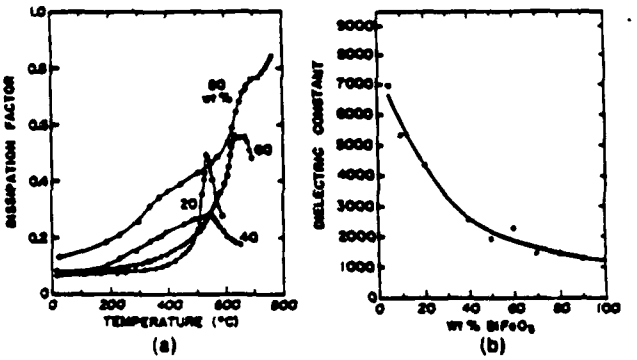

FIGURE 2 (a) Curie point dielectric constant as a function of composition (25°C, 530 MHz), (b) dissipation factor as a function of temperature.[11]

4. Objectives of the Investigation

The objective of this investigation is to produce thin, responsive piezoelectric sheets for hydrophone applications. The $(Pb,Bi)(Ti,Fe)O_3$ / polymer 0-3 composites satisfy all the desired requirements of a good hydrophone material. The high anisotropy of $(Pb_{1-x}Bi_x)(Ti_{1-x}Fe_x)O_3$ compositions in the range x=0.5-0.7 permits considerable hydrostatic sensitivity. 0-3 composites incorporating this filler are, therefore, potentially more responsive than 0-3 designs currently produced containing $PbTiO_3$ or PZT. In addition, very thin sheets of the material may be produced due to the fine particle sizes obtained by quenching the filler powders. The high strain present in ceramics prepared in the x=0.5-0.7 composition range allows for the production of fine particles on quenching with minimal damage to individual crystallites. Sheets made with single crystallites created in this way are found to be more easily poled and to have an enhanced piezoelectric response over composites made with fine particles produced by grinding.

Little has been reported in the literature regarding the piezoelectric properties of materials produced from the $PbTiO_3$-$BiFeO_3$ system. Most studies on the system have been conducted mainly to better determine the nature of $BiFeO_3$ which is difficult to characterize alone. Further, any investigation of the piezoelectric character is restricted by the brittle nature and high conductivity of the material, especially in the prime area of interest near the morphotropic phase boundary. The aim of this investigation is to examine the hydrostatic piezoelectric nature of the binary system as the filler component of a 0-3 composite. The one problem of brittle fracture is resolved and, in fact, exploited in this way. The difficulties related to the high conductivity are alleviated by modifying the filler compositions with small concentrations of a Mn-dopant. The Mn dopant is added in an attempt to counter the electron liberating oxidation, (1), by oxidizing the ferrous ions via the reaction:

$$Mn^{3+} + Fe^{2+} \longrightarrow Fe^{3+} + Mn^{2+} \quad (2)$$

thereby lowering the conductivity of the ceramic.

The hydrostatic piezoelectric performance of composite samples incorporating both the undoped and Mn-doped filler are examined and compared.

5. Preparation of the Ceramic

The $(Pb_{1-x}Bi_x)(Ti_{1-x}(Fe_{1-y}Mn_y)_x)O_3$ powders were prepared by a conventional double-firing process. Green mixtures were batched with compositions in the range x=0.5 - 0.7 with y = 0.0 - 0.025 from the oxides PbO, TiO_2, Bi_2O_3, Fe_2O_3, and MnO_2. The green powders were contained in covered alumina crucibles and subjected to a primary low-temperature firing in air at 800°C for 1.5 hours. The calcined powders were loosely compacted, placed in covered alumina crucibles and subjected to a second firing at 1000°C for 1.5 hours. The pellets were quenched to room temperature directly following the soak period. The quenched samples generally fractured completely upon quenching and required only the lightest grinding with mortar and pestle to break up agglomerates.

The variation of tetragonal lattice parameters with composition was determined by means of an x-ray powder diffraction study and found to be in excellent agreement with that reported in the literature.[10] No changes in lattice parameters were observed, however, for powders with composition x=0.5 containing any concentration of the dopant within the range y = 0.0 - 0.25.

The intergranular nature of the fracture and particle morphology are clearly represented in scanning electron micrographs of powders representing any of the tetragonal compositions investigated. Disruption of the microstructure is observed to occur entirely at the grain boundaries. No fractured particles are observed. Particles produced for all tetragonal compositions are generally discrete, approximately spherical crystallites.

The particle size distribution curves for samples prepared from each composition were determined by means of a Sedigraph 5000D Particle Size Analyzer. Among the samples prepared in the range x = 0.5 - 0.7 without the Mn dopant those with compositions closer to the the phase boundary produced the narrowest distributions with the smallest mean particle size reflecting a more thorough disruption of the microstructure as the strain in the system increases. The mean particle size range is 4-13 μm for compositions x=0.5-0.7, y = 0.0 - 0.025 where the finest particles are produced for powders with compositions x = 0.5, y = 0.01; x = 0.5, y = 0.015; x = 0.5, y = 0.02,(all 4-5 μm) and x = 0.7, y = 0.0, (5 μm).

6. Preparation of the Composite

Composite samples were prepared containing 50-60 volume percent $(Pb,Bi)(Ti,Fe)O_3$ filler and 35-45 volume percent polymer from the epoxy based Eccogel series (Eccogel-Series 1365 #25 Emerson and Cuming, Dewey and Almy, Chemical Division, Canton, Ma.). The filler was initially blended with the liquid components of the Eccogel system and compounded by a high-shear hand-mixing technique.

The mixture was then formed and cured. The first series of samples (Series I) were formed into sheets by hot-rolling at a temperature in the range 40-60°C. The formed sheets were initially cured under a low pressure applied by means of an hydraulic press at 90°C for 2.0 hours and then post-cured for an additional 3.0 - 4.0 hours at 70°C. The second series of samples (Series II) were formed in an one inch diameter die under a pressure of 6000 psi. The pressed discs were then cured in the dies without applied pressure at 80°C for 12 hours.

The cured composite samples were polished with a fine silicon carbide emery paper to a uniform thickness of approximately 0.2-0.5 mm and dried in a 70°C furnace for 2.0 - 3.0 hours. The polished samples were electroded with an air-dry silver paint for poling and for dielectric and piezoelectric testing.

7. Samples Selected for Dielectric and Piezoelectric Measurement

Two series of samples were prepared for dielectric and piezoelectric testing. The series were selected to investigate both the effects of filler composition and Mn-doping of the filler on the degree of poling achieved and on the ultimate hydrostatic piezoelectric response.

The first series was examined in order to monitor the change in piezoelectric response with increasing $BiFeO_3$ content for tetragonal compositions in the vicinity of the morphotropic phase boundary. The samples constituting the second series were prepared incorporating both undoped and Mn-doped $(Pb_{1-x}Bi_x)(Ti_{1-x}Fe_x)O_3$ fillers from the composition x=0.5. The purpose of this second series was to investigate the effects of Mn-doping on the poling and ultimate piezoelectric performance of composites incorporating this filler as well as to determine the concentration of Mn for which the optimum hydrostatic piezoelectric performance of the composite is attained. Investigation of the dielectric and piezoelectric properties included: (a) determination of the optimum poling conditions for each sample, (b) determination of the degree of poling achieved as evidenced by the magnitude of the longitudinal strain coefficient, d_{33}, (c) measurement of low frequency (KHz) dielecric constant and dissipation factor, both before and after poling and, finally, (d) measurement of the hydrostatic piezoelectric coefficients, d_h and g_h.

8. Poling the Composites

The optimum poling temperature, field and time are determined primarily by the relative dielectric constants and conductivities of the composite components, the polymer melting temperature, and the composite integrity. The relative dielectric constants and conductivities of the two composite components in particular affect, to a considerable extent, the degree of poling achieved.[5] The electric field acting on the piezoelectric element within an insulating 0-3 composite will be similar to the applied field only if the dielectric constants of the components are nearly equivalent. This is generally not the case, however, for ceramic/polymer systems where the difference in dielectric constant may be one or two orders of magnitude. In addition, where the conductivity of the ceramic is particularly high, only a very small fraction of the poling field will act on the piezoelectric filler.

The considerable differences in dielectric constant and conductivity between the two components of the composite system establishes the need for a poling field of at least 75 KV/cm to produce any significant poling of the material. The relatively low melting temperature of the Eccogel matrix sets the upper limit for the poling temperature. The optimum poling temperature of 75°C was established on the basis of a general survey made for representative samples selected from the two series and was applied for the poling of all samples investigated.

Optimum poling fields and times were similarly determined by systematically varying the parameters and monitoring the degree of poling achieved and the incidence of breakdown. The results of this study are presented in Table 1. The practical poling field established represents that field strength at which the highest degree of poling is achieved with minimum breakdown. The poling time corresponds to that period required to achieve maximum poling under the influence of the practical field. The magnitudes of the longitudinal strain coefficient, d_{33}, exhibited by samples poled under these conditions are listed for each specimen as an indicator of the degree of poling attained. d_{33} measurements were made on a Berlincourt d_{33} meter (Model CPDT 3300--Channel Products, Inc., Ohio).

TABLE 1 Poling fields, poling periods, and d_{33} coefficients for Series I and Series II samples.

	x	y	Poling E (KV/cm)	Period (min.)	d_{33} (pC/N)
Series I					
50I	0.5	0.0	110	30	85
65I	0.65	0.0	100	15	23
70I	0.70	0.0	100	10	16
Series II					
50IIA	0.5	0.000	100	20	40
50IIB	0.5	0.005	110	25	52
50IIC	0.5	0.010	110	25	67
50IID	0.5	0.015	110	30	48
50IIE	0.5	0.020	110	30	48
50IIF	0.5	0.025	90	30	38

Series I samples were found to be increasingly resistant to poling as the filler composition approached the morphotropic phase boundary. The maximum degree of poling achieved as indicated by the longitudinal strain coefficient, d_{33}, was consequently observed to decrease significantly as the composition became increasingly rich in $BiFeO_3$.

Mn-doping of the x = 0.5 filler was found to significantly affect the poling of composite materials containing the modified ceramic. The degree of poling achieved for all the Series II composite samples containing x = 0.5 fillers with any concentration of the Mn dopant within the range investigated attained higher degrees of poling than the composite containing the undoped x = 0.5 filler poled under similar poling conditions. Composite samples containing Mn-doped x = 0.5 fillers with Mn concentrations in the range y = 0.005 - 0.02 were found to achieve the highest degrees of poling.

9. Dielectric Data

Dielectric constant and dissipation factor were recorded for each sample both before and after poling. The dielectric constant was calculated in terms of the sample dimensions and capacitance. Capacitance and dissipation factor measurements were made at 1 KHz on a Hewlett-Packard 4270A automatic capacitance bridge. The data appear in Table 2.

The dielectric constants for each sample both before and after poling were found to be similar in magnitude. The dielectric constant was observed to decrease somewhat for those samples that attained a sufficiently high degree of poling. This reflects the reorientation of the K_{33} within the piezoelectric filler where the alignment in the poling direction will be manifested by a decrease in the dielectric constant of the composite.

Dissipation factors for all Series I samples were typically about 10% with a slight decrease after poling. A variation of the dissipation factor for poled Series II samples was observed with the lowest losses exhibited by samples 50IIC, 50IID, and 50IIE (y = 0.005-0.020). This suggests that the Mn-dopant does affect the conductivity of the filler within this dopant concentration range.

10. Hydrostatic Piezoelectric Data

Hydrostatic piezoelectric measurement was made by a dynamic technique[18] by which means the voltage coefficient, g_h, was evaluated and the strain coefficient, d_h, subsequently derived. Hydrostatic data are recorded in Table 2. Hydrostatic measurements were taken as a function of pressure on a sample representative of the undoped x = 0.5 filler. The results of that investigation are shown in Figure 3.

The increased inhibition to poling of the Series I samples as the filler composition approaches the morphotropic phase boundary is reflected in the steady decrease of the hydrostatic response from a figure of merit of about 1600 (fm^2/N) for the sample 50I to barely 100 (fm^2/N) for sample 70I. The enhanced poling observed for composite samples incorporating the Mn-doped x =0.5 fillers is also reflected in the high figures of merit attained for samples containing the modified fillers.

TABLE 2 Dielectric and piezoelectric data for Series I and Series II composite samples.

	ε		tanδ		g_h	d_h	$d_h g_h$
	Before	After	Before	After	(pC/N)	(mV/N)	(fm^2/N)
Series I							
50I	90	88	0.13	0.09	25	66	1625
40I	98	98	0.17	0.10	15	30	450
70I	95	95	0.12	0.08	5	15	75
Series II							
50IIA	95	95	0.16	0.11	25	63	1575
50IIB	95	90	0.16	0.08	30	79	2370
50IIC	95	90	0.13	0.08	30	81	2430
50IID	90	95	0.14	0.08	30	81	2430
50IIE	95	90	0.16	0.08	30	79	2370
50II7	95	95	0.13	0.10	30	90	1000

The highest figures of merit within this series were exhibited by the 50IIC and 50IID composites, (2430 fm^2/N), indicating that the optimum dopant concentration is within the range $y = 0.010 - 0.015$. In addition, the hydrostatic response is observed to be highly stable over a broad pressure range. The hydrostatic performance exhibited by the Series II samples, in particular the exceptionally high voltage sensitivity and pressure stability, establishes, therefore, this material's merit as an effective and reliable hydrostatic pressure sensor.

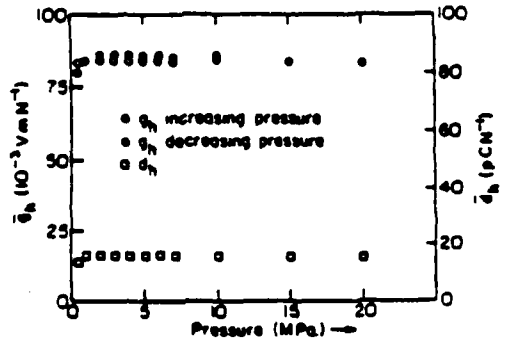

FIGURE 3 Hydrostatic piezoelectric coefficients as a function of pressure (Measurements made at the facilities of the Underwater Sound and Reference Division of the Navy, Orlando, FL).

Acknowledgement

The authors are grateful for the financial support received from the Office of Naval Research and the Celanese Research Company.

References

[1] Hisao Banno and Shigeo Saito, "Piezoelectric and Dielectric Properties of Composites of Synthetic Rubber and $PbTiO_3$ and PZT," Japanese Journal of Applied Physics, 22,Supp. 22-2, 67-69, 1983.

[2] Hisao Banno, "Recent Developments of Piezoelectric Ceramic Products and Composites of Synthetic Rubber and Piezoelectric Ceramic Particles," Ferroelectrics, 5, 3-12, 1983.

[3] R.E. Newnham, L.J. Bowen, K.A. Klicker, and L.E. Cross, "Composite Piezoelectric Transducers," Materials in Engineering, 112, 93, 1980.

[4] R.E. Newnham, A. Safari, J. Giniewicz, and B.H. Fox, "Piezoelectric Sensors," Ferroelectrics, 60, 15-21, 1984.

[5] R.E. Newnham, A. Safari, G.Sa-Gong, and J. Giniewicz, "Flexible Composite Piezoelectric Sensors," Proceedings of IEE Ultrasonic Symposium, 501, 1984.

[6] R.E. Newnham, D.P. Skinner and L.E. Cross, "Connectivity and Piezoelectric-Pyroelectric Composites," Materials Research Bulletin, 13, 525-536, 1978.

[7] Bernard Jaffe, William R. Cook, Jr., and Hans Jaffe, Piezoelectric Ceramics, Academic Press, London and New York, 1971.

[8] H. Kawai, "The Piezoelectricity of Poly(vinylidene Fluoride)," Japanese Journal of Applied Physics, 8, 975, 1969.

[9] S.A. Fedulov, P.B. Ladyzhinski, I.L. Pyatigorskaya, and Yu. N. Venevtsev, "Complete Phase Diagram of the $PbTiO_3$-$BiFeO_3$ System," Soviet Physics-Solid State, 6 (2), 375-377, 1964.

[10] S.A. Fedulov, Yu. N. Venevtsev, G.S. Zhdandov, E.G. Smazhevskaya, and I.S. Rez, "X-Ray and Electrical Studies of the $PbTiO_3$-$BiFeO_3$ System," Soviet Physics-Crystallography, 7 (1),82-86, 1962.

[11] R.T. Smith, G.D. Achenbach, R.Gerson, and W.J. James, "Dielectric Properties of Solid Solutions of $BiFeO_3$ with $Pb(Ti,Zr)O_3$ at High Temperature and High Frequency," Journal of Applied Physics 39 (1), 70-74, 1968.

[12] J. Smit and H.P.J. Wijn, Ferrites, John Wiley and Sons, New York, 1959.

[13] E.P. Wohlfarth, ed., Ferromagnetic Materials (Vol. 2), North Holland Publishing Co.,New York, 1980.

[14] R.F. Soohoo, Theory and Application of Ferrites, Prentice-Hall Inc., New Jersey, 1960.

[15] A.R. Von Hippel, Dielectrics and Waves, John Wiley and Sons, 1954.

[16] J.R. Giniewicz, $(Pb,Bi)(Ti,Fe)O_3$ / Polymer 0-3 Composite Materials for Hydrophone Applications, M.S. Thesis, Pennsylvania State University, 1985.

PREPARATION OF $PbTiO_3$ POWDER FOR A FLEXIBLE 0-3 PIEZOELECTRIC COMPOSITE

Y. H. Lee, M. J. Haun, A. Safari and R. E. Newnham

Materials Research Laboratory
The Pennsylvania State University, University Park, PA 16802

ABSTRACT

Lead titanate powders prepared by three different methods (mixed-oxide, sol-gel and co-precipitation) were synthesized as fillers for 0-3 composite transducers. As starting materials, $Pb(C_2H_3O_2)_2 \cdot 3H_2O$ and $Ti(OC_3H_7)_4$ were used in the sol-gel method, $Pb(NO_3)_2$ an $TiCl_4$ for the co-precipitation technique. The $PbTiO_3$ powder prepared by the co-precipitation method yielded more uniformly shaped powder than the powder prepared by the sol-gel or mixed-oxide method.

0-3 composites were prepared with these powders using Eccogel polymer. X-ray diffraction patterns of the $PbTiO_3$-polymer composites prepared by the co-precipitation method before and after poling indicated that the composites were fully poled. The hydrostatic piezoelectric voltage and charge coefficient, g_h and d_h were about 97 (10^{-3}V-m/N) and 43 (pC/N), respectively. The hydrophone figure of merit $d_h g_h$ was over 4000 ($10^{-15}m^2/N$). These composites showed no significant aging effect.

1. INTRODUCTION

A variety of electromechanical transducers such as hydrophones, air sensors, vibration sensors, pressure and stress sensors depend on the piezoelectric phenomenon exhibited by certain piezoelectric crystals, polarized polymers and composites.

An important class of sensors have as their active sensing element solid shapes of piezoelectric ceramic materials. In the hydrophone application area, the piezoelectrically active ceramic component converts underwater sound pressure waves to electrical signals, which are then amplified and displayed.

The sensitivity of a sound receiver material is characterized by a hydrophone Figure-Of-Merit (FOM), which is commonly derived as the product of the hydrostatic piezoelectric charge (d_h) and voltage (g_h) coefficients.

During the past few years, a number of investigators have examined piezoelectric ceramic polymer composites with different connectivity patterns. The piezoelectric properties of the composites depend, to a large extent, on the connectivity pattern of the constituent phases. A more extensive description of the work on ceramic-polymer composites can be found in recent review papers[1].

One of the simplest types of piezoelectric composites consists of a polymer matrix loaded with ceramic powder. In such a composite the ceramic particles are not in contact with each other while the polymer phase is self-connected in three dimensions (0-3 connectivity). Early attempts to fabricate flexible composites with piezoelectric ceramic particles were made by Kitayama[2], Pauer[3] and Harrison[4].

An improved version of the 0-3 composite was fabricated by Banno[5]. Rather than using PZT as the ceramic filler, pure or modified $PbTiO_3$ was employed, because of its greater piezoelectric anisotropy. The $PbTiO_3$ filler was prepared by water quenching the ceramic, thereby exploiting the high strain present in the material in order to produce fine powders. The average particle size was about 5 μm. The hydrostatic voltage coefficient, g_h, of these pure $PbTiO_3$ composites was found to be comparable to that of PVF_2 polymer (100×10^{-3}Vm/N) and the d_h value was 35 pC/N.

Recently the sol-gel process has been used to prepare $PbTiO_3$ powder for use in 0-3 composites[6,7]. The merits of sol-gel processing such as high purity, molecular homogeneity and lower processing temperatures offered advantages over the conventional mixed-oxide processing method[8].

In this study, $PbTiO_3$ powders were prepared by the mixed-oxide, sol-gel and co-precipitation methods. 0-3 composites were prepared using these powders. Dielectric and

CH2358 0/86/0000 0318 $1 00 © 1986 IEEE

piezoelectric properties of these composites are reported in this paper

2. POWDER PREPARATION

Preparation of $PbTiO_3$ Powders

$PbTiO_3$ powders were prepared by the mixed-oxide, sol-gel and co-precipitation method.

a) Mixed-Oxide Method

Commercially available Alfa Products $PbTiO_3$ was used as the mixed-oxide $PbTiO_3$ powder.

b) Sol-Gel Method

A sol-gel method similar to the procedure described in reference 7 was used to prepare $PbTiO_3$ powder from lead-acetate [$Pb(C_2H_3O_2)_2\ 3H_2O$] and titanium isopropoxide [$Ti(OC_3H_7)_4$]. Figure 1 shows a flow chart of the procedure used to prepare the sol-gel $PbTiO_3$ powder. The lead acetate was dissolved in methoxyethanol ($C_3H_8O_2$) in a three neck reaction flask by heating to approximately 70 °C. To remove the absorbed water a reflux condenser was connected to the reaction flask. The solution was then heated and began to boil at 118 °C. As the water was removed, the temperature of the solution gradually increased to 125 °C (boiling point of methoxyethanol). After cooling the solution to 75 °C, the titanium-isopropoxide was added and again heated to 125 °C.

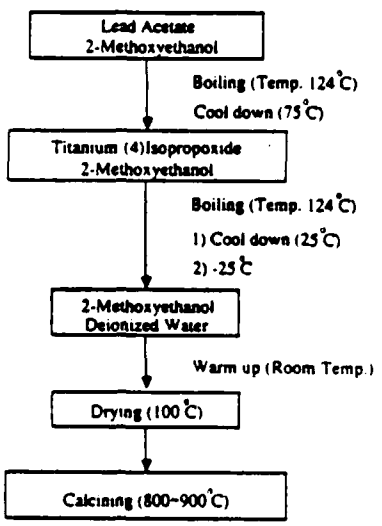

Fig.1. The procedure used to prepare $PbTiO_3$ powder by the sol-gel method.

The solution was cooled to -25 °C with a liquid nitrogen isopropanol bath. The water for hydrolysis (4 moles H_2O per mole alkoxide) was first mixed with an equal amount of methoxyethanol and then added to the cooled solution. By slowly heating the flask up to room temperature the solution gelled. The gel was then heated in a 100 °C oven for 1-2 days until dry. The dried gel was then ground in a mortar and calcined at 800-900 °C for 1 hour.

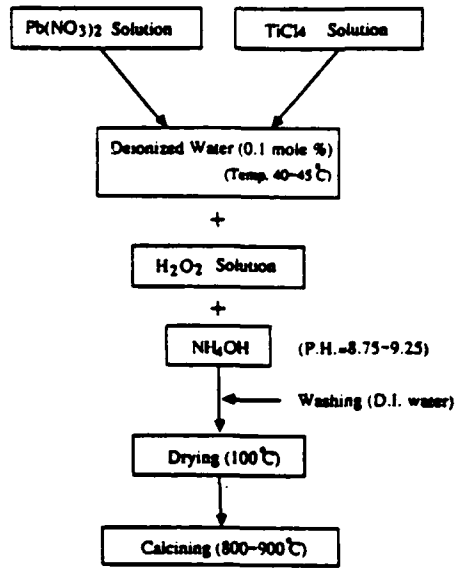

Fig.2. The procedure used to prepare $PbTiO_3$ powder by the co-precipitation method

c) Co-Precipitation Method

Figure 2 shows a flow chart of the procedure used to prepare co-precipitated $PbTiO_3$ powder. The $PbTiO_3$ was formed by precipitation from an aqueous solution in which the reactants were present in 1 molar stoichiometric quantities. Components were combined in the order : 1) $TiCl_4$ solution added to $Pb(NO_3)_2$ solution, 2) H_2O_2 solution added to this solution. The pH of the resulting solution was adjusted to approximately 8.95 to 9.25 by additions of deionized water and NH_4OH. Then the yellow precipitated aqueous solution was washed with deionized water and dried at 100 °C. The dried materials was ground using a mortar and pestle and calcined at 800-900 °C to yield highly crystalline particles.

The SEM micrographs of the powders are shown in Photos 1-3. The particle shape of the powder obtained by the sol-gel method and the mixed-oxide method were more angular than the powder prepared by the co-precipitation

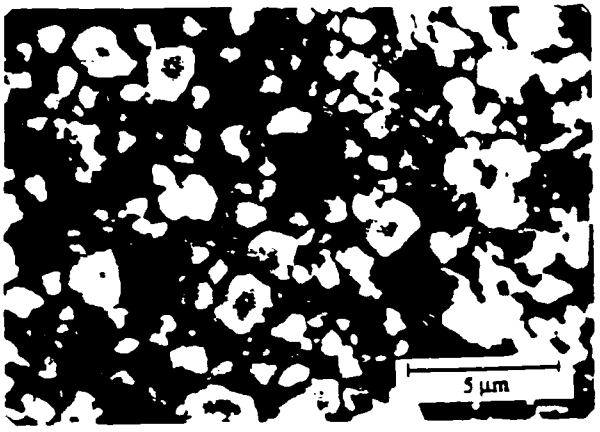

Photo.1. SEM micrograph of the $PbTiO_3$ powder prepared by the mixed-oxide method.

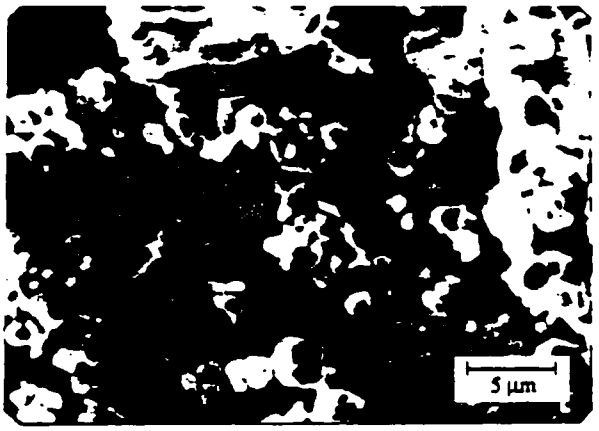

Photo.2. SEM micrograph of the $PbTiO_3$ powder prepared by the sol-gel method.

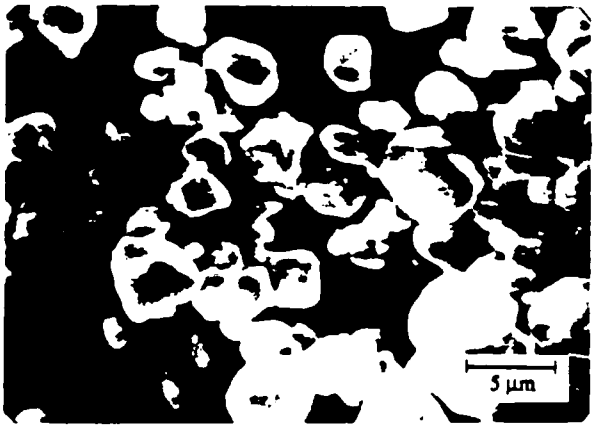

Photo.3. SEM micrograph of the $PbTiO_3$ powder prepared by the co-precipitation method.

method. The powder prepared by the co-precipitation method had a narrower distribution in particle size, than the powders prepared by the mixed-oxide and sol-gel method.

3. 0-3 COMPOSITE FABRICATION

The $PbTiO_3$ powder was dispersed in Eccogel polymer 1365-0 (Emerson and Cuming, W. R. Grace and Co., MA.) to make a 0-3 type composite, as shown in Figure 3. The volume percent of $PbTiO_3$ powder in the composites was about 70 for the mixed-oxide and sol-gel powders, and 67 for the co-precipitation powder. The filler material was mixed with the Eccogel polymer and placed between two sheets of teflon in a 1.25 inch diameter die. The mixture was then pressed with a pressure of 10,000 psi and cured at 80 °C for about 8 hours. Electrodes of an air-dried silver paste were applied on both surfaces of the composites. The composites were poled at 75 °C with a field of 80-115 KV/cm for 30 minutes.

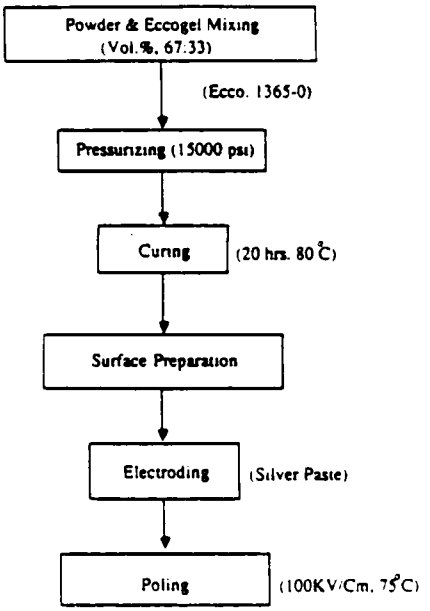

Fig.3. The procedure used to fabricate the $PbTiO_3$-polymer 0-3 composites.

4. EVALUTION OF DIELECTRIC AND PIEZOELECTRIC PROPERTIES

The capacitance and dissipation factor were measured at 1 KHz using a Hewlett-Packard 4270A Multi-Frequency LCR Meter. The d_{33} coefficients were measured dynamically using a Berlincourt Piezo d_{33}-Meter with the electromagnetic driver operating at a frequency of 100 Hz.

The d_h coefficients were determined by the dynamic A.C

technique at a pressure of 100-1000 psi and a frequency of 75 Hz. An electromagnetic driver was used as an A.C. stress generator to apply pressure waves to the sample and a PZT standard, which was also under a static pressure from the hydraulic press. The charges produced from the sample and from the standard were buffered with an impedance converter and the voltages produced were measured on a Hewlett-Packard 3538A Spectrum Analyzer. The ratio of the voltages produced is proportional to the d_h coefficients. By accounting for the sample geometries, the d_h coefficients of the samples were calculated. The d_{31} and g_h coefficients and $d_h g_h$ figure of merit were then calculated from the measured coefficients.

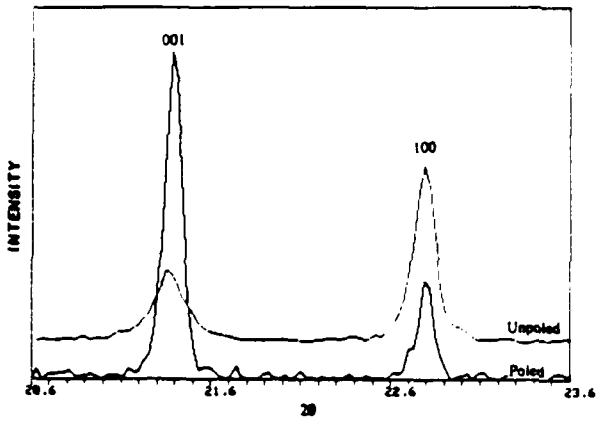

Fig.4. The 001, 100 x-ray diffraction peaks, before and after poling , for a co-precipitation method 0-3 composite.

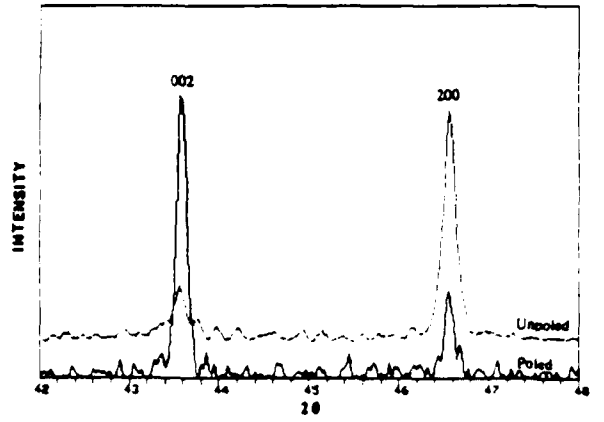

Fig.5. The 002, 200 x-ray diffraction peaks, before and after poling, for a co-precipitation method 0-3 composite.

5. RESULTS AND DISCUSSION

The 001-100 and 002-200 x-ray diffraction peaks from the surface of the composites, before and after poling, were observed to determine the degree of poling. The reversal of the peak intensities indicated that the co-precipitation method composites were more completely poled than the mixed-oxide or sol-gel method composites. Figure 4 and 5 show the reversal of peak intensities for a co-precipitation method composite before and after poling.

Table I Comparison of the dielectric and piezoelectric properties.

0-3 composite	Vol. % PT	Poling Field (KV/Cm)	d_{33} (pC/N)	d_{31} (pC/N)	K_{33}	d_h (pC/N)	g_h (10^{-3} Vm/N)	$d_h g_h$ (10^{-12} m²/N)
Mixed-Oxide Prep	70	115	25	-6.0	45	13	33	430
Sol-Gel Prep	70	80	35	-4.5	50	26	59	1530
Co-Precipitation	67	105	60	-8.7	50	43	97	4170

The dielectric and piezoelectric properties of the three types of 0-3 composites are summarized in Table 1. Also shown in this table are the maximum poling fields that could be applied without electric breakdown. The sol-gel and co-precipitation method composites were poled with lower electric fields than the mixed-oxide method composites, but the degree of poling (as observed by the reversal of the x-ray diffraction peaks) and the piezoelectric coefficients were higher. This was possibly due to the greater purity and homogeneity of the sol-gel and co-precipitation powders.

The lower maximum poling field of the sol-gel method composites may not have allowed these composites to be fully poled, resulting in lower piezoelectric coefficients than the more fully poled co-precipitation method composites. This was possibly due to the non-uniform particle size distribution in the sol-gel powder (some large particles were present, as shown in SEM Photo. 2). The co-precipitation powder was also more regularly shaped than the sol-gel or mixed-oxide powders

The g_h and d_h of the 0-3 composites prepared by the co-precipitation method showed no pressure dependence up to 1000 psi, as shown in Figure 6. These composites also showed no significant aging, as shown in Figure 7 by no change in the x-ray diffraction peak intensities with time.

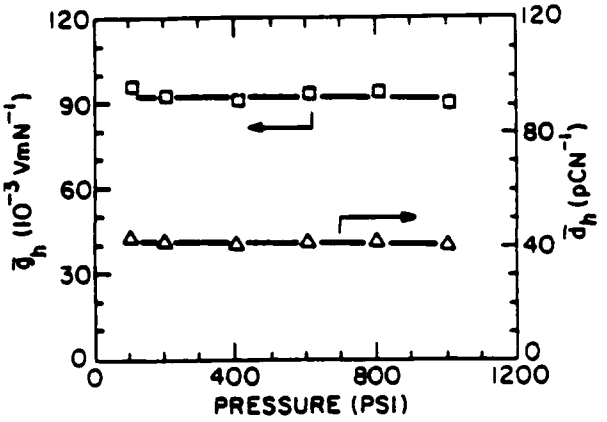

Fig.6. The hydrostatic piezoelectric d_h and g_h coefficients plotted versus pressure at 75 Hz for a co-precipitation method 0-3 composite.

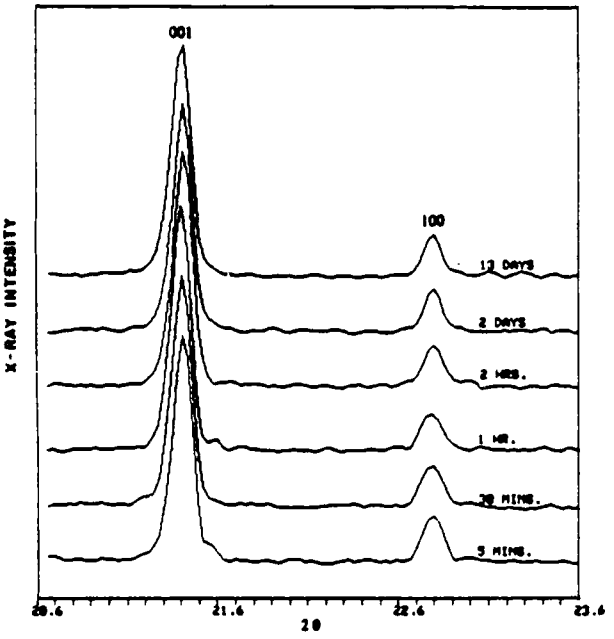

Fig.7. The effect of aging on the 001, 100 x-ray diffraction peaks for a co-precipitation method 0-3 composite.

6. SUMMARY

$PbTiO_3$ powders were prepared using sol-gel and co-precipitation methods. These powders along with a commercial mixed-oxide method $PbTiO_3$ powder were used as filler materials in 0-3 composites. The $PbTiO_3$ powder prepared by the co-precipitation method had more uniformly shaped particles than the sol-gel or mixed-oxide powders. The sol-gel and co-precipitation powders were purer and more homogeneous than the mixed-oxide powder.

X-ray diffraction of the composites before and after poling showed that the co-precipitation method composites were poled more completely than the sol-gel or mixed-oxide method composites, and therefore resulted in the highest piezoelectric coefficients, with a $d_h g_h$ figure of merit of over 4000 ($x10^{-15} m^2/N$). These composites showed no significant pressure or aging effects.

7. ACKNOWLEDGEMENT

The authors are grateful for financial support from the Office of Naval Research and Celanese Research Company.

REFERENCES

[1]. R. E. Newnham, A. Safari, J. Giniewicz and B. H. Fox, Ferroelectrics, 60, 15, (1984).

[2]. T. Kitayama and S. Sugawara, Rept. Proc. Gr. Inst. Elec. Comm. Eng. Japan, CPM 27-17, (1972).

[3]. L. A. Pauer, IEEE Intl. Conv. Rea., 1, (1973).

[4]. W. B. Harrison, Proc. Workshop on Sonar Transducer Materials, Naval Research Lab., (1976).

[5]. H. Banno, Ferroelectrics, 50, 3, (1983).

[6]. S. R. Gurkovich and J. B. Blum, Ferroelectrics, 62, 189, (1985).

[7]. J. B. Blum and S. R. Gurkovich, J. Mater. Sci. 20, 4479, (1985).

[8]. D. L. Monroe, J. B. Blum, A. Safari, Ferroelectrics Letters, Vol.5, pp 39-46 (1986).

COMPOSITE PIEZOELECTRIC PAINTS

K.A. KLEIN, A. SAFARI, R.E. NEWNHAM AND J. RUNT

Materials Research Laboratory
The Pennsylvania State University
University Park PA 16802

ABSTRACT

0-3 composites have been prepared from a water-based suspension of electroceramics and polymer. A typical paint base consisting of a methacrylic copolymer emulsion along with surfactants and rheological agents was used in all formulations. The paint was filled with various concentrations of piezoceramics such as PZT and co-precipitated PbTiO3. The filled emulsion was spread on an appropriate surface, dried and the resultant film electroded and poled. Piezoelectric $\bar{d}$-coefficients, as well as dielectric constant and resistivity were determined for all composites.

INTRODUCTION

Composites of piezoelectric ceramics and polymers have been the focus of much study in the past five to ten years.(1-3) What makes these composites so attractive is their high $\bar{g}_h$(hydrostatic voltage coefficient) and $\overline{d_h g_h}$ (figure of merit) values, compared to the corresponding properties of single phase materials. Consequently, the composites have the potential for use in a number of applications such as in hydrophones or ultrasonic transducers.

As an extension of this work, we have examined composites possessing 0-3 connectivity (ceramic particles in a polymer matrix) for the development of piezoelectric or pyroelectric "paints". The initial question that must be addressed is: is it feasible to load a typical paint vehicle to the levels required to obtain good piezoelectric or pyroelectric activity in the final, dry film? In fact, it is common in flat and ceiling paints to load to 60-80 volume percent pigment.(4) By replacing the pigment with an electroceramic filler one could produce a piezoelectric or pyroelectric paint for large area sensor applications.

One purpose of this paper is to demonstrate the basic principle that one can indeed prepare a ferroelectric paint. Here we present preliminary results of an ongoing investigation in this area.

EXPERIMENTAL

1) Materials and Sample Preparation

The latex emulsion used in this study consisted of a random copolymer of methyl methacrylate and 2-hexyl acrylate (obtained from E.I. duPont de Nemours, Lucite 11018) dispersed in water (60 % solids). Various surfactants and rheological agents were purchased from Polysciences, Inc.. These include sodium carboxy methyl cellulose, hydroxyethylcellulose, sodium lauryl sulfate (an ionic surfactant) and polyethylene oxide (a nonionic surfactant). "Foammaster" defoamer was obtained from Rohm Haas, Inc..

Films were prepared by combining the copolymer emulsion with the surfactants and rheological agents in the proportions designated in ref. 5. The ferroelectric filler was then loaded into the "paint base" and the mixture was allowed to stir for one hour at room temperature. Filler concentrations which resulted in 60 or 70% by volume in the final, dry film were used. Sufficient defoamer was added to eliminate the formation of air bubbles while stirring.

Composites were then prepared by casting the suspension onto brass plates with rough surfaces to ensure good adhesion between the metal and the paint. The films were allowed to air dry for 24 hours, then placed in a vacuum oven at 110 °C for an additional 24 hours. This was done in order to remove all residual water.

Gold-sputtering was used to electrode the films on one side while the brass plate acted as the second electrode. Film thicknesses ranged from

CH2358-0/86/0000-0285 $1.00

0.020-0.050 cm and were suitable for both piezoelectric and dielectric measurements.

All composites were examined with an I.S.I. Super IIIA Scanning Electron Microscope to determine the dispersion of the ceramic particles in the polymer matrix.

2) Poling and Measurements

The poling apparatus consisted of an oil bath and an external power supply. The temperature of the bath was maintained at 75 °C. The voltage was applied stepwise; the specimen was allowed to remain at a particular voltage for 10 minutes, then the field was increased. This process was repeated until the maximum field for a given composite was reached (50-140 kV/cm). This procedure minimized the possibility of electrical breakdown and allowed higher fields to be applied than the "conventional" method.

Measurements of $\bar{d}_{33}$ were made using a Berlincourt Piezo $\bar{d}_{33}$-meter at 100 Hz for each poled sample. $\bar{d}_{33}$ is the composite piezoelectric coefficient which develops as a result of applying a stress parallel to the poling direction. The $\bar{d}_{33}$ values reported here are the average of 10 random measurements (5 on each electroded surface).

To measure the hydrostatic piezoelectric coefficient the composite was placed in an oil chamber. The pressure inside this chamber was raised to 100 psi, and an AC stress generator, which was driven by a function generator adjusted to 50 Hz, provided alternating pressure cycles inside the sample enclosure. The voltage produced by each sample and a standard was displayed on a spectrum analyzer and was recorded. $\bar{d}_h$ was then calculated from the voltage magnitude.

Resistivity and dielectric constant measurements were made using a Hewlett-Packard Model 4270A Automatic Capacitance Bridge at a frequency of 1 kHz at room temperature.

RESULTS AND DISCUSSION

Originally, sodium lauryl sulfate (ionic surfactant) was used in the paint formulation. By examining the breakdown strengths of the polymer with and without this component, it was determined that a much higher field could be applied to the samples if the ionic surfactant was excluded from the paint formulation. (Table 1) All data reported in this paper refer to composites in which the ionic surfactant has been removed and replaced by an equivalent amount of polyethylene oxide. The resistivities of the unloaded samples are also presented in Table 1. Note that the resistivities are relatively low in comparison to PZT and comparable to $PbTiO_3$.(1) The importance of the conductivity of the polymer and ceramic in poling has been pointed out recently by Gururaga, et al.(6) Based on their model, one would expect the ceramic (especially PZT) to experience a relatively large fraction of the applied poling field.

The microstructure of the composites were examined by SEM to determine the dispersion of the ceramic particles in the polymer matrix. The dispersion of $PbTiO_3$ powder in the composites was excellent, indicating that the combination of surfactants and rheological agents utilized were appropriate for this system. (Fig. 1) The PZT filled composites, however, did not show a uniform dispersion of particles throughout the polymer matrix. The micrographs showed two distinct regions; a polymer rich zone and a PZT rich region. This is most likely due to the different particle sizes of the $PbTiO_3$ (4-5 microns) and PZT (submicron). An adjustment clearly needs to be made in the amount of surfactant used in the PZT filled composite.

As shown in Table 2, the dielectric constants for the PZT filled samples are similar to those observed previously (1-3) while the values for the $PbTiO_3$ composites are somewhat higher than those reported in the literature.(1) The resistivities of the PZT and $PbTiO_3$ composites are also listed in Table 2.

The values of $\bar{d}_{33}$ were found to be 20-25 for PZT-polymer composites and 20-35 for $PbTiO_3$ composites. These values are comparable to those reported previously for poled PZT and $PbTiO_3$-polymer composites. Polymers such as those used in this study are frequently suseptible to dissolution or swelling in organic fluids. Consequently, immersion in an oil bath may not be ideal for the poling of these composites. Perhaps by using another technique, such as the corona discharge method (in air), this problem can be alleviated. The hydrostatic voltage coefficient, $\bar{d}_h$, is also listed in Table 2 for each composite. These values are lower than expected on the basis of previous literature values.(1)

The losses for the composites are relatively high ($\tan\delta$ = 0.3-0.4), presumably because the dried paint base is well above its Tg (or α-relaxation). This is in the temperature region where so-called d.c. loss (due to conduction of ionic impurities in the polymer) becomes important. Presently, we are evaluating other candidate paint bases to alleviate this problem. Polymers with Tg's relatively near or above room temperature may be better suited for preparing 0-3 composites with low dielectric losses.

ACKNOWLEDGEMENT

The authors are grateful for financial support received from the Office of Naval Research.

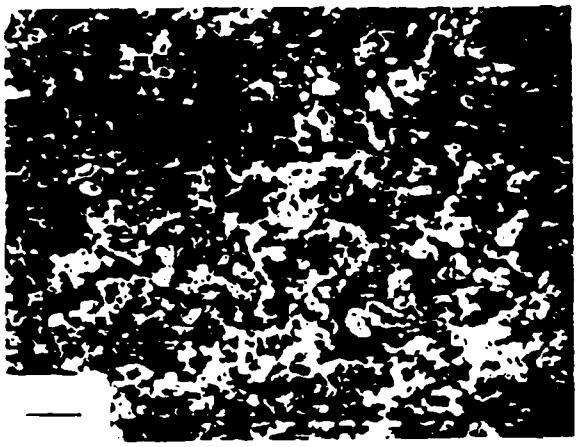

Figure 1. Scanning electron micrograph of 60 volume percent $PbTiO_3$ composite.

TABLE 1

BREAKDOWN STRENGTHS AND RESISTIVITIES OF PURE POLYMER BASE

	BREAKDOWN STRENGTH	RESISTIVITY (ohm cm)
"PURE" COPOLYMER	150 kV/cm	8.3×10^{8}
COPOLYMER + IONIC SURFACTANT	54 kV/cm	2.3×10^{7}
COPOLYMER W/O IONIC SURFACTANT	130 kV/cm	2.0×10^{7}

TABLE 2

DIELECTRIC CONSTANTS, RESISTIVITIES, AND PIEZOELECTRIC COEFFICIENTS FOR PZT AND $PbTiO_3$ COMPOSITES

	K	RESISTIVITY (ohm cm)	$\bar{d}_{33}$	$\bar{d}_h$
60 % PZT	105	4.1×10^{7}	20	7 pC/N
70% PZT	140	4.6×10^{7}	25	6 pC/N
60% $PbTiO_3$	138	9.4×10^{6}	35	5 pC/N
70% $PbTiO_3$	154	9.2×10^{6}	20	4 pC/N

REFERENCES

1) R.E. Newnham, A. Safari, G. Sa-gong and J. Giniewicz; Flexible Composite Piezoelectric Sensors, Ultrasonics symposium (1984).

2) J. Mendiola and B. Jimenez; Review of Recent Work on Ferroelectric Composite Systems. Ferroelectrics, Vol. 53. pp. 159-166(1984).

3) R.E. Newnham, A. Safari, J. Giniewicz, and B.H Fox; Composite Piezoelectric Sensors. Ferroelectrics, Vol. 60, pp. 15-21 (1984).

4) T.C. Patton: Paint Flow and Pigment Dispersion, Wiley (1979).

5) C. Bondy and M. M. Coleman; Film formation and film properties obtained with acrylic, styrene/acrylic and vinyl acetate/VeoVa copolymer emulsions. J. Col. Chem. Assoc., vol. 53, pp. 555-577(1970).

6) T.R. Gururaja, A. Safari, R.E. Newnham and L.E. Cross, Piezoelectric Ceramic-Polymer Composites for Transducer Applications, Review Article (1986).

Mat. Res. Bull., Vol. 21, pp. 1447-1454, 1986. Printed in the USA.
0025-5408/86 $3.00 + .00

3:0: A NEW COMPOSITE CONNECTIVITY

S.M. Pilgrim and R.E. Newnham
Materials Research Laboratory
The Pennsylvania State University, University Park, PA 16802

(Received August 26, 1986; Refereed)

ABSTRACT

A new approach to piezoceramic-polymer composites for piezoelectric applications has been investigated. The resultant composites are analogs of the conventional 0-3 composite structure. An approximately 3-0 connected composite can be prepared by hot pressing large polyethylene spheres and PZT powder. These 3-0 composites may be visualized as an inverse brick wall structure--the "mortar" (PZT) is the high dielectric constant material and the "bricks" (PE) are the low dielectric constant material. In addition, the three connected phase (PZT) is the less compliant. Given such properties and connectivity, two major benefits accrue. The electric field distribution within the composite will be more favorable for poling than in an 0-3 composite. Additionally, applied stress should be concentrated on the PZT phase, thus resulting in increased piezoelectric response.

The poling behavior of these 3-0 composites is improved when contrasted with that of their 0-3 analogs. The applicability of these 3-0 composites will be demonstrated through measurement of their d_{33} and d_h coefficients. The dielectric constant and dielectric loss as functions of frequency and temperature have also been measured.

MATERIALS INDEX:Composite, Piezoelectric, Lead Zirconate Titanate, Polyethylene

Introduction

The advantages of composite materials for improving device performance compared to single phase materials have been demonstrated for a number of disparate applications on several size scales. Mechanical (ABS-acrylonitrile butadiene styrene) materials are based on polymer blends which may be viewed as

composites on the nanometer scale. Piezoelectric transducers are composites on the micron to millimeter scale, whereas reinforced concretes are composites on the centimeter scale. In examining diphasic composites there are ten possible connectivity patterns, where connectivity is defined as the number of dimensions in which a phase is self-connected. In order to describe a composite connectivity, the individual connectivities of the phases are written in order (1). The concept of ordered mixing is also important to composite connectivity (2). Although only ten distinct diphasic connectivities are possible, the convention of placing the active phase first effectively adds eight possible inverted connectivities. Thus the 1-3 piezoelectric composites of Klicker (3,4) are the basis for the 3-1 inverse composites of Safari (5,6). The 0-3 composites (7) can be inverted to form an analogous series of 3-0 composites: 3-0, 3-0-0, 3(03)-0. These 3-0 composites may be viewed as inverse brick wall composites. The "bricks" are an inert, inactive polymer and the "mortar" is a piezoelectric ceramic material. In particular, the 0-3 composite can be inverted to form a 3-0 (Figure 1). The 3-0 connectivity has several possible advantages over 0-3 samples:

1)Improved flux distribution for poling
2)Improved stress distribution
3)Formation of residual stresses.

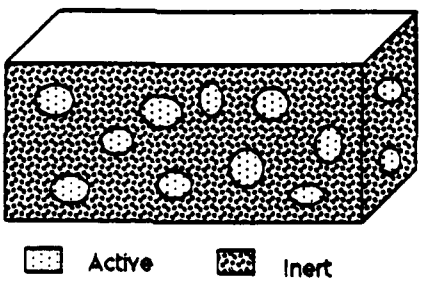

FIG. 1a
0-3 Composite

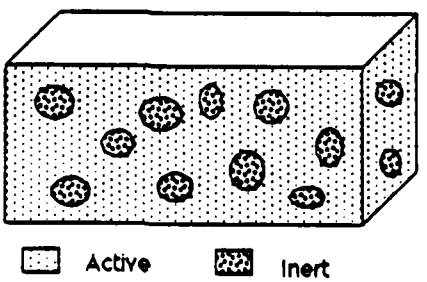

FIG. 1b
3-0 Composite

The electric flux distribution during poling is controlled by the dielectric constants of the component phases in the short time limit and by the component conductivities in the long time limit. The usual 0-3 (PZT-polymer) composites yield very poor electric flux distributions for poling. In these 0-3 composites the polymer matrix is the low dielectric constant phase, the low conductivity phase, and the three connected phase; consequently, the flux concentrates in the polymer at all times. This fact makes it difficult to achieve sufficient field in the PZT to pole it effectively. In the 3-0 case the inverse conditions exist. The PZT matrix is the high dielectric constant phase, the high conductivity phase, and the three connected phase. Although the Maxwell-Wagner conditions cause distortion of the flux near the polymer phase, flux continuity requires passage through the PZT (Figure 2) This makes it easier to achieve sufficient poling fields in the PZT in a 3-0 composite than in a 0-3.

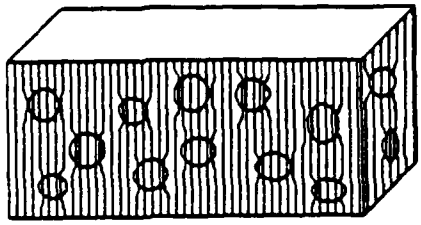

FIG. 2
Electric Field in a 3-0 Composite of PZT and PE

The stress distribution is enhanced analogously to that in a 1-3 or 3-1 configuration, i.e. the low compliance phase (PZT) bears a disproportionally large share of the stress, thus improving the piezoelectric response.

The higher coefficient of thermal expansion of the polymeric component tends to introduce residual stress and circumferential voiding which aid the stress concentrating effect and partially decouple d_{31} from d_h. This decoupling is not as substantial as that found in the 3-1 and 3-2 composites (6). In addition to decoupling d_3, and d_h, the porosity does have a deleterious effect on the pressure stability of the 3-0 samples. The impedance matching characteristics of the 0-3 composites are retained in the 3-0's.

Composites and Materials

The three connectivities: 3-0, 3-0-0, 3(03)-0, are formed from four materials. The piezoelectric phase in each composite was PZT 501A from Ultrasonic Powders. This is a soft PZT with a particle size of 3-6 μm. The inert polymer phase in each composite was Marlex 6001 polyethylene from Phillips Petroleum. This polyethylene has a high molecular weight and a Tm of 135°C. The bead size was approximately 6 mm. The 3-0-0 composites included an inactive conductive filler: Black Pearls 2000 from Vulcan. The 3(03)-0 composites possessed a three dimensionally connected phase which was itself a 0-3 composite of PZT and Eccogel 0 from Emerson and Cuming. Eccogel 0 is a highly flexible two component potting epoxy.

Fabrication

Dry, sieved (<200 mesh) PZT, sufficient to form a 1-2 mm layer was loaded into a 1.8 cm diameter steel die. After mechanical levelling and shaking to achieve a high tap density, ten to twenty polyethylene beads were loaded and symmetrically arranged on the PZT layer. Additional PZT to fill the interstices between the polyethylene was added and shaken mechanically. An upper layer (1-2 mm) of PZT was then added and shaken to achieve a high density.

This three layer sandwich was then uniaxially hot pressed at 190°C and 200 MPa for times ranging from 15 to 60 minutes. Periodic reductions in pressure were used to aid the removal of entrapped air. Thermal gradients were minimized by physically flipping the die at fifteen minute intervals. After pressing, the composites were slow cooled within the die. Cooling prior to removal from the die was necessary to prevent warping and cupping in the thinner composite samples. Subsequent to removal from the die, the composites were polished to 600 grit emery paper to yield flat parallel surfaces. This polishing also served to remove the majority of the polymer skin on the external surfaces. If the polymer skin is not removed it acts as a low dielectric constant capacitor in series with composite, which prevents poling of the composite. Electroding for poling was done with air dry silver paint.

Sample processing for 3-0-0 composites was carried out in the same manner as with the 3-0 composites except for the addition of 0.4 to 1.5 vol% carbon. This carbon was added in two different ways. In the 3-0-0A samples the carbon was added to the PZT and Spex milled for 10 minutes; whereas, in the 3-0-0B samples the carbon was added to the polyethylene beads and Spex milled for 10 minutes. The resulting 3-0-0A composites thus possessed a carbon PZT matrix phase-- a more conductive matrix phase than the 3-0's. The 3-0-0B samples incorporated polyethylene beads whose surfaces were carbon coated into the PZT matrix. These samples are large scale versions of the composites of Tokuoka (8).

Dry, sieved (<200 mesh) PZT, was mixed with 35 vol% Eccogel 0 by Brabender mixing. This mixing process does not incorporate porosity. The resulting 0-3 composite paste was added to ten to twenty polyethylene beads and hand mixed without incorporating air bubbles. The raw composites were pressed at 25°C and 200 MPa for 30 minutes and cured without pressure for 8 hours at 70°C.

Poling and Piezoelectric Coefficients

All composites were poled in silicone oil at DC fields of 10--100 kV/cm at 100°C for 10 to 30 minutes. Stepping the field upward by 5 kV/cm steps was required to avoid failure of the composites. Resulting d_{33} values as measured on a Berlincourt d_{33} meter are given in Table 1. Quasistatic d_h values were measured, but were less than 5 pC/N. These poor hydrostatic coefficients are a result of the residual porosity.

TABLE
Piezoelectric Data for Various 0-3 Type Composites

SAMPLE	Vol% PZT	d_{33} pC/N
3-0 #10	56	18
3-0 #12	59	8
3-0 #16	47	23
3-0-0A #1	25	5
3-0-0B#25	38	24

Electrical Data

Dissipation factors and dielectric constants were measured on a 4274A Hewlett Packard multifrequency LCR meter as a function of temperature (-25 to 125 C) at four frequencies (100Hz, 1kHz, 10kHz, 100kHz). Plots of these data for 3-0 composite #16 are shown in Figure 3. Solid lines are heating runs and dotted lines are the subsequent cooling run. Electrical data for 3-0-0A composite #1 is shown in Figure 4. Figures 5 and 6 show the electrical data for 3-0-0B composite #25 and for 3(03)-0 composite #17 respectively.

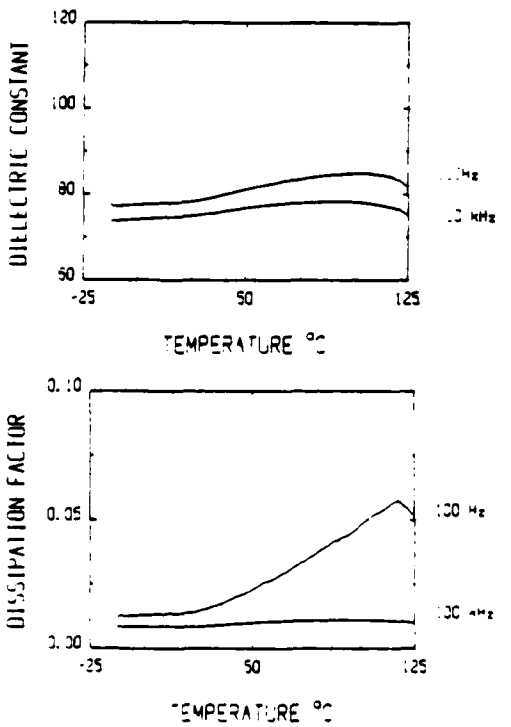

FIG. 3
Electrical Data for 3-0 Composite #16 at 100Hz and 100kHz

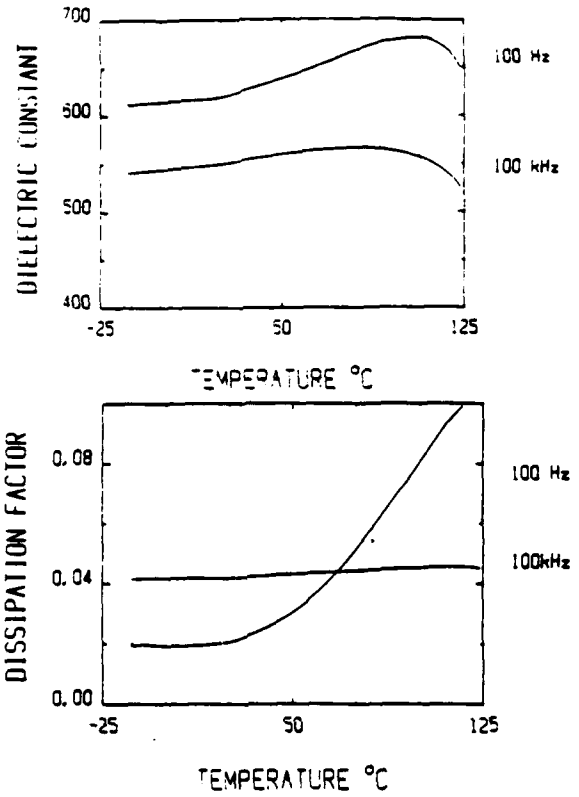

FIG. 4
Electrical Data for 3-0-0A Composite #1 at 100Hz and 100kHz

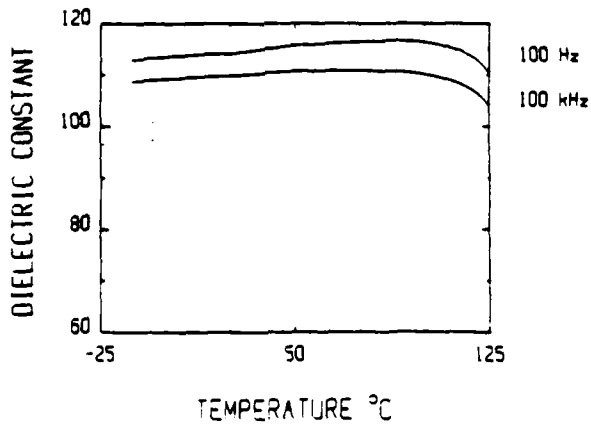

FIG. 5A
Electrical Data for 3-0-0B Composite #25 at 100Hz and 100kHz

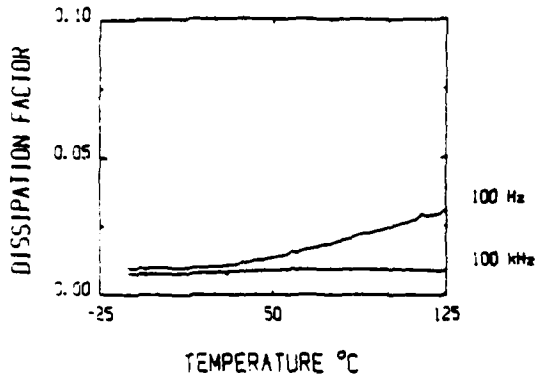

FIG. 5B
Electrical Data for 3-0-0B Composite #25 at 100Hz and 100kHz

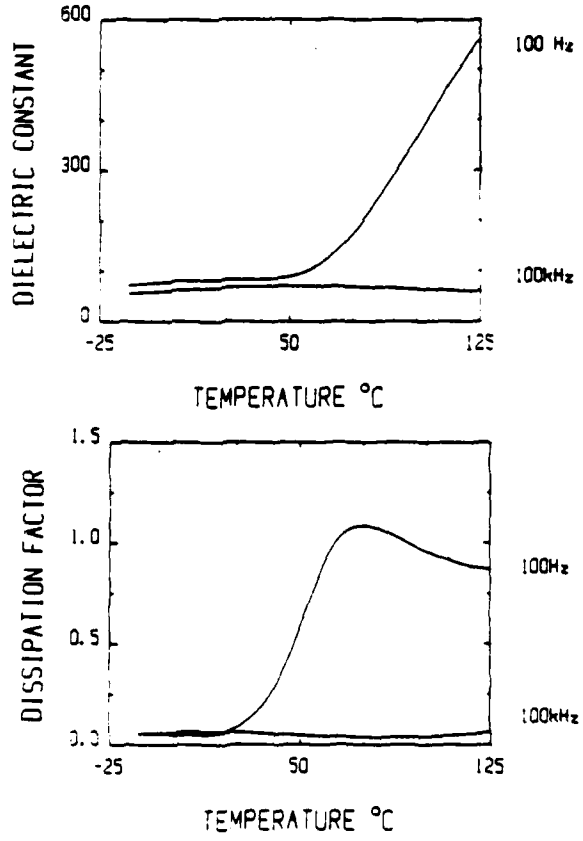

FIG. 6
Electrical Data for 3(03)-0 Composite #17 at 100Hz and 100kHz

The electrical and piezoelectric properties of the 3-0, 3-0-0, and 3(03)-0 composites are not yet consistently reproducible. Processing variations are large and processing variables are difficult to adequately control. A comparison of the d_{33} values for 3-0 composites #12, #10, and #16 (Table 1) clearly illustrates this variability. Samples with low d_{33} show large losses. Good samples (d_{33}>15pC/N) show acceptable losses in the 3-0 and 3-0-0 cases. The huge losses in the 3(03)-0 case (Figure 6) are attributed to the Eccogel 0. Residual open and closed porosity weakens the composites compared to 0-3 samples, although the 3-0 composites are not particularly fragile.

Summary

PZT-PE composites of 3-0 connectivity have been made and show promise for competition with 0-3 composites. Large d_{33} coefficients (>20pC/N) are achievable for <50 vol% PZT. This results from better electric field distribution during poling and from stress concentration on the PZT active phase. Residual open porosity precludes attainment of good hydrostatic piezoelectric coefficients. However,it should be possible to reduce the porosity below the 4-10 vol% in the present composites.

Acknowledgements

Funding provided by the Office of Naval Research.

References

1. R.E. Newnham, D.P. Skinner, and L.E. Cross, Mater. Res. Bull., 13, 525 (1978).

2. J.A. Hersey, Powder Tech., 11, 41 (1975).

3. K.A. Klicker, J.V. Biggers, and R.E. Newnham, J. Am. Ceram. Soc., 64, 5 (1981).

4. K.A. Klicker, Ph.D. Thesis, The Pennsylvania State University, 1980.

5. A. Safari, A. Halliyal, and R.E. Newnham, Mater. Res. Bull., 17, 301 (1982).

6. A. Safari, Ph. D. Thesis, The Pennsylvania State University, 1982.

7. R.E. Newnham, A. Safari, G. Sa-gong, J. Giniewicz, Proc. 1984 IEEE Ultrasonics Symposium, 501 (1985).

8. K. Tokuoka, M. Senna, and H. Kuno, J. Mater. Sci., 21, 493 (1986).

3-0: A NEW COMPOSITE CONNECTIVITY

S.M. Pilgrim and R.E. Newnham

Materials Research Laboratory
The Pennsylvania State University, University Park, PA 16802

Abstract

A new approach to piezoceramic-polymer composites for piezoelectric applications has been investigated. The resultant composites are analogs of the conventional 0-3 composite structure. An approximately 3-0 connected composite can be prepared by hot pressing large polyethylene spheres and PZT powder. These 3-0 composites may be visualized as an inverse brick wall structure--the "mortar" (PZT) is the high dielectric constant material and the "bricks" (PE) are the low dielectric constant material. In addition, the three connected phase (PZT) is the less compliant. Given such properties and connectivity, two major benefits accrue. The electric field distribution within the composite will be more favorable for poling than in an 0-3 composite. Additionally, applied stress should be concentrated on the PZT phase, thus resulting in increased piezoelectric response.

The poling behavior of these 3-0 composites is improved when contrasted with that of their 0-3 analogs. The applicability of these 3-0 composites will be demonstrated through measurement of their d_{33} and d_h coefficients. The dielectric constant and dielectric loss as functions of frequency and temperature have also been measured.

1. Introduction

The advantages of composite materials for improving device performance compared to single phase materials have been demonstrated for a number of disparate applications on several size scales. Mechanical (ABS-acrylonitrile butadiene styrene) materials are based on polymer blends which may be viewed as composites on the nanometer scale. Piezoelectric transducers are composites on the micron to millimeter scale, whereas reinforced concretes are composites on the centimeter scale. In examining diphasic composites there are ten possible connectivity patterns, where connectivity is defined as the number of dimensions in which a phase is self-connected. In order to describe a composite connectivity, the individual connectivities of the phases are written in order [1]. The concept of ordered mixing is also important to composite connectivity [2]. Although only ten distinct diphasic connectivities are possible, the convention of placing the active phase first effectively adds eight possible inverted connectivities. Thus the 1-3 piezoelectric composites of Klicker [3,4] are the basis for the 3-1 inverse composites of Safari [5,6]. The 0-3 composites [7] can be inverted to form an analogous series of 3-0 composites: 3-0, 3-0-0, 3(03)-0. These 3-0 composites may be viewed as inverse brick wall composites. The "bricks" are an inert, inactive polymer and the "mortar" is a piezoelectric ceramic material. In particular, the 0-3 composite can be inverted to form a 3-0 (Figure 1) The 3-0 connectivity has several possible advantages over 0-3 samples:

1)Improved flux distribution for poling
2)Improved stress distribution
3)Formation of residual stresses.

The electric flux distribution during poling is controlled by the dielectric constants of the component phases in the short time limit and by the component conductivities in the long time limit. The usual 0-3 (PZT-polymer) composites yield very poor electric flux distributions for poling. In these 0-3 composites the polymer matrix is the low dielectric constant phase, the low conductivity phase, and the three connected phase; consequently, the flux concentrates in the polymer at all times. This fact makes it difficult to achieve sufficient field in the PZT to pole it effectively. In the 3-0 case the inverse conditions exist. The PZT matrix is the high dielectric constant phase, the high conductivity phase, and the three connected phase. Although the Maxwell-Wagner conditions cause distortion of the flux near the polymer phase, flux continuity requires passage through the PZT (Figure 2) This makes it easier to achieve sufficient poling fields in the PZT in a 3-0 composite than in a 0-3.

The stress distribution is enhanced analogously to that in a 1-3 or 3-1 configuration, i.e. the low compliance phase (PZT) bears a disproportionally large share of the stress, thus improving the piezoelectric response.

The higher coefficient of thermal expansion of the polymeric component tends to introduce residual stress and circumferential voiding which aid the stress concentrating effect and partially decouple d_{31} from d_h. This decoupling is not as substantial as that found in the 3-1 and 3-2 composites [6]. In addition to decoupling d_{31} and d_h, the porosity does have a deleterious effect on the pressure stability of the 3-0 samples. The impedance matching characteristics of the 0-3 composites are retained in the 3-0's.

2. Composites and Materials

The three connectivities: 3-0, 3-0-0, 3(03)-0, are formed from four materials. The piezoelectric phase in each composite was PZT 501A from Ultrasonic Powders. This is a soft PZT with a particle size of 3-6 μm. The inert polymer phase in each composite was Marlex 6001 polyethylene from Phillips Petroleum. This polyethylene has a high molecular weight and a Tm of 135°C. The bead size was approximately 6 mm. The 3-0-0 composites included an inactive conductive filler: Black Pearls 2000 from Vulcan. The 3(03)-0 composites possessed a three dimensionally connected phase which was itself a 0-3 composite of PZT and Eccogel 0 from Emerson and Cuming. Eccogel 0 is a highly flexible two component potting epoxy.

CH2358-0/86/0000-0314 $1.00

3. Fabrication

Dry, sieved (<200 mesh) PZT, sufficient to form a 1-2 mm layer was loaded into a 1.8 cm diameter steel die. After mechanical levelling and shaking to achieve a high tap density, ten to twenty polyethylene beads were loaded and symmetrically arranged on the PZT layer. Additional PZT to fill the interstices between the polyethylene was added and shaken mechanically. An upper layer (1-2 mm) of PZT was then added and shaken to achieve a high density.

This three layer sandwich was then uniaxially hot pressed at 190°C and 200 MPa for times ranging from 15 to 60 minutes. Periodic reductions in pressure were used to aid the removal of entrapped air. Thermal gradients were minimized by physically flipping the die at fifteen minute intervals. After pressing, the composites were slow cooled within the die. Cooling prior to removal from the die was necessary to prevent warping and cupping in the thinner composite samples. Subsequent to removal from the die, the composites were polished to 600 grit emery paper to yield flat parallel surfaces. This polishing also served to remove the majority of the polymer skin on the external surfaces. If the polymer skin is not removed it acts as a low dielectric constant capacitor in series with composite, which prevents poling of the composite. Electroding for poling was done with air dry silver paint.

Sample processing for 3-0-0 composites was carried out in the same manner as with the 3-0 composites except for the addition of 0.4 to 1.5 vol% carbon. This carbon was added in two different ways. In the 3-0-0A samples the carbon was added to the PZT and Spex milled for 10 minutes; whereas, in the 3-0-0B samples the carbon was added to the polyethylene beads and Spex milled for 10 minutes. The resulting 3-0-0A composites thus possessed a carbon PZT matrix phase-- a more conductive matrix phase than the 3-0's. The 3-0-0B samples incorporated polyethylene beads whose surfaces were carbon coated into the PZT matrix. These samples are large scale versions of the composites of Tokuoka [8].

Dry, sieved (<200 mesh) PZT, was mixed with 35 vol% Eccogel 0 by Brabender mixing. This mixing process does not incorporate porosity. The resulting 0-3 composite paste was added to ten to twenty polyethylene beads and hand mixed without incorporating air bubbles. The raw composites were pressed at 25°C and 200 MPa for 30 minutes and cured without pressure for 8 hours at 70°C.

4. Poling and Piezoelectric Coefficients

All composites were poled in silicone oil at DC fields of 10--100 kV/cm at 100°C for 10 to 30 minutes. Stepping the field upward by 5 kV/cm steps was required to avoid failure of the composites. Resulting d_{33} values as measured on a Berlincourt d_{33} meter are given in Table 1. Quasistatic d_h values were measured, but were less than 5 pC/N. These poor hydrostatic coefficients are a result of the residual porosity.

5. Electrical Data

Dissipation factors and dielectric constants were measured on a 4274A Hewlett Packard multifrequency LCR meter as a function of temperature (-25 to 125 C) at four frequencies (100Hz, 1kHz, 10kHz, 100kHz). Plots of these data for 3-0 composite #16 are shown in Figure 3. Solid lines are heating runs and dotted lines are the subsequent cooling run. Electrical data for 3-0-0A composite #1 is shown in Figure 4. Figures 5 and 6 show the electrical data for 3-0-0B composite #25 and for 3(03)-0 composite #17 respectively.

The electrical and piezoelectric properties of the 3-0, 3-0-0, and 3(03)-0 composites are not yet consistently reproducible. Processing variations are large and processing variables are difficult to adequately control. A comparison of the d_{33} values for 3-0 composites #12, #10, and #16 (Table 1) clearly illustrates this variability. Samples with low d_{33} show large losses. Good samples (d_{33}>15pC/N) show acceptable losses in the 3-0 and 3-0-0 cases. The huge losses in the 3(03)-0 case (Figure 6) are attributed to the Eccogel 0. Residual open and closed porosity weakens the composites compared to 0-3 samples, although the 3-0 composites are not particularly fragile.

5. Summary

PZT-PE composites of 3-0 connectivity have been made and show promise for competition with 0-3 composites. Large d_{33} coefficients (>20pC/N) are achievable for <50 vol% PZT. This results from better electric field distribution during poling and from stress concentration on the PZT active phase. Residual open porosity precludes attainment of good hydrostatic piezoelectric coefficients. However,it should be possible to reduce the porosity below the 4-10 vol% in the present composites.

References

[1] R.E. Newnham, D.P. Skinner, and L.E. Cross, "Connectivity and Piezoelectric-Pyroelectric Composites," Mater. Res. Bull., vol. 13, pp. 525-536, 1978.

[2] J.A. Hersey, "Ordered Mixing: A New Concept in Powder Mixing Practice, "Powder Tech., vol. 11, pp. 41-44, 1975.

[3] K.A. Klicker, J.V. Biggers, and R.E. Newnham, "Composites of PZT and Epoxy for Hydrostatic Transducer Applications," J. Am. Ceram. Soc., vol. 64, pp. 5-9, 1981.

[4] K.A. Klicker, "Piezoelectric Composites with 3-1 Connectivity for Transducer Applications"; Ph.D. Thesis, The Pennsylvania State University, 1980.

[5] A. Safari, A. Halliyal, and R.E. Newnham, "Transverse Honeycomb Composites Transducers," Mater. Res. Bull., vol. 17, pp. 301-308, 1982.

[6] A. Safari, "Perforated PZT-Polymer Composites with 3-1 and 3-2 Connectivity for Hydrophone Applications"; Ph. D. Thesis, The Pennsylvania State University, 1982.

[7] R.E. Newnham, A. Safari, G. Sa-gong, J. Giniewicz, "Flexible Composite Piezoelectric Sensors," in Proc. 1984 IEEE Ultrasonics Symposium, 1985, pp. 501-506.

[8] K. Tokuoka, M. Senna, and H. Kuno, "Preparation of Inorganic/Polymeric Composite Microspheres by Direct Suspension Polymerization," J. Mater. Sci., vol. 21, pp. 493-496, 1986.

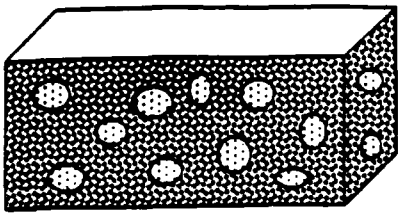

Figure 1a. 0-3 Composite

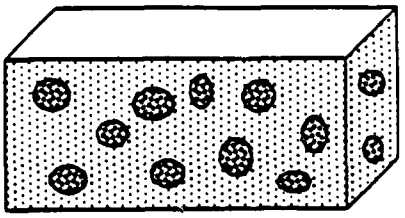

Figure 1b. 3-0 Composite

Figure 1. 0-3 and 3-0 Composites

Active Inert

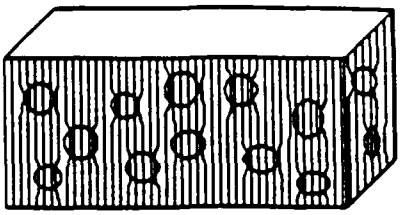

Figure 2. Electric field in a 3-0 composite of PZT and PE.

Table 1. Piezoelectric data for various 0-3 type composites.

SAMPLE		vol% PZT	d_{33} pC/N
3-0	#10	56	18
3-0	#12	59	8
3-0	#16	47	23
3-0-0A	#1	25	5
3-0-0B	#25	40	5
3(03)-0	#17	38	24

Figure 3. Electrical data for 3-0 composite #16.
3a. Dielectric constant vs. temperature at 100 Hz and 100kHz.

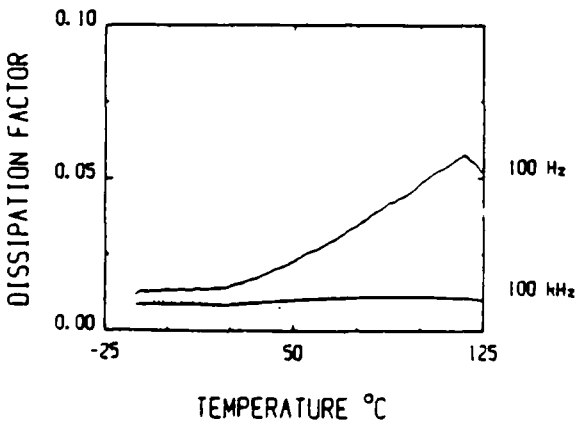

3b. Dissipation factor vs. temperature at 100 Hz and 100kHz.

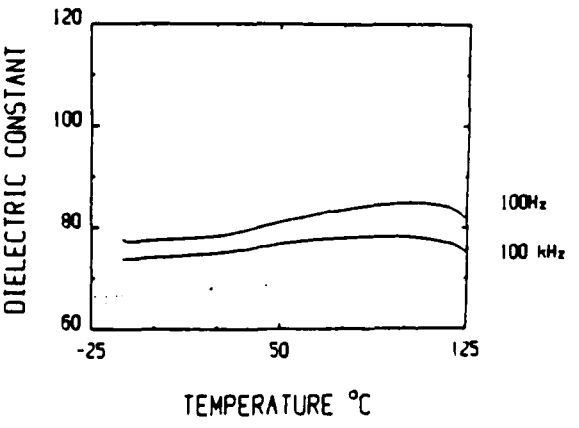

Figure 4. Electrical data for 3-0-0A composite #1.
4a. Dielectric constant vs. temperature at 100 Hz and 100kHz.

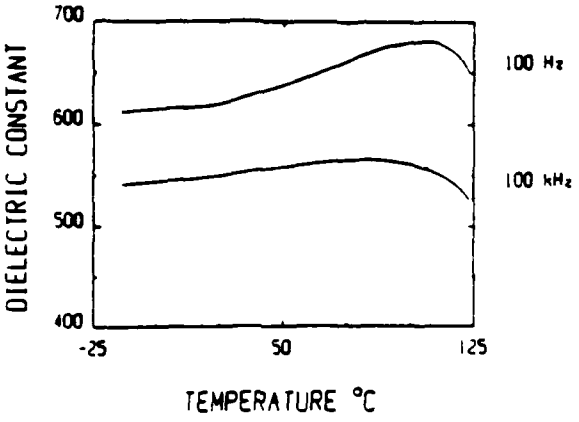

4b. Dissipation factor vs. temperature at 100 Hz and 100kHz.

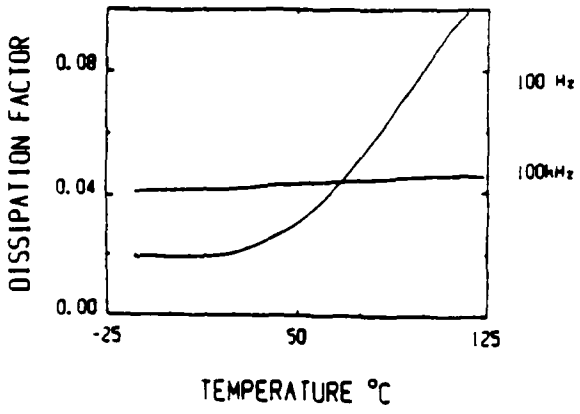

Figure 5. Electrical data for 3-0-0B composite #25.
5a. Dielectric constant vs. temperature at 100 Hz and 100kHz.

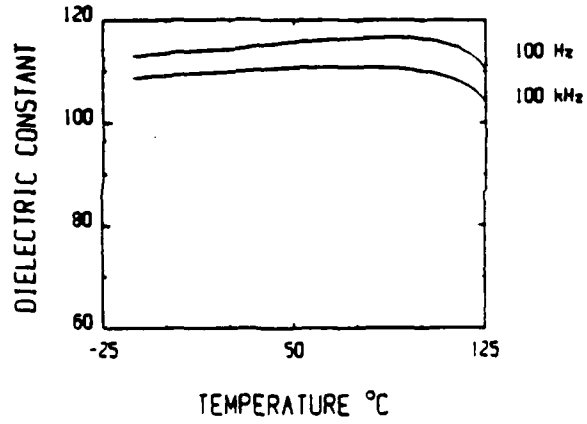

5b. Dissipation factor vs. temperature at 100 Hz and 100kHz.

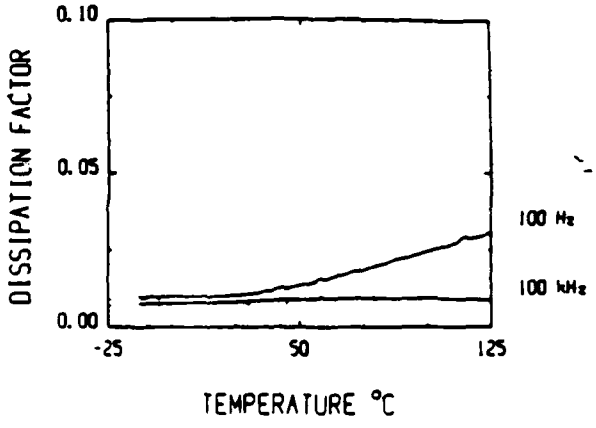

Figure 6. Electrical data for 3(03)-0 composite #17.
6a. Dielectric constant vs. temperature at 100 Hz and 100kHz.

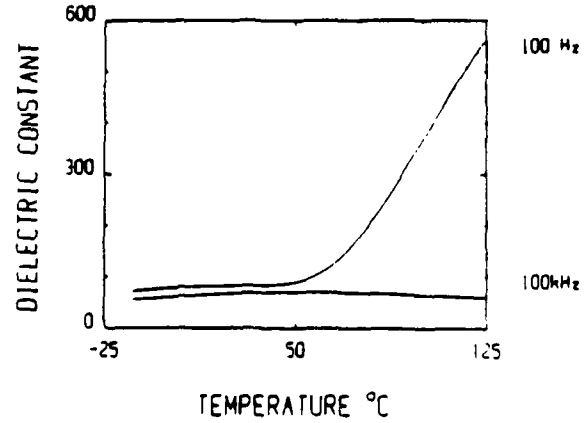

6b. Dissipation factor vs. temperature at 100 Hz and 100kHz.

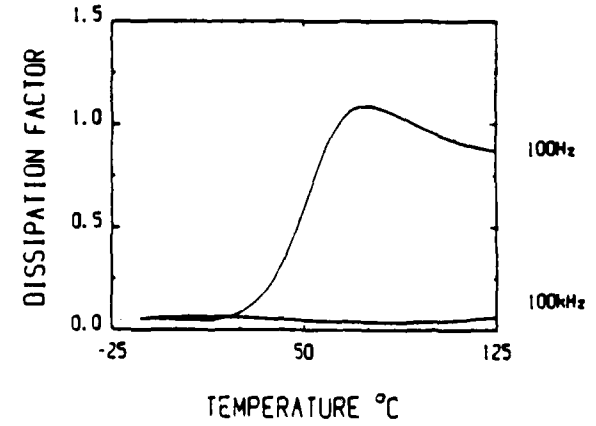

Funding provided by the Office of Naval Research.

0-3 PIEZOELECTRIC CERAMIC-POLYMER COMPOSITES PREPARED BY A NEW METHOD: FIRED COMPOSITES

A. Safari, T.R. Gururaja, C. Hakun, A. Halliyal and R.E. Newnham

Materials Research Laboratory
The Pennsylvania State University
University Park, PA 16802

Abstract

In composites with 0-3 connectivity, a loading of more than 60 volume percent piezoelectric filler is required to achieve useful piezoelectric properties. A limitation of the presently used fabrication procedure is the difficulty in preparing composites with such high loading. A new method of preparing 0-3 composites is presented in this paper in which more than 70 Vol% filler particles can be incorporated easily. Conventional and corona discharge poling techniques were used to electrically polarize the composites. Dielectric and piezoelectric properties of these composites are presented in this paper.

1. Introduction

Lead zirconate titanate (PZT) ceramics are used extensively as a piezoelectric material despite their several disadvantages. PZT has a large piezoelectric d_{33} coefficient but its hydrostatic piezoelectric coefficient $d_h(=d_{33}+2d_{31})$ is low because d_{31} has negetive sign and the magnitude of $d_{31}\simeq 1/2\ d_{33}$. Moreover, its high permittivity ($\varepsilon=2000\ \varepsilon_o$) lowers the voltage coefficients $g_{33}(=d_{33}/\varepsilon)$ and $g_h(=d_h/\varepsilon)$ and hence makes it a poor acoustic pressure sensors. In addition, the high density of PZT (7900 Kg/m^3) makes it difficult to obtain good impedance matching with water. PZT is also brittle ceramic and for underwater hydrophone applications a more compliant material with better shock resistance is desirable.

One approach to overcome these problems is to replace single phase ceramics with composites made from piezoelectric ceramics and flexible polymers. The polymer phase lowers the density and permittivity and increases the elastic compliance. Over the past few years several investigators have examined piezoelectric ceramic-polymer composites with different connectivity patterns. A review of the earlier work on ceramic-polymer composites for piezoelectric devices can be found elsewhere [1,2].

Among a variety of composites with different connectivities studied so far, the simplest type are with 0-3 connectivity. A composite with 0-3 connectivity consists of a three-dimensionally connected polymer matrix loaded with piezoelectrically active ceramic particles. This type of composite does not have the desirable stress concentration factor found in other connectivity patterns, so the hydrostatic figure of merit is not large. However, certain distinctly advantageous features of these composites make them an extremely interesting system.

Perhaps one of the most attractive features of the 0-3 design is its versatility in assuming a variety of forms including thin sheets, extruded bars and fibers, and certain molded shapes. This type of composite is also easy to fabricate and amenable to mass production. By using the right kind of polymer, the composite can be made flexible to conform to curved surfaces.

Early attempts to fabricate flexible composites of PZT ceramic particles and polymer were made by Harrison [3]. The d_{33} coefficient of these composites were comparable with PVDF. An improved version of the 0-3 composite was synthesized by Banno, et al. [4]. Rather than using PZT as the ceramic filler, pure or modified lead titanate was employed because of its greater piezoelectric anisotropy. The lead titanate filler was produced by water-quenching the ceramic, thereby exploiting the high strain present in the material in order to produce fine powders. The average particle size was about 5μm. To fabricate composite bodies, the piezoelectric powders and chloroprene rubber were mixed and rolled into 0.5mm thick sheets at 40°C using a hot roller, and then heated at 120°C for 20 minutes under a pressure of 13 kg/cm^2. The composites were poled at 60°C in silicone oil in a field of 100 kV/cm field for 1 hour. It was shown in this study that loading in excess of 60 volume percent filler is required to achieve useful piezoelectric properties. A limitation of the presently used

CH2358-0/86/0000-0305 $1.00

fabrication procedures such as hot rolling and warm die pressing a mixture of ceramic particles and polymer is the difficulty in obtaining higher loadings of the filler in the composite.

In this paper, a new method of preparing 0-3 composites with loadings in excess of 70% filler is described. This procedure has proved to be advantageous for improved poling and consequently, a better piezoelectric response. The composites were poled by both conventional and corona discharge technique. The advantages of Corna discharge technique for poling 0-3 composites will be discussed.

2. Composite Preparation and Poling

Piezoelectric filler materials used in this study were PZT-501A powder obtained from Ultrasonic Powder Inc. and $PbTiO_3$ (PT) powder prepared by co-precipitation technique [5]. To prepare composites, 100gm of the filler material was mixed with 7gm of 15 wt% PVA solution in water, and pressed into pellets (thickness = 0.2 to 0.3cm, diameter = 2.5cm) at 1.4×10^8 N/m^2 pressure. The pellets were placed on an alumina plate and heat treated at different temperatures from 150° to 800°C to either partially or fully burn out the PVA binders. After cooling, the pellets were placed in a plastic container and impregnated with Spurrs epoxy or Eccogel polymer under vacuum. The composites were then cured for 12 hours at 60°C. After curing, the composites were lapped on both sides to ensure uniform thickness. From the density measurements, the loading of the filler material was estimated to be 70 percent by volume. The composites prepared by this new method will be referred to as 'Fired Composites' to distinguish from composites prepared by other methods.

The fired composites were electroded with air-dried silver paste and poled by both conventional and Corona discharge technique. In the conventional method, poling was carried out in a stirred oil bath at 80°C by applying a field of 50 Kv/cm for 10 min.

The experimental arrangement for Corona poling is illustrated in Figure 1. A large DC potential was applied to a set of needles (thirty-two in our apparatus) which act as field intensifiers, causing an ionization of surrounding gas molecules. One surface of the sample to be poled was electroded and placed on a grounded metal plate. The charge from the needles was sprayed on the unelectroded surface creating an electric field. A grid with a positive bias was positioned in between the sample and the discharge needles to control the intensity of the charge. Only highly-charged ions penetrate the grid and drift to the surface of the unelectroded sample.

Composite samples were poled with a voltage of 40KV applied to the needles, and 10KV applied to the grid. The samples were held at 120°C during the poling process. Initial effort to pole the composite after the polymer impregnation resulted only in a partial polarization. It was found that poling performed on the fired ceramic compacts prior to polymer impregnation yielded superior piezoelectric response and hence, this sequence for poling was used in our study.

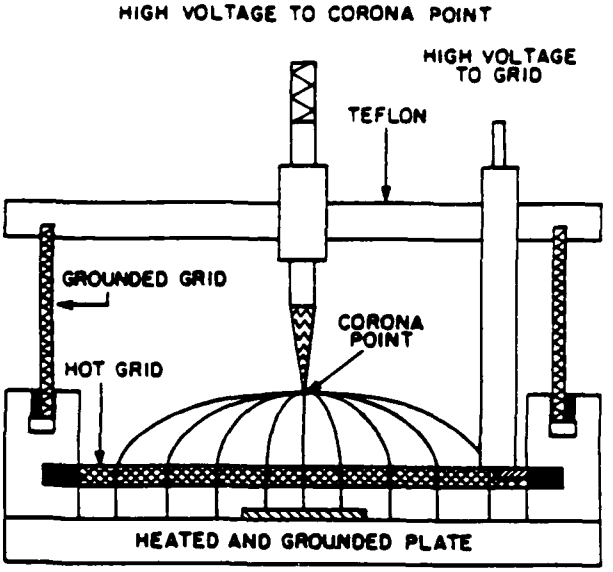

Figure 1. Schematic diagram of Corona poling apparatus.

3. Measurements

The capacitance and dissipation factor were measured at 1KHz using HP-4270A LCR meter. The $\bar{d}_{33}$ coefficient was measured at 100Hz using a Berlincourt d_{33}-meter. The $\bar{d}_h$ coefficient was determined using the dynamic AC technique [6]. Using the measured value of $\bar{d}_h$, $\bar{g}_h$ was calculated from the relation $\bar{g}_h = \bar{d}_h/\varepsilon$.

4. Results and Discussion

In this section, at first, the dependence of dielectric and piezoelectric properties of PZT-polymer composites on firing temperature is discussed. A comparison is made of the properties of the composites poled by conventional and corona discharge techniques. Finally, the properties of composites prepared using co-precipitated $PbTiO_3$ filler material are presented.

The $\bar{d}_{33}$ and dielectric constant of the PZT-Eccogel (1365-25) polymer composite as a function of the firing temperature of PZT pellets are shown in Figures 2 and 3. As will be described later, of the several polymers tested, composites with Eccogel 1365-25 polymer showed the highest $\bar{d}_{33}$ values. For samples poled by both conventional and corona discharge method, $\bar{d}_{33}$ increases gradually with increase in firing temperature up to 600°C, and sharply above 600°C. The sharp increase in $\bar{d}_{33}$ might be due to improved particle

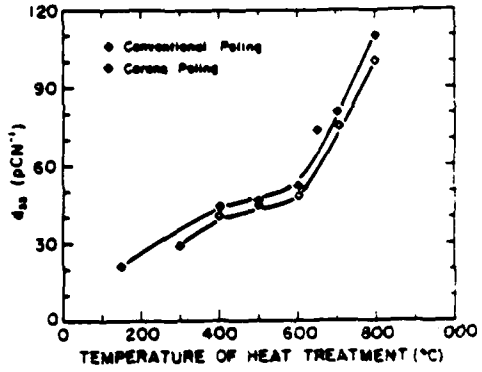

Figure 2. $\bar{d}_{33}$ vs. firing temperature: comparison of Corona discharge and conventional poling methods.

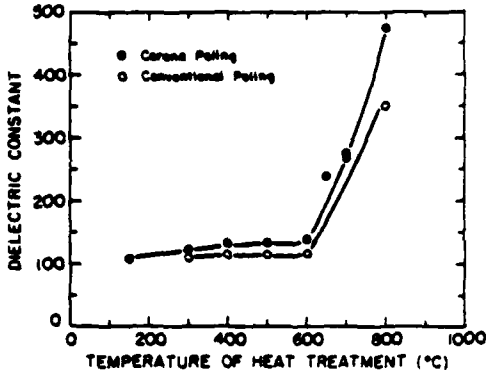

Figure 3. Dielectric constant vs. firing temperature of fired composites; comparison of corona discharge and conventional poling methods.

contact on firing the pellets to a higher temperature. The dielectric constant of the composites remains unchanged up to 600°C and increases sharply above 600°C. At a given temperautre, both $\bar{d}_{33}$ and dielectric constant of the composites poled by Corona discharge are 10-15% higher than those composites poled by conventional method.

Three types of polymers namely Eccogel 25, Eccogel 80 and Spurrs epoxy were used to find an appropriate polymer for the fired compdsite. $\bar{d}_{33}$ values as a function of firing temperature for PZT powder compacts (porous PZT), are compared with composites made from three different polymers in Figure 4. All the samples were poled by corona discharge. It can be seen that, at a given temperature, $\bar{d}_{33}$ of porous PZT decreases when it is impregnated with a polymer. Of the three

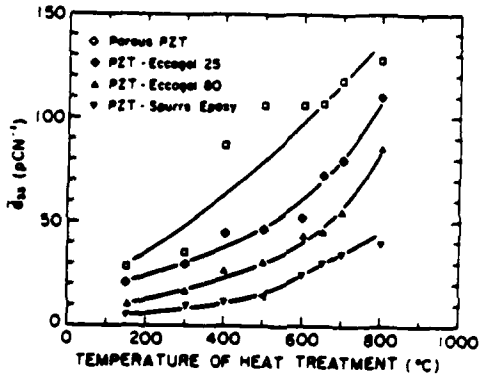

Figure 4. Effect of firing temperature on $\bar{d}_{33}$ of porous PZT compacts and fired composites with different polymers.

polymers chosen in this study, composites with more compliant polymer (Eccogel-25) resulted in a maximum $\bar{d}_{33}$ value.

Figure 5 shows the variation of $\bar{g}_{33}$ with firing temperature of the fired composites. $\bar{g}_{33}$ increases with increase in firing temperature and shows a maximum at about 600°C corresponding to the temperature at which there was a sharp increase in dielectric constant and $\bar{d}_{33}$. Table 1 compares the dielectric and piezoelectric properties of the fired PZT polymer composites with those of the composite prepared by mixing PZT and polymer and warm die pressing. It is clear from the table that $\bar{d}_{33}$ and $\bar{d}_h$ values of the fired composite are higher than those prepared by the regular method. Especially noteworthy are the $\bar{d}_h\bar{g}_h$ figure of merit of the fired composite which is five times larger than the corresponding values for the composite prepared by regular method. It should be noted at this point that PZT is not an ideal riller material for 0-3 composites

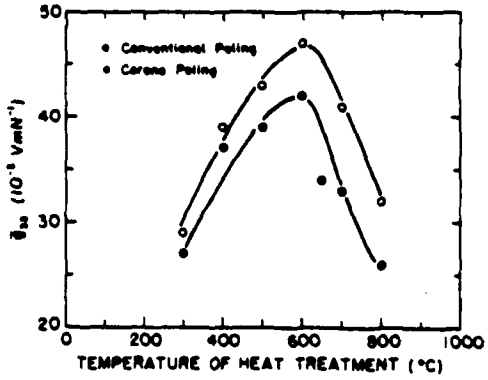

Figure 5. Effect of firing temperature on $\bar{g}_{33}$ of fired composites: comparison of Corona discharge and conventional poling methods.

for hydrostatic applications [2]. PZT was selected for the present study to demonstrate the advantages of the new method to prepare 0-3 composites.

Initial work on preparing fired composites using more suitable filler material such as $PbTiO_3$ powder is very encouraging. $PbTiO_3$ powder prepared by co-precipitation method and calcined at 900°C were used. The composites were prepared by the procedure described in Section 2, and poled at 50Kv/cm for 10 min. As indicated in Table 1, $\bar{g}_h$ and $\bar{d}_h\bar{g}_h$ values of $PbTiO_3$-polymer composite are 70 x 10^{-3} VmN^{-1} and 1750 x 10^{-15} m^2N^{-1}, respectively. These values are much larger than those reported on $PbTiO_3$-polymer composites [7]. The intensity of 002 and 200 x-ray diffraction peaks from the surface of the fired $PbTiO_3$-polymer composite were recorded both before and after poling as shown in Figure 6. A complete reversal of the intensities of the two peaks indicated almost saturation poling in these composites.

5. Summary

0-3 composites using PZT and PT as filler material have been prepared by a new method. We refer to these composites as 'Fired Composites'. This method is simple and can be easily adapted for mass production. Composites with loadings in excess of 70 Vol% piezoelectric ceramic filler could be prepared. The $\bar{d}_h\bar{g}_h$ figure of merit of fired PZT-polymer composites were five times larger than that of composites prepared by the regular method. In fired composites with $PbTiO_3$ filler material, almost saturation poling was achieved and $\bar{d}_h\bar{g}_h$ of these composites were 1750 x 10^{-15} m^2N^{-1}.

6. Acknowledgement

The authors are grateful for financial support from the Office of Naval Research.

TABLE 1: Dielectric and Piezoelectric Properties of Fired Composites

composite	K	tanδ	$\bar{d}_{33}$	$\bar{d}_h$	$\bar{g}_h$	$\bar{d}_h\bar{g}_h$	Vol% Filler
PZT-Polymer*	100	0.03	45	10	10	100	70
PZT-Polymer**	270	0.06	90	35	15	525	70
$PbTiO_3$-Polymer**	40	0.05	70	25	70	1750	70

*Prepared by mixing and warm die pressing method
**Prepared by fired method
Units: $\bar{d}_{33}$, $\bar{d}_h$: pCN^{-1}; $\bar{g}_h$:10^{-3} VmN^{-1},
$\bar{d}_h\bar{g}_h$:$10^{-15}m^2N^{-1}$

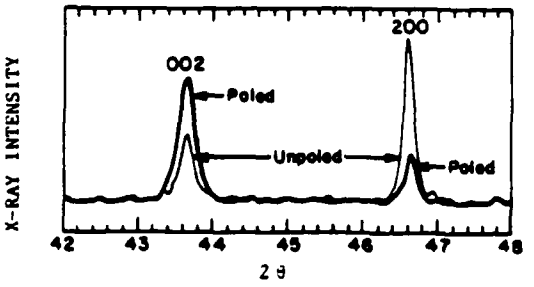

Figure 6. 002 and 200 X-ray diffraction peaks taken on surfaces of the composite before and after poling.

7. References

1. R.E. Newnham, L.J. Bowen, K.A. Klicker and L.E. Cross, Composite Piezoelectric Transducers, Mat. in Eng. Vol. 112, p. 93 (1980).

2. R.E. Newnham, A. Safari, J. Giniewicz, and B.H. Fox, Composite Piezoelectric Sensors, Ferroelectrics, Vol. 60, pp. 15-21 (1984).

3. W.B. Harrison, Flexible Piezoelectric Organic Composites, Proceedings of the Workshop on Sonar Transducer Materials, Naval Research Laboratories (1976).

4. H. Banno, Recent Development of Piezoelectric Ceramic Products and Composites of Synthetic Rubber and Piezoelectric Ceramic Particles, Ferroelectrics, Vol. 5, p. 3 (1983).

5. Y.H. Lee, M.J. Haun, A. Safari and R.E. Newnham, in Proc. 1986 IEEE International Symposium on Applications of Ferroelectrics.

6. A. Safari, Perforated PZT-Polymer Composites with 3-1 and 3-2 Connectivity for Hydrophone Applications, Ph.D. Thesis, The Pennsylvania State University (1983).

7. R.Y. Ting, Naval Research Laboratoy, Private Communications.

POLING STUDY OF $PbTiO_3$-POLYMER COMPOSITES

G. Sa-Gong, A. Safari and R.E. Newnham

Materials Research Laboratory
The Pennsylvania State University
University Park, PA 16802

Abstract

Poling piezoelectric ceramic-polymer composites with 0-3 connectivity is difficult because to the high dielectric constant of most of the ferroelectric filler materials, and the high resistivity of the polymer matrix. To aid in poling this type of composite, conductivity of the polymer phase can be controlled by adding small amounts of a semiconductor phase such as germanium, carbon or silicon. In this study, flexible piezoelectric composites of $PbTiO_3$ powder and Eccogel polymer were developed using small amounts of a semiconducting phase. These composites poled rapidly at low voltages, resulting in properties superior to composites prepared without a conductive phase. The effect of addition of various conductive phases with different volume percentages on the dielectric and piezoelectric properties of the composite are discussed here.

1. Introduction

A hydrophone is an underwater microphone or transducer used to detect underwater sound. The sensitivity of a hydrophone is determined by the voltage that is produced by a hydrostatic pressure wave. The hydrostatic voltage coefficient g_h relates the electric field appearing across a transducer to the applied hydrostatic stress, and is therefore a useful parameter for evaluating piezoelectric materials for use in hydrophones. Another piezoelectric coefficient frequently used is the hydrostatic strain coefficient d_h which describes the polarization resulting from hydrostatic stress. The g_h coefficient is related to the d_h coefficient by the relation, $g_h = d_h/\varepsilon_o K$ where ε_o is the permittivity of free space and K is the relative permittivity of the material.

A useful 'figure of merit' for hydrophone materials is the product of hydrostatic strain coefficient d_h and hydrostatic voltage coefficient g_h. The product $d_h g_h$ has the units of m^2N^{-1}.

Over the past few years several investigators have examined piezoelectric ceramic-polymer composites with different connectivity patterns. A summary can be found in references [1].

The simplest type of piezoelectric composite consists of a polymer matrix loaded with ceramic powder. In this type of composite, the particles are not in contact with each other and the polymer phase is self connected in all three dimensions, the so-called 0-3 connectivity [2]. In many ways the 0-3 composites are similar to polyvinylidene fluoride [PVF_2=$(CH_2$-$CF_2)_n$]. Both consist of a crystalline phase embedded in an amorphous matrix and both are reasonably flexible.

Early attempts to fabricate flexible composites of piezoelectric ceramic particles and polymers were made by Kitayama [3], Pauer [4], and Harrison [5]. The d_{33} of these composites were comparable with PVDF, but the d_h value was lower than those of solid PZT and PVDF polymer.

0-3 composites with improved properties have been prepared by Banno et al. by using pure $PbTiO_3$ powder as a filler material instead of PZT [6]. To fabricate composite the piezoelectric powders and chloroprene rubber were mixed and rolled into 0.5mm thick sheets at 40°C using a hot roller, and then heated at 190°C for 20 minutes under a pressure of 13 kg/cm^2. The composites were poled at 60°C in silicone oil in a field of 100 kV/cm field for 1 hour.

One difficulty with this type of composite is that the piezoelectric particles are smaller in diameter than the thickness of the composite. For fine-grain piezoelectric powder in a polymer matrix, very large poling fields are needed to achieve sufficient poling [6]. The reason for the large fields required for poling will be made clear from the following discussion.

For a 0-3 composite consisting of spherical grains embedded in a matrix, the electric field E_1, acting on an isolated spherical grain is given by:

$$E_1 = \frac{3K_2}{K_1+2K_2} E_o$$

In this equation, K_1 and K_2 are the dielectric constants of the spherical piezoelectric grains and the polymer matrix, respectively, and E_o is an

CH2358-0/86/0000-0281 $1.00

externally applied electric field. For a 0-3 composite of PZT powder and polymer, K_1 is about 2000 and K_2 about 5. In such a composite with an external field of 100 kV/cm, the electric field acting on the piezoelectric particles is only about 1 kV/cm which is insufficient to pole the composite. According to the above equation $E_1 \sim E_o$ only when the dielectric constant of the piezoelectric phase approaches that of the polymer phase. Most of the ferroelectric materials have very high dielectric constants and hence the above condition cannot be satisfied.

The importance of conductivity to poling can be assessed by applying Maxwell-Wagner model [7] to the 0-3 composites. A 0-3 composite with alternating piezoelectric ceramic grains and thin layers of polymer between the two electrodes can be approximated to a 2-layer Maxwell-Wagner model. The dielectric permittivity, conductivity and effective thickness of the ceramic and polymer are (K_1, σ_1, and d_1) and (K_2, σ_2, and d_2), respectively.

When a DC voltage is suddenly applied, the initial field distribution corresponds to electrostatic requirement of constant flux density ($D_1 = D_2$). In this condition, the ratio of the voltage V_1 on the phase 1 (ceramic) to the applied voltage V is given by

$$\frac{V_1}{V} = \frac{1}{\frac{K_1 d_2}{K_2 d_1} + 1}$$

This ratio is small because K_1 (piezoelectric ceramic) is usually much larger than K_2 (polymer).

When a DC poling voltage is applied for a period longer than the relaxation time, the voltage ratio is given by

$$\frac{V_1}{V} = \frac{1}{\frac{\sigma_1 d_2}{\sigma_2 d_1} + 1}$$

This ratio is small unless $\sigma_2 > \sigma_1$ or $d_2 \ll d_1$.

One way to aid poling is to raise the conductivity of the polymer matrix. This can be achieved by adding a small amount of a conductive third phase to the polymer composite. Addition of a conductive phase to the composite may create a continuous electric flux path between PZT particles. This in turn increases the field on the high K ferroelectric filler, making poling easier.

The effect of small additions of carbon germanium or silicon on ease of poling PZT-polymer composite was studied by us earlier [8]. It was observed that a duration of five minutes is sufficient for poling of the composites. This was a substantial improvement compared to poling conditions of 100 kV/cm for one hour used previously [6].

In the present study flexible piezoelectric composite of $PbTiO_3$ powder and Eccogel polymer were developed using small amount of germanium, carbon or silicon. These composites can be poled very quickly at shorter time. The effect of addition of various conductive phases with different volume percent on dielectric and piezoelectric properties of composite are reported in this paper.

2. Sample Preparation

$PbTiO_3$ powder obtained from Ferro Corporation (Independence, Ohio) and Eccogel polymer (an epoxy obtained from Emerson and Cuming) were used as piezoelectric filler and matrix respectively. The third semiconductor phase is fine-grained carbon, germanium or silicon (Alpha Product). To prepare the composites, $PbTiO_3$ was mixed with one of the semiconductor phases and dry ball-milled for two hours. The polymer matrix was then added to the particulate phases and mixed by hand with a spatula. The mixture was then placed in a mold and the composite formed under a pressure of 7500 PSI (50MPa). After curing, the composite was polished lightly to ensure that the faces of the composite were parallel. Electrodes of air-dried silver paste (Materials for Electronics, Inc., Jamaica, New York) were applied to the surfaces of the composite. The samples were poled at 100°C in a stirred oil bath. The effect of the magnitude of the poling field and its duration on the piezoelectric coefficients will be discussed later.

3. Measurements

The capacitance and dissipation factor were measured at 1 kHz using a Hewlett-Packard 4270A Multi-Frequency LCR Meter. The $\bar{d}_{33}$ coefficient was measured using a Berlincourt Piezo d_{33}-meter.

The $\bar{d}_h$ coefficient was determined using the dynamic A.C. technique. An electromagnetic driver was used as an A.C. stress generator to apply pressure waves to the sample and a PZT standard, which were kept under a static pressure from the hydraulic press. The charge produced by the sample and standard were buffered with an impedance converter, and the voltages produced were measured on a Hewlett-Packard 3585A Spectrum Analyzer. The ratio of the voltages is proportional to the $\bar{d}_h$ coefficients. Accounting for the area of the sample and PZT standard, the d_h coefficient of the sample was calculated. Using the measured values of $\bar{d}_h$, the hydrostatic piezoelectric coefficient $\bar{g}_h$, was calculated from the relation, $\bar{g}_h = \bar{d}_h/\varepsilon_o K$.

The electrical resistivity of the composites was measured at the poling temperature using a Keithly electrometer Model 616.

4. Results and Discussion

Figure 1 shows the electrical resistivities of the germanium-polymer, carbon-polymer and

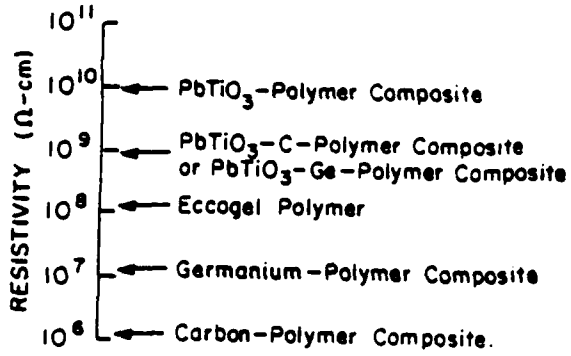

Figure 1. Resistivity of the Eccogel polymer (1365-0) and several different composites measured at the poling temperature.

$PbTiO_3$-polymer composites with and without conductive phases all measured at the poling temperature (100°C). The resistivity of the Eccogel polymer decreased by an order of magnitude when a small amount of carbon or germanium was added. The resistivity of the $PbTiO_3$-polymer composite with carbon or germanium also decreased, as expected.

The intensity ratios of the 001/h00 x-ray diffraction peaks from the surface of the composite was monitored both before and after poling (Fig. 2) in order to detect the possible contribution of domain reorientation on poling. A complete reversal of the intensities of the 001 and 100 peaks with a slight change in the intensity ratio of 002 and 200 peak were observed for germanium additive composites. This indicates the degree of polarization has not been fully achieved.

Table 1 summarizes the results of the dielectric and piezoelectric measurements on the $PbTiO_3$-polymer composites with different

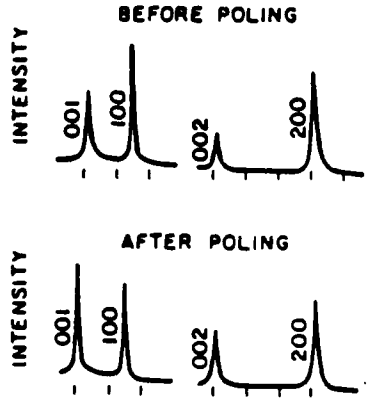

Figure 2. Intensity of the 001 and h00 x-ray diffraction peaks from the surface of the composite before and after poling.

Table 1. Dielectric and Piezoelectric Properites of $PbTiO_3$-Polymer* Composites with Various Conductive Phase Additions

Composites	tanδ	K_{33}	$\bar{d}_{33}$	$\bar{g}_h$	$\bar{d}_h$	$\bar{g}_h\bar{d}_h$
$PbTiO_3$(75)** polymer (25)	0.06	55	24	21	10	210
$PbTiO_3$(66)-Ge(4)-polymer (30)	0.08	60	34	44	24	1056
$PbTiO_3$(73)-C(2) polymer (25)	0.11	63	27	31	17	527
$PbTiO_3$(73.5) -Si(1.5) polymer (25)	0.09	50	33	33	15	495

*Polymer: Eccogel (1365-0)
**( ): Volume percent of ceramic, polymer or semiconductive phase
units: $\bar{d}_{33}$, $\bar{d}_h$-pCN^{-1}; $\bar{g}_h$-$10^{-3}VmN^{-1}$; $\bar{g}_h\bar{d}_h$-10^{15} m^2N^{-1}

conductive phase additives. The corresponding values for $PbTiO_3$-polymer composite without a conductive phase additives are also listed for comparison.

The tangent δ and dielectric constant of the composites with and without conductive phase are similar but the $\bar{d}_{33}$, $\bar{g}_h$ and $\bar{d}_h$ coefficients of the composites with germanium, carbon or silicon are higher than those of composite without conductive phase. Especially noteworthy are the $\bar{g}_h$ and $\bar{g}_h\bar{d}_h$ values of $PbTiO_3$-polymer of composites prepared with germanium. It is found that in $PbTiO_3$ composites, the poling result of the composite with germanium additives were better than other semiconductive additives.

The change in $\bar{d}_{33}$ coefficient is plotted in Figure 3 as a function of the poling voltage for a composite containing 66 vol% $PbTiO_3$, 4 vol% germanium and 30vol% Eccogel 1365-0. All the

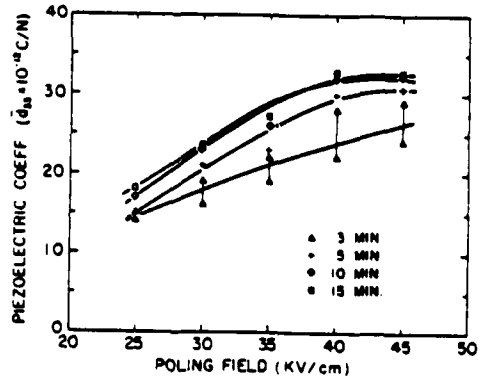

Figure 3. Variation of piezoelectric $\bar{d}_{33}$ coefficient of $PbTiO_3$-Germanium Eccogel composite with poling field.

composites were poled at 100°C for different times. $\bar{d}_{33}$ increases with increasing poling voltage and saturate at about 45 KV/cm. It is observed that a duration of ten minutes is sufficient for poling of the composites.

Figures 4 and 5 show the variation of dielectric constant, loss tangent, $\bar{d}_{33}$, $\bar{g}_h$, $\bar{d}_h$ and $\bar{g}_h\bar{d}_h$ coefficients with volume percent germanium in the $PbTiO_3$-Eccogel composites. Dielectric constant and loss tangent increase slowly with increases of volume percent of germanium. $\bar{d}_{33}$, $\bar{d}_h$ and $\bar{g}_h$ coefficients increase with increasing in germanium content and show a maximum at about 4 volume percent. When the amount of the germanium in the composite exceeds 4 vol%, the loss tangent raises making it difficult to apply the large voltages required for poling. The $\bar{d}_h\bar{g}_h$ product for the composites with 4 vol% germanium is about 1090 (10^{-13} m^2/N) which is five times larger than that of composite without germanium.

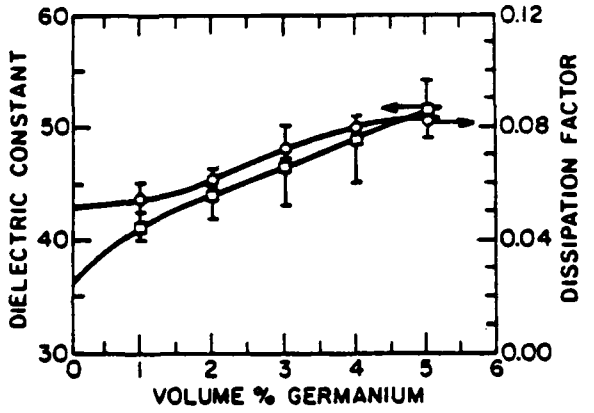

Figure 4. The change in the dielectric constant and dissipation factor with Volume percent of germanium in $PbTiO_3$-polymer composite.

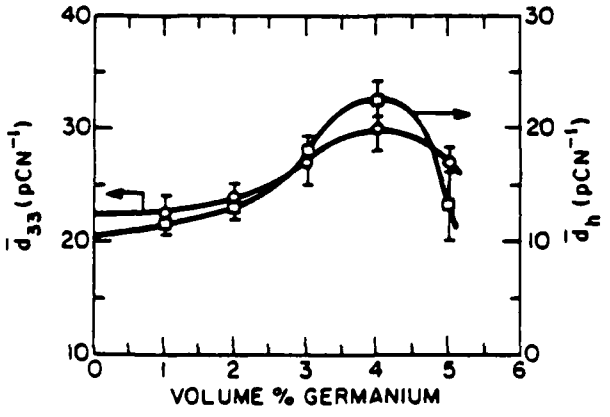

Figure 5. The $\bar{d}_{33}$ and $\bar{d}_h$ coefficients plotted as a function of volume percent germanium in $PbTiO_3$-polymer composite.

5. Summary

$PbTiO_3$-Eccogel piezoelectric 0-3 composites have been poled rapidly by adding a second phase filler such as germanium. A small amount of germanium decreases the resistivity of Eccogel polymer matrix and reduces the poling field to 45 kV/cm. Only ten minutes are required for poling these composites. This is a big improvement over normal poling conditions (100 kV/cm, 1 hour). The hydrostatic voltage coefficient $\bar{g}_h$ and figure of merit $\bar{g}_h\bar{d}_h$ of $PbTiO_3$-germanium-Eccogel composites are two and five times larger than those of composites without germanium additives.

6. Acknowledgement

The authors are grateful for financial support received from the Office of Naval Research and Celanese Research Company.

7. References

1. R.E. Newnham, A. Safari, J. Giniewicz, and B.H. Fox, Composite Piezoelectric Sensors, Ferroelectrics, Vol. 60, pp. 15-21 (1984).

2. R.E. Newnham, D.P. Skinner, and L.E. Cross, Connectivity and Piezoelectric-Pyroelectric Composites, Mat. Res. Bull., Vol. 13, 525 (1978).

3. Kitayama Toyoki, Flexible Piezoelectric Materials, Seramikkusu 14(3), p. 209 (1979).

4. L.A. Pauer, Flexible Piezoelectric Material, IEEE Int. Conf. Res. 1 (1973).

5. W.B. Harrison, Flexible Piezoelectric Organic Composites, Proceedings of the Workshop on Sonar Transducer Materials, Naval Research Laboratories (1976).

6. H. Banno, Recent Development of Piezoelectric Ceramic Products and Composites of Synthetic Rubber and Piezoelectric Ceramic Particles, Ferroelectrics, Vol. 5, p. 3 (1983).

7. A.R. Von Hippel, Dielectrics and Waves, John Wiley and Sons (1954).

8. G. Sa-Gong, A. Safari, S.J. Jang and R.E. Newnham, Poling Flexible Piezoelectric Composites, Ferroelectrics, Vol. 5, pp. 131-142 (1985).

ETCHED PIEZOELECTRIC STRUCTURES

S. Trolier, C. Geist, A. Safari,
R.E. Newnham, Q.C. Xu

Materials Research Laboratory
Pennsylvania State University
University Park PA 16802

ABSTRACT

Miniaturized piezoelectric devices can be fabricated from wafers of lead zirconate titanate (PZT) using techniques developed by the semiconductor industry for the production of integrated circuitry. Patterns generated in a polymeric photoresist are transferred to the surface of the substrate by selective chemical etching of the ceramic. In this fashion, complex device geometries can be obtained with relative ease.

The behavior of PZT in several acidic solutions was examined in an attempt to derive an etchant suitable for microfabrication. Concentrated HF, HCl, H_2SO_4, HNO_3, H_3PO_4, and aqua regia were investigated, and it was found that hydrochloric acid combined a high etching rate and a compatability with commercially available photoresists. Powdery residues found on the surface of the wafers after etching with HCl were identified by x-ray diffraction as pure PZT, suggesting that the acid dissolves around grain boundaries, freeing grains rather than etching through them. This was confirmed by scanning electron microscopy. Although this limits the minimum feature size, it also eliminates many of the restrictions on device geometry due to the use of isotropic etchants.

INTRODUCTION

The technology necessary for the production of miniaturized devices has been developed for and is universally exploited by the semiconductor industry in the production of integrated circuitry. Although many other fields could benefit from the ability to microfabricate components, little work has been done to transfer the available knowledge to other systems. This study, then, was in large part designed to determine if the photolithographic process could be adapted to ceramic materials. Lead zirconate titanate (PZT) was chosen since miniaturized piezoelectric devices could be employed as frequency generators or accelerometers.

TECHNIQUE

Nearly all microprocessing techniques involve the selective removal of material. In order to accomplish this, a two step process is employed wherein a pattern masking portions of the surface is first delineated so that unprotected areas can then be etched away. [1] The process, pictured in Figure 1, is thus largely analogous to the production of pictures by the printing plate method.

Replication of a desired pattern, or lithography, by conventional methods necessitates the use of an energy sensitive barrier, called a resist, and an activating light source. Most commonly, this procedure entails coating a substrate with a uniform layer of photosensitive material and projecting a light through film patterned with a design. Upon exposure to light, the photoresist undergoes a chemical reaction in which either exposed or unexposed regions (corresponding to negative and positive resists, respectively) are rendered insoluble in developing solution. Thus, on developing, a pattern duplicating the original film is generated.

Once the pattern has been delineated in the resist, the design must somehow be engraved into the substrate. Most frequently, this is accomplished using wet chemical etching.

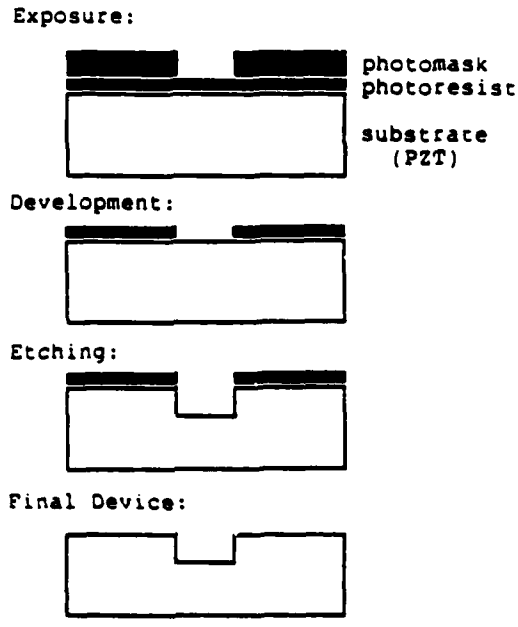

Fig. 1 Photolithography process

0736-0000-0707 $1.00 © 1986 IEEE

DESIGN OF THE STUDY

In order to implement chemical etching it is necessary to find a reagent which readily dissolves the substrate while leaving the patterned resist intact. That was the first goal of this study.

To test the validity of this processing technique, a piezoelectric resonator was designed. If the cantilever structure of Figure 2 is electroded as shown in Figure 3, a wagging mode can be established in which individual cantilevers vibrate in a horizontal plane. Each cantilever is paired with one of a matched length so that when the distance between the two is small, their motions interact. In this way, when the two cantilevers are either exactly in phase or 180° out of phase, the conditions for resonance or anti-resonance are fulfilled. This in turn narrows the width of the resonance frequency peak, leading to a higher mechanical Q. A design symmetric about a center bar is mandated so that the condition for clamping is met at the fixed end of each cantilever. The resonant frequency can then be calculated from:

$$f = \beta^2 \frac{T}{\ell^2} \sqrt{\frac{E}{12\rho}}$$

f = resonance frequency
β = constant
T = thickness
ℓ = cantilever length
ρ = density

Such a device could potentially serve as a frequency generator, a filter, or an accelerometer.

EXPERIMENTAL PROCEDURE

Samples for the etching studies were prepared by layering 30 2.8 mil tape cast sheets (prepared by TAM Ceramics Inc. from a PZT 501 powder) carrier side down and laminating in a warm press at 65°C and 15,000 psi for one minute. Following a five day binder burnout cycle at 500°C, the samples were fired with a four hour ramp to 1285°C, a one hour soak, and a slow cooling rate. Any roughened or irregular edges were smoothed by polishing with a coarse powder.

Before the etching studies were carried out, each sample was immersed in concentrated HCl at 45°C for 5 minutes both to clean the surface and to remove damaged areas. Sample dimensions were determined with micrometers so that nominal surface areas and densities could be calculated.

The etching process was carried out by holding the specimen in acid for 60 seconds with a pair of plastic tweezers. After the allotted time had elapsed, the sample was immediately washed to remove any remaining acid. The specimen was then cleaned ultrasonically, dried under a stream of forced air, and weighed to the nearest 0.0002g. This was repeated until a constant slope of cumulative mass loss per surface area versus time was observed. In all cases, the surface area occluded by the tweezers was considered negligible. The temperature was maintained at a constant value within ±0.5°C in a water bath.

Samples for the microfabrication studies were prepared either in a manner similar to those for etching, or as disks by dry pressing. After sintering, the samples were polished to the desired thickness using a series of alumina powders. Once polished, samples were poled in an oil bath at 110°C by subjecting them to a field intensity of 20kV per cm for 12 minutes, cleaned ultrasonically, and dried under flowing air.

Prior to applying the photoresist, Shipley Microposit 1470, the samples were spun on an Integrated Technologies P-6000 Spin Coater at 4000rpm for 20 seconds to remove dust. Then, working under yellow lights, enough photoresist was placed on the disk to cover two thirds of the surface and the spin cycle was repeated. The second face was coated in a similar fashion. All samples were then placed in a light tight container and baked for 20 minutes at 80°C. The dried photoresist was exposed by holding the sample under a matrix of four white light sources (two 300W, two 375W bulbs arranged in a square such that the distance between sample and sources was approximately 2 feet.) for 5 minutes.

Photomasks for the process were manufactured by generating an enlarged negative image of the pattern with a laser printer and photographing the resultant with Kodak Technipan film. The film was developed with Kodak D-19 Developer in order to achieve maximum contrast. These photomasks were then placed on the resist coated wafer and held in place with a glass flat during exposure.

After exposure, the wafers were developed in Shipley Microposit Developer MF-312 for 1 1.2 minutes with light agitation, so that exposed areas were removed. They were then post-baked for 20 minutes at 80°C to further harden the remaining resist.

Once this had been accomplished, the disks were placed in a bath of warm concentrated HCl. Because one side of the disk was fully coated with the resist, etching took place solely through the areas exposed by developing. The solution was stirred lightly in order to continuously present fresh acid to the disk surface. Intermittently, the wafer was pulled from the acid and sprayed with deionized water to dislodge adherent grains. Pinholes in the disk began to appear after approximately one hour of etching, and individual cantilevers were completely freed inside of half an hour thereafter.

Completion of the etching of larger channels was marked by a tearing of the unpatterned photoresist film. After etching, the remaining resist was removed with a spray of acetone.

Electrodes were hand painted onto the device surface using a suspension of silver particles. One side of the device was fully electroded; on the other, each cantilever was patterned with a split electrode. Electrical connections were made as shown in Figure 3.

Resonant frequency data were collected using a Hewlett Packard 4192A LF Impedance Analyzer.

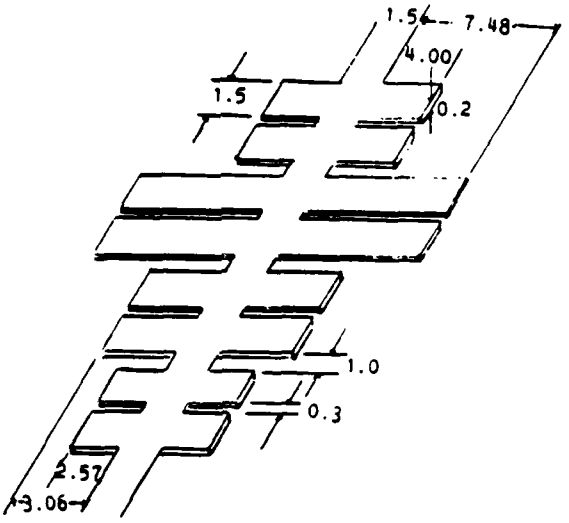

Fig. 2 Resonator design

RESULTS AND DISCUSSION

Preliminary data on the etching of PZT in various acids is presented in Table 1. Concentrated HCl was found to possess a comparatively rapid etching rate for the PZT substrate while leaving the photoresist largely untouched, and so was chosen for further study. More accurate values for the etching rate of PZT in HCl are presented in Table 2.

Table 1: Preliminary Data for Etching of PZT

Acid	Temperature (^{o}C)	Etching rate ($gxcm^{-2}xmin^{-1}$)
H_3PO_4	45-48	$2x10^{-4}$
HNO_3	43-45	$9x10^{-5}$
HCl	42-48	$4x10^{-3}$
H_2SO_4	42-48	$3x10^{-4}$
$0.5H_3PO_4$-0.5HCl	49-50	$3x10^{-4}$
$0.25H_3PO_4$-0.75HCl	49-51	$4x10^{-4}$

Table 2: Etching of PZT in HCl

Temp. (^{o}C)	Etching Rate ($gxcm^{-2}xmin^{-1}$)	Etching rate ($micronsxmin^{-1}$)
30±0.5	$2.1x10^{-3}$	1.4
45±0.5	$3.5x10^{-3}$	2.3
60±0.5	$4.7x10^{-3}$	3.0

In all cases contact with HCl resulted in the formation of a whitish powder on the surface of the laminate, so that thorough ultrasonic cleaning was necessary to remove it from small crevices. X-ray diffraction identified the powder as pure PZT, suggesting that HCl etches by dissolving around the grains, freeing them rather than etching through them. Further support for this hypothesis is offered by SEM micrographs of etched disks, which evince angular surfaces composed of whole grains and negligible rounding of individual grain apices. Although this does limit the minimum feature size to some small multiple of the grain size, it does permit a wider range of geometries to be accessed than would most etchants. Normally, with an isotropic etchant, any trench will be at least twice as wide as it is deep. Indeed, Brodie and Muray [1] suggest that any film to be etched through should be patterned with features no smaller than three times the film thickness. By using a grain boundary specific etchant, however, much better aspect ratios (depth of trench over width of opening) have been achieved. For instance, the separation between matched cantilevers in the resonator design is 0.3mm, only 1 1/2 times the thickness of the sample. There is no reason to believe, at present, that even higher aspect ratios cannot be obtained.

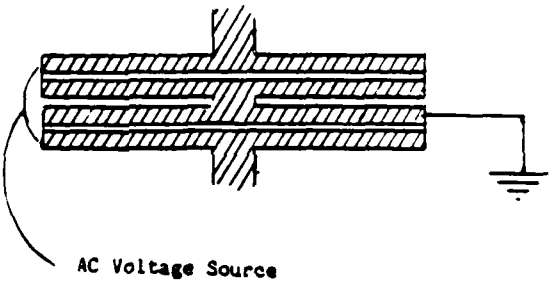

Fig. 3 Electrode Pattern for Resonator

A completely etched resonator is pictured in Figure 4. As can be seen, the reproduction of the patterned photomask is faithful, and indeed, any imperfections in the geometry are attributable to flaws (scratches or trapped dust particles) in the photoresist. Although the finest feature size demanded for this application was 0.3mm, the technique is capable of much better resolution (circa 1-7 microns with a collimated UV light source) [3]-[5] and in more recent work trenches with linewidths of approximately 0.1mm have been obtained. It is hoped that eventually features with dimensions of 2 to 5 times the grain size will be possible.

Measurements of conductance, capacitance, admittance, and phase angle versus frequency were made for the resonator and it was found that resonant frequency peaks were both narrow and easily distinguished from background readings. For the smallest set of cantilevers pictured in Figure 4, resonance occured at 76.6 kHz and anti-resonance at 77.3 kHz, giving a mechanical Q=36.5 and a coupling coefficient=0.134. It is hoped that by further decreasing the distance between cantilevers of matched length, Q will increase further.

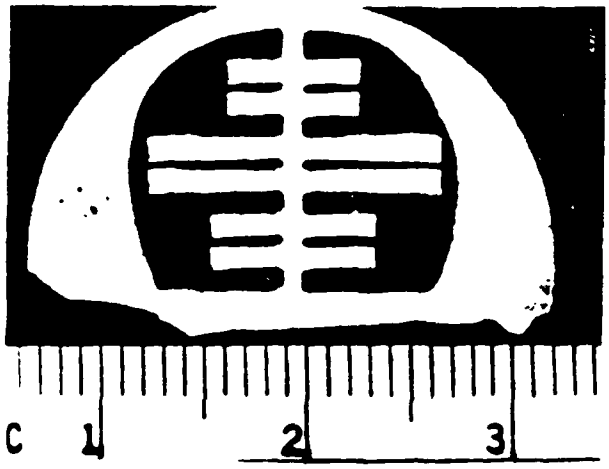

Fig. 4 Piezoelectric Resonator
(Numbered divisions in cm)

CONCLUSIONS

As can be seen from this paper, the coupling of photolithography with chemical etching is a viable processing technique for ceramic materials. The method is readily adapted to a variety of two dimensional patterns and is particularly suited to small feature sizes. Devices fabricated by this technique would be difficult, and perhaps impossible, to replicate by any conventional processes. The use of grain boundary specific etchants further broadens the range of potential geometries by permitting much higher aspect ratios to be attained.

REFERENCES

[1] I. Brodie and J.J. Muray, The Physics of Microfabrication. New York: Plenum Press, 1982.

[2] Ibid. p.251

[3] Ibid. pp. 267-270

[4] King, "Future Developments for 1:1 Projection Photolithography," IEEE Trans. Electron. Devices ED-26 (4) p. 711 (1979).

[5] Bruning, "Performance Limits in 1:1 UV Projection Lithography," J. Vac. Sci. Technol., 16 1925 (1979).

This material is based upon work supported under a National Science Foundation Graduate Fellowship.

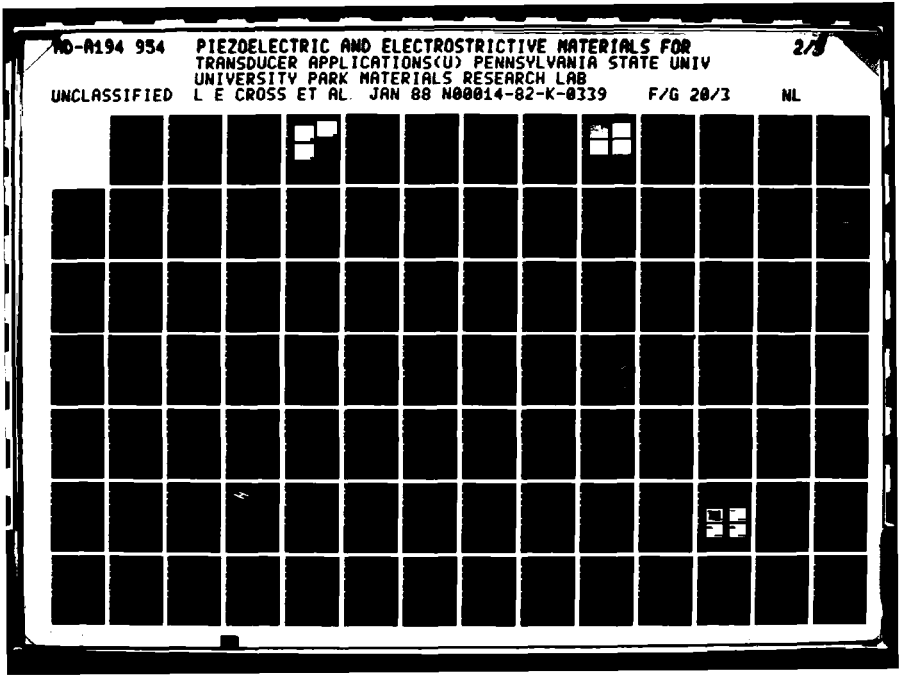
AD-A194 954 PIEZOELECTRIC AND ELECTROSTRICTIVE MATERIALS FOR
TRANSDUCER APPLICATIONS(U) PENNSYLVANIA STATE UNIV
UNIVERSITY PARK MATERIALS RESEARCH LAB
UNCLASSIFIED L E CROSS ET AL. JAN 88 N00014-82-K-0339 F/G 20/3 NL
2/3

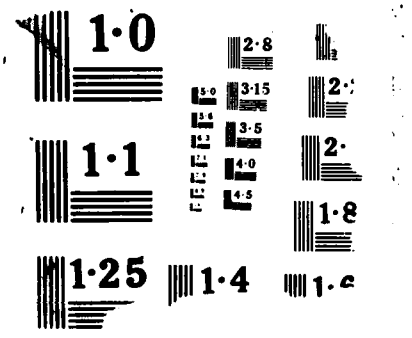
1·0
1·1
1·25
2·8
3·15
3·5
4·0
4·5
1·4
1·8

PIEZOELECTRIC GLASS-CERAMICS AS LOW TEMPERATURE-COEFFICIENT SAW SUBSTRATE MATERIALS

J.M. Browne, C.W. Lee, and J.R. McColl
GTE Laboratories, Inc.
40 Sylvan Rd.
Waltham, MA 02254 U.S.A.
and

E. Yio, A. Halliyal, and A.S. Bhalla
Materials Research Laboratory
Pennsylvania State University
University Park, PA 16802 U.S.A.

ABSTRACT

Surface acoustic wave (SAW) properties of piezoelectric glass-ceramics based on fresnoite ($Ba_2Si_2TiO_8$) are examined in this paper. Fresnoite-based formulations are prepared initially in the glass form, then thermally processed to produce glass-ceramics having a well-oriented fibrous grain structure at the surface; this surface region is piezoelectric owing to the fact that the surface region has polar as well as crystallographic orientation. This class of materials can therefore serve as SAW substrates.

Because the composition of this glass-ceramic system can be varied over wide ranges, it is possible to modify the piezoelectric phase and/or to use a composite approach to tailor SAW properties for specific applications. In this paper, we show that addition of excess titania as well as silica to the fresnoite glass-ceramic system yields SAW coupling coefficients approaching 1.2% combined with exceptionally low temperature coefficients of resonance over a wide temperature range.

INTRODUCTION

A number of piezoelectric materials have been developed for surface acoustic wave (SAW) devices over the past twenty years. Desirable materials properties for application to SAW include

- Low temperature coefficient of resonance (TCR)
- SAW electromechanical coupling coefficient (k^2) matched to bandwidth requirement
- Low attenuation, consistent material quality, etc.

An undesirable tradeoff between coupling coefficient and temperature coefficient exists for most of the widely used SAW materials. For example, ST-quartz exhibits near-zero TCR but has weak coupling. Lithium niobate, with a hign coupling coefficient needed for large bandwidth applications, has a large TCR value of -72 ppm/°C for the popular 128° YX cut. Lithium tantalate, the most widely used medium-coupling SAW substrate material, also has a relatively large TCR value of -35 ppm/°C. Therefore, there is a need for medium to large coupling materials with low TCRs.

A number of attempts have been made to employ conventionally processed piezoelectric ceramics as SAW substrates, but attenuation is generally high in ceramics. The most promising attempt to utilize ceramics as SAW substrates has been the work of the Hitachi group(1-3), which has prepared modified lead titanate ceramics with near-zero TCR and low propagation losses.

Recently, a new technique for preparing glass-ceramics with oriented crystallites has been described(4-6). In this technique, glasses are recrystallized such that the resulting glass-ceramics have both crystallographic and polar orientation. Glass-ceramic pyroelectric detectors and piezoelectric resonators have been demonstrated. Two of the advantages of this processing route to piezoelectric materials are its potentially low processing cost and the freedom to adjust composition and recrystallization conditions to optimize specific properties. Studies to optimize pyroelectic(7) and bulk piezoelectric(6) properties have already been carried out.

Fresnoite ($Ba_2TiSi_2O_8$) is a polar but nonferroelectric material with tetragonal (P4bm) structure. Its single-crystal SAW properties have been characterized(8,9); for Z-cut X-propagating Fresnoite, k^2 is 1.6%, while the TCR is -50 ppm/°C. Ito, et. al.(10,11), showed that the TCR magnitude could be reduced to ≈-20 ppm/°C by partial substitution of Sr for Ba.

Recently, Lee, et. al.(12), showed that fresnoite glass-ceramic could be prepared with SAW properties comparable to those of the Z-cut single crystal. They reported k^2=1.1% and TCR=-60 ppm/°C. They speculated that the TCR magnitude might be reduced by Sr doping by analogy to single-crystal results.

In this paper, we report the results of an investigation of compositional variation of fresnoite-base glass-ceramics on their SAW properties. This report focuses on the glass composition $2.08BaO-0.15CaO-xTiO_2-2.9SiO_2$, with x varied from 0.9 to 1.2. We observe a remarkable variation in depth of oriented crystallinity, coupling constant k^2, and temperature coefficient of resonance.

CH2358-0/86/0000-0300 $1.00 © 1986 IEEE

EXPERIMENTAL

The glass-ceramic sample preparation was identical to that reported by Lee., et. al.(12) For all of the samples reported here, crystallization was carried out by raising the temperature from room temperature to 500°C at 100°C/hr, holding at this annealing temperature for 1 hr, then raising the temperature at 225°C/hr to 950°C, holding at this crystallization temperature for 2 hrs. Samples were investigated by x-ray diffraction both in glass-ceramic form for textural analysis, and powder form for phase identification. All x-ray powder pattern lines could be indexed as fresnoite lines, except for a few very weak lines observed for x=0.9 (titania-deficient). The lattice plane spacings observed for all of the glass-ceramic samples agreed to four decimal places with those measured for a powdered single fresnoite crystal. X-ray textural analysis indicated a regularly increasing degree of c-axis ordering normal to the sample surface as x increased from 0.9 to 1.2.

Microstructure analysis confirms the x-ray textural analysis. The optical micrographs in Figure 1 show that the depth of c-axis orientation depends on titania mole ratio x as follows:

x	depth(μm)
0.9	70-140
1.0	40-190
1.2	250-600

The depth of orientation for x=0.9 is mostly 70 μm with excursions to 140 μm, while the depth for x=1.0 is mostly 190 μm with excursions to 40 μm. Note that approximately 50 μm of oriented material has been removed by polishing in sample preparation. We also note that extensive microcracking is prevalent in the unoriented crystallized regions.

SAW measurements were carried out as decribed by Lee, et. al.(12) Uniform aluminum interdigital transducers with 19.5 periods, 1 mm aperture, and 30 μm wavelength were fabricated on polished ceramic substrates. With this wavelength, IDT center frequencies were about 89 MHz. Coupling coefficients were obtained by measuring the vector impedance of IDTs at their center frequency with an HP 4191A rf impedance analyzer, with careful correction for package and fixture stray capacitance and bonding wire inductance. The values of k^2 were extracted from the impedance data with the crossed-field model formula(13):

$$G = 4Nk^2\omega C/\pi, \qquad (1)$$

where G and C are the measured conductance and capacitance of the IDT, respectively. For propagation loss measurements, four high quality IDTs were selected in a row so that insertion loss could be measured between successively further apart IDTs (intermediate IDTs were etched away after they had been used). Plots of insertion loss vs IDT separation yielded propagation loss. Temperature coefficient of resonance (TCR) data were obtained with the help of an HP 8505A network analyzer stabilized with an HP 8660C frequency synthesizer. The frequency was set to the IDT center frequency, then as sample temperature was ramped at 0.7 °C/min, the frequency f was varied under computer control to maintain constant SAW device output phase ϕ. Thus, the temperature coefficient of resonance is defined as

$$TCR = \frac{1}{f}\left(\frac{\partial f}{\partial T}\right)_{\phi} \qquad (2)$$

For most samples, data were obtained between -20 and 200°C.

RESULTS & DISCUSSION

The data on k^2 are presented in Table I; k^2 for the titania-rich glass-ceramic is comparable to that obtained by Lee, et. al.(12), for Ti-stoi-

Material / Property	Fresnoite Glass-Ceramic (Lee, 1984)	Ti-Rich Fresnoite Glass-Ceramic (This Work)	Ti-Deficient Fresnoite Glass-Ceramic (This Work)	ZX-Fresnoite Single Crystal (Melngailis, et al., 1978)	YZ-$LiNbO_3$ (Slobodnik, 1976)	128° YX $LiNbO_3$ (Shiokawa, et al., 1976)	ST-Quartz (Slobodnik, 1976)	Lead Titanate (Uyemura, Nagatsuma, and Takeuchi, 1981)	YZ-$LiTaO_3$ (Slobodnik, 1976)
SAW Coupling Coefficient (%)	1.13	1.16±0.14	0.79±0.14	1.6	4.5	5.6	0.16	2.2	0.74%
Velocity (m/s)	2630	2660	2641	2678	3488	3993	3158	2810	
Attenuation at 89 MHz (dB/cm)	2.2	1.1	3.5	—	<0.1	<0.1	<0.1	0.6 (100 MHz-Fine Grain)	—
Temperature Coefficient of Resonance @ 25°C (ppm/°C)	-60	-7	-66	-58	-94	-72	<1	<1	-35

Table I. SAW Properties

chiometric glass ceramic, while the value of k^2 for the Ti-deficient sample is considerably decreased. The low value of k^2 for the Ti-deficient sample probably derives from the decreased depth of oriented microstructure apparent in Figure 1.

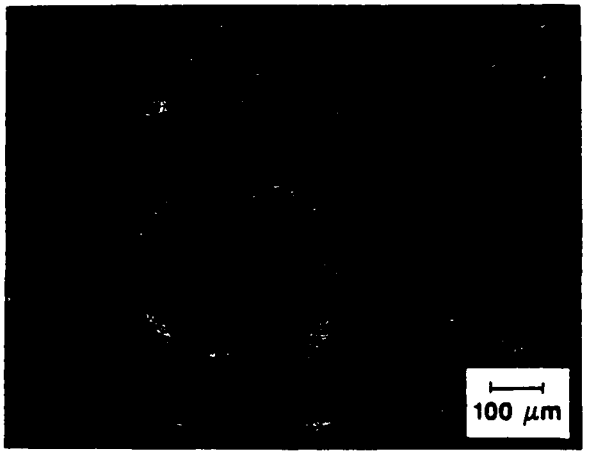

Figure 1a. Microstructure of titanium deficient fresnoite glass-ceramic with composition $2BaO\text{-}0.15CaO\text{-}2.9SiO_2\text{-}0.9TiO_2$.

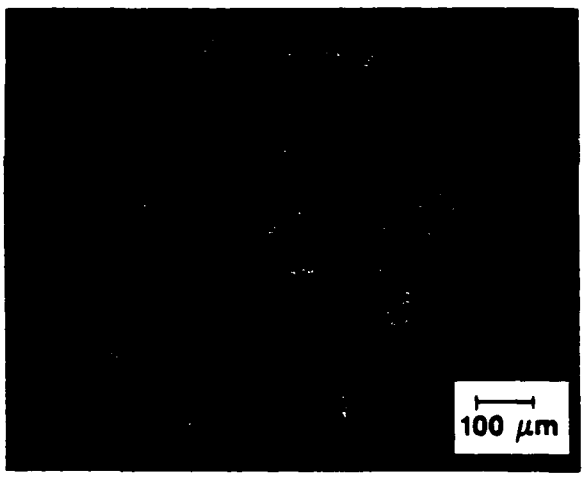

Figure 1b. Microstructure of titanium stoichiometric fresnoite glass-ceramic with composition $2BaO\text{-}0.15CaO\text{-}2.9SiO_2\text{-}1.0TiO_2$.

Even though the Ti-stochiometric and Ti-rich samples have essentially the same values for k^2 at ≈89 MHz, the Ti-rich sample would undoubtedly maintain its k^2 value at lower frequencies where the surface wave would extend further into the substrate, while k^2 for the Ti-stoichiometric sample would decrease.

Calculations performed by Yamauchi(8) and Melngailis(9) indicate that power flow angle is essentially zero and k^2 is essentially constant in fresnoite for SAW propagation directions perpendicular to <001>. Thus, the fact that k^2 in the best glass-ceramic samples is ≈27% lower than k^2 for single crystal fresnoite is not due to the random azimuthal orientation of crystallites in

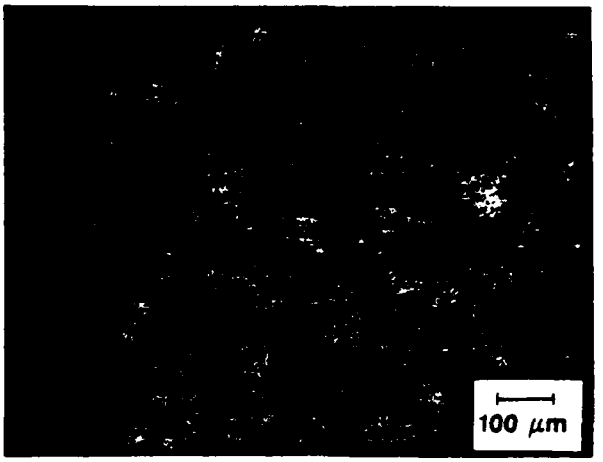

Figure 1c. Microstructure of titanium rich fresnoite glass-ceramic with composition $2BaO\text{-}0.15CaO\text{-}2.9SiO_2\text{-}1.2TiO_2$.

the glass ceramics. C-axis misorientation of 25° would be required to explain this ≈27% reduction. By inspection of Figure 1 it is clear that the c-axes of fresnoite grains in the glass-ceramic are oriented within ≈5° with respect to the surface normal, so that misorientation cannot explain the difference in k^2 values between the single crystal and glass-ceramic. The most probable explanation is dilution of piezoelectric properties by glass phase, as well as the limited depth of crystalline orientation.

Attenuation data are also presented in Table I. The Ti-rich sample has the lowest attenuation, while the Ti-stochiometric and -deficient samples have higher, comparable values. It is likely that two effects, subsurface microcracking and scattering from misoriented grains below the depth of c-axis orientation, are both dominant attenuation mechanisms. The high degree of microcracking in the Ti-stochiometric sample and the low orientation depth in the Ti-deficient sample appear to fortuitously yield comparable attenuation. This subsurface cracking is probably responsible for the observation by Lee, et. al.(12), that spurious bulk waves are strongly attenuated.

Temperature coefficient data are presented in Figures 2 and 3; data obtained with a Z-cut single crystal are included for reference. The curves for Ti-deficient and Ti-stoichiometric glass-ceramic are almost identical with each other, and are very similar to the curves for the single crystal. This reflects the fact that the origin of the piezoelectric effect is common for the three materials: Z-oriented fresnoite. We note that the "wiggles" in the single crystal data in Figure 3 are due to phase shifts induced by bulk wave interference; no attempt to reduce bulk wave interference by back-surface treatment was made; this was unnecessary for the glass-ceramics because of their bulk-wave attenuation. The curves for Ti-rich glass-ceramic are qualitatively different. The magnitude for TCR is much lower for this sample, and the low magnitude is maintained

over a much wider temperature range. These curves were confirmed by measurements on four samples.

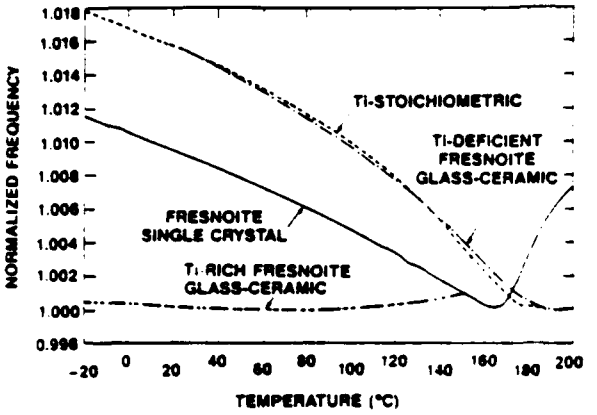

Figure 2. Temperature dependence of normalized frequency adjusted to yield constant SAW device output phase as temperature varies.

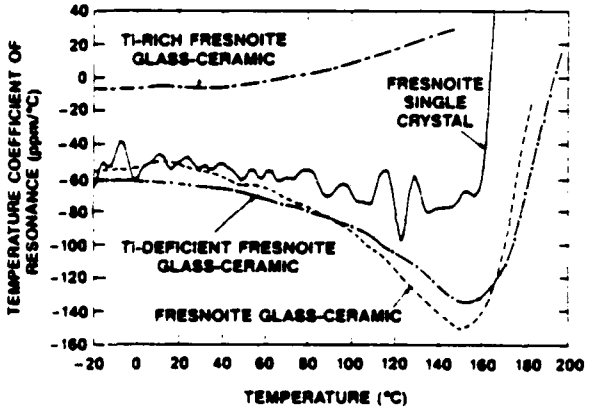

Figure 3. Temperature dependence of temperature coefficient of resonance defined by Eq. (2).

We have not yet found a convincing explanation for the low magnitude of TCR in the Ti-rich glass-ceramic sample. We do not detect a second crystalline phase or lattice constant shift in the fresnoite phase. We do notice a slight difference in preferred orientation between the Ti-rich and Ti-stoichiometric glass-ceramics, both of which were well-oriented within the penetration depth of the Cu Kα x-rays. In both samples, c-axis reflections clearly dominated all other reflections. In the Ti-rich glass-ceramic, a-axis reflections, although weak, were noticably stronger than off-axis reflections, whereas in the Ti-stoichiometric sample, all non-c-axis reflections had about the same magnitude. However, we have no evidence that this slight difference in texture is responsible for the dramatic difference in TCR. The explanation may simply lie in the amount and composition of glass phase.

SUMMARY & CONCLUSIONS

We have demonstrated in this paper how the freedom to vary composition in glass-ceramics can be used to advantage to improve SAW properties in the fresnoite system. A fresnoite glass-ceramic with excess titania and silica was developed which has an electromechanical coupling coefficient k^2 of 1.16%, comparable to the single-crystal value of 1.6%. The temperature coefficient of resonance is dramatically reduced to -7 ppm/°C at room temperature. The low magnitude of the TCR is maintained over a remarkable temperature range. In addition, bulk waves are strongly suppressed, while SAW propagation loss is reasonable. Thus, the SAW properties of the glass-ceramic appear to be superior to those of the single crystal from which it was derived. Fortunately, the low magnitude TCR occurs for a composition for which oriented recrystallization proceeds to a maximum depth.

This glass-ceramic appears to fill a need for a medium-coupling SAW substrate material with low TCR. Available medium coupling materials are lithium tantalate, berlinite, and modified lead-titanate ceramic(1-3). Properties of these materials are given in Table I. Lithium tantalate is commercially available, and is therefore the preferred material for medium-bandwidth SAW applications. However, its relatively high TCR is a disadvantage. An advantage of fresnoite glass-ceramic over ferroelectric ceramics such as lead titanate is that because it is not ferroelectric, it cannot depole or age.

It is probable that the TCR magnitude of fresnoite glass-ceramics can be further reduced by additional compositional or processing modifications. We are currently proceeding with further titania concentration variations, as well as substitution of Sr for Ba.

ACKNOWLEDGEMENTS

We wish to thank Dr. L.E. Cross of Penn State for encouragement and guidance, and Mr. M. Downey of GTE Labs for x-ray analysis.

This work was supported in part by the National Science Foundation under Grant DMR-8303906.

REFERENCES

1. S. Jyomura, K. Nagatsuma, and H. Takeuchi, J. Appl. Phys. 52, 4479 (1981).

2. Y. Ito, H. Takeuchi, S. Jyomura, K. Nagatsuma, and S. Ashida, Appl. Phys. Lett. 35, 595 (1979).

3. Y. Ito, H. Takeuchi, K. Nagatsuma, S.Jyomura, and S. Ashida, J. Appl. Phys. 52, 3223 (1981).

4. A. Halliyal, A.S. Bhalla, R.E. Newnham, L.E. Cross, and T.R. Gururaja, J. Mater. Sci. 17, 295 (1982).

5. A. Halliyal, A.S. Bhalla, and R.E. Newnham, Mat. Res. Bull. 18, 1007 (1983).

6. A. Halliyal, A. Safari, A.S. Bhalla, R.E. Newnham, and L.E. Cross, J. Am. Cer. Soc. 67, 331 (1984).

7. A. Halliyal, A.S. Bhalla, R.E. Newnham, and L.E. Cross, J. Am. Cer. Soc. (in press).

8. H. Yamauchi, J. Appl. Phys. 49, 6162 (1978).

9. J. Melngailis, J.F. Veaclino, A. Thunjunwala, T.8. Reed, R.E. Fahey, and E. Stern, Appl. Phys. Lett. 36, 894 (1980).

10. Y. Ito, K. Nagatsuma, and S. Ashida, Appl. Phys. Lett. 36, 894 (1980).

11. Y. Ito, K. Nagatsuma, and S. Ashida, Jpn. J. Appl. Phys. 20, 163 (1981).

12. C.W. Lee, L.J. Bowen, J.M. Browne, A. Halliyal, A.S. Bhalla, and E Ylo, Proc. IEEE Ultrasonics Symp., 285 (1984).

13. W.R. Smith, H.M. Gerard, J.H. Collins, T.M. Reeder, and H.J. Shaw, IEEE Trans. Microwave Theory and Techniques MTT-17, 856 (1969).

PIEZOELECTRIC PROPERTIES AND MICROSTRUCTURE OF GLASS-CERAMICS IN THE BaO-SrO-SiO_2-TiO_2 SYSTEM

E.E. Ylo III, M. Wheeler, A. Halliyal, A.S. Bhalla, and R.E. Newnham

Materials Research Laboratory, The Pennsylvania State University, University Park, PA 16802 USA

Abstract

Previous studies have shown that fresnoite ($Ba_2TiSi_2O_8$) glass-ceramics with oriented crystallites are promising candidate materials for pyroelectric detectors and surface acoustic wave devices. A detailed investigation of the properties and microstructure of glass-ceramics in the $Ba_{2-x}Sr_xTiSi_2O_8$ solid solution has been carried out. Glasses of several compositions were prepared and recrystallized through a heating schedule to produce an oriented region of crystallites perpendicular to the surface, 100-500μm in depth. The microstructure of the glass-ceramics was examined by scanning electron microscopy. Their dielectric and piezoelectric properties were studied.

1. Introduction

In the recent past, a new technique for preparing glass-ceramics with oriented crystallites of a polar phase has been investigated with the objective of fabricating inexpensive, large area sensor elements for application in pyroelectric detectors and piezoelectric devices[1-4]. Through a suitable thermal process, glass is converted to a glass-ceramic consisting of a grain-oriented polar crystalline phase in a glassy matrix. The macroscopic polarity thus developed gives rise to both piezoelectric and pyroelectric activity with markedly different properties from those of poled ferroelectric ceramics. Earlier studies have shown that these glass-ceramics are promising materials for piezoelectric resonators[2], hydrophones[5,6], pyroelectric devices[7], and surface acoustic wave (SAW) substrates[8].

Several glass-forming polar materials have been prepared in glass-ceramic form. Some of the systems studied include Li_2O-SiO_2, Li_2O-SiO_2-B_2O_3, BaO-SiO_2-TiO_2, BaO-GeO_2-TiO_2, and SrO-SiO_2-TiO_2. Among the crystalline phases recrystallized from the glasses are $Li_2Si_2O_5$, $Li_2B_4O_7$, $Ba_2TiSi_2O_8$, $Sr_2TiSi_2O_8$, and $Ba_2TiGe_2O_8$. One or more of these polar phases are obtained in the glass-ceramic, depending on the composition of the glass. The compositions of the glasses were optimized by compositional variations to obtain glass-ceramics with good physical properties[2,5].

Fresnoite ($Ba_2TiSi_2O_8$) single crystals are promising as SAW substrates, with its SAW properties intermediate between those of $LiNbO_3$ and $LiTaO_3$[9,10]. Modified fresnoite glass-ceramics have also been shown to be viable candidate materials for hydrophones[5,6] and SAW devices[8].

Recently, Ito and coworkers[11,12] have shown that the temperature coefficient of delay (TCD) of fresnoite single crystals can be lowered through the partial substitution of strontium for barium. Crystals of composition $(Ba_{2-x}Sr_x)TiSi_2O_8$ with uniform Sr concentration can be grown by edge-defined film-fed growth (EFG), for the compositions ranging from $x = 0$ to 0.8. Z-cut crystals with a strontium concentration of $x = 0.8$ gave a TCD value of 20 ppm/°C with practically no reduction in the SAW coupling coefficient(k_s^2), and look to be very useful for SAW devices.

In compositions with $x \geq 1.0$, $SrSiO_3$ and $SrTiO_3$ also crystallize along with the fresnoite phase, making it impossible to grow pure strontium titanate silicate single crystals by the usual crystal growing techniques. However, x-ray diffraction studies on

CH2358-0/86/0000-0406 $1.00

ceramic samples indicated that all compositions with x= 0 to 2.0 prepared by conventional ceramic processing techniques give single-phase fresnoite-type structure. The results indicated that Sr substituted for Ba, and a complete solid solution for the ceramics occurred.

In the present work, polar glass-ceramics in the $Ba_2TiSi_2O_8$-$Sr_2TiSi_2O_8$ solid solution system were prepared by recrystallizing the glasses. The microstructure, dielectric, and piezoelectric properties of these glass-ceramics are presented in this paper. Surface acoustic wave properties will be reported later.

2. Experimental Details

Glasses of compositions (2-x)BaO-xSrO-0.15CaO-2.9SiO_2-TiO_2 with x= 0.0, 0.2, 0.6, 1.0, 1.4, 1.8, 2.0 were prepared. Reagent grade $BaCO_3$, $SrCO_3$, $CaCO_3$, $SiO_2 \cdot nH_2O$, and TiO_2 were mixed by ball milling in an alcohol medium, and the mixture was dried. The batch was then melted in a platinum crucible in a globar furnace at 1430°C for 6-10 hours. The glass was poured into a graphite mold to form pellets about 1 cm in diameter and 7 cm thick. Glass samples were annealed at 500°C, well below the nucleation temperature to avoid bulk nucleation.

The typical heat-treatment cycle employed for crystallizing glasses is shown in Figure 1. The temperature was increased up to 500°C slowly and held there for one hour to avoid thermal shock. Then the temperature was raised to the crystallization temperature (950°C) quickly to minimize bulk nucleation. Glasses were crystallized at 950°C for two hours and cooled to 800°C, where they were held for six hours to anneal the glass-ceramics. The glass-ceramics were then slowly cooled to room temperature.

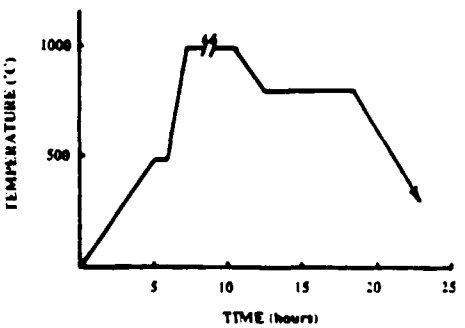

FIGURE 1 Recrystallization schedule for Ba-Sr fresnoite glass-ceramics

To examine the microstructure of the glass-ceramics, samples were polished and etched with 2% HF solution to reveal the oriented growth of crystallites. The samples were then studied using a scanning electron microscope.

For dielectric and piezoelectric measurements, samples in the form of circular disks, having dimensions of about 10 mm in diameter and 0.5 mm thick, were prepared by sectioning the oriented portion of the glass-ceramics. Gold electrodes were sputtered on the polished surfaces. The dielectric constants were calculated by measuring the capacitance of the samples using an LCR bridge*. The piezoelectric constant d_{33} parallel to the crystal growth direction was measured with a d_{33}-meter**. Electromechanical coupling factor was measured by the gain-bandwidth method as described by Holland and EerNisse[13].

3. Results and Discussion

SEM micrographs of selected glass-ceramic samples are shown in Figure 2. The length of the crystallites in the oriented region varied between 100 to 500 μm, with the length being less in glass-ceramics containing higher Sr concentration. Also, a slight curvature in the growth of the crystallites was observed in Sr-rich glass-ceramics.

The variation of the dielectric and piezoelectric properties of glass-ceramics with mole fraction of SrO is shown in Figures 3-6. The dielectric constant, K_{33}, is in the range 10 to 16, with the dissipation factor remaining very low near 0.1 %. As for the piezoelectric d_{33} coefficient, the range is 4 to 16 pC/N, with the composition 0.2BaO-1.8SrO-0.15CaO-2.9SiO_2-TiO_2 showing the highest d_{33}. This composition has a high piezoelectric g_{33} voltage coefficient (110 x 10^{-3} Vm/N) compared to PZT ceramics because of its low dielectric constant. The planar coupling coefficient, k_p, decreases with SrO whereas the planar frequency constant, N_p, is about 3500 m-Hz for all compositions.

* Hewlett-Packard 4274A LCR Meter
** Berlincourt d_{33}-meter, Channel Products (Model CPDT 3300)

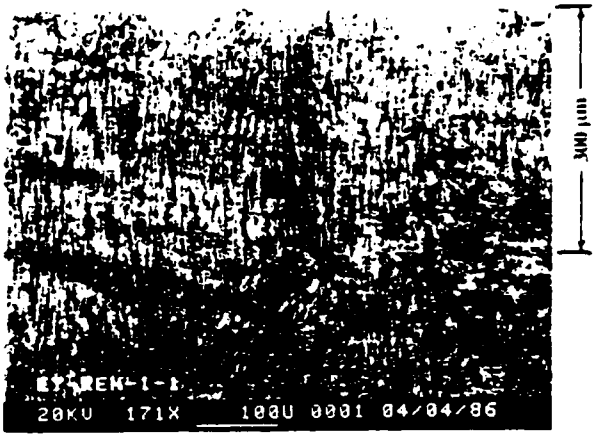

$2.0BaO \cdot 0.15CaO \cdot 2.9SiO_2 \cdot 1.0TiO_2$

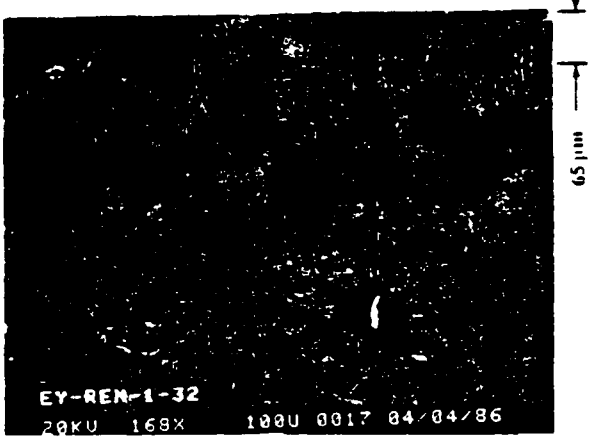

$1.0BaO \cdot 1.0SrO \cdot 0.15CaO \cdot 2.9SiO_2 \cdot 1.0TiO_2$

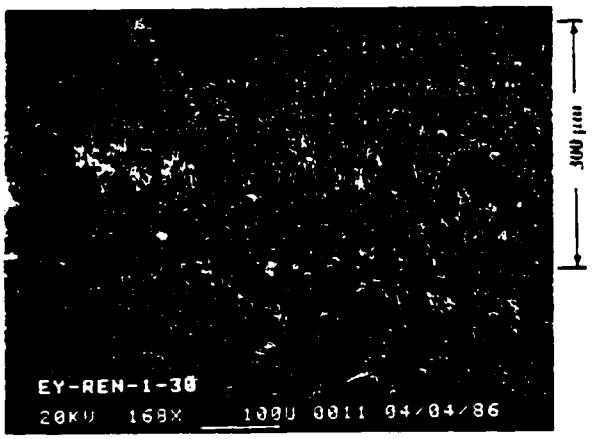

$0.2BaO \cdot 1.8SrO \cdot 0.15CaO \cdot 2.9SiO_2 \cdot 1.0TiO_2$

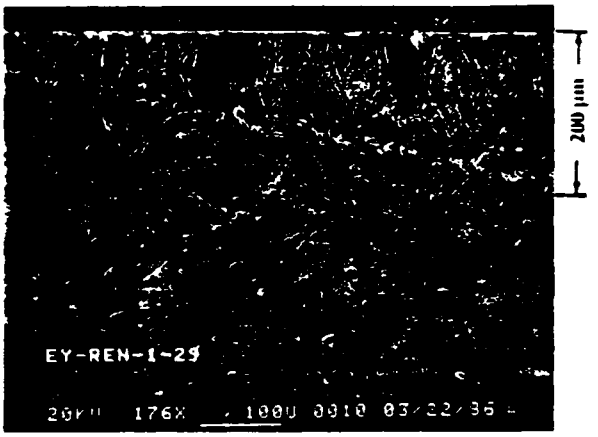

$2.0SrO \cdot 0.15CaO \cdot 2.9SiO_2 \cdot 1.0TiO_2$

FIGURE 2 SEM micrographs of the oriented region in Ba-Sr fresnoite glass-ceramics.

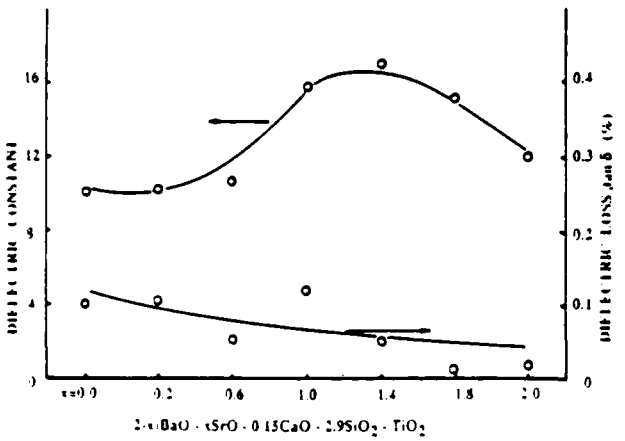

FIGURE 3 The dielectric constant, K_{33}, and the dissipation factor for Ba-Sr fresnoite glass-ceramics (1 kHz, room temperature).

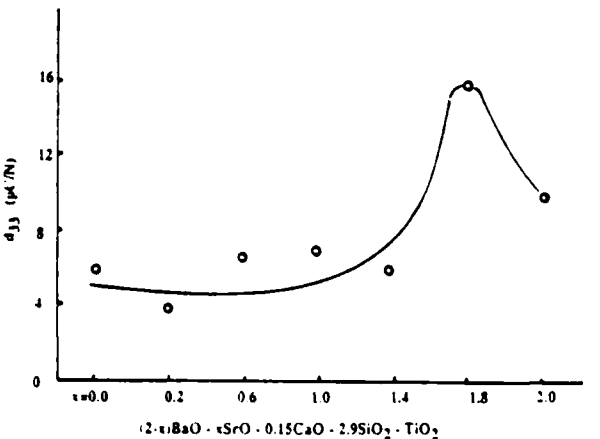

FIGURE 4 The piezoelectric constant, d_{33}, for Ba-Sr fresnoite glass-ceramics

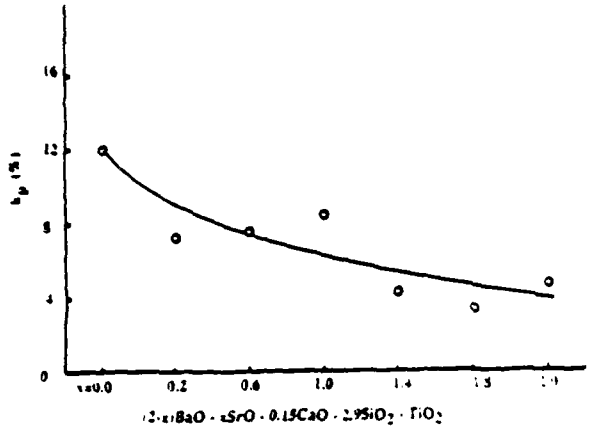

FIGURE 5 The planar coupling coefficient, k_p, for Ba-Sr fresnoite glass-ceramics.

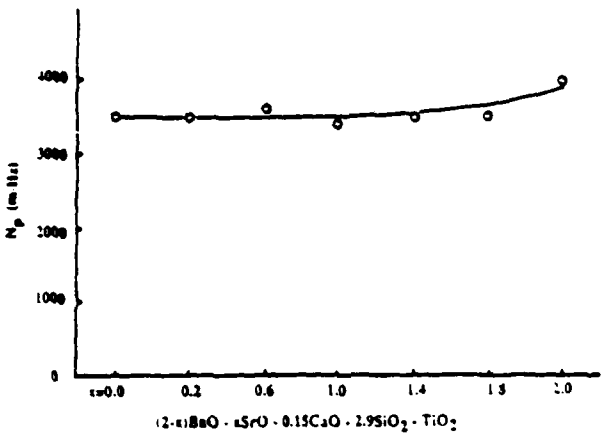

FIGURE 6 The planar frequency constant, N_p, for Ba-Sr fresnoite glass-ceramics.

From the present study, it is clear that we can prepare polar glass-ceramics in the fresnoite system, by replacing Ba with Sr, in the entire solid solution range. Although the length of the oriented crystallites and the planar coupling coefficient decrease with the addition of Sr, the piezoelectric d_{33} coefficient increases.

The surface acoustic wave properties of fresnoite glass-ceramics of composition 2.0BaO-0.15CaO-2.9SiO2-TiO2 have been reported[8]. This composition showed a SAW coupling coefficient of 1.1 % and a temperature coefficient of delay of 60 ppm/°C. In $Ba_{2-x}Sr_xTiSi_2O_8$ single crystals, a decrease in the TCD has been observed with the addition of Sr. We can expect a similar behavior in the modified fresnoite glass-ceramics. The surface acoustic wave properties of polar glass-ceramics in the Ba-Sr fresnoite system will be reported in the future.

4. Summary

Glass-ceramics in the $Ba_{2-x}Sr_xTiSi_2O_8$ solid solution have been prepared. The length of the oriented region ranged between 100 to 500um; glass-ceramics with higher Sr concentration had crystallites that exhibited curvature. The piezoelectric d_{33} coefficients were in the range 6 to 16 pC/N, and the planar coupling coefficients were in the range 12 to 6 %. The composition 0.2BaO-1.8SrO-0.15CaO-2.9SiO2-TiO2 showed a high piezoelectric g_{33} voltage coefficient (110x10^{-3} Vm/N). These glass-ceramics are useful for SAW devices.

Acknowledgments

This work was supported by the National Science Foundation Grant DMR-8303906.

REFERENCES

1. G.J. Gardopee, R.E. Newnham, and A.S. Bhalla, Ferroelectrics 33, 155 (1981).
2. A. Halliyal, A.S. Bhalla, and R.E. Newnham, and L.E. Cross, IEEE Ultrasonics Symposium, 315 (1981).
3. A. Halliyal, A.S. Bhalla, and R.E. Newnham, L.E. Cross, and T.R. Gururaja, J. Mater. Sci. 17, 295 (1982).
4. A. Halliyal, A.S. Bhalla, and R.E. Newnham, Mat. Res. Bull. 18, 1007 (1983)
5. A. Halliyal, A. Safari, A.S. Bhalla, R.E. Newnham, and L.E. Cross, J. Am. Ceram. Soc. 67, 331(1984).
6. R.Y. Ting, A. Halliyal, and A.S. Bhalla, Appl. Phys. Lett. 44, 852 (1984).
7. A. Halliyal, A.S. Bhalla, L.E. Cross, and R.E. Newnham, J. Am. Cer. Soc. (submitted)
8. C.W. Lee, L.J. Bowen, J.M. Browne, A. Halliyal, A.S. Bhalla, and E. Ylo,III, Proc. IEEE Ultrasonic Symposium, 285 (1984).
9. H. Yamauchi, J. Appl. Phys. 49, 6162 (1978).
10. J. Melngailis, J.F. Veaclino, A. Thunjunwala, T.B. Reed, R.E. Fahey, and E. Stern, Appl. Phys. Lett. 32, 203 (1978).
11. Y. Ito, K. Nagatsuma, and S. Ashida, Appl. Phys. Lett. 36, 894 (1980).
12. Y. Ito, K. Nagatsuma, and S. Ashida, Jap. J. Appl. Phys. 20, 163 (1981).
13. R. Holland and E.P. EerNisse, Trans. on Sonics and Ultrasonics 16, 173 (1969).

Phase Transitions, 1986, Vol. 7, pp. 1–8
0141-1594/86/0701-0001/$15.00/0
© 1986 Gordon and Breach Science Publishers, Inc.
Printed in the United Kingdom

TiO—Epoxy Composite Thermistors

K. A. HU, J. RUNT, A. SAFARI and R. E. NEWNHAM

Materials Research Laboratory, The Pennsylvania State University, University Park, PA 16802

(*Received October 9, 1985*)

TiO powder was incorporated into a rigid epoxy matrix to produce composite materials that exhibit unusually large PTC resistivity increases of up to ten orders of magnitude. The composites have a room-temperature resistivity (1–5 Ω-cm) that is comparable with commercial carbon-black-loaded polyethylene thermistors.

INTRODUCTION

Thermistors (temperature-dependent resistors) are used as temperature sensors, as protection against current or voltage surges, as flow meters and automatic gain elements. We have recently shown that composite thermistors consisting of VO_2, V_2O_3, VO or Ti_2O_3 in combination with various polymers exhibit unusually large positive temperature coefficient (PTC) effects. (Bueche, 1973) For example, the magnitude of the PTC anomaly for 56 volume percent V_2O_3 in an epoxy is approximately 9 orders of magnitude. (Bueche, 1973) compared with approximately 4–6 orders for commercial carbon black-loaded polyethylene thermistors. (Doljack, 1981) The best V_2O_3-epoxy composites have a room temperature resistivity of 10 to 20 Ω-cm, about the same as that of $BaTiO_3$ PTC ceramics (Herbert, 1982) but somewhat higher than the carbon black-loaded materials (~ 5 Ω-cm).

In order to lower the room temperature resistivity, we have explored TiO as a potential filler material. The room-temperature resistivity of single crystal TiO ($\sim 2 \times 10^{-4}$ Ω-cm) is at least an order of magnitude lower than the other transition metal oxide fillers we have examined previously. (Hu, Runt, Safari and Newnham, 1985) TiO-epoxy composites exhibited large PTC effects localized over a relatively narrow temperature range and resistivities at room temperature of 1–5 Ω-cm.

EXPERIMENTAL

The matrix for all composites described in this paper was a rigid epoxy ('Spurr' epoxy) obtained from Polysciences, Inc. The specific formulation is as follows:

10 gm. vinylcyclohexane dioxide
4 gm. diglycidyl ether of polypropylene glycol
26 gm. nonenyl succinic anhydride
0.4 gm. dimethylaminoethanol

Optical grade TiO (99 – % purity) was obtained from Alfa Products. The as-received powder (particle size ~ 850 μm) was ground to an average particle size of 25 μm. Composites containing 50 volume percent TiO were fabricated by mixing the epoxy precusrors and TiO and curing at either 85 or 100 C for 8 hours. Air-dry silver electrodes were used on all composites.

The d.c. resistivity of the composites was measured as a function of temperature (from 0 to 130 C) with a Keithley digital electrometer Model 616. a.c. resistivities were recorded over the same temperature range using a Hewlett-Packard Model 4274 LCR meter at 0.1 and 1 kHz.

RESULTS AND DISCUSSION

The a.c. resistivity as a function of temperature for the 50% TiO composite cured at 100 C is shown in Figure 1. The a.c. resistivity is only ~0.5 Ω-cm in the temperature range of 0 to 80 C, then increases sharply by about 8 orders of magnitude over a range of about 20 . The frequency dependence of the resistivity observed at high temperatures has been noted previously[5] and can be explained in terms of a Maxwell-Wagner effect resulting from the diphasic conductor-insulator nature of the composite. The d.c. resistivity at room temperature can be as low as 1-5 Ω-cm while the PTC anomaly can be as large as 10 orders of magnitude. Thus of all the transition metal oxides we have examined, TiO provides the most desirable composite thermistor properties.

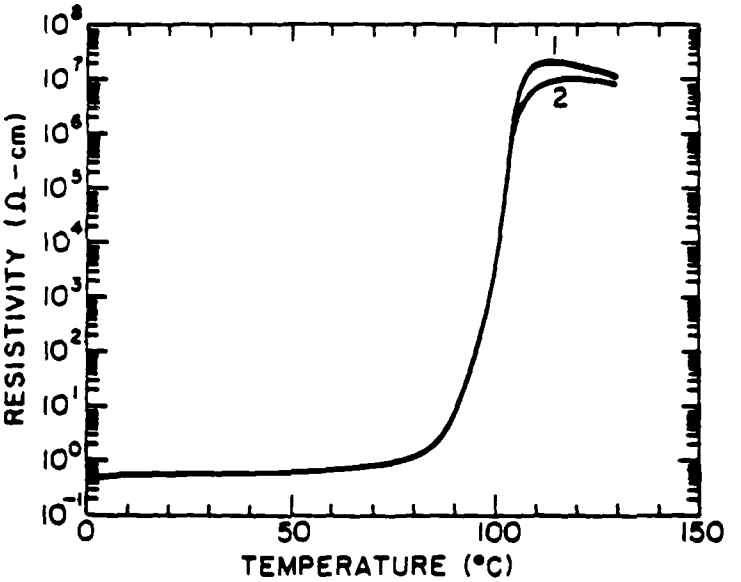

FIGURE 1 a.c. resistivity versus temperature for a 50 volume percent TiO-epoxy composite cured at 100 C. Curve 1 – 100 Hz, curve 2 – 1 kHz.

Finally, Figure 2 summarizes the reproducibility of a 50% composite cured at 100 C upon repeated cycling from 0 to 130 C. Room temperature resistivity increases slightly after the initial heating while the magnitude of the PTC anomaly remains effectively constant. Upon cycling an additional 30 times, one observes a more significant increase in room temperature resistivity (approximately an order of magnitude) and a slight drop in the magnituide of the PTC anomaly.

SUMMARY

Composites consisting of 50 volume percent TiO and a rigid epoxy were found to exhibit large PTC resistivity increases in the temperature range of 85 to 105 C. The magnitude of the PTC effect can be as large as 10 orders of magnitude. In addition, the room-temperature resistivity is considerably lower than $BaTiO_3$ PTC ceramics and comparable to commercial carbon-black filled polyethylene thermistors.

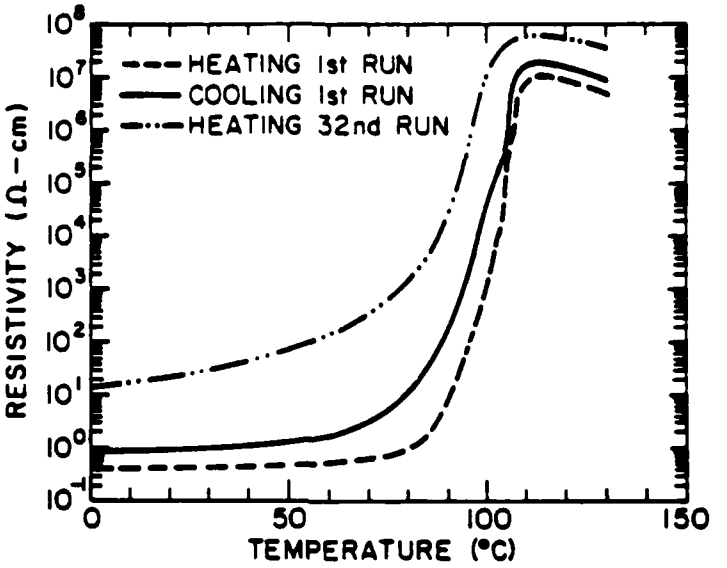

FIGURE 2 Reproducibility of resistivity–temperature behavior : repeated temperature cycling for a 50 volume percent TiO-epoxy composite : at 100 C. a.c. resistivities measured at 1 KHz

Acknowledgments

The authors would like to acknowledge the partial support of Dr. Louis Toth of NSF under the contract No. DMR 8512145 and Dr. Manfred Khan of NRL.

References

1. Hu, K. A., J. Runt, A. Safari and R. E. Newnham. Electroceramic-Polymer Composite Thermistors. (1985) *Ferroelectrics*. Submitted for publication.
2. Doljack, F. A. (1981) Polyswitch PTC Devices – A New Low-Resistance Conductive Polymer-Based PTC Device for Overcurrent Protection. *IEEE Trans. Comp., Hybrids, Manufact. Tech.*, **4**, 372.
3. Herbert, J. M. (1982). *Ferroelectric Transducers and Sensors*. Ch. 5. Gordon and Breach, New York.
4. Morin, F. J. (1959) Oxides Which Show a Metal-to-Insulator Transition at the Neel Temperature. *Phys. Rev. Lett.*, **3**, 34.
5. Bueche, F. (1973) A New Class of Switching Materials. *J. Appl. Phys.*, **54**, 532.

V_2O_3 COMPOSITE THERMISTORS

D. Moffatt, J. Runt, A. Safari, R. E. Newnham

Materials Research Laboratory
Pennsylvania State University
University Park, PA 16802

Abstract

The semiconductor to metal phase transition found in vanadium (III) oxide, V_2O_3, was incorporated into a composite thermistor which exhibits an NTC as well as a PTC resistance effect. The composites were prepared using V_2O_3 and several polymers including a flexible epoxy, a polyurethane and crystalline polyethylene. These composites showed large PTC resistivity effects of up to eight orders of magnitude. Depending on the type of polymer chosen, the transition temperature at which the PTC phenomenon occurs can be changed. In addition, an NTC effect was observed at the temperature of the semiconductor to metal transition of the metal oxide filler. The resistivity versus temperature curve resembles a square well with three different conducting ranges: semiconductor to metal to insulator. Finally, the percolation curves for polyethylene composites were found to be a function of filler particle size.

1. Introduction

A thermistor is a temperature dependent resistor that can be used in such applications as temperature sensors, flow meters, and protection devices against current or voltage surges. Potential thermistor materials are ones that exhibit a large change in resistivity with temperature. These include doped $BaTiO_3$[1] and composites consisting of carbon black [2] or transition metal oxides (such as TiO, VO_2, and V_2O_3) [3,4].

Doped $BaTiO_3$ ceramics show a large positive temperature coefficient (PTC) of resistance and have been widely used. However, they are limited by their relatively high room temperature resistivity (~100 Ω - cm) [1] and high manufacturing costs. An alternative composite material consisting of carbon black- loaded crystalline polymers (such as polyethylene) have proven successful. These composites exhibit a modest PTC as well as low room temperature resistivity (~ 1-5 Ω - cm).

An important concept often used to describe the behavior of metal-insulator composites is percolation. This allows one to understand the change in resistivity as a function of volume percent filler in such composite materials. The percolation threshold is defined as the filler volume fraction at which the resistivity, indicative of the insulating phase, begins to decrease (see Figure 1). This is associated with the point at which the filler particles begin to form conductive paths. As the concentration of filler is increased through the percolation region, more conductive paths are created through the composite. This region of filler concentration is where one would expect to see the largest PTC effects. Once the saturation region is reached, there are a large number of conductive paths, resulting in low resistivities. In addition, this is the region in which one would normally expect the PTC phenomenon to diminish.

For metal-insulator composites where the insulating phase is a crystalline polymer (such as polyethylene or a nylon), the PTC phenomenon is generally observed at the polymer melting point (T_m). At T_m, there is a discontinuous change in the specific volume with temperature and the magnitude of the change is a function of the degree of crystallization of the polymer. At room temperature the filler particles are essentially in contact, giving rise to a low resistivity. As the temperature increases, a large change in volume occurs at the melting point of the polymer. The polymer expands more quickly than the conductive particles, separating the grains and resulting in a rapid increase in resistivity of between 1 and 8 orders of magnitude [5,6].

Very little work has been done on the PTC effects in metal-insulating composites consisting of amorphous polymer matrices. As pointed out by Voet [2] a strong PTC effect in such composites is usually not anticipated, except when the filler concentration is in the critical range. In this range a major resistivity change results from minor changes in interparticle distances.

In this paper we review some of our recent research on a new class of composite thermistor. Transition metal oxide/ polymer composites have been fabricated with a variety of conducting oxides. Here, we focus on vanadium (III) oxide (V_2O_3) / polymer composites. In combination with amorphous or crystalline polymers, V_2O_3 composites exhibit both large NTC (negative temperature coefficient) and PTC effects.

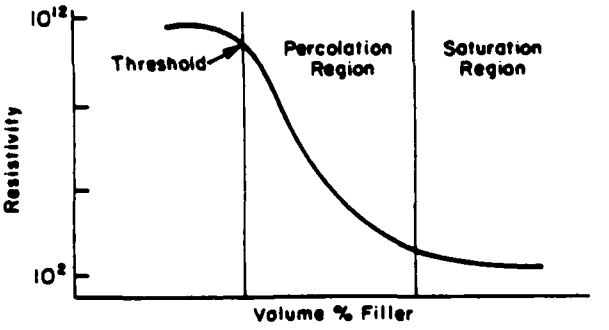

FIGURE 1: A typical percolation curve which relates resistivity to volume percent filler in the composite.

0353-0673/86/0000-0673 $1.00

2. Experimental Procedure

Two types of vanadium (III) oxide, V_2O_3, were used in our research. The first, a powder supplied by Alfa Products, had rod-like particles with an average length-to-width ratio of 3.13 and an average size of approximately 1.3 by 4.1 μm. The second powder, V_2O_3 obtained from Aldrich Chemical Company, also consisted of rod-like particles with a length-to-width ratio of 3.85 and an average size of about 0.8 by 3.4 μm. From all indications, the chemical composition of each powder was identical. These two powders were combined with a number of amorphous and crystalline polymers such as a flexible epoxy (Eccogel 1365-45, obtained from Emerson - Cuming; T_g ~ -30°C), a polyurethane (obtained from Dexter Hysol; T_g ~ 15°C), and polyethylene (T_m~130°C). The composites containing the amorphous polymers were mixed for 30 minutes and pressed at room temperature for two minutes at 12,000 psi. The epoxy composites were cured at 80°C for 18 hours while those with polyurethane were cured at 85°C for two hours. Composites made with the semi-crystalline polymer polyethylene were mixed in a Brabender mixer at 140°C for 20 minutes and hot pressed for 30 minutes at ~200°C. All samples were polished and sputtered gold electrodes were applied. Finally, a.c. resistivity as a function of temperature was measured at 1000 and 10000 Hz using an Hewlett Packard 4274A Multi-Frequency LCR Meter over a temperature range of -150 to 150 °C.

3. Results and Discussion

Figure 2 shows the percolation threshold for the Aldrich V_2O_3 / polyethylene composites to be located at about 10 - 15 volume percent filler. In addition, the percolation region extends from approximately 10 to 30 volume percent. The individual measurements of resistivity versus temperature are illustrated in Figure 3. The 30, 40, and 50 volume percent samples exhibited relatively large PTC phenomena located near the T_m of polyethylene. This phenomenon decreases and disappears at concentrations less than about 20 volume percent. The room temperature resistivity for the highest filler concentration is 30 to 40 Ω - cm. At V_2O_3 concentrations greater than about 30 volume percent, the magnitude of the PTC is 7 to 8 orders.

The corresponding plots for the Alfa powder are shown in Figures 4 and 5. The percolation threshold is higher for this V_2O_3, located near 20 - 25 volume percent. In contrast to the Aldrich powder, the saturation region begins at 40 volume percent. Room temperature resistivity (50 - 60 Ω - cm) and PTC intensity (~8 orders of magnitude) are very similar to those found in the Aldrich / polyethylene composites. Again, large PTC effects are observed for concentrations greater than 30 volume percent but are basically absent for those equal to or less than this concentration. The general character of the resistivity versus temperature curves do not change from one powder to the other.

Figure 6 shows the relationship between composites prepared with 50 volume percent of the Alfa V_2O_3 and two amorphous polymers, a flexible epoxy and a polyurethane, as described in the experimental section. For the epoxy composite, the PTC is more dramatic, occurs near room temperature, and has an intensity of ~5 orders of magnitude. The room temperature resistivity is relatively high, however this corresponds to an area within the PTC transition. The resistivity at temperatures less than 0°C is near 10^3 Ω -cm, which is considerably larger than polyethylene composites of the same volume fraction. The polyurethane composite, on the other hand, has a broader PTC transition centered near 75°C (~ 4 orders in magnitude). Clearly, the resistivity versus temperature curves for the various composites show a significant variation in transition temperature and overall character as a function of polymer type.

For the two amorphous polymers, the PTC temperature seems to scale with the glass transition temperature (T_g). However, previous work suggests that there appears to be no correspondence between T_g and the location of the PTC transition [3,4].

The resistivity versus temperature response for the polyurethane and epoxy composites also illustrates the low temperature NTC effect found in many transition metal oxide composites [3,4]. For V_2O_3, there is a semiconductor to metal phase transition that occurs at about -100°C that corresponds to a change in shape of the lattice and a delocalization of the electrons. The location of the NTC is approximately the same for both polyurethane and epoxy composites, but there is some difference in magnitude. The resulting resistivity curve, especially in the case of the epoxy composite, has a square well shape. In addition to the low temperature NTC, an NTC effect is also observed at temperatures above the PTC transition. This decrease in resistivity follows a path similar to that of the pure polymers.

For comparative purposes, the resistivity versus temperature behavior of a 50 volume percent polyethylene composite is also shown in Figure 6. The PTC transition for the polyethylene composite occurs over a narrow temperature range compared to that of the amorphous polymers. In addition, although not seen in this figure, the V_2O_3 / polyethylene composites exhibit an NTC transition at about -100°C, similar to the other composites. A dramatic NTC above the PTC transition temperature is also observed (not shown); however, this can be eliminated by crosslinking the polyethylene [3]. Note that the polyurethane and epoxy composites are crosslinked initially.

With crystalline polymer matrices, the mechanism of the PTC phenomenon is generally associated with the melting of the polymer and consequent large volume change. However, note that for the polyurethane and epoxy composites, as well as composites with other non-crystalline matrices [3, 4], that the PTC is observed at filler concentrations which are well above the region normally associated with observations of large PTC effects in amorphous polymer composites. If the PTC is believed to be a result of thermal expansion, one would not expect to see the PTC phenomenon over such a wide range of filler concentrations. Further work is in progress to help us understand more clearly the nature of the PTC effect in these metal oxide / amorphous polymer composites.

4. Conclusions

Significant NTC and PTC resistance effects were observed for V_2O_3 composites prepared with both amorphous and crystalline polymers. The location of the PTC phenomenon is determined by the choice of polymer matrix. Two types of V_2O_3 have been utilized to illustrate that the characteristics of the powder influence the resistivity behavior. Finally, the mechanism for the crystalline polymer composites appeared to be due to thermal expansion, as evidenced by the sharp PTC transition at the melting point of polyethylene. A similar conclusion concerning amorphous polymer composites can not be assumed.

5. Acknowledgments

The authors would like to thank the National Science Foundation (grant no. DMR-8512147) and the Naval Research Laboratory (grant no. N00014-86-C-2028) for their support of this work.

6. References

[1] W. Heywang, "Resistivity Anomaly in Doped Barium Titanate", J. Am. Ceram. Soc., 47 (10), 484, (1964).

[2] A. Voet, "Temperature Effect of Electrical Resistivity of Carbon Black Filled Polymers", Rubber Chemistry and Technology, 54, 42, (1980).

[3] K.A. Hu, J. Runt, A. Safari, and R.E. Newnham, "Electroceramic - Polymer Composite Thermistors", Ferroelectrics, In Press.

[4] K.A. Hu, J. Runt, A. Safari, R.E. Newnham, "Composite Thermistors", Mater. Sci. Res. Ser., In Press.

[5] J. Meyer, Polym. Eng. Sci., 133, 42 (1973).

[6] M. Narkis, A. Ram, and F. Flashner, "Resistivity Behavior of Filled Electrically Conductive Crosslinked Polyethylene", Polym. Eng. Sci., 18, 459, (1978).

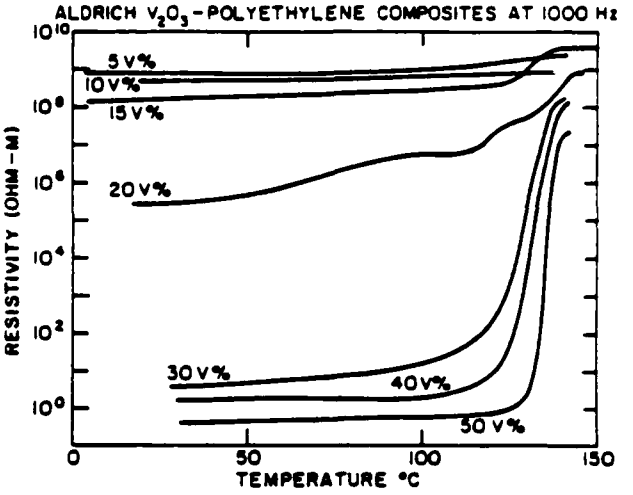

FIGURE 3: Resistivity versus temperature behavior at 1000 Hz for several different compositions of Aldrich V_2O_3 / polyethylene composites.

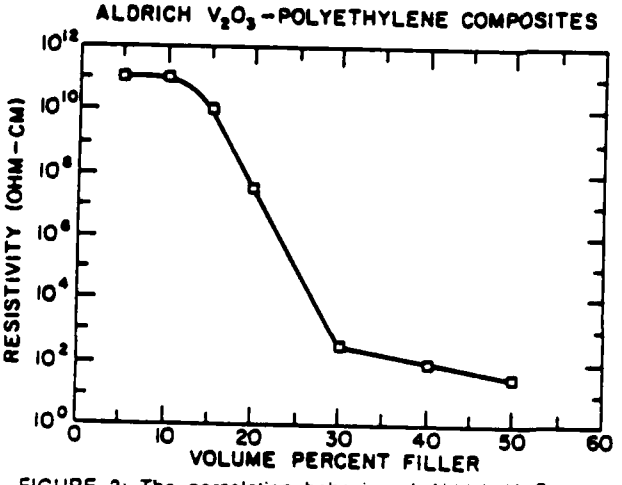

FIGURE 2: The percolation behavior of Aldrich V_2O_3 / polyethylene composites.

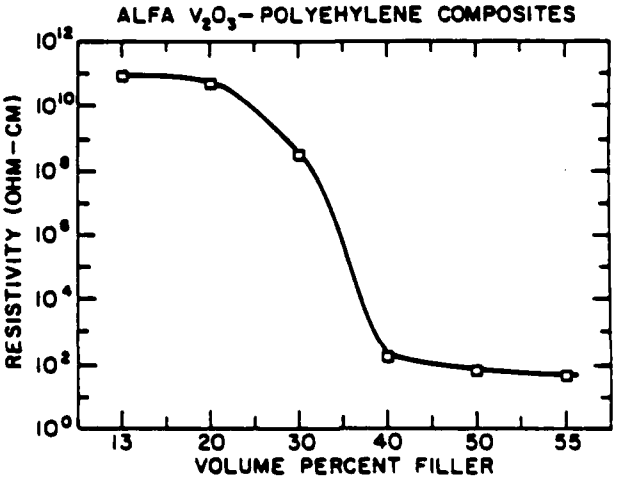

FIGURE 4: The percolation behavior of Alfa V_2O_3 / polyethylene composites.

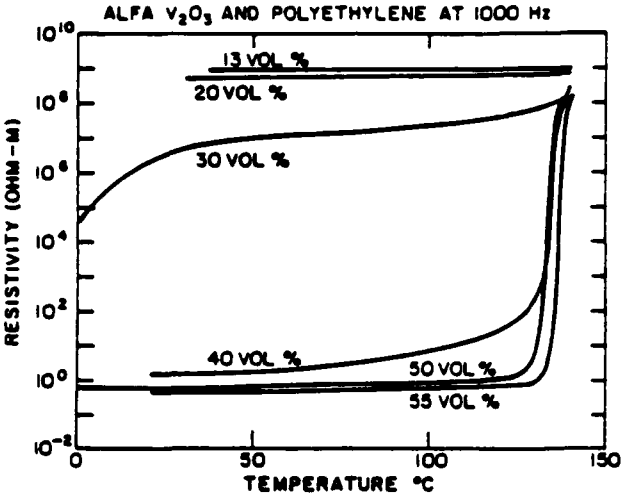

FIGURE 5: Resistivity versus temperature behavior at 1000 Hz for several different compositions of Alfa V_2O_3 / polyethylene composites.

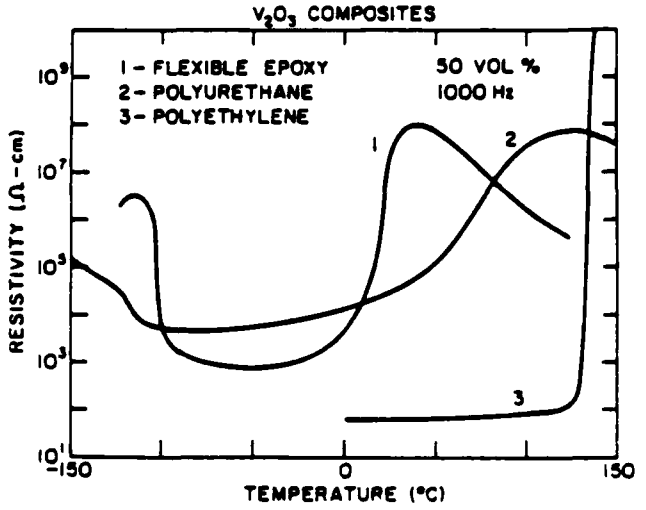

FIGURE 6: Resistivity versus temperature behavior for two types of Alfa V_2O_3 / amorphous polymer composites and Alfa V_2O_3/ polyethylene composites.

ELECTROSTRICTIVE MATERIALS

COMPLETE DETERMINATION OF ELECTROSTRICTION TENSOR COMPONENTS OF $KMnF_3$ SINGLE CRYSTALS AT ROOM TEMPERATURE

Y. Sun*, W.W. Cao, W.Y.Pan, Z.P.Chang, and L.E.Cross¶

Materials Research Laboratory
The Pennsylvania State University
University Park, PA 16802 U.S.A.

*: Also affiliated with Department of Physics.
¶: Also affiliated with Department of Electrical Engineering.

Electrostriction is the basic electromechanical coupling effect in centric crystals, and is therefore of considerable fundamental interest. When it is remembered that the very widely used $PbZrO_3$-$PbTiO_3$ poled ceramic piezoelectric transducers are in effect polarization biased electrostrictors, the phenomenon also becomes of very strong practical importance. Taking the first steps towards an atomistic understanding of the electrostriction effect, Achar et al. (1981) in this laboratory, applied the shell model to the incipent ferroelectric and improper ferroelastic perovskite $SrTiO_3$. For this crystal overall agreement with theory was not good, even though the trend of the temperature dependence is correct, Achar and Barsch (1987). A possible reason for the discrepancy was suggested to be in the large anisotropic polarizability of the oxygen ion. To test this hypothesis it is clearly desirable to move to a non-oxide perovskite and part of the reason for this study was to provide experimental data to test this hypothesis. The crystal chosen for study is potassium manganese fluoride $KMnF_3$, one of the most widely studied of the halide perovskites. For this crystal the second and third order elastic constants have been measured as a function of temperature, Cao (1987), necessary input data for the shell model calculation. A further advantage to chosing $KMnF_3$ is the possibility it affords to study the influence of the improper ferroelastic phase change upon the electrostriction behavior. In many ways this study could be complementary to that of the perovskite oxides which encompass ferroelectric phase changes. The ultimate goal might be to combine soft electrical and mechanical modes in a single material so as to enhance the strain and reduce stress concentration for efficient electrically controlled high strain actuators.

In centric materials, odd rank tensors vanish according to Neumann's principle. Using the elastic Gibbs free energy function with stress (denoted as X), electric field (E), and temperature (T) as the independent variables, one can derive the following in heuristic notation

$$x = s X + M E E$$
$$D = \varepsilon_0 K E + 2 M E X = (\varepsilon_0 K + 2 M X) E$$

One can also use stress and polarization (P) as the independent variables and obtains

$$x = s X + Q P P$$

For cubic symmetry, Q and M are related by

$$Q = M \frac{1}{[\varepsilon_0 (K - 1)]^2}$$

M is mostly used by electrical engineers, which tells how much strain is developed under unit electrical field. On the other hand, Q is used by physicists, which tells how much strain is developed by introducing polarization in the materials. As the electrostriction coefficient M appears in both equations for x and D, two methods for measuring the electrostriction coefficients are possible--the direct method and the converse method. The direct method is to measure the electrically induced strain. The widely used experimental techniques include the strain gage method and the ultrasensitive dilatometer method which employs either a Michelson interferometer, Zhang, Pan et al (1987) or a capacitor dilatometer, Uchino and Cross (1980[1]). The strain gage method is only sensitive to large strain but to minute strain. The dilatometer method is well suited for the oxide perovskite based materials which have large M coefficients. However, it becomes extremely difficult for low permittivity materials such as $KMnF_3$ with small M coefficients, because one has to avoid the mechanical resonance induced in the specimen holder and must perform measurements under very low electrical and mechanical noise environment. On the other hand, the converse method is to measure the minute changes in the dielectric permittivity in the materials induced by external mechanical stresses, where the difficulty is to make the precise measurements of dielectric permittivity. The General Radio 1621 precision capacitance measurement system does provide sufficient sensitivity and stability to handle this problem. Generally the converse method is easier and more stable than the direct method. For the direct method the equation is

$$2 M_{ijkl} = \frac{\partial^2 x_{ij}}{\partial E_K \partial E_l}$$

while for the converse method

$$2 M_{ijkl} = \frac{\partial \varepsilon_{kl}}{\partial X_{ij}}_E$$

where ε_{kl} are the dielectric permittivity components. Since the measurable quantity is the capacitance

$$C = \frac{\varepsilon_0 K A}{d}$$

one obtains

$$\frac{\partial \ln C}{\partial X} = \frac{\partial \ln K}{\partial X} + \frac{\partial \ln (A/d)}{\partial X}$$

The two terms on the right side are denoted as

$$B_i = \frac{\partial \ln K}{\partial X}$$

$$S_i = \frac{\partial \ln (A/d)}{\partial X}$$

B_i and S_i are respectively linear combinations of the electrostriction coefficients and linear combinations of compliance tensor components. Both B_i and S_i depend on the crystal orientations, which are denoted by the subscript i. For convenience, the Voigt notation is used on the second order tensor. $KMnF_3$ has m3m symmetry. Therefore a second order tensor such as the electrostriction tensor M has the following form

$$M = \begin{bmatrix} M_{11} & M_{12} & M_{12} & 0 & 0 & 0 \\ M_{12} & M_{11} & M_{12} & 0 & 0 & 0 \\ M_{12} & M_{12} & M_{11} & 0 & 0 & 0 \\ 0 & 0 & 0 & M_{44} & 0 & 0 \\ 0 & 0 & 0 & 0 & M_{44} & 0 \\ 0 & 0 & 0 & 0 & 0 & M_{44} \end{bmatrix}$$

where M_{11}, M_{12}, and M_{44} are in matrix notation and are related to tensor notation by $M_{11} = M_{1111}$, $M_{12} = M_{1122}$, and $M_{44} = 4M_{1212}$. Samples in disk form were prepared with the major faces (100), (110), and (111). Uniaxial stress was applied perpendicular to the major faces of the disk.. From Preu and Haussuhl (1983), the effective electrostriction coefficients are

$$M'_{100} = M_{11} = \frac{\varepsilon_0 K}{2}[\frac{1}{C}(\frac{\partial C}{\partial X}) + (s^T_{11} + 2s^T_{12})],$$

$$M'_{110} = \frac{1}{2} M_{11} + \frac{1}{2} M_{12} + \frac{1}{4} M_{44} = \frac{\varepsilon_0 K}{2}[(\frac{1}{C} \frac{\partial C}{\partial X})_{110} + \frac{1}{2} (s^T_{44} - 2s^T_{12})],$$

$$M'_{111} = \frac{1}{3} M_{11} + \frac{2}{3} M_{12} + \frac{1}{3} M_{44} = \frac{\varepsilon_0 K}{2}[(\frac{1}{C} \frac{\partial C}{\partial X})_{111} + \frac{1}{3} (2s^T_{44} - s^T_{11} - 2s^T_{12})]$$

If the sample is under hydrostatic pressure, the appropriate coefficient is

$$M_h = M_{11} + 2M_{12} = \frac{\varepsilon_0 K}{2}[(- \frac{1}{C} \frac{\partial C}{\partial p}) - (s^T_{11} + 2s^T_{12})]$$

The s^T_{ij}'s are isothermal elastic compliances, which are calculated from the adiabatic elastic constants measured by the ultrasonic pulse superposition technique, Cao (1987).

There have been several uniaxial stress compressometers for the electrostriction measurements, Meng and Cross (1984), Preu and Haussuhl (1983). Typically single crystal disks having geometry of diameter/thickness being 23 mm/1.5 mm were prepared. Then gold sputtering or aluminum evaporation technique is used to make electrodes on the surfaces of samples. A guard ring electrode is used to prevent an apparent enhancement in the dielectric permittivity due to the fringe field. However, to be effective, the width of the guard should be at least twice as large as the thickness. For a 23 mm/1.5 mm geometry the guard should be 3.5 mm wide.

Unfortunately the $KMnF_3$ single crystal is very fragile. The crystal can easily crack in the process of cutting and polishing and also under stresses. To surmount this problem, smaller single crystals about 9 mm in diameter and 2.0 mm in thickness are used--not too thin to crack under mechanical stresses. However, this leaves little room for the guard ring; therefore one makes the electrode covering the whole surfaces. It will be shown in the discussion that such two terminal geometry is also adequate for converse electrostriction measurements on $KMnF_3$.

The uniaxial compressometer built by Meng and Cross (1985) was modified. A schematic drawing of the compressometer and associated equipment is shown in Fig. 1. For measurement of the capacitance, a General Radio 1621 capacitance measuring system was used. In the figure are shown the main parts of the sample holder and the system for stress application. The system is designed to keep the pressure homogeneous and strictly uniaxial, the temperature stable for the period of measurement, and mechanical vibration isolated. The connections to the sample capacitance terminals are completely electrically shielded. The uniaxial stress is derived from a dead weight and is applied to the sample through a suitable lever arm. In the pressure cell, ram extenders are used, which are made of ordinary glass and cut strictly in the same diameter as the sample. A very thin mylar gasket is used between the bronze anvil and the ram surfaces to take up any surface roughness. Elaborate temperature control was found unnecessary for the system since the thermal capacity of the massive stressing jig was sufficient to smooth out any temperature fluctuations in the ambient in the already temperature controlled room.

The $KMnF_3$ single crystals were grown by a modified Bridgman method. The starting materials KHF_2 and MnF_2 in stoichiometric proportion were pre-heated at 350 ^{o}C for 6 hours. The diameter/thickness dimensions of the samples for (100), (110), and (111) orientations are, respectively, 9.13 mm/2.27 mm, 7.45 mm/1.64 mm, and 7.45 mm/ 1.45 mm. The results are shown in Fig. 2 and summarized in Table 1. The electrostriction measurements were made under reasonable stress loadings well inside the elastic limit of $KMnF_3$ single crystals. The value Q_h $=0.22\ M^4C^{-2}$ (having (X, D) as independent variables)is taken from Uchino, Cross, et al (1984) so as to give a check on the present measurements. M_{11}, M_{12}, and M_{44} are calculated by a least square fit, the fitting error is found to be less than 0.8%.

It can be concluded from the following four arguments that the present sample geometry gives reliable results. First a linear dependence of $\Delta C/C$ on the stress X was obtained. Second, the

capacitance was found to be decreasing with stress, which is opposite to the influence of the fringe field. The fringe field would rather increase the capacitance when a uniaxial stress is applied. Therefore the fringe field effect is at least not dominant. Third, the present data agree well (i.e., within 0.8%) with the Q_h value in the literature. Finally, the measurements on two (111) were made. One with 3 terminals and 23 mm/1.5 mm in diameter /thickness geometry, and the other with 2 terminals and 7.44 mm/1.5 mm geometry. The results of these two measurements agree well with each other within 13%.

In Table 2 the electrostriction coefficients are summarized. As can be seen, and compared with data for other compounds, the electrostriction coefficients are very much structure dependent; those of the fluorites CaF_2, BaF_2, and SrF_2 are very much alike, and so are those of the perovskites. However, the magnitude of electrostriction coefficients Q's depends upon the ionic charges. The larger the ionic charge, the smaller the magnitude of electrostriction coefficients Q--this is reasonable because if one assumes that a certain ionic shift causes the same elastic strain in fluorides and oxides on the basis of an intuitive "ion rattling" model, then the electrostriction Q coefficients in fluorides are expected to be larger because the lower valencies in fluorides result in smaller induced polarizations.

A number of neutron scattering, Gesi et al (1972) and ultrasonic experiments, Furukawa et al (1970) have been made around the improper ferroelastic phase transition at 186 K of $KMnF_3$, which gives information on the dynamics of the soft mode involving the tilting of the MnF_6-octahedra. It is interesting to measure the temperature dependence of the electrostriction coefficients in order to determine the influence of the ferroelastic phase transition on the electrostriction effect. This work is now under way.

The authors gratefully acknowledge the suggestion and guidance provided by Professor G.R. Barsch. This work has been supported by the Office of Naval Research under Contract No. N00014-82-K-0339.

References

Achar, B.N.N., Barsch, G.R., and Cross, L.E., Phys. Rev. B24 (1981) 1209.

Achar, B.N.N. and Barsch, G.R., to be published (1987).

Cao, W.W., Ph.D. thesis, the Pennsylvania State University (1987).

Furukawa, Minoru, et al, J. Phys. Soc. Jpn. 29 (6) (1970) 1528.

Gesi, K., Axe, J.D. and Shirane, G., Phys. Rev. B. 5 (5) (1972) 1933.

Meng, Z.Y. and Cross, L.E., J. Applied Phys., 57 (2) (1985) pp488-491.

Meng, Z.Y., Y.M. Sun and Cross, L.E., Materials Lett. Vol.12, No. 6A & B (1984) pp544-546.

Preu, P. and Haussuhl, S., Solid State Comm.45 (7) (1983) pp619-623.

Uchino, Kenji and Cross, Leslie E., Ferroelectrics 27 (1980[1]) pp35-39.

Uchino, Kenji, Cross, L.E., et al, Phys. Rev. B 29 (12) (1984) pp6921-6925.

Uchino, K., Cross, L.E., et al, J. Applied Physics 51 (2) (1980^2) pp1142-1145.
Zhang, Q.M., Pan, W.Y., et al, to be published (1987).

Table 1. Experimental results of $KMnF_3$ single crystals.

	$1/C\,(\partial C/\partial X)_i$ ($10^{-11}Pa^{-1}$)	S_i ($10^{-11}Pa^{-1}$)	M_i ($10^{-21}M^{-2}V^2$)
(100)	4.708	-1.596	2.723
(110)	4.416	-2.118	2.712
(111)	4.087	-2.293	2.756

Table 2. Electrostriction coefficients of single crystals.

	M_{11}	M_{12}	M_{44}	M_h	Q_{11}	Q_{12}	Q_{44}	Q_h
$KMnF_3$	2.72	-.538	6.58	1.64	.453	-.0896	1.10	.274 *
$BaTiO_3$					.11	-.045		.02 **
CaF_2 ¶	-1.32	1.17	5.07	1.02	-.508	.450	1.95	.392
SrF_2 ¶	-1.16	1.09	5.38	1.02	-.331	.311	1.53	.291
BaF_2 ¶	-1.07	1.23	5.94	1.39	-.340	.390	1.88	.441

M cofficients are in unit of 10^{-21} $M^{-2}V^2$ and Q in M^4C^{-2}.
*: from Uchino, et al , 1984.
**: from Uchino ,et al, 1980[2].
¶: from Meng, Sun and Cross, 1984.

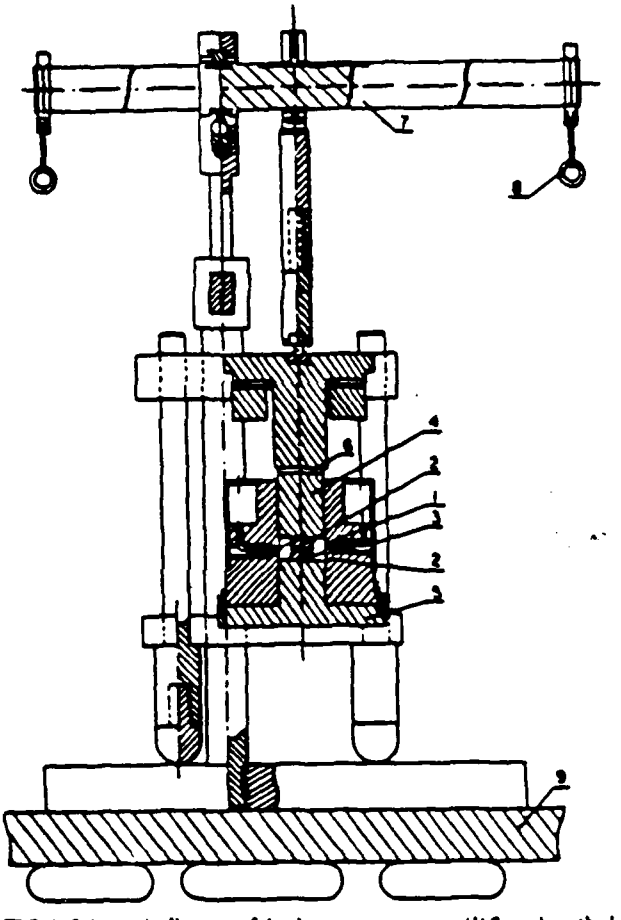

FIG. 1. Schematic diagram of the dc compressometer. (1) Sample with electrodes, (2) stress transmitting ram extenders, (3) coaxial lead, (4) metal rod, (5) metal block, (6) Teflon plate, (7) lever system, (8) dead weight, (9) vibration isolation table.

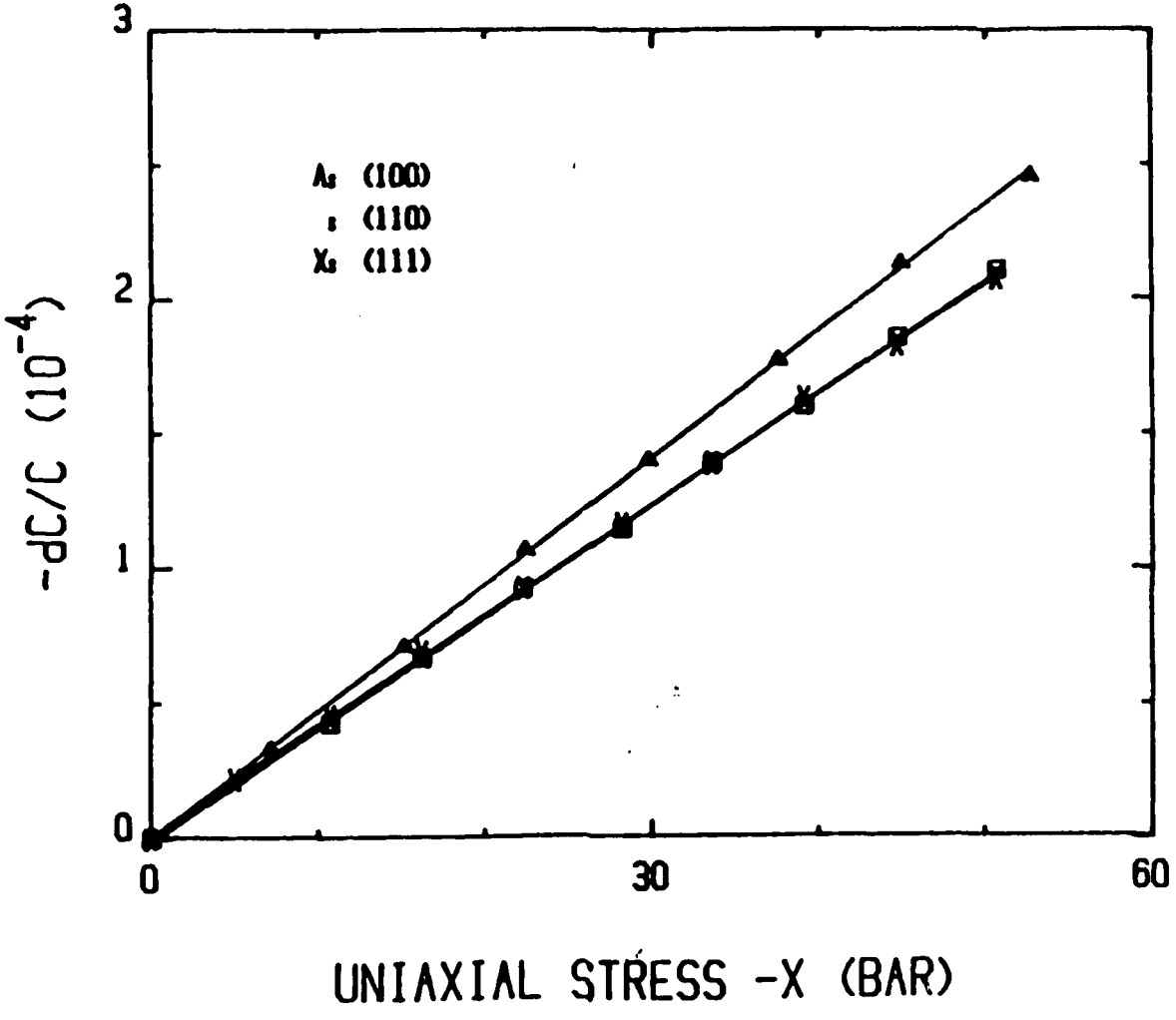
3
2
1
0
0
30
60
-dC/C (10^{-4})
UNIAXIAL STRESS -X (BAR)
As (100)
s (110)
Xs (111)

NORTH-HOLLAND
PHYSICS
PUBLISHING

ELECTROSTRICTION EFFECT IN GLASS

Y. SUN, W.W. CAO and L.E. CROSS

Materials Research Laboratory, The Pennsylvania State University, University Park, PA 16802, U.S.A.

Received 18 February 1986; in final form 10 March 1986

The longitudinal electrostriction tensor component Q_{11} in polarization notation and M_{11} in electric field notation for sodium trisilicate glass and sodium aluminosilicate glass has been measured by the converse method, i.e. by measuring the slope of the uniaxial stress dependence of the dielectric constant at various frequencies. For sodium trisilicate glass, the Q_{11} coefficient strongly depends on the frequency at which the capacitance was measured and shows a maximum near the frequency of 150 Hz, which is the ionic relaxation frequency of the glass. For sodium aluminosilicate glass, the relative change in the dielectric constant in response to a uniaxial stress was, however, found to be much smaller. We construct a sodium ion hopping model to explain qualitatively the results.

Reprinted from MATERIALS LETTERS

ELECTROSTRICTION EFFECT IN GLASS

Y. SUN, W.W. CAO and L.E. CROSS

Materials Research Laboratory, The Pennsylvania State University, University Park, PA 16802, USA

Received 18 February 1986, in final form 10 March 1986

The longitudinal electrostriction tensor component Q_{11} in polarization notation and M_{11} in electric field notation for sodium trisilicate glass and sodium aluminosilicate glass has been measured by the converse method, i.e. by measuring the slope of the uniaxial stress dependence of the dielectric constant at various frequencies. For sodium trisilicate glass, the Q_{11} coefficient strongly depends on the frequency at which the capacitance was measured and shows a maximum near the frequency of 150 Hz, which is the ionic relaxation frequency of the glass. For sodium aluminosilicate glass, the relative change in the dielectric constant in response to a uniaxial stress was, however, found to be much smaller. We construct a sodium ion hopping model to explain qualitatively the results.

1. Introduction

The quadratic electrostriction effect is the basic electromechanical coupling effect in centric crystals and isotropic glasses. There are two alternative experimental approaches to the measurement of electrostriction: the direct method, which is to measure directly the elastic strain induced by a high electrical field and the converse method, in which the thermodynamically equivalent change in dielectric stiffness under mechanical stress is measured. Both methods are very difficult. In the direct method, the electrostrictive strain levels which can be induced at a realizable high electric field on low-permittivity centric crystals are only of the order of 10^{-10}. So that an ultradilatometer or interferometer of the sensitivity of 10^{-13} m is the only possible instrument to measure the minute strain. For the converse method, the need for high sensitivity is transferred to the dielectric measurement. Modern measuring systems like the General Radio 1620 capacitance bridge do have the sensitivity and stability required, but there is now also need for very precise temperature control and the establishment of a truly uniaxial stress upon the sample.

So far, hydrostatic electrostriction coefficients have been measured for several insulator crystals with simple centric structures, but except for high-permittivity perovskite structure oxides, reliable values of the separated tensor components of electrostriction are rare in the literature [1]. In the case of the simple alkali halides, even the signs of the coefficients are in doubt [2,3] and there is considerable uncertainty as to the influence of the defect structure upon the measured values [4].

Glass is interesting because of the amorphous structure and metastability. We can picture the silica glass, from Zachariasen, to be a random but continuous, network of $(SiO_3)^{2-}$ tetrahedra. Thermodynamically, the glass state is metastable, i.e. there is always a crystalline assembly with a lower Gibbs free energy. The measurement of the longitudinal electrostriction coefficient of glass is of interest, because taken in conjunction with hydrostatic measurements, the complete electrostriction tensor can be defined.

It has been suggested that electrostriction is responsible for the unusual effects of electric field upon crack propagation in glass samples, but heretofore, reliable experimental electrostriction data on representative glasses have not been available.

In this work, the converse method for the electrostriction measurement was performed on sodium trisilicate glass and sodium aluminosilicate glass. The

0 167-577x/86/$ 03.50

two glasses are chosen as the samples for this study because the ionic relaxation frequency of these glasses are close to 150 Hz at room temperature, within the range of the General Radio 1620 capacitance measurement system used for the converse electrostriction measurements.

2. Basic principles

M_{ijkl} and Q_{ijkl}, the electrostrictive coefficients in electric field and polarization notations, respectively, are defined by the relations:

$$M_{ijkl} = \tfrac{1}{2}\,(\partial^2 x_{ij}/\partial E_k\,\partial E_l)_X\,. \tag{1}$$

$$Q_{ijkl} = \tfrac{1}{2}\,(\partial^2 x_{ij}/\partial P_k\,\partial P_l)_X \tag{2}$$

and by applying Maxwell's relations to eqs. (1) and (2),

$$M_{ijkl} = \tfrac{1}{2}\,(\partial \delta_{kl}/\partial X_{ij})_P\,, \tag{3}$$

$$Q_{ijkl} = -\tfrac{1}{2}\,(\partial \chi_{kl}/\partial X_{ij})_P\,, \tag{4}$$

where χ_{kl} and δ_{kl} are the components of the dielectric stiffness and dielectric susceptibility, respectively. It may be noted for materials of central symmetry that

$$\chi_{kl} = 1/\delta_{kl} = 1/\epsilon_0(\epsilon_{kl} - 1)\,, \tag{5}$$

where ϵ_0 is the permittivity of free space and ϵ_{kl} the components of the relative permittivity tensor. Thus

$$M_{ijkl} = \tfrac{1}{2}\,\epsilon_0(\partial \epsilon_{kl}/\partial X_{ij})_P\,, \tag{6}$$

$$Q_{ijkl} = [\epsilon_0(\epsilon_{kl} - 1)]^{-2} M_{ijkl}\,, \tag{7}$$

$$= [2\epsilon_0(\epsilon_{kl} - 1)^2]^{-1}\,(\partial \epsilon_{kl}/\partial X_{ij})_P\,. \tag{8}$$

We used a thin circular disk of the specimen for the converse method of measurement. So the capacitance is given by

$$C = \epsilon_0 \epsilon A/d\,. \tag{9}$$

The change of permittivity under the mechanical stress is related to the change in the capacitance and the geometry change under stress:

$$\partial \epsilon/\partial X = \epsilon(C^{-1}\,\partial C/\partial X - S)\,, \tag{10}$$

where S is the appropriate combination of the components of the compliance tensor.

Glass is isotropic, so its dielectric constant tensor and fourth-rank tensor in Voigt notation have the form:

$$\boldsymbol{\epsilon} = \begin{bmatrix} \epsilon & 0 & 0 \\ 0 & \epsilon & 0 \\ 0 & 0 & \epsilon \end{bmatrix}, \tag{11}$$

$$\mathbf{M} = \begin{bmatrix} M_{11} & M_{12} & M_{12} & 0 & 0 & 0 \\ M_{12} & M_{11} & M_{12} & 0 & 0 & 0 \\ M_{12} & M_{12} & M_{11} & 0 & 0 & 0 \\ 0 & 0 & 0 & M_{44} & 0 & 0 \\ 0 & 0 & 0 & 0 & M_{44} & 0 \\ 0 & 0 & 0 & 0 & 0 & M_{44} \end{bmatrix}. \tag{12}$$

where

$$M_{44} = 4M_{1212} = 4 \times \tfrac{1}{2}(M_{11} - M_{12}) = 2(M_{11} - M_{12}). \tag{13}$$

For the longitudinal electrostriction effect, S in eq. (10) is

$$S = -(s_{11}^{\mathrm{T}} - 2s_{12}^{\mathrm{T}}) = ((1)/(9K)) - ((2)/(3\mu))$$

$$= ((1)/(E)) - ((1)/(\mu)) \tag{14}$$

where s_{ij}^{T} is the component of the compliance tensor in Voigt notation, K and μ are the bulk and shear elastic moduli, respectively [5].

3. Experimental procedures

The elastic data and dielectric data for sodium trisilicate glass can be found in refs. [6,7].

We measured the sodium aluminosilicate glass. The elastic data can be obtained by the measurement of the density and the longitudinal and transverse sound speeds in the ultrasonic wave pulse superposition technique. The specimen of thickness 1.393 cm was measured at 20 MHz with an accuracy of one part in 10^4. The elastic data are summarized in table 1. For the dielectric measurement of sodium aluminosilicate glass, we used a sample in the form

Table 1
Density, sound speeds, and elastic data of the sodium trisilicate glass and sodium aluminosilicate glass

Material	ρ (kg/dm^3)	C_l (m/s)	C_t (m/s)	E (10^8 N/m^2)	K (10^8 N/m^2)	μ (10^8 N/m^2)	σ
$Na_2O{\cdot}3SiO_2$ [a]	-	5374	3222	614	365	252	0.219
sodium aluminosilicate	2.42	5329	3329	653	383	269	0.216

[a] Data taken from ref. [6].

of a circular plate 23 mm across and 1.5 mm thick. We evaporated aluminum electrodes on the two planes of less than 1 μm roughness, with a guard gap 0.1 mm wide and 16 mm across made on the "low" electrode.

The dielectric constant and dielectric loss of the glass was measured from 0.1 Hz to 10 MHz. 10 kHz to 10 MHz was covered using a Hewlett–Packard 4274A multi-frequency LCR meter and 100 Hz to 100 kHz using a Hewlett–Packard 4275A multi-frequency LCR meter.

The frequency range of 0.1 Hz to 100 Hz was covered by a Sawyer–Tower circuit with added compensation circuit. We adjust to a horizontal line in the oscilloscope display of D and E when the capacitance and conductance is exactly matched by the parallel combination of a real capacitor and resistor. Such measurement can give a good resolution of 1 pF and 1 MΩ in capacitance and resistance, respectively.

K', K'' and σ (the effective conductivity) as functions of frequency for sodium aluminosilicate glass at room temperature (22°C) are plotted in fig. 1. At low frequencies K' is expected to level off at a value K_0. But the electrode polarization effect becomes dominant with decreasing frequency starting

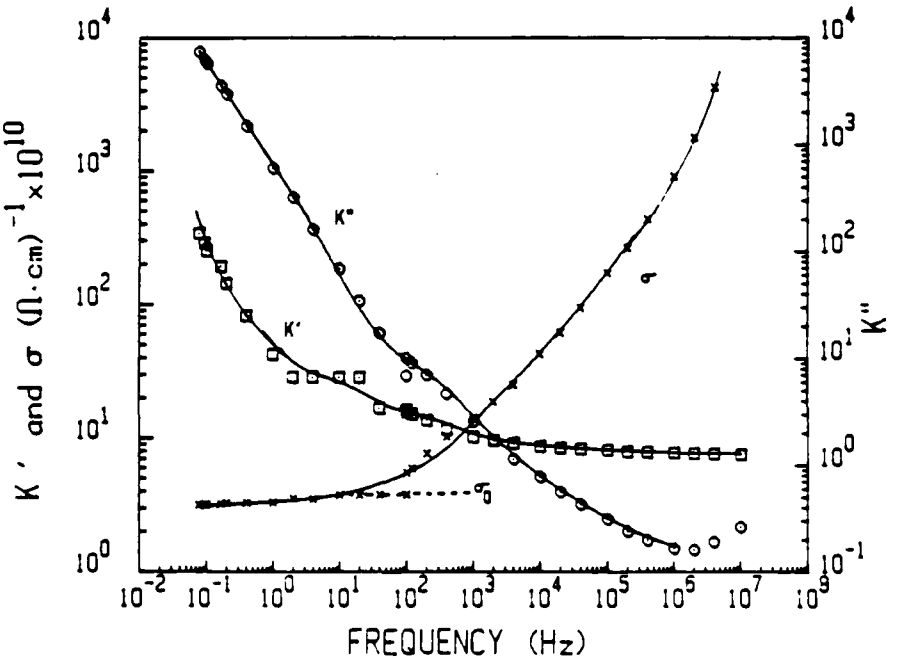

Fig. 1. The real and imaginary parts of the dielectric constants and the effective conductivity of the sodium aluminosilicate glass as a function of frequency.

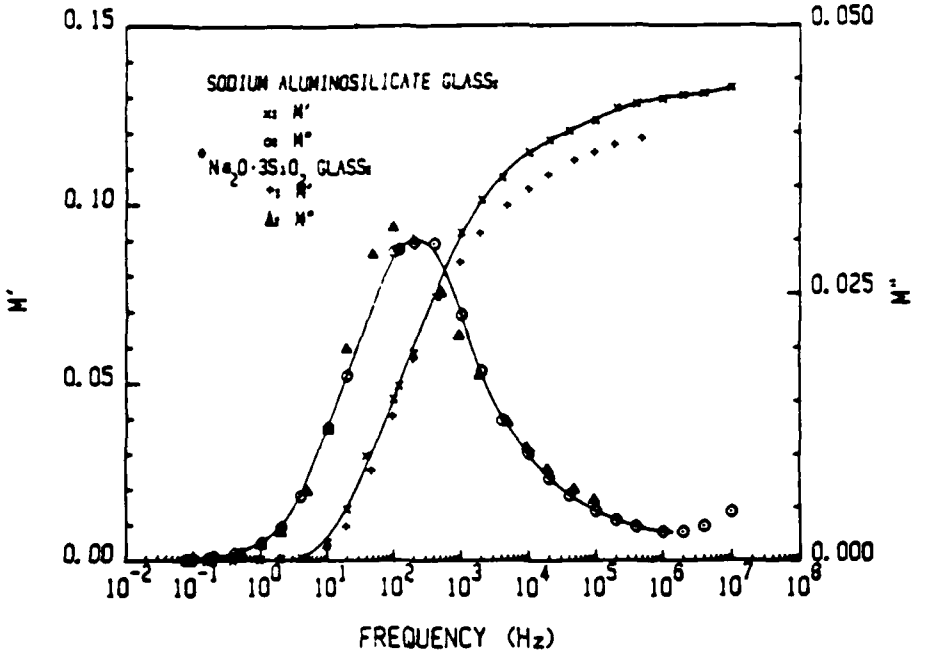

Fig. 2. The real and imaginary parts of the inverse dielectric constants of the sodium alur ›silicate glass and $Na_2O \cdot 3SiO_2$ glass. •: data taken from ref. [6].

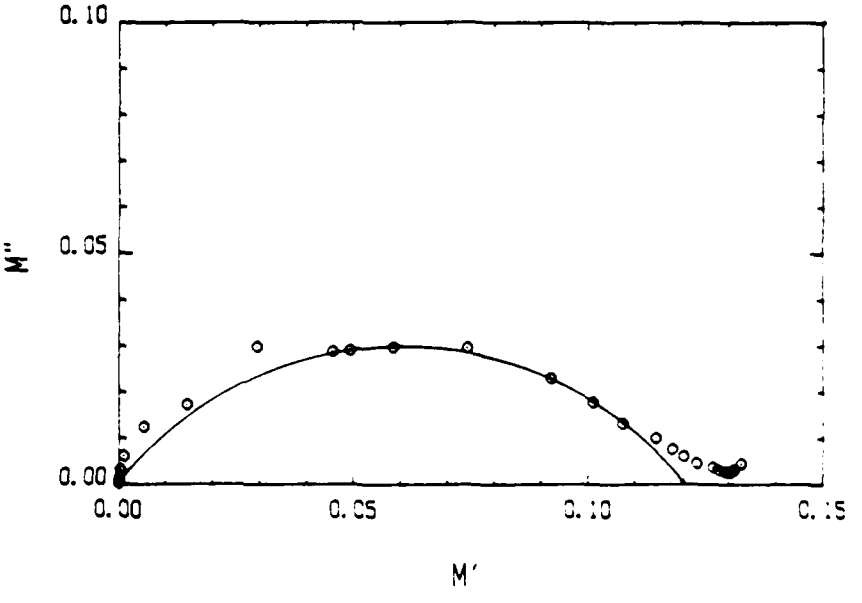

Fig. 3. Cole–Cole plot of the complex inverse dielectric constant of the sodium aluminosilicate glass.

from ≈20 Hz. We can eliminate the electrode polarization effect by using the regime of the complex inverse dielectric constant or electrical modulus, M^*, which is defined as

$$M^* = 1/K^* = 1/(K' - iK'')$$

$$= K'/[(K')^2 + (K'')^2] + K''/[(K')^2 + (K'')^2]$$

$$= M' + M'' . \quad (15)$$

M' and M'' as functions of frequency are shown in fig. 2. They just show relaxation spectra. The M'' curve exhibits a clear peak near 150 Hz, which is the so-called relaxation frequency. The plot of M'' is asymmetric with respect to the peak maximum, and is considerably broader on both sides of the maximum than would be for a single dipole relaxation time. A Cole–Cole plot of M' and M'' is shown in fig. 3.

The dc compressometer designed and built by Meng and Cross [1] was used for the converse method of electrostriction measurement. The capacitance decreases in response to the uniaxial stress in sodium trisilicate glass and sodium aluminosilicate glass. The $Na_2O{\cdot}3SiO_2$ glass was measured at 10 V, various frequencies (fig. 4): the sodium aluminosilicate glass at 10 V, 100 Hz; 30 V, 100 Hz (fig. 5). The data for vitreous silica glass for hydrostatic pressure were obtained by taking the slope $-\epsilon^{-1}(\partial\epsilon/\partial P)_T$ from Reitzel [8].

All data are summarized in table 2.

4. Discussion

We see from table 2 that though sodium trisilicate glass and sodium aluminosilicate glass respond dielectrically to ac electric field in a quite similar manner, they respond to uniaxial stress rather differently. $C^{-1}\partial C/\partial X$ is large in sodium trisilicate and the Q_{11} of the glass strongly depends on the frequency at which the capacitance was measured (fig. 6). $C^{-1}\partial C/\partial X$ of sodium aluminosilicate glass was, however, found to be smaller and the Q_{11} of sodium aluminosilicate glass does not change so much with frequency. We believe that the difference between the sodium trisilicate

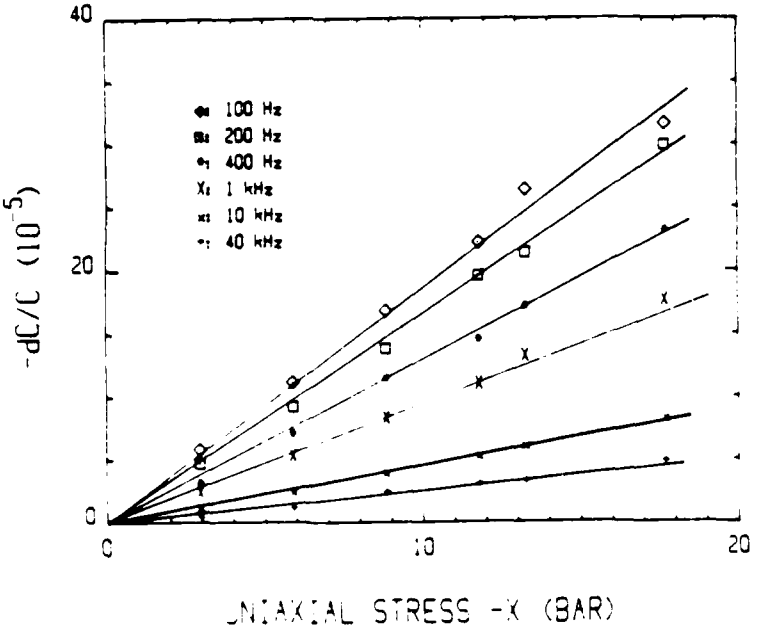

Fig. 4. Uniaxial stress dependence of the relative change of capacitance of $Na_2O\ 3SiO_2$ glass.

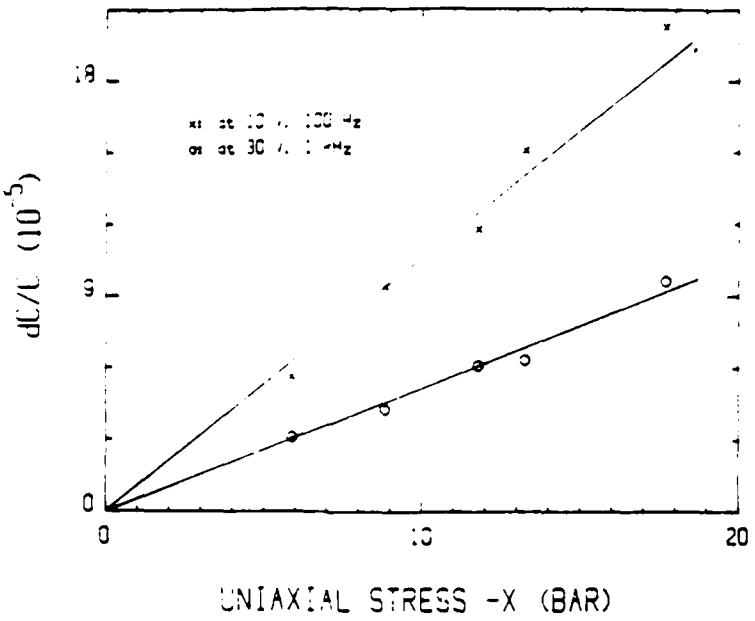

Fig. 5. Uniaxial stress dependence of the relative change of capacitance of the sodium aluminosilicate glass.

Table 2
Electrostrictive coefficients for silica glasses and quartz

Material	f (Hz)	K	$C^{-1}\partial C/\partial X$ (10^{-11} Pa^{-1})	M_{11} (10^{-20} m^2 V^{-2})	Q_{11} (m^4 C^{-2})
$Na_2O{\cdot}3SiO_2$	10^2	15.5	18.1	1.40	0.851
	2×10^2	13.8	17.1	1.19	0.923
	4×10^2	12.13	13.5	0.849	0.874
	10^3	11.3	10.3	0.631	0.765
	10^4	9.36	4.82	0.297	0.541
	4×10^4	8.82	2.95	0.207	0.430
sodium aluminosilicate	10^2	15.7	12.4	1.01	0.599
	10^3	10.2	5.45	0.346	0.519
X-cut quartz	–	4.34 ($\perp c$ axis)	–	-0.06 ± 0.02 [a]	-0.69 ± 0.23

	f (Hz)	K	$-\epsilon^{-1}\partial\epsilon/\partial p$ (10^{-11} Pa^{-1})	M_h (10^{-20} m^2 V^{-2})	Q_h (m^4 C^{-2})	T (°C)
vitreous silica	2.5×10^3	3.8	1.62 [b]	0.0272	0.443	20
	2.5×10^3	3.8	1.35 [b]	0.0227	0.370	138

[a] Data taken from ref. [9] using the direct method.
[b] Data read from ref. [8].

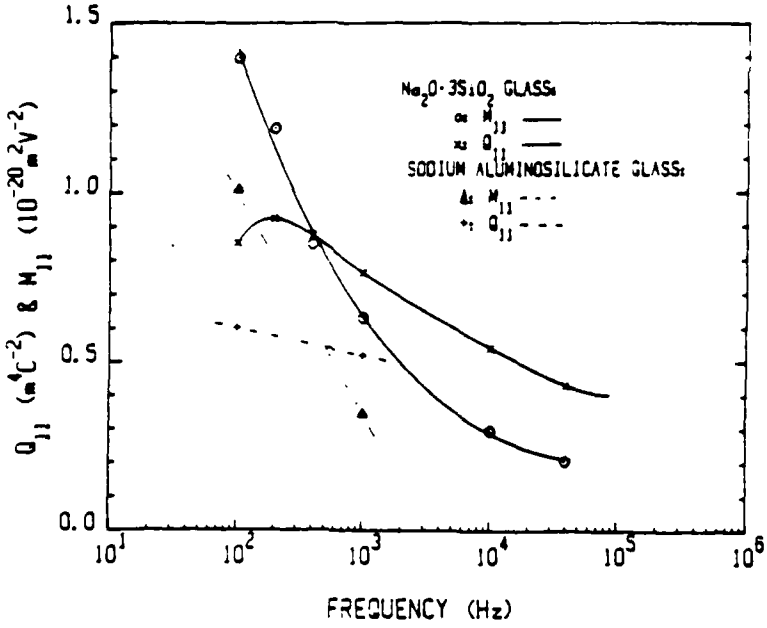

Fig. 6. Longitudinal electrostrictive coefficients of $Na_2O \cdot 3SiO_2$ glass and the sodium aluminosilicate glass as a function of frequency.

and the sodium aluminosilicate may be accounted for qualitatively in the following manner.

In the sodium silicate glass, the extra oxygen introduced by the Na_2O is non-bridging in the silicate structure. The addition of alumina reduces the number of these non-bridging oxygens so that at the Al/Na = 1 ratio all have been eliminated. Earlier literature on the conduction [10] shows that the activation energy for conduction decreases with the reduction in non-bridging oxygen content and is a minimum at the Al/Na = 1 ratio. In these papers, the effect is attributed to the expansion of the coordination shell in the silicate framework about the Na^+ ion, with the reduction in non-bridging oxygen content.

It was proposed that this change in volume of the coordination shell could be electrostatic in origin, or could be due to the modification in the adjustment of orbitals interacting with the sodium ion between bridging and non-bridging oxygens.

Whatever the origin, it is clear that if the Na^+ ion is in an expanded cage, hopping of the Na^+ ion may be accomplished with less effect on the geometry of the cage structure so that in the aluminosilicate the Na polarizability contributes less strongly to electrostriction.

When the sodium ions become immobilized at very high frequency, the electrostriction reponse must be largely that of the unmodified network, and it is interesting to note that in vitreous silica $Q_h \approx 0.443$ $m^4 C^{-2}$, rather close to the highest frequency value of Q_{11} for the trisilicate glass.

Since there is in these measurements a rather clear evidence of the role of the network modifier in changing the electrostrictive response, it will be most interesting to explore the role of alternative but very different network modifiers such as boron, and these studies are now underway.

Acknowledgement

This work was carried out under the Office of Naval Research contract N00014-82-K0339.

References

[1] Z.Y. Meng and L.E. Cross, J. Appl. Phys. 57 (1985) 488
[2] L. Bohaty and S. Haussuhl, Acta Cryst. A33 (1977) 114
[3] P. Preu and S. Haussuhl, Solid State Commun. 45 (1983) 619.
[4] G. Balakrishnan, K. Srinivasan and R. Srinivasan, J. Appl. Phys. 54 (1983) 2875.
[5] J.F. Nye, Physical properties of crystals (Oxford Univ. Press, London, 1979) pp. 134–143.
[6] G.O. Karapetyan, V.Ya. Livshits and D.G. Tennison, Fiz. Khim. Stekla 7 (1981) 188 [English Transl. Soviet J. Glass Phys. Chem. 7 (1981) 131].
[7] V. Provenzano, L.P. Boesch, V. Volterra, C.T. Moynihan and P.B. Macedo, J. Am. Ceram. Soc. 55 (1972) 492.
[8] J. Reitzel, Nature 178 (1956) 940.
[9] B.L. Luymes, Ph.D. Thesis, Eindhoven (1982).
[10] J.O. Isard, Trans. Soc. Glass Tech. 43 (1959) 113.

INVESTIGATIONS OF ELECTROSTRICTION EFFECTS IN GLASS BY UNIAXIAL STRESS COMPRESSOMETER

Y. Sun and L.E. Cross
Materials Research Laboratory
The Pennsylvania State University
University Park, PA 16802 U.S.A.

Abstract

In order to understand the basic principles governing the electrostriction effect, we applied the converse method of electrostriction measurement using a dc uniaxial compressometer on three glasses, i.e. sodium trisilicate, sodium aluminosilicate and Corning 7070 (borosilicate). A most important finding is that the polarization based longitudinal electrostrictive coefficient Q_{11} has opposite sign between the silicate, aluminosilicate and the borosilicate, that is Q_{11} is positive for silicate and aluminosililcate but negative for the borosilicate. Q_{11} of the sodium trisilicate glass shows a strong dependence on the frequency at which the capacitance was measured, with a peak value near 150Hz, which is the ionic relaxation frequency of this glass at room temperature. For the sodium aluminosilicate and the Corning 7070 glass, however, Q_{11}'s show little dependence on the frequency. The results indicate that the hopping of the sodium ion contributes significantly to the electrostriction effect in glass and that Al^{3+} and B^{3+} network modifier ions have different effects on the electrostriction.

Electrostriction is the basic coupling mechanism between dielectric polarization and elastic strain in centric crystals and isotropic insulators. Data are now available for electrostriction constants in a number of ferroelectric crystals, in alkali halides and in fluorite structure crystals. In order to understand the basic principles governing the electrostriction effect, we investigated the electrostriction effect in glass. The purpose of this work is to understand the roles played by alkali ions like sodium, the network modifiers such as Al^{3+} and B^{3+} in the electrostriction effect. In this paper, work is reported which measures the longitudinal electrostriction constants Q_{11} for a number of silicate glasses.

A simplification in the glass system is that they are isotropic since the longitudinal electrostriction data can be combined with hydrostatic coefficients Q_h and M_h, and the whole electrostriction tensor determined. The data are also of practical value, as they can be used to investigate the unusual effects of electric field upon crack propagation in glass, which are believed to be electrostrictive in origin.

We chose sodium trisilicate, sodium aluminosilicate (25.8mol% Na_2O,4.5mol% Al_2O_3, and 69.7mol% SiO_2), and Corning 7070(borosilicate, low thermal expansion) for reasons stated as follows. Sodium ions are quite mobile in glass, they are the so called fast ions. Such a fast mobility of sodium ions gives rise to the ionic relaxation. The first two glasses were chosen because the ionic relaxation in them are near 150Hz at room temperature, within the measuring range of our precision capacitance measurement system. Finally, we contrast the sodium aluminosilicate and Corning 7070 to learn the effect of Al^{3+} and B^{3+}as network modifiers.

The converse method for the measurement of electrostriction was performed on sodium trisilicate, sodium aluminosilicate, and Corning 7070 glass using the uniaxial compressometer designed and built by Meng and Cross[1]. The basic principles for the converse method were described in details elsewhere[1,2]. The point is that the electrostrictive coefficients can be obtained through the measurement of the slope of the capacitance change in response to uniaxial stress.

The elastic data, dielectric data, and the uniaxial stress dependence of the capacitance are needed to calculate the electrostrictive coefficients. Also the dielectric spectra are essential to analyze the ionic relaxation. The elastic data are for calculation of the elastic deformation of the specimen under

[illegible] 0000-0735 $1.00 © 1988 IEEE

uniaxial stress. The elastic and dielectric data for sodium trisilicate glass were found in [3,4], those for Corning 7070 glass were supplied from Corning.

Table I.
The elastic data of the sodium trisilicate glass, the sodium aluminosilicate and Corning 7070 glass.

Materials	E $10^8 N/m^2$	B $10^8 N/m^2$	μ $10^8 N/m^2$	σ
$Na_2O \cdot 3SiO_2$*	614	365	252	219
Sodium aluminosilicate	653	383	269	216
Corning 7070 **	466	278	191	22

*: Data taken from G.O. Karapetyan, et al [3].
**: Data Supplied by Corning.

We measured the sodium aluminosilicate glass. The elastic data can be obtained by the measurement of the density and the longitudinal and transverse sound velocities in the ultrasonic wave pulse superposition technique. The specimen of thickness 1.393 cm was measured at 20 MHz with the accuracy of one in 10^4. The elastic data are summarized in Table I. The dielectric constant and dielectric loss of the glass was measured from 0.1Hz to 10MHz. The frequency range from 10 kHz to 10MHz was covered using a Hewlett Packard 4274A multi-frequency LCR meter and 100Hz to 100kHz using another, Hewlett Packard 4275A multi-frequency LCR meter. The frequency range of 0.1Hz to 100Hz was covered by a Sawyer-Tower circuit with added compensation circuit. Such measurement can give a good resolution of 1 pF and 1MΩ in capacitance and resistance, respectively.

K', K" and σ (the effective conductivity) as functions of frequency for sodium aluminosilicate glass at room temperature (22°C) are plotted in Fig.1. At low frequencies K' is expected to level off at a value K_0. But the electrode polarization effect becomes dominant with decreasing frequency starting from about 20Hz. We can eliminate the electrode polarization effect by using the regime of the complex inverse dielectric constant or electrical modulus, M*, which is defined as:

$$M^* = 1 / K^* = 1 / (K' - iK'')$$

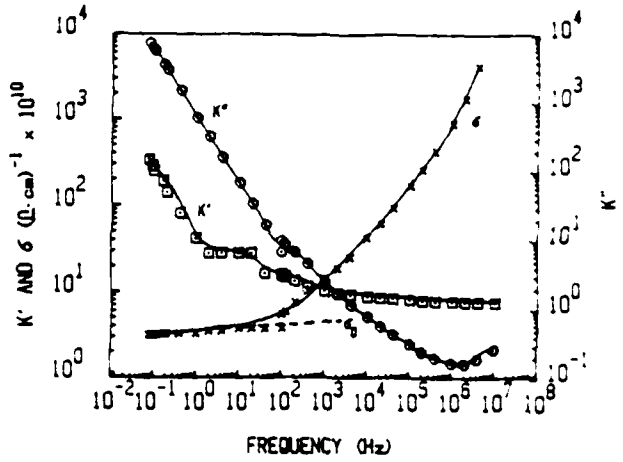

Fig. 1. The real and imaginary parts of dielectric constants and effecuve conductivity of the sodium aluminosilicate glass as functions of frequency.

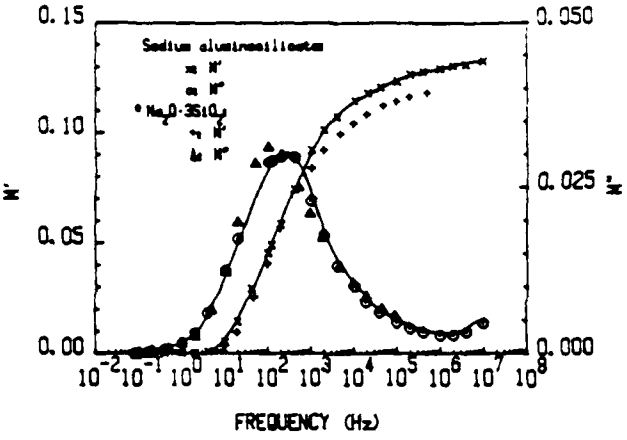

Fig. 2. The real and imaginary parts of the inverse dielectric constants of the sodium aluminosilicate glass and the $Na_2O \cdot 3SiO_2$ glass.
* Data taken from Provenzano, et al [4].

$$= K'/(K'^2 + K''^2) + i\,K''/(K'^2 + K''^2) = M' + i\,M''$$

M' and M'' as functions of frequency are shown in Fig. 2. They just show relaxation spectra. The M'' curve exhibits a clear peak near 150Hz, which is the so-called relaxation frequency. The plot of M'' is asymmetric with respect to the peak maximum, and is considerably broader on both sides of the maximum than would be for a single dipole relaxation time. That means a distribution of relaxation frequencies around 150Hz.

The dc compressometer designed and built by Meng and Cross was used for the converse method of electrostriction measurement. The $Na_2O \cdot 3SiO_2$ glass was measured at 10V and

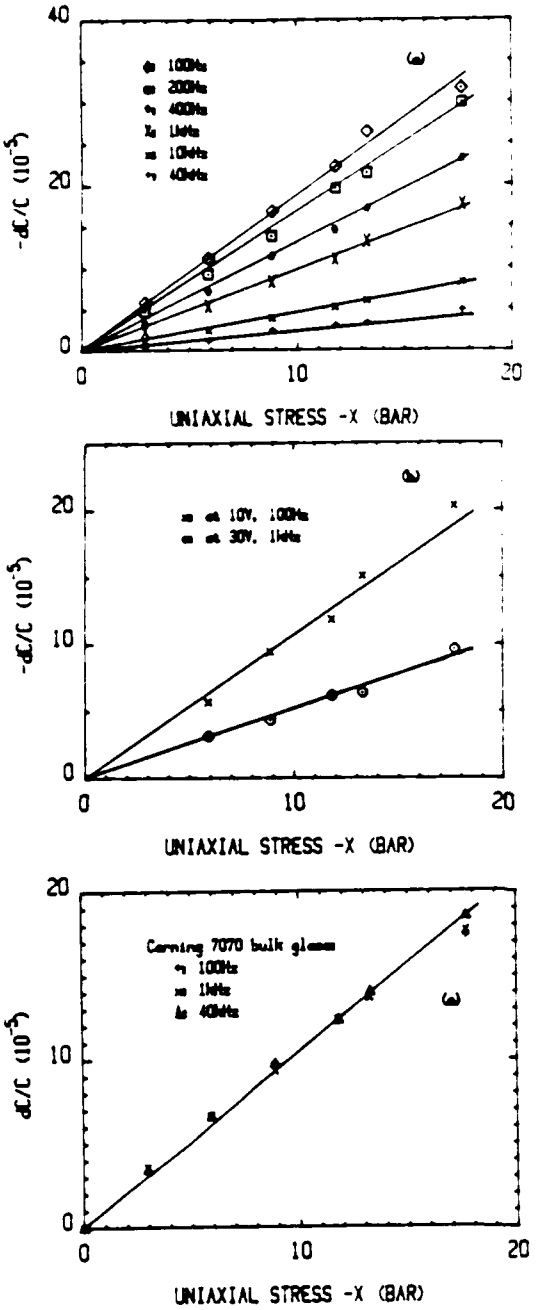

Fig. 3. The relative change in capacitance of glasses in response to uniaxial stress. (a). $Na_2O \cdot 3SiO_2$, (b). the sodium aluminosilicate, and (c). the Corning 7070 glass (borosilicate).

various frequencies (Fig. 3). The sodium aluminosilicate glass at 10V and 100Hz, 30V and 1kHz. The Corning 7070 glass was measured at 10V and 100Hz, 1kHz and 40kHz . The properties of this glass stay almost unchanged in a very wide frequency range at room temperature, which is because there is no ionic relaxation in this glass. The data for vitreous silica glass for hydrostatic pressure were obtained by taking the slope $-1/\varepsilon(\partial\varepsilon/\partial p)_T$ from Reitzel [5]. All data are summarized in Table II.

Table II.
Electrostrictive coefficients of silicate glasses and quartz.

Material	f Hz	K	$1/C \cdot \partial C/\partial X$ $10^{-11}Pa^{-1}$	M_{11} $10^{-20}m^2v^{-2}$	Q_{11} m^4C^{-2}
$Na_2O \cdot 3SiO_2$	10^2	15.5	18.1	1.40	.851
	$2x10^2$	13.8	17.1	1.19	.923
	$4x10^2$	12.1	13.5	.849	.874
	10^3	11.3	10.3	.631	.765
	10^4	9.36	4.82	.297	.541
	$4x10^4$	8.82	2.95	.207	.430
Sodium aluminosilicate	10^2	15.7	12.4	1.01	.599
	10^3	10.2	5.45	.346	.519
Corning 7070	10^2--10^4	4.1	-9.90	-.121	-1.71
X-cut quartz	-	4.34 ($\perp$ c axis)	-	*-.06±.02	-.69±.23

Materials	f Hz	K	$-/\varepsilon \cdot \partial\varepsilon/\partial p$ $10^{-11}Pa^{-1}$	M_h $10^{-20}m^2v^{-2}$	Q_h m^4C^{-2}	t °C
Vitreous silica	$2.5x10^3$	3.8	**1.62	.0272	.443	20
	$2.5x10^3$	3.8	**1.35	.0227	.370	138

*Data taken from Luymes, B.J. using direct method.
**Data read from Reitzel, John.

For the sodium trisilicate glass and sodium aluminosilicate glass there is a decrease in capacitance under uniaxial compression, but an increase in Corning 7070 glass. As is shown in Fig. 4, the polarization based longitudinal electrostriction coefficient Q_{11} of the sodium trisilicate glass shows a strong dependence on the frequency at which the capacitance is measured, with a peak near 150Hz, which is just the ionic relaxation frequency of this glass at room temperature. For the sodium aluminosilicate glass and the Corning 7070 glass, however, Q_{11}'s show little dependence on the frequency. A most important finding is that Q_{11} has opposite sign between the silicate and aluminosilicate and the borosilicate glass. We believe that this may be related to the difference between Al^{3+}-modified and B^{3+}-modified (SiO_2) random networks. It may be of significant interest to now look for glasses which combine these properties so as to have zero electrostriction.

We see from Table II that though sodium trisilicate glass and sodium aluminosilicate glass respond dielectrically to ac electric

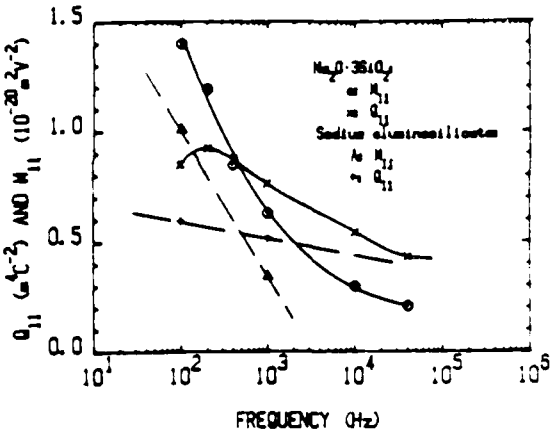

Fig. 4 The longitudinal electrostrictive coefficients of $Na_2O \cdot 3SiO_2$ glass and the sodium aluminosilicate glass as functions of frequency.

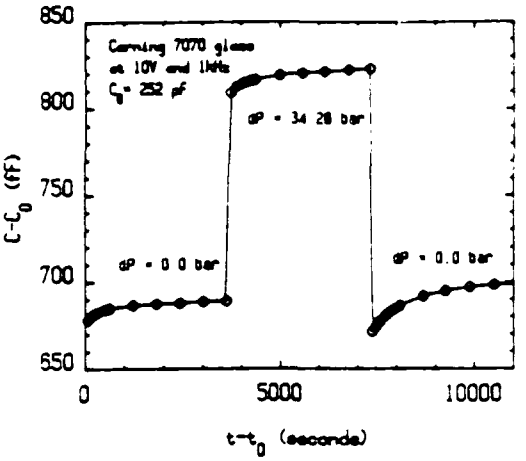

Fig. 5. The aging effect in the capacitance of the Corning 7070 glass.

field in a quite similarly manner, they respond to uniaxial stress rather differently. The magnitude of $1/C \cdot \partial C/\partial X$ is large in sodium trisilicate and the Q_{11} value of this glass strongly depends on the frequency at which the capacitance was measured. $1/C \cdot \partial C/\partial X$ of sodium aluminosilicate glass was, however, found to be smaller and the Q_{11} of sodium aluminosilicate glass does not change so much with frequency. We believe that the difference between the sodium trisilicate and the sodium aluminosilicate may be accounted for qualitatively in the following manner. In the sodium silicate glass, the extra oxygen introduced by the Na_2O is non-bridging in the silicate structure. The addition of alumina reduces the number of these non-bridging oxygens so that at the Al /Na = 1 ratio all have been eliminated. Earlier literature on the conduction [6] shows that the activation energy for conduction decreases with the reduction in non-bridging oxygen content and is a minimum at the Al / Na = 1 ratio. In these papers, the effect is attributed to the expansion of the coordination shell in the silicate framework about the Na^+ ion, with the reduction in non-bridging oxygen content. It was proposed that this change in volume of the coordination shell could be electrostatic in origin, or could be due to the modification in the adjustment of orbitals interacting with the sodium ion between bridging and non-bridging oxygens. Whatever the origin, it is clear that the Na^+ ion is in an expanded cage, hopping of the Na^+ may be accomplished with less effect on the geometry of the cage structure so that in the aluminosilicate the Na polarizability contributes less strongly to the electrostriction.

When the sodium ions become immobilized at very high frequency, the electrostriction response must be largely that of the unmodified network, and it is interesting to note that in vitreous silica $Q_h \sim 0.443\ m^4C^{-2}$, rather close to the highest frequency value of Q_{11} for the trisilicate glass.

The aging effect in capacitance when loading and unloading the uniaxial stress was studied through measurements on the Corning 7070 glass specimen (Fig. 6).. The results can be explained from the elastic after effects in glass. We reduce this effect by taking the capacitance measurement immediately after the loading or unloading though the level of the aging effect is small compared with the increment due to the electrostriction.

Reference

[1] Z.Y. Meng and L.E. Cross, "Determination of the electrostriction tensor components in single-crystal CaF_2 from the uniaxial stress dependence of the dielectric permittivity," J. Appl. Phys. 57 (2) (1985) 488-491.

[2] Y. Sun, W.W. Cao and L.E. Cross, "Electrostriction effect in glass," to be published in Materials Letters 1986.

[3] G.O. Karapetyan, V.Ya. Livshits and D.G. Tennison, Fiz. Khim. Stekla 7 (2) (1981), 188 or see Eng. Trans. Sov. J. Glass Phys. Chem. 7 (2) (1981) 131.

[4] V. Provenzano, L.P. Boesch, V. Volterra, C.T. Moynihan and P.B. Macedo, J. Am. Ceram. Soc. 55 (10) (1972) 492.

[5] J. Reitzel, Nature 178 (1956) 940.

[6] J.O. Isard, Trans. Soc. Glass Tech. 43 (1959) 113.

[7] B.J. Luymes, Ph.D. Thesis, Proetschrif Eindhoven ISBN 90-9000381-9(17 Dec. 1982).

Dielectric ageing effects in doped lead magnesium niobate : lead titanate relaxor ferroelectric ceramics

WUYI PAN, E. FURMAN, G. O. DAYTON, L. E. CROSS
Materials Research Laboratory, The Pennsylvania State University, University Park, Pennsylvania 16802, USA

Earlier studies in the laboratory [1] have shown no evidence of dielectric ageing phenomena in lead magnesium niobate $Pb(Mg_{1/3}Nb_{2/3})O_3$ (PMN) or in lead magnesium niobate : lead titanate solid solutions $(PbMg_{1/3}Nb_{2/3}O_3 : PbTiO_3)$ (PMN : PT) although all compositions up to 13 mol % $PbTiO_3$ addition show ferroelectric relaxor character. Studies of the PLZT relaxor compositions [2], however, and also strontium barium niobate (SBN) materials [3] show significant ageing phenomena. In seeking the difference between these two families of relaxors, it may be noted that the PLZT and SBN are intrinsically "defective" in the sense that in the stoichiometric composition not all sites for the cations are occupied while in the PMN derived compositions the structure is fully "stuffed" and has all lattice sites occupied.

To explore further the role of defects in the ageing phenomena in relaxors, PMN : 10 mol % PT compositions have been fabricated with a 0.1 mol % doping of MnO. The work reported here shows that these doped ceramics show ageing effects similar in many respects to the PLZT relaxor compositions.

Ceramic samples of PMN : 10% PT for use in this study were prepared using the pre-reaction of MgO and Nb_2O_5 to form first the columbite structure precursor in the manner discussed in earlier papers [4, 5]. For the doping studies, MnO was introduced using a dilute $Mn(NO_3)_2$ solution, added to the calcine. Final sintered samples were all above 97% theoretical density and were shown by X-ray diffraction to be free of pyrochlore phase contamination.

For ageing studies, disk-shaped samples were equipped with chrome : gold electrodes on the major faces. Ageing was accomplished by first heating the sample above 150 C to relieve all earlier ageing, then bringing the sample down to a fixed temperature and starting the measuring clock. Room-temperature ageing was carried out in a dessicator in the air-conditioned laboratory space (22 to 28 C). The 40 C ageing runs were carried through in a heated plexol oil bath with temperature fluctuation less than ± 0.5 C. The -15 C runs were carried out in a commercial freezer with a measured temperature variation of ± 2 C. All runs were carried out with the sample under open circuit conditions, connection being made at intervals to establish the capacitance and loss but then relieved for the ageing time.

The permittivity–temperature runs were made in a computer-controlled environment chamber (Delta Design Model 2300) using liquid nitrogen as the coolant. The sample was put into the chamber at a temperature below the ageing temperature, the temperatures were then lowered to -70 C and the dielectric properties were measured during heating at 4 C min. For cooling runs, the samples were heated to 170 C, kept at that temperature for 1 h, then measured as the temperature was lowered at 4 C min down to -70 C. Dielectric properties were measured using the Hewlett packard LCR meter (model 4274A) under computer control covering a frequency range from 100 Hz to 100 kHz with field strength less than 100 V cm^{-1}.

Hysteresis loops were measured with a Sawyer and Tower system [6] under 0.1 Hz frequency driving field. The aged sample was measured without any prior heating above the ageing temperature. The a.c. de-aged sample was measured by applying a 10 Hz field of 20 kV cm^{-1} for 20 min and measuring with 0.1 Hz field. The thermally de-aged sample was measured after heating the sample above the Curie range and measuring as soon as the temperature reached room temperature.

Fig. 1a shows the variation of frequency dispersion with temperature. The curves may be divided into four regions. (i) A low-temperature region (below 10 C) where the frequency dispersions for both aged and deaged samples are similar. (ii) A region of decreasing dispersion (10 to 25 C) ending at the ageing temperature. (iii) A region of very markedly reduced dispersion for the aged samples (25 to 60 C) between the ageing temperature and a temperature above that of the permittivity peaks. The dispersion reduction due to ageing in this region is more pronounced than that observed by Schulze *et al.* [1] in PLZT. (iv) A paraelectric region (about 60 C) with no apparent ageing or dispersion.

In Fig. 1b, the loss tangents against temperature may be divided into three regions. (i) A region where the tan δ of the aged sample are slightly greater than those of the de-aged samples but with similar frequency dispersion. (ii) A region where the tan δ of the aged sample are markedly less than those of de-aged samples especially at the ageing temperature. (iii) A region (above 55 C) where the tan δ for aged and de-aged samples are the same.

Fig. 2 shows the variation of the frequency dispersion with temperature for a PMN – 10% PT relaxor ceramics without MnO doping, which is typical for all undoped samples which do not show ageing.

Fig. 3 shows the effect of ageing time on the dielectric constants. In the vicinity of the ageing temperature, a decrease of the dielectric permittivity with

0261–8028/86 $03.00 + .12

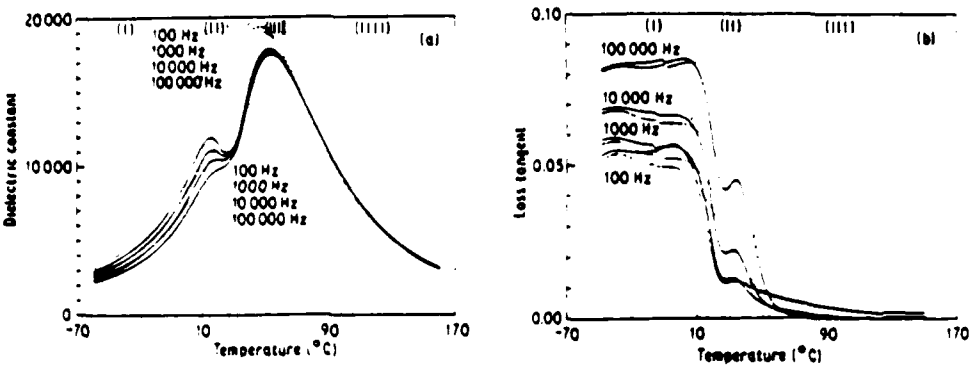

Figure 1 (a) Dielectric permittivity and (b) dielectric loss tangent against temperature for $(PbMg_{1/3}Nb_{2/3}O_3)_{0.9}(PbTiO_3)_{0.1}$ ceramic doped with 0.1 mol % MnO. Solid curves show the data obtained after ageing for 1000 h at 23 °C. Dotted curves show data for a sample freshly de-aged at 160 °C for 30 min. Frequencies of measurement are as illustrated.

increasing ageing time was observed. Below and above this region, the variation of dielectric constant with ageing time is reduced.

Fig. 4 shows the effects of ageing temperature on the dielectric constant against temperature curves. The saddle point occurring at the ageing temperature shifts as the ageing temperature is changed. Low-temperature ageing was observed to have less effect on the dielectric constant as observed in Curve C (Fig. 4) probably because of the much reduced ageing rate at the lower temperature. As observed in Fig. 4, Curve C, a minimum of dielectric constant in the ageing temperature observed for the higher temperatures was not obvious in the curve for the lowest temperature.

Fig. 5a shows the loop of an aged sample. A double *loop with a slim portion in the low-field region* was observed. Fig. 5b shows the loop of the above aged sample after 20 min under a 10 Hz field of 20 kV cm^{-1}. The slim portion gradually disappears. Fig. 5c shows the loop for the thermally de-aged sample. The absence of the waisted loop character is obvious. Fig. 5d shows the loop for a sample which was free from MnO doping. Again a loop with no waisted character was evident immediately upon first application of the field.

The data presented in Fig. 2 confirm that as indicated by earlier measurements there is no obvious ageing effect in a PMN : PT composition. However, in the samples of PMN doped with 0.1 mol % MnO there is now an obvious ageing effect which is in many respects similar to that observed earlier in the relaxor ferroelectric PLZT compositions [2].

It has been suggested that for both normal and relaxor ferroelectrics an essential ingredient of the ageing process is a lattice defect which has polar character [7]. The suggested model is that the polar defect couples to the P_s vector in the domain or microdomain and readjusts its orientation slowly so as to minimize the energy of the system [8]. If defect orientation is thermally activated, ageing proceeds much more slowly at low temperature than at high. Clearly if the energy is minimized for an existing domain orientation, switching from that orientation will be inhibited. Thus if the bulk sample is unpoled, a balanced array of domains will stabilize and the nonpolar state will be preferred, leading to a well defined waist in the hysteresis loop. If, however, the sample is cycled over a saturated loop, the domain vectors will spend almost as much time away from the aged-in polar defect direction as they do in this direction; and thus, slowly the waist of the loop will be lost as the defects randomize.

The suggestion for PMN is that in the stoichiometric composition there is a very low concentration of defects, and thus no obvious ageing. In the MnO doped composition, however, the aliovalent manganese is presumably compensated by oxygen

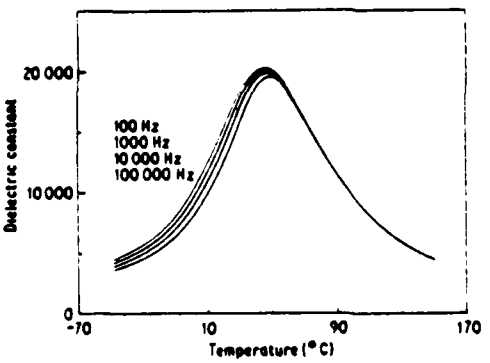

Figure 2 Dielectric permittivity against temperature for a pure $(PbMg_{1/3}Nb_{2/3}O_3)_{0.9}(PbTiO_3)_{0.1}$ ceramic after ageing for 1000 h at 23 °C.

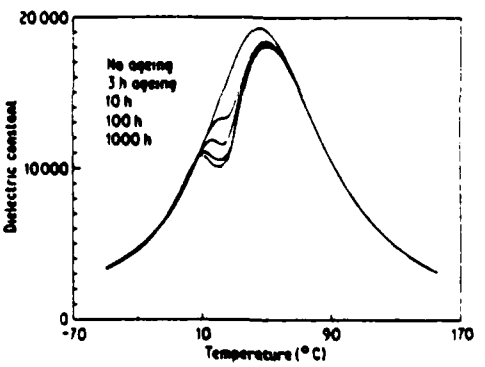

Figure 3 Effects of ageing time on the 100 Hz dielectric permittivity against temperature curves on $(PbMg_{1/3}Nb_{2/3}O_3)_{0.9}(PbTiO_3)_{0.1}$ ceramic doped with 0.1 mol % MnO.

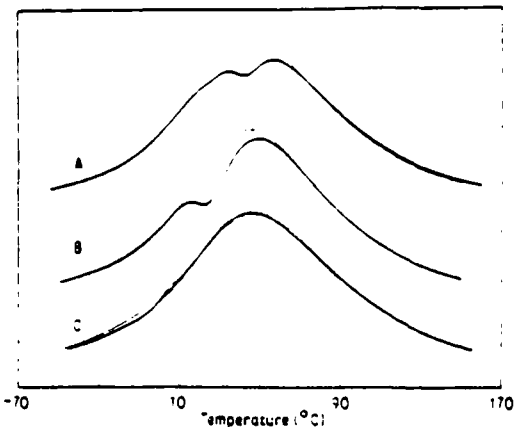

Figure 4 Effect of ageing temperature on the 100 Hz dielectric permittivity against temperature in 0.1 mol% MnO doped PMN 10% PT. Solid curves are for aged samples. Curve A 70 h at 40 °C. Curve B 10 h at 23 °C. Curve C [illegible] °C. Dashed curves are for fresnly de-aged samples.

vacancies providing the thermally activated defect dipole pair which is the essential component for ageing.

Both PMN and PMN PT are relaxor ferroelectrics, and here as in the PLZT relaxors, there is a very obvious preferential ageing of the dispersive component of the permittivity. In PLZT, because of the valence of lanthanum in the solid solution, all samples are necessarily "defective" with lead vacancies the most probable defect species. Thus it is certainly not unexpected that all PLZT relaxors exhibit ageing.

For PMN: + 10% PT 0.1% MnO, the asymmetry of the elimination of the dispersive component for temperatures above that of the ageing temperature, and the re-emergence of ageing below that temperature is extreme and strongly suggests that the polar microregions responsible for the superparaelectric dispersion are stabilized by a volume distribution of defect dipoles. Thus on heating when one is emerging into the paraelectric phase, all material in the polar regions is still aged; on cooling, however, new unaged material will be falling into the polar phase and will therefore be able to reorient under field and re-establish the dispersive component of permittivity.

From the dielectric hysteresis date, it is evident that the high field can effect an amalgamation of microregions into macrodomains which switch with the field, thus eliminating the preferred orientation and effectively de-ageing the sample as in a normal ferroelectric.

References

1. W. A. SCHULZE, J. V. BIGGERS and L. E. CROSS, *J. Am. Ceram. Soc.* **61** (1978) 46.
2. G. BORCHHARDT, J. VON CIEMINSKI and G. SCHMIDT, *Phys. Status Solidi (a)* **59** (1980) 749.
3. G. A. SMOLENSKII, V. A. ISUPOV, A. I. AGRANOVSKA and N. POPOV, *Sov. Phys. Solid State* **2** (1961) 2584.
4. S. L. SWARTZ and T. R. SHROUT, *Mater. Res. Bull.* **17** (1982) 1245.
5. S. L. SWARTZ, T. R. SHROUT, W. A. SCHULZE and L. E. CROSS, *J. Am. Ceram. Soc.* **67** (1984) 311.
6. H. DIAMANT, K. DRENCK and R. PEPINSKY, *Rev. Sci. Instrum.* **28** (1) (1957) 30.
7. K. CARL and K. H. HARDTL, *Ferroelectrics* **17** (1978) 473.
8. K. CARL and K. GESEN, *Proc. IEEE* **61** (7) (1973).

Received 25 November
and accepted 4 December 1985

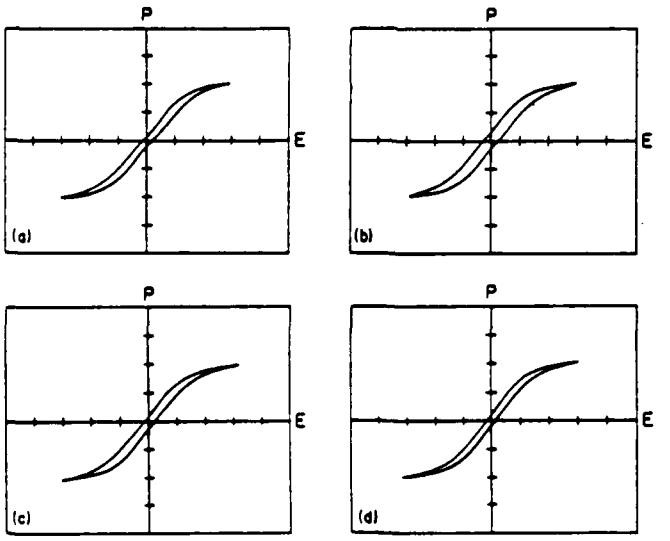

Figure 5 (a) Dielectric hysteresis loop of a 0.1 mol% MnO PMN 10% PT sample aged at 23 °C for 100 h. (b) Hysteresis loop of a.c. de-aged sample driven for 20 min. (c) Hysteresis loop for a sample freshly thermally de-aged by heating to 160 °C for 30 min. (d) Hysteresis in an undoped PMN 10% PT sample.

LOW-TEMPERATURE FIRED LEAD MAGNESIUM NIOBATE

S.L. Swartz
Battelle, Columbus Division

G.O. Dayton and D.K. Laubscher
Materials Research Laboratory
Pennsylvania State University

ABSTRACT

Lead magnesium niobate-lead titanate (PMN-PT) ceramics have been sintered at low temperatures by PbO atmosphere control, or with additions of excess PbO. The densification and dielectric properties were extremely sensitive to sintering conditions and/or the amount of excess PbO. Stoichiometric PMN-PT ceramics could not be densified at 1000°C in air, due to PbO volatilization. However, when sintered in a PbO atmosphere, densities approaching 98% theoretical were achieved at 1000°C, with maximum dielectric constants of 17500. Excess PbO (1 and 3 wt%) allowed for PMN-PT ceramics to be densified at temperatures as low as 900°C in air. However, samples sintered with excess PbO exhibited inferior dielectric properties (lower dielectric constants and transition temperatures, along with significant dielectric ageing), even though most of the PbO was driven off during sintering.

INTRODUCTION

Over the past few years, there has been much interest in lead-based perovskite relaxor ferroelectrics, such as $PbMg_{1/3}Nb_{2/3}O_3$ (PMN), because of their high dielectric constants and their potential for low firing temperatures [1-7]. The development of these materials has been hindered by processing difficulties, i.e., the appearance of a parasitic lead niobate-based pyrochlore phase during ceramic fabrication [1,3,4]. Recently, some improved techniques have been developed that allow for the preparation of pyrochlore-free PMN [1,2,5-7]. One of these methods, referred to as the columbite approach, involves the pre-reaction of MgO and Nb_2O_5 to form the columbite $MgNb_2O_6$, prior to the addition of PbO [1]. This results in the direct formation of perovskite, and the pyrochlore phase is avoided. PMN ceramics prepared by this process were shown to have excellent dielectric properties, as compared to PMN ceramics prepared by conventional mixed oxides processing [2]. The columbite approach has also proven to be an effective and reproducible fabrication technique for several other lead-based complex perovskites [8-11].

The sintering of PMN ceramics is complicated by the loss of PbO through volatilization. If PbO loss is not controlled, the sintering and resultant dielectric properties of PMN ceramics are adversely affected. In this investigation, the control of PbO stoichiometry was attempted with two methods, by sintering stoichiometric PMN ceramics in a PbO atmosphere, and by adding an excess of PbO into the starting compositions, and sintering in air. With these two methods, PMN ceramics with densities of up to 98% theoretical were sintered at temperatures in the range of 900 to 1000°C. The effects of excess PbO on the sintering behavior and dielectric properties, were studied systematically, and the results will be reported in this paper.

The addition of excess PbO to PMN has been employed previously. A liquid-phase at 830°C in the $PbO-Nb_2O_5$ system was reported, and this was exploited to sinter PMN at low temperatures. Excess PbO was added to PMN powders prepared by calcination of oxides, and a complicated firing schedule (maximum temperatures of 900 to 1000°C) resulted in phase-pure PMN with good density and excellent dielectric properties [5,6]. In these studies, the excess PbO was added to stabilize the perovskite phase, and lower sintering temperatures resulted. No systematic study of the effects of excess PbO on the densification, PbO weight loss, and resultant dielectric properties has been reported. In the present investigation, the use of the columbite approach, along with the addition of excess PbO, allowed for such a study to be made.

EXPERIMENTAL PROCEDURE

The compositions studied were based on PMN with 7.5 mole percent $PbTiO_3$. The $PbTiO_3$ was included in the composition to shift the Curie temperature range closer to room temperature (from about -15°C for pure PMN). Intimate mixing was accomplished by vibratory milling in nalgene jars with alcohol and zirconia media for eight hours; this step was carried out before and after any calcination operation. The columbite precursor was prepared by calcination of MgO and Nb_2O_5 at 1000°C for eight hours. PMN-PT batches were weighed-out, with excess PbO amounts of zero, one, and three weight percent. The powders were calcined at 700°C, in open alumina crucibles for four hours. The remainder of the processing included addition of PVA binder, pellet pressing, and binder burnout.

Sintering time studies at temperatures of 900, 950, and 1000°C were carried out on pellets of the two excess PbO compositions. Pellets were placed on zirconia setters which were stacked in a furnace. The furnace was heated to the sintering temperature (in one hour), and setters were removed

after various times ranging from five minutes to four hours. When the same sintering conditions were applied to the stoichiometric PMN-PT samples (without excess PbO), no densification was observed, so a second type of sintering condition was employed for these samples. Pellets were buried (separated by platinum) in coarse PMN powder in a closed alumina crucible, using the method employed in earlier investigations [2,8], and sintered at 1000°C for two hours.

Weight loss was recorded on each sample, and the values for identical samples (typically two for each composition and sintering condition) were averaged. Geometric densities were measured on samples polished parallel with 12 micron alumina. Dielectric measurements were made on the parallel samples with sputtered gold electrodes using the system described in earlier publications [2,8]. Measurements were made on cooling to obtain the non-aged dielectric properties. Ageing phenomena were observed with heating runs; prior to measurement, samples were allowed to age at room temperature for 24 hours after being heated to 100°C. For all of the dielectric measurements, heating and cooling rates were 0.5°C/minute.

RESULTS

No densification occurred when the stoichiometric PMN-PT samples were sintered in air, and significant weight losses were observed. However, when stoichiometric pellets were sintered in a PbO atmosphere (buried in coarse PMN powder), densities of 7.95 g/cc (98% theoretical) were obtained, without significant weight loss. Weight loss and density of the excess PbO samples sintered in air are presented in Table 1. For both excess PbO compositions, weight loss increased with sintering temperature and time, and levelled off close to the weight losses corresponding to the amount of excess PbO in the starting compositions. Generally, densities increased with excess PbO content and sintering temperature. Densities of the 1% PbO samples increased over the first thirty minutes at each sintering temperature. Densification of pellets of the 3% PbO composition was quite rapid and densities were independent of sintering time, except for the first few minutes at 900°C. Densities greater than 7.90 g/cc (97% theoretical) were achieved in some of the 1% PbO samples sintered for the longer times at 1000°C, and in most pellets of the 3% PbO composition sintered at all three temperatures.

The dielectric constant and loss (on cooling), for the stoichiometric PMN-PT sample sintered in a PbO atmosphere is shown in Figure 1. The frequency dependence of the dielectric constant maxima were typical of relaxor ferroelectric, and the transition range was near room temperature, as would be expected from the composition. At 1 kHz, the maximum dielectric constant of 17500 occurred at 23°C. The dielectric loss was also typical of relaxors, with high, frequency-dependent domain losses below the transition. The dielectric curves of this sample were identical upon heating and cooling, indicating no ageing.

Table 1: Weight loss and density of PMN-PT samples sintered with excess PbO.

Temp. (°C)	Time (min)	1% PbO Weight Loss (%)	1% PbO Density (g/cc)	3% PbO Weight Loss (%)	3% PbO Density (g/cc)
900	10	0.43	7.15	0.46	7.40
	20	0.63	7.52	0.85	7.86
	30	0.65	7.66	0.66	7.90
	60	0.89	7.69	1.34	7.95
	90	1.02	7.75	1.67	7.94
	120	1.09	7.74	2.25	7.94
	180	1.07	7.75	2.63	7.90
	240	1.12	7.71	2.78	7.90
950	5	0.44	7.64	0.89	7.96
	10	0.47	7.63	0.85	7.93
	20	0.56	7.79	1.28	7.96
	30	0.66	7.81	1.58	7.95
	60	0.99	7.87	2.49	7.95
	90	1.06	7.86	2.78	7.95
	120	1.10	7.77	2.88	7.93
1000	5	0.88	7.65	1.43	7.82
	10	0.93	7.76	1.55	7.97
	20	0.95	7.77	1.66	7.88
	30	1.03	7.92	2.11	7.90
	60	1.11	7.95	2.80	7.95
	90	1.14	7.88	2.90	7.94
	120	1.19	7.91	2.91	7.95

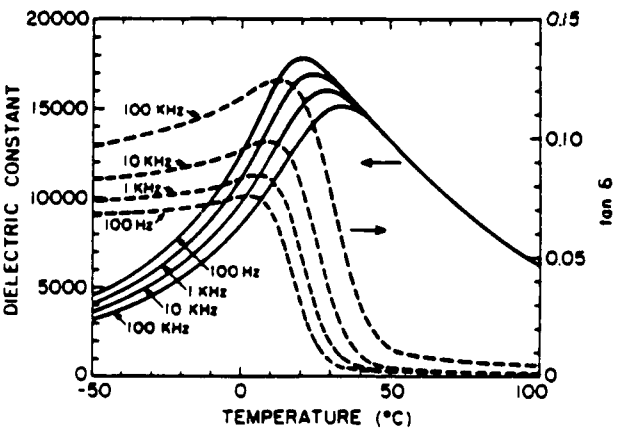

Figure 1: Dielectric constant and loss versus temperature for stoichiometric PMN-PT, sintered at 1000°C for two hours.

Dielectric data (1 kHz) of excess PbO samples appear in Table 2. The maximum dielectric constant and transition temperature (from cooling runs) are summarized. Maximum dielectric constants of the 1% PbO samples were in the range of 10000 to 15000, and those of the 3% PbO samples were lower (5000 to 10000), with significantly lower transition temperatures. Dielectric constants of the 1% PbO samples were largest within the first thirty minutes at each of the sintering temperatures. The longer time decrease of the maximum dielectric

constant was accompanied by a decrease of the transition temperature, especially at higher sintering temperatures. For samples of the 3% PbO composition, after an initial increase over the first few minutes, maximum dielectric constants decreased with longer sintering times, along with further reductions of the transition temperatures.

The lower dielectric constants and transition temperatures observed with increasing sintering time and excess PbO content were also accompanied by broadening of the temperature dependence. The temperature dependence of the dielectric constant of relaxor ferrolectrics has been described by a diffuseness coefficient, δ [12]. This parameter has units of temperature and is related to the distribution of transition temperatures that are proposed to exist in relaxor ferroelectrics from the existence of micro-heterogeneity. This parameter was calculated from the temperature dependence of the dielectric constant in the paraelectric region, and these data are included in Table 2. These data indicate that the occurrence of lower dielectric constants and transition temperatures corresponded to an increase in the diffuseness parameter.

Table 2: 1 kHz Dielectric data of PMN-PT samples sintered with excess PbO.

		1% PbO			3% PbO		
Temp. (°C)	Time (min)	K_{MAX}	T_C(°C)	δ(°C)	K_{MAX}	T_C(°C)	δ(°C)
900	10	10900	23	49.4	4300	18	72.8
	20	12000	24	48.8	9100	17	56.9
	30	13100	23	45.8	9500	17	55.6
	60	12500	22	51.4	9980	12	61.9
	120	10700	21	57.3	9640	9	69.8
	240	11400	22	51.9	9110	9	66.1
950	10	13000	24	48.4	7760	14	63.0
	20	14200	22	48.8	9440	14	68.2
	30	14000	22	52.3	8810	10	76.0
	60	13100	20	57.3	7850	7	86.9
	120	12900	18	57.3	9050	7	79.9
1000	10	14500	20	46.5	9120	13	67.9
	20	14700	20	47.0	9100	10	60.5
	30	13000	20	47.2	8180	6	69.4
	60	12400	17	51.8	8580	2	86.4
	120	12200	20	55.1	9130	5	80.4

No dielectric ageing was observed in the stoichiometric PMN-PT sample, as the dielectric curves were identical upon heating and cooling. However, all of the excess PbO samples exhibited significant dielectric ageing. An example of this phenomenon is shown in Figure 2, where dielectric constant curves obtained on heating and cooling are compared for the 1% PbO sample sintered at 1000°C for one hour. The dielectric constant is depressed in the region near room temperature, where the sample was aged. Generally, the ageing increased with sintering temperature, time, and excess PbO content, following the same trend of the decreased dielectric constants and transition temperatures.

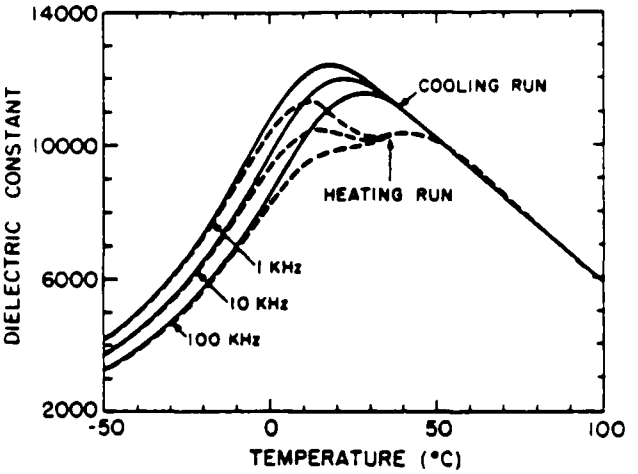

Figure 2: Dielectric constant on heating and cooling, showing ageing in the 1% PbO sample, sintered at 1000°C for one hour.

DISCUSSION OF RESULTS

PbO was extremely important to the sintering of these PMN-PT ceramics. It was not possible to sinter stoichiometric PMN-PT ceramics (without excess PbO) at 1000°C in air, because PbO loss was rapid enough to hinder the sintering process. However, sintering the same pellets in a PbO atmosphere at the same temperature resulted in densities of 98% theoretical and excellent dielectric properties. Also, the excess PbO improved the sintering of the PMN-PT ceramics, allowing for densification to better than 97% theoretical at temperatures as low as 900°C. However, the improved sintering was at the cost of lower dielectric constants and transition temperatures, and significant dielectric ageing.

The degraded dielectric properties of excess PbO samples may have been caused by the presence of an amorphous, PbO-rich grain boundary phase, which has previously been identified in PMN ceramics by TEM analysis [13]. In the present study, the addition of excess PbO may have enhanced this grain boundary phase, even though most of the excess PbO was driven off during sintering. However, the presence of a grain boundary phase cannot explain the decrease of transition temperature or the large increase in the diffuseness, observed with sintering time.

The lower dielectric constants and transition temperatures, the increased diffuseness, and the appearance of ageing in the excess PbO samples are most likely related. These phenomena could have resulted from a change in the defect structure of the PMN-PT grains caused by an interaction of the excess PbO with the PMN-PT grains during sintering. If this is true, then the actual time during the sintering process at which the excess PbO is driven off would be important. This possibly explains why the dielectric properties of similar PMN-PT

ceramics, prepared with excess PbO, were improved when a complex sintering schedule was employed [5,6]. This also points to the need for an investigation of the effect of heating rates on the sintering and dielectric properties.

This investigation has revealed that dielectric ageing is a serious problem in PMN ceramics prepared by adding excess PbO as a sintering aid. Dielectric ageing has been observed in PMN ceramics doped with MnO [14], and it has been suggested that any B-site acceptor dopant will induce ageing in PMN [15]. The ageing observed in the present study is similar in that it was most likely caused by a change in the defect structure. However, in this case, the experimental evidence points to defects on the A-site. To date, the existence and/or absence of dielectric ageing in PMN ceramics prepared with excess PbO has not been reported in the literature [4,5]. The general trend over the past few years has been to report the temperature dependence of dielectric properties based on cooling runs, and this would obscure any ageing phenomena if they were present. The results of this study suggest that ageing in PMN ceramics is an important parameter, and that it should be considered in more detail in any processing study.

SUMMARY

The results of this investigation are summarized below:

1) PMN-PT ceramics, prepared by the columbite approach were sintered in the range of 900 to 1000°C, by sintering in a PbO atmosphere, or by adding excess PbO and sintering in air.

2) The largest maximum dielectric constant (17500 at 1 kHz and 23°C) was achieved in a stoichiometric PMN-PT sample sintered in a PbO atmosphere at 1000°C for two hours, and this sample did not exhibit dielectric ageing.

3) Excess PbO samples sintered in air exhibited severely degraded dielectric properties (lower dielectric constants and transition temperatures, along with significant dielectric ageing).

4) The control of PbO stoichiometry was extremely important to the sintering and resultant dielectric properties of these PMN-PT ceramics.

5) Dielectric ageing is an important consideration when deciding the effectiveness of any processing technique for PMN ceramics.

REFERENCES

1. S.L. Swartz and T.R. Shrout, "Fabrication of Perovskite Lead Magnesium Niobate," Mat. Res. Bull. 17, 1245-1250 (1982).

2. S.L. Swartz, T.R. Shrout, W.A. Schulze, and L.E. Cross, "Dielectric Properties of Lead Magnesium Niobate Ceramics," J. Am. Cer. Soc. 67 (5), 311-315 (1984).

3. M. Lejeune and J.P. Boilot, "Formation Mechanism and Ceramic Process of the Ferroelectric Perovskites: $Pb(Mg_{1/3}Nb_{2/3})O_3$ and $Pb(Fe_{1/2}Nb_{1/2})O_3$," Cer. Int. 8 (3), 99-103 (1982).

4. M. Lejeune and J.P. Boilot, "Influence of Ceramic Processing on the Dielectric Properties of Lead Magnesium Niobate Ceramics," Cer. Int. 9 (4), 119-122 (1983).

5. M. Lejeune and J.P. Boilot, "Low Firing Dielectrics Based on Lead Magnesium Niobate," Mat. Res. Bull. 20, 493-499 (1985).

6. M. Lejeune and J.P. Boilot, "Optimization of Dielectric Properties of Lead Magnesium Niobate Ceramics," Bull. Am. Cer. Soc. 64 (4), 679-682 (1985).

7. G. Desjardin, M. Halmi, J.M. Haussonne, and B. Raveau, "Nouveaux Materiaux Dielectriques a Base de Condensateurs Multicouches de Type II," presented at Sciences of Ceramics, Orleans, France (1985).

8. D.J. Voss, S.L. Swartz, and T.R. Shrout, "The Effects of Various B-Site Modifications on the Dielectric and Electrostrictive Properties of Lead Magnesium Niobate Ceramics," Ferroelectrics 50 (1/2/3/4), 203-208 (1983).

9. T.R. Shrout, M.J. Haun, and S.L. Swartz, "Dielectric Properties in the $PbFe_{1/2}Nb_{1/2}O_3$-$PbNi_{1/3}Nb_{2/3}O_3$ Solid Solution System," Bull. Am. Cer. Soc. 63 (6), 808-810,820 (1984)

10. L.C. Veitch, "Dielectric Properties of Lead Nickel Niobate," B.S. Thesis, The Pennsylvania State University, University Park, PA (1983).

11. P. Groves, "Fabrication and Characterization of Ferroelectric Perovskite Lead Indium Niobate," to be published.

12. K. Uchino, L.E. Cross, S.J. Jang, and R.E. Newnham, "Electrostrictive Effect in Lead Magnesium Niobate Single Crystals," J. Appl. Phys. 51 (2), 1142-1145 (1980).

13. E. Goo, G. Thomas, T. Yamamoto, and K. Okazaki, "Microstructure of Lead-Magnesium-Niobate Ceramics," to be published.

14. W. Pan, E. Furman, G.O. Dayton, and L.E. Cross, "Dielectric Ageing Effects in Doped Lead Magnesium Niobate: Lead Titanate Ceramics," to be published.

15. T.R. Shrout, "A Review of the Processing of Lead-based Ferroelectric Relaxors for Capacitors," to be published.

ACKNOWLEDGEMENTS

The authors would like to thank Jenny Nicol and Gaylord Shawver for their contributions to the research, and Tom Shrout for helpful discussions.

DIELECTRIC AGING EFFECTS IN DOPED LEAD MAGNESIUM NIOBATE: LEAD TITANATE RELAXOR FERROELECTRIC CERAMICS

W.Pan G. O. Dayton and L. E. Cross
Materials Reseach Laboratory
The Pennsylvania State University
University Park, PA 16802

Abstract

No obvious dielectric aging effects have been observed in pure $.9Pb(Mg_{1/3}Nb_{2/3})O_3$:.$1PbTiO_3$ relaxor ferroelectric ceramics in this study. The addition of small amounts of MnO however, induces aging effects. Aging effects preferentially reduce the dispersive component of the weak field permittivities above the aging temperature. Isothermal aging rates are observed to increase with increasing doping level. Dielectric constants vs the logarithm of time at constant temperature level out with time. The origin of aging for this type of relaxor material can be explained in terms of the volume stabilization of the polar vectors in polar micro-regions by the defect dipoles introduced by the doping.

Introduction

If domain stabilization due to defect dipoles interacting with the polarization vectors is regarded as the major contributor to aging in normal ferroelectics[1], a similar phenomenon may be expected to occur in relaxor ferroelectrics. Thus, it is not surprising that relaxors such as PLZT [2] and SBN[3] which by their chemical nature must have a highly defective structure show strong aging effects. In a macroscopically defect free (fully stuffed structure) like $Pb(Mg_{1/3}Nb_{2/3})O_3$, charged defects may be eliminated by very careful preparation so that this mechanism should not occur.

For these micro- polar systems, the strain associated with the onset of ferroelectricity will be miniscule so that the strain destablization of the domain structure which may contribute to aging in normal macro-domain ferroelectrics should also be absent.

Thus, in relaxors like PMN, if the defect concentration can be kept very low, it may be possible to have no significant aging effects within the diffused phase transition temperature range.

To further explore the role of defects in the aging phenomena in relaxors. .9PMN: .1PT compositions have been fabricated in both pure and MnO doped forms. This work reports the aging behaviours for these ceramics.

Experimental Procedure

Ceramic samples of .9 PMN: .1PT for this study were prepared using pre-reaction of MgO and Nb_2O_5 to first form the columbite structure precursor in the manners discussed in earlier papers[4,5]. For the doping study, MnO was introduced using a dilute $Mn(NO_3)_2$ solutions added to the calcine. Pure, defect free samples require some care in preparation. The best result can be obtained when the original oxides are pure, batching is done with regard to loss on ignition, processing is free from contimination and lead volatilization is carefully controlled. Final sintered samples were all above 97% of theoretical density and were shown by X-ray diffraction to be free of pyrochlore phase contamination. Aging was accomplished by first heating the samples above 160^0C to relieve all earlier aging, then bring the samples down to a fixed temperature and starting the measuring clock. Dielectric constants vs temperature measurements were begun from lower temperature up to study aging and from higher temperature down to study deaging. Isothermal aging was

CH2358-0/86/0000-0645 $1.00

carried out in an insulated chamber containing a coil connected to a constant temperature water bath[6]. The temperature variation monitored by a digital thermometer was shown be ±0.1C.

Experimental Results

Fig.1 shows the weak field (5v/cm) dielectric constants vs temperature for .1%(wt) MnO doped sample. The solid curves show the data obtained after aging 1000 hours at room temperature. The dotted curves show the data for the sample freshly deaged at 160°C for 30 minites. It is observed that from the aging temperature up, the magnitude and dispersive component of the weak field permittivities have been greatly reduced.Below the aging temperature, however, the magnitude and dispersion of dielectric constants are unaffected by aging. In contrast, Fig.2 shows dielectric constants vs temperature for the pure composition aged and measured in exactly the same manners as the doped and aged sample. The sample can be seen to be almost completely free of aging. Fig.3 shows the dielectric constant reduction as a function of the logarithm of time for different amounts of MnO doping. Differences in dielectric constants in the freshly deaged states among the samples with different MnO doping were taken into account by dividing the data by the initial dielectric constant data. An increasing slope with increasing doping level is observed. The pure composition is shown to be almost free of aging. Fig.4 shows dielectric constants as a function of the logarithm of time. A leveling out of dielectric constants with the logarithm of time is observed.

Summary and Discussion

The data presented in Fig.2 and Fig.3 confirms that there are no obvious aging effects in pure 0.9 PMN: 0.1PT ceramic in the vicinity of the average Curie temperature. Aging effects appear in doped samples and increase with increasing doping level which clearly suggests the role of defect dipoles. Magnese ions were added in the valence 2 form which may survive at elevated temperature because they are already in their most reduced form . The size of Mn^{2+} is comparable to the B ion in perovskite structure. For every Mn^{2+} sitting in a B site, an oxygen vacancy is generated. A defect dipole will be formed by the vacancy charge and Mn^{2+}. The orientation of the dipole can be adjusted by oxygen vacancy diffusion from one face center site to the other in the perovskite unit cell. Domains can be stabilized under the local field provided by the defect dipoles.

The retention of dispersion below the aging temperature is a characteristic of relaxor ferroelectrics. Paraelectric to ferroelectric transitions continue below the aging temperature producing fresh micropolar regions which can dominate weak field dielectric properties. Above the aging temperature, however, polar regions become increasingly more unstable and convert to paraelectric phases. Neither the stabilized polar regions nor the paraelectric phase regions show dispersion at the frequencies used. Therefore, the dispersive component is greatly reduced at and above the aging temperature.

Fig.4 shows the nature of isothermal aging. Unlike normal ferroelectrics such as $BaTiO_3$ ceramics[7], this ceramic shows dielectric aging which is nonlinear with respect to the logarithm of time. It is well known that at the beginning of aging, errors in measuring the zero time can contribute to the nonlinearity at early stage[6]. The aging behaviours at first few minites are difficult to ascertain. In this study, the nonlinearity at times longer than 60 minites has been very reproducible. Such behaviour suggests that this material is composed of the regions that show quite high aging rates in conjunction with the regions that show little or no aging. The theory that relaxor ferroelectrics are composed of chemically heterogeneous regions with a range of Curie temperatures is currently well accepted[8]. We may therefore suppose that polar regions are predominately responsible for aging and that paraelectric regions of the material age very slowly or not at all. The non-aging regions make a greater and greater contribution to the observed permittivity until a constant value is approached at extended time.

Acknowledgement

We wish to thanks E. Furman for some of interesting discussions and Q. Y. Jiang for her help in measurements.

Reference

[1] Sadayuki Takahashi."Effects of Impurity Doping in Lead Zirconate-Titanate Ceramics". Ferroelectrics Vol.41 PP.143-156 (1982)

[2] W. A. Shulze, J. V. Biggers and L. E. Cross. "Aging of Dielectirc Dispersion in PLZT Relaxor Ceramics" J. Amer. Ceram. Soc. 61 (1978) PP 46-49

[3] G. Borchhardt, J. Von Cieminski and G. Schmidt. "Aging of Strontiun Barium Niobate and PLZT Ceramics". Phys. Stat. Sol. (a) 59.PP 749 (1980)

[4] S. L. Swartz and T. R. Shrout."Frabrication of Perovskite Lead Magnesium Niobate". Mat. Res. Bull 17 (1982) PP 1245-1250

[5] S. L. Swartz, T. R. Shrout, W. A. Schulze and L. E. Cross."Dielectric Properties of Lead Magnesium Niobate Ceramics" J. Amer. Ceram. Soc. 67 (1984) PP 311-315

[6] W. A. Schulze and J. V. Biggers."Dielectric Aging in the PLZT System". Ferroelectrics, Vol.9 PP 203-207 (1975)

[7] K.W. Plessner. " Aging of Dielectric Properties of Barium Titanate Ceramics." Proc. Phy. Soc. B69 PP1261 (1956)

[8] N. Setter and L.E.Cross. " The Role of B-Site Cation Disorder in Diffuse Phase Transition Behavior of Perovskite Ferroelectrics". J. Appl. Phys.51(8) PP 4356-60 (1980)

Figures

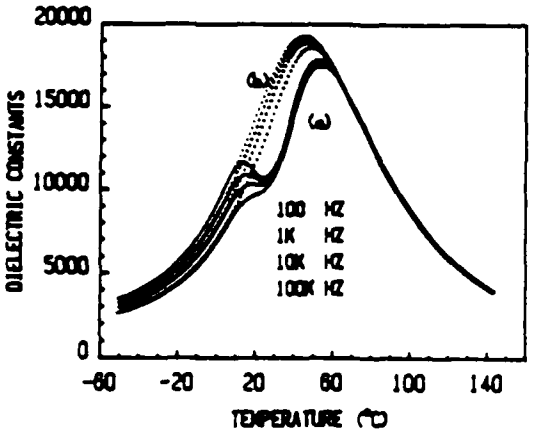

FIG.1 Dielectric constants vs temperature for .1%(WT) MnO doped .9PMN.1PT. (a) The sample aged at room temperature for 1000hrs. (b) The thermal deaged sample.

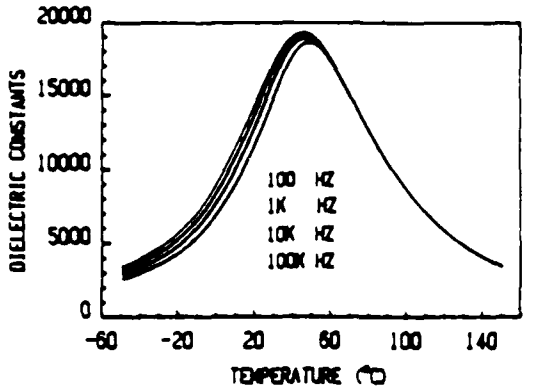

FIG.2 Dielectric constants vs temperature for pure .9PMN.1PT aged at room temperature for 1000hrs.

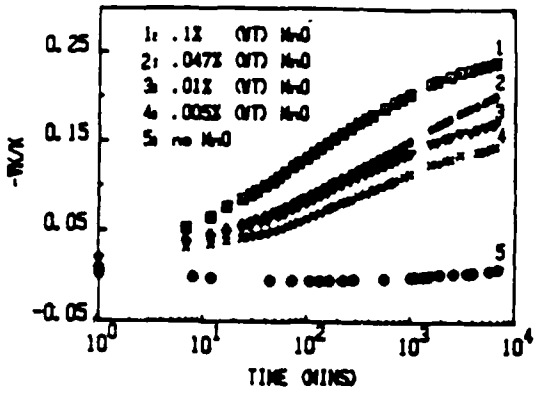

FIG.3 Fractional reduction of dielectric constants vs logarithm of time for .9PMN.1PT with different MnO doping at 37.5 °C (Frequency 1KHz).

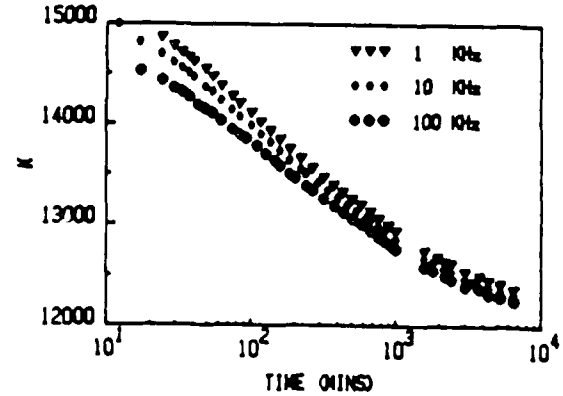

FIG.4 Dielectric constants vs logarithm of time for .1%(WT) MnO doped .9PMN.1PT at 37.5 °C

STABILITY OF PEROVSKITE PHASE IN $Pb(Zn_{1/3}Nb_{2/3})O_3$ AND OTHER $A(B'B'')O_3$ PEROVSKITES

A. Halliyal, T.R. Gururaja, U. Kumar and A. Safari

Materials Research Laboratory
The Pennsylvania State University
University Park, PA 16802

Abstract

It is difficult to prepare ceramics of $Pb(Zn_{1/3}Nb_{2/3})O_3$ (PZN) and several other lead based $A(B'B'')O_3$ perovskites in perovskite form due to the formation of a stable lead niobate pyrochlore phase. In this study two approaches have been employed to stabilize perovskite structure in PZN. In the first approach perovskite PZN was prepared by the addition of small amount of a stable perovskite compound (7 mol% of $BaTiO_3$, 10 mol% $SrTiO_3$). In the second approach perovskite PZN-PT was prepared by either quenching or slow cooling a mixture of molten PZN and PbO flux. The kinetics of the transformation of perovskite to pyrochlore phase was studied.

1. Introduction

PZN is a ferroelectric crystal with a partially disordered perovskite structure. It undergoes a diffuse phase transition near 140°C. The crystal symmetry is rhombohedral (ferroelectric) at room temperature and cubic (paraelectric) above 140°C [1,2]. The solid solution between PZN with rhombohedral symmetry and $PbTiO_3$ (PT) with tetragonal symmetry, has a morphotropic phase boundary (MPB) near 9 mole% PT. Single crystals with compositions near MPB show unusually large dielectric, piezoelectric and electrostrictive coefficients [3,4]. PZN and PZN-PT single crystals can be grown rather easily by a flux method.

Unfortunately, it is very difficult to prepare pure PZN or PZN-PT ceramics with the perovskite structure by conventional ceramic processing. The product obtained by solid state reaction at about 1100°C is largely a cubic pyrochlore phase of the type $Pb_3Nb_4O_{13}$. The presence of pyrochlore phase is detrimental to both dielectric and piezoelectric properties. The formation of pyrochlore phase has been observed in a number of $A(B'B'')O_3$ type ferroelectric compounds with perovskite structure.

The problem of pyrochlore formation has been studied extensively in $Pb(Mg_{1/3}Nb_{2/3})O_3$ (PMN) ceramics [5,6]. By following a different processing scheme, Swartz and Shrout were able to stabilize perovskite structure in PMN. The reaction sequence used by them is as follows:

$$MgO + Nb_2O_5 \xrightarrow{1000°C} MgNb_2O_6$$

$$MgNb_2O_6 + 3PbO \xrightarrow{900°C} 3Pb(Mg_{1/3}Nb_{2/3})O_3$$

In this method, MgO is pre-reacted with Nb_2O_5 to form $MgNb_2O_6$ which has columbite structure. $MgNb_2O_6$ is then reacted with PbO to obtain 100% pure perovskite PMN ceramics. By this processing scheme also (by reacting $ZnNb_2O_6$ with PbO) it is not possible to prepare PZN in pure perovskite form.

In the next section an analysis of the stability of perovskite structure in a number of ABO_3 or $A(B'B'')O_3$ perovskites is given by considering the structure field map and ionic nature of chemical bonds. The possibility of stabilizing perovskite structure in PZN by adding only a small amount of second perovskite compound is examined.

2. Stability of Perovskite Structure

The stability of different crystal structures belonging to a particular class of compounds can be studied by structure field maps [7]. Structure field maps provide a useful way of correlating ionic radii with structure types. A structure field map of ABO_3 compounds near the perovskite region is shown in Fig. 1. Here r_A is the radius of the larger cation and r_B is the radius of smaller cation. Several ABO_3 type ferroelectric oxides are marked in this diagram. It is clear that all the compounds under consideration fall well within the ideal perovskite region of the structure field map. However, it is difficult to prepare PMN, PZN, PFN, PFW, PNN and PIN in perovskite form by the usual ceramic processing techniques. Preparation of ceramics of these

CH2305-5/86/0000-0437 $1.00

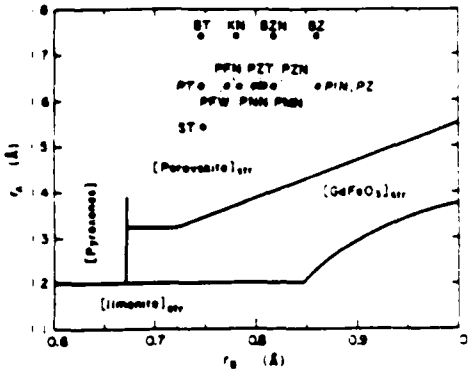

Figure 1. Structure field map of perovskites. BT:$BaTiO_3$, ST:$SrTiO_3$, PT:$PbTiO_3$, KN:$KNbO_3$, BZ:$BaZrO_3$, PZ:$PbZrO_3$, PZT:$Pb(Zr_{1/2}Ti_{1/2})O_3$, PMN:$Pb(Mg_{1/3}Nb_{2/3})O_3$, PZN:$Pb(Zn_{1/3}Nb_{2/3})O_3$, PFN:$Pb(Fe_{1/2}Nb_{1/2})O_3$, PFW:$Pb(Fe_{2/3}W_{1/3})O_3$, PNN:$Pb(Ni_{1/3}Nb_{2/3})O_3$, PIN:$Pb(In_{1/2}Nb_{1/2})O_3$, BZN:$Ba(Zn_{1/3}Nb_{2/3})O_3$.

materials by mixed oxide method yields a mixture of perovskite and pyrochlore phases. For an ABO_3 compound to form a stable perovskite structure the ionic radii of the cation should be within proper limits and the cations-anions should form strong mutual ionic bond.

Goldschmidt has proposed the concept of tolerance factor to describe the stability limits of a crystal structure in terms of the ionic radii [8]. For the perovskite structure, the tolerance factor t is given by

$$t = \frac{r_A + r_O}{\sqrt{2}(r_B + r_O)} \qquad (1)$$

Here r_A and r_B are the ionic radii of cations A and B and r_O is the ionic radius of oxygen. The perovskite structure is stable if t is large.

The second factor to be considered is the ionic character of the chemical bonds in the compound. The percentage of ionic character of the bonds is proportional to the electronegativity difference between cations and anions.

For several ABO_3 compounds with perovskite structure, the tolerance factor were calculated using equation (1) and the ionic radii proposed by Shannon and Prewitt [9,10]. The electronegativity differences of cation A and oxygen (χ_{A-O}) and cation B and oxygen (χ_{B-O}) were calculated using Pauling's electronegativity scale [11]. For $A(B'B'')O_3$ type perovskites, a weighted average value was used for r_B and χ_{B-O}. A plot of average electronegativity difference $(\chi_{A-O}+\chi_{B-O})/2$ vs. the tolerance factor is shown in Fig. 2. For the perovskite compounds under consideration the tolerance factor t is within the limits $0.96<t<1.06$. A few interesting observations can be made from Fig. 2 [1]. $BaTiO_3$ and $KNbO_3$, have both large tolerance factor and large electronegativity difference and hence these compounds should have stable perovskite structure [2]. For PMN, PZN, PFN, PFW, PNN and PIN, both the tolerance factor and electronegativity difference are small and hence they may not form perovskite structure easily.

It should be more difficult to stabilize PZN in perovskite form than PMN which is in accordance with experimental results. PMN can be prepared in perovskite form by repeated calcination or by the reaction sequence proposed by Swartz and Shrout [5]. It is not possible to stabilize PZN in perovskite form by these techniques. $PbTiO_3$ has slightly higher electronegativity difference and larger tolerance factor than PZN. In the solid solution system (1-x) PZN-xPT, compostions can be stabilized in perovskite form if $x>0.25$. The reason for this is evident from Fig. 2. The addition of PT to PZN increases both the tolerance factor and the electronegativity difference. Since $BaTiO_3$ has the largest electronegativity difference and tolerance factor it should be possible to stabilize PZN or PMN in perovskite form by adding a smaller percentage of $BaTiO_3$ than $PbTiO_3$. It has been shown that 6 to 7 mole% of $BaTiO_3$ is sufficient to stabilize PZN in perovskite structure [12]. Table 1 gives the amount of different oxides needed to stabilize perovskite structure in PZN by conventional ceramic processing. The minimum amount of oxides needed to stabilize perovskite phase may vary slightly depending on the conditions followed in ceramic processing. The phase relations and dielectric properties of ceramics in the PZN-$BaTiO_3$ [12], PZN-$SrTiO_3$ [13,14], PZN-$BaTiO_3$-$PbTiO_3$ [15] system have been reported. Most of the compositions in the above solid solution systems show a diffuse phase transition with an increase in Curie temperature with increasing

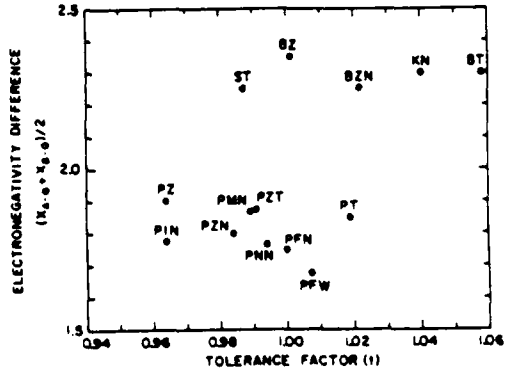

Figure 2. Plot of electronegativity difference vs. tolerance factor.

TABLE 1. Amount of additives needed to stabilize perovskite phase in PZN

Additive	Mole%
$BaTiO_3$	6- 7
$SrTiO_3$	9-10
$PbTiO_3$	25-30
$BaZrO_3$	15-18
$Ba(Zn_{1/3}Nb_{2/3})O_3$	15
Replacing Pb with K	10
$PbZrO_3$	55-60

frequency, characteristic of ferroelectric relaxors.

The second approach to stabilize perovskite PZN by either quenching or slow cooling a mixture of PZN and PbO flux, is discussed in the next section.

3. Preparation of Perovskite Phase PZN-PT Powder by Flux Method

In PZN-PT system, single crystals near MPB (9 mol% PT) can be grown easily in PbO flux. This indicates that perovskite phase can be stabilized in molten flux environment in this system. In the present work PZN-PT powder near MPB was prepared by two different methods taking advantage of the stability of perovskite phase in PbO flux.

In the first method, one mole of 0.91 PZN-0.09 PT was mixed with two moles of PbO flux and heated to 1150-1200°C in a platinum crucible and held at this soak temperature for 3-4 hours. The molten mass was poured into a beaker containing water. The water quenched powder was leached in boiling acetic acid for a few hours to remove PbO flux and filtered. The x-ray diffraction pattern of dried powder revealed pure perovskite type structure, but the diffraction peaks were not very sharp, probably because the powder was not completely crystalline due to rapid quenching from 1200°C. Attempts to improve the crystallinity of the powder by annealing at 600°C led to partial formation of pyrochlore phase. Studies on the perovskite to pyrochlore phase transformation after heat treatment will be discussed in the next section.

In the second method, the molten mixture was cooled in the furnace at approximately 200°C/hr. The solidified mass in the crucible was leached in boiling acetic acid PZN-PT powder of particle size varying from micron to millimeter size was obtained by this process. The x-ray diffraction patterns of the powder showed sharp peaks corresponding to perovskite phase. The sharp x-ray diffraction peaks indicated that the crystallinity of the powder obtained by furnace cooling was superior to that obtained by water quenching. Chemical analysis of the powders showed that water quenched powder was deficient in ZnO and had excess of Nb_2O_5 compared to the stoichiometric composition. The composition of furnace cooled powder was very close to the stoichiometric composition. Further details about experimental procedure can be found in ref. [16].

4. Perovskite to Pyrochlore Phase Transformation

Heat treatment of PZN-PT powder prepared by flux method resulted in a partial transformation of perovskite to pyrochlore phase. Detailed studies were performed to understand the kinetics of the phase transformation.

For the heat treatment studies, a fast-firing furnace system developed by Fox et al. [17] was used. A digitally controlled stepper motor was used to inject samples to the required temperature zone in a horizontal tubular furnace in five minutes. The sample was held at the soak temperature for different periods of time and then withdrawn to room temperature in five minutes. This controlled temperature profile firing system enabled to carry out precise heat treatment on the samples. The relative amounts of perovskite and pyrochlore phases were determined using powder x-ray diffraction patterns of samples by measuring the major x-ray peak intensities for perovskite and pyrochlore phases [(110) and (222) respectively]. The percentage of perovskite phase was calculated using the following equation:

$$\% \text{ Perov} = \frac{100 \times I_{perov}}{(I_{perov}+I_{pyro})}$$

The results of the heat treatment studies are listed in Table 2. From the Table it is clear that water quenched powder transforms to pyrochlore phase on heat treatment more easily than furnace cooled powder. A heat treatment of the powders at 600°C for 15 minutes resulted in 85% pyrochlore phase in the case of water quenched powder, whereas only 9% of the furnance cooled powder transformed to pyrochlore phase. Only 20% of furnace cooled powder transformed to pyrochlore phase on heating to 900°C for 15 minutes.

TABLE 2. Effect of heat treatment on perovskite to pyrochlore transformation of PZN-PT powder

Temperature	Duration	Water Quenched Powder % Perovskite	Furnace Cooled Powder % Perovskite
500°C	15	57	97
	30	44	—
	60	35	95
600°C	15	16	91
	30	15	90
	60	12	—
700°C	15	—	86
900°C	15	—	80

Heat treatment of calcined powders in the PZN-$BaTiO_3$ and PZN-$SrTiO_3$ system also indicated transformation of perovskite phase to pyrochlore phase in samples containing smaller amounts of $BaTiO_3$ or $SrTiO_3$. The fraction of pyrochlore phase as a function of heat treatment temperature is shown in Fig. 3 for 0.95 PZN-0.05 ST [13]. The transformation of perovskite to pyrochlore phase was not observed in compositions containing a higher fraction of $BaTiO_3$ or $SrTiO_3$.

5. Pyrochlore Formation in $A(B'B'')O_3$ Perovskites

The formation of stable pyrochlore phase has been observed in ceramic preparation of a number of $A(B'B'')O_3$ type perovskites in addition to PMN and PZN. Many of these compounds are promising materials for multilayer capacitors because of their high dielectric constant and low firing temperature [18,19]. The use of these ferroelectric materials in ceramic form for capacitor, transducer or micropositioner applications is restricted because of the formation of pyrochlore phase. By the processing scheme suggested by Swartz and Shrout [5], perovskite structure can be stabilized in $Pb(Ni_{1/3}Nb_{2/3})O_3$, $Pb(Fe_{1/2}Nb_{1/2})O_3$, $Pb(Sc_{1/2}Nb_{1/2})O_3$, $Pb(Sc_{1/2}Ta_{1/2})O_3$, $Pb(Mg_{1/3}Ta_{2/3})O_3$ and a few other compounds. But this processing scheme fails to stabilize perovskite structure in several other perovskites like PZN, $Pb(Zn_{1/3}Ta_{2/3})O_3$, and $Pb(In_{1/2}Nb_{1/2})O_3$. For such perovskite compounds, the addition of a small amount of stable perovskite compound such as $BaTiO_3$ or $SrTiO_3$ can be used to stabilize perovskite structure.

6. Conclusions

From the present investigation it is clear that in $A(B'B'')O_3$ perovskites a large tolerance factor and a large fraction of ionic bonding are necessary to stabilize the perovskite structure. Several of these comounds such as $Pb(Mg_{1/3}Nb_{2/3})O_3$, $Pb(Zn_{1/3}Nb_{2/3})O_3$ and $Pb(In_{1/2}Nb_{1/2})O_3$ are difficult to synthesize in perovskite form by the usual ceramic processing. $BaTiO_3$ or $SrTiO_3$ seem to be excellent additives to stabilize perovskite structure in these compounds.

The stability of perovskite phase and the kinetics of transformation of perovskite to pyrochlore phase were studied in $Pb(Zn_{1/3}Nb_{2/3})O_3$. It has been shown that only about 7 mole% of $BaTiO_3$ and 10 mole% of $SrTiO_3$ are needed to stabilize perovskite phase in PZN. Perovskite phase could also be stabilized in PZN in molten PbO flux. Perovskite PZN-PT powder prepared by molten flux method converts partially to pyrochlore structure on heat treatment at temperatures greater than 500°C. It is clear that both thermodynamics of the system and kinetics of the perovskite to pyrochlore phase transformation should be considered in order to understand the stability of perovskite structure in PZN and other similar $A(B'B'')O_3$ perovskite compounds.

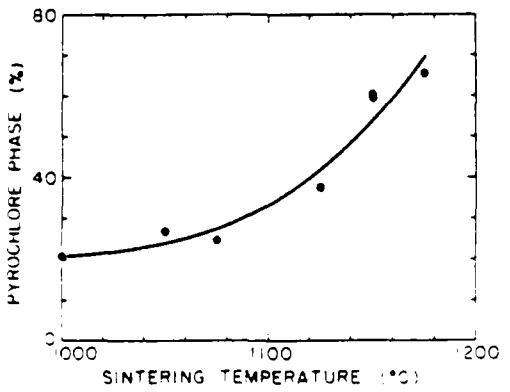

Figure 3. Percentage of pyrochlore phase vs. sintering temperature for 0.95PZN-0.05$SrTiO_3$.

7. Acknowledgement

The authors are grateful to the Office of Naval Research for the financial support for this work.

8. References

1. Y. Yokomizo, T. Takahashi and S. Nomura, J. Phys. Soc. Jpn. 28, 1278 (1970).

2. J. Kuwata, K. Uchino and S. Nomura, Ferroelectrics 22, 863 (1979).

3. J. Kuwata, K. Uchino and S. Nomura, Jpn. J. Appl. Phys. 21, 1298 (1982).

4. S. Nomura and J. Kuwata, Mat. Res. Bull. 14, 769 (1979).

5. S.L. Swartz and T.R. Shrout, Mat. Res. Bull. 17, 1245 (1982).

6. S.L. Swartz, T.R. Shrout, W.A. Schulze and L.E. Cross; J. Am. Cer. Soc., 67, 311 (1984).

7. O. Muller and R. Roy, 'Crystal Chemistry of Nonmetallic Materials', Springer-Verlag, NY, 1974.

8. V.M. Goldschmidt, Geochemische Verteilungsgesetze der elemente I-IX, Skrift. Norske, Vid. Akad. Oslo, I Mat-Naturv. kl.

9. P.D. Shannon and C.T. Prewitt, Acta Cryst. B25, 925 (1969).

10. R.D. Shannon and C.T. Prewitt, Acta. Cryst. B26, 1046 (1970).

11. L. Pauling, 'The Nature of Chemical Bonds', Cornell University Press, NY 1960.

12. A. Halliyal, U. Kumar, R.E. Newnham and L.E. Cross, J. Am. Cer. Soc. (submitted).

13. J. Belsick, B.S. Thesis, The Pennsylvania State University, 1986.

14. O. Furukawa, Y. Yamashita, M. Harata, T. Takahashi and K. Inagaki, Jpn. J. Appl. Phys. 24, 96 (1985).

15. A. Halliyal, U. Kumar, R.E. Newnham, and L.E. Cross, J. Am. Cer. Soc. (submitted).

16. T.R. Gururaja, A. Safari and A. Halliyal, J. Am. Cer. Soc. (submitted).

17. B.H. Fox, G. Dayton, P. Moses and J.V. Biggers, Bull. Am. Ceram. Soc. 64, 1141 (1985).

18. M. Yonezawa, Bull. Am. Cer. Soc. 52, 1375 (1983).

19. T.R. Shrout, S.L. Swartz and M.J. Haun, Cer. Bull. 63, 809 (1984).

Dielectric and Piezoelectric Properties of $Pb(Zn_{1/3}Nb_{2/3})O_3$-$PbTiO_3$-$BaTiO_3$ Ceramics

S.L. Baumler, A. Halliyal, and R.E. Newnham

Materials Research Laboratory
Pennsylvania State University
University Park, Pennsylvania 16802

Abstract

Previous studies in the (1-x)$Pb(Zn_{1/3}Nb_{2/3})O_3$-x$PbTiO_3$ system have shown the existence of a morphotropic phase boundary near x=0.09. Single crystals of this composition grown in the perovskite form using PbO flux method show excellent piezoelectric and dielectric properties. However it is difficult to prepare polycrystalline ceramics near the morphotropic phase boundary because of the stability of a competing lead niobate pyrochlore phase. Recently, it has been shown that the formation of the pyrochlore phase can be suppressed by the addition of a small amount of $BaTiO_3$. In the present study, compositions near the morphotropic phase boundary were prepared in the perovskite form by the addition of 5 mole percent $BaTiO_3$. The location of the morphotropic phase boundary and the dielectric and piezoelectric properties of selected compositions in this system are described.

1. Introduction

$Pb(Zn_{1/3}Nb_{2/3})O_3$ (hereafter designated PZN) is a disordered perovskite showing a diffuse phase transition from a cubic paraelectric to a rhombohedral ferroelectric phase near 140°C [1-3]. Perovskite $PbTiO_3$ (hereafter designated PT) is also a ferroelectric material showing a transition from a cubic paraelectric to a tetragonal ferroelectric phase at 490°C. Compositions in the PZN-PT solid solution system exhibit a morphotropic phase boundary, MPB, between the rhombohedral and tetragonal phases at approximately 9 mole percent PT [3]. The dielectric and piezoelectric properties of materials near the MPB, as expected, are anomalously high. Single crystals and polycrystalline ceramics of such compositions have been prepared in the perovskite form by using a PbO flux growth method [4] and special high pressure techniques [5], respectively. However, polycrystalline ceramics cannot be obtained by standard solid state reaction without the formation of a more stable lead niobate pyrochlore phase. The presence of this pyrochlore phase is found to be detrimental to the dielectric and piezoelectric properties.

In a recent study it has been shown that the addition of only 6 to 7 mole percent of $BaTiO_3$ (hereafter designated BT) stabilizes the perovskite structure in PZN [6]. In the present work, ceramics in the PZN-PT system near the morphotropic phase boundary were prepared by stabilizing the perovskite phase with the addition of 5 mole percent BT. The location of the morphotropic phase boundary was determined and the dielectric and piezoelectric properties of selected compositions were investigated.

2. Experimental Procedure

Ceramic samples along the (.95-x)PZN - xPT - .05BT composition line, as shown in Figure 1, were prepared using reagent grade chemicals by a two stage mixed oxide technique [7]. In the first stage a precursor columbite phase ($ZnNb_2O_6$) was prepared by mixing ZnO and Nb_2O_5 in stoichiometric ratio and calcining at 1000°C for 4 hours. In the second stage the precursor was mixed in stoichiometric ratios with PbO, $BaCO_3$, and TiO_2, and processed as outlined in Figure 2. An excess of 0.5 weight percent PbO was added to compensate for PbO volatility during calcining and sintering. After calcination at 900°C for 4 hours, the calcined slug was crushed and ball milled. A polyvinyl alcohol (PVA) binder was mixed with the powders and pellets 12 mm in diameter and 2-3 mm thick were pressed at 10,000 psi. The binder was burned out by a slow heating process at 500°C for 3 hours.

Compositions with x = 0.04, 0.07, 0.10 were sintered at 1050°C to 1150°C at 25°C intervals. Pellets were placed on platinum foil in an enclosed alumina crucible and sealed with alumina cement. To further reduce PbO volatility, sintering was performed in a lead rich atmosphere by placing a small amount of an equimolar mixture of PbO and ZrO_2 in the crucible. The samples were heated to sintering temperature at 220°C/hr and held for 1, 2, or 4 hour(s) soak times and cooled in the furnace with the power off. Powder X-ray diffraction patterns of calcined powders and the sintered discs were analyzed to determine the lattice constants, appropriate structure, and the presence of pyrochlore.

In preparation for dielectric and piezoelectric measurements sample discs were polished flat and parallel and electroded with sputtered gold. An air drying silver paste was also applied to insure good electrical contact. Dielectric measurements were made using an automated system in which a temperature control box (Model 2300, Delta Design, Inc.) and LCR meters (Model 4274A and Model 4275A LCR meter, Hewlett-Packard, Inc.) were controlled by a microcomputer (Model 9816, Hewlett-Packard, Inc.). Dielectric constant and dissipation factors were determined at 100 Hz, 1 kHz, 10 kHz, and 100 kHz as the samples were cooled from 230°C to -100°C at a rate of 2 to 4 degrees per minute.

For piezoelectric measurements poling was performed on selected samples by cooling from above the transition temperature to room temperature in a stirred oil bath with an applied field of 20 kV/cm. The piezoelectric coefficients were measured on a Berlincourt d_{33}-meter (Model CPDT 3000, Channel Products, Inc.). The planar coupling coefficient k_p, frequency constant N_p, and mechanical quality factor Q were calculated by a resonance - anti-resonance technique [8] using a spectrum analyzer (Model 3585A, Hewlett-Packard, Inc.).

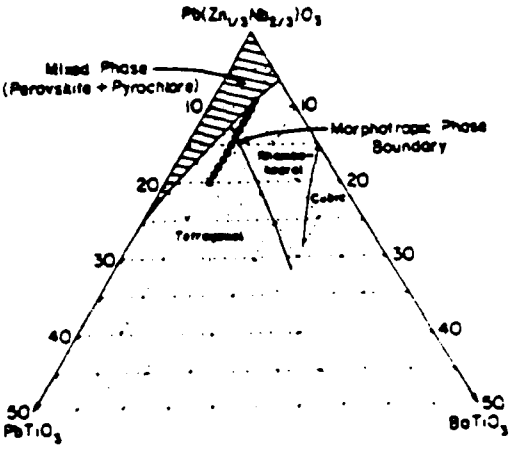

Figure 1 Phase diagram for the PZN - PT - BT ternary system. Compositions investigated in this study are marked by solid circles.

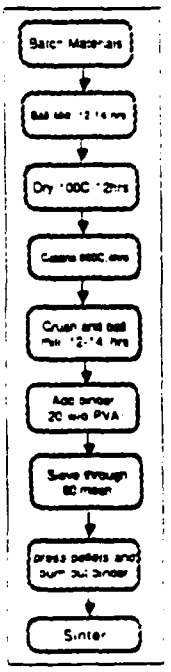

Figure 2 Processing steps for the second stage of materials preparation

3. Results and Discussion

As determined by powder X-ray diffraction, pyrochlore phase was present only in compositions with x = 0.04 and 0.05. The pyrochlore phase present was found to be of the anion deficient $Pb_3Nb_4O_{13}$ form. The perovskite phase was stabilized in compositions containing more than 5 mole percent PT. Observed by X-ray diffraction, splitting of the (002) peak begins to occur in the 7 mole percent PT composition as indicated in the plot of lattice constants versus composition shown in Figure 3. This is evidence that the morphotropic phase boundary between the rhombohedral and tetragonal phases lies between the 6 and 7 percent PT compositions.

All samples were found to sinter to greater than 92% of theoretical density with optimum firing condition being 1100°C for 2 hours. It is important to note that samples fired above 1125°C melted.

Plots of the variation of dielectric constant and dissipation factor as a function of temperature and frequency for the 6% and 10% PT compositions are shown in Figures 4 and 5, respectively. The curves indicate behavior typical of relaxor ferroelectrics with a broad dielectric maxima and with the peak values decreasing with increasing measurement frequency. Also typical of relaxors the temperature of the dielectric maxima increased with increasing frequency. The dielectric behavior of the 15% PT composition, shown in Figure 6, clearly indicates a more normal, or ordered, ferroelectric behavior. This increase in order with the PT content is also evident from the nonlinearity and dispersion of the Curie temperatures (T_c's) as shown in Figure 7. Discrepancies in the T_c's for the 4 and 5 percent compositions were probably due to the presence of pyrochlore. The peak dielectric constants varied from 9000 to 15000 (@100 Hz with the highest values occurring at the 6 mole percent PT composition. This is in agreement with the X-ray results indicating the location of the MPB to be somewhere between 6 and 7 mole percent PT compositions.

The values of the piezoelectric coefficient d_{33}, electromechanical coupling coefficient k_p, frequency constant N_p, and mechanical quality factor Q measured on selected samples are listed in Table I. Compositions near the morphotropic phase boundary showed d_{33} values greater than 500 pC/N and k_p values up to 45%. Work is now in progress to optimize the poling conditions to further improve piezoelectric properties. Our preliminary work indicates the possibility of finding compositions in this system with properties comparable to those of modified PZT ceramics [9] with the advantage of considerably lower firing temperatures.

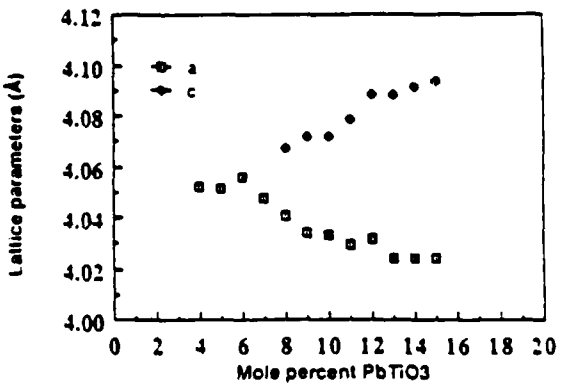

Figure 3: Lattice parameters as a function of composition

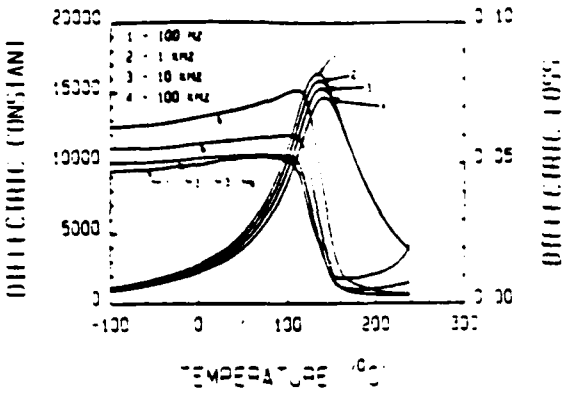

Figure 4 Dielectric constant and loss as a function of temperature and frequency for 0.89 PZN - 0.06 PT - 0.05 BT

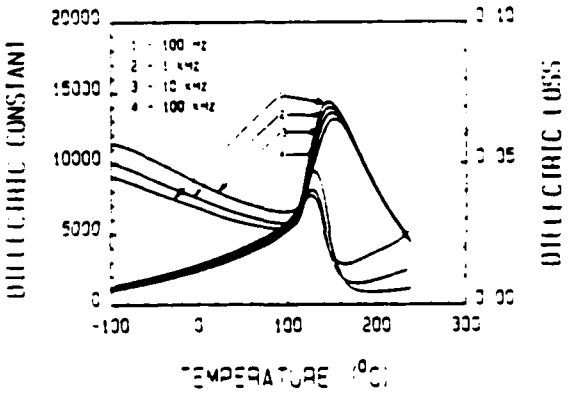

Figure 5 Dielectric constant and loss as a function of temperature and frequency for 0.85 PZN - 0.10 PT - 0.05 BT

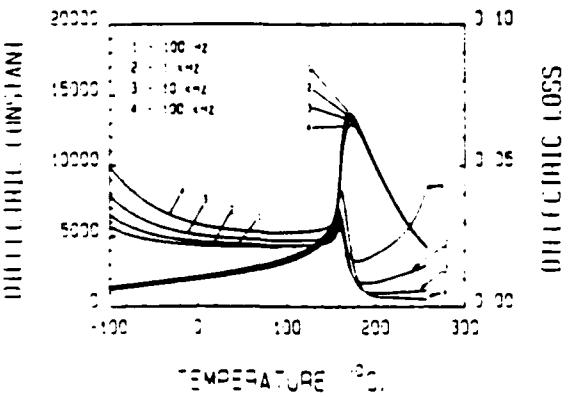

Figure 6 Dielectric constant and loss as a function of temperature and frequency for 0.80 PZN - 0.15 PT - 0.05 BT

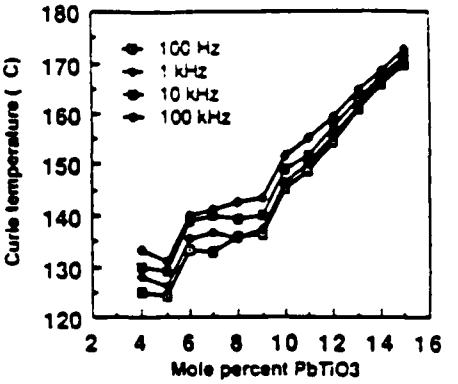

Figure 7 : Curie temperature as a function of composition.

Composition PZN - PT - BT	d_{33} (pC/N)	k_p (%)	N_p (m-Hz)	Q
89 - 6 - 5	425	42	2080	64
88 - 7 - 5	500	45	2050	64
84 - 11 - 5	405	44	2050	61

Table I Piezoelectric properties of selected PZN - PT - BT compositions.

4. Summary

1.) The perovskite phase was stabilized in the PZN-PT system by the addition of a small amount $BaTiO_3$

2.) The location of the morphotropic phase boundary with 5 mole percent $BaTiO_3$ was determined to be between 6 and 7 mole percent $PbTiO_3$ as determined by X-ray diffraction and dielectric properties.

3.) The dielectric behavior was typical of relaxor ferroelectrics showing more ordered, or normal, behavior with increasing $PbTiO_3$ content.

4.) Peak dielectric constants as high as 15,000 (@100 Hz) were found for compositions near the morphotropic phase boundary. Maximum d_{33} and k_p values obtained were ~ 400 to 500 pC/N and ~ 45%, respectively, but optimization of poling conditions is still required.

References

[1] Y Yokomizo, T Takahashi, and S Nomura, "Ferroelectric properties of $Pb(Zn_{1/3}Nb_{2/3})O_3$," J Phys Soc Jpn 28 (5), 1278-84 (1970).

[2] J. Kuwata, K Uchino and S Nomura, "Diffuse phase transitions in lead zinc niobate," Ferroelectrics 22 863-867 (1979)

[3] J Kuwata, K Uchino and S Nomura, "Dielectric and piezoelectric properties of 0.91 $Pb(Zn_{1/3}Nb_{2/3})O_3$ - 0.09 $PbTiO_3$ single crystals," Jap J Appl Phys 21 (9), 1298-1302 (1982)

[4] J Kuwata, K Uchino, and S Nomura, "Phase transitions in the $Pb(Zn_{1/3}Nb_{2/3})O_3$ - $PbTiO_3$ system," Ferroelectrics 37 579-582 (1981)

[5] Y Matsuo, H Sasaki, S Hayakawa, F Kanamura and M Koizumi, "High pressure synthesis of perovskite type $Pb(Zn_{1/3}Nb_{2/3})O_3$," J Am Cer Soc 52 (9), 516-517 (1969)

[6] A Halliyal, U. Kumar, and R E. Newnham, "Stabilization of perovskite phase and dielectric properties of ceramics in the $Pb(Zn_{1/3}Nb_{2/3})O_3$ - $BaTiO_3$ system," to be published.

[7] S. L Swartz and T R Shrout, "Fabrication of perovskite lead magnesium niobate," Mat. Res. Bull., 17 1245-1250 (1982)

[8] "IRE standards on piezoelectric crystals Determination of the elastic, piezoelectric and dielectric constants - the electromechanical coupling factor," Proc IRE 46 764-773 (1958).

[9] B Jaffe W R Cook Jr and H Jaffe Piezoelectric Ceramics Academic Press London and New York, 1971

PHENOMENOLOGY AND PROPERTIES OF CONVENTIONAL CERAMIC PIEZOELECTRICS

A PHENOMENOLOGICAL THEORY FOR THE SECOND ORDER TRANSITION REGION OF THE PZT SOLID SOLUTION SYSTEM

M.J. Haun, Z.Q. Zhuang, S.J. Jang, H.A. McKinstry and L.E. Cross

Materials Research Laboratory
The Pennsylvania State University
University Park, PA 16802

Abstract

A second tricritical point, where the transition changes from first to second order, was found to occur near or possibly at the morphotropic phase boundary between the tetragonal and rhombohedral phases in the PZT solid solution system. A second order transition region occurs between this tricritical point and another tricritical point that was previously shown to occur at the $Pb(Zr_{0.94}Ti_{0.06})O_3$ composition. A phenomenological theory was developed for this second order transition region. Using an equation derived from the theory, the spontaneous tilt angle of the oxygen octahedra in the low temperature rhombohedral phase was calculated from experimental spontaneous strain data, that was determined from x-ray diffraction.

1. Introduction

The Landau:Ginsburg:Devonshire theory for the single cell region of the PZT solid solution system developed by Amin, et al. [1] was extended to include the low temperature rhombohedral phase field [2], which exhibits composition having both ferroelectric polarization and tilted oxygen octahedra. This theory assumed that the phase transitions were first order.

However, at the cubic-rhombohedral boundary, a tricritical point has been shown to exist at the $Pb(Zr_{0.94}Ti_{0.06})O_3$ composition, where the transition changes from first to second order [3-5]. For $PbZrO_3$ to the tricritical point the transition was shown to be first order, and a region of second order behavior occurs from the tricritical point over to at least the $Pb(Zr_{0.88}Ti_{0.12})O_3$ composition [6].

Experimental spontaneous strain data for $PbTiO_3$ and several PZT compositions in the tetragonal phase field over to the morphotropic phase boundary indicate that the cubic-tetragonal phase transition is first order. A second tricritical point should therefore occur between $Pb(Zr_{0.88}Ti_{0.12})O_3$ and the morphotropic boundary.

To find the second tricritical point, pure homogeneous sol-gel derived PZT powders were prepared for several compositions in the rhombohedral phase field. The lattice parameters of these compositions were determined as a function of temperature from high temperature x-ray diffraction, and were used to calculate the spontaneous strain. The results of these calculations and the development of a phenomenological theory for the second order transition region will be described.

2. Elastic Gibbs Free Energy Function

An additional term ($\tau d\theta$) was added to the elastic Gibbs free energy G to account for the oxygen octahedral tilting [2,7]:

$$dG = -SdT + EdP - xdX + \tau d\theta \qquad (1)$$

where τ is the torque responsible for the tilt $d\theta$.

The energy function was expanded in a three-dimensional power series of P and θ, assuming isothermal conditions. The coefficients of the energy function are limited by the symmetry of the paraelectric phase: m3m for PZT. Using reduced notation.

$$\begin{aligned}
\Delta G = {} & \alpha_1(P_1^2+P_2^2+P_3^2)+\alpha_{11}(P_1^4+P_2^4+P_3^4) \\
& + \alpha_{12}(P_1^2P_2^2+P_2^2P_3^2+P_3^2P_1^2) + \alpha_{111}(P_1^6+P_2^6+P_3^6) \\
& + \alpha_{112}[P_1^4(P_2^2+P_3^2)+P_2^4(P_1^2+P_3^2)+P_3^4(P_1^2+P_2^2)] \\
& + \alpha_{123}P_1^2P_2^2P_3^2+\beta_1(\theta_1^2+\theta_2^2+\theta_3^2)+\beta_{11}(\theta_1^4+\theta_2^4+\theta_3^4) \\
& + \gamma_{11}(P_1^2\theta_1^2+P_2^2\theta_2^2+P_3^2\theta_3^2) - 1/2\ s_{11}(X_1^2+X_2^2+X_3^2) \\
& - s_{12}(X_1X_2+X_2X_3+X_3X_1) - 1/2\ s_{44}(X_4^2+X_5^2+X_6^2) \\
& - Q_{11}(X_1P_1^2+X_2P_2^2+X_3P_3^2) - Q_{12}[X_1(P_2^2+P_3^2)+X_2(P_3^2+P_1^2) \\
& + X_3(P_1^2+P_2^2)] - Q_{44}(X_4P_2P_3+X_5P_1P_3+X_6P_1P_2) \\
& - R_{11}(X_1\theta_1^2+X_2\theta_2^2+X_3\theta_3^2) - R_{12}[X_1(\theta_2^2+\theta_3^2)+X_2(\theta_3^2+\theta_1^2) \\
& + X_3(\theta_1^2+\theta_2^2)] - R_{44}(X_4\theta_2\theta_3+X_5\theta_1\theta_3+X_6\theta_1\theta_2) \qquad (2)
\end{aligned}$$

where α_1 and the α_{ij} and α_{ijk} are the dielectric stiffness and higher order stiffnesses, β_1 and β_{11} are the octahedral torsion constants, γ_{11} is a polarization-tilt angle coupling coefficient, the s_{ij} are the elastic compliance coefficients, the Q_{ij} are cubic electrostriction constants, and the R_{ij} are rotostriction coupling constants between the stress and the square of the tilt angle.

The three solutions of Equation (2), which are of interest in the second order transition region are:

$$\text{Cubic:}\quad P_1^2 = P_2^2 = P_3^2 = 0, \quad \theta_1^2 = \theta_2^2 = \theta_3^2 = 0 \qquad (3)$$

$$\Delta G = 0 \tag{4}$$

Rhombohedral (HT): $P_1^2=P_2^2=P_3^2\neq 0,\quad \theta_1^2=\theta_2^2=\theta_3^2=0$ (5)

$$\Delta G = 3\alpha_1 P_3^2 + \delta P_3^4 + \xi P_3^6 \tag{6}$$

$$P_3^2 = \frac{-\delta/3+(\delta^2/9-\alpha_1\xi)^{1/2}}{\xi} \tag{7}$$

where $\delta = 3(\alpha_{11}+\alpha_{12})$, and (8)

$$\xi = 3\alpha_{111}+6\alpha_{112}+\alpha_{123}. \tag{9}$$

Rhombohedral (LT): $P_1^2=P_2^2=P_3^2\neq 0,\ \theta_1^2=\theta_2^2=\theta_3^2\neq 0$ (10)

$$\Delta G = 3P_3^2+\delta P_3^4+\xi P_3^6+3\beta_1\theta_3^2+3\beta_{11}\theta_3^2+3\gamma_{11}P_3^2\theta_3^2 \tag{11}$$

P_3^2 and θ_3^2 were determined from the following two equations:

$$\alpha_1 + 2/3\ \delta P_3^2 + \xi P_3^4 + \gamma_{11}\theta_3^2 = 0 \tag{12}$$

$$\beta_1 + 2\beta_{11}\theta_3^2 + \gamma_{11}P_3^2 = 0 \tag{13}$$

The spontaneous elastic strains ($x_i = dG/dX_i$) for the three solutions, under zero stress conditions, were derived from Equation 2:

Cubic $x_1 = x_2 = x_3 = x_4 = x_5 = x_6 = 0$ (14)

Rhombohedral (HT)

$$x_1=x_2=x_3=(Q_{11}+2Q_{12})P_3^2,\ x_4=x_5=x_6=Q_{44}P_3^2 \tag{15}$$

Rhombohedral (LT)

$$x_1 = x_2 = x_3 = (Q_{11}+2Q_{12})P_3^2 + (R_{11}+2R_{12})\theta_3^2,$$

$$x_4 = x_5 = x_6 = Q_{44}P_3^2 + R_{44}\theta_3^2 \tag{16}$$

3. Evaluation of the Coefficients of the Energy Function

All of the coefficients in Equations (6) and (11) were assumed to be independent of temperature, except the dielectric stiffness constant α_1, which was given a linear temperature dependence based on the Curie-Weiss law.

$$\alpha_1 = \frac{T-T_o}{2\varepsilon_o C}, \tag{17}$$

where C is the Curie constant, ε_o is the permittivity of free space, and T_o (for a second order transition) is equal to the Curie or transition temperature T_c.

The transition temperature T_c was determined from a cubic least squares fit [1] of the experimental PZT phase diagram [8]:

$$T_c = (211.8+486.0x-280.0x^2+74.42x^3)\,^\circ C, \tag{18}$$

where x is the mole fraction of $PbTiO_3$ in PZT.

The Curie constant C was assumed to be independent of composition and equal to $2\times10^5\,^\circ C^{-1}$. This value was determined from dielectric constant measurements on a single crystal of $Pb(Zr_{0.9}Ti_{0.1})O_3$ [9].

The fourth (δ) and sixth (ξ) order rhombohedral dielectric stiffness constants were determined from spontaneous strain data. Pure homogeneous sol-gel derived powders of $Pb(Zr_xTi_{1-x})O_3$ with x equal to 0.6, 0.7, 0.8 and 0.9 were prepared, as described in reference 10. The spontaneous strain $x_4(=(90-\alpha_R)/90$, where α_R is the rhombohedral angle) was calculated from high temperature x-ray diffraction patterns of the four compositions listed above, as shown in Figure 1. The microcomputer automated diffractometer that was used and the analysis of the x-ray patterns are described in Reference 11.

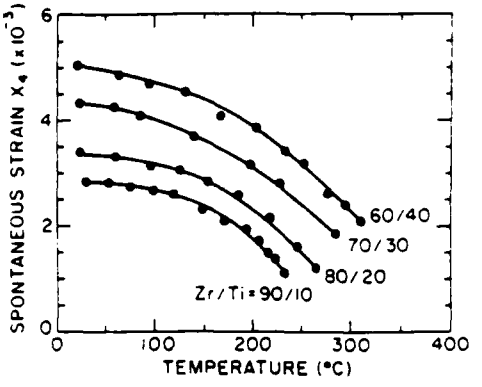

Figure 1. The spontaneous strain x_4 plotted versus temperature. For clarity the PZT 80/20, 70/30, and 60/40 data were shifted up by 0.5, 1.0, and 1.5, respectively.

The spontaneous polarization (P_3) of the high temperature rhombohedral phase was calculated from the strain (x_4) data using Equation (15). The electrostriction constant Q_{44} was assumed to be independent of composition and temperature, and equal to 0.02 m^4/C^2. This value was calculated from spontaneous polarization data on a single crystal of $Pb(Zr_{0.9}Ti_{0.1})O_3$ [12].

The spontaneous polarization calculated from the strain data was then used with Equation (7) to find values of the fourth (δ) and sixth (ξ) order dielectric stiffness constant that gave the best fit of the data. The values obtained are plotted versus composition in Figure 2, along with linear least square fits of the constants:

$$\delta = (-1.781+18.70x)\cdot10^8\ m^5/C^2F \tag{19}$$

$$\xi = (3.068-6.601x)\cdot10^9\ m^9/C^4F \tag{20}$$

Whatmore, et al. [4] showed that on the $PbZrO_3$ side of the first tricritical point the fourth and sixth order constants were negative and positive, respectively. The fourth order constant was shown to decrease in magnitude and go to zero at the tricritical point, causing the transition to change from first to second order.

Figure 2 shows that the fourth order constant becomes positive and continues to increase for compositions to the right of the tricritical point. The sixth order constant is shown to decrease across the rhombohedral phase field, and from a linear least square fit of the data goes to zero near the morphotropic phase boundary.

If the sixth order constant goes to zero and becomes negative in the rhombohedral phase field, then a second tricritical point would occur. In this case, eighth order terms would have to be

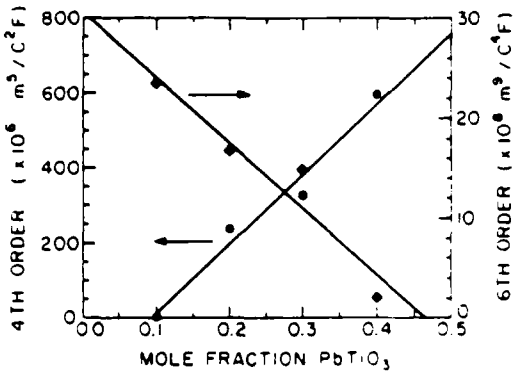

Figure 2. The fourth and sixth order rhombonedral dielectric stiffness constants plotted versus composition.

included in the energy function to keep the energy from going to negative infinity.

However, if the sixth order constant remains positive throughout the rhombohedral phase field, then a different type of second to first order behavior would occur. The order of the paraelectric - ferroelectric transition would change from second to first at the morphotropic boundary, where second order behavior would occur on the rhombohedral side, and first order behavior on the tetragonal side.

The tilt angle related constants β_1 and β_{11}, and the polarization - tilt angle coupling coefficient γ_{11} were related to three new constants T_R, $P_{RLT(TR)}$, and and $\theta_{RLT(TR)}$ at the high to low temperature rhombohedral phase transition using Equations (12) and (13), and by equating the energies of the two phases at the boundary. T_R is the phase transition temperature between the high and low temperature rhombohedral phases, and was determined from a quadratic least squares fit of the experimental phase diagram [8]:

$$T_R = (-36.5+1815x-4636x^2)°C \qquad (21)$$

$P_{RLT(TR)}$ and $\theta_{RLT(TR)}$ are the spontaneous polarization and tilt angle of the low temperature rhombohedral phase at the transition temperture T_R. The transition at T_R is of first order [6]. $P_{RLT(TR)}$ was related to the spontaneous polarization of the high temperature rhombohedral phase at T_R ($P_{RHT(TR)}$) using experimental spontaneous polarization data from a single crystal of $Pb(Zr_{0.9}Ti_{0.1})O_3$ [12]:

$$P_{RLT(TR)} = 1.09\ P_{RHT(TR)} \qquad (22)$$

This relation was then assumed to be independent of composition.

$\theta_{RLT(TR)}$ was determined from experimental spontaneous tilt angle data. Unfortunately, the tilt angle has only been determined for $Pb(Zr_{0.9}Ti_{0.1})O_3$ at 25 and 60°C [13,14], and for $Pb(Zr_{0.6}Ti_{0.4})O_3$ at 9K [15] using neutron diffraction. However, Equation (16) can be used to determine the spontaneous tilt angle from spontaneous strain data, which can be determined from x-ray diffraction.

The electrostriction Q_{44} constant was calculated in the high temperature rhombohedral phase from the spontaneous strain data and single crystal spontaneous polarization data, as described above. The rotostriction constant R_{44} was also assumed to be independent of composition and temperature, and equal to $-3x10^{-5}$ deg^{-2}. This value was calculated at 25 and 60°C for $Pb(Zr_{0.9}Ti_{0.1})O_3$ from the experimental spontaneous strain, polarization, and tilt angle data [14].

The spontaneous polarization of the low temperature rhombohedral phases was approximated by assuming that it was 1.09 times the spontaneous polarization of the high temperature phase at any temperature (see Equation 22). The tilt angle was then calculated from Equation (16) using the experimental strain data (Figure 1) for the $Pb(Zr_xTi_{1-x})O_3$ compositions with x = 0.7, 0.8, and 0.9. In Figure 3 the calculated tilt angle data for $Pb(Zr_{0.9}Ti_{0.1})O_3$ is plotted, along with the tilt angle data determined from neutron diffraction [13,14].

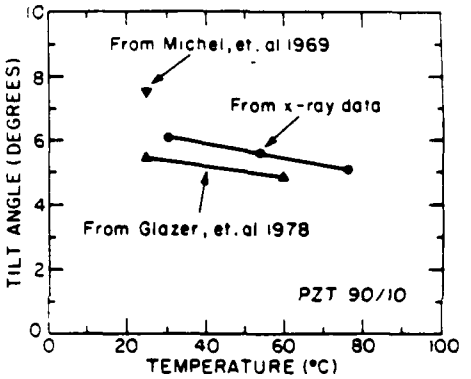

Figure 3. The spontaneous tilt angle plotted versus temperature for $Pb(Zr_{0.9}Ti_{0.1})O_3$.

$\theta_{RLT(TR)}$ was determined for x = 0.7, 0.8, and 0.9 by fitting the calculated tilt angle data for each of these three compositions. The compositional dependence of $\theta_{RLT(TR)}$ was then determined from a quadratic fit of this data:

$$\theta_{RLT(TR)} = 4.006-13.275x+28.25x^2 \qquad (23)$$

4. Theoretical Calculations

The theory developed in Section 2 and the values of the coefficients determined in Section 3 were used to calculate the energies and spontaneous polarizations and tilt angles for the high and low temperature rhombohedral phases. Figure 4 shows a comparison of the theoretical and experimental phase diagrams. The solid curves are the calculated phase boundaries, and the data points are from the experimental phase diagram [8].

The calculated spontaneous polarization was plotted versus temperature in Figure 5. The calculated values for the $Pb(Zr_{0.9}Ti_{0.1})O_3$ composition are in much better quantitative agreement with the experimental single crystal data [12], than the first order theory that was previously developed.

The spontaneous tilt angle was plotted versus temperature in Figure 6. The solid curves are the theoretical calculations, and the data points are

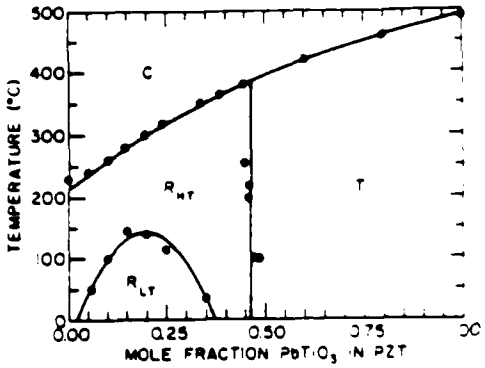

Figure 4. Superposition of the theoretical and experimental phase diagrams.

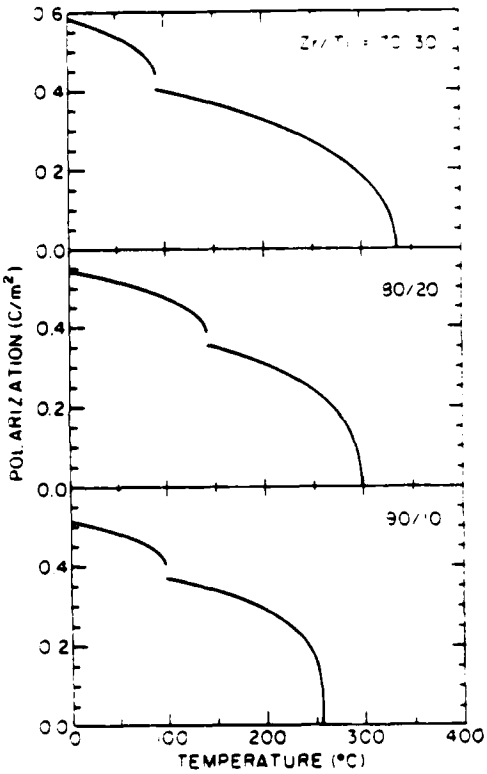

Figure 5. The spontaneous polarization plotted versus temperature.

from the experimental spontaneous strain data using Equation (16), as described in Section 3.

5. Summary

A second tricritical point was found to occur near or possibly at the morphotropic phase boundary. Additional spontaneous strain measurements will be needed to determine more precisely where the second tricritical point occurs.

The spontaneous tilt angle of the oxygen octahedra in the low temperature rhombohedral phase was calculated from experimental spontaneous strain

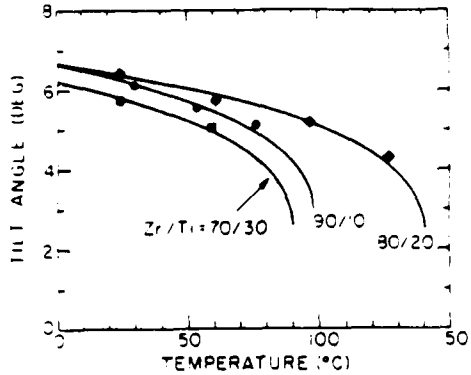

Figure 6. The spontaneous tilt angle plotted versus temperature.

data. The calculated tilt angle data was in good agreement with neutron diffraction data.

A phenomenological theory was developed for the second order region of the PZT solid solution system. The experimental and theoretical phase diagrams were shown to agree very well. The calculated spontaneous polarization for the $Pb(Zr_{0.9}Ti_{0.1})O_3$ composition was in much better quantitative agreement with single crystal data, than the first order theory that was previously developed.

References

[1] A. Amin, M. Haun, B. Badger, H. McKinstry and L.E. Cross, Ferroelectrics, 65, 107 (1985).

[2] M. Haun, T. Halemane, R.E. Newnham, and L.E. Cross, Jpn. J. Appl. Phys. 24, 209 (1985).

[3] R. Clark and A.M. Glazer, Ferroelectrics, 14, 695 (1976).

[4] R.W. Whatmore, R. Clarke, and A.M. Glazer, J. Phys. C: Solid State Phys., 11, 3089 (1978).

[5] K. Roleder and J. Handerek, Phase Transitions, 2, 285 (1982).

[6] R. Clarke, A.M. Glazer, F.W. Ainger, D. Appleby, N.J. Poole, and S.G. Porter, Ferroelectrics, 11, 359 (1976).

[7] T.R. Halemane, M.J. Haun, L.E. Cross and R.E. Newnham, Ferroelectrics, 62, 149 (1985).

[8] B. Jaffe, W. Cook, and H. Jaffe, Piezoelectric Ceramics, London, Academic Press (1971).

[9] R. Clarke and R.W. Whatemore, J. Cryst. Growth, 33, 29 (1976).

[10] Z.Q. Zhuang, M.J. Haun, S.J. Jang, and L.E. Cross, Proc. ISAF 1986.

[11] M.J. Haun, Y.H. Lee, H.A. McKinstry and L.E. Cross, Proc. 35th Annual Denver X-Ray Conference, 1986, to be published in Vol. 31 of Advances in X-Ray Analysis.

[12] R. Clarke and A.M. Glazer, Ferroelectrics, 12, 207 (1976).

[13] C. Michel, J. Moreau, G. Achenback, R. Gerson, and W. James, Solid State Comm., 7, 865 (1969).

[14] A.M. Glazer, S.A. Mabud, and R. Clarke, Acta Cryst., B34, 1060 (1978).

[15] A. Amin, R.E. Newnham, and L.E. Cross, J. Solid State Chemistry, 37, 248 (1981).

MODIFIED LEAD ZINC NIOBATE CERAMIC ELECTROSTRICTORS FOR MICROPOSITIONER APPLICATIONS

U. Kumar, A. Halliyal and L.E. Cross

Materials Research Laboratory
The Pennsylvania State University
University Park, PA 16802, USA

Abstract

Properties of a number of compositions in (1-x-y)$Pb(Zn_{1/3}Nb_{2/3})O_3$-x $BaTiO_3$-y $PbTiO_3$ systems have been investigated for micropositioner applications. For room temperature applications, ceramics with 0.85 PZN-0.1BT-0.05 PT composition showed optimum properties. Electrostrictive Q_{ij} coefficients, switching speed, strain vs. temperature behavior at constant electric field, dielectric and pyroelectric properties are reported here. These properties are compared with those of 0.9PMN-0.1PT which is currently the favored electrostrictive ceramic for room temperature applications.

1.0 Introduction

Lead zinc niobate (PZN) is one of the few relaxor type ferroelectric materials with a high transition temperature (140°C). PZN single crystals show a very high dielectric constant near the transition temperature (70,000 at 120 Hz) [1]. The crystal has rhombohedral symmetry below 140°C and cubic symmetry above this transition temperature. It forms solid solutions with $PbTiO_3$ (PT) and has a morphotropic phase boundary (MPB) at a composition close to 9 mole% of PT. Single crystals of 0.91 PZN - 0.09 PT show excellent electromechanical properties [2].

PZN ceramics have not yet been synthesized in pure perovskite form. Recently it has been shown that an addition of 6 to 7 mole% of $BaTiO_3$ (BT) stabilizes the perovskite structure [6]. Phase stability and dielectric properties of ceramics in PZN-BT and PZN-BT-PT systems have been reported elsewhere [3,4].

Several compositions in the PZN-BT-PT system were analyzed for electrostrictive applications. Ceramics with 0.85 PZN-0.1BT-0.05PT composition showed optimum properties for room temperature micropositioner applications. Dielectric, pyroelectric and electrostrictive properties of this composition are presented in this paper. A detailed account of properties of several compositions in the PZN-BT-PT system will be published later.

2. Sample Preparation

Details of the procedure followed for ceramic preparation can be found in references 3 and 4. Briefly, powders of lead oxide, barium carbonate, niobium oxide, zinc oxide and titanium oxide were mixed in stoichiometric ratio in a ball mill with alcohol. One wt% excess of PbO was added to compensate for PbO loss during calcination and sintering. The calcined powder was ball milled and mixed with PVA binder and pellets of 12mm diameter and 2-3mm thickness were pressed. After binder burn out, sintering was carried out at 1150°C/1h in a sealed alumina crucible with PbO-ZrO_2 source. Care was taken to keep the total wt. loss below 1 wt% during calcination and sintering. Powder x-ray diffraction patterns taken on calcined powder and sintered ceramics showed pure perovskite structure.

3. Measurements

Capacitance of circular gold electroded samples were measured at various temperatures using a computer controlled measuring system and a Delta Design furnace. From the accumulated data dielectric constant was calculated. Pyroelectric current was measured by heating a poled sample from -25°C to 125°C. A 4°C/min constant heating rate was provided by a Delta Design furnace controlled by a Hewlett Packard computer. Pyroelectric coefficient was calculated from the accumulated pyroelectric current data.

Electrostrictive properties were studied by strain gage method [5]. A polyimide foil strain gage was cemented on a rectangular sample with gold electrodes. An alternating electric field (E) at 0.1Hz was applied to the sample and the strain (s) was measured by forming a Wheatstone bridge with three other strain gages and by amplifying the offset introduced by electric field. Simultaneously hysteresis plots of electric field vs. polarization (E vs. P) were recorded using a Sawyer-Tower circuit. Using a digital storage oscilloscope polarization vs. strain plots (P vs. s) were also recorded. All the above measurements were made at various temperatures. Electrostrictive Q_{ij} coefficients were calculated using the relation $s_j = Q_{ij}P_i^2$.

0000-0683 $1.00

Details of the measurement of switching speed using a square pulse can be found elsewhere [6]. A Hewlett Packard 214B pulse generator and Cober high powder pulse generator were used to produce square pulse and a Nicolet digital storage oscilloscope was used to record the signals.

4. Results and Discussions

Variation of dielectric constant and pyroelectric coefficient with temperature for ceramics with composition 0.85 PZN - 0.1BT - 0.05PT are shown in Fig. 1. Significant difference in dielectric maxima (T_{max}) and pyroelectric coefficient maxima (T_t) can be noticed. In relaxor ferroelectric materials with rhombohedral structure, T_{max} and T_t need not be the same. In the PLZT system, differences of up to 100°C have been reported [7]. Since depolarization occurs at T_t, pure electrostrictive behavior can be expected at temperatures above T_t instead of T_{max}.

In Fig. 2, electric field vs. transverse strain (E vs. s_{12}), electric field vs. polarization (E vs. P) and polarization vs. strain (P vs. s_{12}) are plotted at four different temperatures. Even though a small hysteresis in strain is observed in E vs. s plot, almost no hysteresis is observed in P vs. s plot at 25°C. From s vs. P^2 plots at different temperatures, it

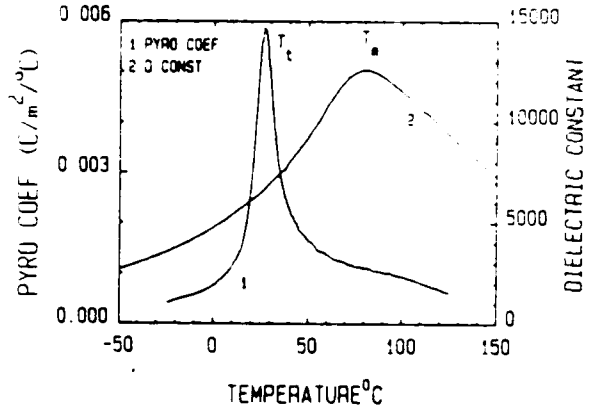

Figure 1. Dielectric (100 Hz) and pyroelectric properties.

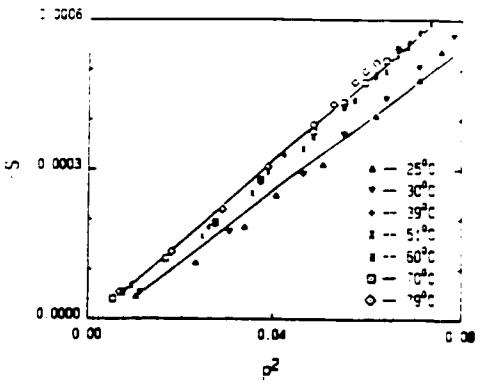

Figure 3. Transverse strain vs. P^2 plots.

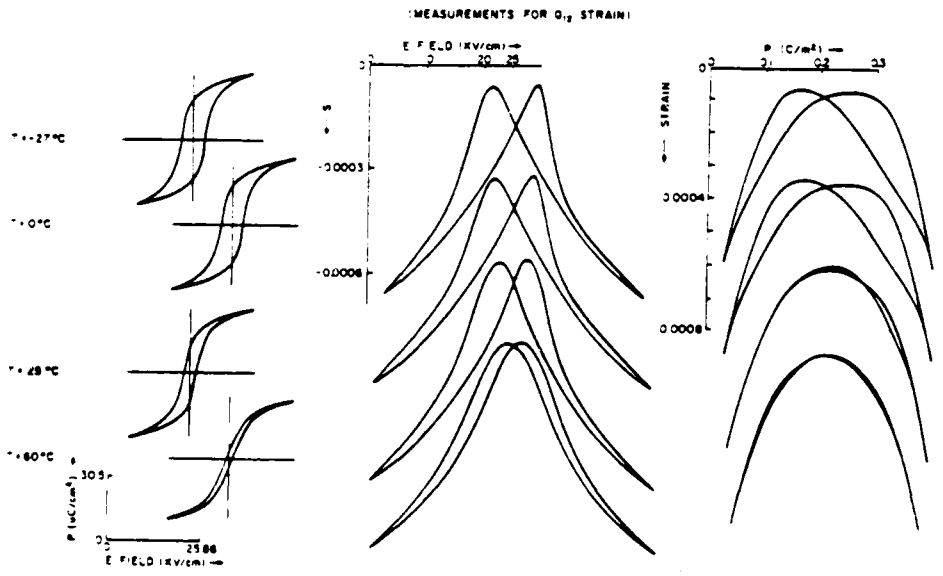

(a) P vs. E HYSTERESIS (b) s vs. E (c) s vs. P

Figure 2. Electric field vs. transverse stain, electric field vs. polarization and polarization vs. strain plots.

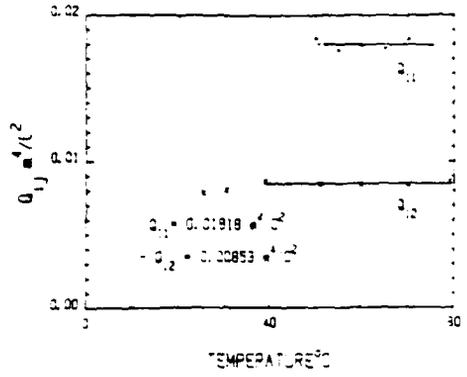

Figure 4. Longitudinal and transverse Q coefficient vs. temperature.

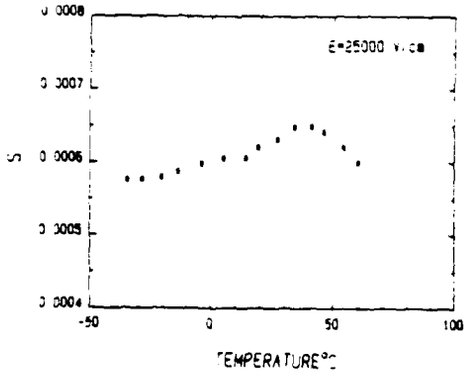

Figure 5. Strain vs. positive bias field at various temperature.

is obvious that pure electrostrictive behavior is observed above 40°C (Fig. 3). A least square fit analysis showed the magnitudes of Q_{11} and Q_{12} to be 0.018 m^4/C^2 and -0.0085 m^4/C^2 respectively (Fig. 4). These values are comparable to the magnitudes reported for other relaxor materials [8].

The effects of applying a bias field on transverse strain were studied. A 25 kV/cm field was applied in the positive direction at 0.1Hz. The results of the measurement are plotted in Fig. 5. Very slim reproducible curves were noticeable at all temperatures. The variation of maximum strain with temperature is shown in Fig. 6. Since the peak value occurs near 40°C, the temperature coefficient of strain was not calculated.

An electric field of about 100 kV/cm can be applied very easily - if the material is prepared in multilayer configuration. From the equation $s_{12} = -Q_{12}P^2$, it can be shown that a polarization of 0.36 C/m^2 is needed to get 0.1% transverse strain. To calculate the corresponding electric field, the following thermodynamic equation was used.

$$E = \alpha P + \beta P^3 + \nu P^5 \qquad (1)$$

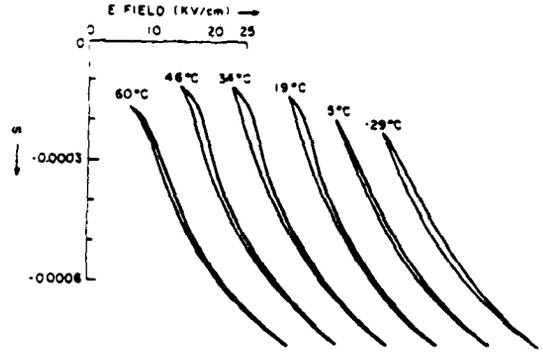

Figure 6. Variation of maximum strain vs. temperature for 25 kV/cm bias field (calculated from Figure 5).

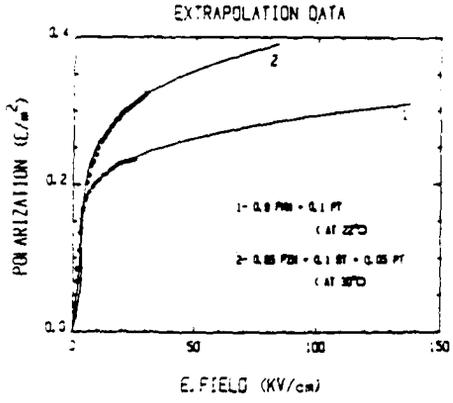

Figure 7. Extrapolation of electric field vs. polarization.

Since relaxor ferroelectrics do not show either a first order or second order characteristic, in the normal sense, no restrictions were put on α, β, or ν. P vs. E plots were used to calculate α, β and ν. Knowing α, β and ν, electric field values were extrapolated to a higher polarization value. A similar analysis was carried out for 0.9PMN-0.1PT also (Fig. 7). An electric field of about 70 KV/cm is sufficient to get the needed polarization of 0.36 c/m^2 for the 0.85PZN-0.1BT-0.05PT composition. To achieve the same strain in 0.9PMN-0.1PT greater than 200 KV/cm is needed.

Faster switching speed is one of the important criteria for micropositioner applications. Switching speed was measured by applying a pulse to the samples and measuring the decay current [6]. PZN showed a switching speed of approximately 1.5μ sec at an applied field of 25KV/cm. For a comparison a 0.9PMN-0.1PT sample under similar conditions showed a switching speed of approximately 3.5μ sec.

5. Conclusions

Electrostrictive properties of PZN ceramics of composition 0.85PZN-0.1BT-0.05PT were investigated for micropositioner applications. The electrostrictive Q coefficients of this composition are comparable to PMN based ceramics. Lower dielectric constant, approximately 50% larger transverse strain for the same applied electric field and comparable switching speed make the PZN compositions preferable to PMN based ceramics (Table 1). In a multilayer configuration, a transverse strain of 10×10^{-4} can be expected at approximately 70 kV/cm in PZN compositions and at least twice this strain can be expected in a longitudinal configuration.

TABLE 1 Comparison of the Properties of 0.85 PZN - 0.1BT - 0.05PT and 0.9PMN - 0.1PT Ceramics

	PZN - BT - PT	PMN - PT
Room Temperature Dielectric Constant	7000	25000
T_{max} at 100 Hz	75°C	30°C
T_t	27°C	0°C
Q_{11}	0.018 m^4/C^2	0.022 m^4/C^2
Q_{12}	-0.0085 m^4/C^2	-0.009 m^4/C^2
Transverse strain at 25KV/cm	6.1×10^{-4}	4.0×10^{-4}
Calculated E. Field for $s_{12} = 10 \times 10^{-4}$	70KV/cm	>200KV/cm
Switching speed	1.5 μ sec	3.5 μ sec

6. Reference

[1] Y. Yokomizo, T. Takahashi and S. Nomura, J. Phys. Soc. Japan 28, 1278 (1970).

[2] J. Kuwata, K. Uchino and S. Nomura, Ferroelectrics 37, 579 (198).

[3] A. Halliyal, U. Kumar, R.E. Newnham and L.E. Cross, Submitted to J. Am. Ceram. Soc.

[4] A. Halliyal, U. Kumar, R.E. Newnham and L.E. Cross, Submitted to J. Am. Ceram. Soc.

[5] K. Uchino, S. Nomura, L.E. Cross, S.J. Jang and R.E. Newnham, J. Appl. Phys. 51, 1142 (1980).

[6] W.J. Merz, Physical Review 95, 690 (1954).

[7] H.M. O'Bryan and A.H. Meitzler, J. Am. Ceram. Soc. 55, 504 (1972).

[8] S. Namura and K. Uchino, Ferroelectrics 41, 117 (1982).

Multilayer Actuator Design

W. B. Carlson , S.E. Trolier, A.Safari, R. E. Newnham , L.E. Cross

Materials Research Laboratory
The Pennsylvania State University
University Park, Pa.16802

Abstract

A finite difference method of analyzing actuators for electrostrictive and piezoelectric materials will be discussed. Recent analysis of devices via numerical techniques and applications to electromechanical systems are demonstrated. Operating parameters and ceramic systems for multiphase devices are proposed which show performance criteria for actuator applications. Examples of the numerical treatment of specific devices such as axial positioners and linear resonators will be included.

1. Introduction

Lead zirconate titanate (PZT) and barium titanate ($BaTiO_3$) are two widely used materials in the electroceramics industry. PZT is used principally in electromechanical applications while $BaTiO_3$ is used primarily as a capacitor dielectric. Recently the non-linear response of these materials been investigated for multilayer devices. The piezoelectric response of etched PZT devices and the elasto-electric response of multilayer electrostrictive materials have been modeled using the Finite Difference method.

This paper reviews research at the Materials Research Laboratory on the modeling of electroceramic materials. A description of the finite difference method (FD) as applied to the response of electroceramic materials and the results of electric field analysis for multilayer high permittivity materials is presented. Analysis depicting linear elastic fracture in ceramics are shown. Frequency response of admittance for a poled and etched PZT device is compared with numerical analysis.

2. Problem Description

Many materials exhibit the nonlinear electrostrictive effect evident in polarizable solids; examples include glasses and electroceramics such as barium titanate. In addition piezoelectric materials like poled lead zirconate titanate ceramics exhibit a linear response to an applied strain or electric field, as shown in Figure 1. These electromechanical effects are useful in both the electronic and mechanical control industries. Because of a high dielectric constant, ceramic $BaTiO_3$ is widely used in the capacitor industry. Its function ,however, is limited by its breakdown voltage as well as its temperature stability and charge storing capability. Internally, although a ceramic is traditionally considered to be a homogeneous material, it is actually a heterogeneous multiphase system with embedded processing and packaging flaws. Such a material contains pores, delaminations ,and misplaced electrodes due to inconsistencies in the processing, see Figure 2. The packaging and integration of components on a circuit board brings additional problems. All of these flaws taken together or singly may result in premature degradation of the component, device , or entire circuit module , therefore it is important to identify critical design features which may have deleterious effect on the overall performance. In addition multiple layer systems employed as actuators, resonators, and sensors must be correctly designed for accurate determination of motion as in positioner applications and mechanical resonator applications.

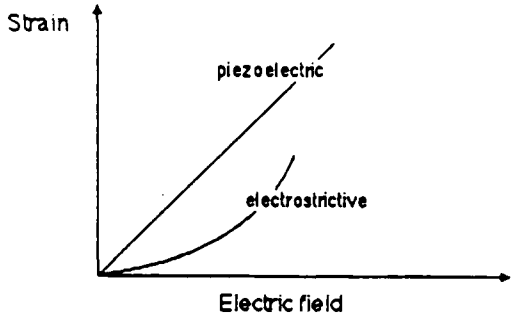

Fig. 1 Piezoelectric and Electrostrictive Behavior

A Finite Difference computer model has been used to analyze non-conductive multilayer capacitors and actuators. This model applies to devices which can be represented in two dimensions with embedded second phases of gaseous inclusions or conductor material of arbitrary geometries. Results for electrostatic analysis of multilayers are represented as the ratio of local electric field concentrations to the applied field. Electrostrictive and piezoelectric strains can be calculated knowing the appropriate electromechanical properties. These types of studies are intended to delineate the electric field induced internal stresses which may lead to mechanical fracture as well as electrical breakdown .

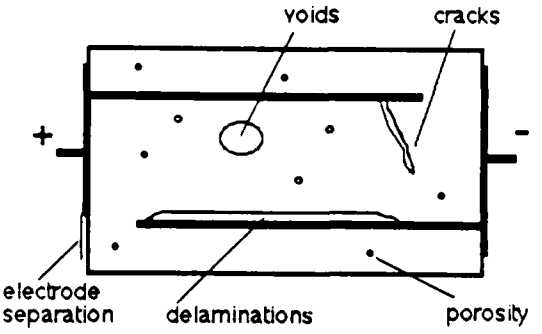

Fig. 2 Processing Flaws in Ceramic Multilayers

CH2353-0/86/0000-0641 $1.00

Identification of stress fields could result in alternative manufacturing techniques and improved quality control, which would identify and eliminate harmful flaws. Improved electromechanical actuator or resonator designs will be possible by tailoring electrode patterns to precise performance specifications for frequency and energy dissipation requirements.

The FD technique is applied to a continuum that may be divided into a finite number of discrete nodes with each node representing an unknown scalar value. Discretized equations at the nodal points are then used to replace the continuuum differential equations. Figure 3 depicts the discretized media and the form of the linear differential equation. Solution of the equations may then be found via direct or iterative linear algebra procedures. The precision of the FD technique will be dependent on the manner of discretization of the domain, the computing machine, and the method of solution. The technique used here depends on a rectilinear mesh, although, polar discretization and nonlinear dielectric[1] has also been treated by other investigators.

In this paper we have applied the FD method to investigate two types of problems, an electrostatics problem with applications to steady-state actuator design and a mechanical dynamics problem for resonators. In the first problem the electric field results and the electro-mechanical properties are used to determine stress and strain distributions within a $BaTiO_3$ ceramic with gaseous inclusions. In the second problem the FD method is used to predict the frequency response of etched PZT ceramic with arbitrary electrode patterns.

3. Electrostatic and Electromechanical Analysis

For field problems analyzed in this publication the Laplace equation was treated by the method of central differences. This is a 'divided difference' scheme and is commonly used to analyze continuum problems. The simultaneous solution of all equations will yield the potential at all nodal points in the field. Boundary conditions are specified for both the perimeter of the field and the embedded gaseous phases or conductors. Symmetry conditions are applied where permitted. In this analysis the conductor is treated as a constant potential surface and the far field condition is approximated. The accuracy of the far field assumption is dependent on the distance from the inclusion and the boundary condition at the inclusion. In some cases the interphase boundary condition at the inclusion may be approximated if the ratio of permittivities between the two phases is large. This is shown in the comparison between a closed-form and a numerical solution of a circular inclusion between two electrodes, figure 4.

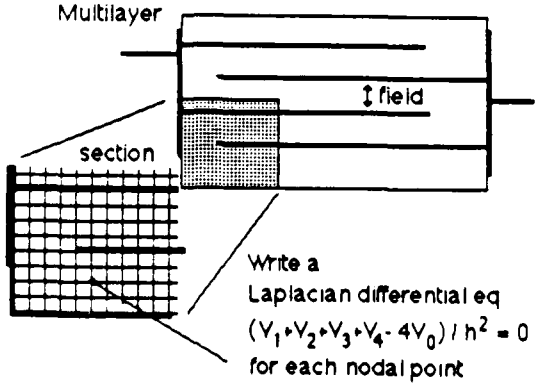

Fig. 3 Multilayer Capacitor Analysis

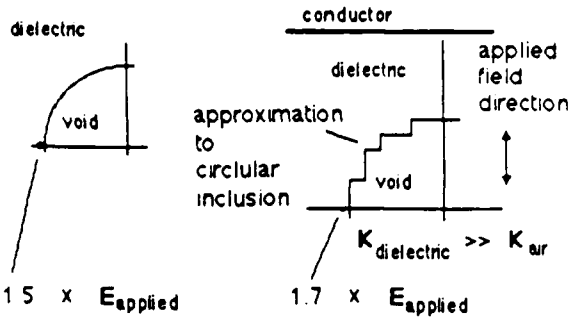

Fig. 4 Accuracy of approximate numerical method

Beside the assumptions in the numerical calculations, there are further restrictions placed on the geometrical resolution. In the continuum each phase is assumed to be homogeneous, however the grain size in the actual ceramic will alter the electric field and thereby place a lower limit on the validity of the numerical results. The nodal discretization will therefore be limited by the physical nature of the material. The analysis has been applied to flaws in uniform and non-uniform fields where the permittivity of the flaw is much lower than that of the surrounding dielectric. Initial checks were made with closed-form spherical solutions. These closed form solutions were derived for flaw geometries in uniform and static fields and then compared to the numerical results.

Multilayer actuator configurations were analyzed in order to determine the variation of strain in the margins due to the non-uniformity of the electric field. Results of the electrical field analysis are directly applied to the constituitive electromechanical equations in order to analyze electrostriction. The constitutive equations for piezoelectric and electrostrictive effects are

$$x = d^t E + sX + ME^2$$

$$P = k_r k_0 E - k_0 E + dX$$

where x is the strain, d is the piezoelectric matrix, E the electric field, s the elastic compliance, X the stress, and M the electrostrictive matrix. In the second equation the P is the polarization, k_r the relative permittivity, and k_0 the permittivity of free space. Figures 5 and 6 depict the configuration analyzed and the equipotential contours for a hypothetical specimen including a delamination on one of the conductors. The total deformation is the sum of the incremental deformations across each discrete volume. To preclude fracture a low elastic stiffnesspolymer may be required for the margin region. From the field potentials it is possible to determine critical areas in the design of the actuator as well as the deformation of the device.

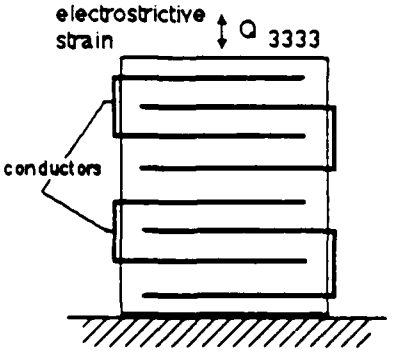

Fig. 5 Multilayer Actuator Configuration

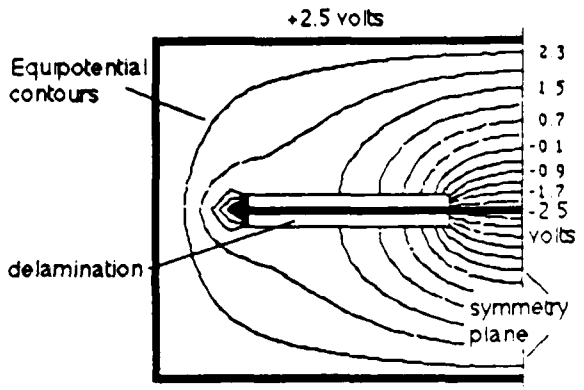

Fig. 6 Electric Potential Analysis of a Multilayer

Particularly interesting phenomena in void formation, crack propagation, and fatigue due to electrical loading may be studied. In the case of linear elastic fracture the local electric field in the dielectric will transform the mechanical stress intensity factor by imposing an additional strain component which may aid or hinder crack propagation. Electrical, mechanical, and thermally induced strains must be superimposed to determine the likelyhood of the material to propagate a crack. For this study, no numerical analysis was performed to determine deformation in the conductors or to calculate residual thermal strains from processing. The elastic and electrical interaction may be demonstrated in design diagrams like Figure 7. This diagram relates the mechanical fracture strength due to an edge crack of indicated geometry to the applied electric field and the crack length. Here crack propagation will be governed by the residual stress near the critical crack and the extent of the crack. The geometry at the tip of the flaw will deform as shown in Figure 8 causing a decrease in the strength of the ceramic. This was demonstrated by others[2].

In addition to mechanical integrity the electrical field may directly initiate gaseous breakdown via entrapped voids or delaminations. Field strengths may rise to such levels that partial discharges may result in the gas within the inclusion. Inception of gaseous discharge may be estimated using Paschen's theory.

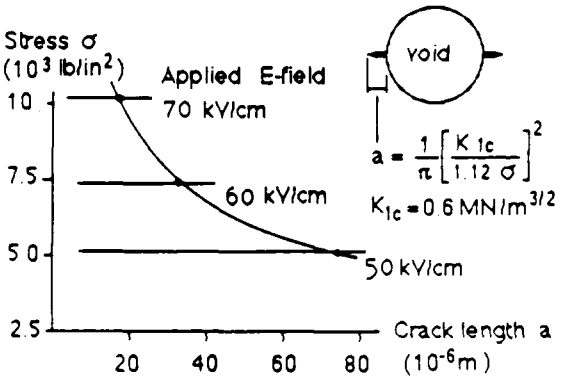

Fig.7 Stress Near Void due to Electric Field

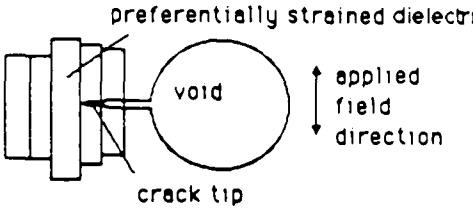

Fig.8 Enhanced Electrostriction near Crack

4. Dynamical Resonator Analysis

An analytical description of an electrostrictive mechanical resonator may be obtained by combining the constitutive electrostrictive equations with the mechanical equations of motion. The mechanical force balance may be written as

$$M\ddot{U} + C\dot{U} + KU = F$$

where U are the displacements and $\dot{U}$, $\ddot{U}$ its time derivatives. M the mass in the system, C the damping in the system, K the elastic spring stiffness, and F the mechanical force. From the electrical force balance an elongation of the system due to charge separation occurs:

$$K_{uv} V = F$$

where K_{uv} is the piezoelectric stiffness from electric potential change. If only the nonlinear electromechanical effect is represented in the material the electrostrictive stiffness matrix would replace the piezoelectric matrix and the force balance becomes:

$$K_{uv} V^2 = F.$$

Of course the full electromechanical resonator expression will require the expansion of all higher order potential terms, inelastic mechanical force terms usually being neglected. In such a system the full formulation ignoring damping and including cross coupling between electromechanical stiffnesses may be written as

$$M_{uu}\ddot{U} + K_{uu}U + K_{uv}V + K_{vv}V^2 = F.$$

Figure 9 shows the electromechanical resonator matrix formulation if only piezoelectric resonance terms are involved.

$$\begin{bmatrix} M_{uu} & 0 \\ 0 & 0 \end{bmatrix}\begin{bmatrix} \ddot{U} \\ \ddot{V} \end{bmatrix} + \begin{bmatrix} K_{uu} & K_{uv} \\ K_{vu}^t & -K_{vv} \end{bmatrix}\begin{bmatrix} U \\ V \end{bmatrix} = \begin{bmatrix} F \\ Q \end{bmatrix}$$

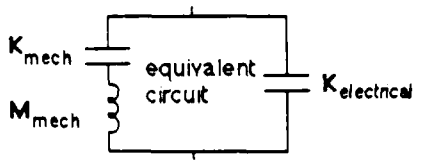

Fig. 9 Matrix Formulation of Piezoelectric Resonator

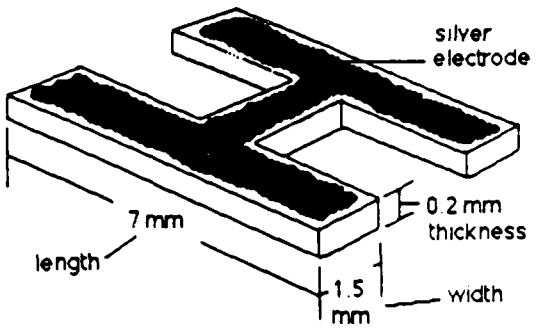

Fig. 10 Poled and Etched PZT Ceramic Resonator

The eigenvalue problem was solved for a undamped system consisting of a poled and etched PZT sample. Figure 10 shows the sample configuration and dimensions. The sample was electroded on the top and bottom surfaces and an impedance analyzer was used to determine the resonant frequencies. From the numerical analysis it was determined that the midpoint of the resonant and antiresonant frequencies for the width mode across a representative section would be 1.6 MHz . Other anlaytically determined frequencies were the length mode at 250 KHz and the half length mode at 480 KHz. Experimental results are plotted in Figure 11. All experimental resonator results seem to substantiate the numerical model to within limitations of the processing accuracy of the etched and electroded sample dimensions. Testing of the etched resonator is continuing to determine loss performance and electrostrictive recovery period.

5. Conclusions

It has been demonstrated that electrical and mechanical characteristics of actuators and resonators are being successfully analyzed. In particular device performance has been determined via numerical analysis for certain well defined ceramic systems namely barium titanate and lead zirconate titanate. Both internal degradation mechanisms as well as overall device performance is being determined for multilayer ceramic electromechanical actuators. Work has begun on the dynamical characterization of PZT resonators for specific device applications.

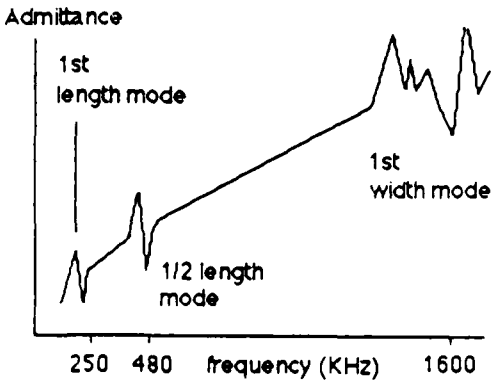

Fig. 11 Frequency Spectrum of etched PZT
1st modes only

6. Acknowledgements:

I would like to acknowledge the support of the Center for Dielectric Studies at the Materials Research Laboratory of The Pennsylvania State University.

7. References

[1] A. Lioris, A. Prieto, and J.C. Torres, "Calculation of Potential Distribution in Homogeneous Anisotropic Nonlinear Dielectrics," J. Appl. Phys. 54(11), pp. 6610-6614, Nov. 1983.

[2] T. Yamamoto, H. Sato, H. Igarashi, and K. Okazaki, "Stress Anisotropy of PLZT Ceramics Induced by Polarization," Japanese J. of Appl. Phys. ,vol.22 suppl.22-2 ,pp. 70-72, 1983.

LOW TEMPERATURE DIELECTRIC, PIEZOELECTRIC AND ELASTIC PROPERTIES OF PURE (UNDOPED) PZT CERAMICS

Z.Q. Zhuang, M.J. Haun, S.J. Jang and L.E. Cross

Materials Research Laboratory
The Pennsylvania State University
University Park, PA 16802

Abstract

Pure (undoped) PZT ceramic samples at compositions across the ferroelectric region of the phase diagram have been prepared from sol-gel derived fine powders. Excess lead oxide was included in the PZT powders to obtain dense (95-96 percent of theoretical density) ceramics with large grain size ($\gtrsim$ 7μm), and to control the lead stoichiometry.

The dielectric, piezoelectric, and elastic properties were measured from 4.2 to 300K. At very low temperatures, the extrinsic domain wall and thermal defect motions "freeze out." The low temperature dielectric data will be used to separate the sixth order dielectric stiffness coefficients in a phenomenological theory. The extrinsic contribution to the properties can then be separated from the single domain properties derived from the theory.

1. Introduction

Piezoelectric lead zirconate titanate (PZT) ceramics have been used in a wide range of applications since the 1950's [1]. However, the growth of good quality single crystals of PZT for compositions across the entire phase diagram has not been accomplished. Clarke and Whatmore [2] have described the previous attempts at growing single crystals of $PbZr_xTi_{1-x}O_3$, and have found that crystals of reasonable quality can be grown within the ranges $1 \gtrsim x \gtrsim 0.84$ and $0.25 \gtrsim x \gtrsim 0$, but were unsuccessful for values of x between these two ranges.

Due to the lack of PZT single crystal data, the development of a phenomenological theory of PZT has been complicated and involved indirect methods of determining the coefficients of an energy function [3-5]. Additional experimental data is needed to separate the sixth order dielectric stiffness coefficients [5]. Dielectric constant measurements on ceramic samples at low temperatures, where the extrinsic domain wall and thermal defect motions "freeze out" [6,7], may provide this data.

Pure homogeneous PZT ceramic samples at compositions across the phase diagram have been prepared from sol-gel derived fine powders. The low temperature dielectric, piezoelectric, and elastic properties were measured from 4.2 to 300K. The procedure used to prepare the sol-gel powders and ceramic samples, along with the low temperature measurement apparatus, will be described in the next section. The results of the measurements will then be discussed.

2. Experimental Procedure

A sol-gel method similar to the procedure described in Reference 8 was used to prepare PZT compositions with four to eight mole percent excess lead oxide, depending on the composition. The starting chemicals were lead acetate $[Pb(C_2H_3O_2)_2 \cdot 3H_2O]$, titanium isopropoxide $[Ti(OC_3H_7)_4]$, and zirconium n-propoxide $[Zr(OC_3H_7)_4]$.

The lead acetate was dissolved in methoxyethanol ($C_3H_8O_2$) in a three neck reaction flask. To remove the adsorbed water, a reflux condenser was connected to the reaction flask, and the solution was heated until the temperature reached 125°C (the boiling point of methoxyethanol). After cooling the solution to 75°C, the titanium isopropoxide and zirconium n-propoxide were added, and again heated to 125°C to drive off excess methoxyethanol.

The solution was cooled to -25°C with a liquid nitrogen isopropanol bath. The water for hydrolysis (4 moles H_2O per mole alkoxide) was first mixed with an equal amount of methoxyethanol, and then added to the cooled solution. By slowly heating the flask up to room temperature (or higher depending on composition), the solution gelled. The gel was then heated in a 100°C oven for one to two days until dry.

The dried gels were calcined at 800°C for one hour. The calcined powders were then ground, and pressed into pellets without binder under a pressure of 50,000 psi. The green pellets, with four to eight mole percent excess lead oxide, were sintered on platinum sheets in a set of alumina crucibles with a lead source powder. The samples were sintered at a range of temperature from 1000 to 1260°C for 20 to 60 hours depending on the composition. The sintered ceramic samples had densities of 95 to 96 percent of theoretical density, and average grain sizes larger than 7 μm.

X-ray diffraction patterns of the calcined powders showed that both perovskite PZT and lead oxide were present. However, after sintering, no lead oxide diffraction peaks could be detected, indicating that the excess lead oxide was volatilized during sintering.

0000-0394

Coexistence of the tetragonal and rhombonedral phases was found from x-ray diffraction to occur for compositions one mole percent on either side of the morphotropic boundary. This is much narrower than the coexistence region normally achieved from the mixed oxide method, but not as narrow as that reported for a coprecipitation method [9].

The ceramic samples were sputtered with gold electrodes, and poled with electric fields of 20 to 40 KV/cm for 4 to 30 minutes. The piezoelectric strain coefficient d_{33} was then measured using a Berlincourt Piezo-d_{33} meter to determine the completeness of poling. The poled discs were cut into bars, cylinders, and discs according to the I.R.E. Standards [10].

The apparatus used for the low temperature measurements was composed of an Air Products and Chemicals model LT-3-110 cryogenics system, which can stably control the temperature from 4.2 to 300K. The dielectric and resonance properties were measured on a Hewlett Packard 4270A automatic digital capacitance bridge and 3585A Spectrum analyzer. The samples with thermal-resistance wire attached as leads, were shielded in a copper enclosure. The samples were first cooled down to 4.2K, and then the measurements were made during heating to 300K. The I.R.E. standard method [10] for piezoelectric resonance measurements was used for the calculations.

3. Results and Discussion

The dielectric constant at room temperature was plotted versus composition for poled (measured parallel to the poling direction) and unpoled ceramic samples in Figure 1. The peak in the dielectric constant occurs close to the morphotropic phase boundary between the tetragonal and rhombohedral phases at a composition of approximately $Pb(Zr_{0.52}Ti_{0.48})O_3$. By poling the samples the dielectric constant increased and decreased for the tetragonal and rhombohedral compositions, respectively.

The increase of the dielectric constant when poling the tetragonal samples was previously explained [11] as being due to the elimination of the effect of compression of the 180-degree domains. This occurs due to the virtually complete 180-degree domain reorientation along the poling direction, and dominates the decrease in dielectric constant from 90-degree domain reorientation.

For the rhombohedral compositions, the dielectric constant decreases when poling the samples. This net decrease occurs, because the decrease of the dielectric constant due to the 71 (109) degree domain reorientation dominates the effect of the removal of compression [11].

The dielectric constant and dissipation factor for several PZT compositions are plotted versus temperature in Figure 2. The dielectric constants

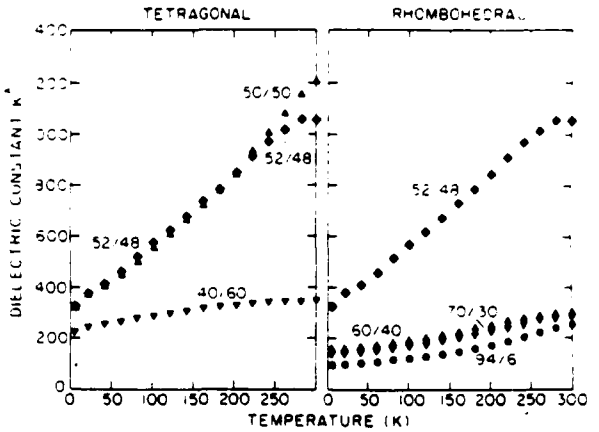

(a)

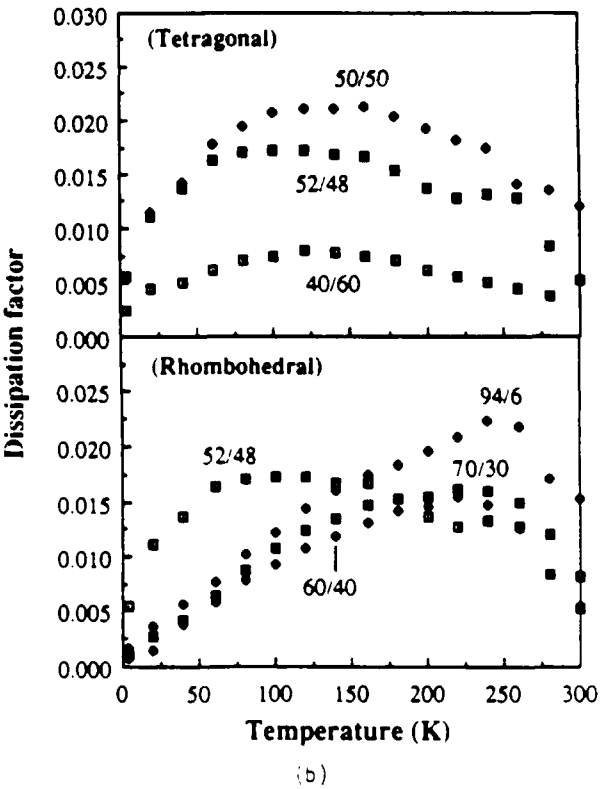

(b)

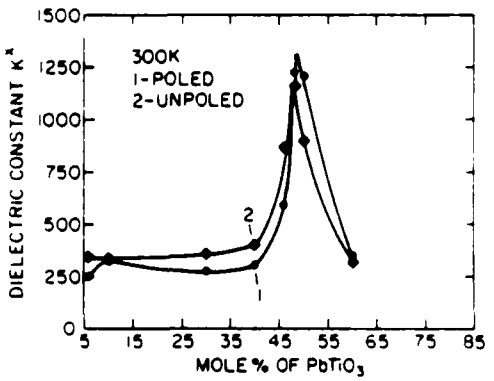

Figure 1. The dielectric constant for poled and unpoled ceramic samples at room temperature plotted versus composition.

Figure 2. The a) dielectric constant and b) dissipation factor for several PZT compositions plotted versus temperature.

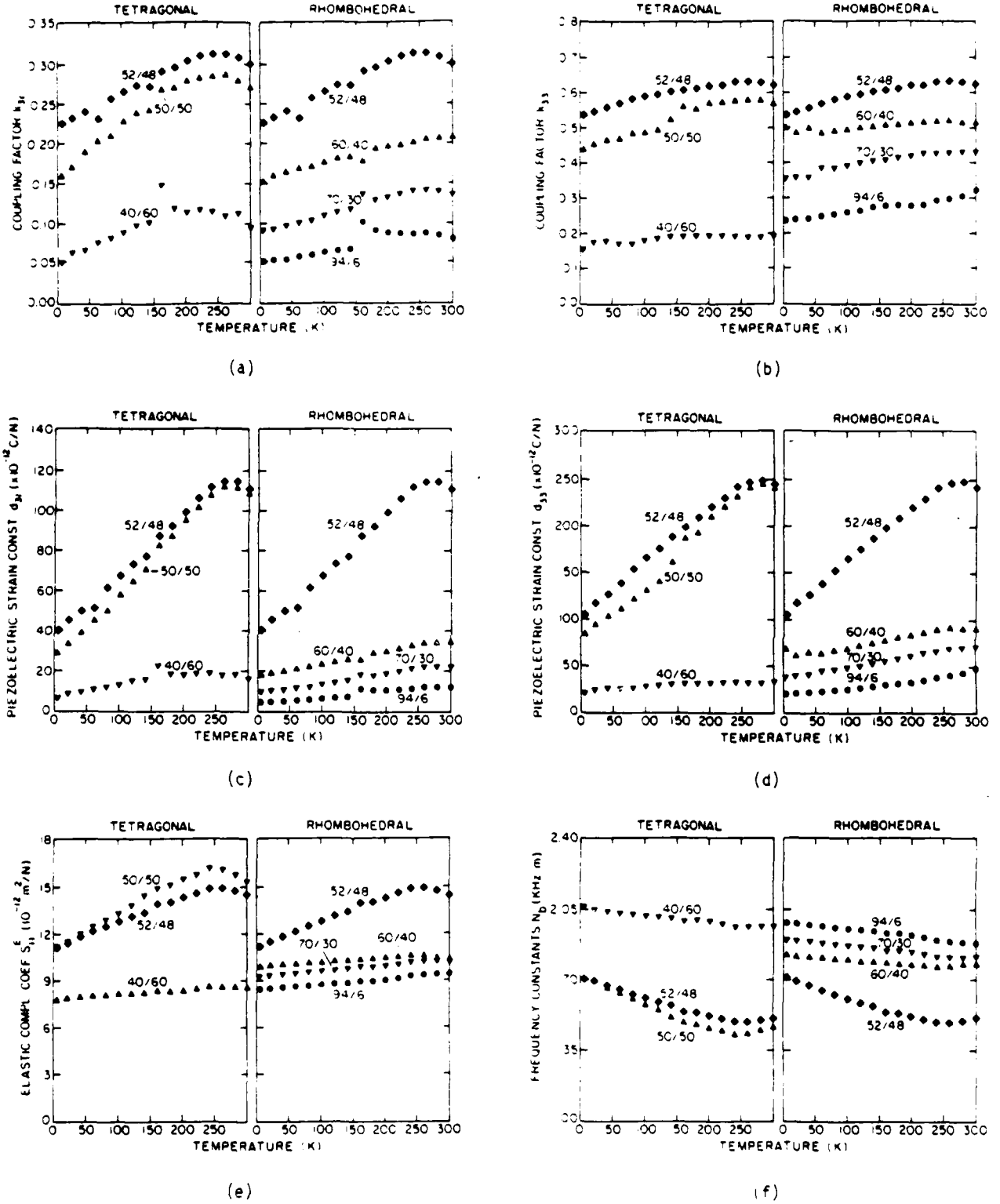

Figure 3. The coupling factors a) k_{31} and b) k_{33}, piezoelectric strain coefficients c) d_{31}, and d) d_{33}, e) elastic compliance coefficient s_{11}^E, and f) frequency constant N_b for several PZT compositions plotted versus temperature.

of the compositions close to the morphotropic boundary showed a much stronger temperature dependence than the composition away from the boundary.

Broad peaks in the dissipation factor versus temperature were found to occur at 225 to 250K for the rhombohedral compositions, and at 100 to 150K for the tetragonal compositions. The different activation energies for domain wall motion in the tetragonal and rhombohedral samples would possibly account for these loss peaks, and is presently under further investigation. The PZT 52/48 composition, which showed coexistence of both tetragonal and rhombohedral phases, had loss peaks in both temperature ranges.

Figure 3 shows the temperature dependence of the coupling factors k_{31} and k_{33}, piezoelectric strain coefficients d_{31} and d_{33}, elastic compliance coefficient s^E_{11}, and frequency constant N_b. The compositions close to the morphotropic boundary again showed the largest temperature dependence.

The compositional dependence of the elastic compliance coefficient s^E_{11} and the frequency constant N_b at 4.2 and 300K are shown in Figure 4. The effect of the morphotropic boundary between the tetragonal and rhombohedral phases can be seen in this figure, along with the effect of the morphotropic boundary between the ferroelectric rhombohedral and antiferroelectric orthorhombic phases near the PZT 94/6 composition.

4. Summary

A sol-gel method was used to prepare pure PZT powders across the ferroelectric region of the phase diagram. Excess PbO was included in the powders to obtain dense (95 to 96 percent of theoretical density) ceramics with large grain size ($\geq$ 7μm), and to control the lead stoichiometry during sintering. X-ray diffraction showed a narrow coexistence region of tetragonal and rhombohedral phases of approximately one mole percent on either side of the morphotropic boundary.

The dielectric, piezoelectric, and elastic properties were measured from 4.2 to 300K. At very low temperatures the domain wall and thermal defect motions "freeze out." The compositions near the morphotropic phase boundary had the largest temperature dependence. Dielectric loss peaks were found to occur from 225 to 250K for the rhombohedral compositions, and from 100 to 150K for the tetragonal compositions.

The low temperature dielectric data will be used to separate the sixth order dielectric stiffness coefficients in a phenomenological theory of PZT. The extrinsic contributions to the properties can then be separated from the intrinsic single domain properties derived from the theory.

References

[1] B. Jaffe, W.R. Cook, and H. Jaffe, Piezoelectric Ceramics. London, Academic Press, 1971.

[2] R. Clarke and R.W. Whatmore, J. Cryst. Growth, Vol. 33, pp. 29-33, 1976.

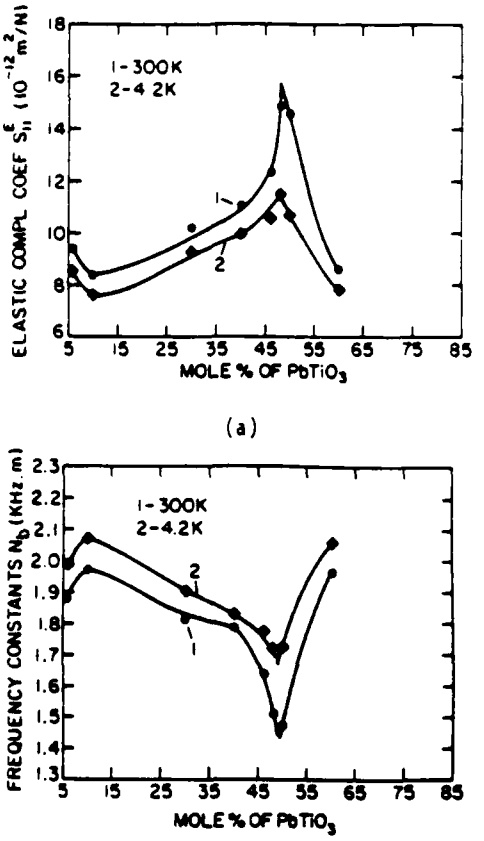

Figure 4. The a) elastic compliance coefficient s^E_{11} and b) frequency constant N_b at 4.2 and 300K plotted versus composition.

[3] A. Amin, M.J. Haun, B. Badger, H. McKinstry, and L.E. Cross, Ferroelectrics, Vol. 65, pp. 107-130, 1985.

[4] M.J. Haun, T.R. Halemane, R.E. Newnham and L.E. Cross, Proc. IMF-6, Jpn. J. Appl. Phys. (accepted).

[5] M.J. Haun, Z.Q. Zhuang, S.J. Jang, H.A. McKinstry, and L.E. Cross, Proc. of ISAF 1986.

[6] X.L. Zhang, Z.X. Chen, L.E. Cross, and W.A. Schulze, J. Mat. Sci., Vol. 18, pp. 968-972, 1983.

[7] J.N Kim, M.J. Haun, S.J. Jang, and L.E. Cross, J. High Tech. Ceramics (accepted).

[8] J.B. Blum and S.R. Gurkovich, J. Mat. Sci., Vol. 20, pp. 4479-4483, 1985.

[9] K. Kakegawa, J. Mohri, T. Takahashi, H. Yamamura, and S. Shirasaki, Solid State Comm., Vol. 24, pp. 769-772, 1977.

[10] "I.R.E. Standards on Piezoelectric Crystals: Measurements of Piezoelectric Ceramics, 1961," Proc. I.R.E., Vol. 49, pp. 1161-69, 1961.

[11] A.V. Turik, M.F. Kupriyanov, E.M. Sidorenko, and S.M. Zaitsev, Sov. Phys. Tech. Phys., Vol. 25 (10), pp. 1251-1254, 1980.

ELECTRICAL PROPERTIES OF GRAIN-GROWN PLZT CERAMICS

D.N. Huang*, Z.W. Yin*, and L.E. Cross

Materials Research Laboratory
The Pennsylvania State University
University Park, PA 16802

Abstract

8/65/35 PLZT ceramics with different grain size distribution were prepared by long time heat treatments in a PbO atmosphere. After thermal etching, image analyses were carried out for these specimens and their electrical properties were measured. Experimental results showed that the grain boundaries give rise to large effects on the electrical properties of the PLZT ceramics. An explanation for the grain boundary effects in these PLZT is suggested.

1. Introduction

The research work on fabrication, properties, phase transitions and applications of $(Pb,La)(Zr,Ti)O_3$ (PLZT) solid solutions have been an attractive topic since 1970. However, they are still attractive today due to their diffuse phase transition behavior and the developing need for a more complete explanation of these interesting dispersion phenomena.

Investigations of the effects of grain size on the electrical and optical properties of PLZT ceramics have been carried out by Okazaki[1][2] etc. and a space-charge field mechanism was suggested to explain the grain-size dependencies of some ferroelectric properties. However, the largest grain size sample in their works is only 14 μm and the mean grain size of the sample was measured by the linear-intercept method.

In the present work, hot-pressed transparent 8/65/35 PLZT ceramic slug was used as original material, through different process of heat treatment, ceramic specimens with different grain size distributions were prepared and a Quantimet 900 Micro-Image Automatic Quantitative Analyser was used for image analysis[3], using S_v, the total interface area in unit volume of ceramic material instead of mean grain size to discuss the effect of grain boundaries on the properties of these ceramic materials.

Table 1.
Image Analysis Date of PLZT Ceramic Specimens with Different Grain Sizes.

Specimen No.	Total Number Counted	Grain Length (L) Mean (μm)	Grain Length (L) Std. Dev. (μm)	Grain Breadth (B) Mean (μm)	Grain Breadth (B) Std. Dev. (μm)	Roundness (F) Mean	Roundness (F) Std. Dev.	S_v mm^2/mm^3 Mean	S_v mm^2/mm^3 Std. Dev.
1*	4000	5.35	2.25	3.86	1.68	1.38	0.228	0.658	0.014
2	7914	19.0	9.21	13.9	7.52	1.35	0.188	0.159	0.033
3	4456	25.4	13.5	18.6	9.90	1.41	0.351	0.130	0.003
4	2866	31.1	15.1	23.0	12.2	1.36	0.232	0.103	0.0035

*Original hot-pressed sample.

*Visiting Scientists from Shanghai Institute of Ceramics, Shanghai, China.

2. Experimental Results from Image Analyses

Table 1 shows the statistical results of image analysis of 4 specimens which were obtained by different processes of heat treatment. The parameters measured are grain size related parameters length distribution (L) and breadth distribution (B), grain shape related parameter roundness distribution (F) and the total interface area in unit volume (S_v), etc. For measuring L, B, and F, data from 2800-8000 grains in different fields were taken to get the results. For each S_v measurement, the result is the average value of the data from more than twenty measurements of different fields.

It can be seen from Table 1 for grains in hot-pressed specimen (No. 1) after different heat treatments, the average length increases from 5.35 μm to 31.1 μm, average breadth from 3.66 μm to 23.0 μm, and S_v from 0.658 decreased to 0.103. However, the shape related parameter roundness remains unchanged, at about 1.4. This means that in present heat treatment conditions, the growth of grain does not change its crystalline habit. The grains are equivalent to elongated cubes (as calculated, for a two dimensional cube F = 1.31). No overheating phenomena were evident such as pores occluded or grain boundaries broaden or density decreased. The transparency of the ceramic remain essentially unchanged.

3. Dielectric and Ferroelectric Measurements of Grain-Grown Specimens

The samples used for electrical measurements are plates of 0.2 mm thickness with electrodes around 4 mm in diameter. The dielectric properties were measured by a computerized automatic measuring system with Hewlett-Packard's microprocessor-based equipment. The temperature dependence of dielectric constant and loss tangent were measured by a multifrequency LCR meter HP4274A in the frequency range of 10^2-10^5 Hz, with basic accuracy of 0.1%. The polarization and biased pyroelectric currents were measured with a HP4140B picoampere meter. A Delta design Model 2300 environment chamber covered the temperature range from -150 to 200°C, using liquid nitrogen as a coolant. Temperatures were measured with a Fluke 8502A digital multimeter via a platinum resistance thermometer mounted directly on the ground electrode of the sample fixture. A HP9825A desktop computer was used for on-line control of automatic measurements through a HP6904B multiprogrammer interface. All the data were recorded on flexible magnetic discs. The hysteresis loops below T_t of the hot-pressed and grain-grown specimens were measured by using the Sawyer-Tower circuit at 0.1 Hz, P_r and E_c were evaluated from the loops.

The typical curves of the temperature dependence of the weak field dielectric constant and loss of the depoled or prepoled original hot-pressed and grain-grown samples are shown in Figure 1. The behavior measured at different frequencies of the grain-grown samples is shown in Figure 2.

Figure 3 shows the linear relationship of T_m and T_t with $1/S_v$, the reciprocal of the total interface area in unit volume of the ceramic material. Figures 4 and 5 show respectively the $1/S_v$ dependences of dielectric constant measured at different frequencies and of polarization at different temperatures. Figures 6 and 7 show respectively the typical curves of temperature dependences of polarization and current density with different bias fields for the grain grown specimens. From these figures, the bias field dependences of polarization and transition temperatures for different grain-size specimens were obtained, these are shown in Figures 8 and 9. The hysteresis loops of hot-pressed and grain-grown specimens are shown in Figure 10.

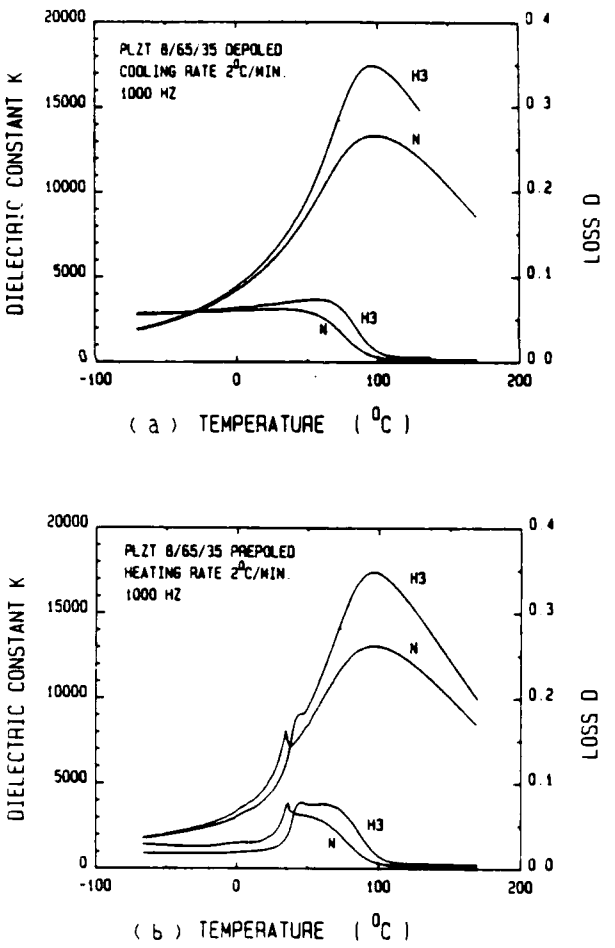

Fig. 1. Typical curves of the temperature dependence of the dielectric constant and loss of the depoled or prepoled 8/65/35 PLZT samples. N - normal hot-pressed sample. H-Grain-grown sample by heat treatment. (a) Depoled, (b) Prepoled.

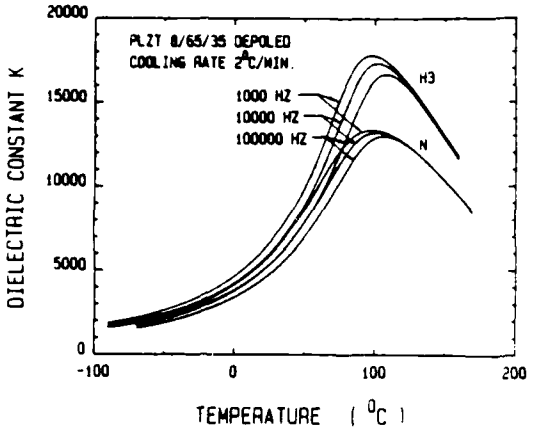

Fig. 2. Typical curves of the temperature dependence of dielectric constant measured at different frequencies of the grain-grown 8/65/35 PLZT sample.

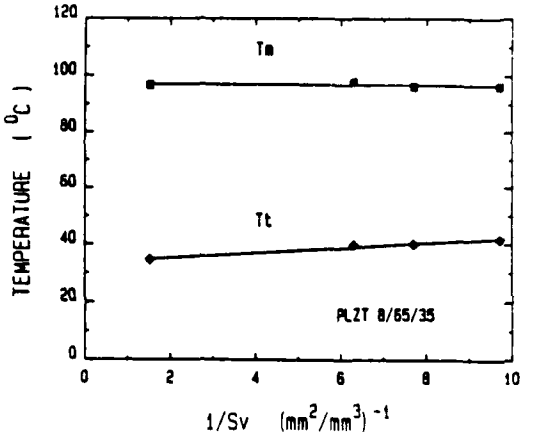

Fig. 3. The linear relationship of T_m and T_t with $1/S_v$, the reciprocal of the total interface area in unit volume of the PLZT ceramic material.

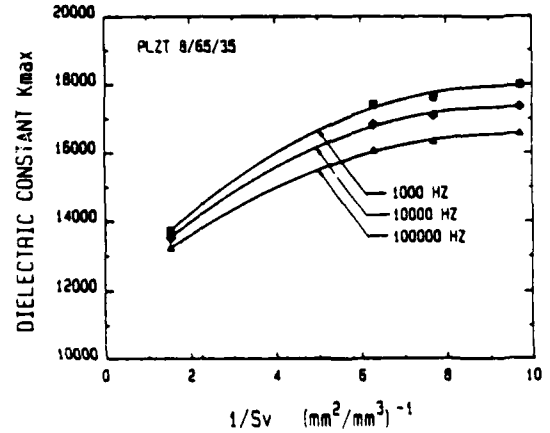

Fig. 4. The relationship curves of dielectric constant against $1/S_v$ measured at different frequencies of 8/65/35 PLZT samples.

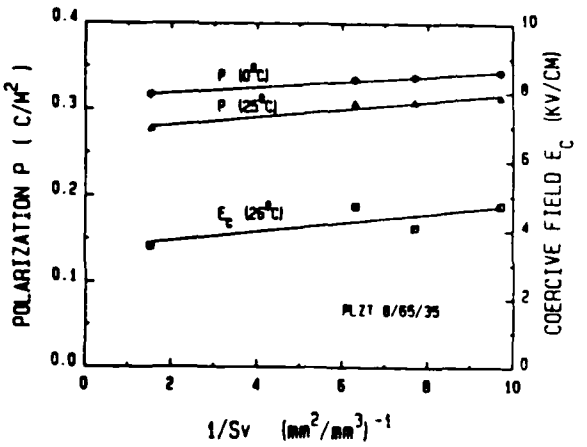

Fig. 5. The relationship curves of polarization against $1/S_v$ at different temperatures of 8/65/35 PLZT samples.

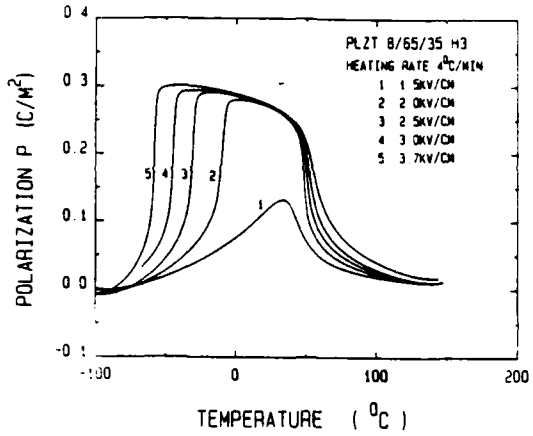

Fig. 6. Typical curves of temperature dependence of polarization under different bias field of 8/65/35 PLZT ceramics.

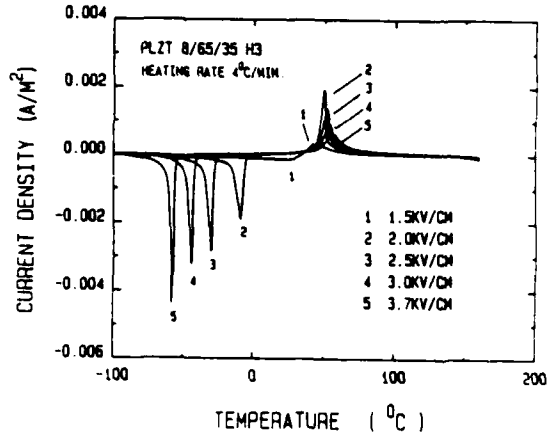

Fig. 7. Typical curves of temperature dependence of current density under different bias field of 8/65/35 PLZT ceramics.

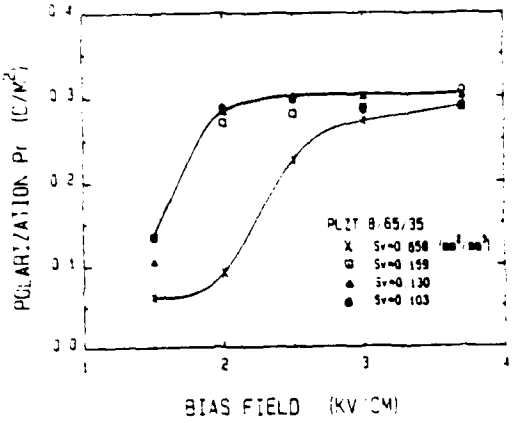

Fig. 8. The bias field dependence of polarization for different grain size specimen of 8/65/35 PLZT ceramics.

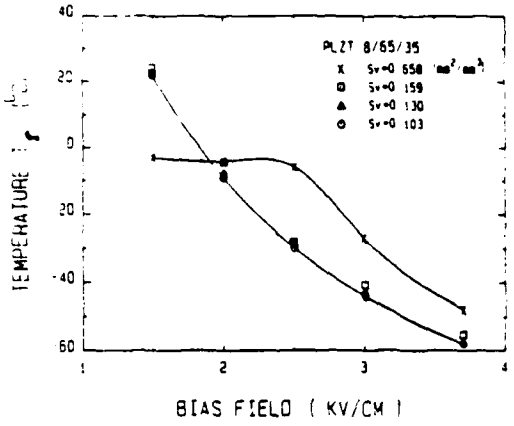

Fig. 9. The bias field dependence of transition temperature T_t for different grain size specimens of 8/65/35 PLZT ceramics.

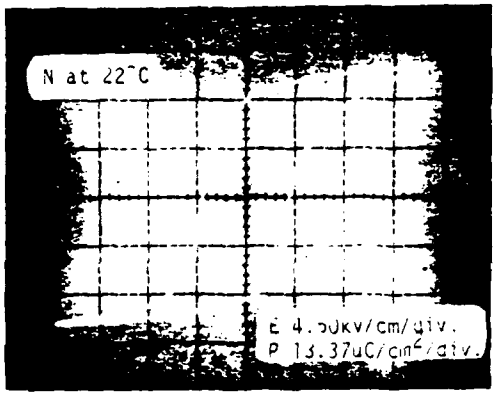

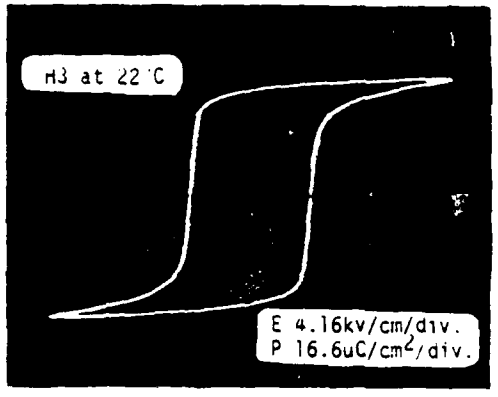

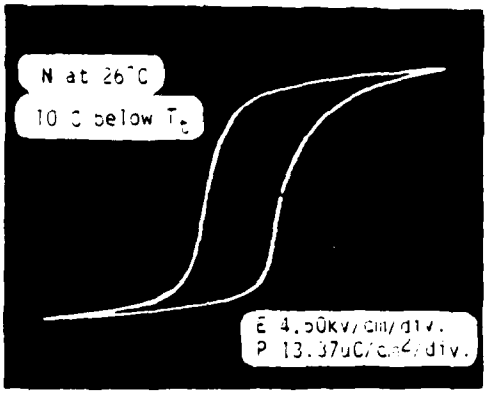

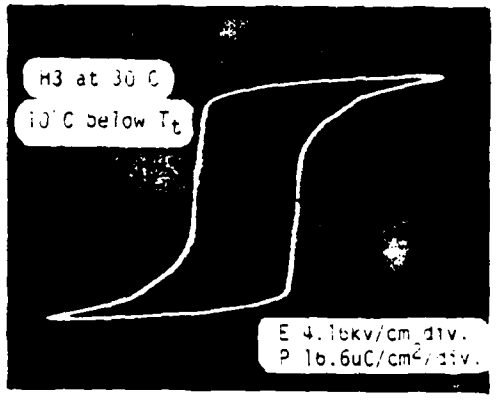

Fig. 10. The hysteresis loops below T_t of the hot-pressed and grain-grown 8765/35 PLZT specimens. P_r and E_c were evaluated from the loops.

4. Chemical Analysis Data of Hot-Pressed and Grain-Grown Specimens

For verifying the possible variation of chemical composition of the samples after long time heat treatments in PbO atmosphere, all samples were chemically analysed after each treatment by the x-ray fluorescence spectrum analysis. The chemical composition data were calculated and summarized in Table 2. The error in chemical analysis is within 1% for Pb and La, within 0.5% for Zr and Ti.

6. Proposed-Model

The dielectric data strongly suggest that there is a 'region' of reduced dielectric polarizability in the vicinity of the grain boundary in these PLZT ceramics. On this model, increasing the grain size reduces the area of grain boundary, and thus the volume of lower permittivity which is electrically connected in series with the bulk of the grain.

Table 2. Chemical Analysis Data for Hot-pressed and grain-Grown 8/65/35 PLZT Specimens

Specimen No.	State of Treatment	Calculated Chemical Formula
N	Original hot-pressed sample	$Pb_{.89}La_{0.76}\square_{.038}(Zr_{.665}Ti_{.335})O_3$
H_1	72 hrs. heat treatment at 1340°C	$Pb_{.86}La_{.068}\square_{.034}(Zr_{.663}Ti_{.337})O_3$
H_2	120 hrs. heat treatment at 1340°C	$Pb_{.88}La_{.068}\square_{.034}(Zr_{.662}Ti_{.338})O_3$
H_3	168 hrs. heat treatment at 1340°C	$Pb_{.88}La_{.080}\square_{.040}(Zr_{.667}Ti_{.333})O_3$

5. Summary of Experimental Results

From Fig. 1 to Fig. 10 and Table 2, the following results were obtained for the grain-grown specimen as compared with that of hot-pressed PLZT ceramics:

1. The grain-grown specimen has higher dielectric constant at T_m and higher loss in the α phase region but less in the β phase region than that of the finer grain hot-pressed specimen.

2. The T_t temperature will go up as the grain size of the specimen increases and there is a linear relationship between T_t and $1/S_v$. However, the T_m temperature remains almost unchanged for different grain size specimens.

3. The relaxation effect is more pronounced for grain-grown specimens, and will reach equilibrium after the S_v decreases to near 0.1 mm^2/mm^3.

4. Both the remanent polarization P_r and coercive field E_c are higher for grain-grown specimens and the hysteresis loop becomes more rectangular than that of the hot-pressed specimen.

5. At a constant heating rate and constant bias, T_f [4] shifts to a lower temperature for the grain-grown specimen, and its temperature range of macrodomain state becomes broadened, as compared with that of hot-pressed specimen.

6. The chemical composition of the specimen remains fundamentally unchanged after long time heat treatment in PbO atmosphere.

In relaxor ferroelectrics like these PLZTs, it has been suggested [4] that a major part of the polarizability, particularly at temperatures near T_m comes from the thermal reorientation of polar micro-regions too small to be completely stable, i.e. a superparaelectric effect. These polar regions are assumed to arise from heterogeneity in the composition giving rise to a sharply changing volume distribution of Curie points and thus at any temperature in the 'Curie Range' a volume distribution of micro-polar regions in a high permittivity perovskite matrix phase.

If the micro-regions are small, the energy barriers separating the different states also became small and when $v \sim [200Å]^3$ these barriers become comparable to kT and the polar vectors reorient thermally with a relaxation character. In perfect macroscopic crystals, all domain states in a ferroelectric phase are energetically equivalent (a necessary feature for ferroelectricity) and these equivalences are defined by elements of the prototypic point symmetry. For the compositionally heterogeneous crystal, the local symmetry at a given polar region will not be the same as the global crystal symmetry, due to the differing composition gradients around the region. Thus the prefered vector directions for P_s will not be energetically exactly equivalent nor will they necessarily conform exactly to those prescribed by the prototypic form.

On this model the polar micro-region will have a prefered orientation corresponding to the deepest minimum in energy and its contribuiton to the total polarizability will decrease as the local anisotorpy (differential well depth) increases.

We would suggest that in a ceramic, the grain boundary must modify the local composition gradients giving rise to higher anisotropy in polar micro-regions close to the boundary.

Consequences of such an anisotropy would be:

1. A strong grain size dependence of ε_{max} at T_m.

2. Higher anisotropy will lead to an earlier breakup of the poled state on heating, thus T_t should increase with grain size.

3. Anisotropy will preferentially remove the relaxation component of the polarization, so that grain grown samples should have stronger relaxation than hot pressed samples.

4. Increased anisotropy makes poling more difficult but encourages depoling, thus P_s and E_c should be larger in the less anisotropic grain grown samples.

5. At a constant heating rate under DC bias, anisotropic samples will be harder to pole and easier to depole, thus T_f shifts down and T_t shifts up in the grain grown material.

It is evident from the above as compared to the experimental findings that qualitatively the model of anisotropic polar micro-regions could account for all of the observed phenomena if as appears rather logical, the composition gradient becomes steeper near the grain boundary. Clearly, however, the model is at this stage only one of several possible working hypothesis and much works remains to extend and to quantify the proposed internal structure of micro-polar regions.

References

[1] K. Okazaki and K. Nagata, J. Am. Cer. Soc., Vol. 56 (2), pp. 82-86 (1973).

[2] K. Okazaki, H. Igarashi, K. Nagata and A. Hasegawa, Ferroelectrics, Vol. 7, pp. 153-155 (1974).

[3] Z.W. Yin, D.N. Huang, X.T. Chen, X.Q. Chen and X.L. Zhou, to be published.

[4] Yao Xi, Chen Zhili and L.E. Cross, J. Appl. Phys., 54 (6), pp. 3399-3403 (1983).

[5] B.H. Chu, H.K. Ao, X.S. Zhen and Z.W. Yin, Proc. First China-U.S. Seminar on Microstructure and Properties of Ceramic Materials, Science Press, Beijing, China, p. 410 (1985).

THE EFFECTS OF HYDROSTATIC PRESSURE ON POLARIZATION REVERSAL IN SOFT Nb:PZT CERAMICS

Q. LI*, W. Y. PAN and L. E. CROSS
Materials Research Laboratory
The Pennsylvania State University
University Park, PA 16802

ABSTRACT

For a soft niobium-doped PZT ceramic (Ultrasonic Powders type 501A), the changes with hydrostatic pressure of polarization and activation field for domain wall motion have been investigated in the range of 0 to 6 kbar. The application of hydrostatic pressure decreased the spontaneous polarization, remanent polarization, coercive field, and activation field for domain wall motion. The changes of activation field with hydrostatic pressure show different characteristics in fine and coarse grain specimens. The fine grain showing a nonlinear dependence and the coarse grain a linear dependence on pressure.

1. INTRODUCTION

Because of the strong interdependence between the lattice strain and the spontaneous electric polarization, pressure is an important variable in the study of ferroelectric properties. There has been a number of studies on the effects of hydrostatic pressure on the properties in ferroelectric materials such as $BaTiO_3$ [1-3], $SrTiO_3$ [3-5], $PbTiO_3$ [6,7], TGS [8,9], KDP [10,11], and PZT [12-14]. However, these works, in general, were concentrated on the study of Curie temperature and macroscopic ferroelectric properties under hydrostatic pressure.

So far the work by Hayashi [15] is the only study of domain wall dynamics under hydrostatic pressure. He measured the change of activation field α for domain wall motion in $BaTiO_3$ and TGS single crystals under hydrostatic pressure σ, and found that the value of α decreased linearly with increasing hydrostatic pressure in $BaTiO_3$ but increased linearly in TGS. Our work aims at studying the effect of hydrostatic pressure on activation field of domain wall motion in PZT ceramics.

2. EXPERIMENTS

The raw material was commercial Nb:PZT 52/48 powder produced by Ultrasonic Powders, Inc. The ceramic discs sintered at 1285°C for a half hour and at 1315°C for 3 hours were 7.48 g/cm^3 and 7.55 g/cm^3 in density and 2 μm and 10 μm in average grain size respectively.

It was found that the specimens with an irregular shape were favorable for preventing the radial-mode piezoelectric oscillation. The specimens used in the study were made into irregular plates of about 1 mm^2 in area and 200-300 μm in thickness.

The experiments were performed in a 6 kbar hydrostatic pressure system. This consisted of a pressure generator and a specimen chamber interconnected by a steel capillary. Silicone oil was used as the transmitting medium. A square wave pulse generator and a high voltage amplifier were used to generate a square pulse up to 1500 volts. The rise time is shorter than 20 nsec. The voltage response across a small resistor (~3Ω) in series with the specimen was examined on the oscilloscope (Nicolet 204A).

*Visiting scientist from the Institute of Solid State Physics Nanjing University, China.

3. RESULTS

(a) Effects of Hydrostatic Pressure on Coercive Field and Remanent Polarization

The hysteresis loops under various hydrostatic pressure up to 6 kbar were measured at 25°C. The application of pressure evidently reduced the spontaneous and remanent polarizations, and the coercive field. It may be noted that they change nonlinearly with hydrostatic pressure as shown in Figure 1, at least for lower pressure. However, the changes of P_r and E_c with temperature measured within a range of room temperature to 80°C were linear.

(b) Effect of Applied Field on Switching Transient Under Fixed Hydrostatic Pressure

Under any fixed hydrostatic pressure, if a positive or negative square pulse was applied to the specimen, we can observe a switching current signal with a peak, except for incompleted switching at low field. The contour of switching pulse is very similar to the results in ferroelectric single crystals such as $BaTiO_3$ [16,17], TGS [18], but different from that in PZT 65/35 ceramics measured by Masuda et al. [19] in which there is not any explicit peak on the switching current curves.

Figure 2 illustrates a typical set of switching current-time curves for various applied fields at 25°C and 3.5 kbar. With increasing applied field, the position of peak is shifted towards the left part, the peak is increased and the switching time is reduced.

Figure 3 shows the peak switching current i_{max} as a function of applied field at room pressure. It may be found that the peak switching current i_{max}, under lower applied field used in the experiment, is satisfied with the well-known equation

$$i_{max} \sim e^{-\alpha/E} \quad . \tag{1}$$

At the same time, the experiment showed that the switching time t_s, at which the switching current was attenuated to 10% of the maximum, was also satisfied with the following relation

$$t_s \sim e^{\alpha/E} \quad . \tag{2}$$

(c) Effect of Hydrostatic Pressure on Activation Field

(1) Fine grain specimen

For the specimens with fine grain structure (about 2 μm), the experiments under hydrostatic pressure up to 6 kbar showed that the switching rate was increased remarkably. Figure 4 is a typical example at 2 kV/mm. With increasing hydrostatic pressure, the switching current peak was shifted towards the left part of the plot, and the peak switching current was raised. However, it should be pointed out that because of the remanent polarization decreasing with increasing pressure, the peak switching current doesn't always increase with pressure. At higher field (>2.3 kV/mm), the peak current even may decrease with pressure as shown in Figure 5.

Figure 6a and b are plots of α versus σ in which the values of α are obtained according to equation (1) and (2) respectively. Although there are some quantitative differences between both sets of α, the qualitative features are the same. The changes of α with hydrostatic pressure are nonlinear, particularly under the pressure less than 3 kbar. During increasing hydrostatic pressure, the value of α decreases at a slower and slower rate and approaches a constant, for example, at 6.5 kV/mm in Figure 6a.

(2) Coarse grain specimens

For the coarse grain specimens in which the average grain size is about 10 μm, the switching processes were much faster than that in fine grain samples. The peak position t_s, in most of the experiments, was about 0.2 μsec, so that we often couldn't resolve the shift of peak as changing applied field or pressure. However, the switching current i_{max} still changes with applied field and pressure. Figure 7 and Figure 8 are

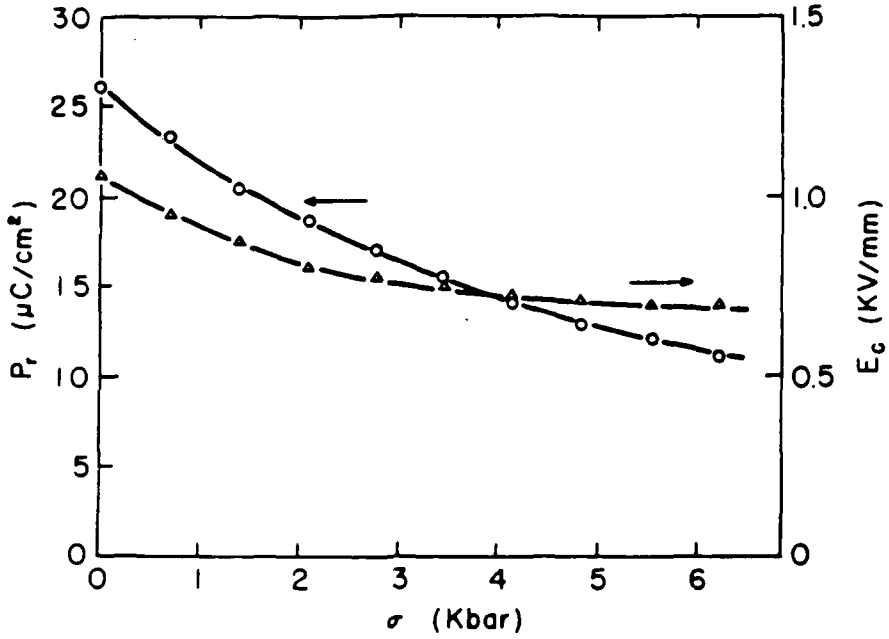

Figure 1 Hydrostatic pressure dependences of remanent polarization and coercive field in fine grain PZT ceramics.

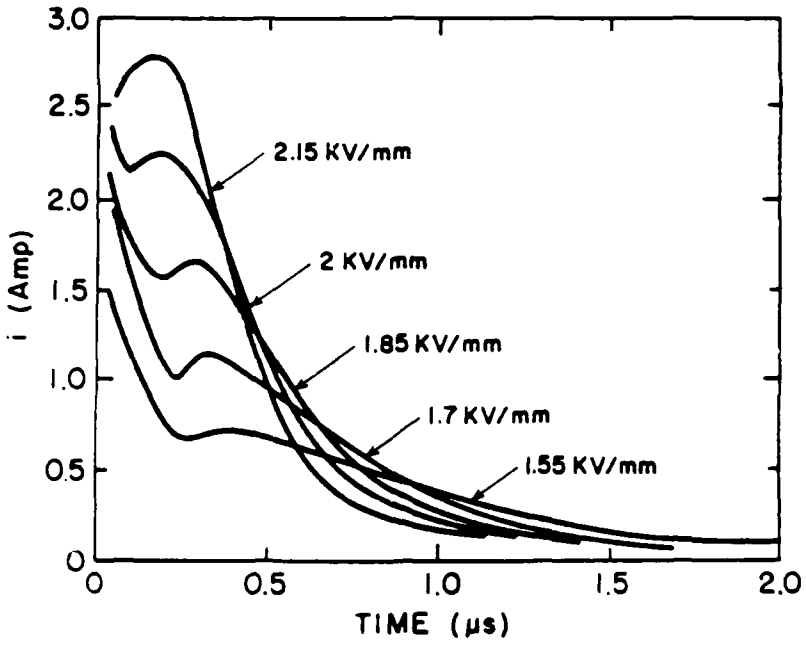

Figure 2 Switching current-time curves for various applied fields at 3.5 kbar in fine grain PZT ceramics.

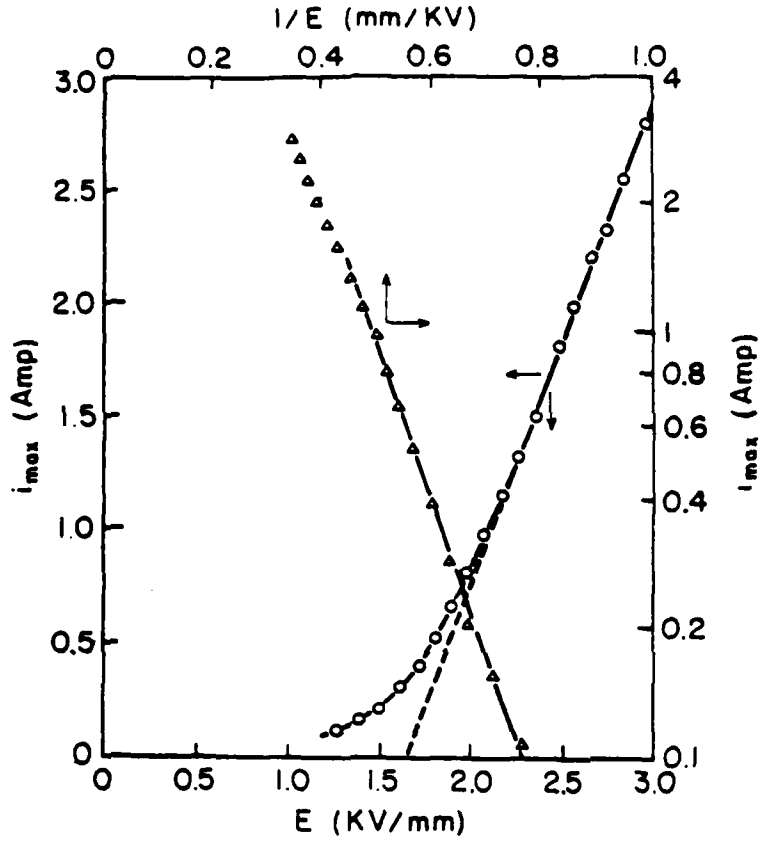

Figure 3 Peak switching current versus applied field in a specimen with 4 μm grains.

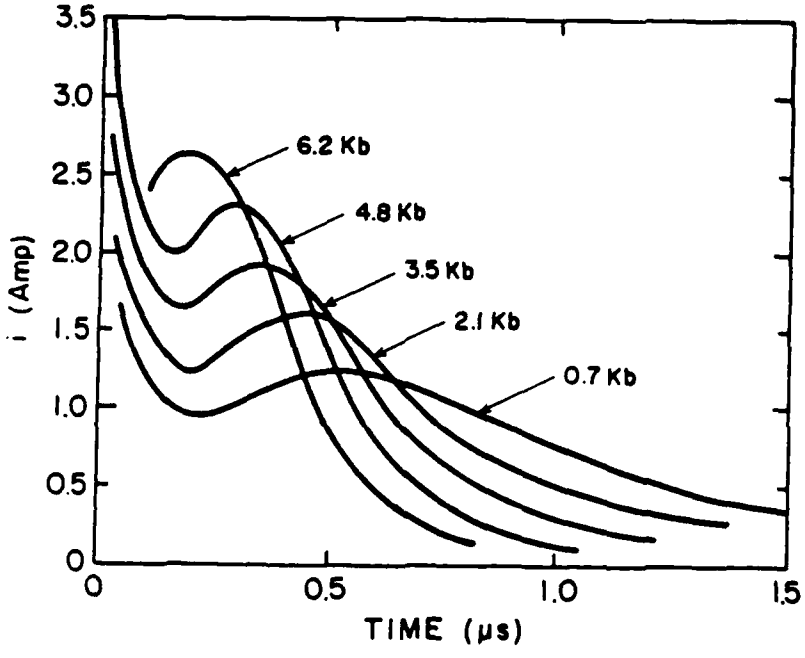

Figure 4 Switching current-time curves at 2 kV/mm and various hydrostatic pressures in fine grain PZT ceramics.

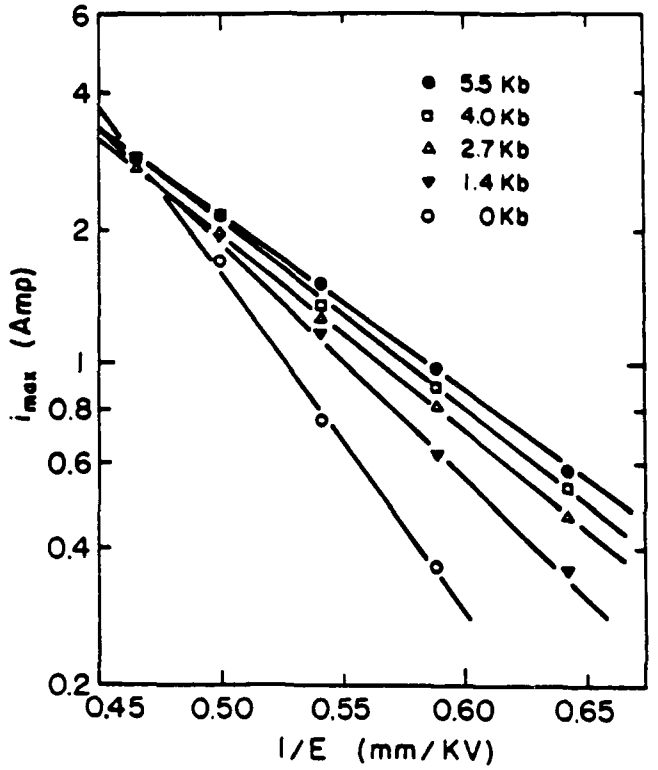

Figure 5 Applied field dependence of peak switching current under various hydrostatic pressures in fine grain PZT ceramics.

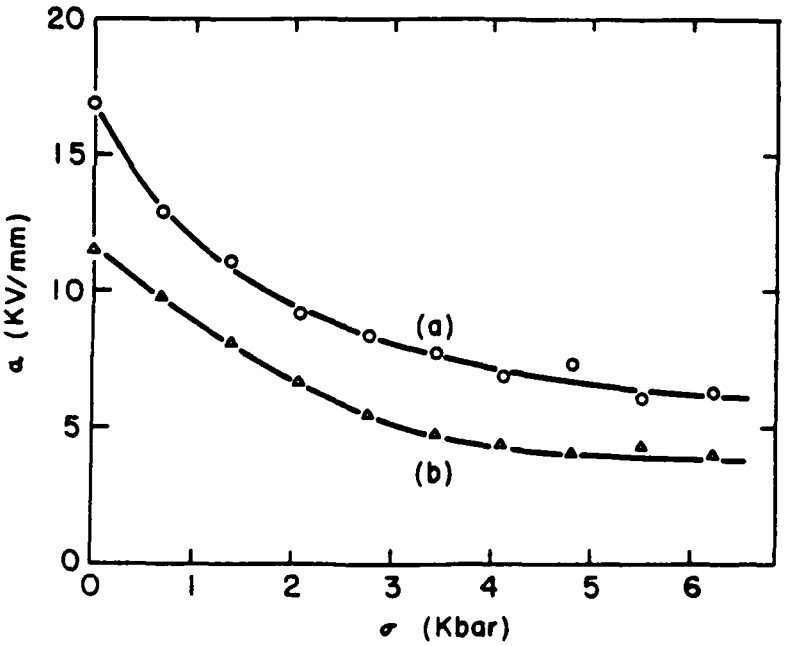

Figure 6 Activation field versus hydrostatic pressure in fine grain PZT ceramics (a) obtained from i_{max}, and (b) obtained from t_s.

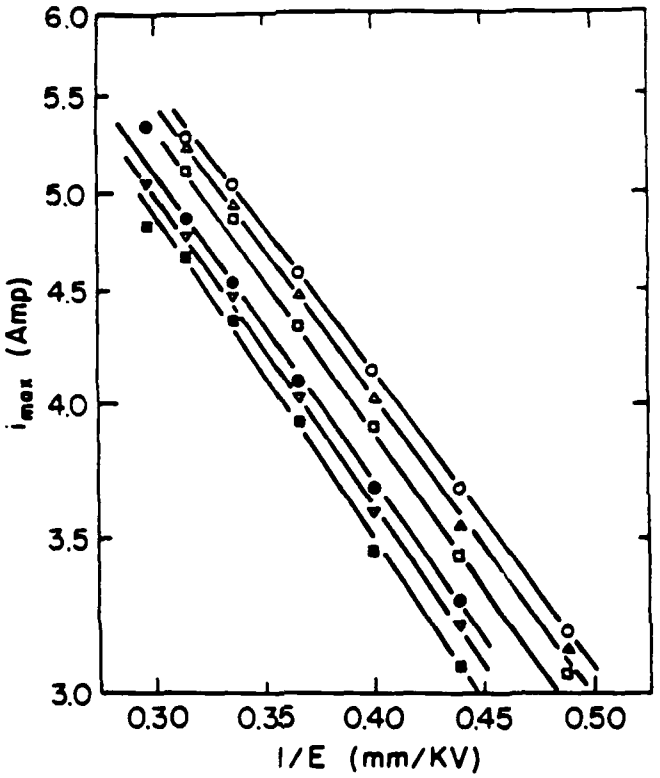

Figure 7 Applied field dependence of peak switching current under various hydrostatic pressures in coarse grain PZT ceramics.

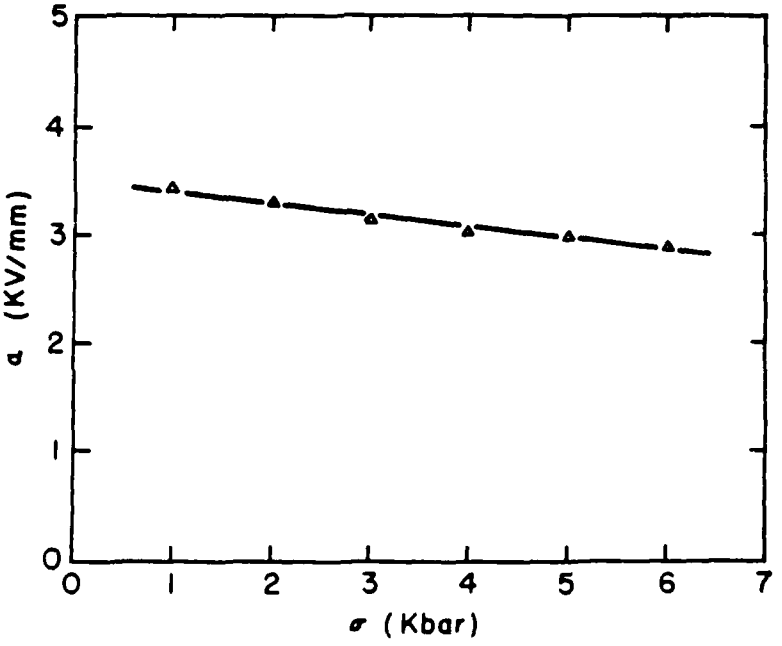

Figure 8 Hydrostatic pressure dependence of activation field in coarse grain PZT ceramics.

the plots of i_{max} versus 1/E and α versus σ respectively. It must be noted that the effect of hydrostatic pressure on activation field of domain wall motion is very different from previously, α changes linearly with pressure, and is always less than that in fine grain samples, especially at lower hydrostatic pressures.

4. DISCUSSION

(a) Using the square pulse field method developed by Merz [16], our results for commercial Nb:PZT 52/48 and pure PLZT 8/65/35 [17] ceramics showed well-defined switching current peaks. However, the switching transients in PZT 65/35, PLZT 5/65/35 ceramics measured by Masuda et al. [19] didn't show any switching current peak. This is not surprising if we examine the rise time of their pulse source which at 5 μsec is much longer than t_{max} and even longer than t_s in our experiment.

(b) The applied field dependence of switching process (t_{max}, t_s, i_{max}) is similar to that in many ferroelectric crystals. Therefore, it may be expected that the two steps which are involved in the switching process for ferroelectric crystals, nucleation of ferroelectric domains and growth of these domains, are also the elemental processes of polarization reversal in PZT ceramics.

(c) The activation field for domain wall motion clearly decreases with increasing hydrostatic pressure, similar to that in $BaTiO_3$ but of opposite sign to the effect in TGS. Probably a major reason for this difference is that in the perovskites the Curie point T_c decreases with pressure while in TGS it increases, thus the perovskite is pushed closer to T_c where α is reduced while TGS is moved away.

(d) The fine grain ceramics were made at lower sintering temperature and shorter soaking time than the coarse grain ceramics, so they should contain much more defects such as grain boundaries, pores, dislocations, etc. It may be predicted that the interaction between defects and domain walls will hinder the domain wall motion and hence increase the activation field of domain wall motion. The fact that the activation field α, at any hydrostatic pressure, is always larger in fine grain specimens than in coarse ones tends to confirm this deduction.

(e) The difference in the rate of change of α between fine and coarse-grained samples may, we believe, be traced to the effect of the morphotropic phase boundary which is close to the composition used. X-ray diffraction experiments show that in samples with the same nominal starting composition there is more tetragonal phase in the fine-grain ceramic, and more rhombohedral phase in the coarse-grained ceramic. Under hydrostatic pressure, the rhombohedral phase is stabilized at higher pressure so that it is natural to expect larger change with pressure in the fine-grained sample. Probably it is this phase conversion which gives rise to the nonlinear effect saturating at nearly the slope observed for α versus P in the coarse-grained ceramics.

(f) In these commercial type PZT samples with compositions close to the morphotropic boundary, four kinds of domain walls (71°, 109°, 180° in the rhombohedral and 180° and 90° in the tetragonal state) occur. The crystallite axes are random and phase switching under both field and pressure are possible. Clearly the overall phenomena are necessarily complex and a full quantitative explanation of the behavior cannot be expected.

ACKNOWLEDGEMENTS

We would like to thank Mr. Z. C. Zhuang and Professor D. N. Huang for helpful discussions. Financial support by the Office of Naval Research under Contract No. N00014-82-K-0339 is gratefully ackowledged.

REFERENCES

1. W. J. Merz, *Phys. Rev.* 77, 52 (1950).
2. J. Klimowski and J. Pietrzak, *Proc. Phys. Soc.* **75**, 456 (1960).
3. G. A. Samara, *Phys. Rev.* **151**, 378 (1966).
4. A. J. Bosman and E. E. Havinga, *Phys. Rev.* **129**, 1593 (1963).
5. E. Hegenbarth and C. Frenzel, *Cryogenics* **7**, 331 (1967).
6. S. S. Kahalkina and L. F. Vereshehagin, *Soviet Phys. Dokl.* **7**, 310 (1962).
7. G. A. Samara, *Bull. Am. Ceram. Soc.* **44**, 638 (1965).
8. F. Jona and G. Shirane, *Phys. Rev.* **117**, 139 (1960).
9. O. K. Gulish and I. N. Polandov, *Sov. Phys. Solid State* **20**, 2131 (1978).
10. E. Hegenbarth and S. Ullmer, *Cryogenics* **7**, 306 (1967).
11. G. A. Samara, *Phys. Lett.* **25A**, 664 (1967).
12. H. T. Martirena and J. C. Burfoot, *Ferroelectrics* **7**, 151 (1974).
13. H. T. Martirena and J. C. Burfoot, *J. Phys. C: Sol. State Phys.* 7, 3182 (1974).
14. G. W. Timco and H. H. Schloessin, *Ferroelectrics* **11**, 409 (1976).
15. M. Hayashi, *J. Phys. Soc. Japan* **8**, 348 (1970).
16. W. J. Merz, *Phys. Rev.* **95**, 690 (1954).
17. H. H. Wider, *Phys. Rev.* **99**, 1161 (1955).
18. E. Fatuzzo, *Phys. Rev.* **127**, 1999 (1962).
19. Y. Masuda, A. Baba, M. Jyumonji, and K. Kasai, *Japanese J. Appl. Phys.* **22**, Supplement 22-2, 118 (1983).

TEMPERATURE BEHAVIOR OF THE COMPLEX PIEZOELECTRIC d_{31} COEFFICIENT IN MODIFIED LEAD TITANATE CERAMICS

D. DAMJANOVIC, T.R. GURURAJA, S.J. JANG and L.E. CROSS
Materials Research Laboratory, The Pennsylvania State University, University Park, PA 16802, USA

Received 17 July 1986

Piezoelectric properties of modified lead titanate ceramics were investigated in an effort to explain the large electromechanical anisotropy observed in these materials. While the thickness coupling factor is approximately constant with temperature, the planar coupling factor becomes zero near room temperature, probably indicating a change in sign of the piezoelectric d_{31} coefficient. It is shown that for an accurate description of the electromechanical behavior of modified lead titanate ceramics, all material constants relevant for the planar coupling mode (s_{11}^E, s_{12}^E, d_{31}) must be taken as complex. Possible contributions to the complex d_{31} are discussed.

1. Introduction

Modified lead titanate ceramics have recently received a great deal of attention as promising materials for transducer arrays [1,2]. Unlike most piezoelectric ceramics, such as PZT, whose planar coupling factor (k_p) is in excess of 0.50, some of the modified lead titanates show vanishingly small planar coupling factor at room temperature [1–3]. However, the thickness coupling factor (k_t) for both types of materials is approximately 0.50. Among the compositions reported in the literature, the samarium- and calcium-modified lead titanates have exceptionally high electromechanical anisotropy, i.e. high k_t/k_p ratio. The properties of these ceramics have been measured at room temperature and their potential applications described, however, little was discussed about the possible mechanisms responsible for the observed electromechanical anisotropy [1,2]. The only data on temperature dependence of the electromechanical properties were reported by Xue et al. [3]. This paper is a report on the preliminary investigations of the temperature behavior of the complex piezoelectric properties of calcium- and samarium-modified lead titanate ceramics.

2. Materials preparation and measurements

Ceramics with compositions

$(Pb_{0.94}Sm_{0.15})(Ti_{1-x}Mn_{0.02})O_3$

and

$(Pb_{0.76}Ca_{0.24})[(Co_{1/2}W_{1/2})_{0.04}Ti_{0.96}]O_3$

were prepared by conventional processing using mixed oxide powders [2,3]. Sintered ceramics in the form of discs were poled up to 60 kV/cm at 150°C in silicon oil for 5 min. These poling conditions were necessary to obtain a saturation of the thickness coupling coefficient to about 0.45–0.50, the piezoelectric coefficient d_{31} to about 55–60 pC/N and the planar coupling coefficient k_p of less then 0.01 at room temperature for both compositions. Therefore, the k_t/k_p was close to 50 at room temperature. The planar coupling coefficient was calculated from the measured frequencies of the series (f_s) and the parallel (f_p) resonance of a thin disk using the equation derived by Mason [4]. The thickness coupling coefficient was calculated from the ratio of the overtone frequency f_2 to the fundamental frequency f_1 of the thickness mode series resonance, f_2/f_1, using table 2 in Onoe et al.'s paper [5]. All impedance measurements were performed using an HP 4192A LF impedance analyzer interfaced with a computer. The

0 167-577x/86/$ 03.50

piezoelectric d_{31} coefficient was measured with a Berlincourt piezo d_{31} meter.

3. Results and discussion

Figs. 1 and 2 show planar and thickness coupling factors as a function of temperature for Sm- and Ca-modified lead titanate ceramics. An interesting behavior was that the thickness coupling factor remains approximately constant with temperature, while the planar coupling factor goes through zero near room temperature. It then increases below and above this temperature reaching a maximum value of approximately 0.04 at the ends of the investigated temperature range. Similar behavior of k_t was reported earlier by Xue et al. [3] for Sm-doped lead titanate ceramics.

One could attempt to explain the observed disappearance of the resonance for the planar coupling mode by considering the temperature dependence of relevant material constants. The planar coupling factor is related to the transverse coupling factor k_{31}, which in turn is related to piezoelectric constant d_{31}, elastic compliance s_{11}^E and dielectric permittivity ε_{33}^T as given by the relation [6]:

$$k_p = k_{31}\left(\frac{2}{1-\sigma^E}\right)^{1/2} = \frac{d_{31}}{(s_{11}^E \varepsilon_{33}^T)^{1/2}}\left(\frac{2}{1-\sigma^E}\right)^{1/2}, \qquad (1)$$

where σ^E is the Poisson ratio. k_{31} and d_{31} could be calculated using a sample in the shape of a thin rectangular bar with the direction of polarization perpendicular to its length. The admittance of such a sample near the fundamental harmonic for the lengthwise vibration is given by [6]:

$$Y = \mathrm{i}\frac{\omega l w}{t}\left(\varepsilon_{33}^T - \frac{d_{31}^2}{s_{11}^E}\right) - \mathrm{i}\frac{2wd^2}{(\rho s_{11}^E)^{1/2}}\tan[\tfrac{1}{2}\omega l(\rho s_{11}^E)^{1/2}]. \qquad (2)$$

where the parameters have their usual meaning [6]. From eqs. (1) and (2) it is seen immediately that the disappearance of the resonance and the associated coupling factor k_p at a certain temperature is possibly due to a zero value of the piezoelectric constant d_{31}. Such a possibility could be realized by a change of the sign of d_{31} or by d_{31} going through zero as its extremum point. To measure the material coefficients in eqs. (1) and (2) as functions of temperature, an iterative method described by Smits [7] was used. This iterative method enables us to measure the values of the complex material constants s_{11}^E, ε_{33}^T and d_{31}, defined as $m = m' - \mathrm{i}m''$, by using eq. (2) and the values of the admittance $Y = G - \mathrm{i}B$ at three frequencies near the resonance.

A plot of susceptance B versus conductance G of the transverse mode resonance of a rectangular bar at a temperature close to where $k_p \approx 0$ is shown in fig. 3 for Sm-modified lead titanate. Experimental data are represented by full circles. Assuming all material coefficients to be complex, the theoretical fit to the experimental data, as in curve (a) in fig. 3, was obtained by Smits' iterative method. Curve (b) in

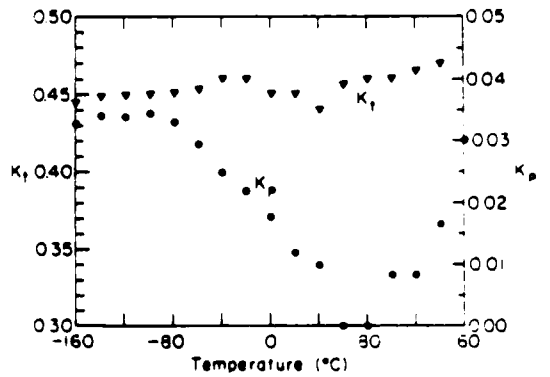

Fig. 1. Planar and thickness coupling factors for Sm-modified lead titanate as a function of temperature.

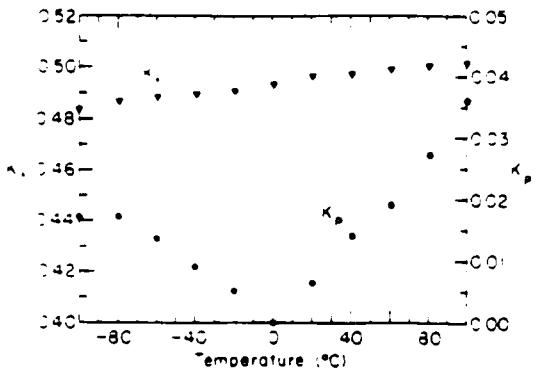

Fig. 2. Planar and thickness coupling factors for Ca-modified lead titanate as a function of temperature.

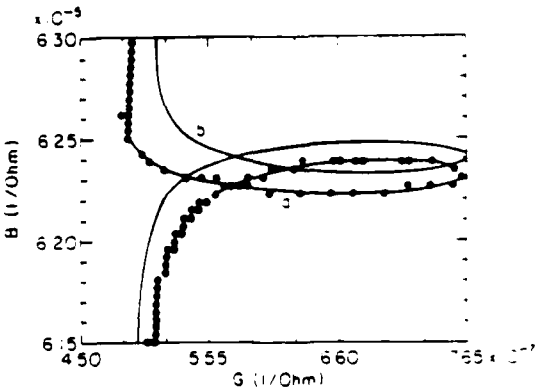

Fig. 3. Susceptance, B, versus conductance, G, loop for Sm-modified lead titanate at 90 °C. Dots represent experimental points. Curve (a) theoretical fit using Smits' method. Curve (b) theoretical fit assuming $d_{31}'' = 0$.

fig. 3 is obtained by taking the imaginary part of d_{31} equal to zero and using the real part for d_{31} and complex values for s_{11} and ε_{33} obtained by the iterative method. From fig. 3 it is clear that the imaginary part of the piezoelectric constant is necessary for a good fit to the data, especially at temperatures where k_p becomes very small. The analysis was performed to exemplify the effect of the imaginary part of d_{31} on the resonance spectrum. The iterative method allows us to calculate only the product $d_{31}'d_{31}''$ and the difference $(d_{31}')^2-(d_{31}'')^2$ from which we evaluate the real and imaginary components of d_{31}, without getting their signs independently. However, as is seen in fig.

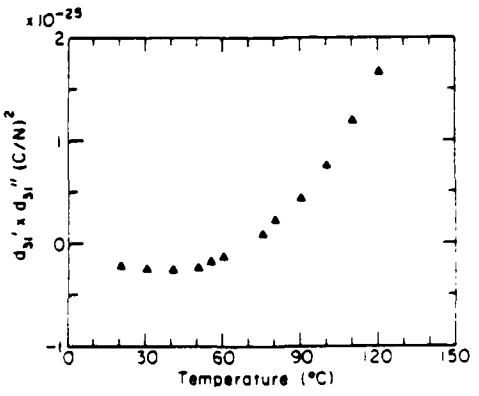

Fig. 4. $d_{31}'d_{31}''$ product obtained by the iterative method showing that either d_{31}' or d_{31}'' but not both, changes sign at the temperature of minimum k_p for Sm-modified lead titanate.

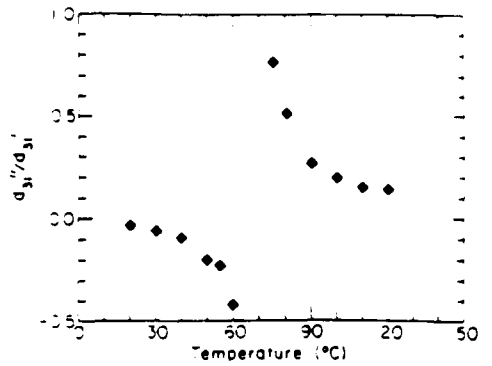

Fig. 5. d_{31}''/d_{31}' ratio for Sm-modified lead titanate as a function of temperature.

4, the product $d_{31}'d_{31}''$ changes its sign indicating that either real or imaginary part of d_{31} changed sign. Analysis of our data, as explained below, suggests that it is more likely to be the real component of d_{31}. Fig. 5 shows that the ratio $|d_{31}''/d_{31}'|$ increases rapidly as the temperature of zero k_p is approached. This means that d_{31}' approaches zero at least as fast as d_{31}'', i.e. if d_{31}'' assumes a value of zero and changes its sign, then d_{31}' should be zero too. However, according to eq. (2), if both real and imaginary components of d_{31} are equal to zero, a linear relationship in G versus frequency is expected. Fig. 6 shows plots of conductance G versus frequency in the temperature range from 60 to 80 °C, where k_p goes through zero. From fig. 6, it is clear that the signal at the resonance frequency never disappears completely. Moreover, the conductance versus frequency curve observed at 70 °C, where it was difficult to perform a fit due to scattering in data, implies that $d_{31}'' \neq 0$ and $d_{31}' \approx 0$. Therefore, it follows from the above considerations that the real component of d_{31} is the one that passes through zero and changes sign, somewhere between 65 and 75 °C, while the imaginary component d_{31}'' remains non-zero throughout the investigated temperature range.

Finally, fig. 7 shows the temperature dependence of d_{31}' and d_{31}'' with signs chosen according to analyses above. No anomalies were observed in the temperature behavior of complex ε_{33} and s_{11}, but their imaginary parts are necessary to obtain a good fit to the resonance data.

The probable change of the sign of d_{31} and the

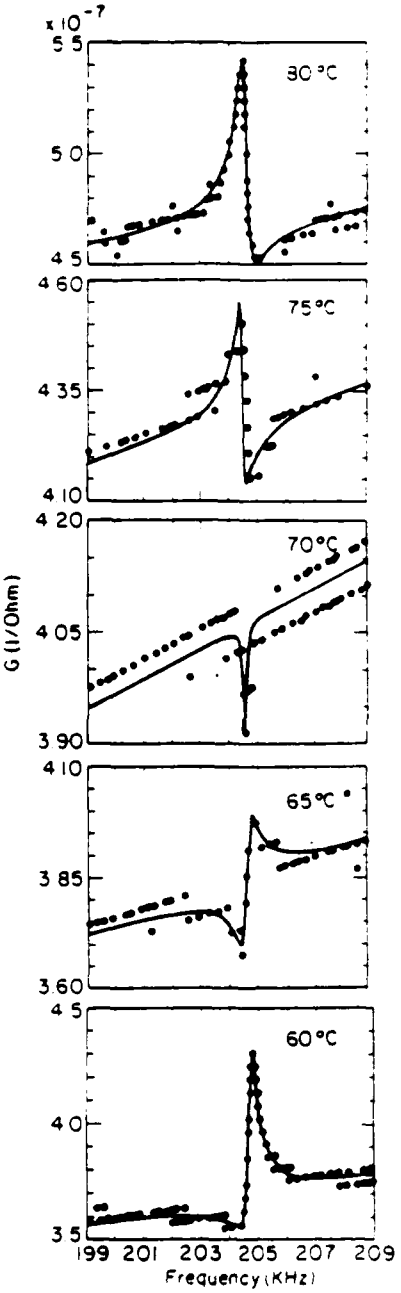

Fig. 6. Plots of conductance (G) versus frequency near the temperature where ε_{33} goes through minimum for Sm-modified lead titanate. Dots are experimental points and solid line is a fit to data. Scattering in the data is due to the resolution of the impedance analyzer.

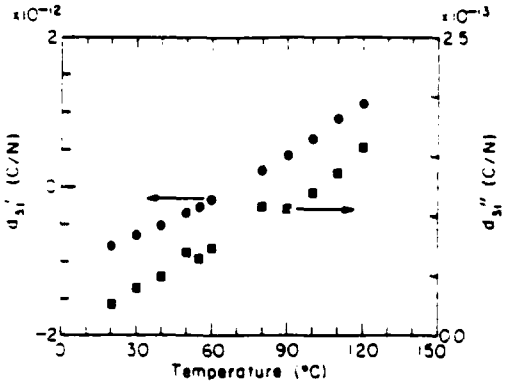

Fig. 7. Real and imaginary components of the piezoelectric d coefficient as a function of temperature for Sm-modified lead titanate.

simultaneous presence of the substantial imaginary component of the complex piezoelectric coefficient together with elastic and dielectric losses in these materials, suggest extrinsic contributions to the apparent d_{31} piezoelectric coefficient. Such contributions, if different in sign, could cancel each other giving zero d_{31} or change its sign with temperature. While the origins of the dielectric and elastic losses in the piezoelectric ceramics are well understood, more studies on possible mechanisms of the piezoelectric relaxation have been done only recently. It has been shown [8–15] that any defects in a piezoelectric material that are responsive both to the elastic and electric fields (such as certain point defects, 90° domains, second phase in the piezoelectric polymer materials, etc.) are a source of piezoelectric relaxation through the coupling of the elastic and dielectric losses. Consequently, it is possible to define the complex material coefficients m^* [8]:

$$s^*_{11} = s'_{11} - \Delta s_{11} - \mathrm{i}s''_{11},$$

$$\varepsilon^*_{33} = \varepsilon_{33} - \Delta\varepsilon_{33} - \mathrm{i}\varepsilon''_{33},$$

$$d^*_{31} = d_{31} - \Delta d'_{31} - \mathrm{i}d''_{31}, \qquad (3)$$

where m' represents the value of a coefficient at frequencies far above the relaxation frequency and $\Delta m - \mathrm{i}m''$ is the relaxational contribution of the defects. Using the requirement that the power dissipation in a passive material must be positive, Holland

[9] has shown that the imaginary parts of the diagonal elements of elastic compliance and dielectric permittivity matrices must be positive. There are no similar constraints on the sign of the imaginary part of the piezoelectric coefficients. However, certain relationships, such as $s_{ij}\varepsilon_{ij} \geq (d_{ij})^2$, must be satisfied. Therefore, an ideal (a loss free) dielectric or elastic material will also be ideal in its piezoelectric properties. Using symmetry arguments, Nowick and Heller [10] have derived certain selection rules showing that some but not all the piezoelectric coefficients can undergo the piezoelectric relaxation, depending both on the symmetry of defects and the symmetry of crystal. Furthermore, Arlt and Dederichs [11] have investigated the domain wall contribution to the d_{31} in ferroelectric ceramics assuming no other coupled elastic and electric mechanisms. For the perovskite-type ceramics, they have shown this contribution to d_{31} to be negative. In some cases the piezoelectric relaxation can be described by a simple Debye-type relaxation. Examples of this type of relaxation in a piezoelectric coefficient are found in $AgNa(NO_2)$ due to relaxational motion of NO_2 molecules [12], in the epoxy–PZT composite due to dc conductivity in the epoxy phase [13], in the ferroelectric ceramics due to 90° domain wall motion [11], etc. In the multiphase materials, such as polymers, the mechanisms of the piezoelectric relaxation are, in general, much more complex [12,14].

Considering the discussion above, it is clear that the existence of the imaginary component of the piezoelectric coefficient indicates the presence of extrinsic contributions to the piezoelectricity in these materials, regardless of the actual mechanisms involved. Knowing that in the perovskite ferroelectric ceramics the intrinsic d_{31} is considered to be negative, the hypothesis of a change of sign of d_{31} with temperature due to a positive contribution, is particularly attractive. A possibility of a change of sign of piezoelectric coefficient with temperature has been demonstrated in organic materials [15] and single crystals such as $AgNa(NO_2)$ [12]. However, it is unknown to us that such piezoelectric behavior has ever been observed in ceramics or oxide single crystals. To resolve this question in the case of the materials investigated in this study it would be sufficient to determine the sign of d_{31} directly, for example by strain versus electric field measurements, at two temperatures, above and below the temperature where resonance disappears. It should be mentioned here that Xue et al. attempted to measure a change of sign of d_{31} for Sm-modified lead titanate [3]. No change in sign was observed in the limited temperature range were k_p was small. This could be explained by the fact that the measurements were performed at about 10 Hz of the applied electric field, which was far below the frequency of planar mode resonance at approximately 100 kHz. As we have shown above, modified lead titanate ceramics investigated in this study have significant piezoelectric imaginary component indicating possible piezoelectric relaxation, in which case low-frequency properties could be very different from those at higher frequencies.

We point out that although our data strongly suggest that the apparent d_{31} measured at the resonance frequency changed its sign with temperature, it is necessary to perform additional experiments for a full interpretation of the observed phenomena. The mechanisms which lead to piezoelectric relaxation in ceramics are in general poorly understood. With more knowledge, it could be that alternative explanations will become possible.

In summary, the existence of significant piezoelectric imaginary component in modified lead titanate ceramics was shown, indicating extrinsic contributions to the piezoelectric d_{31} coefficient. Disappearance of the resonance for the planar coupling mode is attributed to a probable change in sign of the piezoelectric d_{31} coefficient.

Acknowledgement

This work was supported by the North American Philips Co. The authors are grateful to Dr. G. Arlt, Technische Hochschule Aachen, for his suggestions and discussions during his visit to MRL, Penn State University, in February 1986. The authors are also indebted to Dr. W.A. Smith and Dr. R.E. Newnham, for discussions and many useful ideas. The work by Mr. Paul Moses on computer interfacing is highly appreciated.

References

[1] H. Takeuchi, S. Jyomura, E. Yamamoto and Y. Ito, J. Acoust. Soc. Am. 72 (1982) 1114.
[2] Y. Yamashita, S. Yoshida and T. Takahashi, Japan. J. Appl. Phys. Suppl. 22-2 (1983) 40.
[3] W.R. Xue, J.N. Kim, S.J. Jang, L.E. Cross and R.E. Newnham, Japan. J. Appl. Phys. Suppl. 24-2 (1985) 718.
[4] W.P. Mason, Phys. Rev. 74 (1948) 1134.
[5] M. Onoe, H.F. Tiersten and A.H. Meitzler, J. Acoust. Soc. Am. 35 (1963) 36.
[6] D.A. Berlincourt, D.R. Curran and H. Jaffe, in: Physical acoustics, Vol. 1, Part A, ed. W.P. Mason (Academic Press, New York, 1964) pp. 225–240.
[7] J.G. Smits, IEEE Trans. Sonics Ultrasonics 23 (1976) 393.
[8] G. Arlt, Ferroelectrics 40 (1982) 149.
[9] R. Holland, IEEE Trans. Sonics Ultrasonics 14 (1967) 18.
[10] A.S. Nowick and W.R. Heller, Advan. Phys. 14 (1965) 101.
[11] G. Arlt and H. Dederichs, Ferroelectrics 29 (1980) 47.
[12] K. Hamano and T. Yamaguchi, Ferroelectrics 42 (1982) 23.
[13] T. Furukawa and E. Fukada, Japan. J. Appl. Phys. 16 (1977) 433.
[14] R. Hayakawa and Y. Wada, in: Advances in polymer science, Vol. 11 (Springer, Berlin, 1973) pp. 1–55.
[15] E. Fukada, Ferroelectrics 60 (1984) 285.

AD-A194 954 PIEZOELECTRIC AND ELECTROSTRICTIVE MATERIALS FOR TRANSDUCER APPLICATIONS(U) PENNSYLVANIA STATE UNIV UNIVERSITY PARK MATERIALS RESEARCH LAB

UNCLASSIFIED L E CROSS ET AL. JAN 88 N00014-82-K-0339 F/G 20/3 NL

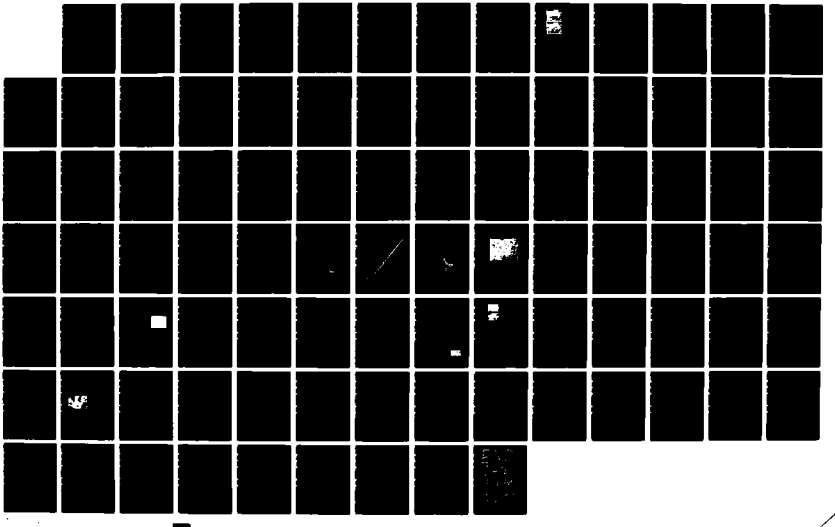

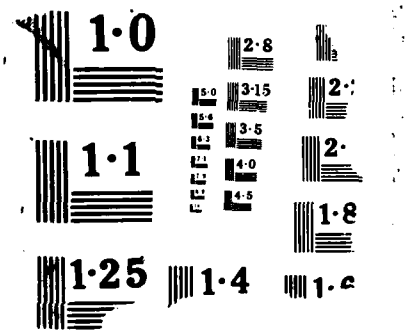
1·0
1·1
1·25
1·4
2·8
3·15
3·5
4·0
4·5
2·
1·8

ELECTROMECHANICAL ANISOTROPY IN MODIFIED LEAD TITANATE CERAMICS

D.Damjanovic, T.R.Gururaja, S.J.Jang and L.E.Cross

Materials Research Laboratory
The Pennsylvania State University
University Park, PA 16802

ABSTRACT

Lead titanate ceramics modified by Sm and Ca were investigated as materials with exceptionally large electromechanical coupling anisotropy. Both ceramic materials exhibited a minimum of the planar coupling coefficient at certain temperatures whereas the thickness coupling coefficient was essentially a constant over the investigated temperature range. The dielectric, piezoelectric and elastic constants related to the planar coupling mode were all considered to be complex in order to correctly describe the behavior of the ceramics near the resonance. The minimum of the planar coupling coefficient is attributed to a probable change in sign of the d_{31} piezoelectric coefficient with temperature.

1. INTRODUCTION

The conventional piezoelectric ceramics, such as PZT, with large electromechanical coupling coefficients are desired in many piezoelectric applications. In some cases, however, materials with more directional piezoelectric properties are preferred. In materials for ultrasonic transducer arrays, for example, it is essential to supress the coupling of the thickness to lateral modes, i.e. a small d_{31} and a large d_{33} are desired. Similarly, when a large hydrostatic piezoelectric coefficient, $d_h = d_{33} + 2d_{31}$, is required, it is again necessary to have a large piezoelectric anisotropy (large d_{33}/d_{31}) since the coefficients d_{33} and d_{31} are opposite in sign ($d_{33} > 0$, $d_{31} < 0$). Recently, lead titanate based ceramics have been reported with unusually large ratio of the thickness, k_T, to the planar, k_P, coupling coefficients, and consequently a large ratio d_{33}/d_{31} [1,2]. The measurements of the electromechanical properties of samarium modified lead titanate showed this ratio to be temperature dependent with k_P becoming zero at certain temperatures [3]. As a possible reason for the high anisotropy in piezoelectric coefficients, the crystal lattice anisotropy [1], and the 90° domain rotation [2] were suggested. No extensive studies on this subject, however, have been yet reported. It was the objective of this work to investigate the electromechanical properties of Ca and Sm modified $PbTiO_3$ ceramics and possibly understand the mechanisms responsible for the anisotropic behavior. It is hoped that a better understanding of the electromechanical anisotropy in the modified lead titanates would provide us with methods of developing other materials with similar properties.

2. MATERIAL PREPARATION AND MEASUREMENTS

Two compositions of the modified lead titanate ceramic were selected for this study, namely $(Pb_{0.85}Sm_{0.15})(Ti_{0.94}Mn_{0.02})O_3$ and $(Pb_{0.76}Ca_{0.24})[(Co_{1/2}W_{1/2})_{0.04}Ti_{0.96}]O_3$. Both compositions have a tetragonal symmetry with the lattice parameters a = 3.902 Å, c = 4.072 Å and a = 3.896 Å, c = 4.041 Å respectively. The ceramics were prepared by the conventional way from mixed oxide process. The samarium modified composition was calcined at 850 - 900 °C for 6 hours and then pressed disks were fired at 1230 °C for 3 hours. The calcium modified ceramics were calcined at 900 °C for 2 hours and sintered at 1130 °C for approximately 7 hours. The density of the fired ceramics was around 95 % of the theoretical. Electroded ceramics were poled with an electric field up to 60 kV/cm at 150 °C in silicon oil for 5 minutes. These poling conditions were necessary to obtain a saturation of the thickness coupling coefficient k_T to 45 - 50 %, the piezoelectric coefficient d_{33} to about 60 pC/N and the planar coupling coefficient k_P of less than 1 %. Thus, the ratio k_T/k_P was close to 50 at room temperature (Fig. 1). These poled ceramics in the form of disks or long thin bars were then used for measurements of dielectric, elastic and piezoelectric properties of the material. k_P was calculated from the measured frequencies of the series and parallel resonance frequency of a thin disk using the equation derived by Mason [4]. k_T was calculated from the ratio of the overtone frequency f_2 to the fundamental frequency f_1 of the thickness mode series resonance, f_2/f_1, using Table II in Onoe et al.'s paper [5]. The complex dielectric permittivity ε_{33}, the elastic compliance s_{11} and the piezoelectric coefficient d_{31} at the resonant frequency of the length extensional mode for a bar were calculated using Smits' method [6]. Vector impedance measurments for the above calculations were performed on an HP 4192A LF Impedance Analyzer interfaced with a computer.

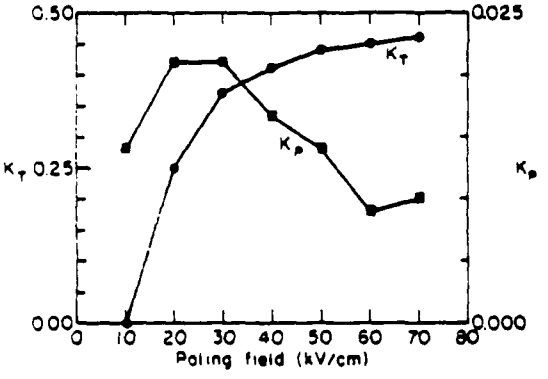

Fig. 1. Thickness, k_T, and planar, k_P, coupling coefficients as functions of poling field for Sm modified lead titanate.

CH2358 0 86 0000-0344 $1 0.0 ◯ 1986 IEEE

3. RESULTS AND DISCUSSION

The electromechanical coupling coefficients of the samarium and calcium modified lead titanates as a function of poling field exhibit an unusual behavior. The planar coupling factor increases initially and then decreases to a very small value with poling field above 50 kV/cm. However, the thickness coupling coefficient increases to approximately 50 % (Fig.1). As a possible explanation for the anisotropy, Yamashita et al. [2,7] suggested such behavior in calcium modified lead titanate to be caused by the reorentation of 90° domains. Indeed, they showed that a substantial increase in dimensions (up to 0.3 %) of ceramic samples occured as they were poled indicating 90° domain switching. The large stress that accompanies 90° domain switching was considered as a possible reason for the large anisotropy in coupling factors and the small value of the mechanical factor Q_m at poling fields at which k_p became vanishingly small. They also observed that specimens with lower resistivity showed a smaller planar coupling coefficient. Xue et al. showed, however, the k_p to be a strong function of temperature for samarium modified lead titanate [3], becoming zero only at certain temperatures

Fig. (2) and (3) show the thickness and planar coupling coefficients for materials investigated in this study as a function of temperature. Both materials exhibited a minimum in their planar coupling coefficient, reaching ~4 % at the ends of the investigated temperature range while their thickness coupling coefficients remained approximately constant over the investigated temperatures. Describing the conversion of electric into elastic energy, and vice versa, the electromechanical coupling coefficients are always defined as positive values. Piezoelectric coefficients in general , however, may be either positive or negative. From the definition of the planar coupling coefficient [8]:

$$k_p = \frac{d_{31}}{(s_{11}^E \varepsilon_{33}^T)^{1/2}} \left(\frac{2}{1-\sigma^E}\right)^{1/2} = k_{31}\left(\frac{2}{1-\sigma^E}\right)^{1/2} \quad (1)$$

(where σ is Poisson's ratio) it is, therefore, seen immediately that resonance can disappear if d_{31} becomes zero , either by changing its sign or by going through zero as an extremum point. For the measurement of material coefficients in Eq.(1) we have used the method described by Smits[6]. This method allows us to calculate the complex material coefficients s_{11}, d_{31}, ε_{33} (i.e. the real parts and their losses) at the resonant frequency of the length extensional coupling mode of a bar. The method consists of measuring the admittance $Y = G + jB$ at three frequencies near the resonance and calculating, in an iterative way, the material coefficients defined as $m = m' - jm''$, using the Equation (2) [8]:

$$Y = j\frac{\omega w l}{t}\left(\varepsilon_{33}^T - \frac{d_{31}^2}{s_{11}^E}\right) + j\frac{2wd_{31}^2}{(\rho s_{11}^E)^{1/2} s_{11}^E t}\tan\frac{\omega l}{2}(\rho s_{11}^E)^{1/2} \quad (2)$$

which describes the resonant behavior of a bar (The notations have their usual meanings). These experiments demonstrated that imaginary components of all three material coefficients are necessary for a good fit to the resonance data, especially at temperatures where planar coupling mode becomes small (Fig. 4.). Furthermore, our data show that even when the resonant signal of admittance Y seems to disappear completely, a weak signal in the conductance G was still observed [9]. Our analysis [9] led to the conclusion that the real part of d_{31} changed its sign near the

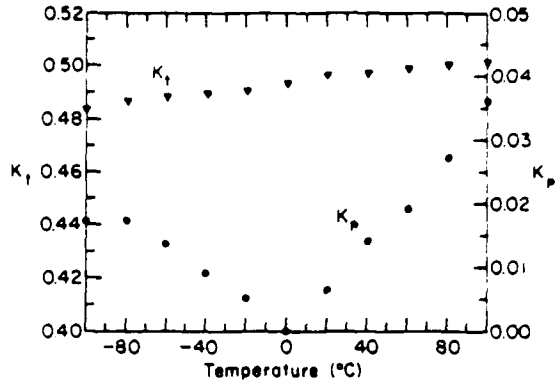

Fig. 2. Planar and thickness coupling coefficients as functions of temperature for Ca modified lead titanate.

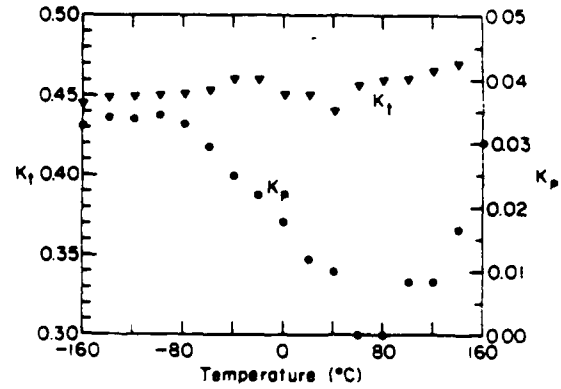

Fig. 3. Planar and thickness coupling coefficients as functions of temperature for Sm modified lead titanate.

temperature where k_p became small but its imaginary component remained nonzero (Fig. 5.). No anomalies were apparent in the behavior of the complex elastic and dielectric coefficients. However, their imaginary components are necessary for a good fit to the data. The mechanical quality Q_m was calculated as the ratio $s_{11}'/s_{11}'' \; (\approx f_m/2\Delta f)$ [6] of the real and imaginary parts of elastic compliance. Figure 6 shows that the mechanical quality of the samarium modified lead titanate ceramics remained high over the investigated temperatures suggesting that a small k_p is not necessarily accompanied by a decrease in the mechanical quality.

The presence of a significant imaginary component of the piezoelectric coefficient in these modified lead titanates suggests possible piezoelectric relaxation mechanisms which could lead to several contributions to the apparent d_{31}. Such contributions, if different in sign could cancel each other giving zero d_{31} or change its sign with temperature [9,10]. Our experience shows that the temperature where k_p goes through a minimum depends strongly on the poling conditions, the sintering schedule and other processing parameters. Not all of the samples showed the disappearance of the planar coupling mode at investigated temperatures (generally, -180 °C to +150 °C). All samples, however, showed a large

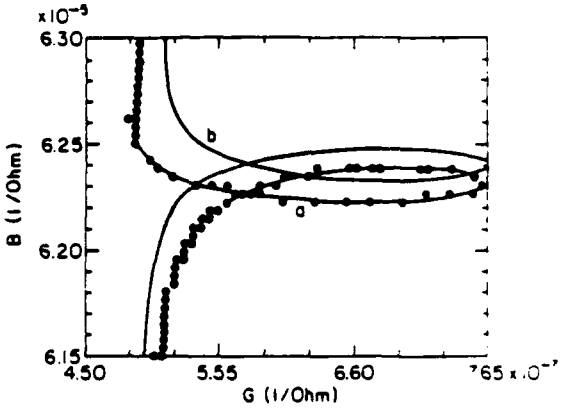

Fig. 4. Susceptance, B, vs. conductance, G, loop for Sm modified lead titanate, at 90 °C; dots represent experimental points.
a) Theoretical fit assuming a nonzero d_{31}" (Smit's method).
b) Theoretical fit assuming d_{31}"=0.

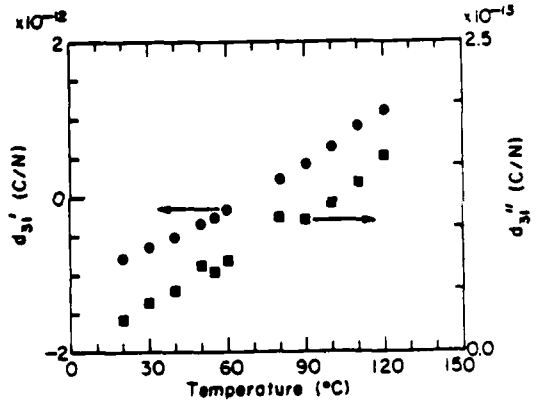

Fig. 5. Real, d_{31}', and imaginary, d_{31}", piezoelectric coefficients as functions of temperature for Sm modified lead titanate.

electromechanical anisotropy, i.e. a large k_T/k_P ratio. This suggests that there are probably two mechanisms responsible for the electromechanical anisotropy in these materials: one mechanism, possibly related to tetragonality, is responsible for the high piezoelectric anisotropy observed in these lead titanate based ceramics. The other mechanism, strongly dependent on processing conditions, seems to be responsible for the temperature dependence of k_P and the change of sign of d_{31}. This latter mechanism could be related to a piezoelectric relaxation through some kind of defects present in these ceramics [10].

It has been proposed that ceramics with high coercive fields, such as modified lead titanates, crack under high poling fields. Such cracks, if oriented parallel to the poling direction, could cause a large difference in the behavior of d_{31} and d_{33}. Measurements are being performed similar to those described above taking poling field as a parameter. Even at 10 kV/cm of applied field we have observed a minimum in the planar coupling coefficient and the disappearance of the resonance signal at low temperatures, appearing again as temperature was further decreased. Assuming that poling field of 10 kV/cm was not sufficient to produce microcracks in a sample, this

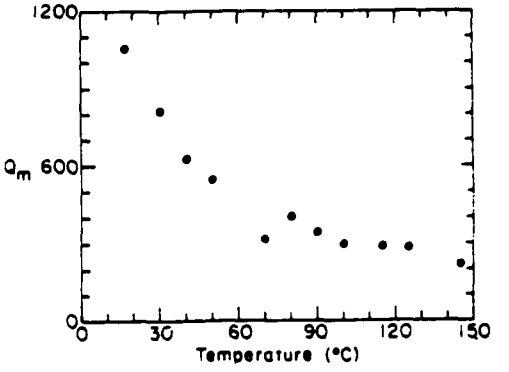

Fig. 6. Mechanical quality Q_m as a function of temperature for Sm modified lead titanate.

experiment shows that (although development of cracks with increased poling field is expected) the cracking of sample by applying poling field is not essential for the observed temperature behavior.

4. CONCLUSIONS

Similarities in the electromechanical coupling behavior between Ca and Sm modified lead titanate ceramics were demonstrated. The temperature behavior of the planar coupling mode is strongly dependent on poling and processing conditions. A zero planar coupling mode at certain temperatures is probably due to a change in the sign of the piezoelectric coefficient. A large electromechanical anisotropy was present in all the samples of the compositions used in this study, regardless of processing conditions. This indicates that more than one mechanism is responsible for the electromechanical coupling properties of these materials.

ACKNOWLEDGEMENTS

This work was supported by the North American Philips Co. The authors are grateful to Dr. G. Arlt, Technische Hochschule Aachen, for his suggestions and discussions during his visit to MRL, Penn State, in February 1986. The authors are also indebted to Dr. W.A. Smith and Dr. R.E. Newnham, for frequent discussions and many useful ideas. The work by Mr. Paul Moses on computer interfacing was highly appreciated.

REFERENCES:

[1] H. Takeuchi, S. Jyomura, E. Yamamoto and Y. Ito, J. Acoust. Soc. Am. 72 (1982) 1114.

[2] Y. Yamashita, S. Yoshida and T. Takahashi, Japan. J. Appl. Phys. 22 (1983) 40, Suppl.22-2.

[3] W.R . Xue, J.N. Kim, S.J. Jang, L.E. Cross and R.E. Newnham, Japan. J. Appl. Phys. 24 (1985) 718, Suppl. 24-2.

[4] W.P. Mason, Phys. Rev. 74 (1948) 1134.

[5] M. Onoe, H.F. Tierstein and A.H. Meitzler, J.Acoust. Soc. Am. 35 (1963) 36.

[6] J.G. Smits, IEEE Transactions SU 23 (1976) 393.

[7] Y. Yamashita, T. Takahashi and S. Yoshida, Ferroelectrics 54 (1984) 131.

[8] D.A. Berlincourt, D.R. Curran and H. Jaffe, in: Physical Acoustics vol. 1,part A, ed. W.P. Mason (Academic Press, New York, 1964) p.225-240.

[9] D. Damjanovic, T.R. Gururaja, S.J. Jang and L.E. Cross, to be published

[10] G. Arlt, Ferroelectrics 40 (1982) 149.

ELECTROMECHANICAL PROPERTIES OF CALCIUM MODIFIED LEAD TITANATE CERAMICS

K.Takeuchi*, D.Damjanovic, T.R.Gururaja, S.J.Jang and L.E.Cross

Materials Research Laboratory
The Pennsylvania State University
University Park, PA 16802

ABSTRACT

Some of the modified lead titanate ceramics exhibit large electromechanical anisotropy (i.e. large k_t/k_p). However, their piezoelectric constant d_{33} (≈60pC/N) is not large. The primary cause of the low d_{33} is due to the relatively low dielectric constant K (≈200) of these materials. In this paper the calcium modified lead titanate ceramics were investigated to increase their d_{33} by increasing K with ion modifications while retaining their large k_t/k_p by optimizing the processing conditions. A large d_{33} (≈92pC/N) with large K (≈456) and an infinite k_t/k_p were obtained in the composition $Pb_{0.66}Ca_{0.34}Ti_{0.94}(Co_{1/2}W_{1/2})_{0.06}O_3$ + 0.01 MnO sintered for 30 hrs and poled at 50kV/cm.

1. Introduction

Lead zirconate titanate $Pb(Zr,Ti)O_3$ solid solutions (PZT) are widely used for transducers because of their large piezoelectric constants. However, PZT ceramics have a complication in some applications such as underwater hydrophones and ultrasonic imaging transducers. PZT ceramics have a large planar coupling factor (k_p) in the lateral direction and a large thickness coupling factor (k_t) in the poling direction, so the ultrasonic waves from both effects interfere with each other.

Ceramics with large electromechanical anisotropy (i.e. large k_t/k_p) have large k_t and negligibly small k_p. They can transmit ultrasonic wave in the poling direction sharply with high efficiency without interference from lateral modes. Two compositions with large k_t/k_p have been intensively studied. They are calcium modified lead titanate $(Pb,Ca)(Ti,Co,W)O_3$ [1] and samarium modified lead titanate [2]. Although they have large k_t, their piezoelectric constant (d_{33}) in that direction is not large. In other words, they are efficient but not sensitive.

It was the objective of this study to find ceramics with large k_t/k_p and d_{33}. According to the literature [1], calcium modified lead titanate was likely to meet these requirements with some modifications. The piezoelectric constant d_{33} is related to the longitudinal coupling factor (k_{33}) by the equation $d_{33}^2 = \kappa_{33}^2 K \varepsilon_0 s_{33}^E$, where ε_0 is the permittivity of free space and s_{33}^E is the elastic compliance. Since $k_{33} \approx k_t$ applies in materials with low k_p, $k_{33}^2 = k_t^2 + k_p^2 - k_t^2 k_p^2$ [3]). It's apparent that the low d_{33} in the modified lead titanate ceramics is due to their relatively low dielectric constant K (≈200), providing s_{33}^E does not change drastically. The system with 24 mole % calcium has $k_t/k_p \approx 12$ and $d_{33} \approx 68$ pC/N [1]; however, d_{33} seems to be increased while retaining its large k_t/k_p by replacing lead by calcium up to 36 mole % because K increases more than twofold with minimal changes to the k_t and k_p. In addition to the ion modifications, the processing conditions (poling temperature and sintering time) were studied to optimize the properties. It was previously reported that k_p decreased with higher poling electric field in the calcium modified lead titanate [4] and with grain size, which generally increases with sintering, in neodymium modified lead titanate [5]. In this study, samples of $(Pb,Ca)(Ti,Co,W)O_3$ system with high calcium content were prepared and the influences of the ion modifications and processing conditions were investigated to maximize d_{33} and k_t/k_p.

2. Sample Preparation and Measurement

Samples were prepared from oxide powders by conventional sintering technique. Using formula $Pb_{1-X}Ca_XTi_{1-Y}(Co_{1/2}W_{1/2})_YO_3$ + 0.01 MnO (X=0.34-0.38, Y=0-0.06), the weight of materials PbO, CaO or $CaCO_3$, TiO_2, $Co(OH)_2$, WO_3, and MnO were calculated. One mole % of MnO was added to increase the resistivity of the samples [4]. Two mole % of PbO was added to compensate for the lead evaporation during sintering. The weighted raw materials were ballmilled for 24 hrs in a plastic bottle with zirconia balls and alcohol, dried, and calcined in an alumina crucible at 850°C for 2 hrs. The calcined lump was ground in a mortar, sieved, then mixed with several wt.% of deionized water. The wet calcined powder was pressed at 1×10^8 N/m² (≈1000 kg/cm²) in a cylindrical die (1.905 cm in diameter) into green disks. The green disks were sintered in a covered alumina crucible at an optimized sintering temperature of 1100 °C. Sintering was performed for 1, 5, and 30 hrs for each composition to see the influence of sintering time. To study the effect of ion modification, the sintering time which gave the largest K was selected for each composition. Sintered disks were lapped to 0.9-1.3 mm thick, polished, and gold-electroded on both faces by sputtering. The electroded disks were poled in an oil bath at elevated temperature with an electric field of 50 kV/cm for 5 minutes. The poling was performed at several temperatures to decide the optimum poling temperature.

Powder X-ray diffraction patterns were obtained on crushed and ground sintered disks using Cu-Kα radiation. The lattice constants a (a=b for tetragonal) and c were calculated from the diffraction peaks. Coupling factors were measured by resonance method using HP 4192A LF Impedance Analyzer. The planar coupling factor was calculated from the series and parallel resonance frequencies [6] of a thin disk using the equation derived by Mason [7]. The thickness coupling factor was calculated from the ratio of the overtone frequency to the fundamental frequency of the thickness mode series resonance using Table II in Onoe et al.'s paper [8]. The dielectric constant was calculated from the capacitance at 1 kHz and the dimension of the sample. The piezoelectric constant was measured at 100Hz by Berlincourt Piezo d_{33} Meter. The transition temperature (T_c) was given by the temperature at which K reached its maximum value.

* Nissan Motor Company, Tokyo, Japan

3. Experimental Results and Discussion

For the study of the calcium modification effects, Y was fixed at 0.04 and X was chosen at 0.34, 0.36, and 0.38 for each composition. Over 93% of theoretical density was obtained in each sample. The dielectric constant was over 411 and k_p remained low at 4.1% within X of below 0.36 as shown in Fig.1. Although k_t decreased slightly, it retained large k_t/k_p (=11-13). The piezoelectric constant of 96pC/N at X=0.34 and 105pC/N at X=0.36 were larger than previously reported data (d_{33}=68 pC/N) of the composition which had k_t/k_p=12 and K=200 [1]. However, the amount of calcium X=0.36 seemed to be the limit for the large k_t/k_p of this system with Y=0.04 because k_p jumped to 20% at X=0.38.

It should be noted that, although T_c did not change smoothly, Curie temperature (T_0) decreased smoothly between X=0.36 to X=0.38 as shown in Fig. 2. The decrease of T_c may indicate the decrease of atomic displacement and spontaneous polarization (P_s) in the crystal [9]. It can be understood that, although these compositions form similar cubic crystal structures at high temperature, there is a slight difference in the formation of the tetragonal crystal structure between the composition of X=0.36 and X=0.38, and this difference may be related to the electromechanical anisotropy. The decrease of k_t may be caused by the decrease of P_s which is the origin of the ferroelectric effects.

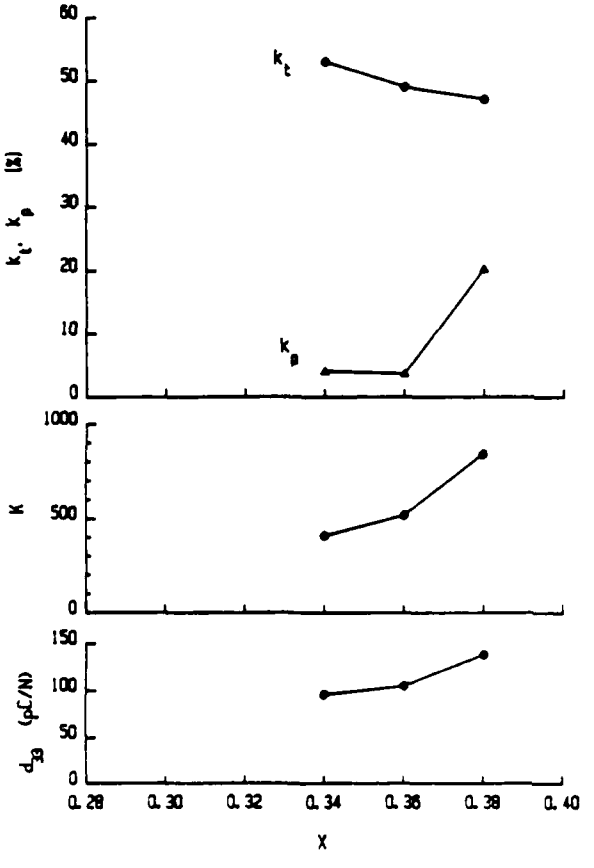

Fig. 1 Coupling factors, dielectric constant, and piezoelectric constant as a function of calcium amount X in $Pb_{1-X}Ca_XTi_{0.96}(Co_{1/2}W_{1/2})_{0.04}O_3$ + 0.01 MnO

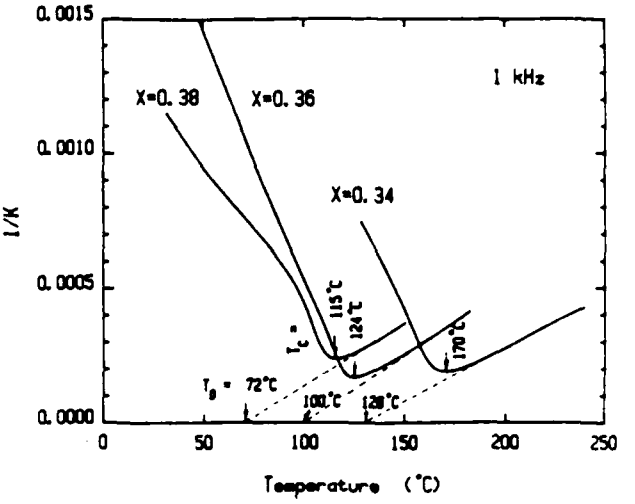

Fig. 2 Reciprocal of dielectric constant as a function of temperature in $Pb_{1-X}Ca_XTi_{0.96}(Co_{1/2}W_{1/2})_{0.04}O_3$ + 0.01 MnO

The axial ratio or tetragonality (c/a) decreased from 1.021 at X=0.34 to 1.012 at X=0.38. This tendency indicates that the relaxation of crystal distortion takes place with addition of calcium. The difference of c/a between 1.017 at X=0.36 and 1.012 at X=0.38 can be another possibility to make the difference in the electromechanical anisotropy. The tetragonality at X=0.38 is close to that, c/a=1.010 [10], of $BaTiO_3$ which does not have electromechanical anisotropy. The X-ray patterns of the compositions with X=0.36 and X=0.38 showed that there was no distinctive difference in symmetry except tetragonality between the two. $PbTiO_3$ has large c/a which resists 90° domain rotation when external electric field is applied and gives poor poling performance which results in small k_t and d_{33}. Addition of calcium in $PbTiO_3$ reduced c/a and resulted in large k_t, K, and d_{33}; however, it also reduced P_s and k_t as was discussed. This implies that it is difficult to expect further increase of d_{33} by addition of calcium.

For the study of the cobalt and tungsten modificaiton effects, X was fixed at 0.34 and Y was chosen at 0, 0.04, and 0.06 for each composition. It is seen in Fig.3 that both k_t and k_p increased, so the electromecchanical anisotropy did not change with Y. The increase of k_t seems to be caused by the reduction of c/a which decreased from 1.030 at Y=0 to 1.016 at Y=0.06 by the same reason as the effects of calcium. The large increase of d_{33} may be caused by the increase of both k_t and K. The slight decrease of k_t at Y=0.06 seems to be resulted from the decrease of P_s as was seen from the decrease of T_c which decreased from 225°C at Y=0 to 121°C at Y=0.06. The cobalt and tungsten gave almost the same effects as calcium to the properties of $PbTiO_3$.

For the study of the poling temperature effects, the poling electric field was fixed at 50kV/cm. The poling temperature is usually taken high enough, so that the domain rotation can easily take place. For some compositions, the k_p decreased with poling temperature. The composition with X=0.34 and Y=0.06 sintered 30 hrs had k_p=0.7% after poling at 80°C, but k_p became negligibly small or k_p=0% after poling at 100°C. The domain orientation appears to be related to the electromechanical anisotropy.

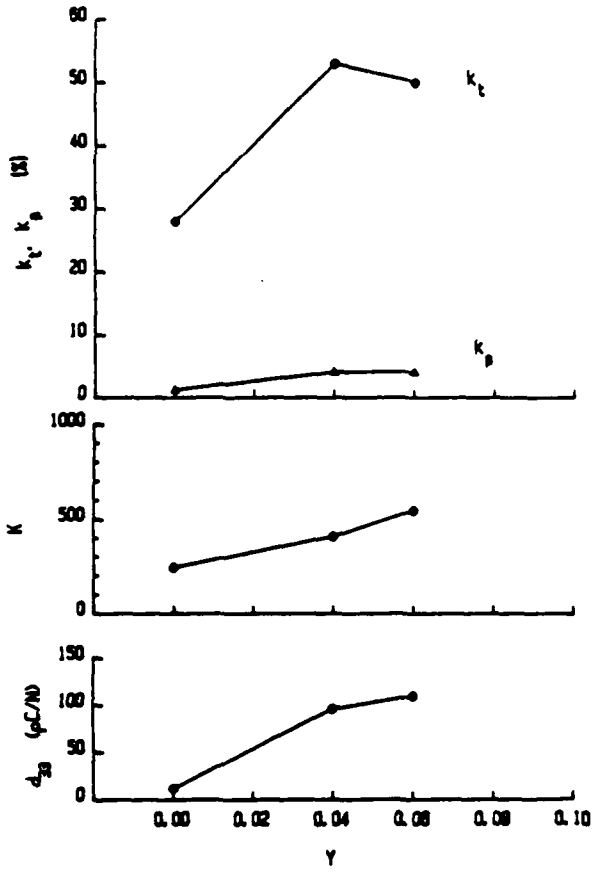

Fig. 3 Coupling factors, dielectric constant, and piezoelectric constant as a function of cobalt and tungsten amount Y in $Pb_{0.66}Ca_{0.34}Ti_{1-Y}(Co_{1/2}W_{1/2})_YO_3$ + 0.01 MnO

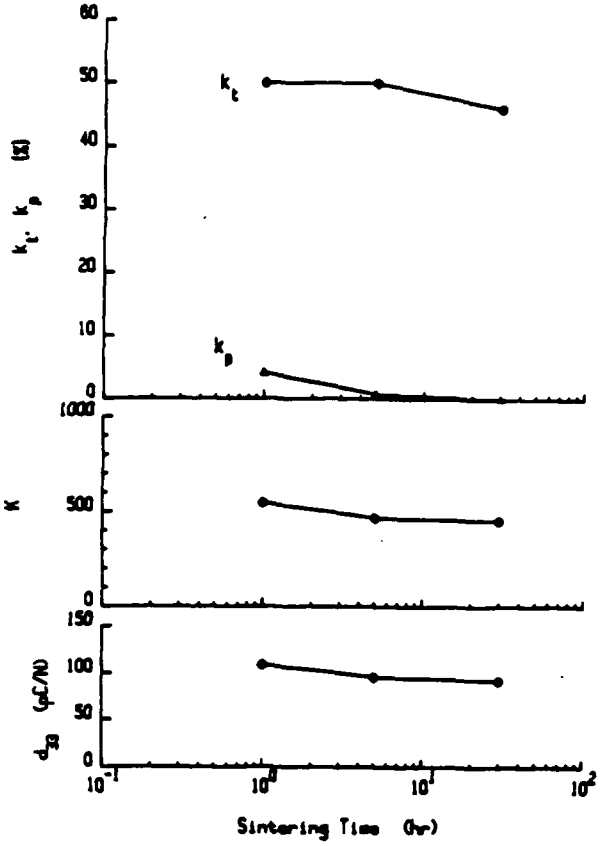

Fig. 4 Coupling factors, dielectric constant, and piezoelectric constant as a function of sintering time in $Pb_{0.66}Ca_{0.34}Ti_{0.94}(Co_{1/2}W_{1/2})_{0.06}O_3$ + 0.01 MnO

For the study of the sintering time effects, the samples with X=0.34 and Y=0.06 were sintered for 1 hr, 5 hrs, or 30 hrs. It is seen in Fig.4 that coupling factors (k_t and k_p), K, and d_{33} slightly decreased with sintering time. It is noted that k_p decreased to 0% with 30 hr sintering. The transition temperature and the lattice constants did not change with sintering. The scanning electron micrographs (x1000) in Fig. 5 show the sintered surfaces of the samples sintered for 1 hr or 30 hrs. Both samples have uniform grains, and the average grain size of 1 hr sintered sample is 3 μm and that of 30 hr sintered sample is 10 μm. The grain size appears to be related to the electromechanical anisotropy. This 30 hr sintered composition had larger d_{33} (=92pC/N) than previous composition which had d_{33}=62.8pC/N and infinite k_t/k_p ratio [4].

Table 1 shows two compositions which have an infinite electromechanical anisotropy in (Pb,Ca)(Ti,Co,W)O_3 system. The piezoelectric constant is increased about 50% with higher ion modifications in this work. It is interesting to note that the different compositions with different crystal shape, tetragonality (c/a) and atomic displacement (from T_c), have same infinite electromechanical anisotropy.

Table 1 Properties of $Pb_{1-X}Ca_XTi_{1-Y}(Co_{1/2}W_{1/2})_YO_3$ + 0.01 MnO (+ additive) system with k_p=0

	X=0.24, Y=0.04 (+ 0.02 MnO)	X=0.34, Y=0.06 (+ 0.01 MnO)
k_t (%)	53	46
k_p (%)	0	0
K	200	456
D (%)	2.2	1.6
d_{33} (pC/N)	62.8	92
T_c (°C)	260	123
c/a	1.040	1.017
ρ (g/cm^3)	7.00	6.42
grain (μm)	8.0	10
Reference	[4]	this work

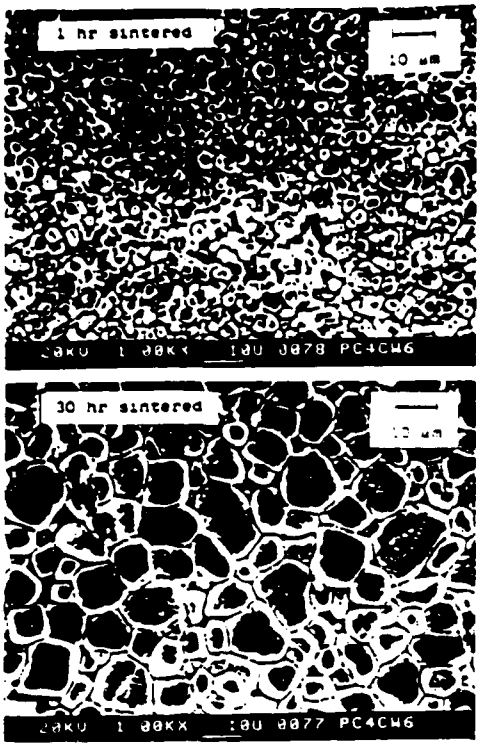

Fig. 5 Scanning electron micrographs (x1000) on the sintered surface of $Pb_{0.66}Ca_{0.34}Ti_{0.94}(Co_{1/2}W_{1/2})_{0.06}O_3$ + 0.01 MnO

4. Conclusions

(1) The piezoelectirc constant of lead titanate ceramics was raised by ion modifications while retaining the large electromechanical anisotropy. The increased piezoelectric constant comes from the increased dielectric constant due to the reduced tetragonality. The tetragonality and the atomic displacement appear to be related to the electromechanical anisotropy.

(2) The electromechanical anisotropy was increased by the processing conditions. The domain orientation and the grain size appear to be related to the electromechanical anisotropy.

(3) The piezoelectric constant and the electromechanical anisotropy were maximized by ion modifications, poling temperature, and sintering time. A maximum d_{33} (=109pC/N) and an acceptably large k_t/k_p (=12) were obtained in the composition $Pb_{0.66}Ca_{0.34}Ti_{0.94}(Co_{1/2}W_{1/2})_{0.06}O_3$ + 0.01 MnO with 1 hr sintering. A large d_{33} (=92 pC/N) and an infinite k_t/k_p were obtained in the same composition with 30 hr sintering.

ACKNOWLEDGEMENTS

We would like to thank Mr. F.J. Opalko for his suggestions and to the staff of the Materials Research Laboratory for their help in the experiments. The financial support of this research was provided by North American Philips Corporation.

BIBLIOGRAPHY

[1] Y.Yamashita, K.Yokoyama, H.Honda, and T.Takahashi, Japan. J. Appl. Phys., vol. 20, Suppl. 20-4, pp. 183-187, 1981.

[2] H.Takeuchi, S.Jyomura, E.Yamamoto, and Y.Ito, J. Acoust. Soc. Am., vol. 72, pp. 1114-1120, 1982.

[3] B.Jaffe, W.R.Cook, and H.Jaffe, "Piezoelectric Ceramics," Academic Press, London and New York, 1971, p. 29.

[4] Y.Yamashita, S.Yoshida, and T.Takahashi, Japan. J. Appl. Phys., vol. 22, Suppl. 22-2, pp. 40-42, 1983.

[5] S.Jyomura, K.Nagatsuma, and H.Takeuchi, J. Appl. Phys., vol. 52, pp. 4472-4478, 1981.

[6] "IRE Standards on Piezoelectric Crystals," Proc. IRE, vol. 49, pp. 1161-1169, 1961.

[7] W.P.Mason, Phys. Rev., vol. 74, pp. 1134-1147, 1948.

[8] M.Onoe, H.F.Tiersten, and A.H.Meitzeler, J. Acoust. Soc. Am., vol. 35, pp. 36-42, 1963.

[9] S.C.Abrahams, S.K.Kurtz, and P.B.Jamieson, Phys. Rev., vol. 172, pp. 551-553, 1968.

[10] H.D.Megaw, Proc. Phys. Soc., vol. 58, pp. 133-152, 1946.

ANTIFERROELECTRIC TO FERROELECTRIC SWITCHING IN LEAD ZIRCONATE TITANATE STANNATE CERAMICS

W Pan and L. E. Cross

Materials Research Laboratory
The Pennsylvania State University
University Park, PA 16802

Abstract

Electric field induced switching from antiferroelectric to ferroelectric states in several ceramics compositions in the modified Lead Zirconate Titanate Stannate family was investigated at room temperature. The Maximum volume expansion observed was .26%. The degradation effects (under repeated electric switching) saturate and can be kept to less than 20% in the volume switching for properly prepared samples. The switching can be completed within 40 microseconds just above the transition field and becomes very fast as the electric field increases. Hydrostatic pressure increases the transition field but the reduction of the induced ferroelectric polarization remains small until the transiuon field approaches the applied driving field.

Introduction

Ceramics in the Lead Zirconate Titanate Stannate family have been studied extensively in the past 20 years for many actual and potential applications in energy conversion.[1,2] More recently[3,4], interest has begun to focus upon the electrostriction phenomenon in antiferroelectrics and the possible use of the antiferroelectric to ferroelectric switching in transduction. However, the speeds of the switching reported in the past were quite slow and quite different[4,5] probably due to the limitation in power of the pulse generator used. It is the purpose of this paper to report the volume expansions and the switching speeds measured by more reliable methods Furthermore, to model the real situation in application, the switching behaviours as a function of repeated switching (degrdation effects) and hydrostatic pressure are also reported to verify the real applicability of this family of ceramics compositions for electrostriction applications.

Sample Preparation and Measurements

The compositions chosen for study were:

(1) $Pb_{.99}(Zr_{.57}Ti_{.05}Sn_{.38})Nb_{.02}O_3$

(2) $Pb_{.92}Sr_{.05}La_{.02}(Zr_{.54}Ti_{.16}Sn_{.30})O_3$

(3) $Pb_{.92}Mg_{.05}La_{.02}(Zr_{.59}Ti_{.11}Sn_{.30})O_3$

(4) $Pb_{.97}La_{.02}(Zr_{.66}Ti_{.09}Sn_{.25})O_3$

(5) $Pb_{.97}La_{.02}(Zr_{.53}Ti_{.12}Sn_{.35})O_3$

The differnt compositions were made up from reagent grade mixed oxides. Calcing temperatures were in the range 750 to 900^{0}C. The disks were cold pressed using a small amount of PVA binder and fired at 1350^{0}C in PbO atomsphere provided by excess $PbZrO_3$ in closed containers.

Polarization field relations were measured using a balanced Sawyer and Tower network. A bonded strain guage

techniqe was used for both longitudinal and transverse strain measurements. Hydrostatic pressure was generated in an air-driven intensified pump. Plexol was used as the pressure medium. For kinetics study, the pulses generated by a pulse generator (Hewlett Packard type 214) were amplified by a high power (9kw) pulse amplifier (Cober Model 604 A) which can supply maximum current of 6 amperes if the pulse width is less than 2 miliseconds and the pulse amplitude is less than 1500 volts.

Experiment Results

Composition 1,4 and 5 exhibied clear polarization switchings but 2 and 3 did not under field levels up to 50 kv/cm. The volume expansions for composition 1 and 5 are .16% and .26% respectivly which are in good agreement with the values reported by Uchino and Berlincourt[4,5] for this family of compounds. Fig.1 shows the longitudinal and transverse strains vs electric field for composition 5. Fig.2 shows the polarization hysteresis loops under low frequency(.1Hz) AC field for different hydrostatic pressures. It is evident that the transition field increases with increasing hydrostatic pressure but the reduction of the ferroelectic polarization with increasing hydrostatic pressure is not obvious until the transition field approaches the applied field as shown in Fig.3. The switching currents and speeds for different electric fields are shown in Fig.4 and Fig 5. The increasing speed with increasing electric field is evident. The switching current and speeds as a function of hydrostatic pressure under constant electric field are shown in Fig.6 and Fig.7. The effects of hydrostatic pressure are just opposite to the overvoltage effects. Fig.8 shows the degradation of the induced strain and polarization as a function of number of switching cycles. A saturation of degradation is indeed observed. More than 80% of the initial strain is still observed after 4,320,000 switchings for some of the best samples. The ratio of strain to the square of polarization remains constant which suggests that the electrostrictive constant is free from degradation.

Discusion

The electric field induced volume expansion measured in this study confirmed the earlier results measured by Uchino and Berlincourt[4,5] for this family of antiferroelectric compounds. Although the longitudinal and transverse strain are not much greater than that of .9PMN:.1PT electrostrictive ceramics, the transverse strain is positive which offers greater advantage over .9 PMN:.1PT ceramics for hydraulic amplification application. It is observed that the switching can be completed within 2 microseconds by an easily achievable electric field. Such a speed is the typical order of magnitude of switching in ferroelectrics. Because the hydrostatic pressure increases the transition field and elongates the switching time. Extra electric field is necessary for high stress application.

Acknowledgment

We wish to thank Q. Jiang, Q. Li, E. Furman and P. Moses for their helps. Support for this work is acknowledged from Air Products and Chemicals on contract 063-166-P-A.

References

[1] B. Jaffe, W. R. Cooke, Jr. and H. Jaffe, Piezoelectric Ceramics, Acadamic Press, 1971

[2] D. Berlincourt, H. H. Krueger, B. Jaffe, "Stability of phases in modified lead zirconate with variation in pressure, electric field, temperature and composition." Phy. Chem. Solids. 25 pp. 659-674, 1964

[3] K. Uchino, L. E. Cross, R. E. Newnham, "Electrostrictive effects in paraelectric-ferroelectric-antiferroelectric phase transition". Japan. Journal of Applied Physics 19 pp. L425 -L428, 1980

[4] K. Uchino, S. Nomura, "Electrostriction in PZT family antiferroelectrics". Ferroelectrics 50 pp. 517-520, 1983

[5] D. Berlincourt, "Transducers using forced transitions between ferroelectric and antiferroelectric states." IEEE Transactions on Sonics and Ultransonic. Vol. SU-13 No.4 Oct. pp. 116-125, 1966

Figures

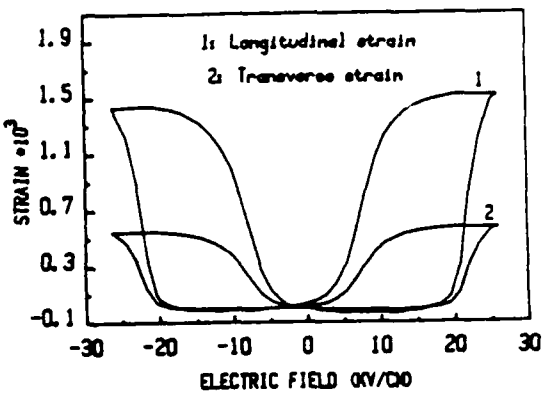

FIG. 1 Longitudinal and transverse strain vs. electric field for composition 5

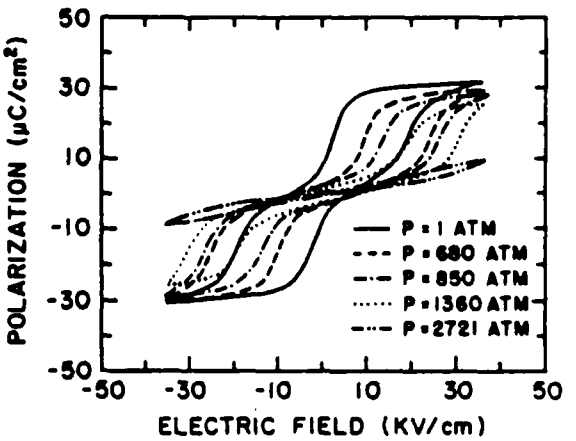

FIG. 2 P-E Hysteresis loops under different hydrostatic pressures for composition 5

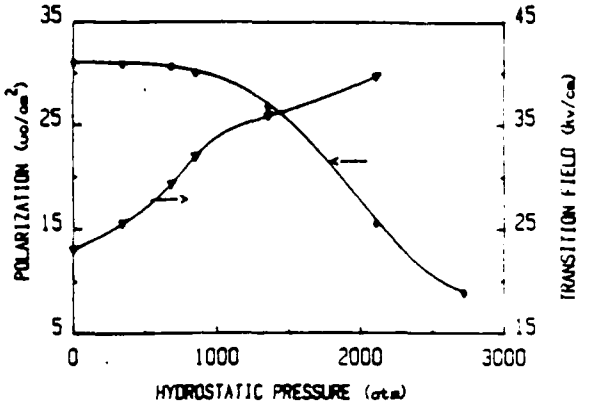

FIG. 3 Field (33kv/cm) induced polarization and transition fields as a function of hydrostatic pressure for composition 5

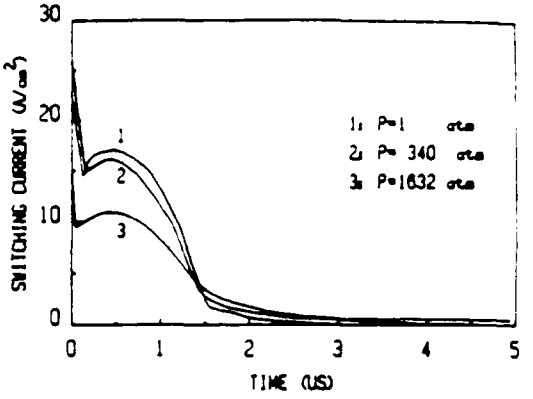

FIG. 6 Switching currents under different hydrostatic pressure for composition 5

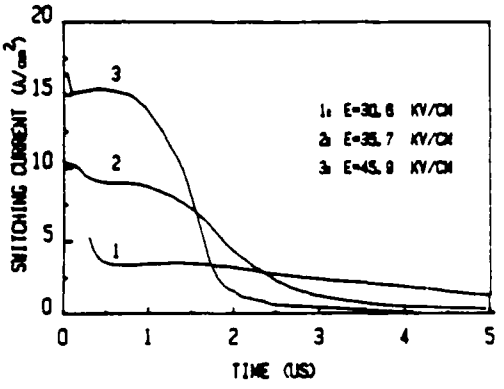

FIG. 4 Switching currents under different electric fields for composition 5

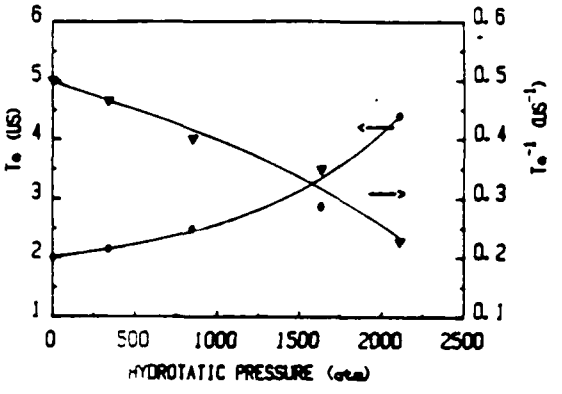

FIG. 7 Times and reciprocal times for the transitions vs. hydrostatic pressure for composition 5 (Electric field of the pulses 51 kv/cm)

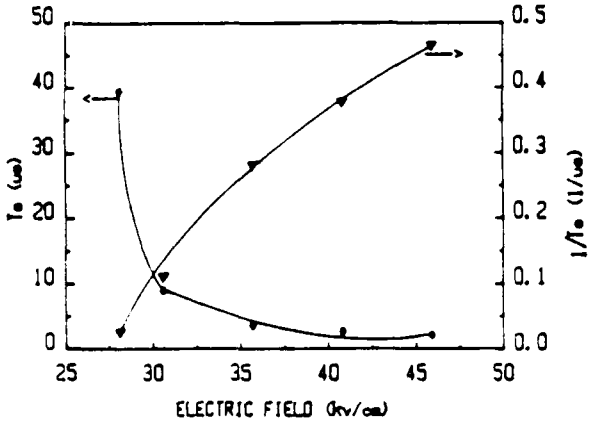

FIG. 5 Times and reciprocal times for the transitions as a function of electric field for composition 5

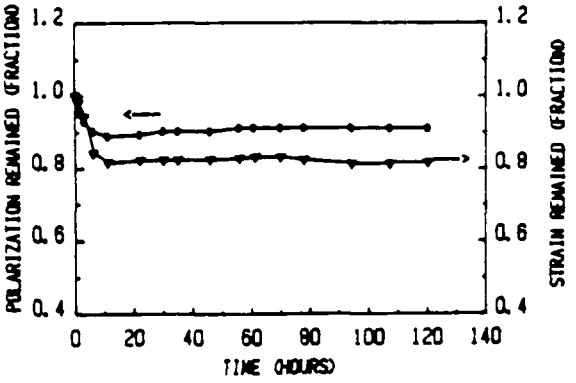

FIG. 8 Polarization and strain vs. electric field (10HZ) driving time for composition 5

ASSOCIATED PROGRAMS

A REVIEW OF THE FABRICATION OF LEAD-BASED FERROELECTRIC RELAXORS FOR CAPACITORS

Thomas R. Shrout and Arvind Halliyal

Materials Research Laboratory
The Pennsylvania State University
University Park, PA 16802

ABSTRACT

Compositions in the perovskite family, having the general formula $Pb(B_1,B_2)O_3$, known as relaxor ferroelectrics are of considerable interest. Their high dielectric constants, broad maximas and relatively low firing temperatures have made them promising candidate materials for multilayer ceramic capacitors. However, such materials have always been extremely difficult to reproducibly fabricate without the appearance of a pyrochlore phase which can be detrimental to the dielectric properties. A review of recent work on both the kinetics and thermodynamics of the perovskite structure in relation to pyrochlore is discussed. It is believed such an understanding will enable the implementation of relaxor dielectrics into the present day multilayer capacitor industry.

I. INTRODUCTION

The multilayer ceramic capacitor industry is growing rapidly as the result of the continuing miniaturization of integrated electronic circuits. The driving force behind the capacitor industries growth are the obvious advantages of multilayer ceramic capacitors as compared to aluminum and tantalum electrolytic capacitors, including compact design, high reliability, relatively large capacitance, and low cost. For the past forty years, the primary materials utilized for multilayer ceramic capacitors have been modified $BaTiO_3$ and other various titanates[1]. Such materials generally require high firing temperatures (>1300°C) making it necessary to use expensive internal electrodes, such as Pd. Great strives in the capacitor industry have been made to continuously reduce the materials cost of the multilayers, paying particular attention to reducing the cost of internal electrodes[2], by (1) the addition of fluxes to reduce the sintering temperature thus allowing the use of less expensive Ag:Pd alloys, (2) the use of non-noble metals such as Ni and Cu requiring a reducing atmosphere[3,4] during firing, (3) the lead injection process in which molten lead is impregnated into porous layers to act as the electrodes[5,6].

By these efforts a significant reduction in the cost of ceramic multilayer capacitors has been achieved but there still remains the limitation of capacitance volumetric efficiency. The capacitance volume efficiency or packing density is approximately proportional to the dielectric constant (k) and inversely proportional to the square of the thickness (t) of the active dielectric. Thus to further improve the "compactness" of multilayers capacitors, there are obviously two alternatives: (1) Reduce the thickness of the active dielectric and/or (2) utilize a ceramic material with a high dielectric constant. Presently, multilayers have active dielectric layers with a thickness typically in the range of 20 to 35 μm which appears to be the

lower limit for present day wet lay down and other tape casting techniques. Such lower limits are not necessarily due to limitations of the fabrication processes, but are due to other stringent capacitor requirements set by the E.I.A. (Electronics Industry Association) such as dielectric breakdown strength, capacitance/bias percent change, etc.

In the fabrication of multilayer capacitors there are certain limitations in the dielectric thickness and with the upper limit of the dielectric constant (k), for modified $BaTiO_3$ around 10,000, much of the recent research work is focused on other families of dielectric materials having unusually high dielectric constant. The perovskite ferroelectric relaxors is one such family. Of particular interest for capacitors are the lead (PbO) based relaxors having the general formula $Pb(B_1,B_2)O_3$, where B_1 is typically a low valence cation, e.g. Mg^{+2}, Zn^{+2}, Fe^{+3}, Ni^{+2}, Sc^{+3}, and B_2 a high valence cation, e.g. Ti^{+4}, Nb^{+5}, Ta^{+5}, W^{+6}. For simplicity, the term relaxor here will refer only to complex lead-based perovskites. The earliest and best known lead-based relaxor $Pb(Mg_{1/3}Nb_{2/3})O_3$ (hereafter designated PMN) was first synthesized in the late 1950's by Smolenski and co-workers[7]. Studies of the dielectric properties of PMN, as well as many other relaxors, have shown that such compounds exhibit a broad maximum in the dielectric constant or a diffuse phase transition (see Figure 1). The origin of such diffuse phase transition is believed to be a distribution of Curie points in the material due to compositional fluctuation, or micro-inhomogeneity (disorder) in the B-site cations.

As shown in Figure 1, the dielectric maxima of a relaxor ferroelectric is broad in comparison with a normal or ordered relaxor ferroelectric material. The temperature of the dielectric maximum for relaxors increases with increasing frequency, thus no one Curie temperature can be given for

ferroelectric relaxors without reference to the appropriate test frequency. Another characteristic of relaxors is the frequency dispersion in the dielectric loss, which occrs at a slightly lower temperature than the dielectric maxima, and is also larger than that of the ordered dielectric below T_c. It has been reported that the degree of ordering can be varied in certain relaxor materials such as $Pb(Sc_{1/2}Ta_{1/2})O_3$ (PST) and $Pb(Sc_{1/2}Nb_{1/2})O_3$ (PSN) by thermal annealing[8-10], but for most of the ferroelectric relaxors ordering can be varied only compositionally[11-13]. Since the perovskite structure is very forgiving compositionally, varying degrees of ordering of ions in the B site can be obtained by forming solid solutions with relaxor end members that exhibit normal dielectric behavior such as $Pb(Fe_{1/2}Nb_{1/2}O_3)$ (PFN) or with end members such as $PbZrO_3$ (PZ), $PbTiO_3$ (PT), etc. In Figure 2 is shown a typical plot of Curie temperature, T_c, as a function of frequency for a solid solution between a disordered end member ($Pb(Ni_{1/3}Nb_{2/3})O_3$ (PNN)) and the end member (PFN), which is actually compositionally disordered but shows nearly normal dielectric behavior in the frequency range of interest. As is apparent from the figure, the expected linearity in T_c was not observed, as a result of the strong frequency dispersion observed in the low temperature disordered end member.

The properties of relaxor dielectrics such as high dielectric constants (up to 30,000), broad dielectric maxima and relatively low firing temperatures, which allows the use of low cost Ag:Pd electrodes, have made them promising candidate materials for capacitor. Presented in Table 1 are many recent relaxor compositions reported from patents and publications proposed for utilization in capacitors. Some commercially available relaxor based compositions and actual multilayer capacitors comprising of various relaxor dielectric materials are also presented. The commercially available dielectrics and capacitors in general are based on the appropriate patent(s).

Most of the compositions listed in Table 1 are simply solid solutions of known end members, with one end member being a T_c shifter which adjusts the dielectric maximum closer to room temperature to meet appropriate EIA standard specifications e.g. Z5U, Y5V, Y5S, etc. Many of the compositions reported in the various publications are very similar and differ only in the amount of additives, such as MnO_2, SiO_2, Li_2O etc., which are added to improve the electrical resistivity, reduce the firing temperature, or to reduce the temperature coefficient of capacitance.

Interestingly, the vast amount of research on relaxor dielectrics for capacitors has occurred only in recent years. The question arises, what has delayed the commercial utilization of relaxors in the capacitor industry until now? Relaxor ferroelectrics offer several obvious advantages, but there are several disadvantages in using relaxors for capacitors when compared to $BaTiO_3$ based materials.

Some disadvantages of relaxors for use in multilayer capacitors are:

1) Strong dependence of dielectric properties on frequency.

2) High dielectric loss - (ferroelectric region)

3) PbO is a major constituent - (volatile, toxic)

4) Mechanically weak.

The most significant disadvantage, however, is the fact that many perovskite relaxors are extremely difficult to reproducibly fabricate/process without the appearance of a stable pyrochlore phase, which often leads to poor dielectric properties. In this paper a review of the recent work done to prepare reliable and useful ferroelectric relaxors for capacitors is presented. An analysis of the stability of the perovskite structure and the conditions under which pyrochlore phase(s) form is presented.

II. PROCESSING OF RELAXOR DIELECTRICS

As discussed in the previous section, much of the delay in the practical development of relaxors for capacitors is due to the difficulty in preparing single phase complex $Pb(B_1B_2)O_3$ perovskite ceramics. If the ceramic preparation is done by following conventional mixed oxide process, formation of stable lead-based pyrochlore type phase(s) typically occurs. The pyrochlore phase(s) severely degrade the dielectric properties and are the primary cause for the variation in dielectric properties for a given relaxor composition reported in the literature.

Previous studies have shown that in order to understand the causes for the formation of pyrochlore phase, we should consider both the thermodynamics and reaction kinetics of the perovskite relaxor systems. A description of the reaction kinetics and the stability of the perovskite phase considering thermodynamics is presented in the following sections.

III. KINETICS

To date there have been only a few studies regarding formation mechanism and reaction kinetics of relaxor compounds with much of the work being done on the relaxor PMN. The large dielectric constant and broad transition temperature of PMN near room temperature makes it one of the more attractive materials for capacitors and has been widely investigated. The kinetics of the formation process of PMN are presented in this section. It is believed that the reaction kinetics in PMN are representative of many other niobate relaxors as well as their tantalate analogues.

From earlier work it is clear that the formation of perovskite PMN is directly related to the reactivity of the refractory oxide MgO, (or in the case of other relaxors the refractory B site cations), in relation to other phases belonging to the binary system $PbO-Nb_2O_5$.

A reaction sequence for the formation of PMN, as well as solid solutions of PMN-PZ-PT was first proposed by Inada[34]. From extensive DTA and X-ray diffraction studies, he concluded that the perovskite PMN was formed not by the direct formation of oxides, but by the repetition of the following reactions:

$$PbO + Nb_2O_5 \xrightarrow[exo]{530\text{-}600^\circ C} Pb_{1.5}Nb_2O_{6.5}\ (P_{1.5}N_2) - \text{anion deficient cubic pyrochlore} \quad (1)$$

$$Pb_{1.5}Nb_2O_{6.5} + PbO \xrightarrow[exo]{600\text{-}700^\circ C} Pb_2Nb_2O_7 - \text{rhombohedral pyrochlore} \quad (2)$$

$$Pb_2Nb_2O_7 + MgO \xrightarrow[endo]{700\text{-}800^\circ C} \text{PMN perovskite} + Pb_{1.5}Nb_2O_{6.5} \quad (3)$$

In equation 1, the initial reaction between PbO and Nb_2O_5 results in the formation of cubic pyrochlore, where upon further reaction with PbO results in the formation of a rhombohedral pyrochlore $Pb_2Nb_2O_7$ (P_2N) (equation 2). The rhombohedral pyrochlore then reacts with MgO at higher temperature to form perovskite PMN, with the reappearance of cubic pyrochlore phase. Inada concluded that to obtain single phase PMN, it is necessary to prevent the evaporation of PbO, which would slow down the above reactions, and to repeat the process of calcining, crushing and calcining. The reaction sequence proposed by Inada is similar to that proposed for PFN, by Kassarjian[35], and Yonezawa[36], except that in PFN a $2PbO{\cdot}Fe_2O_3$ (P_2F) phase also forms and that the perovskite PFN appears to form more easily than perovskite PMN.

Lejeune and Boilot[37] have reported a somewhat different reaction sequence for the formation of PMN and PFN, than that proposed by Inada. They reported that the reaction of PbO and Nb_2O_5 leads to the formation of 3 types of pyrochlore phases, $Pb_3Nb_2O_8$ (P_3N), P_2N and $P_{1.5}N_2$, and further reaction between P_2N with PbO forms a lead rich P_3N pyrochlore with the $P_{1.5}N_2$ cubic

pyrochlore phase being stable. At about 830°C, a liquid phase was found to form and P_3N reacted with MgO to form perovskite PMN with the P_3N_2 phase being unaltered.

Swartz and Shrout[38], have reported a somewhat different reaction sequence for the formation of PMN than that of either Inada or Lejeune. In their work, only the cubic pyrochlore $P_{1.5}N_2$ was observed, which in turn reacted with PbO and MgO to form perovskite PMN. Swartz and Shrout also confirmed that MgO was incorporated into the cubic pyrochlore structure having an approximate formula of $Pb_{1.83}Nb_{1.21}Mg_{0.29}O_{6.34}$[39]. The exact amount of MgO that can be incorporated into the pyrochlore structure is not yet known. E. Goo and G. Thomas[40], H.C. Wang, et al.[41] and Chan, et al.[42] have also reported partial incorporation of MgO in the pyrochlore phase. From the works mentioned above, it is clear that perovskite PMN does not form by a direct reaction of oxides, but by subsequent reactions through pyrochlore phase(s), and that the cubic pyrochlore is very stable and is never completely eliminated. Also, the formation of PMN could be accelerated by excess additions of PbO and also MgO.

Differences in the aforementioned reaction sequences in the formation of PMN could be due to the dependence of reaction kinetics on various processing parameters, such as particle size and surface area of the raw materials, heating rates, etc.

Lejeune, et al.[43] and other investigators[44,45] have reported the effect of various processing parameters on the composition and amount of phases formed in the preparation of PMN. Results of various ceramic processing studies are given in Table II. As can be expected from the reaction sequences[1-3], processes that reduce the volatility of PbO, such as shorter sintering times and, closed crucible firings, lead to an increased amount of perovskite phase. Conversely, processes that lead to PbO loss, as

in longer sintering times lead to an increased amount of pyrochlore phase as is evident form the following reverse reaction:

$$3\ PMN \rightarrow 2(PMN) + Pyrochlore + PbO \qquad (4)$$

From the above reaction as well as other reactions in which pyrochlore phase forms, free PbO will be present in the ceramics unless driven off through volatilization. The presence of free PbO is commonly observed in the grain boundaries and at triple points, as shown in a schemtaic illustration of the microstructure for PMN[40] (Figure 3). It is believed that this relatively weak amorphous PbO grain boundary phase gives rise to the characteristic intergranular fracture frequently observed in relaxors. Along with the amorphous PbO being at the grain boundary, small grains of pyrochlore are also observed. It has been reported that depending on the ceramic process pyrochlore phase can also be found in the form of large discrete grains[42].

From Table II, it is also apparent that ceramic processes that improve the reactivity of the refractory oxide MgO, e.g. finer raw materials, mixing/milling (disperability) and sol-gel technique, increase significantly the amount of perovskite PMN. The importance of the distribution of MgO in the formation of PMN is clearly depicted from an X-ray fluorescence (Figure 4) and a TEM photomicrographs (Figure 3) where discrete unreacted MgO particles can be seen in the perovskite grains. The MgO particles being poorly dispersed and/or simply too refractory allows PbO and Nb_2O_5 particles to react favorably to form pyrochlore phase.

Hence from ceramic processing studies described in Table II, it is clear that the cubic pyrochlore phase is extremely stable. The pyrochlore phase could not be completely eliminated even by highly reactive processes, such as sol-gel technique.

To completely eliminate the cubic pyrochlore phase, it has been shown that an addition of up to 6 wt% excess PbO[47] is necessary. Excess PbO accelerates the formation of PbO rich pyrochlore phases, $Pb_2Nb_2O_7$ or $Pb_3Nb_2O_8$[37] (Equation 2). The addition of excess MgO (at least 5 mole%)[48-50], also helps to eliminate the pyrochlore phase by compensating for poor dispersability and reactivity. Additives such as Pb based fluxes PbF_2 and $Pb_5Ge_3O_{11}$ which increase the amount of PbO, also reduce the fraction of pyrochlore phase[46]. Such additives are commonly used in PMN based commercial relaxors listed in Table 1, such as TAM's composition. Also, the PMN-PFN patent by Wheeler[26] is based on a solid solution of PMN with a formula of $Pb(Mg_{1/2}Nb_{1/2})O_3$ and non-stoichiometric PFN, which is effectivley PbO and MgO excess. The effect of eliminating pyrochlore phase on the dielectric properties can be seen in Figure 5. Here the dielectric constant drastically increases[51] due to the elimination of pyrochlore phase by the addition of excess PbO.

Even though the cubic pyrochlore phase can be eliminated by the addition of excess PbO or MgO, the resulting PMN perovskite phase will be non-stoichiometric, which is not desirable. The importance of obtaining a stoichiometric perovskite PMN composition is evident by the vast variation in physical and dielectric properties reported for PMN in the literature and summarized in Table III. It is clear that PbO and MgO deficiency can result in excessive amount of pyrochlore phase which causes poor densification and greatly degrades dielectric properties. Discrete grains of pyrochlore phase (estimated k of ~ 120[39]), would have little effect on the dielectric properties of the relaxor, but the presence of free PbO (k ~ 20) in the grain boundary, (Figure 3), will lower the overall dielectric constant giving rise to the observed grain size dependency of k as reported by Swartz, et al.[57]. Excess PbO not only aids in the elimination of pyrochlore, but enhances

densification through liquid phase sintering. However, excess PbO in the grain boundary can lead to unwanted reduction in k, IR degradation, and aging[51-57] The detrimental effects of excess PbO on the dielectric properties can be avoided if the excess PbO is driven off through volatilization during the early stages of sintering[55]. Excess PbO also can lead to slight shifts in T_c (+1-2°C/wt%[57]) and increased diffuseness/broadness of the transition[43,57]. As with excess PbO, various PbO based fluxes, that are commonly employed in the fabrication of PMN can also lead to reduced dielectric constant and other detrimental effects.

Excess MgO has been found to promote grain growth and to enhance k. Such grain growth is believed to be the result of elimination of pyrochlore phase from the grain boundary region which inhibits grain growth. As with excess PbO, excess MgO also results in slight shifts in T_c[52]. The addition of acceptor dopants, such as Mn, and Fe, which are commonly added to relaxor formulations, also cause a higher aging rate of dielectric properties. The mechanism by which excess PbO, and other dopants cause aging is not yet clear.

Columbite-(Wolframite) Precursor Method

In order to obtain stoichiometric perovskite PMN, it was concluded by Swartz and Shrout[38] that the intermediate pyrochlore phase(s) reaction must be eliminated. In order to achieve this, a novel approach whereby the two refractory B site oxides MgO and Nb_2O_5 were prereacted to form the columbite $MgNb_2O_6$ prior to reaction with PbO as shown in the following set of reactions:

$$MgO + Nb_2O_5 \xrightarrow{\sim 1000°C} MgNb_2O_6 \qquad (5)$$

$$MgNb_2O_6 + 3PbO \xrightarrow[exo]{\sim 700°C} 3\ (PMN) \qquad (6)$$

In the above reaction sequence, the pyrochlore formation is bypassed leading to the direct formation of PMN. Naturally the success of this approach depends upon various ceramic process parameters, such as reactivity of MgO, mixing, and controlling PbO volatility. Preparation by this method always shows substantial improvement in the amount of perovskite phase compared to conventional mixed oxide processing as shown in Table IV. Stoichiometric PMN ceramics, completely free of pyrochlore phase, can be prepared easily by this method.

The columbite method is believed to be successful in preparing PMN ceramics, with perovskite structure, for the following reasons:

(1) The refractory oxides, MgO and Nb_2O_5 are dispersed essentially on an atomic scale. From Table II and Figures 3 and 4, it is clear that the dispersion of MgO is very critical in supressing the formation of pyrochlore phase.

(2) In order for PbO to react with $MgNb_2O_6$ to form pyrochlore, it would first have to liberate Nb_2O_5. The kinetics of this reaction appears to be slow enough to prevent pyrochlore formation.

The dielectric properties of PMN ceramics prepared by this method are, in general, consistently superior compared to those prepared by conventional mixed oxide process[56].

The process of pre-reacting the B site cations, either to form Columbite phase $B_1B_2O_3$ or to form Wolframite phase $B_1B_2O_4$ has been successfully applied to many other relaxors, such as presented in Table IV, PNN[59], PFN[13], PMT[53] and PST[53], and for many solid solution systems[60]. As with PMN, the dielectric properties were found to be superior, as a result of reduction in the amount of cubic pyrochlore phase. This method, however, was only partially successful for PIN[61] and totally unsuccessful for a number of relaxors such as $Pb(Zn_{1/3}Nb_{2/3})O_3$ (PZN), $Pb(Cd_{1/3}NB_{2/3})O_3$ (PCN) and

$PB(ZN_{1/3}TA_{2/3})O_3$ (PZTa)[53]. From the preceding discussion it is clear that in order to understand the stability of the perovskite phase and the formation of pyrochlore phase in ferroelectric relaxors, we should consider the thermodynamics as well as the reaction kinetics.

IV. THERMODYNAMICS

Of all the ABO_3 structures, the compounds of the perovskite family are probably the most numerous and of technological importance. Numerous authors have studied the stability of perovskite structure with respect to other structures[62]. The perovskite structure has the general formula: $A^{XII}B^{VI}O_3^{VI}$. Here, the roman numerals represent the corresponding cation:anion coordination number (CN). The two basic requirements for the stability of the perovskite structure are: (1) the ionic radii of the cations should be within proper limits and (2) the cations-anions should have a strong mutual ionic bond. The first requirement relates to the perovskite unit cell size. Goldshmidt[63] proposed the concept of a tolerance factor where the tolerance factor 't' is given by:

$$t = \frac{r_A + r_O}{2(r_B + r_O)} \tag{7}$$

where r_A, r_B, r_O are the respective ionic radii. Goldschmidt concluded that the perovskite structure may be expected within the limits t = 0.77 to 0.99, if ionic radii based on octahedral coordination are considered. If the ionic radii are corrected for the difference in coordination number, the limits of t are 0.94 to 1.06.

The second requirement relates to the amount of ionic bonding. The amount of ionic bonding is proportional to the difference between the electronegativity of the cations and anions. Similar to the analysis

presented by Halliyal, et al.[64,65] the tolerance factor and electronegativity differences for several known ABO_3 type perovskite compounds were calculated and are plotted in Figure 6. The tolerance factors were calculated using equation 7 using ionic radii suggested by Shannon and Prewitt[66]. For compounds containing more than one B site cation, as with the relaxors, the weighted average was used for r_B. A weighted average was again used for determining the electronegativity difference using Pauling's[67] electronegativity scale as expressed in the following equation:

$$(X_{A-O}+X_{B-O})/2 \qquad (8)$$

where X_{A-O} is the electronegativity difference between A site cation and oxygen and X_{B-O}, the electronegativity difference between the B site cations and oxygen. As shown in Figure (6), it is clearly evident that compounds such as $BaTiO_3$ and $KNbO_3$ having both high tolerance factor and high electronegativity difference (strong ionic bonding) should be extremely stable perovskites structures, as they are well known to be. For PbO based $A(B_1B_2)O_3$ perovskite compounds, both the tolerance factor and electronegativity difference are small, thus they should be less stable perovskites. This observation agrees quite well with experimental data in regard to the ease of preparation of these compounds with perovskite structure. Experimentally, the relative ease of fabrication of the lead based perovskites roughly follows the sequence[11,12,53,68]:

PZN < PCN < PIN < PSN < PNN < PMN < PFN < PFW < PZ < PT

In other words, PZN is the most difficult relaxor perovskite to prepare in single phase perovskite form. In fact, it is well known that perovskite PZN cannot be fabricated by conventional mixed oxide ceramic processing. However, the above sequence of difficulty does not quite fit empirically as shown in

Figure 6. Perhaps for compounds such as PZ and PZN, other bonding and structural parameters, such as electron configuration, cation valence stability, ordering parameters, etc. should also be considered.

To further investigate the stability of lead based complex perovskites, one should also look at the pyrochlore structure. The pyrochlore structure is normally of the type $A_2^{VIII}B_2^{IV}O_6^{V}O^{IV}$, where the A site cation is now 8 coordinated. A number of these compositions also frequently form an anion deficient pyrochlore structure where one of the oxygens is missing giving the general formula $A_2^{VI}B_2^{IV}O_6$. In many of these defect pyrochlores, the vacant anion site is partially filled. Due to the missing oxygen atom, the CN of the A cation (typically Pb^{+2}), drops from 8 to 6. It has been suggested[69,70] that Pb-Pb bonding across the oxygen vacancy is responsible for this defect structure or alternately, the inherent covalency of these phases favors the defect structure. From Figure 6, it is clear that PbO based perovskite compounds tend to be more covalently bonded than other perovskites such as $BaTiO_3$ (BT), and $SrTiO_3$ (ST). Thus perhaps one would expect PbO based perovskites to favor covalently bonded structure such as the anion deficient pyrochlore. Perhaps the affinity of the pyrochlore structure towards covalency is the primary reason why the perovskite PZN is extremely difficult to form. In PZN, the Zn^{+2} cation prefers four-fold coordination as in Wurtzite ZnO, which is strongly covalently bonded. Based on the thermodynamic argument, we can conclude that if lead based perovskites can be made more ionic or if the tolerance factor is increased, the problem of pyrochlore formation can be eliminated.

Furukawa, et al.[70] and Halliyal, et al.[64] both observed that since $BaTiO_3$ has the highest electronegativity difference and tolerance factor, the addition of a small amount of BT should stabilize the perovskite structure in

PZN. As listed in Table V, only 6-7 mole% of BT[64] was required to stabilize perovskite PZN whereas 10 mole% of BZN[72], 10 mole% K_2O[73]0, 10 mole% of $SrTiO_3$[74], 30 mole% of PT[75,76] and up to 55 mole% of PZ[76] was required to stabilize perovskite PZN. Also included in the table are calculated values of the electronegativity differences ΔX and tolerance factor t.

The improvement in the dielectric constant of PZN ceramics as a function of additions of $BaTiO_3$[64] can be seen in Figure 7. An addition of 7 mole% of $BaTiO_3$ completely eliminates the formation of pyrochlore phase resulting in a large increase in dielectric constant. PZN based compositions modified with BT and or ST have already been developed for capacitors, as presented in Table I.

Many investigators have observed that cerain compositional modification of relaxors, e.g. PMN-PT[44], Li_2O doped PIN[61] and PMN[77], etc. were easier to fabricate in perovskite form. Perhaps such modifications also effectively increase the ionicity and/or tolerance factor which help in stabilizing the perovskite structure, as with the various PZN modification.

Summary

A review of recent literature on lead based ferroelectric relaxors reveals that over the past few years lead based dielectric materials are becoming increasingly important for multilayer ceramic capacitors. Extensive research work on the studies of preparation and dielectric properties of lead based relaxors has enabled to reproducibly fabricate relaxors which were in the past plagued by the inevitable formation of a parasite pyrochlore phase. Efforts have been made to understand the problem of pyrochlore formation and the stability of the perovskite phase both kinetically and thermodynamically.

In several relaxors like PMN, the formation of the perovskite phase is primarily related to the reactivity of the refractory oxides in relation to

the other phases in the $PbO-Nb_2O_5$ binary system. Kinetically, ceramic processes that improve the reactivity of MgO, such as better milling/mixing - dispersability and processes in which the PbO volatility is controlled by reduction in firing time, or by firing the ceramic in PbO rich atmosphere, enhance the formation of perovskite phase. It has also been observed that the addition of excess PbO, and MgO or lead-based fluxes could lead to the elimination of the pyrochlore phase, but yield non-stoichiometric ceramics which show undesirable dielectric properties such as aging. To obtain stoichiometric perovskite relaxors such as PMN, PNN, etc. a novel approach referred to as the Columbite/Wolframite precursor method can be adopted. In this method the refractory B site cations are prereacted prior to the reaction with PbO, thus eliminating the unwanted pyrochlore phase. However, this approach fails to yield perovskite ceramics for PZN, PZT, PIN and PCN, which leads one to conclude that the stability of the perovskite phase is probably thermodynamic in nature. Thermodynamically, the stability of the perovskite ABO_3 structure is found to be dependent on the Goldschmidt tolerance factor, which relates ideal cation sizes for the stability of the perovskite structure and the ionicity of the perovskite structure. An analysis of the electronegativity and tolerance factor of several ABO_3 type compounds revealed that perovskite compounds with both large tolerance factor and electronegativity differences such as $SrTiO_3$ and $BaTiO_3$ are very stable perovskites. The lead based relaxor compounds which have lower tolerance factor and lower electronegativity diffference than $SrTiO_3$ and $BaTiO_3$ are found to be difficult to synthesize in perovskite form. Such compounds tend to form a more covalently bonded pyrochlore structure, $Pb_2Nb_2O_7$ or the anion deficient pyrochlore $Pb_{1.5}Nb_2O_{6.5}$ phase. Increasing the tolerance factor and electronegativity difference of such compounds by the addition of $BaTiO_3$ or $SrTiO_3$, is found to be highly successful in stabilizing the perovskite

structure. It is clear that the problem of pyrochlore formation in the preparation of perovskite lead based relaxors is primarily thermodynamic in nature for relaxors such as PZN, PIN, PCN, and perhaps to a lesser extent for other relaxors such as PMN, and PNN in which the pyrochlore formation strongly depends on the reaction kinetics.

Regardless of whether the formation of the pyrochlore phase in perovskite relaxors is thermodynamic or kinetic, the dielectric and physical properties of relaxors are strongly dependent on the ability to control and understand the nature of the pyrochlore formation in order to reproducibly fabricate relaxors with the perovskite structure.

Suggestions for Future Work

(1) From the studies performed on the relaxor PMN, it is clear that the reaction kinetics plays an extremely important role in the formation of pyrochlore phase. Particularly, improving the reactivity and dispersability of the refractory oxide MgO suppresses the formation of pyrochlore phase. Further work should be done in order to understand the effect of high energy milling and better mixing of the raw materials using techniques like attrition milling on the reaction kinetics of relaxors. Also, non-conventional ceramic processing methods such as molten salt, co-precipitation and hydrothermal techniques can be used to prepare highly reactive powders of relaxors to understand the reaction kinetics better. Perhaps, such techniques may permit the preparation of thermodynamically unstable relaxor perovskites such as PZN.

(2) To further evaluate the thermodynamic nature of the perovskite stability the stabilization of the perovskite phase for relaxors such as PIN, PZTa, and PCN with additions of $SrTiO_3$ or $BaTiO_3$ could be evaluated. A similar study of examination of ionicity and tolerance factor needs to be done for the pyrochlore structure family also.

(3) The role of processing variables on corresponding variation in phase content and dielectric and physical properties of the ceramics should be investigated in commercial multilayer capacitors, paying particular attention to mechanical strength, IR degration, aging, and Ag^+ migration from the electrodes.

Acknowledgements

The authors would like to acknowledge Dr. L.E. Cross, Dr. S.J. Jang, Dr. W.A. Schulze, Dr. Scott Swartz, Dr. S. Venkataramani and Truman Rutt for all their help in the world of relaxor dielectrics.

REFERENCES

1. J.M. Herbert, "Ceramic Dielectrics and Capacitors," Electrocomponent Science Monographs, Vol. 6, Gordon and Breach, NY (1985).
2. W.R. Buessem and T.I. Prokopowicz, "Electrode and Materials Problems in Ceramic Capacitors," Ferroelectrics 10, 225-230 (1981).
3. J.M. Herbert, "Method of Making Ceramic Dielectric Material," U.S. Patent #2,934,442 (1959).
4. I. Burn and G.H. Maher, "High Resistivity $BaTiO_3$ Ceramics Sintered in CO-CO_2 Atmospheres," J. Mat. Sci. 10, 633-640 (1975).
5. T.L. Rutt, "Ceramic Capacitors," U.S. Patent 3,679,950 (1972).
6. T.L. Rutt and J.A. Syne, "Fabrication of Multilayer Ceramic Capacitor by Metal Impregnation," IEEE Trans. on Parts, Hybrids, and Packaging, PHP-9, 144-147 (1973).
7. G.A. Smolenskii and A.I. Agranovuskaya, "Dielectric Polarization of a Number of Complex Compounds," Soviet Physics - Solid State 1, 1429-1437 (1959).
8. N. Setter and L.E. Cross, "The Role of B-Site Cation Disorder in Diffuse Phase Transition Behavior on Perovskite Ferroelectrics," J. Appl. Phys. 51 [8], 4356-4360 (1980).
9. C.G.F. Stenger, F.L. Scholten, and A.J. Burggraf, "Ordering and Diffuse Transitions in $Pb(Sc_{0.5}Ta_{0.5})O_3$ Ceramics," Sol. State Comm. 32, 898-992 (1979).
10. N. Setter and L.E. Cross, "The Contribution of Structural Disorder to Diffuse Phase Transitions in Ferroelectrics," J. Mat. Sci. 15 [a], 2428-2482 (1980).
11. Landolt-Bornstein, Ferroelectrics and Related Substances, New Series, Vol. 16, Springer-Verlag Berlin, Heidelberg, NY (1981).

12. F.S. Galasso, Structure, Properties and Preparation of Perovskite Type Compounds, Pergamon Press, NY (1969).

13. T.R. Shrout, S.L. Swartz and M.J. Haun, "Dielectric Properties in the $Pb(Fe_{1/2}Nb_{1/2})O_3$-$Pb(Ni_{1/3}Nb_{2/3})O_3$ Solid Solution System," Amer. Cerm. Soc. Bull. 63 [6], 808-810 (1984).

14. S. Fujiawara, K. Furukawa, N. Kikachi, O. Iizawa and H. Tanaka, "High Dielectric Constant Type Ceramic Composition," U.S. Patent 4,265,668 (1981).

15. O. Iizawa, S. Fujiwana, H. Ueoka, K. Furukawa, N. Kikuchi and H. Tanaka, "High Dielectric Constant Type Ceramic Composition," U.S. Patent 4,235,635 (1984).

16. K. Furukawa, S. Fujiwara, N. Kikachi, O. Iizawa and H. Tanaka, "High Dielectric Constant Type Ceramic Composition Consisting Essentially of $Pb(Fe_{1/2}Nb_{1/2})O_3$-$Pb(Mg_{1/3}Nb_{2/3})O_3$." U.S. Patent 4,216,102 (1980).

17. S. Fujiwara, K. Furukawa, N. Kikuchi, O. Iisawa, H. Tanaka and H. Ueaka, "High Dielectric Composition Consisting Essentially of $Pb(Fe_{1/2}Nb_{1/2})O_3$-$Pb(Mg_{1/3}Ta_{2/3})O_3$." U.S. Patent 4,216,103 (1980).

18. M. Yonezawa and T. Ohno, "Ceramic Compositions Having High Dielectric Constant," U.S. Patent 4,078,938 (1978).

19. M. Yonezawa and T. Ohno, "Ceramic Compositions Having High Dielectric Constants," U.S. Patent 4,236,928 (1980).

20. Miyamoto and M. Yonezawa, "Ceramic Compositions," Jpn. Patent (in Japanese) Sho60-33258 (1985).

21. K. Takahashi and Harata, "High Permittivity Ceramic Compositions," Jpn. Patent (in Japanese) Sho59-181407 (1984).

22. Y. Yamishita, T. Takahashi and M. Harata, "High Dielectric Contant Type Ceramic Composition," European Patent 0,121,161 (1984).

23. Y. Yamashita, O. Furukawa, M. Harata, T. Takahashi and K. Inagaki, "A New Lead Perovskite Y55 Dielectric for Multilayer Ceramic Capacitor," Jpn. J. Appl. Phys. 24, 1027-1029 (1985).

24. Y. Yamashita, K. Inagaki, K. Handa and T. Watanase, "A Large Capacitance Y5U MLC Based on Modified Lead Zinc Niobate," (to be published in Ferroelectrics).

25. Y. Sakabe and y. Hamaji, "Ceramic Dielectric Compositin," U.S. Patent 4,339,544 (1982).

26. J.M. Wheeler, "Ceramic Capacitors and Dielectric Compositions," U.K. Patent 2,126,575 (1984).

27. J.M. Wheeler and D.A. Jackson, "Dielectric Composition," U.K. Patent 2,127,187A (1984).

28. H. Ohuchi and Y. Mitsuo, "High Permittivity Ceramic Compositions," Jpn. Patent (in Japanese) Sho59-107959 (1984).

29. Tsuta and Yasuo, "Manufacturing Method of High Permittivity Ceramic Compositions," Jpn. Patent (in Japanese) Sho59-203759 (1984).

30. H. Ohuchi and Y. Matsuo, "High Permittivity Ceramic Compositions," Jpn. Patent (in Japanese) Sho-59-111201 (1984).

31. M. Nishita, H. Ohuchi and y. Matsuo, "High Permittivity Ceramic Compositions," Jpn. Patent (in Japanese) Sho 59-54665 (1984).

32. R.J. Bouchand, "Dielectric Powder Compositions," U.S. Patent 4,048,546 (1977).

33. H.D. Pack and A.E. Brown, "Ceramic Composition for Dielectric in Multilayer Capacitors," U.S. Patent #4,550,088 (1985).

34. M. Inada, "Analysis of the Formation Process of the Piezoelectric PCM Ceramics," Japanese National Technical Report, 27 [1], 95-102 (1977).

35. M.J. Kassarjian, "A Lead-Iron-Niobate Dielectric Ceramic for Low Firing Temperature Capacitors," M.S. Thesis, The Pennsylvania State University (1984).

36. M. Yonezawa and T. Ohno, "Perovskite Formation Processes and Properties of the System $Pb(Fe_{2/3}W_{1/3})O_3$-$Pb(Fe_{1/2}Nb_{1/2})O_3$," Proceedings of the Japan-U.S. Study Seminar on Dielectrics ad Piezoelectrics," T-8, 1-5 (1982).

37. M. Lejeune and J.P. Boilot, "Formation Mechanism and Ceramic Process of the Ferroelectric Perovskites: $Pb(Mg_{1/3}Nb_{2/3})O_3$ and $Pb(Fe_{1/2}Nb_{1/2})O_3$," Ceram. Intl. 8 [3], 99-104 (1982).

38. S.L. Swartz and T.R. Shrout, "Fabrication of Perovskite Lead Magnesium Niobate," Mat. Res. Bull. 17, 1245-1250 (1982).

39. T.R. Shrout and S.L. Swartz, "Dielectric Properties of Pyrochlore Lead Magnesium Niobate," Mat. Res. Bull. 18, 663-667 (1983).

40. E. Goo and G. Thomas, "Microstructure of Lead-Magnesium-Niobate Ceramics,"

41. H.C. Wang, W.A. Schulze and P.F. Johnson, "SEMS Characterization of the Role of Excess PbO and MgO in Lead Magnesium Niobate," presented at 87th Annual American Ceramic Society in Chicago, IL (1986).

42. H.M Chan, A. Gorton, C. Jie, D.M. Smyth and M.P. Harmer, "Processing Microstructure and Properties of the Relaxor Materials $Pb(Mg_{1/3}Nb_{2/3})O_3$:$PbTiO_3$ and $Pb(Mg_{1/2}W_{1/2})O_3$·$PbTiO_3$," Presented at Amer. Ceram. Soc. Mtg., Chicago, IL (1986).

43. M. Lejeune and J.P. Boilot, "Influence of Ceramic Processing on Dielectric Properties of Perovskite Type Compound: $Pb(Mg_{1/3}Nb_{2/3})O_3$," Ceram. Intl. 9 [4], 119-122 (1983).

44. S.J. Jang, "Electrostrictive Ceramics for Electrostrictive Applications," Ph.D. Thesis, The Pennsylvania State University (1980).

45. T.W. Dekleva, "Preparation of Pyrochlore-Free PMN, and the Chemistry Involved in the Gels Involved," (to be published).

46. "Perovskite et Pyrochlores Au Ploms PZN $(PbZn_{1/3}Nb_{2/3})O_3$: PFN $(PbFe_{1/2}Nb_{1/2})O_3$ et PMN $(PbMg_{1/3}Nb_{2/3})O_3$ Condensateurs Multicouches a Haute Constante Dielectrique," Crystals Chem. and Phys. 8, 469-491 (1983).

47. M. Lejeune and J.P. Boilot, "Ceramics of Perovskite Lead Magnesium Niobate," Ferroelectrics 54, 191-194 (1984).

48. Yao Xi, private communication.

49. M. Nagase, "Formation of $Pb[(Mg_{1/3}Nb_{2/3})TiZr])O_3$ Ceramic and Effect of Excess MgO," (Japanese) Matsushita Electric Co., Wireless Lab. Report IDI-6137 (1968).

50. K. Furukawa, S. Fujiwana, and T. Ogasawara, "Dielectric Properties of $Pb(Mg_{1/3}Nb_{2/3})O_3$-$PbTiO_3$ Ceramics for Capacitor Materials," Proceedings of the Japan-U.S. Study Seminar on Dielectric and Piezoelectric Ceramics, P.T.-4 (1982).

51. S.L. Swartz, T.R. Shrout, W.A. Schuzle and L.E. Cross, "Dielectric Properties of Lead Magnesium Niobate Ceramics,"

52. M. Lejeune and J.P. Poilot, "Low Firing Dielectrics Based on Lead Magneisum Niobate," Mat. Res. Bull. 20, 493-499 (1985).

53. Thomas Shrout, private communication.

54. Scott Swartz, private communication.

55. M. Lejeune and J.P. Boilot, "Optimization of Dielectric Properties of Lead-Magnesium Niobate Ceramics," Am. Ceram. Soc. Bull. 64 [4], 679-682 (1986).

56. M. Lejeune and J.P. Boilot, "$Pb(Mg_{1/3}Nb_{2/3})O_3$ (PMN) Multilayer Capacitors," Journal De Physique-Colloque C1 47, C1-895 (1986).

57. S. Swartz, G.O. Dayton and D. Laubscher, "Low Temperature Fired Lead Magnesium Niobate," (to be published in Ferroelectrics).

58. W. Pan, E. Furman, L.E. Cross and G.O. Dayton, "Aging Effect in MnO Doped $Pb(Mg_{1/3}Nb_{2/3})O_3$ + 10% $PbTiO_3$ Relaxor Ceramics," (to be published in Ferroelectrics).

59. L. Veitch, "Dielectric Properties of $Pb(Ni_{1/3}Nb_{2/3})O_3$, B.S. Thesis, The Pennsylvania State University, University Park, PA (1982).

60. D.J. Voss, S.L. Swartz, and T.R. Shrout, "The Effects of Various B-Site Modifications on the Dielectric and Electrostrictive Properties of Lead Magnesium Niobate Ceramics," Ferroelectrics 50, 203-208 (1983).

61. P. Groves, "Fabrication and Characterization of Ferroelectric Perovskite Lead Indium Niobate," to be published in Ferroelectrics.

62. O. Muller and R. Roy, "Crystal Chemistry on Non-Metallic Materials," Springer-Verlag, NY (1974).

63. V.M. Goldschmidt, Schrifter Norske Videnskaps - Akad. Oslo 1: Matemot. Naturuid. Klasse, No. 2 (1926).

64. A. Halliyal, U. Kumar and R.E. Newnham, "Stabilization of Perovskite Phase and Dielectric Properties of Ceramics in the $Pb(Zn_{1/3}Nb_{2/3}O_3$-$BaTiO_3$ System," Submitted to J. Amer. Ceram. Soc.

65. A. Halliyal, T.R. Gururaja, U. Kumar and A. Safari, "Stability of Perovskite Phase in $Pb(Zn_{1/3}Nb_{2/3})O_3$ and Other $A(B'B'')O_3$ Perovskites," to be published in Ferroelectrics.

66. R.D. Shannon and C.T. Prewitt, Acta Cryst. B25, 925 (1969); Acta Cryst. B26, 1046 (1970).

67. L. Pauling, "The Nature of Chemical Bonds," Cornell University Press, NY (1960).

68. A.I. Agranovskaya, "Physical-Chemicl Investigations of the Formation of Complex Ferroelectrics with the Perovskite Structure," Bull. Acad. Sciences - Phys. Series, 1271-1277 (1960).

69. J.M. Longo, P.M Raccah and J.B. Goodenough, "$Pb_2M_2O_{1-x}$ (M = Ru, Ir, Re) - Preparation and Properties of Oxygen Deficient Pyrochlore," Mat. Res. Bull. 4, 191-202 (1969).

70. A.W. Sleight, "$AgPbO_3$: Chemical Characterization and Structural Considerations," Mat. Res. Bull. 4, 377-380 (1969).

71. O. Furukawa, Y. Yamashita, M. Harata, T. Takahashi, and K. Inagaki, "Dielectric Properties of Modified Lead Zinc Niobate Ceramic," Jpn. J. of Appl. Phys. 24, 96-99 (1985).

72. S. Nomura and H. Arima, "Dielectric and Piezoelectric Properties in the Ternary System of $Pb(Zn_{1/3}Nb_{2/3})O_3$-$Ba(Zn_{1/3}Nb_{2/3})O_3$-$PbTiO_3$," Jpn. J. Appl. Phys. 11 [3], 358 (1977).

73. L. Hanh and S. Nomura, "Ferroelectric and Piezoelectric Properties of $xPb_{1-y}K_y(Zn_{1/3}Nb_{2/3})O_{3-y/2}$-$(1-x)PbTiO_3$ Solid Solutions," Jpn. J. Appl. Phys. 15 [6], 1059 (1976).

74. J. Belsick, B.S. Thesis, The Pennsylvania State University (1986).

75. B. Jaffe, W.R. Cook, Jr. and H. Jaffe, "Piezoelectric Ceramics," pp. 237-242., Academic Pres, NY (1971).

76. M. Lanagan, D. Anderson and D. Moffatt, (to be published).

77. G. Desgardin, M. Halmi, J.M. Haussonne and B. Raveau, "Nouveax Materiaux, Dielectrique A Box De Perovskite Au Plans ?????" (to be published).

FIGURE CAPTIONS

Figure 1. Typical dielectric behavior for "disordered" and "ordered" relaxors. The example presented is for a disordered and thermally annealed crystals of $Pb(Sc_{1/2}Ta_{1/2})O_3$ (PST)[8].

Figure 2. Curie temperature as a function of frequency in the binary system $xPb(Fe_{1/2}Nb_{1/2})O_3-(1-x)Pb(Ni_{1/3},Nb_{2/3})O_3$[13].

Figure 3. A schematic illustration of the microstructure in PMN ceramics[40].

Figure 4. An x-ray fluorescence micrograph of MgO (white regions) in PMN ceramics[46,53].

Figure 5. The dielectric constant k (1 kHz) as a function of temperature for PMN ceramics with approximately 8% pyrochlore (A) and pyrochlore free (B) PMN prepared with excess PbO[50].

Figure 6. Plot of electronegativity difference vs tolerance factor for several perovskite compounds.

Figure 7. Variation of the dielectric constant k (1 kHz) with temperature for (1-x) PZN-xBT compositions.

Table I. Relaxor Compositional Families* for Capacitors.

Patents and Publications	Manufacturer (Assignee)
PMN-PT[14] PFW-PZ[15] PMN-PFN[16] PFN-PMT[17] +PMN-PT+PbO based flux	TDK, Ltd.
++PFW-PFN[18] ++PFW-PFN-PZN[19] PMWN-PNN-PT[20]	NEC (Nippon Electric Co.)
PFN-Ba,Ca(CuW)-PFW[21,22] PZN-PT-ST[23]	Toshiba Co.
PZN-BT-ST[24] PMN-PZN-PT[25]	Marcon Electronic Co.
PMN-PFN-PT[26] +++PMN-PFN-PT[27]	STL (Standard Telephone Lab.)
PMN-PZN-PFN[28] PMN-PFW-PT[29] PNN-PFN-PFW[30,31]	Matushita Co.
+PMW-PT-ST[32]	E.I. DuPont de Nemours
++PMN-PFN-PGe[33]	Union Carbide Co.

+Commercially available powder.
++Multilayer capacitors.
+++Compolsition licensed to Transelco Co.

+Composition Designations: PMN-$Pb(Mg_{1/3}Nb_{2/3})O_3$, PT-$PbTiO_3$, PZ-$PbZrO_3$, PFW-$Pb(Fe_{2/3}Nb_{1/3})O_3$, PFN-$Pb(Fe_{1/2},Nb_{1/2})O_3$, PMT-$Pb(Mg_{1/3}Ta_{1/3})O_3$, PZN-$Pb(Zn_{1/3}Nb_{2/3})O_3$, PNN-$Pb(Ni_{1/3}Nb_{2/3})O_3$, Ba,Ca(CuW)-$Ba,Ca(Cu_{1/2}W_{1/2})O_3$, PMW-$Pb(Mg_{2/3}W_{1/3})O_3$, PW-$PbWO_4$, ST-$SrTiO_3$, PbGe-lead germanate flux.

Table II. Influence of Ceramic Processing on PMN Perovskite Formation.

Process/Conventional	Parameter A -> B	% Perovskite PMN* A -> B	Comment
Ball Milling/Mixing	MgO -> $MgCO_3$	42% -> 81%[43]	Improved Reactivity and Dispersability
	Water -> Acetone	51% -> 81%[43]	
Calcination	# Cycles 1 vs 3	60% -> 90%[43]	---
	800°C -> 1000°C	68% -> 76%[38]	---
	Air O_2	77% -> 85%[43]	Help Prevent Anion Deficient Pyrochlore Formation
Sintering	Heating Rate - 770°C/min vs. 5°C/min	49% -> 77%[43]	---
	1050°C/6 hrs vs. 1050°C/24 hrs	81% -> 60%[43]	PbO Loss
	Open Crucible vs Closed Crucible 1100°C/20 hrs.	33% - 80%[34]	PbO Source
Sol-Gel Processing[45]	Calcine 700-800°C/1 hr.	~90%	Improved Reactivity

*Relative Amount of Perovskite Phase Determined from X-Ray Diffraction:

$$\% \text{ Perovskite} = \frac{I_{(110)\ \text{Perov}}}{I_{\text{Perov}} + I_{(222)}\text{Pyrochlore}}$$

Table III. Effect of "Non-Stoichiometry" on the Dielectric Properties of PMN Ceramics.

Parameter	Effect	Comment
PbO Deficiency	Reduction in k[37]	Promotes formation of Pyrochlore and poor densification
MgO Deficiency	Reduction in k[53]	Promotes pyrochlore
PbO Excess	Reduction of k[51,57] Insulation Resistance (IR) Degraded[52,53] *Enhanced k and IR[52,54,55] Increase in Aging[57]	Excess PbO in grain boundary Promotes densification and perovskite phase (*Excess PbO must be driven off through volatilization)
MgO Excess	Increase in k[50,57]	Promotes grain growth and elimination of pyrochlore phase

Table IV. Fabrication of PMN and Various Relaxor Using Columbite (Wolframite) Precursor Method.

Conventional/Columbite (Wolframite)	% Perovskite Phase Conventional/Columbite (Wolframite)
$3PbO+MgO+Nb_2O_5/3PbO+MgNb_2O_6$	70% -> 100%[38,33]
$3PbO+MgO+Ta_2O_5/3PbO+MgTa_2O_6$	60% -> 100%[53]
$3PbO+NiO+Nb_2O_3/3PbO+NiNb_2O_6$	80% -> 100%[59]
$3PbO+Sc_2O_3+Ta_2O_5/3PbO+ScTaO_4$	60% -> 100%[53]
$3PbO+In_2O_3+Nb_2O_5/3PbO+InNbO_4$ (Excess In_2O_3)	20% -> 70%[61] ~95%

Table V. Electronegativity/Tolerance Factors of PZN and Stabilized PZN Perovskites.

Composition	$\Delta\chi$	t
PZN	1.8	0.984
0.94 PZN-0.6BT	1.83	0.988
0.9PZN-0.1BZN	1.845	0.988
$Pb_{1-y}K_y(Zn_{1/3}Nb_{2/3})O_{3-y/2}$ (y=0.1)	1.849	0.988
0.9PZN-0.1ST	1.845	0.9845
0.70PZN-0.30PT	1.815	0.995
0.45PZN-0.55PZ	1.855	0.973
2.25PZN-0.75PMN	1.850	0.988

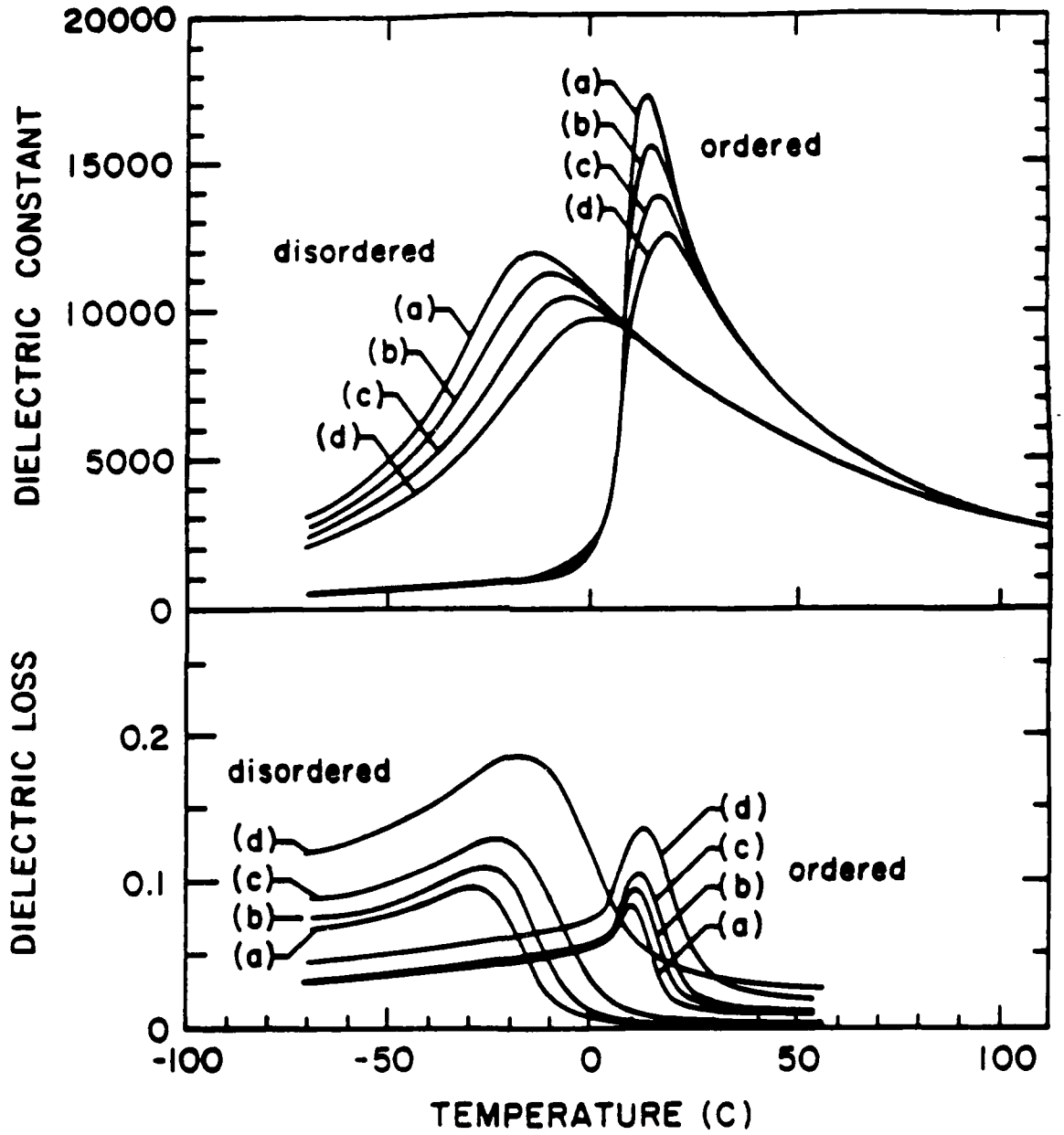
20000
15000
10000
5000
0
DIELECTRIC CONSTANT
(a)
(b)
(c)
(d)
ordered
disordered
(a)
(b)
(c)
(d)
0.2
0.1
0
DIELECTRIC LOSS
disordered
(d)
(c)
(b)
(a)
(d)
(c)
(b)
(a)
ordered
-100
-50
0
50
100
TEMPERATURE (C)

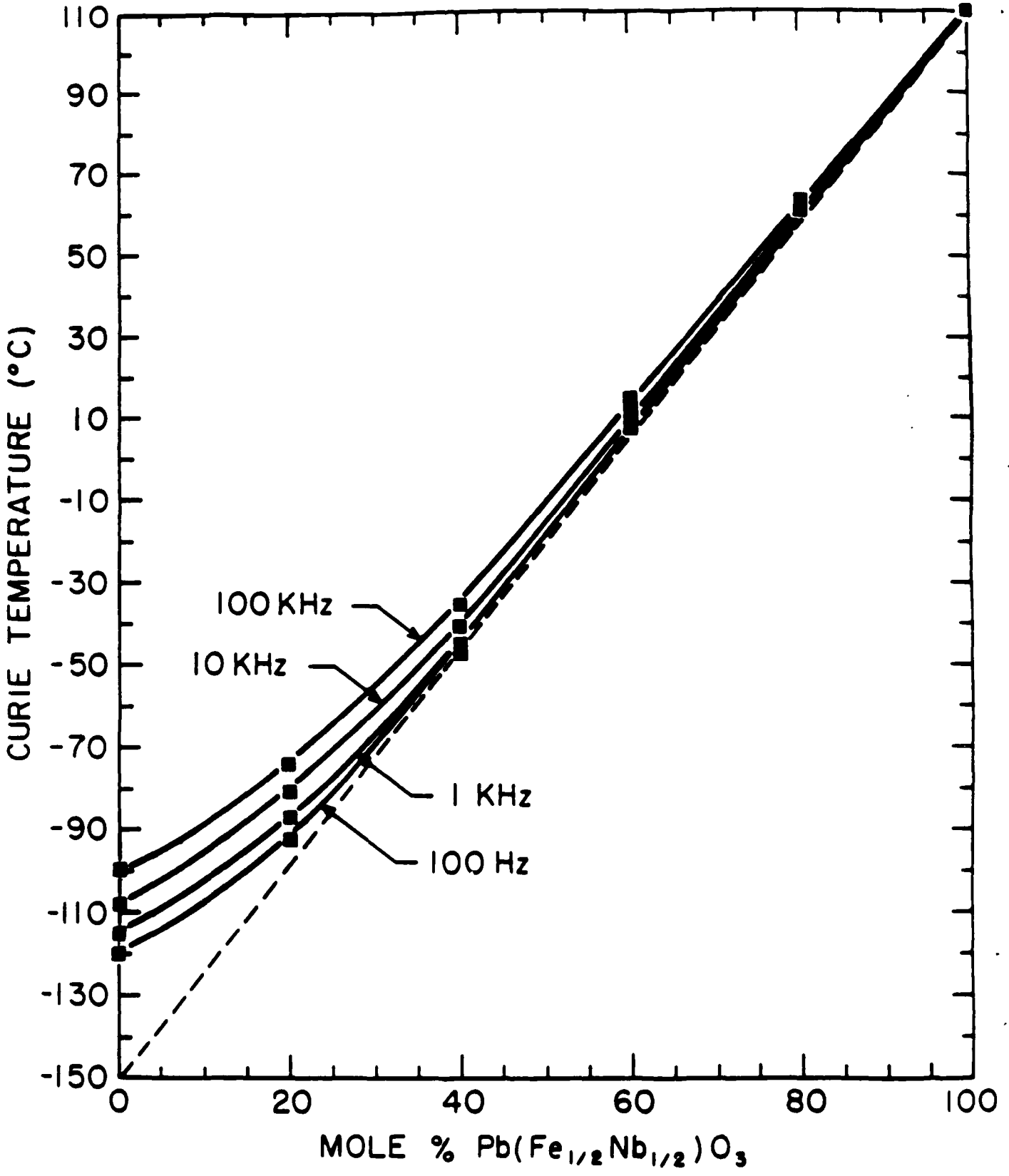
110
90
70
50
30
10
-10
-30
-50
-70
-90
-110
-130
-150
CURIE TEMPERATURE (°C)
100 KHz
10 KHz
1 KHz
100 Hz
0
20
40
60
80
100
MOLE % Pb(Fe1/2Nb1/2)O3

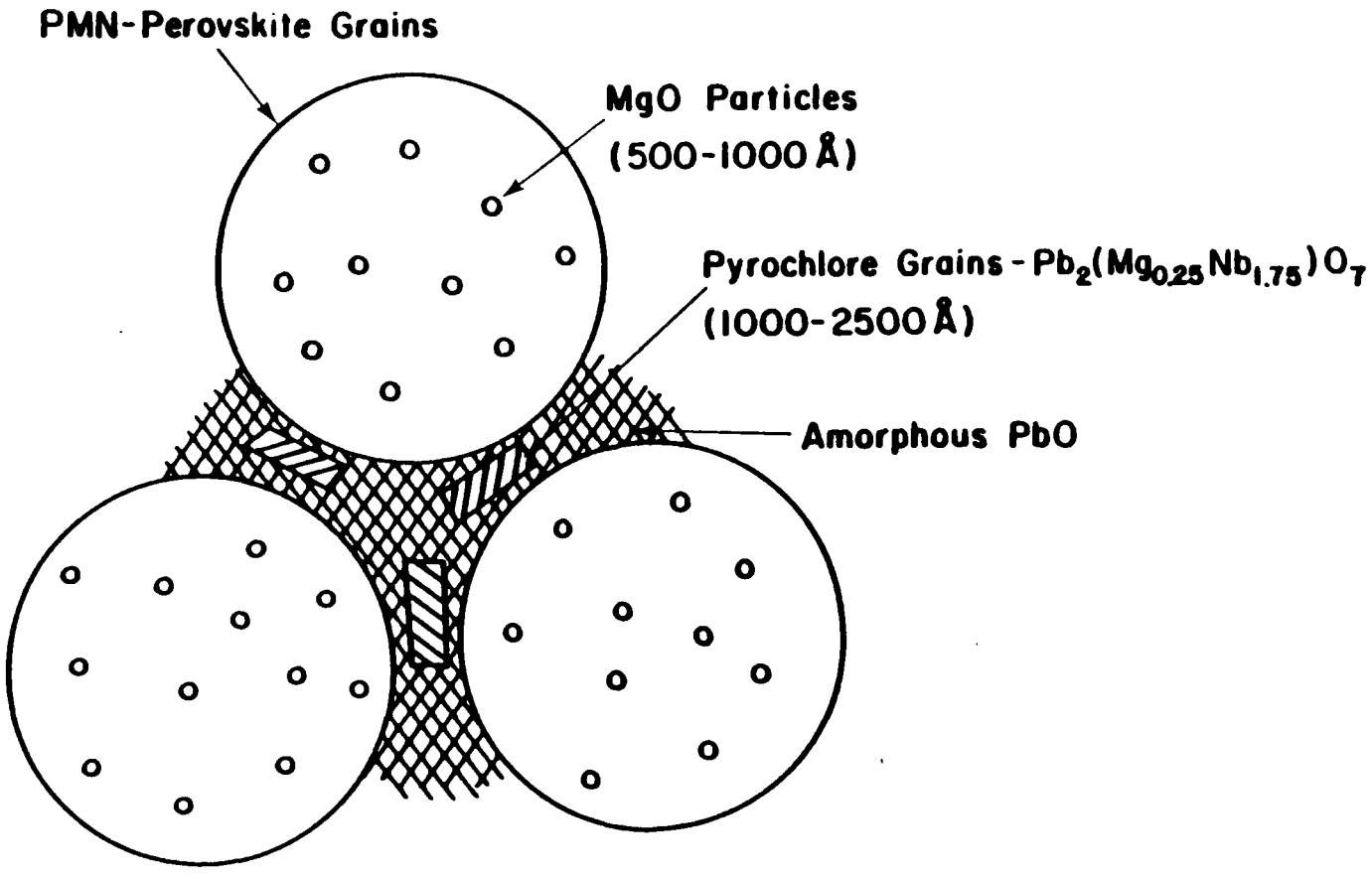
PMN-Perovskite Grains
MgO Particles
(500-1000 Å)
Pyrochlore Grains - $Pb_2(Mg_{0.25}Nb_{1.75})O_7$
(1000-2500 Å)
Amorphous PbO

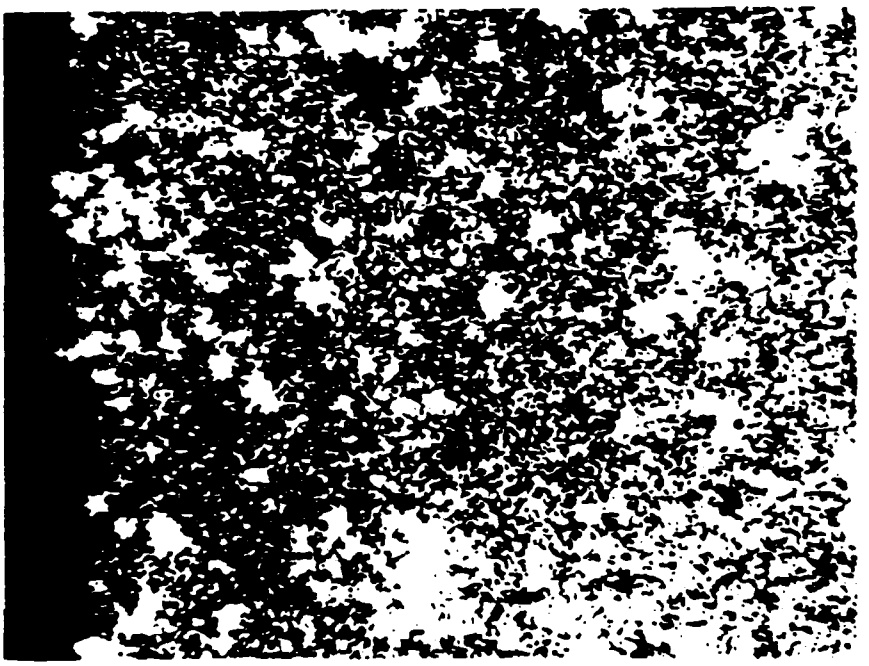

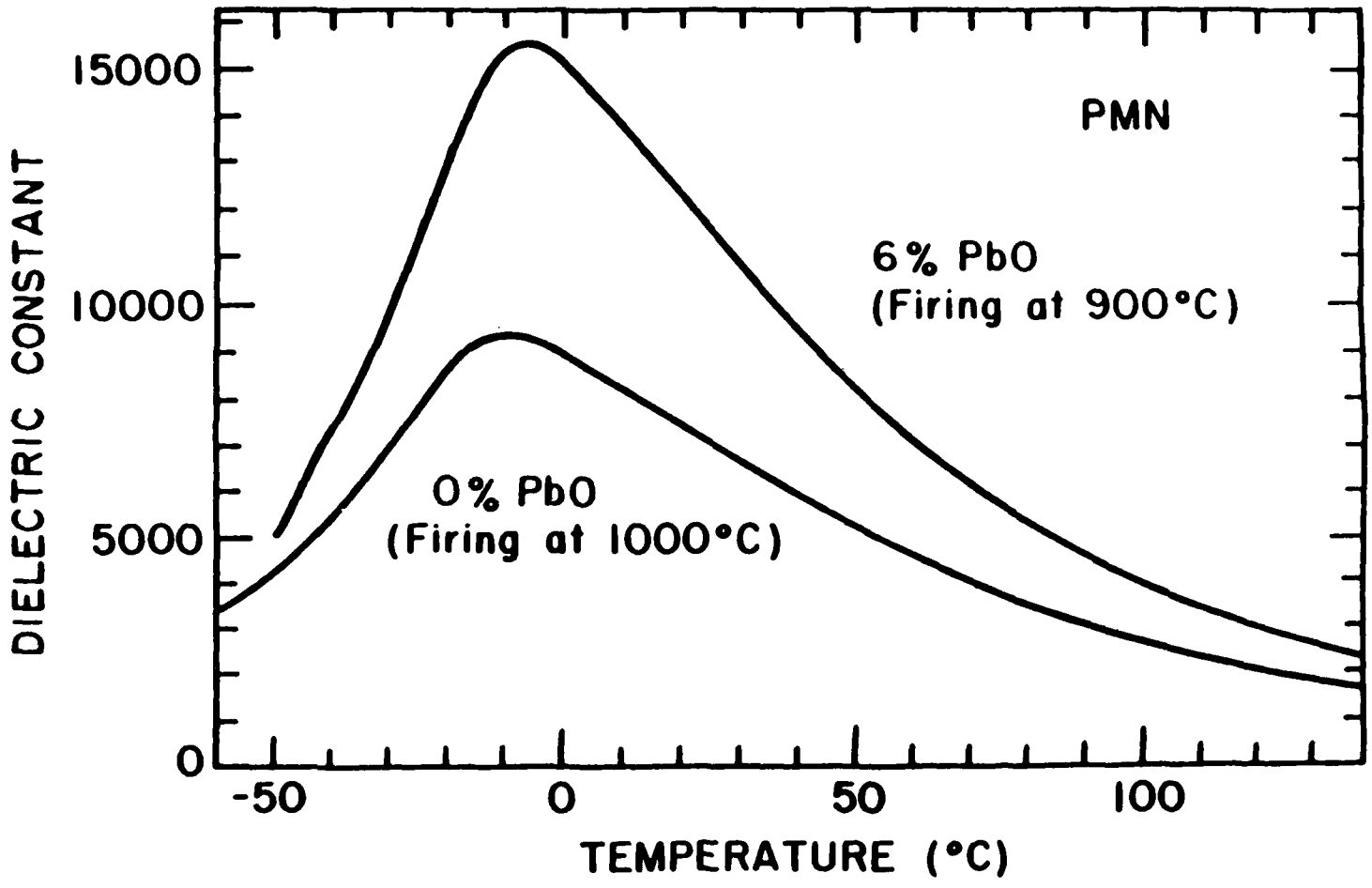
15000
10000
5000
0
DIELECTRIC CONSTANT
PMN
6% PbO
(Firing at 900°C)
0% PbO
(Firing at 1000°C)
-50
0
50
100
TEMPERATURE (°C)

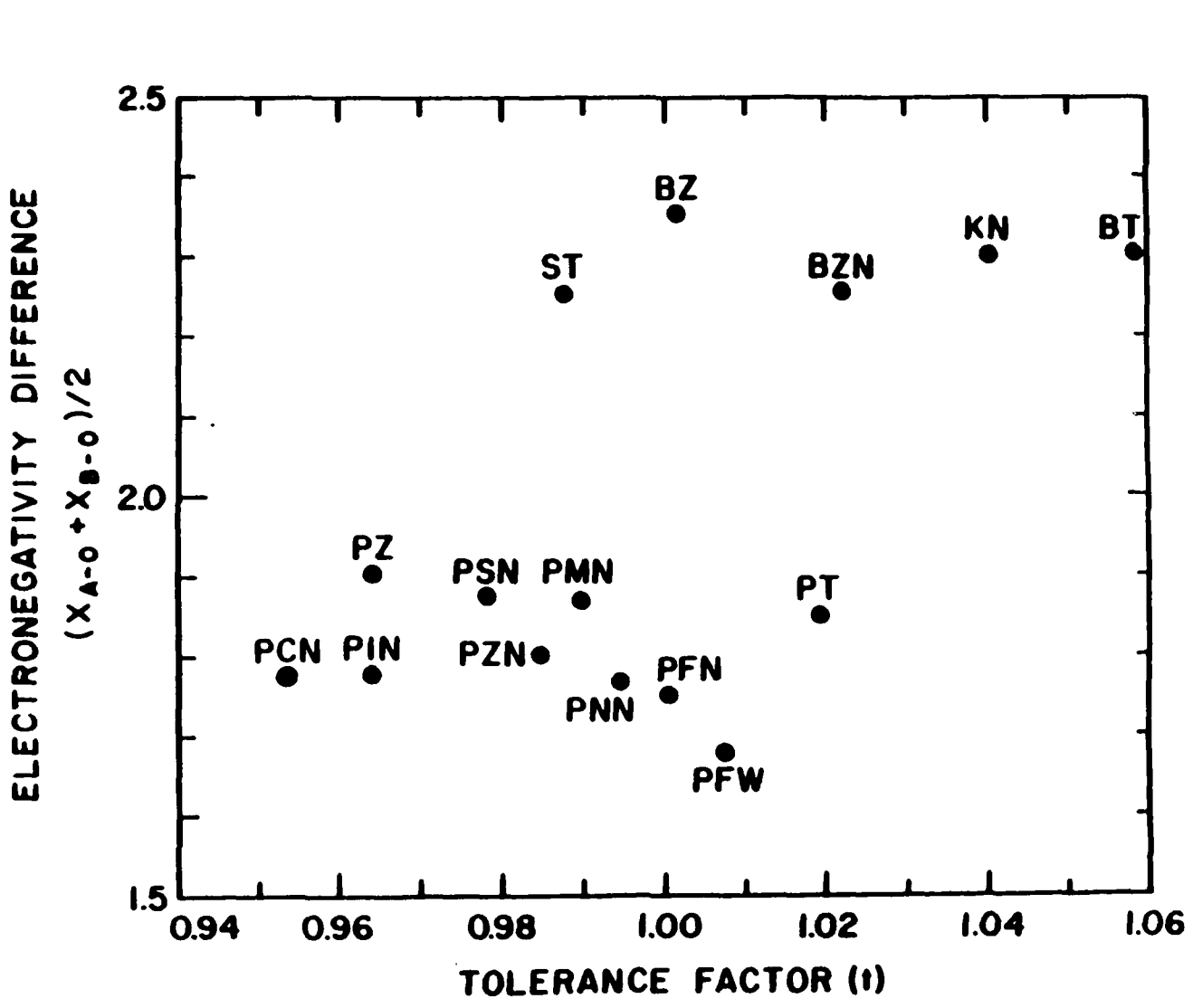
2.5
2.0
1.5
ELECTRONEGATIVITY DIFFERENCE
$(X_{A-O} + X_{B-O})/2$
BZ
KN
BT
ST
BZN
PZ
PSN
PMN
PT
PCN
PIN
PZN
PFN
PNN
PFW
0.94
0.96
0.98
1.00
1.02
1.04
1.06
TOLERANCE FACTOR (t)

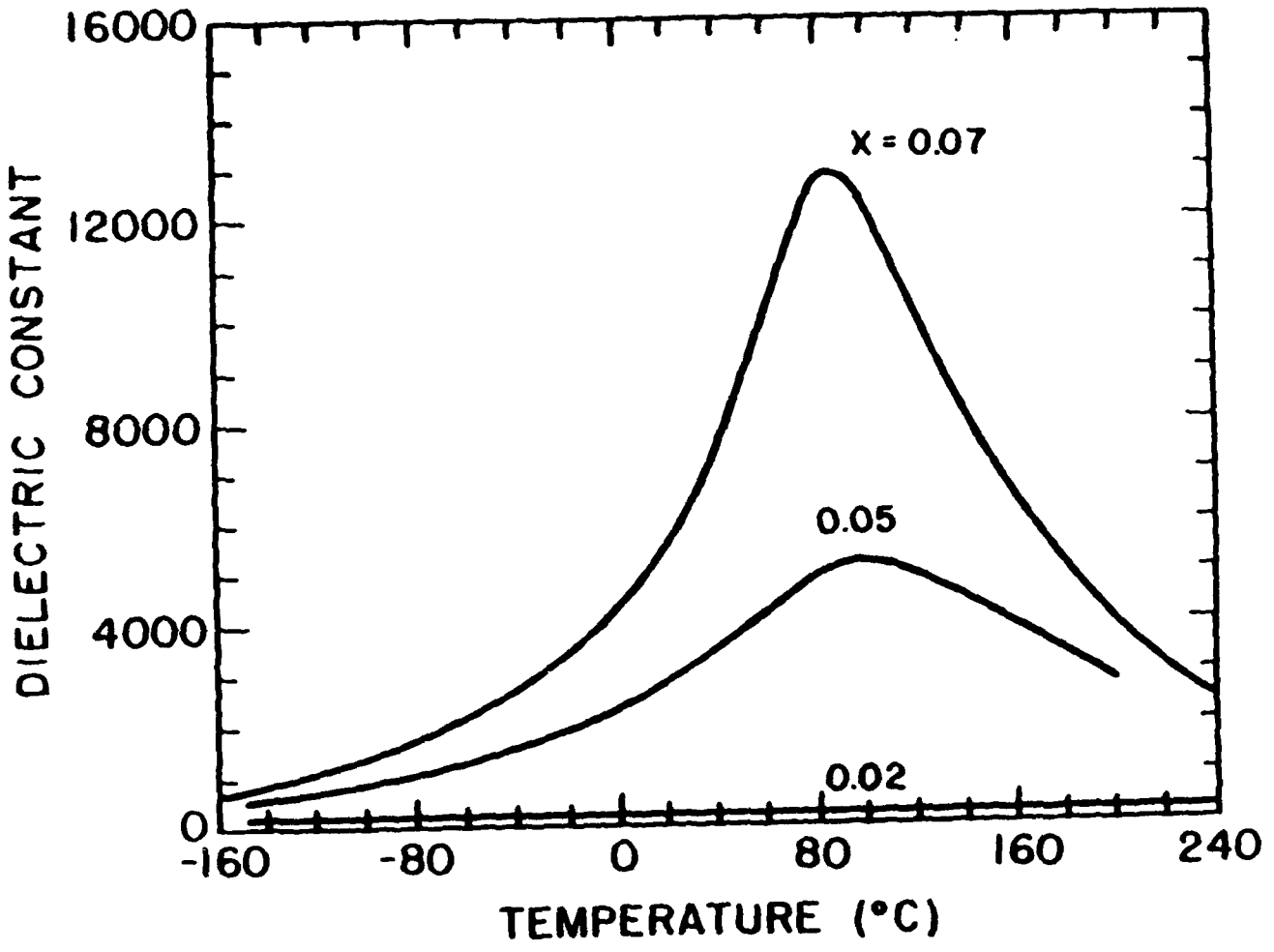
16000
12000
8000
4000
0
DIELECTRIC CONSTANT
X = 0.07
0.05
0.02
-160
-80
0
80
160
240
TEMPERATURE (°C)

GROWTH AND DIELECTRIC PROPERTIES OF LEAD BARIUM NIOBATE SINGLE CRYSTALS AND MORPHOTROPIC PHASE BOUNDARY

M. Adachi*, S.G. Sankar, A.S. Bhalla, Z.P. Chang and L.E. Cross

Materials Research Laboratory
The Pennsylvania Sate University
University Park, PA 16802

Abstract

Single crystals of lead barium niobate (PBN) belonging to the tetragonal tungsten bronze structures possess many desirable properties for potential applications in electro-optic, piezoelectric and pyroelectric devices. In the solid solution $PbNb_2O_6$-$BaNb_2O_6$, substitution of barium for lead first decreases the orthorhombic distortion and later stabilizes the tetragonal structure. A morphotropic phase boundary exists at about $Pb_{0.6}Ba_{0.4}Nb_2O_6$. Current understanding based on phenomenological calculations on related materials indicate that electro-optic and dielectric properties of PBN should exhibit considerable enhancement near the morphotropic phase boundary and that they should be largely temperature-independent over a reasonably large range of temperature. As a result of this motivation, we have grown single crystals of $Pb_{1-x}Ba_xNb_2O_6$ employing Czochralski technique. Results of dielectric constant of two compositions in the orthorhombic structure with x = 0.37 and 0.40 and one composition in the tetragonal structure with x = 0.65 are reported in this paper. These results largely confirm the predictions made by the phenomenological thermodynamic theory.

1. Introduction

Among the various ferroelectric materials, a number of niobates having tetragonal or related orthorhombic tungsten-bronze structure have attracted a great deal of attention due to their potential applications in electro-optic, nonlinear optic, bulk wave and surface acoustic wave devices [1]. The tungsten-bronze materials with over 150 individual end member compositions and with numerous possible solid solutions offer one of the most versatile, extensive and potentially useful families of oxygen octahedra based ferroelectrics [2].

One of the tungsten-bronze ferroelectrics, $PbNb_2O_6$ was discovered by Goodman in 1953 [3]. After this discovery, a great deal of effort on related materials took place. Device applications in quantum electronics, ultrasonics and related fields were explored. In the solid solution $PbNb_2O_6$-$BaNb_2O_6$ system, the substitution of Ba for Pb first decreases the orthorhombic distortion and then stabilizes a tetragonal structure with compositions up to $Pb_{0.2}Ba_{0.8}Nb_2O_6$. A morphotropic phase boundary exists near the composition $Pb_{0.6}Ba_{0.4}Nb_2O_6$ [4]. Properties of single crystals with compositions close to the boundary are of major importance from fundamental as well as technological viewpoints. Considerable effort has been devoted in this Laboratory to elucidate the behavior of materials near the morphotropic phase boundary employing phenomenological thermodynamic calculations [5,6]. This paper describes the growth conditions of single crystals of $Pb_{1-x}Ba_xNb_2O_6$ with x = 0.37, 0.40 (orthorhombic) and with x = 0.65 (tetragonal). The first two compositions are in the vicinity of the morphotropic phase boundary and the third composition is far away from the boundary (see Fig. 1).

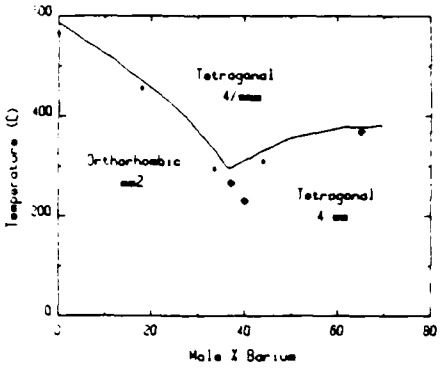

Figure 1. Phase diagram of $Pb_{1-x}Ba_xNb_2O_6$. The smooth line is based on work using ceramic samples (Ref. 5). The asterisks are based on single crystals (Ref. 8,9). Filled diamonds are from present work.

2. Experimental

Single crystals of $Pb_{1-x}Ba_xNb_2O_6$ were grown by the Czochralski technique from melts using CRYSTALOX MCGS3 crystal growth system containing a sealed enclosure. The starting compositions are specified here by the value of x in formula

*Present Address: Department of Electronics, Faculty of Engineering, Kyoto University, Sakyo, Kyoto 606, Japan.

$Pb_{1-x}Ba_xNb_2O_6$. The attempted values for x in this study are 0.37, 0.40 and 0.65. The raw materials were Specpure grade PbO, $BaCO_3$ and Nb_2O_5 obtained from Johnson-Matthey, Inc. These oxides were weighed, mixed well in the appropriate stoichiometry and ball-milled together with ethanol for about 12 to 24 h in a small polyethylene container. The resulting slurry was air dried and then fired in an alumina crucible at 1050°C for 3 h. The fired product was crushed in a mortar and pestle. An excess of 10 wt% PbO was added into the above crushed powder to compensate for losses due to volatilization during the crystal growth. These powders were re-mixed, dried and fired at 750°C for 10 h. This procedure was adopted to ensure that lead was in a fully oxidized state before being placed in the platinum crucible. The mixture was loaded in the platinum crucible and melted by rf-heating. The crucible was 40 mm in both diameter and height, and was supported in an alumina crucible. A platinum after-heater was employed to reduce vertical and radial thermal gradients above the melt surface and to minimize heat losses from the crucible. As seed materials, both Pt wires and PBN crystals were used [7,8]. The pulling axis was chosen parallel to the a-axis in order to minimize cracking taking place during the growth. The growth rates were ~2 mm/hr with a rotation of 10-15 rpm. All growth experiments were carried out in an O_2 pressure of around 24 psi to reduce volatilization of PbO. The grown crystals were annealed in-situ by programming the over a 48 hour period.

X-ray diffraction measurements were performed by means of a diffractometer using Ni filtered CuKα radiation. Lattice constants a, b, and c were calculated using reflection peaks in the 2θ = 20 to 60° range.

The dielectric constants ε (c⊥) and ε (c//) were measured at 10, 100, 1,000 and 10,000 kHz using HP 4275A frequency LCR meter under full program control from room temperature to 400°C.

3. Results and Discussion

Transparent and pale-yellow single crystals of PBN have been obtained in this study. In spite of a number of attempts, it was not possible to grow reasonably large and crack-free crystals. Crystals often contained cracks presumably due to the thermal stress unavoidably generated when cooled below the Curie temperature. However, several single crystals of approximately 10x5x5 mm sizes were recovered for further characterization. The easy direction of crystal growth was determined to be along <110>.

Compositions of single crystals grown in this work have been determined by chemical analysis. X-ray powder diffraction analyses on two crystals showed that $Pb_{0.35}Ba_{0.65}Nb_2O_6$ belonged to the tetragonal structure with room temperature lattice constants a = b = 12.57 and c = 3.966 Å. Similarly, x-ray powder diffraction analyses of $Pb_{0.60}Ba_{0.40}Nb_2O_6$ indicated that it belonged to orthorhombic structure with lattice constants a = 17.71, b = 17.89 and c = 3.919 Å.

The temperature dependence of dielectric constants ε (c⊥) and ε (c//) and loss (tan δ) were determined on unpoled [001] and [100] or [010] plates at frequencies 10, 100, 1000, and 10,000 kHz. For $Pb_{0.35}Ba_{0.65}Nb_2O_6$, ε (c⊥) and ε (c//) are equal to ε^T_{11} and ε^T_{33}, respectively. On the other hand, ε (c//) is ε^T_{33}, but ε (c⊥) is not equal to ε^T_{11} or ε^T_{22} for samples with the orthorhombic structure because they were not poled in the present study. The temperature dependence of dielectric constants at 10 kHz are shown in Figs. (2)-(4). As can be seen from Fig. (2), the dielectric constants $\varepsilon^T_{11}/\varepsilon_0$ and $\varepsilon^T_{33}/\varepsilon_0$ at room temperature were 196 and 286, respectively. The constant ε^T_{33} shows marked anomaly at the transition point of 370°C. On the other hand, the dielectric constant ε^T_{11} does not show any anomaly and decreases gradually with increasing temperature. This temperature behavior and large anisotropy of ε^T_{33} and ε^T_{11} is typical of most tetragonal ferroelectric bronzes such as $K_3Li_2Nb_5O_{15}$ [3].

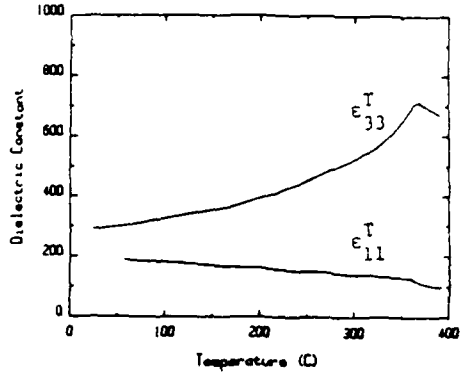

Figure 2. Dielectric constant (ε^T_{33} and ε^T_{11}) vs. temperature for tetragonal $Pb_{0.35}Ba_{0.65}Nb_2O_6$ measured at a frequency of 10 kHz.

In Figs. 3 and 4, the constant ε (c⊥) display marked anomalies at transition points and constants ε^T_{33} show very little anomalies at the transition temperatures. In Figs. 3 and 4, two characteristic features may be noted. One is that the Curie temperature moves markedly to higher temperature and the peak of dielectric constant ε (c⊥) broadens and its value becomes smaller with decreasing x. The other feature is that the Curie temperature of 235°C for $Pb_{0.6}Ba_{0.4}Nb_2O_6$ is the minimum value in the $PbNb_2O_6$-$BaNb_2O_6$ system [4]. Therefore, the sample $Pb_{0.6}Ba_{0.4}Nb_2O_6$ is very close to the reported morphotropic phase boundary. Little frequency dependence of the dielectric constants was observed in all the samples investigated in this study from room temperature to their Curie temperatures.

It may be noted that according to thermodynamic phenomenological theory, the dielectric stiffness in the orthorhombic form is given by

$$X^T_{33} = 2a_{30}(T-\theta_3) + 4a_{13}P_1^2$$

where a's are thermodynamic constants and P_1 is the polarization. In compositions near the morphotropic phase boundary and at temperatures just below θ_1, when T becomes less than θ_3 the first term in the above expression will be

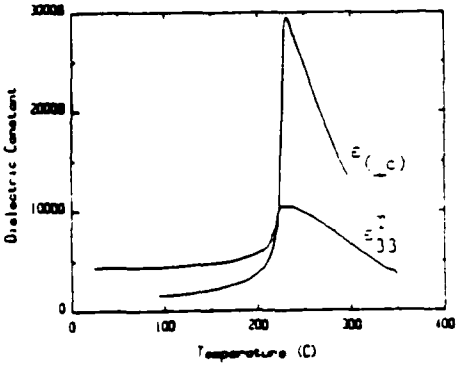

Figure 3. Dielectric constant (ε^T_{33} and $\varepsilon_{\perp c}$) vs. temperature for orthorhombic $Pb_{0.63}Ba_{0.37}Nb_2O_6$ measured at a frequency of 10 kHz.

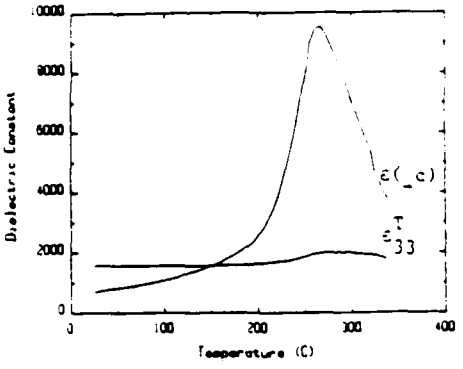

Figure 4. Dielectric constant (ε^T_{33} and $\varepsilon_{\perp c}$) vs. temperature for orthorhombic $Pb_{0.60}Ba_{0.40}Nb_2O_6$ measured at a frequency of 10 kHz.

negative. Since P_1^2 increases more slowly than linear below θ_1, the linearly increasing magnitude of the first negative term destabilizes the polarization and χ^1_{33} becomes very small. Consequently the dielectric constant ε_{33} becomes large. Also in view of the balance of positive and negative terms the above expression, the temperature dependence of these large values of dielectric constant should be smaller than in normal ferroelectrics. An examination of the temperature dependence of the dielectric constant for the two orthorhombic compositions (see Figs. 3 and 4) reveal that the above predictions based on simple phenomenological calculations are confirmed in practice.

4. Conclusions

Single crystals with compositions $Pb_{0.63}Ba_{0.37}Nb_2O_6$, $Pb_{0.60}Ba_{0.40}Nb_2O_6$ and $Pb_{0.35}Ba_{0.65}Nb_2O_6$ have been grown. The first two crystals belong to orthorhombic structure, mm2 symmetry and the third composition belongs to tetragonal structure, 4mm symmetry. Dielectric constant measurements indicate that the orthorhombic crystals show reasonably large dielectric constants which are fairly temperature independent in conformity with the phenomenological thermodynamic theory. Further work exploring the low temperature behavior of these crystals is in progress.

5. Acknowledgement

This work is supported by the Office of Naval Research and Rockwell International.

References

1. M.H. Francombe and B. Lewis, "Structural, Dielectric and Optical Properties of Ferroelectric Lead Metaniobate," Acta Cryst., Vol. 11, pp. 696-703, 1958.
2. Landolt Bornstein, Ferroelectrics and Related Substances, K.H. Hellwege and A.M. Hellwege, Eds., New York, Springer-Verlag, 1981.
3. G. Goodman, "Ferroelectric Properties of Lead Metaniobate," J. Amer. Ceram. Soc., Vol. 36, pp. 368-372, 1953.
4. E.C. Subbarao, G. Shirane and F. Jona, "X-ray, Dielectric and Optical Study of Ferroelectric Lead Metatantalate and Related Compounds," Acta Cryst., Vol. 13, pp. 226-231, 1960.
5. A. Amin and L.E. Cross, "The Ferroic Phase Transition Behavior of $PbZr_{0.6}Ti_{0.4}O_3$," Ferroelectrics, Vol. 50, pp. 237-241, 1983.
6. M.J. Haun, Z.Q. Zhuang, S.J. Jang, H.A. McKinstry and L.E. Cross, "A Phenomenological Theory for the Second Order Transition Region of the PZT Solid Solution System," Proceedings of this Symposium.
7. T.R. Shrout, L.E. Cross and D.A. Hukin, "Ferroelectric Properties of Tungsten bronze Lead Barium Niobate Single Crystals," Ferroelectrics Letters, Vol. 44, pp. 325-330, 1983.
8. T.R. Shrout, H.C. Chen and L.E. Cross, "Dielectric and Piezoelectric Properties of Tungsten Bronze Lead Barium Niobate Single Crystals," European Meeting on Ferroelectrics EMF5, Spain, 1983.

GROWTH AND PYROELECTRIC PROPERTIES OF ALANINE AND PHOSPHORUS SUBSTITUTED TRIGLYCINE SELENATE (TGSe) SINGLE CRYSTALS

X.S. Lin , A.S. Bhalla, and L.E. Cross

Materials Research Laboratory
The Pennsylvania State University
University Park, PA 16802

Abstract

Phosphorus and alanine doped triglycine selenate (LATGSeP) crystals have been grown with partial substitution of H_2SeO_4 with H_3PO_4. LATGSeP has higher pyroelectric coefficients and dielectric constant than those of TGSe, and its pyroelectric figure of merit ($2.2x10^{-5}$ C/m^2K) is similar in magnitude to those obtained on ATGSP and ATGSAs crystals. Single crystal LATGSeP grown at 35°C under optimum conditions were crack-free and colorless.

The triglycine sulphate (TGS) family of ferroelectric crystals has many attractive features for a number of pyroelectric applications. Various dopants or substitutions for the $(SO_4)^{2-}$ group have been extensively tried in order to enhance the pyroelectric properties of TGS [1].

In the TGS family, triglycine selenate (TGSe) has recently become of major interest since its very high pyroelectric coefficient and high dielectric permittivity at room temperature have shown a good compatibility with some CCD readout schemes for pyroelectric imaging [2-3].

In this paper we report a) the growth of alanine and phosphorus substituted single crystals of TGSe at about 35°C and b) the result of dielectric and pyroelectric properties measured as a function of temperature. The computed pyroelectric figure of merit p/K of ATGSeP showed an improvement of the p/K values obtained on TGSe single crystals.

Pure TGSe crystals are very difficult to grow from water solution. In solution containing high concentration of the selenate, decomposition leads to precipitation of finely divided selenium which contaminates the growing crystals. This problem can be reduced by growing crystals in a refrigerated water bath at ~5°C, but controlling the growth rate is difficult and the procedure is also inconvenient. Addition of alanine to solution raises the viscosity so the crack-free crystals are in general very difficult to grow [4].

Single crystals of LATGSeP were grown by slow cooling of the saturated solution with composition $(NH_2CH_2COOH)_{3(1-y)}\cdot(NH_2CH(CH_3)COOH)_{3y}\cdot(1-x)H_2SeO_4\cdot xH_3PO_4$.

In our present attempts, single crystals of LATGSeP were grown from bath at about 35°C and control chemically the decomposition of LATGSeP solutions. Unfortunately for high substitution of PO_4^{3-} the crystals became more susceptible to mechanical cracking. Low level substitutions of phosphates resulted in unclear crystals with poor pyroelectric properties. Only the crystals with appropriate phosphorus content and low growth rate exhibit excellent pyroelectric properties.

The differences in crystal growth habits compared to those of pure TGSe have been observed. The ±b faces of crystals were prominent while a faces were elongated than those of pure TGSe.

Thin samples were cut and polished to a thickness ~0.5 - 1 mm and were coated on both sides with sputtered gold electrodes 4 mm in diameter. Pyroelectric and dielectric properties were measured on these plates in the temperature range from -10~40°C. Pyroelectric coefficients were measured by Byer-Roundy technique [5] and dielectric measurements were made by using the multi-frequency LCR bridge [1].

Figure 1 (a) (b) and (c) show the plots of p versus T, P_s versus T, and M (p/K) versus T behavior on LATGSeP crystals.

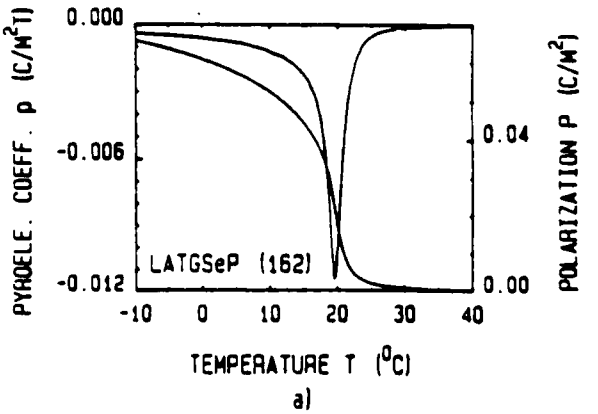

a)

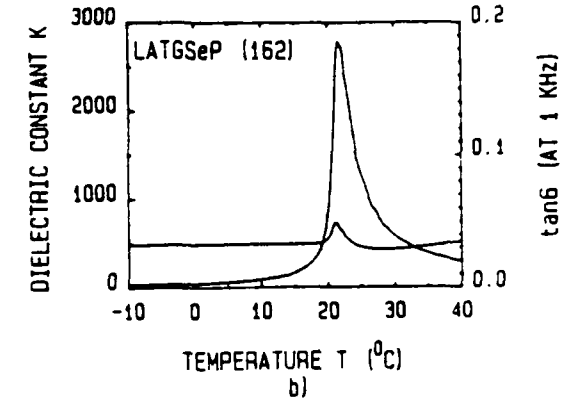

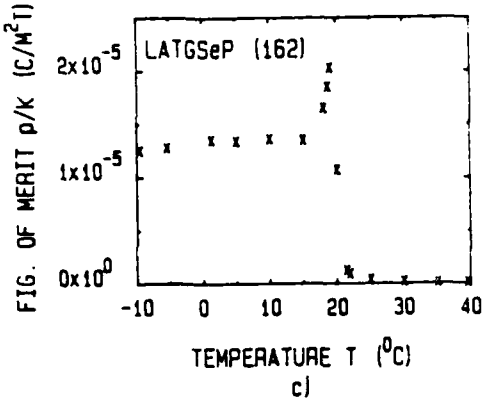

Figure 1. Temperature dependence of polarization P, p, k, and p/k of LATGSeP single crystals.

The best pyroelectric figure of merit M in the case of LATGSeP is similar in magnitude to those obtained on ATGSP crystals.

Table 1 summarizes the results of the experiments and shows the comparison with the corresponding values of the TGS family [1,4].

The Curie point is 21.5°C which is 1°C lower than that of pure TGSe. The pyroelectric coefficient of LATGSeP at (T_c-1.5°C) is about 15×10^3 $\mu C/m^2$-K compared to the pure TGSe crystal value of 3.5×10^3 $\mu C/m^2$-K.

Alanine doped crystals of LATGSeP showed no sign of depoling after repeated heating through T_c, (about 30°C above T_c). Figure 2 shows the hysteresis loop, and internal bias of about 4 kV/cm in LATGSeP single crystals.

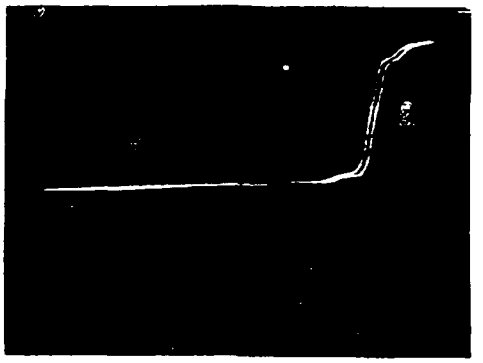

Figure 2. The hysteresis loop of LATGSeP single crystal.

The chemical analysis of the phosphorus content in crystals of LATGSeP showed that only 0.02wt% of P was incorporated in the crystals. It is evident that the small content of phosphorus in the single crystals can markedly effect the pyroelectric and dielectric properties of TGSe. The results on pure TGSe and TGSeP are compared in

Table 1. Pyroelectric Properties of the TGS Family (Optimum Temperature).

Material	K	p ($\mu C/m^2$ K)	P_s ($\mu C/cm^2$)	T_c (°C)	p/K (10^{-5} C/m^2 K)
TGS	30	330	3.0	49	1.1
DTGS	19	270		62	1.4
TGFB	14-16	210-140		73	1.5
DTGFB	11-14	190-240	4.3	75	1.7
LTGS	40	400	3.7	49	1.0
MTGS	40	560	4.6	49	1.2
ATGSP (25°C)	30-32	650	5.0	51	2.0
ATGSAs (25°C)	32	700	6.0	51	2.1-2.3
ADTGSP	22	460	5.3	60	2.1
ADTGSAs	23	500	6.2	62	2.2
LATGSeP (-6°C)	31-41	400	5-7	21.5	1.3
(20°C)	900	10^4			2 ~ 2.2

Table 2. There is a significant improvement in the figure of merit (p/K) of TGSeP over that of pure TGSe.

Table 2. Some Properties of TGS, TGSe and LATGSeP Crystals.

	TGS	TGSe		LATGSeP	
T_c (°C)	49.5°C	22.5		~21.5	
K_{max}	7.5×10^4 (1.6 kHz)	4.6×10^4 (1.6 kHz)		$2.0 \sim 3.7 \times 10^3$ (1.0 kHz)	
K	38 (21°C)	420 (21°C)	36 (-6°C)	412~922 (20°C)	31~45 (-6°C)
p (C/m^2-K)	3.5×10^{-4}	42×10^{-4}	2.1×10^{-4}	150×10^{-4}	5×10^{-4}
M = p/K (C/m^2-K)	11×10^{-6}	10×10^{-6}	5.8×10^{-6}	19.7~21.9 $\times 10^{-6}$	8~13 $\times 10^{-6}$
P_s ($\mu C/cm^2$)	3.2	~4			~6

There is no significant change in the T_c of TGSe as a result of phosphorus doping but the value of P_s of TGSeP single crystals showed an increase of about 50% over that of pure TGSe. Similar results have been observed in the case of TGS and TGSP. This increase as reported earlier, could be due to the temperature dependence of β, γ,.... and can be explained by the inclusion of the higher order terms in the Devonshire function for describing the energy function for this family.

We wish to thank Mr. H. Gong for chemical analysis.

References

[1] A.S. Bhalla, C.S. Fang, and L.E. Cross, Materials Letters 3 (1985) 475.
[2] K.L Bye, P.W. Whipps, E.T. Keve, and M.R. Josey, Ferroelectrics 7 (1976) 179-181.
[3] G.M. Loiacono, A. Shaulov, D. Dorman, J. Jacco and G. Kostecky, J. Crystal Growth 60 (1982) 29.
[4] K.L. Bye, P.W. Whipps, E.T. Keve and M.R. Josey, Ferroelectric 11 (1976) 525-534.
[5] R.L. Byer and C.B. Roundy, Ferroelectrics 3 (1972) 333.

GROWTH, DIELECTRIC AND PYROELECTRIC PROPERTIES OF $0.9Pb(Zn_{1/3}Nb_{2/3})O_3$-$0.1PbTiO_3$ SINGLE CRYSTALS

C.P. Chang, A.S. Bhalla and L.E. Cross

Materials Research Laboratory
The Pennsylvania State University
University Park, PA 16802

Abstract

Single crystals of $0.9Pb(Zn_{1/3}Nb_{2/3})O_3$-$0.1PbTiO_3$ were grown using the flux method. The dielectric property along the pseudocubic [111] and [100] directions was measured as a function of temperature and frequency. The effects of poling and DC bias field were investigated. The pyroelectric property along these two directions was also measured.

1. Introduction

The $Pb(Zn_{1/3}Nb_{2/3})O_3$-$PbTiO_3$ (PZN-PT) system is known to have a near morphotropic phase boundary between the tetragonal and rhombohedral phase in the range of 9 to 9.5 mole% $PbTiO_3$. Crystals with more than 9.5% $PbTiO_3$ show tetragonal symmetry, while those with less than 9% $PbTiO_3$ show rhombohedral symmetry [1]. Crystals with 9% $PbTiO_3$ were found to have very large dielectric and piezoelectric constants [2].

In this paper the growth and characterization of crystals with starting compositions 0.9PZN-0.1PT are discussed. The dielectric and pyroelectric properties along the pseudocubic [111] and [100] directions and the effects of poling and DC bias field on the dielectric behavior are also investigated.

2. Crystal Growth

Single crystals of $0.9Pb(Zn_{1/3}Nb_{2/3})O_3$-$0.1PbTiO_3$ (PZN0.1PT) were grown from molten PbO flux by slow cooling. Starting materials were PbO, ZnO, Nb_2O_5 and TiO_2 in stoichiometric proportion. A compound to flux ratio of 1:2 in mole was used. The charge was placed in a platinum crucible and heated to 1230°C. After a soaking period of 5 hrs, the charge was slowly cooled at a rate of 3-5°C/hr to 900°C and then to room temperature in 24 hrs. The PbO flux was removed by dissolving in hot acetic acid.

The crystals obtained are mostly in the form of an arrowhead or irregular in shape with a linear dimension of 1 to 3 mm, and have brown color. Some smaller crystals also show rectangular faces and have lighter color. Back reflection Laue technique reveals that the pseudocubic [111] direction is along the direction of the arrowhead and the [100] direction is normal to the rectangular face. X-ray powder diffraction patterns do not index as a single phase. Imposing a rhombohedral symmetry results in the parameters a = 4.050Å and α = 80°54' which account for certain lines, whereas imposing a tetragonal symmetry results in a = 4.028Å, c = 4.084Å which account for the rest of the lines. These values agree very well with the values for the two phases as shown in Fig. 1 in Reference [1], indicating that both the rhombohedral and tetragonal phases coexist. In the above analysis, a computer program using Appleman's least-squares method for cell refinement [3] was used.

Composition analyses by electron microprobe were performed on arrowhead-shaped and rectangular samples from two growth trials. The composition for each sample was obtained from averaging the values at five locations, the two arrowhead-shaped samples have 0.113 and 0.117 parts of Ti in the oxide form while the two rectangular ones have 0.117 and 0.129 parts. The overall average of Ti is found to be .119 parts whereas Zn is less than the proportion in the starting formula $PbZn_{.3}Nb_{.6}Ti_{.1}O_3$. Loss of ZnO through evaporation took place during growth due to the higher initial temperature.

3. Dielectric Properties

Samples in platelet form with the major face normal to the pseudocubic [111] or [100] direction were prepared. Back reflection Laue method was used in orienting samples. The dielectric constant K and loss along the pseudocubic [111] and [100] directions were measured as a function of temperature at four frequencies: 0.1, 1, 10 and 100 KHz and for unpoled and poled states. Poling was effected by cooling the sample from 200°C to 0°C under a DC field of 10 KV/cm. Figs. 1 and 2 show the dielectric constant and loss as a function of temperature for unpoled samples in the [111] and [100] directions, respectively. They show the behavior of a relaxor type ferroelectric. Near room temperature there is a diffused transition from the rhombohedral to tetragonal phase, and at 175°C a transition from the tetragonal to cubic phase with increasing temperature.

Figs. 3 and 4 show the effect of poling. Poling along the [111] and [100] directions has a very different effect on the K vs T curves. When poled along [111], K rises sharply at the rhombohedral to tetragonal (R-T) phase transition, reaching a value of 12,000 slightly above the

CH2358-0/86/0000-0482 $1.00 © 1986 IEEE

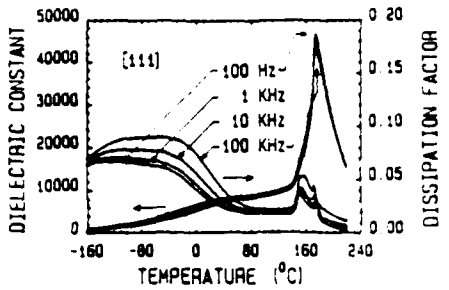

Figure 1. Dielectric constant and loss in [111] direction.

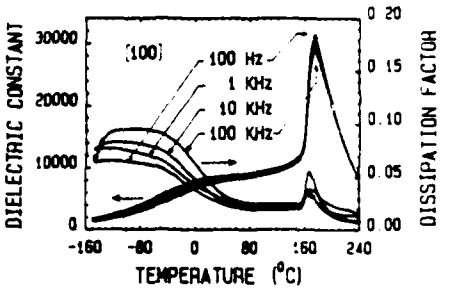

Figure 2. Dielectric constant and loss in [100] direction.

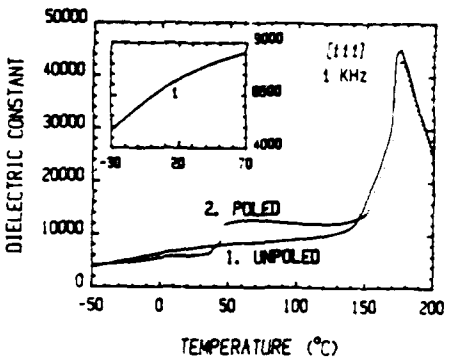

Figure 3. Effect of poling in [111] direction.

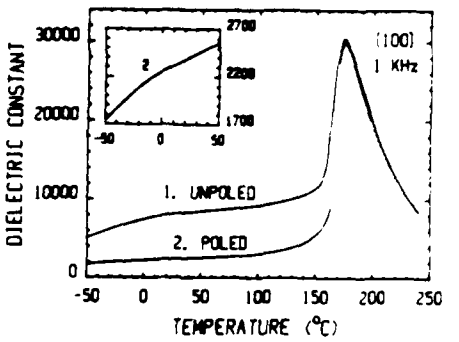

Figure 4. Effect of poling in [100] direction.

transition. For the diffused R-T transition in the unpoled state, if one defines a transition temperature T_{R-T} by the intersection of the tangents on both sides of the transition, it is seen that poling shifts T_{R-T} from 23° to 47.3°C. When poled along [100], K is reduced by a factor of 4 in the temperature range between 20 and 140°C in which the tetragonal phase is stable in the unpoled state and T_{R-T} is shifted from 15° to -16°C as shown in the inset of Fig. 4. There is no sharp change of K at T_{R-T}.

Figs. 5 and 6 show the effect of DC bias field on poled samples. For [111] samples, bias field shifts T_{R-T} and T_{T-C} toward higher temperatures. For [100] samples, bias field shifts T_{T-C} toward higher temperature but shifts T_{R-C} toward lower temperature. The rates of shifting are shown in Table 1.

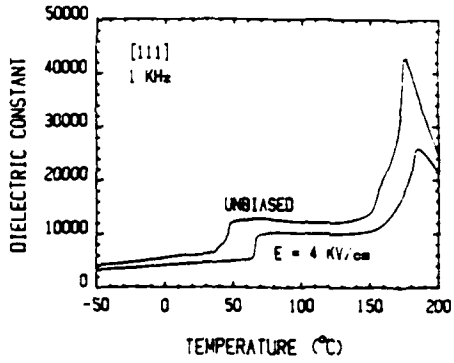

Figure 5. Effect of DC bias field in [111] direction.

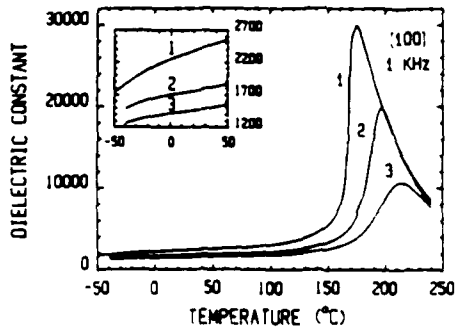

Figure 6. Effect of DC bias field in [100] direction. 1. Bias = 0, 2. 5.3 kV/cm, 3. 10.5 kV/cm.

Table 1. Rate of Shifting (in units of °C cm/kV).

	dT_{R-T}/dE	dT_{T-C}/dE
[111]	4.9	2.6
[100]	-0.9	4.9

Since the polarization in the rhombohedral phase is along [111], and in the tetragonal phase along [100], poling and DC bias field in the [111] or [100] direction tend to extend the temperature range for the rhombohedral or tetragonal phase respectively. Large change in dielectric constant K//[111] due to the shifting of T_{R-T} by DC bias field as in the temperature range between 50 and 65°C in Fig. 5 has potential applications especially if the transition temperature can be lowered to room temperature either by some dopants or change in composition.

4. Pyroelectric Properties

Prior to the pyroelectric measurements, the samples were poled by cooling from 220 to -50°C under a DC field of 10 kV/cm. The pyroelectric current was measured during heating to allow for the calculation of the pyroelectric coefficient and polarization. The results are shown in Figs. 7 and 8. In the [111] samples, pyroelectric coefficient peaks appear at both the R-T and T-C transition, the polarization also shows corresponding sharp changes. In the [100] sample, there is only a peak at the T-C transition, no peak appears at the R-T transition and the polarization curve at the corresponding temperature does not show any sharp change.

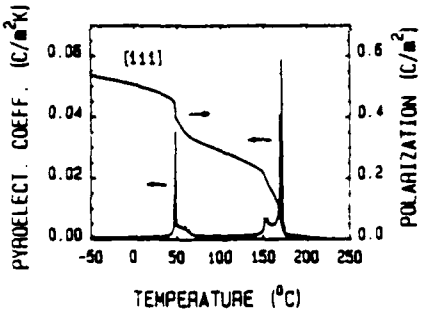

Figure 7. Pyroelectric property in [111] direction.

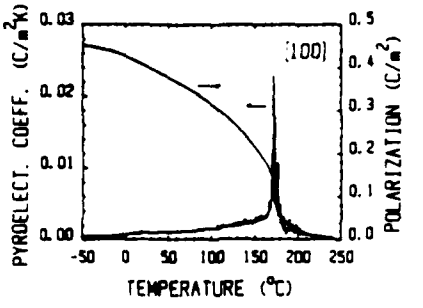

Figure 8. Pyroelectric property in [100] direction.

5. Results

1. PZN10%PT is a relaxor type ferroelectric. Near room temperature it has a very large dielectric constant (K ~ 8000) but a small temperature coefficient.

2. Poling along the [111] and [100] directions has a very different effect on the dielectric behavior. Poling along the [111] direction introduces a sharp rise of K at T_{R-T}, with increasing temperature, from 8,000 to 12,000 and results in a very flat portion of the K vs T curve in the temperature range between 50 to 150°C. Poling in the [100] direction, on the contrary, reduces K by almost a factor of 4 in the temperature range between 20 and 140°C in which the tetragonal phase is stable. No sharp change in K appears at the R-T transition.

3. Both the [111] and [100] DC bias field shift the dielectric constant peaks at the T-C transition toward higher temperature and reduces the dielectric constant. However, at the R-T transition, the [111] DC bias field shifts it toward higher temperature, while the [100] field shifts it toward lower temperature. Hence, the [111] or [100] DC bias field extends, respectively, the temperature range in which the rhombohedral or tetragonal phase is stable.

4. Pyroelectric coefficient in the [111] direction has peaks at both the R-T and T-C transitions, whereas in the [100] direction there is no peak at the R-T transition.

References

[1] S. Nomura, T. Takahashi, and Y. Yokomizo, "Ferroelectric Properties in the System $Pb(Zn_{1/3}Nb_{2/3})O_3$-0.9$PbTiO_3$," J. Phys. Soc. Jpn., Vol. 27, p. 262 (1969).

[2] J. Kuwata, K. Uchino, and S. Nomura, "Dielectric and Piezoelectric Properties of 0.91$Pb(Zn_{1/3}Nb_{2/3})O_3$-0.09$PbTiO_3$ Single Crystals," Jpn. J. Appl. Phys., Vol. 21, pp. 1298-1302 (1982).

[3] H.T. Evans, Jr., D.E. Appleman and D.S. Handwerker, Report #PB216188 (1973). U.S. Dept. of Commerce, National Tech. Infn. Ctr., 5285 Port Royal Road, Springfield, VA 22151.

DIELECTRIC PROPERTIES OF RF SPUTTERED BISMUTH TITANATE THIN FILMS

P.K. Ghosh, A.S. Bhalla, and L.E. Cross

Materials Research Laboratory
The Pennsylvania State University
University Park, PA 16802

Abstract

In these studies, crystalline films of $Bi_4Ti_3O_{12}$ were deposited by RF sputtering in argon:oxygen gas using heated substrates. Using a gas pressure of 20 mtorr, preliminary experiments indicated bismuth loss from the films and this was compensated by enriching the bismuth content in the target.

To achieve high dielectric constant and low loss comparable to single crystal values, a substrate temperature of 450°C was required. For these conditions, pinhole-free films with permittivity $\epsilon_R > 200$ and $\tan\delta < 2\%$ could be obtained quite reproducibly suggesting the potential use of this material in thin film capacitors.

1. Introduction

Bismuth-titanate ($Bi_4Ti_3O_{12}$) is the one member of the large family of bismuth oxide layer structure ferroelectrics which exhibits switchable spontaneous electric polarization along all three axial directions. The high Curie temperature of 675°C and the mica-like morphology of the sheet structure suggest the potentially as a stable thin film dielectric with high dielectric strength. Cummins and Cross [1,2] showed that $Bi_4Ti_3O_{12}$ in the ferroelectric phase, below 675°C, belongs to a monoclinic symmetry, point group m. The spontaneous polarization lies in the monoclinic a-c plane at angle of approximately 4.5 degrees with the major crystal surface resulting a major component of 50 $\mu C/cm^2$ along the a-axis and a minor component of 4 $\mu C/cm^2$ along the c-axis. Reversal of c-axis polarization component rotates optical indicatrix through an angle of 42° producing a large change in the extinction angle. These properties lead to various interesting electro-optic properties useful in optical memory [3] or display applications [4].

Several attempts [5-10] have been made to prepare stoichiometric $Bi_4Ti_3O_{12}$ films in order to duplicate its single crystal properties. Various preparation techniques, including RF sputtering, were used for the $Bi_4Ti_3O_{12}$ thin film preparation. In this paper we report the preparation of thin films of $Bi_4Ti_3O_{12}$ and their dielectric properties.

2. Preparation

$Bi_4Ti_3O_{12}$ thin films were prepared by RF sputtering technique. It has been reported in the literature [6] that the pure $Bi_4Ti_3O_{12}$ target results in non-stoichiometric films and films from various target with excess Bi show that in general for each target there is a temperature range over which pure $Bi_4Ti_3O_{12}$ can be obtained. In this study $Bi_4Ti_3O_{12}$ films were prepared using a ceramic $0.8Bi_4Ti_3O_{12} + 0.2Bi_{12}TiO_{20}$ target in different plasma gas atmospheres. Films were deposited on various substrates, such as, plain glass slides, SnO_2 coated glass slides, Au-coated glass slides, Pt-coated glass slides, and Si-wafers.

$Bi_4Ti_3O_{12}$ thin films were first deposited on unheated substrates. As-grown films, irrespective of the preparation conditions, in general are amorphous in nature. Figure 1 shows the microstructure of an as-grown film. Post deposition annealing of these films result in cracking of the film as shown in Figure 2. Several sets of films were then deposited on heated substrates. Various substrate temperatures were used for deposition as listed in Table 1. Films are continuous and free from cracks.

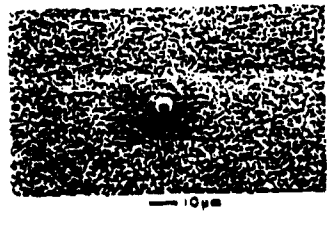

Figure 1. Microstructure of a $Bi_4Ti_3O_{12}$ thin film deposited on unheated substrates.

CH2058-0/86/0000-0596 $1.00 © 1986 IEEE

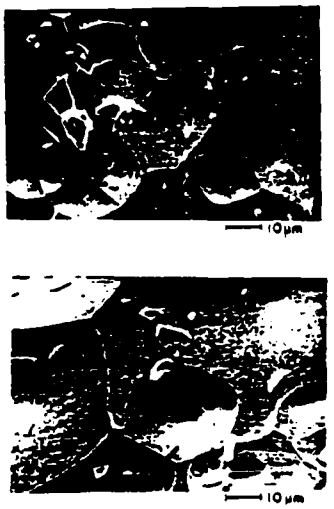

Figure 2. Microstructure of an annealed $Bi_4Ti_3O_{12}$ thin film deposited on unheated substrate.

Table 1. Deposition Conditions for the $Bi_4Ti_3O_{12}$ Films made by RF Sputtering on Heated Substrates.

RF Power (watts)	Gas Pressure O_2 (mtorr)	Gas Pressure Ar (mtorr)	Substrate Temperature (°C)
100/12	10	10	96
100/11	10	10	124
100/11	10	10	240
100/11	10	10	325
100/12	10	10	356
100/12	10	10	414
100/12	10	10	461
100/12	10	10	503
100/10	10	10	552

3. Experimental Results

A computer controlled HP4274A LCR meter was used for the measurements of dielectric constants and dissipation factors. The films deposited on SnO_2 coated substrates were used for the electrical measurements. A sputtered Au counter electrode was deposited on such films. Figure 3 shows the general low dielectric constant and high dissipation factor of $Bi_4Ti_3O_{12}$ thin films grown on unheated substrate. This behavior could be the result of their amorphous nature and probable departure from stoichiometry.

Figure 4 shows the effect of substrate temperature on the dielectric properties. Dielectric constant gradually increases with substrate temperature and at certain zone of substrate temperature dielectric constant of the $Bi_4Ti_3O_{12}$ thin films is as high as that of its single crystal form. Dissipation factor, as shown in Figure 5, at first increases but then gradually decreases with the increase of substrate temperature, this could be due to the formation of intermediate metastable phases. After about 400°C of substrate temperature, dissipation factor does not vary much and has a value less than 2%. Figure 6 shows the dielectric constant and loss vs. temperature, at different frequencies, of a $Bi_4Ti_3O_{12}$ thin film prepared in the substrate temperature zone mentioned above. A comparison of dielectric values of $Bi_4Ti_3O_{12}$ thin films with its single crystal form show that values are quite comparable.

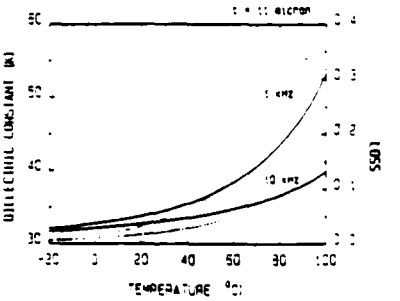

Figure 3. Temperature dependence of dielectric constant and dissipation factor of $Bi_4Ti_3O_{12}$ thin film deposited on unheated substrate.

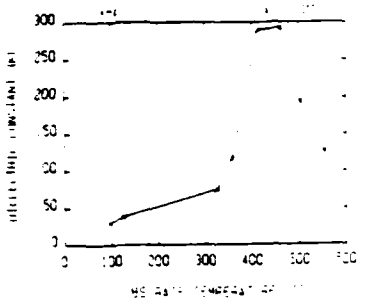

Figure 4. Effect of substrate temperature on the dielectric constant of $Bi_4Ti_3O_{12}$ thin film.

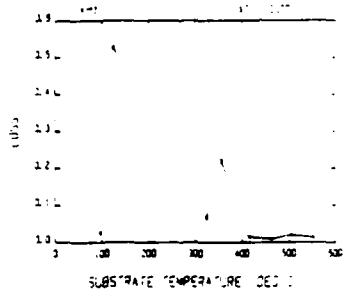

Figure 5. Effect of substrate temperature on the dielectric loss of $Bi_4Ti_3O_{12}$ thin films.

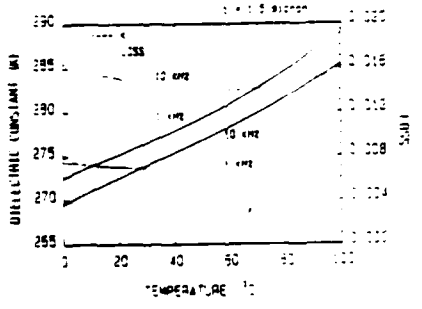

Figure 6. Temperature dependence of dielectric constant and loss of a $Bi_4Ti_3O_{12}$ thin film deposited on heated substrate.

4. Summary

$Bi_4Ti_3O_{12}$ thin films were prepared by RF sputtering with a Bi excess ceramic target. It is shown that for a particular preparation condition there is a zone of substrate temperature for the preparation of $Bi_4Ti_3O_{12}$ thin films to achieve high dielectric constant and low loss. $Bi_4Ti_3O_{12}$ thin films with a capacitance of 0.2 $\mu F/cm^2$ and loss < 2% were prepared reproducibly.

References

[1] S.E. Cummins and L.E. Cross, Appl. Phys. Lett., 10 (1), 14 (1967).

[2] S.E. Cummins and L.E. Cross, J. Appl., 39 (5), 2268 (1968).

[3] S.E. Cummins, Proc. IEEE, 55 (8), 1536 (1967).

[4] S.E. Cummins, Proc. IEEE, 55 (8), 1537 (1967).

[5] W.J. Takei, N.P. Formigoni, and M.H. Francombe, Appl. Phys. Lett., 15 (8), 256 (1969).

[6] W.J. Takei, N.P. Formigoni, and M.H. Francombe, J. Vac. Sci. Tech., 7 (3), 442 (1970).

[7] S.Y. Wu, W.J. Takei, M.H. Francombe, and S.E. Cummins, Ferroelectrics, 3, 217 (1972).

[8] M.H. Francombe, J. Vac. Sci. Tech., 11 (1), 130 (1974).

[9] W.J. Takei, S.Y. Wu, and M.H. Francombe, J. Crys. Growth, 28, 188 (1975).

[10] S.Y. Wu, J. Appl. Phys., 50 (6), (1979).

TESTING TECHNIQUES FOR SONOCHEMISTRY IN FLOW-THROUGH TRANSDUCERS

C.W. Nies, T.R. Gururaja, and R.E. Newnham

Materials Research Laboratory
The Pennsylvania State University, University Park, PA 16802 U.S.A.

Abstract

Sonochemistry, or the enhancement of chemical reactivity via ultrasound, is gaining interest for chemical processing. This technique takes advantage of acoustic cavitation stimulated in the liquid. The purpose of this study is to explore testing techniques using simple transducers for continuous sonication systems.

Two tests for characterization were examined: acoustic noise measurement and I_3^- production in a sonicated solution of NaI. These tests were used to evaluate lead zirconate titanate (PZT) ring transducers poled in the radial direction. It was found that the acoustic test gave information about the types of cavitation occurring in the liquid, while the chemical test indicated the presence of transient cavitation, by which chemical reactivity is affected. Continuous sonochemistry could be carried out at slow flow rates in these rings; resonant frequency and channel dimensions controlled the intensity of the cavitation occurring in them.

1. Introduction

Sonochemistry is best described as the stimulation or enhancement of chemical reactions via ultrasonic stimulation of liquid precursors. Examples of sonochemical reactions include the shearing of aromatic rings [1], the synthesis of thioamides [2], and the reduction of metal carbonyls [3]. As this technique gains interest, more efficient designs for sonicating equipment will be needed, particularly in the area of continuous processing. The purpose of this study is to explore possible tests and simple transducer configurations for continuous sonochemical processing.

The chemical effects of ultrasonics have been attributed to acoustic cavitation - the formation, growth and collapse of small oscillating bubbles in the liquid, caused by the changing pressure conditions. When a nucleating bubble comes under the influence of the rarefaction phase of a pressure wave passing through the liquid, the bubble expands to form a cavitation bubble. In an oscillating sound field at low pressure amplitudes, the bubble ideally grows by rectified diffusion to a resonant size as it oscillates nonlinearly about its equilibrium radius before collapsing (stable cavitation). At higher pressure amplitudes, the bubble expands rapidly to a maximum size and collapses violently (transient cavitation). Each type of cavitation occurs at a particular pressure threshold determined by the liquid characteristics.

Cavitation is a common phenomenon in liquids, and there are a number of excellent reviews on the subject [4,5]. It depends directly on such variables as ambient temperature and pressure, ultrasonic frequency and intensity, solvent surface tension and vapor pressure, and the presence of nucleation bubbles, from which cavitation bubbles form. Chemical effects generally require transient cavitation. The rapid collapse of these bubbles creates "hot spots" which are of short duration (< 7 nsec) but are capable of reaching temperatures and pressures estimated at 10000 K and 10000 atmospheres [6]. Because of these rapidly changing conditions, vapor-phase, liquid-vapor, and liquid-phase reactions are possible near transient bubbles.

Lead zirconate titanate (PZT) compositions are the most commonly used materials today for sonication transducers. Hard PZTs (having high coercive fields) are preferred because of the strenuous voltage conditions employed. The most common type of transducer available is the "sandwich" transducer, in which conical metal end pieces are bolted to PZT disc transducers. This sandwich is then driven at a resonant frequency determined by the dimensions of the transducer. The advantages of this type of design over monolithic PZT transducers are greater efficiency due to better heat removal and larger vibrational amplitudes. The design considerations for this type of transducer have been reviewed by van Randeraat and Setterington [7]. Jaffe [8] proposed piezoelectric ceramic tubes and parabolic transducers as early as 1950; however, these are not commonly used today.

2. Experimental Procedure

For this study, two techniques for characterizing cavitation were examined: a study of the acoustic spectrum emitted by the transducers, and a simple sonochemical test involving the measurement of I_3^- produced in a solution of NaI by sonication. The acoustic test (reviewed by Apfel [5]) involved analyzing the acoustic spectrum produced in a liquid by an ultrasonic driver transducer at varying levels of driving voltage. For this test, a perforated composite hydrophone was used in conjunction with a Hewlett-Packard 3585-A spectrum analyzer protected by a 100x voltage probe. The noise levels in the acoustic spectrum at the fundamental driving frequency (f_r), the second harmonic frequency ($2f_r$), the sub-harmonic frequency ($0.5f_r$), and the background noise (measured near $1.25f_r$) were then recorded. Figure 1 shows a sample spectrum of a cavitating liquid, indicating the location of these peaks.

The chemical test used was the production of iodide trimer (I_3^-) in a 1 M solution of sodium iodide undergoing cavitation:

$$3\,I^- \rightarrow I_3^-$$

The procedure for this test is described by Suslick et al. [9]. Measurements were made with the reactant solution at 20° C. The relative amounts of I_3^- in each sample were determined by measuring the absorbance spectrum at 353 nm, using a Cary 2300 UV/VIS/IR spectrophotometer. Each sonicated sample

3 shows the changes at these frequencies with increasing peak to peak voltage for each transducer, using a flow rate of 2 ml/min.

Figure 3.A shows the variation of the acoustic spectrum with applied voltage for the 1" ring. The onset of the sub-harmonic peak and a sharp rise in the background noise (indications of transient cavitation) can be seen at 100 V. In addition, the insulating varnish on the inside surface of the ring was chipped away in some spots by the cavitation produced. Figure 3.B shows similar data for the 1.5" ring. In this case, however, the subharmonic is only weakly present and the background does not rise sharply to indicate the onset of cavitation in the system. An examination of the transducer showed no sign of interior chipping to indicate erosion by cavitation. Figure 3.C shows the variation of the acoustic spectrum of the 2" ring with operating voltage. The subharmonic and background noise can be seen to rise at 60 V. An audible hiss could be heard emanating from this transducer, and chipping was observed on the inner surfaces of this transducer. All figures show the onset of the second harmonic, which is taken to indicate stable cavitation, at much lower intensities.

Figure 4 summarizes the results of the chemical tests on the rings. The graph shows a noticeable rise in the production of iodide trimer in the vicinity of an applied voltage of 60 V (3 W input power for the 2" ring, and a small rise at 100 V (5 W input power) for the 1" ring. This indicates a correspondence between the change in the subharmonic and background noise and the production of I_3^-. No rise is noted in the case of the 1.5" ring, corresponding to the lack of background and subharmonic rise for the voltages employed. Because of the 2" ring's high chemical yield, the production of I_3^- was measured with reactant flow rate through the transducer at a driving voltage of 80 V peak to peak (5.5 W input power), as shown in figure 5. Production of iodide trimer drops sharply but is still visible at higher flow rates.

Differences in the test results for each transducer can be ascribed to their different sizes. The 2" transducer operates at the lowest frequency, and thus has the lowest cavitation threshold. It also has the largest internal cavity, so for similar flow rates, reactants will undergo cavitation for a longer time. Absence of cavitation in the 1.5" ring is unusual, but is probably explained by the production of distructive interference in the ring; no calculations were performed to confirm this, however.

It can be seen that each test has its own advantages and disadvantages. Acoustic testing provides a great deal of information in that it can tell the observer what type of cavitation is occuring in the system and gives some information on the degree of cavitation in the system. It also delivers this information immediately, making the test useful for rapidly changing conditions. It cannot provide information on the length of sonication, and is best conducted with small hydrophones in order to perturb the acoustic field as little as possible. The iodide trimer test is capable of detecting the relative intensity of transient cavitation and the relative duration of sonication, making it useful for flow rate studies. Transducer size doesn't limit the applicability of this test; however, temperature control is important for uniform results, and no indications of stable cavitation are given. These tests complement each other well for evaluating the transducers.

The results of the ring tests indicate the possibility of monolithic flow-through transducers being developed in the

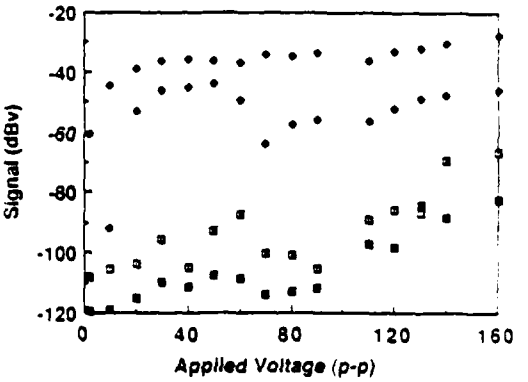

Figure 3A. 1" Ring.

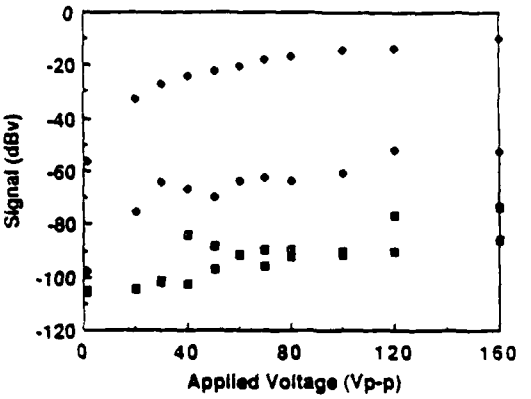

Figure 3B. 1.5" Ring.

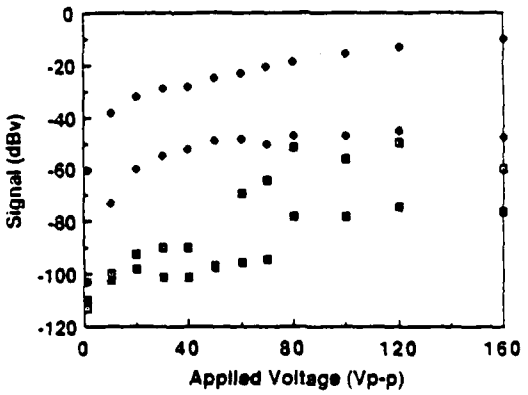

Figure 3C. 2" Ring.

Figure 3. Variation of Acoustic Spectrum with Applied Voltage at Selected Frequencies for Ring Transducers (◆ - Fundamental, ● - Second harmonic, ■ - Subharmonic, ■ - Background).

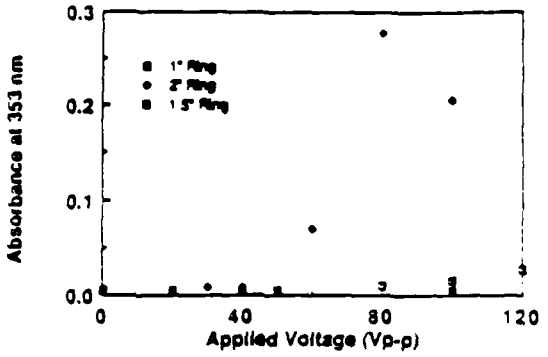

Figure 4. Production of Iodide Trimer at Varying Voltages for Ring Transducers.

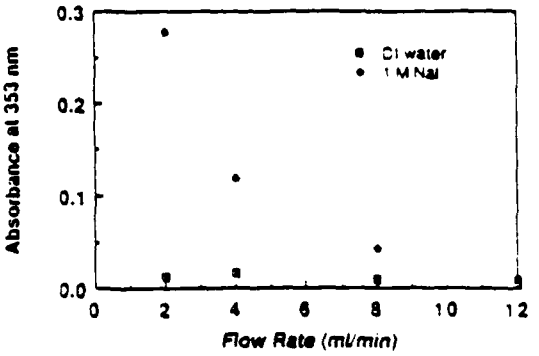

Figure 5. Variation in Iodide Production with Flow Rate for 2" Ring Transducer

future. The major stumbling block for this set of transducers appears to be the low flow rate needed to produce sufficient amounts of chemical products. One way of obtaining higher output might be to have a number of these transducers connected in series to increase flow rates, or in a parallel pipe array to increase throughput. In these cases the power required must be multiplied by the number of transducers used. A more fruitful course of action is to increase the efficiency of the transducer design. For example, the thickness mode in the rings was the most efficient for producing cavitation in these transducers. Obtaining low frequencies with this mode is difficult because it requires increasing the wall thickness of the transducer when it would be more advantageous to decrease the size in order to make the elements part of an array. However, if the radial "breathing" mode could be exploited for use in these transducers, lower frequencies would be available which could be translated into lower power requirements for cavitation and more energetic bubbie collapses. Another approach would be to improve standing wave production in the liquid. This approach offers a method of achieving higher intensities without large increases in power input. One other way of improving the transducers may be to utilize a composite configuration. The original drawbacks of PZT, having to do with poor heat removal from large blocks of piezoelectric ceramics, were originally solved using the "sandwich" configurations. Designs more conducive to continuous processing may be developed if novel monolithic ceramics are again investigated.

4. Summary

In order to evaluate transducers for sonochemistry conveniently, simple cavitation tests were for comparison purposes. The acoustic test delivers information on the types of cavitation occuring in the liquid. It also delivers this information immediately, making the test useful for relatively rapidly changing conditions. The iodide trimer test indicates only transient cavitation, but can also be used to evaluate the duration of sonication for a given intensity. The tests on prototype ring transducers demonstrated the effectiveness of the cavitation tests and the feasibility of simple flow-through transducers.

Many opportunities are available in continuous sonochemistry for industrial-scale production, an area still somewhat in its infancy. As these types of uses for sonication expand, flow-through sonochemistry will become a goal well worth pursuing.

5. Acknowledgements

The authors would like to express their appreciation to Dr. Peter Lewin of Drexel University for his advice and Dr. Ahmad Safari for his help in fabricating useful hydrophones for this study. Funding was provided by the Office of Naval Research for this study.

References

[1] L. Zechmeister and L. Wallclave, "On the cleavage of benzene, thiophene, and furan rings by means of ultrasonic waves," J. Amer. Chem. Soc., vol. 77, pp. 2853 - 2855, 1955.

[2] S. Raucher and P. Klein, "Ultrasound in heterogeneous organic reactions. An improved procedure for the synthesis of thioamides," J. Org. Chem., vol. 46, pp. 3558-3559. 1981.

[3] K.S. Suslick, J.W. Goodale, H.H. Wang and P.F. Schubert, "Sonochemistry and sonocatalysis of iron carbonyls," J. Amer. Chem. Soc., vol. 105, pp. 5781-5785, 1983.

[4] I.E. El'piner, Ultrasound: Its Physical, Chemical and Biological Effects (translation F.L. Sinclair), Consultants Bureau, New York, 1964.

[5] R.E. Apfel, "Acoustic Cavitation" in Methods in Experimental Physics: Ultrasonics, Academic Press, 1981, pp. 355 - 411.

[6] E.A. Neppiras and B.E. Noltingk, "Cavitation produced by ultrasonics: theoretical conditions for the onset of cavitation", Proc. Phys. Soc. London, Sect. B, vol. 64, 1951, pp. 384-395.

[7] J. van Randeraat and R.E. Setterington, Piezoelectric Ceramics Application Book, N.V. Philips, Eindhoven, The Netherlands, 1974, pp.123-145.

[8] H. Jaffe, "Titanate ceramics for electromechanical purposes," Ind. and Eng. Chem., vol. 42, pp. 264-268, 1950.

[9] K.S. Suslick, P.F. Schubert, and J.W. Goodale, "Chemical dosimetry of ultrasonic cavitation," in Proc. IEEE Ultrason. Symp., vol. 1, 1981, pp. 612-616.

THE EFFECT OF OCTAHEDRALLY- COORDINATED CALCIUM ON THE FERROELECTRIC TRANSITION OF $BaTiO_3$

Z.Q.Zhuang, M.P.Harmer and D.M.Smyth

Materials Research Center, Lehigh University, Bethlehem, PA 18015, U.S.A.

R.E.Newnham

Materials Research Laboratory

The Pennsylvania State University, University Park 16802, U.S.A.

Abstract

The effect of the B-site calcium ion on the ferroelectric transition of $BaTiO_3$ ceramics was investigated by X-ray diffraction, TEM, SEM, and by measurements of dielectric properties and equilibrium electric conductivity. It was found that the c/a ratio decreases continuously to near unity with increasing amount of Ca ion on the B site up to 5%, and that the broadened and diffused Curie peak moves to room temperature for the composition with 5% of Ca ion on the B site and 6% on the A site. A thermodynamic model has been developed to explain this effect.

Introduction

Several previous investigations have been carried out on the structure and dielectric properties of Ca-doped barium titanate. In 1952, Berlincourt and Kulesar [1] found that Ca addition to $BaTiO_3$ caused only negligible changes in the Curie point. Two years later, McQuarrie and Behnke[2] reported that Ca-doped $BaTiO_3$ showed a slight decrease of the Curie point. In 1961 Mitsui and Westphal[3] through the dielectric and X-ray studies of $Ba_{1-x}Ca_xTiO_3$ demonstrated that the Curie point of $Ba_{1-x}Ca_xTiO_3$ increases from130.7°C for pure $BaTiO_3$ up to 136.1°C for x=0.08 and then decreases slightly for continuously increasing Ca concentration up to 25%. A similar statement on the Ca-doped $BaTiO_3$ appears in the book by Jaffe, Cook and Jaffe[4]. Wakino, Minai and Sakabe[5] have investigated Ca-doped $BaTiO_3$ multilayer ceramic capacitors for use with base metal electrodes, which can be sintered in a reducing atmosphere.

The present investigation centers on the dielectric properties, defect chemistry, and microstructure of acceptor-doped barium titanate. Microstructure examination was carried out to elucidate the ferroelectric behavior, together with a 4-point DC technique for the measurement of the equilibrium electric conductivity, and the measurement of dielectric properties. It is speculated that the broadened Curie peak shifting effect is caused by the lattice distortion caused by replacing Ti with the larger Ca ion, acting in the same manner as a hydrostatic pressure[6] .

Experimental Procedure

Samples were prepared by the liquid-mixing technique which is a modification of the process developed by Pechini[7]. The starting chemicals were titanium tetraisoproxide, barium carbonate, and calcium carbonate. After polymerization with the addition of citric acid, and calcination at 900°C for 5 hours, the calcined powder was ground, cold pressed into pellets, and sintered in air in an electric furnace, to form dense ceramic samples of $Ba_{1-x}Ti_{1-y}Ca_{x+y}O_{3-y}$ with x ranging from 0 - 6% and y from 0 - 5%. Dielectric measurements were carried out on circular disks 0.04cm thick and 1 cm in diameter. Sputtered gold or platinum electrodes were employed. An automated capacitance bridge was used in the determination of dielectric constant. X-ray diffraction analysis was carried out on an APD3600 Automated X-ray Powder Diffractometer with CuKα radiation, using crushed powder from freshly sintered ceramic disks. Lattice parameters were determined using the 400α_1 and 004 α_1 diffraction peaks. Electrical conductivity measurements were performed using a 4-point DC technique described elsewhere[8]. For SEM examination, the specimens were thermally etched at 1000°C to 1200°C for 30 minutes. For TEM examination, the specimens were thinned on an Argon

Ionic Thinner until a specimen with a thickness of about 1000 Å was obtained.

Results and Discussion

Figure 1 shows the changes in Curie point of barium titanate ceramics of composition $Ba_{1-x}Ti_{1-y}Ca_{x+y}O_{3-y}$ with x (0-5%) and y (0-5%). It can be seen that the transition temperature T_c depends on the concentration of Ca on the B site and that T_c is 126.7°C for pure barium titanate. T_c lies near room temperature for ceramics containing 6% Ca on the A site and 5% Ca on the B site. The change of Curie point with the concentration of Ca on the B site, and also on both the A and B sites, is shown schematically in Fig.2.

Based on high angle X-ray diffraction patterns, values of c, a, c/a and the unit cell volume of $Ba_{0.95}Ti_{1-x}Ca_{0.05+x}O_{3-x}$ ceramics in the tetragonal phase at room temperature are presented in Table 1. From Table 1, we conclude that the c/a ratio decreases with increasing amount of Ca on the B site; the tetragonality at room temperature approaches a cubic unit cell for the composition $Ba_{0.94}Ti_{0.95}Ca_{0.11}O_{2.95}$. We interpret these results as an internal lattice distortion of the materials, caused by the substitution of Ca for Ti (Fig.3). In Fig.3, the arrows indicate the directions of the internal stresses p.

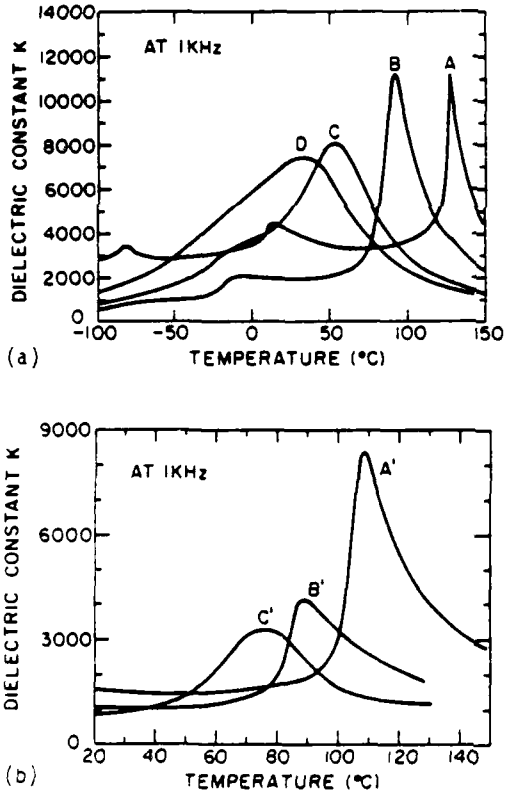

Fig.1. The temperature dependence of dielectric constant K of barium titanate ceramics with compositions of (a). $Ba_{0.95}Ti_{1-x}Ca_{0.05+x}O_{3-x}$: (A) pure, (B) x=0.01, (C) x=0.02 and (D) x=0.04 ; and of (b): (A') $BaTi_{0.99}Ca_{0.01}O_{2.99}$, (B') $BaTi_{0.98}Ca_{0.02}O_{2.98}$ and (C') $BaTi_{0.97}Ca_{0.03}O_{2.97}$. All measured at 1000Hz.

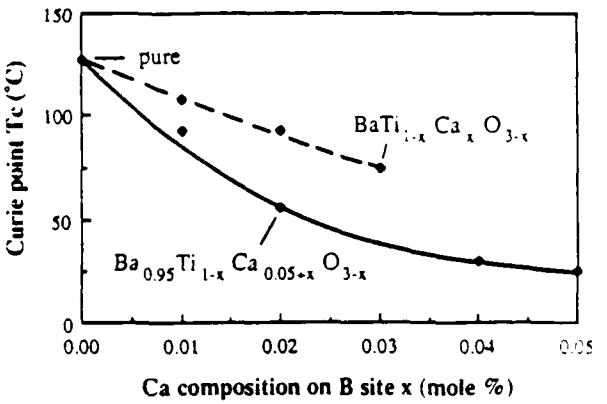

Fig.2. The lowering of Curie point T_c with the concentration of Ca ion (on the B site and on both the A site and the B site).

Additional evidence comes from changes in domain configurations with Ca concentration on the B site (Fig.4). Domains can easily be seen in pure barium titanate, and in Ca-A-site-doped barium titanate ceramics (Fig.4(a) and (b)). But

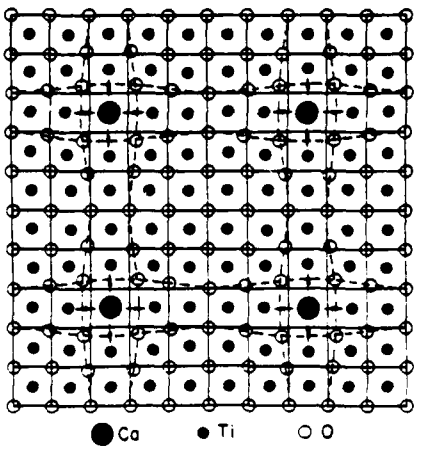

Fig.3. A two-dimensional view of the structure of Ca-doped $BaTiO_3$, showing the localized expansion of the unit cell caused by the substitution of Ca for Ti in the octahedral sites of the perovskite structure.

it is very difficult to examine the domain structure under TEM in heavily-doped barium titanate ceramics (fig.4(e) and (f)), because of the c/a ratio decreasing with the increasing of Ca concentration on the B site.

Table1. Lattice parameters of $Ba_{0.95}Ti_{1-x}Ca_{0.05-x}O_{3-x}$ ceramics at room temperature

		x				
	undoped	0	0.01	0.02	0.03	0.04
c(Å)	4.0400	4.0356	4.0270	4.0192	4.012	4.012
a(Å)	3.9964	3.9904	3.9980	4.0056	-----	-----
c/a	1.0109	1.0113	1.0073	1.0030	-----	-----
V(Å^3)	64.52	64.26	64.368	64.487	-----	64.58

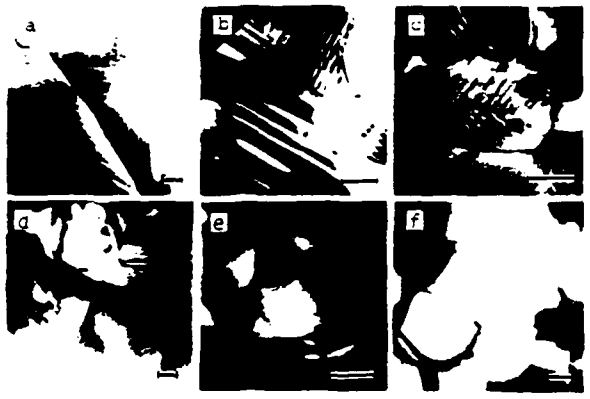

Fig.4 . The variation of the domain configuration of Ca-doped barium titanate ceramics with the increase of the concentration of Ca on the B sites: (a). pure, (b). $Ba_{0.95}Ca_{0.05}TiO_3$, (c). $Ba_{0.95}Ti_{0.98}Ca_{0.07}O_{2.98}$, (d). $Ba_{0.95}Ti_{0.97}Ca_{0.08}O_{2.97}$, (e). and (f). $Ba_{0.95}Ti_{0.96}Ca_{0.09}O_{2.96}$. In the pure and slightly doped ceramics, the domains can be easily seen because of their larger size. With increasing Ca concentration on the B site, the domains become vanishingly small. The observed domain sizes vary from 0.3 μm to 0.06 μm.The scale bar is 0.5 μm in every picture.

Measurement of the equilibrium electric conductivity demonstrated acceptor-doped behavior in Ca-B-site-doped barium titanate ceramics(Fig.5). In the case of Ca substitution for Ba and Ti ions, the reaction

$$2CaO \text{ -----} > Ca_{Ba} + Ca_{Ti}'' + 2O_O + V_O \qquad (1)$$

in which a Ca ion substitution for a Ti ion creates an oxygen vacancy $V_O^{\cdot\cdot}$. At the minimum of the equilibrium electric conductivity curve,

$$[V_O] = [Ca_{Ti}''] >> n \text{ and } p \qquad (2)$$

When combined with the oxidation and reduction reactions, we have

$$d \log Po_2^o / d \log [Ca_{Ti}''] = -2 \qquad (3)$$

where, Po_2^o stands for the oxygen pressure at the minimum in equilibrium electric conductivity. It is obvious from equation (3) that the position of the minimum should move two orders of magnitude toward lower oxygen pressure for each order of increase in the content of Ca on the B site. Fig.5 shows qualitative agreement with this prediction. In the other words, the shift in position of the minima toward lower oxygen pressure indicates the occupancy of Ca on the B site in the Ca-doped barium titanate ceramics.

According to Goswami and Cross[9], the elastic Gibbs free energy for barium titanate ceramic can be written in the form

$$\begin{aligned} G_1-G_{1O} =& A(P_x^2+P_y^2+P_z^2) + B(P_x^4+P_y^4+P_z^4) + C(P_x^6 \\ &+P_y^6+P_z^6) + D(P_x^2P_y^2+P_y^2P_z^2+P_z^2P_x^2) + G(P_x^2P_y^4 \\ &+P_x^4P_y^2+P_y^2P_z^4+P_y^4P_z^2+P_z^2P_x^4+P_z^4P_x^2) \\ &-1/2\, s_{11}(X_x^2+Y_y^2+Z_z^2) - s_{12}(X_xY_y+Y_yZ_z+Z_zX_x) \\ &-1/2\, s_{44}(X_y^2+Y_z^2+Z_x^2)+(Q_{11}X_x+Q_{12}Y_y+Q_{12}Z_z)P_x^2 \\ &+(Q_{12}X_x+Q_{11}Y_y+Q_{12}Z_z)P_y^2+(Q_{12}X_x+Q_{12}Y_y \\ &+Q_{11}Z_z)P_z^2+Q_{44}(X_yP_xP_y+Y_zP_yP_z+Z_xP_zP_x) \end{aligned} \qquad (4)$$

where, X_x, Y_y, Z_z are the normal stress components.

X_y, Y_z, Z_x the shear stress components.

s_{11}, s_{12}, s_{44} the elastic compliance constants.

P_x, P_y, P_z the components of polarization.

Q_{11}, Q_{12}, Q_{44} the electrostrictive coefficients.

A, B, C, D, G the coefficients of the free energy function and G_{1o} the free energy of the unstressed, unpoled solid.

For hydrostatic stress -p

$$X_x = Y_y = Z_z = -p \qquad (N/m^2)$$

$$Y_z = X_y = Z_x = 0$$

The Curie Weiss law in the paraelectric phase under stress can be written as

$$K = C/(T-T_\theta) \qquad (5)$$

where, $T_\theta = [T_o - 2\varepsilon_o p (Q_{11}+2Q_{12})_o C_o] / [1 + 2\varepsilon_o \alpha \cdot p (Q_{11}+2Q_{12})_o C_o]$ (6)

In this expression, $(Q_{11}+2Q_{12})_o$ is the value of the electrostrictive coefficients at zero temperature. C_o and T_o the unstressed Curie Weiss constant and Curie Weiss temperature, T_θ the ferroelectric Curie Weiss temperature in the stressed state.Therefore, we can consider the transition temperature under stress to be a function of stress p and proportional to it. It is obvious from eq.(6) that the transition temperature decreases linearly with the increase of hydrostatic stress p.

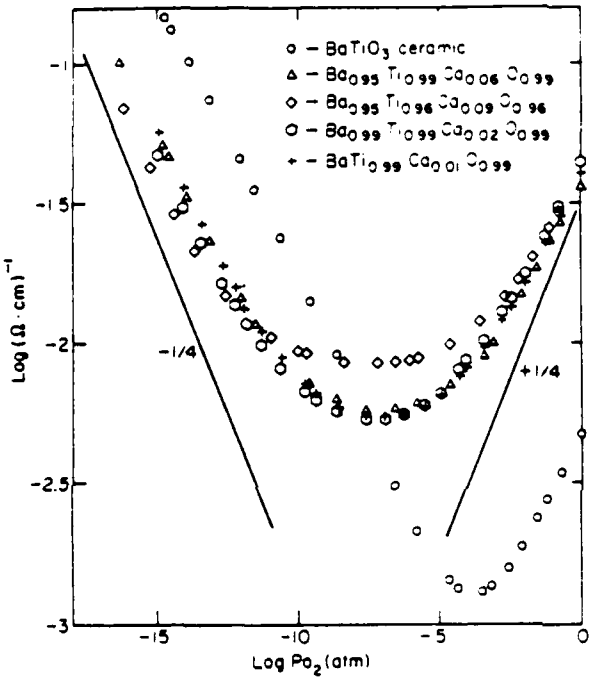

Fig.5. Equilibrium electric conductivity at 1000°C of barium titanate ceramics undoped and Ca-doped.

As mentioned in the previous section, the Ca occupancy on B site causes a distortion of the unit cell and a model of the distorted lattice is shown in Fig. 3. As shown in Fig.3, it could be seen that the unit cell in which a Ca ion occupies the B site expands and exerts a compressive stress p on the adjacent unit cells which are compressed. The former can be treated as a tension source. Therefore, the Curie temperature of Ca-B-site-doped barium titanate ceramics will decrease with concentration of Ca on B site due to the internal stress , as described by eq.6. And from Fig.1 and Fig.2, it is obvious that the lowering of the transition temperature for a given change in the Ca composition (0-5%) on B sites was more pronounced when there was Ca (about 5%) on A sites. When there are Ca ions on A sites more Ca ions occupy B sites and the lattice distorts more easily.

It is clear from Fig.3 that the compression of the unit cells along the tension directions is not uniform. This leads to a stress distribution along the tension direction causing the Curie temperature to broaden over a range of temperatures, from T_{cm} to T_{cn}, as shown in Fig.1.

Acknowledgement

The authors wish to express the thanks to Professor L.E.Cross for useful discussions and helpful comments on the manuscript, and also to Dr. H.M.Chan, and Dr. E.K.Chang for assistance with the measurement of the equilibrium electrical conductivity.

References

[1]. D.A.Berlincourt, and F.Kulesar, J. Acoust. Soc. Am., Vol.24, pp.709-13, 1952.

[2]. M.C.McQuarrie and F.W.Behnke, J. Am. Ceram. Soc., Vol.37, pp.539-43, 1954.

[3]. T.Mitsui and W.B.Westphal, Phys. Rev., Vol.124, pp.1354-59 1961.

[4]. B. Jaffe, W.R.Cook, and H. Jaffe, "Piezoelectric Ceramics", Academic Press, NY, 1971, p91.

[5]."High-Dielectric Constant Ceramics for Base Metal Monolithic Capacitors", K. Wakino, K. Minai and Y. Sakabe, Murata Manufacturing Co., Ltd., Japan.

[6]. W.J.Merz, Phys.Rev.,Vol.77, pp52-54, 1950.

[7]. M.Pechini, U. S. Pat., 3, 330, 697 (1967).

[8]. N.-H.Chan, R.K.Sharma and D.M.Smyth, J.Am.Ceram. Soc., Vol.65, p167, 1982.

[9]. A.K.Goswami, and L.E.Cross, Phys. Rev., Vol.171, pp549-50, 1968.

INVESTIGATIONS OF CHARGE COMPENSATION IN THE PHOSPHATE, ARSENATE, AND CHROMATE-DOPED TRIGLYCINE SULPHATE (TGS) CRYSTALS: MECHANISM OF ENHANCEMENT OF PYROELECTRIC PROPERTIES

N. S. Dalal*, A. S. Bhalla+ and L. E. Cross+

*Chemistry Department, West Virginia University, Morgantown, WV 26506
+Materials Research Laboratory, The Pennsylvania State University, University Park, PA 16802, USA

Abstract: ESR spectroscopic studies of TGS grown from aqueous solutions containing chromate, phosphate and arsenate ions show that the dopants enter the TGS lattice replacing the sulfate ions and have an extra proton for charge compensation.

INTRODUCTION

Recent studies by Bhalla, Cross and coworkers (1-4) have demonstrated that the doping of triglycine sulfate (TGS) crystals with a few mole % of phosphate, arsenate or chromate entities leads to a significant increase (up to 200%) of their pyroelectric coefficients. Typical results are as follows.

Sample	P ($\mu C/m^2K$)	P/ε ($\mu C/m^2K$)
TGS	330	11
TGS:P	600	18-20
TGS:As	650	20-22
TGS:Cr	~360	~13

The observed large increase in the pyroelectric properties of the doped TGS is highly significant for its use as a pyroelectric detector. However the mechanism by which the dopants modify the pyroelectric behavior of TGS is not yet understood. The present work summarizes our recent spectroscopic studies undertaken for clarifying the atomic structures of the dopants and thereby to understand the microscopic mechanism of the enhancement phenomenon.

METHODOLOGY

We have employed the electron spin resonance (ESR) spectroscopy as a direct, sensitive and non-destructive technique for identifying the oxidation states and, in favorable cases, the atomic structure of the dopant species in the TGS lattice. The ESR technique was selected because other, more conventional, techniques such as IR and Raman techniques were not thought to be suitable for detecting small amounts of the phosphate and arsenate species in the presence of the SO_4^{2-} host, since the bands are expected to be in the same area.

The basis of this work will be discussed for the arsenate doping, since similar considerations apply to the phosphate and the chromate species.

For TGS crystals grown from acidic aqueous solutions containing the arsenate, the following species may be present as the dopant: AsO_4^{2-}, AsO_4^{3-}, $H^+AsO_4^{3-}$, $H_2SO_4^-$ or $H_2AsO_4^{2-}$. Of these AsO_4^{2-}, and AsO_4^{4-} or $(H_2AsO_4)^{2-}$ are paramagnetic and should be directly detectable by ESR spectroscopy (5). Thus the detection of ESR signals and their detailed analysis via the ^{75}As hyperfine couplings (1) could provide direct information on the structure of the dopant. Conversely the absence of ESR signals, while knowing that arsenic is present in the TGS lattice, would eliminate AsO_4^{2-} and AsO_4^{4-} and strongly imply the presence of $HAsO_4^{2-}$ type of diamagnetic species containing an excess proton (H^+) relative to the substituted (SO_4^{2-}) units.

RESULTS

Spectrochemical analysis of the doped TGS crystals showed that As and P were present at a few mole percent level, but no further information was possible regarding the oxidation state or the chemical structure of the dopant.

The ESR measurements, performed at X-band (~9.7 GHz) frequencies using a Bruker ER200D ESR spectrometer, showed the absence of the AsO_4^{2-} as well as AsO_4^{4-} species in the arsenate-doped samples. Similarly ESR studies of the phosphate-doped samples showed the absence of PO_4^{2-} and PO_4^{4-}. Similarly, ESR studies of the chromate-doped samples exhibited no signal, indicating that CrO_4^{2-} is perhaps present. This was confirmed by ESR studies on γ-irradiated samples which exhibited strong signals from CrO_4^{3-} which is known to be formed from CrO_4^{2-} via electron capture on γ-irradiation (1). CrO_4^{3-} (or $HCrO_4^{2-}$) was identified through its g-values around 1.97, as discussed elsewhere (5). Furthermore, detailed studies of the angular dependence of the observed ESR signals, when the TGS crystals were oriented in the various crystal planes with respect to the external, Zeeman (magnetic) field, showed that the CrO_4^{2-} ions substitute for the SO_4^{2-} ions. It may be noted that the very detection of the ESR signals shows that the dopant species must be CrO_4^{3-} (or $HCrO_4^{2-}$), since CrO_4^{2-} is diamagnetic, hence ESR inactive. Further, no measurable H coupling was found, thus suggesting that the chromate-based dopant does not have a proton attached.

TABLE 4

Measured and calculated constrained expansion coefficient a_{3c}

Sample Type	Measured ($X10^{6}K^{-1}$)	Calculated ($X10^{6}K^{-1}$)
Low Draw	3.1±0.1	3.01
High Draw	2.3±0.1	2.38
Voided	2.8±0.1	3.12

TABLE 5

Linear thermal expansion coefficients and calculated secondary pyroelectricity

Sample Type	a_1	a_2	a_3	λ_s^m
Low Draw	0.030	1.69	1.87	-15.3
High Draw	-0.070	1.80	1.21	-3.4
Voided	-0.008	1.63	2.02	-3.3

TABLE 6

Pyroelectric measurements

Sample	λ^m	λ_c^m	$a_{3c}e_{33}^m$	λ_p^m	λ_s^m
Low Draw	-29.3	-29.9	-19.1	-10.8	-18.5
High Draw	-31.0	-34.6	-5.9	-28.7	-2.3
Voided	-18.2	-17.7	-3.7	-14.0	-4.2

TABLE 7

Primary, secondary, dipolar, dimensional and total pyroelectricity

Pyroelectricity $\mu Cm^{-2}K^{-1}$	Low Draw Ratio	High Draw Ratio	Voided Low Draw
λ_p^m	-10.8	-28.7	-14.0
λ_s^m	-18.5	-2.3	-4.2
λ_I^m	-19.9	-24.9	-10.1
$-Pa_3$	-9.4	-6.1	-8.1
λ^m	-29.3	-31.0	-18.2

Combining the ESR and spectrochemical results, it seems clear all three (arsenate, chromate and phosphate) dopants occupy the site of the SO_4^{2-} ions in the TGS lattice. However, while the chromate species substitutes as CrO_4^{2-} (requiring no proton for charge neutrality), the phosphate and the arsenate substitute as $(HPO_4)^{2-}$ and $(HAsO_4)^{2-}$, carrying one proton for charge compensation.

CONCLUSIONS

The TGS crystals grown from acidic, aqueous phosphate, arsenate and chromate solutions contain HPO_4^{2-}, $HAsO_4^{2-}$ and CrO_4^{2-} ions substituting for the SO_4^{2-} units of the TGS lattice. The phosphate and the arsenate-doped crystals exhibit much larger increases in the pyroelectric behavior than that shown by the chromate-doped lattice. The present work suggests that the excess protons that enter the TGS lattice along with the phosphate or the arsenates are the key species for the enhancement of the pyroelectric behavior of the doped lattice. The same model also explains the relatively much smaller enhancement caused by the chromate doping. This model further predicts an enhancement of the pyroelectric properties via the doping of ions such as ClO_4^- which will require the loss of a proton from the TGS lattice for replacing SO_4^{2-}. Some preliminary results obtained very recently from the ClO_4^--doped samples support this contention (6). Further studies are planned for using NMR and ENDOR (electron nuclear double resonance) techniques for directly probing the P-H or As-H interactions (5).

Acknowledgement. We gratefully acknowledge the support from NSF and DOD for this work.

References

1. C. S. Fang, Y. Xi, A. S. Bhalla and L. E. Cross, Ferroelectrics, 51, 9 (1983).

2. A. S. Bhalla, C. S. Fang and L. E. Cross, Materials Science Letters, 3, 12 (1985).

3. A. S. Bhalla, C. S. Fang, Y. Xi, and L. E. Cross, Ferroelectrics, 54, 2 (1984).

4. A. S. Bhalla, C. S. Fang, Y. Xi and L. E. Cross, Appl. Phys. Lett., 43, 10 (1983).

5. N. S. Dalal, Advan. Mag. Reson., 10, 119-215 (1985) contains details of the EPR signal assignments for the PO_4^{4-}, PO_4^{2-}, AsO_4^{4-}, AsO_4^{2-} and CrO_4^{3-} species.

6. A. S. Bhalla and L. E. Cross, In preparation.

ONR DISTRIBUTION LIST

Basic Distribution List
Technical and Summary Reports

Organization	No. Copies
Defense Documentation Center Cameron Station Alexandria, VA 22314	12
Office of Naval Research Attn: Code 471 Department of the Navy 800 N. Quincy Street Arlington, VA 22217	1
Office of Naval Research Attn: Code 470 Department of the Navy 800 N. Quincy Street Arlington, VA 22217	1
Commanding Officer Office of Naval Research Branch Office Building 114, Section D 666 Summer Street Boston, MA 02210	1
Commanding Officer Office of Naval Research Branch Office 536 South Clark Street Chicago, IL 60605	1
Office of Naval Research San Francisco Area Office One Hallidie Plaza Suite 601 San Francisco, CA 94102	1
Naval Research Laboratory Attn: Code 6000 Washington, DC 20375	1
Naval Research Laboratory Attn: Code 6100 Washington, DC 20375	1
Naval Research Laboratory Attn: Code 6300 Washington, DC 20375	1

Organization	No. Copies
Naval Research Laboratory Attn: Code 2627	1
Naval Air Development Center Code 606 Attn: Mr. F.S. Williams Warminster, PA 18974	1
Naval Weapons Center Attn: Library China Lack, CA 93555	1
Naval Air Propulsion Test Center Attn: Library Trenton, NJ 08628	1
Naval Construction Batallion Attn: Materials Division Civil Engineering Laboratory Port Hueneme, CA 93043	1
Naval Electronics Laboratory Attn: Electron Materials Sciences Division San Diego, CA 92152	1
Naval Missile Center Materials Consultant Code 3312-1 Point Mugu, CA 92041	1
Commanding Officer Naval Surface Weapons Center Attn: Library White Oak Laboratory Silver Spring, MD 10910	1
Commander David W. Taylor Naval Ship Research and Development Center Bethesda, MD 10084	1
Naval Oceans Systems Center Attn: Library San Diego, CA 92132	1
Naval Underwater System Center Attn: Library Newport, RI 02840	1
Naval Postgraduate School Attn: Mechanical Engineering Dept. Monterey, CA 93940	1

Organization	No. Copies
Naval Air Systems Command Attn: Code 52031 Washington, DC 20360	1
Naval Air Systems Command Attn: Code 52032 Washington, DC 20360	1
Naval Sea System Command Attn: Code 05R Washington, DC 20362	1
Naval Facilities Engineering Command Attn: Code 03 Alexandria, VA 22331	1
Scientific Advisor Commandant of the Marine Corps Attn: Code AX Washington, DC 20380	1
Army Research Office Box 12211 Attn: Metallurgy and Ceramics Program Triangle Park, NC 27709	1
Army Materials and Mechanics Research Center Attn: Research Programs Office Watertown, MA 02172	1
Air Force Office of Scientific Research/NE Building 410 Bolling Air Force Base Attn: Chemical Science Directorate Washington, DC 20332	1
Air Force Office of Scientific Research/NE Building 410 Bolling Air Force Base Attn: Electronics and Materials Sciences Directorate Washington, DC 20332	1
Air Force Materials Laboratory Wright-Patterson AFB Dayton, OH 45433	1
Library Building 50, Room 134 Lawrence Radiation Laboratory Berkeley, CA 94720	1

Organization	No. Copies
NASA Headquarters Attn: Code RRM Washington, DC 20546	1
NASA Lewis Research Center Attn: Library 21000 Brookpark Road Cleveland, OH 44135	1
National Bureau of Standards Attn: Metals Science and Standards Division Washington, DC 20234	1
National Bureau of Standards Attn: Ceramics Glass and Solid State Science Division Washington, DC 20234	1
National Bureau of Standards Attn: Fracture and Deformation Division Washington, DC 20234	1
Director Applied Physics Laboratory University of Washington 1013 Northeast Fortieth Street Seattle, WA 98105	1
Defense Metals and Ceramics Information Center Battelle Memorial Institute 505 King Avenue Columbus, OH 43201	1
Metals and Ceramics Division Oak Ridge National Laboratory Box X Oak Ridge, TN 37380	1
Los Alamos Scientific Laboratory Box 1663 Attn: Report Librarian Los Alamos, NM 87544	1
Argonne National Laboratory Metallurgy Division Box 229 Lemont, IL 60439	1
Brookhaven National Laboratory Technical Information Division Attn: Research Library Upton, Long Island New York 11973	1

Organization	No. Copies
Office of Naval Research Branch Office 1030 East Green Street Pasadena, CA 91106	1

Supplementary Distribution List A
Electronic, Magnetic and Optical Ceramics

Organization

Advanced Research Project Agency
Materials Science Director
1400 Wilson Boulevard
Arlington, VA 22209

Dr. Don Berlincourt
Channel Products
16722 Park Circle Drive W.
Chagrin Falls, OH 44022

Dr. J.V. Biggers
The Pennsylvania State University
Materials Research Laboratory
University Park, PA 16802

Mr. George Boyer
Sensor Systems Program
Office of Naval Research
Code 222
Arlington, VA 22217

Dr. Dean Buckner
Piezo Products Division
Bulton Industries
Box 4300
Fullerton, CA 92634

Dr. Robert Callahan
Channel Products
839 Ward Drive
Box 3680
Santa Barbara, CA 93105

Professor L.E. Cross
Materials Research Laboratory
The Pennsylvania State University
University Park, PA 16802

Mr. N. Coda
Vice President for Engineering
Erie Technological Products
West College Avenue
State College, PA 16801

Dr. N. Perrone
Code 474
Office of Naval Research
800 N. Quincy Street
Arlington, VA 22217

Dr. Gene Haertling
Motorola Corporation
3434 Vassar, NE
Albuquerque, NM 87107

Dr. W.B. Harrison
Honeywell Ceramics Center
1885 Douglas Drive
Golden Valley, MN 55422

Dr. C.M. Stickley, V.P.
The BDM Corporation
7915 Jones Branch Drive
McLean, VA 22102

Dr. L.L. Hench
Department of Metallurgy
University of Florida
Gainesville, FL 32603

Dr. B.F. Rider
Rockwell International
400 Collins Road NE
Cedar Rapids, IA 52406

Dr. F. Robert Hill
Marine Resources
755 Highway 17 and 92
Fern Park, FL 32730

Dr. B.G. Koepke
Honeywell, Inc.
Corporate Research Center
10701 Lyndale Avenue South
Bloomington, MN 55420

Dr. R. Lapetina
Edo Western Corporation
2645 South 300 West
Salt Lake City, UT 84115

Mr. C. LeBlanc
Naval Underwater Systems Center
TD 121
Newport, RI 02840

Professor R. Roy
Materials Research Laboratory
The Pennsylvania State University
University Park, PA 16802

Dr. Frank Recny
General Electric
Court Street
Plant Building C
Box 1122
Syracuse, NY 13201

Dr. J.H. Rosolowski
General Electric Company
Research and Development Center
Box 8
Schenectady, NY 02301

Dr. P.L. Smith
Naval Research Laboratory
Code 6361
Washington, DC 20375

Dr. R.W. Timme
Naval Research Laboratory
Code 8275
Underwater Sound Reference Division
Box 8337
Orlando, FL 32806

Dr. Charles C. Walker
Naval Sea Systems Command
National Center #3
2531 Jefferson Davis Highway
Arlington, VA 20390

Dr. Paul D. Wilcox
Sandia Laboratories
Division 2521
Albuquerque, NM 87115

The State University of New York at Alfred
Materials Science Division
Alfred, NY 14802

Dr. R. Rice
Naval Research Laboratory
Code 6360

Dr. David C. Hill
Member, Technical Staff
Texas Instruments, Inc.
Attleboro, MA 02703

Dr. S.K. Kurtz
Materials Research Laboratory
The Pennsylvania State University
University Park, PA 16802

Dr. N. Tallan
AFML Wright-Patterson AFB
Dayton, OH 45433

Dr. H.E. Bennett
Naval Weapons Center
Code 3818
China Lake, CA 93555

Dr. Michael Bell
Inorganic Materials Division
National Bureau of Standards
Washington, DC 20234

Dr. R. Bratton
Westinghouse Research Laboratory
Pittsburgh, PA 15235

Dr. Joe Dougherty
Materials Research Laboratory
The Pennsylvania State University
University Park, PA 16802

Dr. James Pappis
Raytheon Co.
Research Division
28 Seyon Street
Waltham, MA 02154

Dr. Perry A. Miles
Raytheon Co., Res. Div.
28 Seyon Street
Waltham, MA 02154

Dr. P.E.D. Morgan
Rockwell Science Center
1049 Camino Dos Rios
Box 1085
Thousand Oaks, CA 91360

Dr. G. Ewell
MS6-D163
Hughes Aircraft Company
Centinela and Teale Streets
Culver City, CA 90230

Dr. George W. Taylor
Princeton Resources, Inc.
Box 211
Princeton, NJ 08540

Mr. John J. Theirmann
Physics International
2700 Merced Street
San Leandro, CA 94577

Dr. Herb Moss
RCA Laboratories
Princeton, NJ 08540

Dr. R.E. Newnham
Materials Research Laboratory
The Pennsylvania State University
University Park, PA 16802

Dr. Charles S. Sahagian, Chief
EM Technology Branch, SSS Division
HQ Rome Air Dev. Center (AFSC)
Deputy for Electronic Technology
Hanscom AFB, MA 01731

Dr. J. Smith
GTE Sylvania
100 Endicott Street
Danvers, MA 01923

Dr. Wallace A. Smith
North American Philips Laboratories
345 Scarborough Road
Briarcliff Manor, NY 10510

Mr. Raymond E. Sparks
Technology Library R220
Delco Electronics Division/GMC
Box 1104
Kokomo, IN 46901

Dr. Manfred Kahn
Senior Scientist, Prod. Dev.
AVX Ceramics
Myrtle Beach, SC 29577

Mr. G. Goodman, Manager
Corporation of Applied Research Group
Globe-Union, Inc.
5757 North Green Bay Avenue
Milwaukee, WI 53201

Dr. A.E. Clark
Naval Surface Weapons Center
White Oak Laboratory
Silver Spring, MD 20910

Director
Applied Research Laboratory
The Pennsylvania State University
University Park, PA 16802

Dr. D. Carson
Code 7122
Naval Ocean Systems Center
San Diego, CA 92152

Dr. C. Hicks
Code 631
Naval Ocean Systems Center
San Diego, CA 92152

Dr. R. Smith
Code 7122
Naval Ocean Systems Center
San Diego, CA 92152

Professor R. Buchanan
Department of Ceramic Eng.
University of Illinois
Urbana, IL 61801

Professor B.A. Auld
Stanford University
W.W. Hansen Laboratories of Physics
Stanford, CA 94306

Dr. S. Musikant
General Electric Co.
3188 Chestnut Street
Philadelphia, PA 19101

Dr. A. Gentile
Hughes Research Labs
3011 Malibu Canyon Road
Malibu, CA 90265

Dr. J. Harrington
Hughes Res. Labs.
3011 Malibu Canyon Road
Malibu, CA 90265

Professor G. Kino
Stanford University
Stanford, CA 94305

Dr. Gordon Martin
2627 Burgener
San Diego, CA 92110

Deborah Graves
Ceramic Engineer
Endevco
Rancho Vie Jo Road
San Juan Capistrano, CA 92675

Army Research Office
Box CM Duke Station
Attn: Met. and Ceram. Div.
Durham, NC 17706

National Bureau of Standards
Inorganic Matls. Division
Washington, DC 20234

National Bureau of Standards
Metallurgy Division
Washington, DC 20234

Naval Air Systems Command
Code 320
Washington, DC 20360

Pacific Missile Test Center
Materials Consultant
Code 4121
Pt. Mugu, CA 93042

Naval Research Lab
Code 6400
Washington, DC 20390

Naval Sea System Command
Code 035
Washington, DC 20362

Naval Ship Engr. Center
Code 6101 CTR BG #2
3700 East-West Highway
Prince Georges Plaza
Hyattsville, MD 20782

Office of Naval Research
Department of the Navy
Code 102
Arlington, VA 22217

Dr. G. Bansal
Battelle Laboratories
505 King Avenue
Columbus, OH 43201

Dr. F.F. Lange
Rockwell International
Box 1085
1049 Camino Dos Rios
Thousand Oaks, CA 91360

Dr. G. Denman
Code LPJ
AFML Wright-Patterson AFB
Dayton, OH 45433

Sheldon Detwiler, Disp. Mgr.
Adv. Technol. Laboratories
13208 Northrup Way
Box 6639
Bellevue, WA 98007

Dr. W.G.D. Frederick
AFML Wright-Patterson AFB
Dayton, OH 45433

Dr. P. Gielisse
University of Rhode Island
Kingston, RI 02881

Mr. G. Hayes
Naval Weapons Center
China Lake, CA 93555

Dr. R.N. Katz
Army Materials and Mechanics
Research Center
Watertown, MA 02171

Dr. P.L. Lall
Office of Naval Research
666 Summer Street
Boston, MA 02210

Dr. P. Land
AFML Wright-Patterson AFB
Dayton, OH 45433

Dr. Eugene A. Larson, Pres.
Blue River Laboratories
Box 442
Lewistown, PA 17044

Dr. George Benthien
Naval Ocean Systems Center
Code 212
San Diego, CA 92152

Mr. K. Letson
Redstone Arsenal
Huntsville, AL 35809

Mr. G. Schmitt
AFML Wright-Patterson AFB
Dayton, OH 45433

Mr. F. Markarin
Naval Weapons Center
China Lake, CA 93555

Mr. K.D. McHenry
Honeywell Corp. Tech. Center
10701 Lyndale Avenue South
Bloomington, MN 55420

Dr. R.R. Neurgaonkar
Rockwell International Science Center
1049 Camino Dos Rios
Box 1085
Thousand Oaks, CA 91360

Norton Company--Library
Industrial Ceramics Division
Worcester, MA 01606

James W. Pell
Manager of Development
Rohe Scientific Corporation
2722 S. Fairview Street
Santa Ana, CA 92704

Dr. R.C. Pohanka
Room 619 Ballston Tower
800 N. Quincy Street
Arlington, VA 22217

Dr. R.A. Queeney
126 Hammond Building
The Pennsylvania State University
University Park, PA 16802

J.J. Rasmussen, Manager
Applied Research Division
Montana Energy and MHD R and D
Box 3809
Butte, MT 59701

Dr. R. Ruh
AFML Wright-Patterson AFB
Dayton, OH 45433

James Runt
313 Steidle Bldg.
The Pennsylvania State University
University Park, PA 16802

Dr. T. Sentementes
GTE Sylvania
100 Endicott Street
Danvers, MA 01923

State University of New York
College of Ceramics
Attn: Library
Alfred University
Alfred, NY 14802

Dr. R.E. Tressler
Ceramic Science Section
226 Steidle Building
The Pennsylvania State University
University Park, PA 16802

Eric Udd
McDonnell Douglas Aston.
5301 Bolsa Avenue
Huntington Beach, CA 92647

Dr. T. Vasilos
AVCO R and Adv. Dev. Div.
201 Lowell Street
Wilmington, MA 01887

Mr. J.D. Walton
Engineering Experiment Station
Georgia Institute of Technol.
Atlanta, GA 30332

Mr. L.B. Weckesser
Applied Physics Laboratory
Johns Hopkins Road
Laurel, MD 20810

Mertan Brooks
Sandia National Labs
Division 7472
Box 5800
Albuquerque, NM 87185

Darnall P. Burks
Sprague Electric Company
Ceramic Capacitor Operations
Box 5327
Wichita Falls, TX 76307

Dr. Kim Ritchie
AVX Corporation
Box 867
Myrtle Beach, SC 29577

Roger T. Dirstine
Unitrode Corporation
580 Pleasant Street
Watertown, MA 02172

END

DATED

FILM

8—88

DTIC